IDENTIFICATION OF SPATIAL MODELS

FOB TEE VIBRATION ANALYSIS OF LIGHTLY DAMPED STRUCTURES

by

PETER THOMAS GLEESON

B.Sc., Liverpool

A thesis submitted for the degree of Doctor of Philosophy
of London University and the Diploma of Imperial College.

Dynamics Section,
Department of Mechanical Engineering,
Imperial College of Science and Technology,
LONDON, S.W.7.

November 1979

ABSTRACT

It is accepted today that the design of structures should include consideration of their vibrational characteristics. It is thus necessary to obtain structural vibration data by measurement or by use of computer predictions and to evaluate and modify the structures so that satisfactory characteristics are ultimately achieved. The amount of data involved is difficult to handle in all but the simplest cases and so relatively simple computer models become necessary to reduce this amount and to facilitate investigation of the effects of changes of design parameters.

Spatial models consist of matrices of mass, stiffness and damping properties expressed in relation to selected coordinates of interest, in particular at points of connection. The lightly damped structures featured in this thesis have the property that their natural frequencies are easily distinguished from each other. The dynamic range of their mobility properties is very large.

The earlier parts of this thesis are concerned with identification of modal parameters which represent the vibration behaviour of specific points on a structure. Extension is then made to the relationship of several points which are related by natural mode shapes. It is shown that such modal data can be converted into a spatial model of the structure. Particular attention is paid to the need to measure rotational mobilities and cope with the limitations of transducers. The use of residues to represent the effects of modes beyond the range of measurement is explored.

The modelling techniques are initially evaluated on error-free data for ideal systems with finite numbers of modes end beams with unlimited numbers of modes.

The latter parts of the thesis are concerned with the application of the foregoing measurement and analysis techniques to physical structures. Good results are obtained for modelling a simple beam assembly and for prediction of the lowest cantilever frequency of a turbine blade based on measurements of its free-free properties.

ACKNOWLEDGEMENTS

The author is most grateful to his supervisor Dr. D.J. Ewins who has provided sustained.stimulus, guidance and encouragement over the long period in which these studies have been carried out.

Many members of the Dynamics Section have helped with practical advice and discussion of experimental and computing problems. Special thanks are due in this regard to past members Dr. M.G. Sainsbury, Dr. J.M.K. Silva and Mr. G. Maleci and present members Ms. B. Hillary and Mr . J. Griffin. The help provided by Mr. R.D. Gunn in the laboratory is particularly acknowledged.

Mention must also be made of present and former colleagues at Middlesex Polytechnic. Dr. A. Chitty gave by his example initial encouragement into the field of research. The Polytechnic authorities as personified by the Course Leader, Dr. E.P. Booth and Dean, Mr. J. Osborne Moss, made available both time allocation and financial support,which are much appreciated. Mr. P. Moore, Mr. I.J.G. Berry and Kr. M.R.E. Bloyce gave valuable support in lightening the author's teaching and administrative load during the final compilation of this thesis.

Thanks are also due to Mr. R.E. Pearson for constructive criticism of the thesis at 2 formative stage and to Mrs. J. Peak for her careful efforts in typing this work. Finally, the author is grateful for the patience and understanding of his wife,Judy, and children, Kate and Paul.

NOMENCLATURE

a	Acceleration (m/s^2): Length (m)
A	Area of cross section (m^2)
$_rA_{ij}$	Modal constant of r^{th} mode, response at i^{th} coordinate to excitation at j^{th} coordinate
AM	Apparent Mass (kg)
AR	Antiresonance
b	Length (m)
C	Cantilever frequency
C_x, C_Y, etc.	Scaling factors
C_r	Residual flexibility ; Complex constant
d	Length (m)
D_r	Complex constant
e	Length (m) ; exponential number
f	Frequency (Hz)
F	Force (N)
g	Acceleration due to gravity (m/s^2)
G	Centroid
h	Height (m)
$[H]$	Hysteretic damping matrix
$[I]$	Unit matrix
I	Mass moment of inertia ($kg\ m^2$) ; area moment of inertia (m^4) ; Inertance $(m/s^2)/N$)
$[I_S]$, $[I_L]$	Inertia matrices for mass cancellation
i, j	Imaginary number $\sqrt{-1}$; number of coordinate
k_r	Stiffness of r^{th} node
$[K]$	Stiffness matrix
l	Length (E)
L	Lower (suffix)
m	Mass
m_r	Mass of r^{th} node

M	Moment (N m)
$[M]$	Ehss matrix
n	Number
N	Number of modes
P	Number of modes ; Point'
q_i	Generalised displacement of i^{th} coordinate
Q_i	Generalised force at i^{th} coordinate
r	Radius (m) ; mode number
R	**Resonance** ; Residue
$[R]$	Matrix of frequency terms
s	Length (m) ; mode number
S	Residue
t	Time (s)
T	Kinetic energy (J)
U	Upper (suffix)
V	Strain energy (J); Voltage
x	Displacement (m)
X	Displacement (m)
Y	Displacement (m)
Y	Mobility (m/s)/N ; Displacement (m)
z	Displacement (m)
Z	Impedance N/(m/s) ; Displacement (5)
α	Receptance (m/N); angle (rad)
β	Arbitrary Constant; angle (rad)
δ	Displacement (m) ; small increment
ϵ	Strain
η	Damping loss factor
θ	Rotational displacement (rad)
λ	Complex number
λ_r	Complex eigenvalue of r^{th} mode

ρ	Mass density (kg/m^3)
σ	Stress (N/m^2)
Σ	Summation
${}_r\phi_i$	i^{th} element cf r^{th} mode shape vector
$[\Phi]$	Mode shape matrix
ψ	Angle (rad)
$[\Psi], [\Psi']$	Alternative mode shape matrices
ω	Frequency (rad/s)
ω_r	Natural frequency of r^{th} mode (rad/s)
Ω	Response frequency (rad/s)
$[\Omega]$	klternative matrix of frequency terms
$\dot{}$	Differential with respect to tine, $\dot{x} = dx/dt$
$\lvert\ \rvert$	Modulus , Determinant
$\lVert\ \rVert$	Norm
$[\ ]$	Matrix
$\{\ \}$	Column vector
$\lceil\ \rfloor$	Diagonal Matrix

CONTENTS

1. INTRODUCTION

1.1 The Need to Model Vibrating Structures

The design of mechanical structures should include consideration of the vibrational properties of the structures and their components. There are recent trends that highlight the desirability of developments in this field. Designs for structures and components, small, large, mechanical, civil, all tend towards the narrowing of safety margins and the use of less massive components. Light structures tead to have higher natural frequencies 2nd consequently are prone to fatigue more quickly than their heavier predecessors. Changes in methods of fabrication, too, contribute to a general increase in the level of vibration since bolted joints which have friction damping are often replaced by welds or by adhesive with small dissipative properties. A parallel tendency is an increasing intrusion of vibrational effects 2nd consequential acoustic ones into the human environment. These netters have been reviewed recently by Grootenhuis (1).

Accepting the need for study of the vibration of structures, it becomes necessary to consider the methods applicable. If the structure can be represented by simple components such 2s beams, plates and shells, then modern computational methods, in particular finite elenent techniques, can be used to Predict vibration properties from design data. Many structures , however, contain components which cannot easily be modelled theoretically either because cf the complexity of their shape (for example, 2 turbine blade) or because of non-linearity and temperature or frequency dependence as exemplified by 2 damped viscoelastic isolation mount. In such cases, direct measurement of vibration is desirable.

Many neasurenent systems are now available and the gathering of vibration data is made easy by automatic recording devices. it is not so easy to make sense of the data or even to gather wisely.

In some applications it may be possible to make direct use of measured data but in most cases data reduction is necessary in order to save storage space and time of computation. It is thus desirable to abstract from the large amount of available information that which best simplifies and characterises the material. This is the essential feature of the modelling process.

Most fields of study involve this or an analogous sequence of steps; the gathering of data, its classification, the evolution of coherent ideas, the testing of hypothetical representations and then refinement of the concepts. One may observe similarities, perhaps, between the development of actuarial tables from population statistics; or the establishment of the authorship of Chapters of the New Testament from consideration of textual fragments or in the modelling of vibrating structures; all have the objective of producing useful order from apparent chaos.

it has to be said that the manufacturers of vibration test equipment can also supply computer programs for modelling the data obtained. Such programs are sophisticated and their complexity discourages the user of the equipment from enquiring too deeply into the validity of the models developed. No doubt, in a najcrity of cases, the results are quite satisfactory but it is desirable, in the author's opinion, for the development engineer designing a structure to understand the process by which a model is obtained so that he can use his experience and judgecent in the selection of data.

The modelling procedures which form a significant part of'this thesis are essentially simple and each step is capable of being tested independently. Computer programs are used but data have to be handled by hand calculator at certain junctures. Such manual work is first done at stages where considerable reductions of data have already taken place, are not onerous and have the advantage of giving insight.

The method is economical in tine of computation. When it works, it works quickly. When it fails, because of error or because damping is heavy, the failure is rapidly apparent. It cannot be used 2s the only analytical ool but is potentially nost valuable when used judiciously.

1.2 Fundamental Concepts

This section consists of a review of the basics of the vibrations of structures, and an introduction to three-dimensional graphical representations of a 'response surface'. A variety of models is discussed as a prelude to the identification of data which is the subject of Chapter 2.

Identification is here defined as the process of determining the parameters of a system from observations of that system's frequency response.

1.2.1 Structural Vibration

A structure* consists of components having properties of mass, stiffness and damping which are distributed in space either in the form of lumped parameters or as a continuous system. The structure may be approximately described by a finite number of time-dependent displacement coordinates showing the instantaneous spatial distribution of its components. Certain of the coordinates might be related by equations of constraint but there will be N independent coordinates, each corresponding to a degree of freedom, which are known as generalised coordinates.

If the structure vibrates, its motion is governed by energy, oscillating between that associated with inertia elements (kinetic energy) and that stored in elastic elements (potential energy). There say also be an input of energy from an external source and there will certainly be in practice a dissipation of energy because of damping. Lightly-damped structures, the subject of this study, may be assumed to dissipate only a small part (say 5% or less) of their energy during each cycle.

Equations of motion can be formulated, for example, by applying the methods of Lagrange to expressions of energy. Such equations relate the forces applied to a structure to its displacements.

---

* Key words are underlined in this Chapter uhen their specific meanings are introduced.

Important properties of the structure are associated with free vibrations which are observed if it is left unconstrained after a disturbance. In such circumstances the vibration will occur at one or more of N discrete natural frequencies which are determined by the mass and stiffness parameters of the structure. *ht* each natural frequency the structure moves in 2 natural or principal mode. The mode shape is defined in terms of the generalised coordinates by a column vector which has arbitrary amplitude but fixed ratios between its elements.

A set of principal coordinates for the structure is so chosen that when it vibrates in a principal mode only one coordinate varies while the others remain zero. Thus principal modes have the property of orthoaonalitv. If 2 principal coordinate is normalised so that it has defined amplitude it is then known 2s a normal coordinate. A set of norm21 coordinates is linearly related by a transformation matrix to the set of generalised coordinates and it is thus possible to recast the equations of motion in terms of the normal coordinates. This procedure has the advantage, because of orthogonality, of uncoupling the equations and making them easier to solve, although they 2re now expressed in mod21 rather than spatial parameters.

When 2 structure is set into motion by applied forces it responds to 2 greater or lesser extent depending on the magnitude and on the time-dependent characteristics of the force, be it random, impulsive, sinusoidal or periodic, No matter what form the force takes it is useful to consider the freouencv response of the structure which involves the relationship between sinusoid21 force 2nd resultant motion. This is not 2 restriction which causes loss of generality because the mathematical relationship between sinusoidal 2nd otherforms of excitation is well established.

The most useful way of quantifying frequency response is to calculate the mobility of the point of interest on the structure. Mobility

is the ratio of harmonic velocity/force and is in generalacomplex quantity expressed in modulus/phase or real/imaginary form. The other response/force quantities in general use are receptance (displacement/force) and inertance (acceleration/force). These three quantities are all measurable on a structure with one or more degrees of freedom since it is possible to arrange that there be only one input force at a *specified* coordinate and then to measure the responses at all coordinates. However, it is not usually possible to constrain the system so that there is only one non-zero response when there are input forces applied at all coordinates. This means that force/response quantities are not directly measurable *for a systen* with more than one degree of freedom. The three force/response quantities are dynamic stiffness (force/displacement), mechanical impedance (force/velocity) and apparent mass (force/acceleration).

The six quantities are known generally as mechanical impedance data (or latterly as mobility data) and their use is an example of the mechanical impedance method. Each is a ahasor quantity, being represented on the Argand diagram by a rotating phasor(as is electrical impedance)but they have the added complication not encountered in the electrical case of being vector quantities requiring description in spatial terms. In the most general case one point on a sinusoidally vibrating structure may have three translational and three rotational coordinates each of which has a time dependence which can be described by a rotating phasor.

The structural vibration concepts briefly summarised above are exhaustively treated in books by Hurty and Eubinstein (2 j and -- Meirovitch (3). iiobility methods are comprehensively introduced by Ewins(4) who gives an extensive list of references. Books by Bishop and Johnson(5) and Salter(6) are classic works in this field. The book by McCallion(7) covers much of the ground and has the advantage over those two 'classic' works of being still in print.

1.2.2 The Response Surface

The frequency response characteristics of several points on a beam are represented in two dinensions in Figure 1.1. The beam is undamped, freely supported and excited et the right-hand tip. Each line represents the linear mobility of a point on the beam 2s 2 function of frequency. Such data can be represented by equation (1.20) of section 1.3 following 2nd can be found by vibration testing,

The positive sections of the curves are those where the response is in phase with the sinusoidal stinulus. Figure 1.1(a) shows the point response for which both stimulus and response are at Z = 1, the right hand tip. In this case the response is in phase with the stimulus on the low-frequency side of the discontinuous change of phase et each resonance. The out-of-phase response at lowest frequency plotted is that appropriate to the high-frequency side of the zero natural frequency of the rigid body mode. Changes cf phase are also observed at the zero-crossings which are characteristic of antiresonances.

The second curve, Figure 1.1(b) has similar features to the first but the resonances are not so pronounced. This is 2transfer response, being the response at Z = 0.75 to force input at Z = 1. Parts (c),(d) and (e) of Figure 1.1 show transfer responses et locations progressively further along the beam from the stiaulus.

The relationships which exist between these curves canbe nore clearly seen by making an ensemble in three dimensions, the third dimension being distance of the response location along the beam. The result is 2 response surface, a general view of which is given 2s Figure 1.2.

In this example twenty-one evenly spaced points have been chosen from the infinite number available for the continuous system and the twenty-one curves are placed along the Z axis according to their spatial

coordinates. Date were calculated at 101 frequencies to give each curve.*

The response surface gives considerable information about the vibration properties of the beam. If it is viewed from 2 location near the Z axis 2s in Figure 1.3 a series of maxima are seen in all the curves at the resonance frequencies which coincide with natural frequencies. In this presentation of linear mobility the discontinuous change of sign of response as the stimulus frequency passes through resonance is clear. It is also seen that away from resonance responses tend to be relatively small.

A view along the frequency axis 2s in Figure 1.4 reveals the rode shapes of the been. The tilted straight line visible et the lowest frequency is indicative of the rigid body mode. At a frequency just below the first resonance the peak mobilities of the twenty-one points define a simple spatial curve showing the first bending rode with a positive maximum. At the next frequency, just above this resonance, a similar curve of opposite sign can be seen. Thus the change of phase on passage through resonance is again apparent. The different amplitudes of the node shape curves are related to the closeness of the stimulus frequency to the natural frequency. The amplitude would, in this undamped case, be unbounded if the forcing frequency was to coincide exactly with the natural frequency. The surface becomes infinitely steep 2s resonance is approached and the amplitude is in practice difficult to estimate although the frequency of resonance can be closely defined. The rode shape can be expressed in terms of the displacement or translation of the curve from 2 neutral position. It can also be defined by the slope or rotation of the curve or by 2 combination of these translations and rotations.

* The data for the response surface were calculated using the author's Fortran program FREBES and the curves were plotted using PICASO graphics developed by Dr. J. Vince at Middlesex Polytechnic. The example chosen was the Long bees of Chapters 4, 6 2nd 7 of this thesis.

The birds-eye view obtained by looking at the surface along the mobility coordinate as in Figure 1.5 reveals clearly the straight parallel lines at which there are changes of sign at resonance. It also reveals that other sign changes occur as mobility passes through zero at antiresonances. It is clear that a resonance affects every part of the systemat the sane frequency but that 2n antiresonance is a localised characteristic. At the point at which excitation is applied, the lower end of the beam in Figure 1.5, antiresonances and resonances alternate, this being a necessary characteristic of point responses. ht the opposite end of the beam there are no antiresonances, the non-zero minimum between resonances having no associated phase change. For intermediate Points on the bean the number of 2ntiresonances decreases with distance from the stimulus, a clear pattern being discernible. In general, transfer responses, involving force input at cne point and response at another include fewer antiresonances as the distance of transfer increases.

A significant effect of changing the driving point in a vibration test is indicated in Figures 1.6, 1.7, 1.8 and 1.9 *which* show the response of the beam to a central excitation. The beam centre is a node - for alternate modes of vibration a point of zero motion — and these modes are therefore not excited. Thus in such cases natural frequencies are not frequencies of resonance.

The response surface represents the large amount of vibration data available as a result of testing. It may be sampled in various ways in order to model the system and thus reduce the data needed to represent the system's vibration characteristics.

1.2.3 Mobility, Modaland Spatial Models

The values of mobility represented on the response surface at one particular frequency correspond to stimulus along cne coordinate and thus correspond to one column of the mobility matrix. There ere N such

columns in the complete mobility matrix $\left[Y(\omega)\right]_{NxN}$ which may be regarded 2s the mobility model of the structure at frequency ω. A model represents the physic21 structure in terms of an array of numbers. When the mobility model is used 2 great deal of data must be stored since there are N^2 complex numbers (or $(N^2 + N)/2$ when the symmetry of the matrix is taken into accountj for each of many frequencies.

Since each element of a mobility matrix can be represented as a summation of modal terms (equation 1.20), it is possible to constructa modal model of a structure which consists of all the modal constants together with the natural frequencies 2nd loss factors. Data for 211 the mod21 constants are contained in the mode shape matrix (equation 1.19). Thus the modal model can be expressed in terms of two NxN matrices with complex elements, the first being 2 diagonal matrix of natural frequencies 2nd mod21 loss factors and the second being the mode shape matrix. The two matrices contain only $(N^2 + N)$ complex numbers in tot21 2nd they are independent of the forcing frequency. Thus the amount of data to be stored for the modal model is very much less than is needed for the mobility model. If the mobility model is needed, for coupling calculations perhaps, it can be regenerated for each chosen stimulus frequency from the modal model. The process of extracting modal data from frequency responses is known as mod21 analysis or system identification.

Modal constants for one element of the mobility model can be identified, as we shall see, from 2 limited sample of data taken along one response line of the response surface, finding the frequencies of resonance and the level of response st interspersed off-resonance frequencies. This is considered in detail in Chapter 2.

It would seem to be an equally valid method of acquiring mod21 data to establish a resonance and to sample each point et resonance - working et right angles, 2s it were, to the identification process indicated

above. Such methods are used in many cases, but they are fraught with practical difficulties.

Chief among these difficulties is the effect of damping. The amount of damping controls the amplitude which can be attained at resonance. In practice, the nature of damping is poorly defined and the various models that have been proposed, viscous, structural, Coulomb, etc. are at best first order approximations. The fundamental conclusion of the investigation by Bishop 2nd Gladwell [8] into resonance testing was that the whole pattern of such testing revolved around the nature Of the damping of the system under test. At that time (1963) there were few experimental date relating to the mechanics 2nd the effects of damping. Silva [9] and Beards [10] report on the current information about damping effects but the problems are by no means solved.

if the damping is light, the case considered in this thesis, the frequencies of resonence are well defined 2nd separated from one another although the amplitudes and mode shapes at resonance are not easy to establish accurately by direct measurement. Fortunately, the method of identification developed in Chapter 2 does not require knowledge of resonence amplitudes, at least in the first instance, since off-resonance data substantially independent of damping effects are used in the calculation of modal constants related to mass and stiffness.

Where damping is heavy, resonances interact 2nd the resolution of mod21 data has to be done mode by mode, or with small groups of modes, by circle fitting polar plots 2s outlined in section 1.3.1. in such an instance the damping parameters are established first and stiffness 2nd mass values subsecuently. The accuracy of the letter data is dependent on the measurement accuracy 2nd the appositeness of the assumed model of damping. This dependence or damping is a severe disadvantage. Although this is an active field of research with recent

work published by Silva [9], Gaukroger et al. [11], Goyder [12], Klosterman [13] and Flannelly et al. [14] among others no one method of analysis has established ore-eminence.

In this work damping is considered to be light 2nd being of secondary importance may often be ignored altogether. This approach is justified for three reasons. The first ic the above-mentioned availability for heavily damped systems of developed analytical techniques, which are time-consuming. The second is that many structural components considered in isolation have negligible damping 2nd exhibit vibration behaviour dominated by their mass 2nd stiffness properties. Thirdly, the analytical procedures developed are economical dtime.

Once the modal model has been calculated, by appropriate methods, one may then consider its utility. Certainly it can be used to regenerate mobility data and, in that form, take part in calculation of the effects of coupling substructures. It does not, however, lend itself tc visualisation of the physical structure or to the investigation of the effects of change of mass or stiffness parameters.

The equations (1.12), howevershowhow the modal model can be transformed into a spatial model in which mass and stiffness elements can be related to coordinates cf interest on the physical structure 2nd used directly for coupling.

The spatial rodel can be used directly in the regeneration of mobility date 2s is indicated in Figure 1.10 showing the relationships between the three models discussed. its chief use is in the design Of structures with specified vibration properties such as the avoidance of particular frequencies of resonance. it is amenable, fcr example, to the methods Of Done et al.[15,16] which establish bounds Of response resulting from the addition of mass or stiffness elements to an existing structure.

As indicated in Figure 1 .10 there are relationships between all three models, mobility, modal and spatial and they facilitate comparisons between experiment end theory, always a necessary part of the engineering design process.

Thus the 'theoretical' route to vibration analysis will start with a mathemati cal spatial model and proceed via natural frequencies, mode shapes and modal damping - the modal model - to predicted response characteristics - the mobility model - and there be compared with experimental data.

The 'experimental' route is the converse. It starts with experimental response data and proceeds vie modal data to the spatial model. Comparisons can be made et any stage although it is current practice to concentrate on the matching of modal data. In Chapters 4 and 7 of this thesis comparisons are found Et all levels.

1.3 Mathematical Preliminaries

1.3.1 Vibrations of an N Degree-of-Freedom System

The equation of motion of a sinusoidally-excited N degree-of-freedom system may be written:

$$-\omega^2 [M] \{q\} e^{i\omega t} + i[H]\{q\}e^{i\omega t} + [K]\{q\}e^{i\omega t} = \{Q\}e^{i\omega t} \qquad (1.1)$$

or $$[K + iH - \omega^2 M]\{q\} = \{Q\}$$

where $[M]$, $[H]$ and $[K]$ are N x N matrices representing mass, hysteretic damping and stiffness respectively, and $\{q\}, \{Q\}$ are complex N x 1 column vectors of generalised displacements and forces respectively, and ω is the frequency of sinusoidal excitation.

The equation of free vibration for the system may be obtained from equation (1.1) by replacing ω by λ, a complex quantity which accounts for damped oscillation, and the applied force vector $\{Q\}$ by $\{0\}$.

Thus $$[K + iH - \lambda^2 M]\{q\} = \{0\} \qquad (1.2)$$

This equation represents an eigenvalue problem and has N solutions each relating to a particular mode of vibration.

The r^{th} mode is characterised by an eigenvalue, λ_r and by an eigenvector $\{\psi\}_r$ which specifies the node shape such that:

$$[K + iH - \lambda_r^2 M]\{\psi\}_r = \{0\} \qquad (1.3)$$

The complete set of solutions may be assembled into N x N matrices:

$[\lambda_r^2]$, the diagonal eigenvalue matrix

and $[\Psi]$, the eigenvector, or mode-shape, matrix.

Since the mode-shape vectors are orthogonal they obey the equations:

$$\{\psi\}_r^T [M]\{\psi\}_s = 0$$
$$\{\psi\}_r^T [K + iH]\{\psi\}_s = 0 \qquad \text{for } r \neq s \qquad (1.4)$$

And

$$\{\psi\}_r^T [M]\{\psi\}_r = m_r$$
$$\{\psi\}_r^T [K + iH]\{\psi\}_r = k_r \qquad \text{for } r = s \qquad (1.5)$$

where $k_r/m_r = \lambda_r^2$ which is generally expressed

$$= \omega_r^2 (1 + i\eta_r) \qquad (1.6)$$

ω_r = natural frequency of r^{th} mode

η_r = damping loss factor of r^{th} mode

m_r = nodal mass of r^{th} node

k_r = nodai stiffness of r^{th} node

Equations (1.4) and (1.5) may be more concisely expressed in terms of the mode shape matrix:

$$\begin{aligned} [\psi]^T [M][\psi] &= [m_r] \\ [\psi]^T [K + iH][\psi] &= [k_r] \end{aligned} \qquad (1.7)$$

Other forms cf normalisation are common. The most popular is mass-normalisation, summarised in the equations:

$$\begin{aligned} [\Phi]^T [M][\Phi] &= [1] = [I] \\ [\Phi]^T [K + iH][\Phi] &= [\lambda_r^2] \end{aligned} \qquad (1.8)$$

for which $\{\phi\}_r = \{\psi\}_r / \sqrt{m_r}$ (1.9)

is also a solution of equation (1.2).

Stiffness-nomalisatioc may also be encountered:

$$\begin{aligned} [\Psi']^T [M][\Psi'] &= [1/\lambda_r^2] \\ [\Psi']^T [K + iH][\Psi'] &= [1] = [I] \end{aligned} \qquad (1.10)$$

with $\{\psi'\}_r = \{\psi\}_r / \sqrt{k_r}$ (1.11)

The mass-normalised node shape vector $\{\phi\}_r$ is used in this work.

The conversion of a modal model to a spatial model is accomplished by rewriting equation (1.8), premultiplying by $[\Phi]^{-T}$ and postmultiplying by $[\Phi]^{-1}$ to get:

$$\begin{aligned} [M] &= [\Phi]^{-T} [\Phi]^{-1} \\ [K + iH] &= [\Phi]^{-T} [\lambda_r^2] [\Phi]^{-1} \end{aligned} \qquad (1.12)$$

Proceeding further by substituting these matrices in equation (1.1) we get:

$$\left(-\omega^2 [\Phi]^{-T}[\Phi]^{-1} + [\Phi]^{-T}[\lambda_r^2][\Phi]^{-1}\right)\{q\} = \{Q\} \quad (1.13)$$

Premultiplying by $[\Phi]^T$ and rearranging:

$$[(\lambda_r^2 - \omega^2)][\Phi]^{-1}\{q\} = [\Phi]^T\{Q\} \quad (1.14)$$

Premultiply by $[1/(\lambda_r^2 - \omega^2)]$ and then $[\Phi]$ to get:

$$\{q\} = [\Phi][1/(\lambda_r^2 - \omega^2)][\Phi]^T\{Q\} = [\alpha]\{Q\} \quad (1.15)$$

where $[\alpha]$ is a matrix of receptance quantities.

If $\{Q\}$ has only one element, in the k^{th} row; we get:

$$[1/(\lambda_r^2 - \omega^2)][\Phi]^T\{Q\} = \begin{Bmatrix} {}_1\phi_k/(\lambda_1^2 - \omega^2) \\ {}_2\phi_k/(\lambda_2^2 - \omega^2) \\ \vdots \\ {}_N\phi_k/(\lambda_N^2 - \omega^2) \end{Bmatrix} Q_k(\omega) \quad (1.16)$$

The response q_j is obtained by premultiplying this column by the j^{th} row of $[\Phi]$

$$\text{Thus } q_j(\omega) = ({}_1\phi_j \; {}_2\phi_j \; \cdots \; {}_N\phi_j) \begin{Bmatrix} {}_1\phi_k/(\lambda_1^2 - \omega^2) \\ \vdots \\ {}_N\phi_k/(\lambda_N^2 - \omega^2) \end{Bmatrix} Q_K(\omega) \quad (1.17)$$

which gives:

$$\frac{q_j(\omega)}{Q_k(\omega)} = \alpha_{jk}(\omega) = \sum_{r=1}^{N} \frac{{}_r\phi_j \; {}_r\phi_k}{(\lambda_r^2 - \omega^2)} \quad (1.18)$$

We define a 'modal constant':

$$ {}_r\phi_j \; {}_r\phi_k = {}_rA_{jk} \tag{1.19} $$

and using equation (1.6) we obtain:

$$ \alpha_{jk}(\omega) = \sum_{r=1}^{N} \frac{{}_rA_{jk}}{\omega_r^2 (1 - (\omega/\omega_r)^2 + i\eta_r)} \tag{1.20} $$

in which the receptance α_{jk} at a particular frequency ω is expressed as the sum of a series of modal terms.

It is interesting to observe from equation (1.19) that the full N x N matrix of modal constants at the r^{th} natural frequency may be obtained from knowledge of the r^{th} N x 1 modal column. This relationship forms the basis of the derivation of modal constants of responses not directly measured as discussed in detail in Chapter 2. The complete matrix $[\alpha]_{N\times N}$ can thus se constructed fro-, knowledge of one column, corresponding to single point excitation.

Polar Plots

The receptance $\alpha_{jk}(\omega)$ as defined in equation (1.20) is a complex expression and as such can be represented on the complex plane by a polar plot such as used by Nyquist [17] or Kennedy and Pancu [18]. The plot shows the locus of α_{jk} as the frequency ω is varied and it is conveniently built up in stages:

Figure 1.11 (a) is a plot of the function:

$$1/(1 - (\omega/\omega_r)^2 + i\eta_r)$$

which is a 'modal circle' whose diameter is $1/\eta_r$.

The expression, ${}_rA_{jk}/\omega_r^2$ is a complex number which can be written $C_r e^{i\theta_r}$. Thus Figure 1.11 (b) represents the function

$$(C_r e^{i\theta_r}) / (1 - (\omega/\omega_r)^2 + i\eta_r)$$

which is a scaled and rotated version of Figure 1.11 (a) whose modal circle has diameter C_r/η_r.

So far we have considered only one mode; the other modes whose natural frequencies do not lie in the range $\omega \simeq \omega_r$ will contribute components which are nearly constant with frequency and which can be represented by a complex constant D_r which has the effect of shifting the rotated modal circle away from the origin as seen in Figure 1.11 (c) which represents the function:

$$D_r + (C_r e^{i\theta_r}) / (1 - (\omega/\omega_r)^2 + i\eta_r)$$

Finally, Figure 1.11 (d) shows the complete function:

$$\sum_{r=1}^{N} (C_r e^{i\theta_r}) / (1 - (\omega/\omega_r)^2 + i\eta_r)$$

which consists of several overlapping and interacting modal circles.

Practical Systems

It is convenient to class measured frequency response data into three categories according to the nature of their polar plots. These categories are:

(a) lightly damped

(b) loosely-coupled nodes

(c) tightly-coupled nodes

In the case of a lightly damped system the modal circles are very large and are swept very rapidly as frequency ω is incremented. It is usual to use the type of plot of log α versus log ω developed by Bode [19]. Bode and Nyquist plots for the three categories are shown in Figure 1.12 .

1.3.2 Mobility and Impedance Matrices

A simple example of the use of mechanical impedance data is given in Figure 1.13 in which a beam substructure has three coordinates of interest, two translational and one rotational.

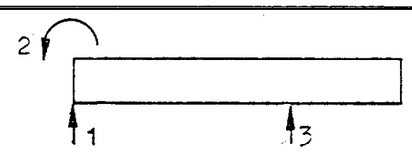

Figure 1.13 Coordinates of interest on a beam substructure.

The responses at the three coordinates are related to the forces which may be applied at those coordinates in the following manner:

$$\begin{Bmatrix} X_1 \\ \theta_2 \\ X_3 \end{Bmatrix} = \begin{bmatrix} (\dot{X}_1/F_1) & (\dot{X}_1/M_2) & (\dot{X}_1/F_3) \\ (\dot{\theta}_2/F_1) & (\dot{\theta}_2/M_2) & (\dot{\theta}_2/F_3) \\ (\dot{X}_3/F_1) & (\dot{X}_3/M_2) & (\dot{X}_3/F_3) \end{bmatrix} \begin{Bmatrix} F_1 \\ M_2 \\ F_3 \end{Bmatrix}$$

or $$\{\dot{X}\} = [Y]\{F\} \qquad (1.21)$$

where all the variables are functions of frequency.

$[Y]$ is the mobility matrix

$Y_{11} = (\dot{X}_1/F_1)$ is a point nobility

$Y_{21} = (\dot{\theta}_2/F_1)$ is a cross mobility

$Y_{31} = (\dot{X}_3/F_1)$ is a transfer mobility

Each element of $[Y]$ measurable since it is possible to apply just one force or moment to the substructure and evaluate the resultant responses.

The relationships between forces and velocities may also be expressed by inverting equation (1.21) to get:

$$\{F\} = [Z]\{\dot{X}\}$$

where $$[Z] = [Y]^{-1}$$

$[Z]$ is the impedance matrix

It is important to remember that the individual elements of $[Z]$ cannot be directly measured but must be found by inverting $[Y]$.*

1.3.3 Coupling of Substructures

The mobility properties of a structure may be predicted from the known mobilities of its substructures by carrying out coupling calculations.

The method may be illustrated by the simple example of Figure 1.14 in which a structure C is formed by connecting substructures A and B at a single coordinate.

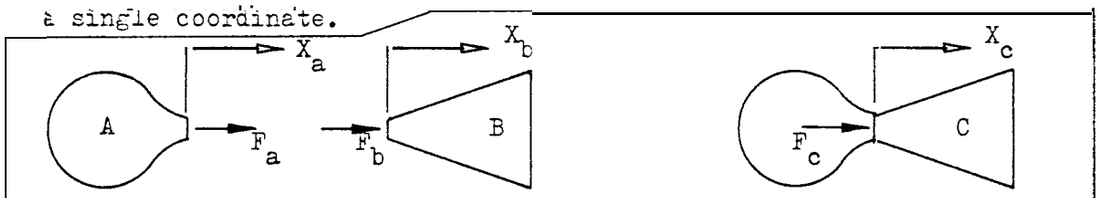

Figure 1.14 A structure formed by addition of substructures.

Excitation and response for each substructure are related by:

$$\dot{X}_a = Y_a F_a \,, \quad \dot{X}_b = Y_b F_b \,, \quad \dot{X}_c = Y_c F_c$$

When the components A and B are added to form C we have:

$$\dot{X}_c = \dot{X}_a = \dot{X}_b \quad \text{and} \quad F_c = F_a + F_b$$

which leads to: $$\frac{1}{Y_c} = \frac{1}{Y_a} + \frac{1}{Y_b}$$

which is, in impedance terms $$Z_c = Z_a + Z_b$$

When the subsystems are coupled at more than one coordinate the equations above become matrix equations:

$$[Y_c]^{-1} = [Y_a]^{-1} + [Y_b]^{-1}$$

or $$[Z_c] = [Z_a] + [Z_b]$$

Thus coupling is carried out by the addition of impedance matrices.

* In some work in this field pseudo-impedances with elements of the form $Z^*_{11} = 1/Y_{11}$ are found. They serve no useful purpose. To avoid confusion such notation should be translated into meaningful mobility terms.

In the general case each substructure will be represented by an impedance matrix referred to coordinates of interest other than those involved in the connections. The coupling technique can be illustrated by using two components: A with n_a coordinates of interest and B with n_b coordinates. The components are coupled at n_c coordinates ($n_c < n_a$ or n_b). The impedance matrices are partitioned so that these coupling coordinates are grouped together.

Thus
$$[Z_a] = \left[\begin{array}{c|c} Z_a^{11} & Z_a^{12} \\ \hline Z_a^{21} & Z_a^{22} \end{array}\right]$$

where the later coordinates are those involved in coupling. The partitioning for B is done so that the earlier coordinates are to be coupled.

The resulting impedance matrix for C has $(n_a + n_b - n_c)$ coordinates and the matrix is composed as follows:

$$[Z_c] = \left[\begin{array}{cc|c} \left[\begin{array}{c|c} Z_a^{11} & Z_a^{12} \\ \hline Z_a^{21} & Z_a^{22} \end{array}\right] & & \begin{array}{c} 0 \\ \hline 0 \end{array} \\ \hline \begin{array}{cc} 0 & 0 \end{array} & & 0 \end{array}\right] + \left[\begin{array}{c|cc} 0 & 0 & 0 \\ \hline 0 & \multicolumn{2}{c}{\left[\begin{array}{c|c} Z_b^{11} & Z_b^{12} \\ \hline Z_b^{21} & Z_b^{22} \end{array}\right]} \\ \hline 0 & & \end{array}\right]$$

$$= \left[\begin{array}{c|c|c} Z_a^{11} & Z_a^{12} & 0 \\ \hline Z_a^{21} & Z_a^{22}+Z_b^{11} & Z_b^{12} \\ \hline 0 & Z_b^{21} & Z_b^{22} \end{array}\right]$$

$$= [Y_c]^{-1}$$

The mobility properties of a structure can thus be found, frequency by frequency, by carrying out matrix calculations based on substructure mobilities. This coupling is the essence of the 'Building Block Method' of Klosterman and Lemon [20] and is facilitated at Imperial College by Sainsbury's computer program COUPLE1 [21]*.

---

* A brief description of each computer program used in this work is provided for reference in Appendix A1.

In this present work much attention is paid to the coupling of two beams at a butt joint. Two coordinates of coupling are necessary in this case, one rotational and one translational. Particular attention is paid to the measurement and use of rotational mobility data.

1.4 Summary of Previous Work

Surveys of System Identification

System identificetion techniques have **Seen established in the** fields of control engineering 2nd aerodynamic stability for many years, and there is now vast literature on the subject [22][23]. Only in the past decade has there been considerable research into the system identification of vibrating structures. Several papers which survey this field of interest have been published. The 1969 paper by Young and On [24] gives an introduction to the field and tabulates the advantages 2nd disadvantages of several identification schemes. Five categories are specified: complete modal information, incomplete nod21 information, transfer function, component modal coupling and response time history product and averaging. Two papers appeared simultaneously in 1972. That by Collins et al. [25] emphasized statistical handling of data and iterative techniques. Their opinion was that modelling techniques had seriously lagged behind analysis capabilities. The paper by Flannelly and Berman [26] was specifically concerned with modelling of aerospace structures. More recently, in 1978, Ewins [27] listed current papers in the field and focussed attention on nobility, nodal 2nd spatial models and the tests by which they might be established experimentally.

In the immediately-following sections previous work is divided into three categories; measurement of mobility data; methods of modal analysis and the synthesis of models. It must be recognised that these categories overlap since, for example, the model sought will influence the selected method of testing, but that there is sone value in making distinctions.

1.4.1 Measurement of Mobility Data

Since a mobility parameter is a ratio of two mechanical quantities it is necessary to make measurements using two transducers, one for force, 2 force gauge, 2nd one fcr motion, most usually an accelerometer.

The usual form of transducing element is piezeolectric although strain gauge and piezo resistive devices are sometimes encountered, especially if measurements have to be made of static quantities or at frequencies below the usual 5 Hz cut off frequency of the piezoelectric transducers.

The standard techniques of using vibration transducers are available from their manufacturers, for example Broch [28] of Bruel & Kjaer and Quackenbush [29] of Endevco. Kerlin and Snowdon [30] report on point impedance measurements. A thorough review-including an extensive bibliography is provided by Ewins [4]. The mobility measurement facilities available to the Dynamics Group of the Mechanical Engineering Department of Imperial College are specified in the work of Sainsbury [31] and Silva [9].

Some part of thework reported in this thesis extends the multi-direction21 measurement techniques developed by Sainsbury. The use of piezoelectric accelerometers 2nd force gauges for measurement of rotations is the subject of Chapter 5.

There 2re many current methods for establishing frequency responses. The classic method involving steady state sinusoid21 forces generated by electrodynamic shakers controlled by variable frequency oscillators is still favoured by experimenters seeking the mode shapes of aerospace structures[32]. It is usuel to employ sever21 shakers carefully adjusted in phase 2nd amplitude so 2s to excite pure modes of the structure under test. The experimental setting up 2nd distribution of force is difficult but the response date eventually obtained require little processing. The multishaker technique was pioneered by Lewis 2nd Wrisley [33] 2nd has been further developed by Fraejis de Veubeke [34], Traill-Nash [35], Asher [36], Ibanez [37], Klosterman [13], de Vries and Beatrix [38], Sloane 2nd McKeever [39], Smith 2nd Woods [40], Gabri 2nd Matthews [41] 2nd Keller and Andress [42]. Bishop 2nd Gladwell [8] provide a critical discussion of the earlier developments.

In many applications it is possible, knowing the derivation properties of the mobility model, to use single-shaker tests to find the complete response data needed.

In recent years, following the development of the Finite Fourier Transform (FFT)* by Cooley and Tukey [43], it has been possible to use minicomputers or microprocessors to calculate, in fractions of one second, the frequency response function associated with 2 non-periodic excitetion such as an impulse or random stimulus. Bamsey [44] has written 2 useful review paper mentioning pure, pseudo- and periodic random excitetion techniques together with sinusoidal testing 2nd impact ('hammer') 2nd step relaxation ('cable release') transient methods. Similar information is presented in the papers of Sissor et al. [45], Peterson and Klosterman [46] and Brown et al. [47].

Impulse excitation with pulses of simple shape are not al-6ays suitable for transient testing, however, because zeroes in the modulus spectre give regions of zero response 2nd uncertainty in neasured data derived by division of Fourier transforms. White [48,49] has developed the rapid frequency sweep technique introduced by Skingle [50] in which, for example, two decades of frequency are swept in one second, the spectrum having a flat modulus and high cut off rates at start and stop frequencies. This type of input, sometimes known as a 'chirp', gives transient results with all modes in the frequency range excited. A critical guide to PST analysis is provided by Williams and Gabri [51] and also Thrane [52,53]. Single point excitation techniques are easier to apply experimentally than multipoint testing but generally require more elaborate analysis as discussed by Leppert et al. [54].

Despite the advantage of FFT methods in speed of testing steady state sine testing is still popular. This method is quite slot: but when controlled by minicomputer can deliver very accurate data in a

---

* Popularly known as Fast Fourier Transform.

reasonable tine, as asserted by Hamma et al [55] and Williams [56] and is the method used for acquisition of experimental data in this present work.

1.4.2 Modal Analysis

The problem of extracting modal date, i.e. resonance frequencies and **mode shapes**, from measured mobilities has been tackled by several investigators. In the general case where damping may not be neglected it is usual to carry out a circle-fitting procedure on data presented in the form of a polar plot. The concept was originally applied to vibration data by Kennedy and Pancu [18] and has been developed for solution using digital computers by Klosterman [13] 2nd latterly by Silva [9] whose method requires only a mini-computer, since the circle-fitting is carried out node by node. in cases cf close modes it may **be** necessary to model several nodes simultaneously and large-computer programs for this purpose have been developed 2nd applied by Gaukroger et al. [57] acd Goyder [12], for example. These methods use least-squrres iterations to converge to a satisfactory result and need initial estinetes of the desired parameters. A consequence of the circle-fitting approach is that modal damping is first calculated and mass 2nd stiffness parameters subsequently. The inherent inaccuracy of the damping model thus affects 211 calculated values.

A least-squares approach is also used by Dat and Heurzec [58] and ' t Mannetje [59] who multiply out equation (1.20) to produce a rational fraction of two polynomials which when suitably weighted, can produce best values *of the* coefficients. The method is suitable for systezs with few resonances only since calculations with polynomials of high degree are unwieldy.

Flannelly et al [60] developed 2 method of modal analysis of damped system. An N x N matrix of complex mobility data was obtained fcr

each node at each of two near-resonance frequencies. Extensive manipulation of real and imaginary parts eventually produced 2 mode shape vector. Repetition of the process over the N modes then gave the complete complex mode shape matrix. The process map be visualised in terms of the response surface 2s identifications of data in 2 series of YZ planes placed at each resonance along tie X or, frequency, axis. The process was checked only by calculations cn computer-simulated rather than experimentally-measured data.

For systems with light damping, simpler methods have been applied. Mobilities of the form of equation (1.20) can be produced by a set of uncoupled oscillators connected in series or connected in parallel to 2 common base. O'Hara & Remmers [61] used this latter model when modelling double cantilever beams. Neubert [62] used a series form with data based on antiresonances rather than resonances, developing an idea of Biot [63] presented in 2 classic paper in 1940. Raney [64] included viscous damping in his model and postulated that data should be measured only near resonances. In effect he found each element of the mass and stiffness matrices of equation (1.7) by considering only one column of the mode shape matrix. Such 2 process provides a curve fit which is valid only around resonances. Raney tested his modelling technique by using computer-simulated data 2nd found it satisfactory, a simple averaging of five estimates of each matrix element being used. It is to be expected that relatively poor results would have been obtained if near-resonance experimental data were used.

Hardenberg [65] formulated 2 matrix expression relating modal constants to measured receptance using the concept of uncoupled oscillators and omitted damping entirely. He successfully modelled the response of 2 free-pinned beam over its first four modes. Hemingway [66] used 2 similar approach but split equation (1.20) into real 2nd imaginary parts and used an iterative technique to estimate modal parameters. His

initial *values,* needed for the iteration, were found by assuming that there was no damping. Thus at the first stage, his method is equivalent to the Hardenberg method which has the advantage of simplicity 2nd speed of computation and provides modal data unaffected by the inaccuracies of damping. This method is extended 2nd its limitations explored in Chapter 2 of this work. As will be seen, it has advantages when applied to experiment21 data obtained in tests on physic21 structures.

1.4.3 Synthesis of Models

There is a well-presented introduction to this topic 'in a paper by Ross (67). He initially distinguishes between low-order models (models of 2 few degrees of freedom) and high-order models, both based on experiment21 vibration data. Low-order models involve matrices of mass stiffness and damping properties which need not have physical significance since their primary function is the accurate modelling of asystem's dynamic response. High order models, on the other hand, are *to* be compared with high-order theoretic21 models (often in terms of finite elements) for which individual matrix elements have physic21 interpretation. There are difficulties, however, because displacement functions used in finite elements rarely equal the true system displacement functions because the *former* are high-strain energy displacements which are poorly approximated by discretizing functions. Boss is mainly concerned with the conversion of the modal node1 expressed in terms of natural frequencies and mode shapes into the spatial model. Reference is made to the methods of Raney (64) and Ibanez (68) which proceed directly from the mobility model to the spatial model.

Ross mentions the case, commonly encountered in experimental work, in which only P of the total of N eigenvectors of 2 system are available, and the inverse of the mode shape vector $[\Phi]$ is not defined. One method for making $[\Phi]$ non-singular is by limiting the number *of*

coordinates used in the modal matrix to 3, the number of vectors determined. This is t-k-e basis of a truncated or incomplete model. The theory of incomplete models is treated by Berman 2nd Flannelly [69] for the particular case of many measurement stations and few natural frequencies; common in aerospace structures. Flannelly et al. [70,71] further considered the properties of truncated models in the prediction cf the effects of changes in system parameters. Returning to the non-singular $[\Phi]$ matrix, Ross considers the addition of (N - P) arbitrary linearly-independent vectors to fill out $[\Phi]$, a technique also suggested by Peterson 2nd Klosterman [46]. But, as Silva [9] comments, this approach creates new problems. In the most common case of a continuous system the idea is impracticable since N tends to infinity. There is much to be said for using a method which is as simple as possible and enables the analyst to exercise maximum control.

Thoren [72] concentrates or the direct identification of 2 low order complete spatial model using Raney's near-resonance technicue already mentioned in section 1.4.2. The method has the defect that the mass matrix is determined as 2 function cf the damping matrix which is liable to have large error. Thoren's comparison of responses predicted from the spatial model with test results shows good agreecent at resonance as one would expect but poor matching in regions away from resonance, although the iineir graphical presentation used tends to suppress the fact.

The pair of papers by Bagley [73,74] deal with 2 very limited 2x2 matrix spatial model representation of a uniform cantilever beam. These papers are, however, significant on two counts. Firstly, an emphasis is puton measurements away from resonance, pref erablyatantiresonances ; thus reducing errors due to shaker connections and to inadequate knowledge of damping mechanisms. Secondly, the procedures were verified by experimental measurements on 2 physical structure.

Flannelly and Giansante [71] carried out tests on a lightly damped bar specimen in order to verify the system identification 'based on the cod21 analysis method [60] referred to in section 1.4.2. The coordinates at which the measurements were made were exclusively translational. They chose response date with forcingfrequencies this time as far 2s possible from the natural frequencies and of a magnitude significantly different (preferably in sign 2s well as magnitude) from that of the rigid body code. The ultimate comparison of regenerated response data with that used for the original identification was very close but the model was not tested in any predictive manner, by coupling to mother substructure or by investigating the effect on frequency response of an added mass, for example.

Goyder [75] recently reported at investigation involving modal analysis and spatial modelling. Thesystem was assumed to have hysteretic damping and the analysis technique depended on the use of near-resonance response data. He concluded that modelling could be used successfully to regenerate measured data and incorporated *a* useful smoothing effect. The regenerated data did tend, however, to be inaccurate in regions of antiresonance. The technique reported involved the identification of the mass matrix as a function of the damping parameters. A particular example of a beam with non-uniform damping led to a spatial model which was inaccurate, because the mathematical model was sensitive to resonances outside the range of measurement.

Thus it can be seer, that there are 2 number of investigators working in the fieid of system identification who are developing techniques 2nd formulation which auite often overlap and at other times are complementary.

1.5 The Scope and Organisation of this Thesis

In the course of this thesis it is intended to demonstrate the feasibility and utility of spatial models with rotational as well as translational coordinates. An underlying philosophy is the desire to achieve simplicity. One may visualise the modelling process as the establishment by measurement of the response surface description of a vibrating structure and then the analysis of that surface remote from resonances so that modal data are revealed which are not affected by damping.

Thus in Chapter 2 the basic identification of one curve in the response surface is done by the one-step solution of a matrix equation. As limitations of frequency range become apparent modifications are introduced at low and high frequencies to mitigate their effects. Corrections for the effects of damping can be made after the mass and stiffness properties of the system are established. The inter-relation of curves in the response surface is then used in order to establish mode shapes which are expressed in terms of rotational and translational spatial coordinates which can be located at points of interest. Spatial modelling is restricted to the case for which the number of coordinates is the same as the number of nodes modelled. The processes involved are demonstrated in Chapter 3 for ideal lumped-parameter mass-spring systems for which the properties of incomplete models are investigated. Further evaluation of the theoretical tools is carried out in Chapter 4 for ideal beams - continuous systems. These are tested by their accuracy in the coupling of substructures.

The latter part of the thesis, commencing with Chapter 5, is concerned with the development and application of the measurement techniques, again with an emphasis on rotations, by which the mobility data of the response surface may be established for physical structures. Experience with measurements on uniform steel beams, the subject of Chapter 6, whose

properties could be accurately predicted, directs the development of exciting blocks for the input and measurement of forces, torques, translations and rotations. Finally, in Chapter 7 the theoretical and practical techniques developed in earlier Chapters are applied to models based on measured data being used for predictive purposes.

Thus the organisation of this thesis may be summarised:

Part 1.	Development of Theoretical Tools	Chapter 2
Tart 2.	Evaluation 0f Theoretical Tools Applied to Ideal Data	Chapters 3, 4
Part 3.	Development of Experimental Tools	Chapter 5
Part 4.	Application of Theoretical end Experimental Tools to Measurements of Vibration of Physical Structures	Chapters 6, 7

The Figures used in illustration and the Tabies of data are in most cases grouped at the ends of the appropriate Chapters.

Figure 1.1 Frequency Responses et Different Points on a Beam
Linear Mobili tv v. Logari thmic Frecuency

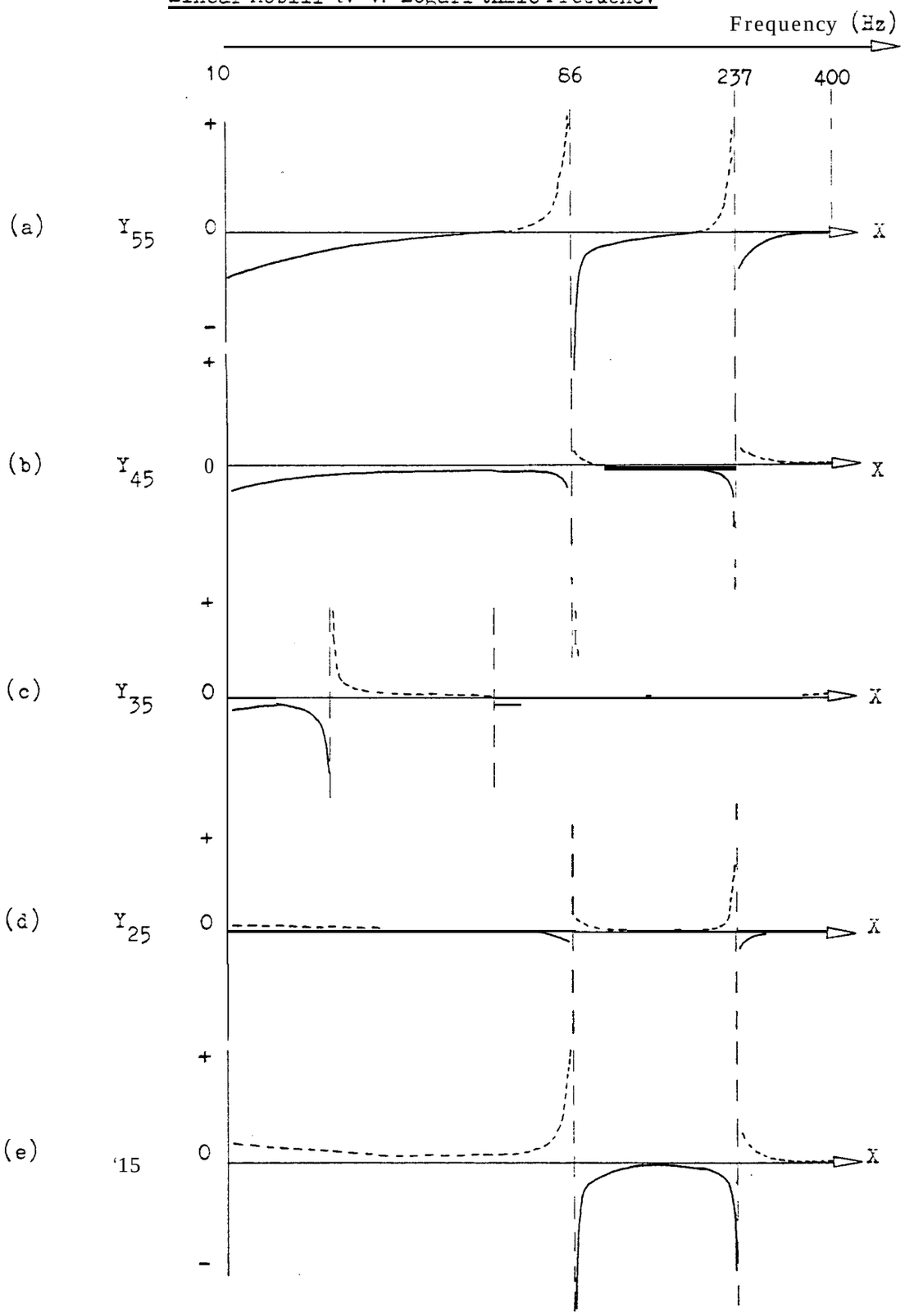

Coordinates 1 , 2, 3, 4, 5 at Z = 0, 0.25, 0.5, 0.75, 1.0 x L, along beam
Stimulus at ZE, tip of bean, coordinate 5
(a) is a Point Response; (b) to (e) ere Transfer Responses

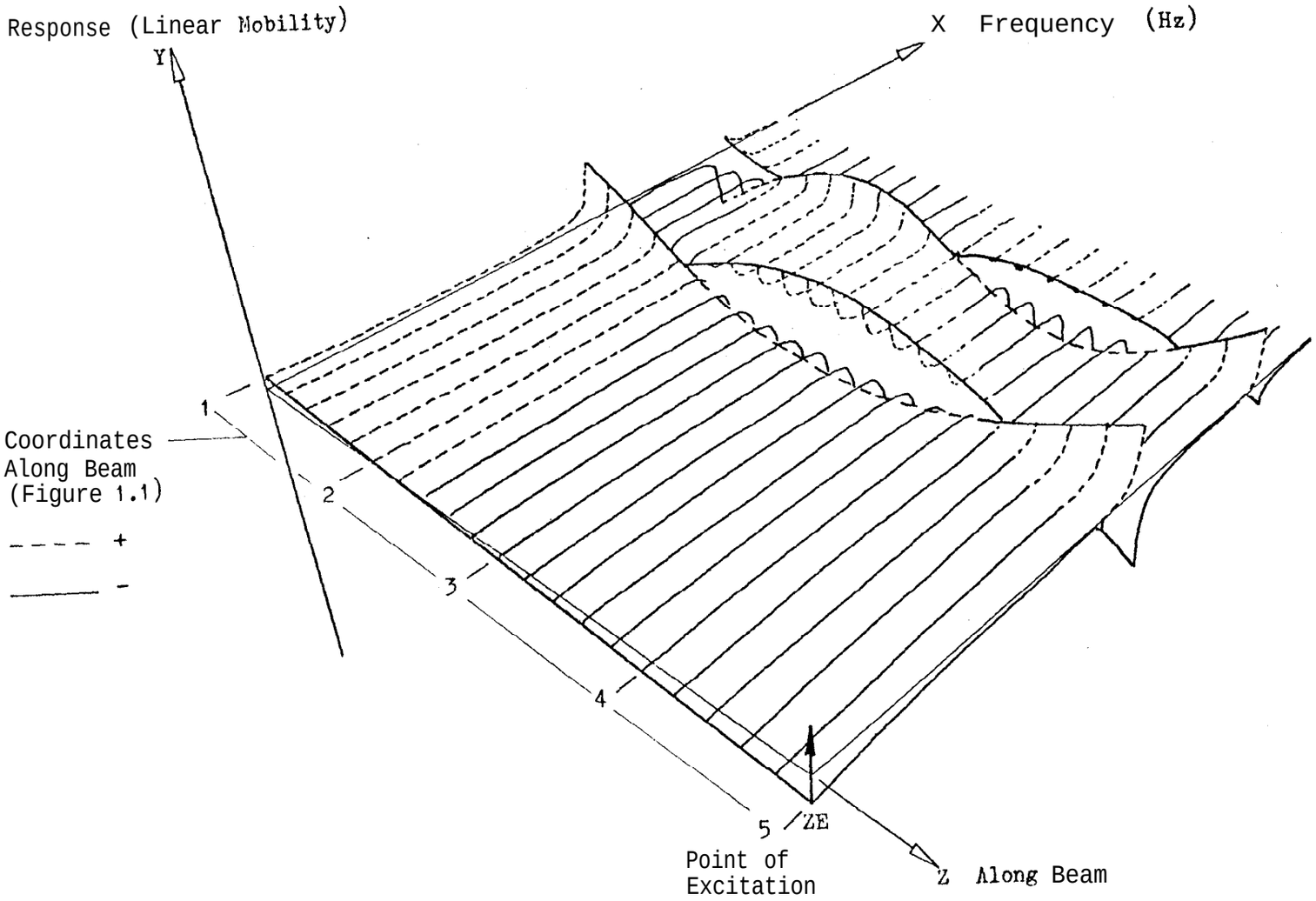

Figure 1.2 General View of Response Surface

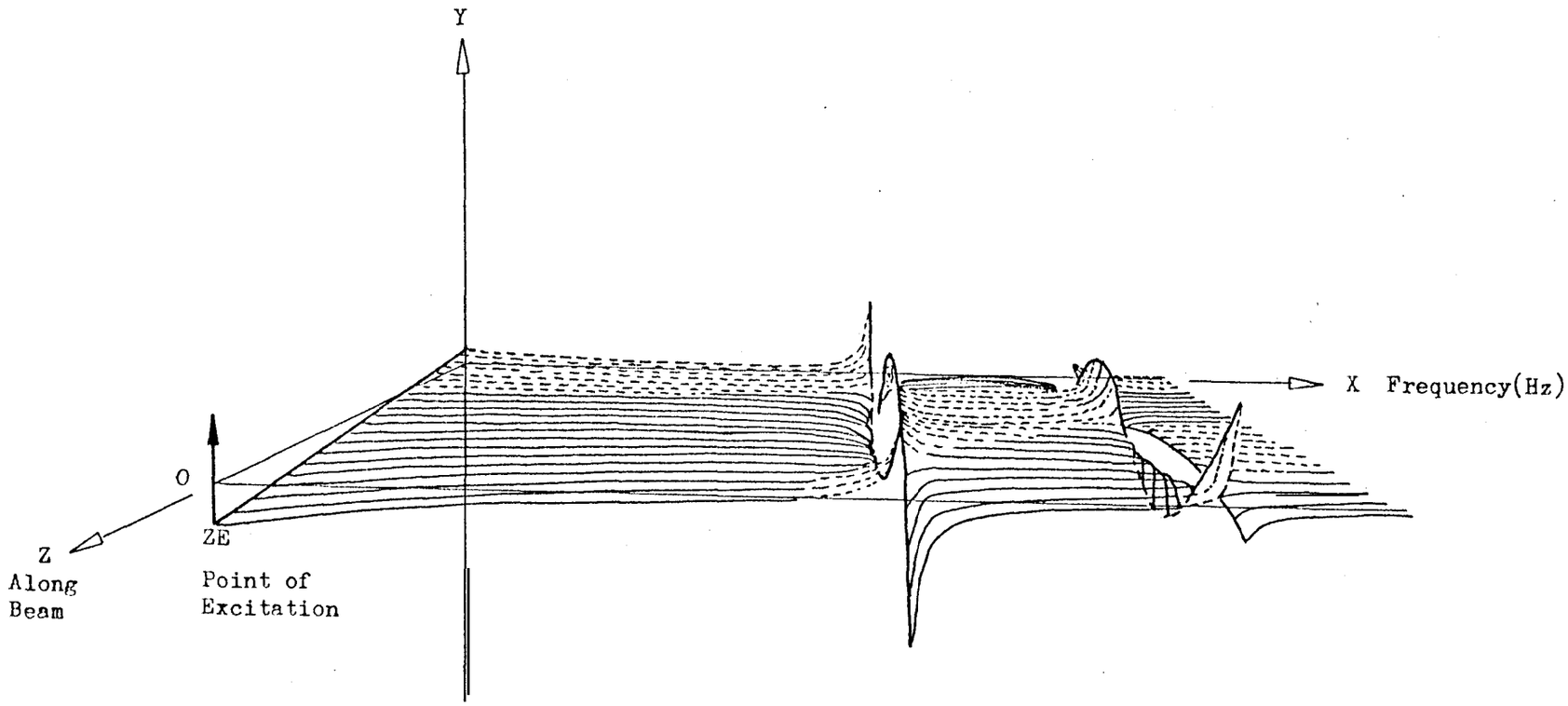

Figure 1.3 Response Surface viewed along Z Axis : Discontinuities at Resonance

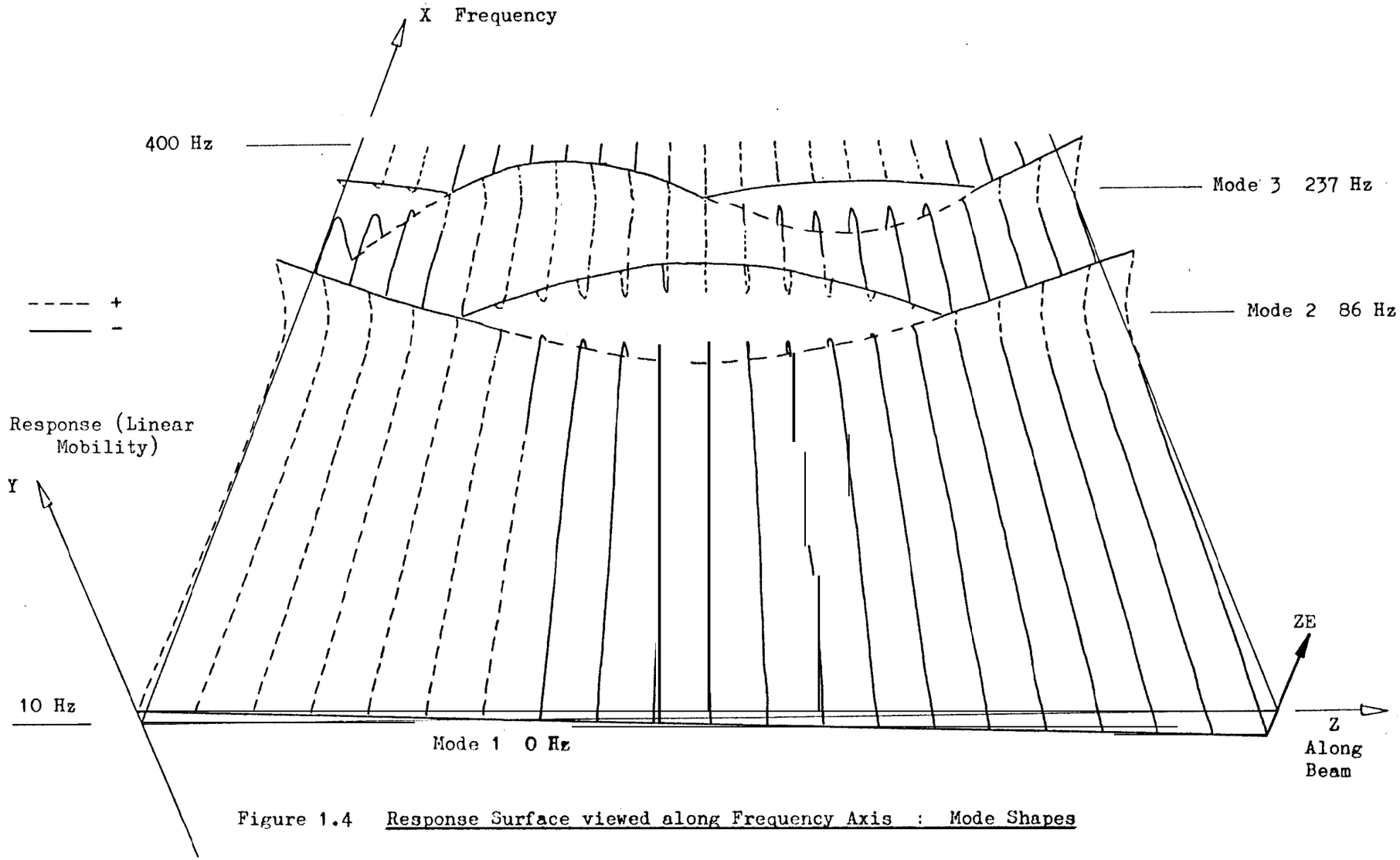

Figure 1.4 Response Surface viewed along Frequency Axis : Mode Shapes

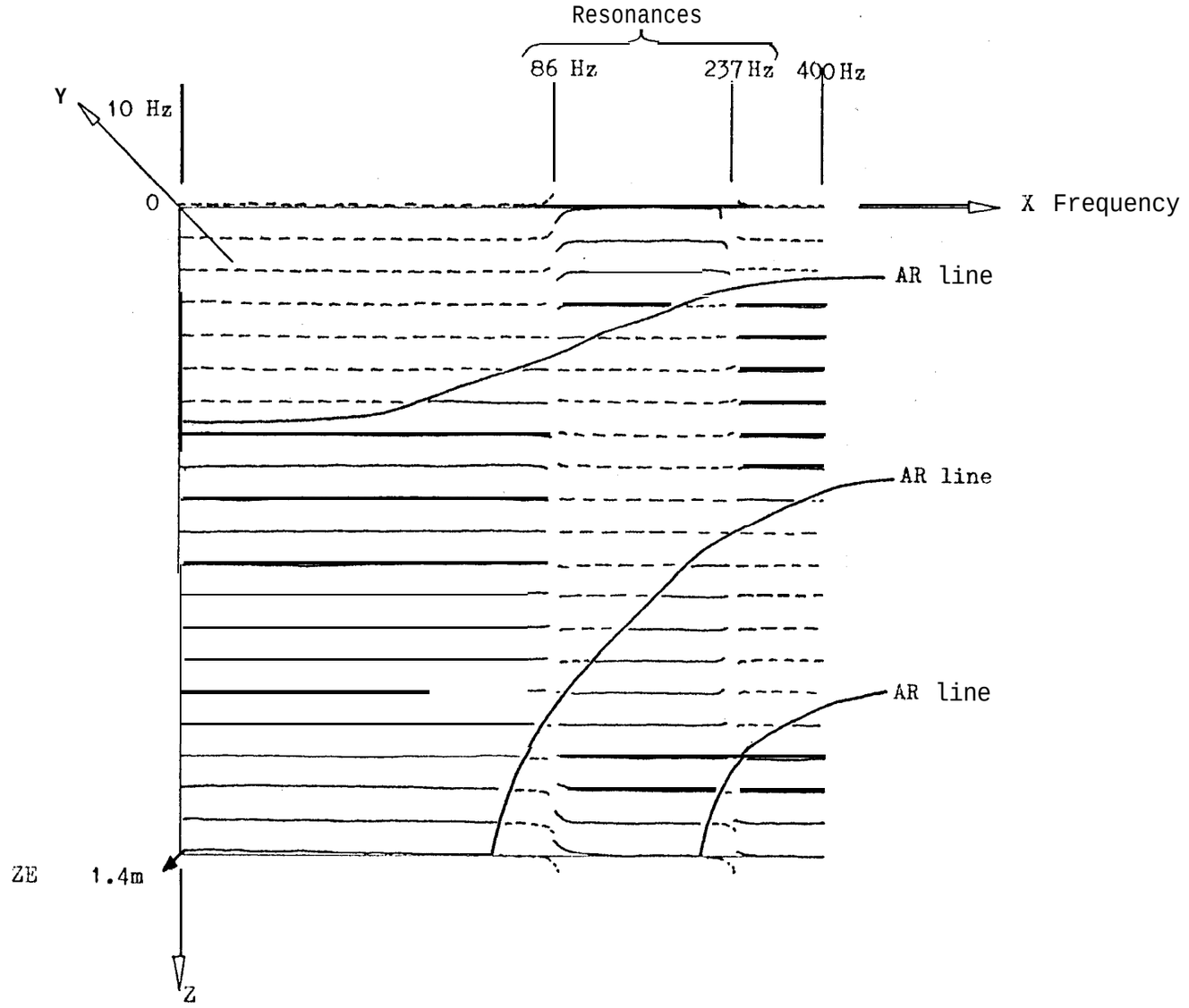

Figure 1.5 Bird's Eye View of Response Surface : Antiresonance Lines

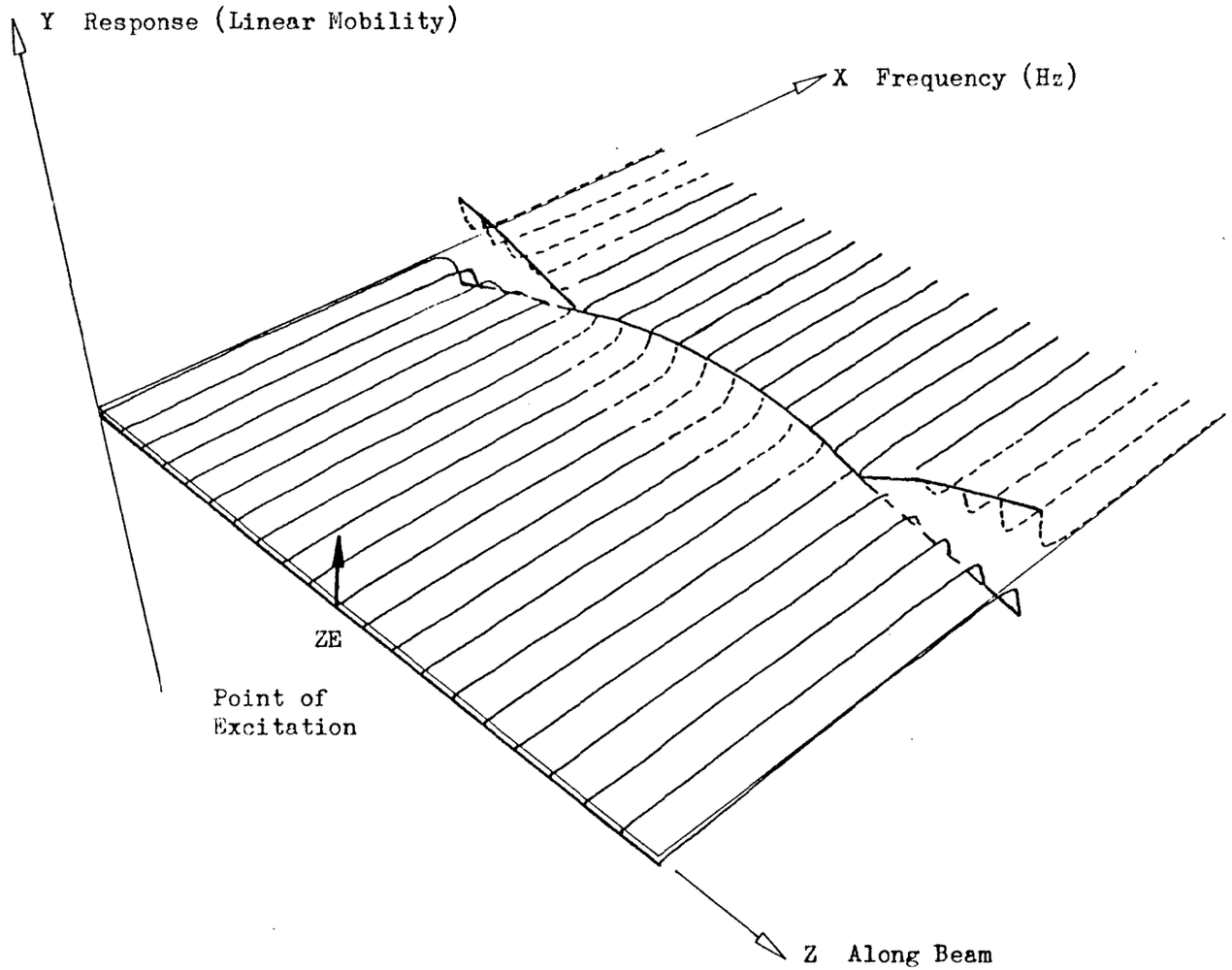

Figure 1.6 General View of Response Surface : Central Excitation

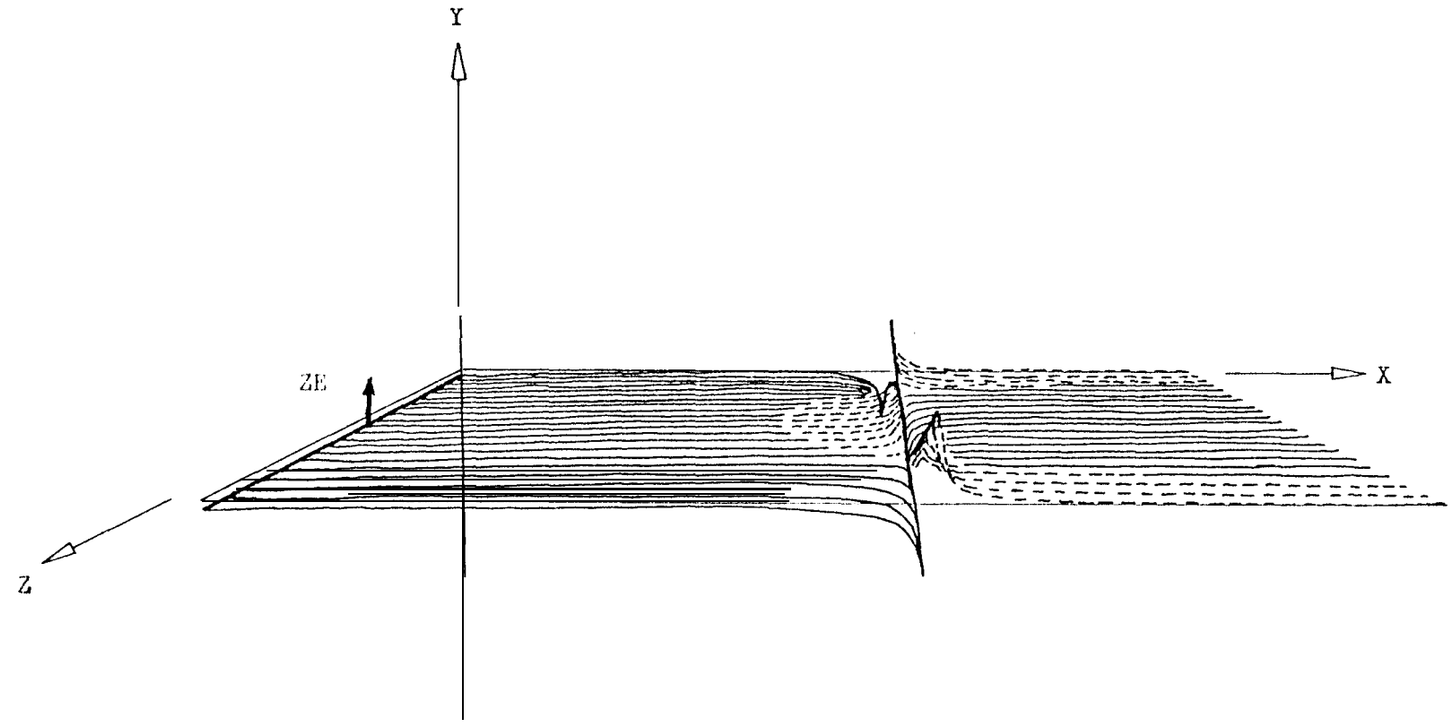

Figure 1.7 Response Surface viewed along Z axis : Central Excitation

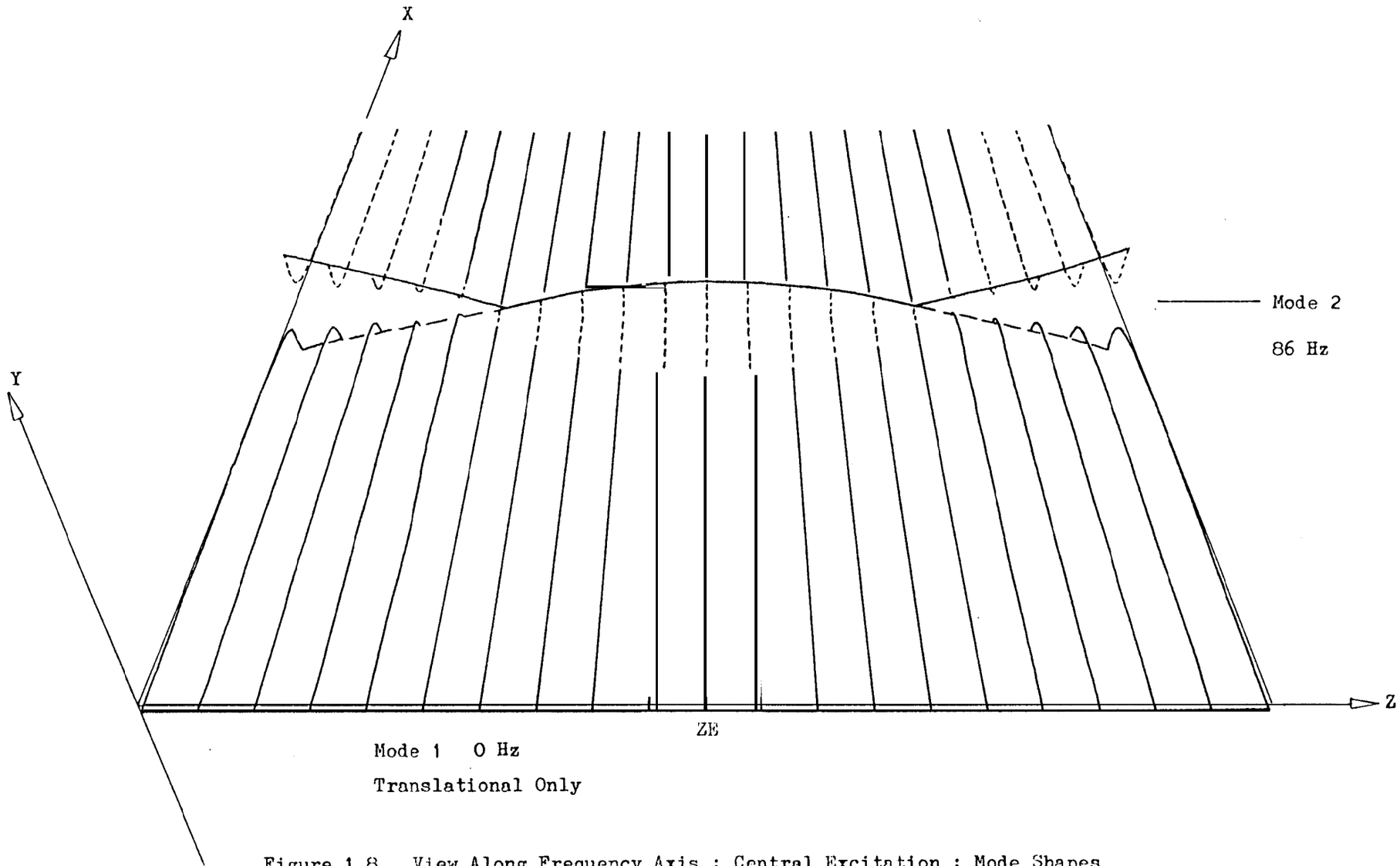

Figure 1.8 View Along Frequency Axis : Central Excitation : Mode Shapes

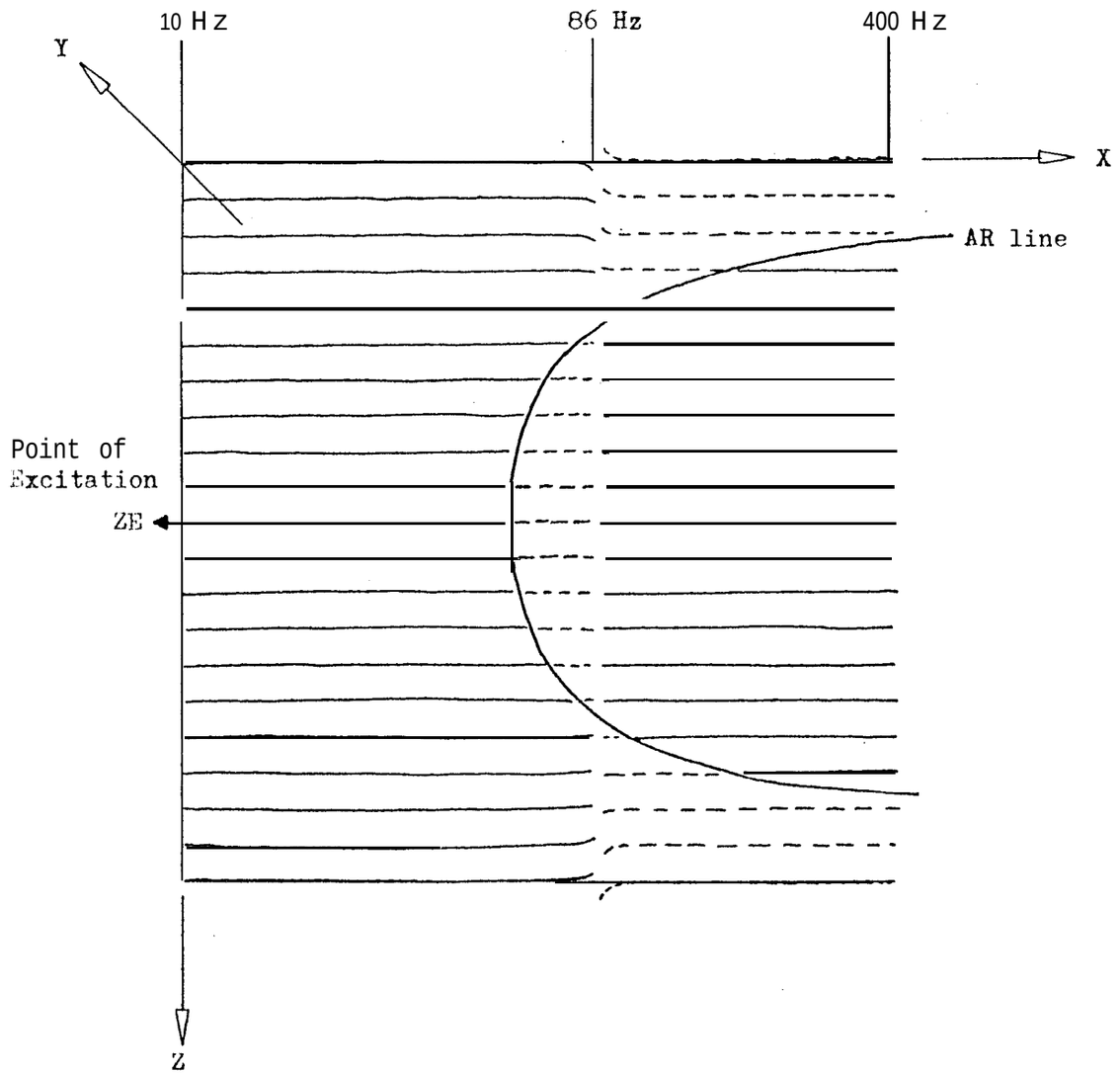

Figure 1.9 Bird's Eye View of Response Surface : Central Excitation
Rotational Body Mode and Second Bending Mode at 236 Hz Not Stimulated

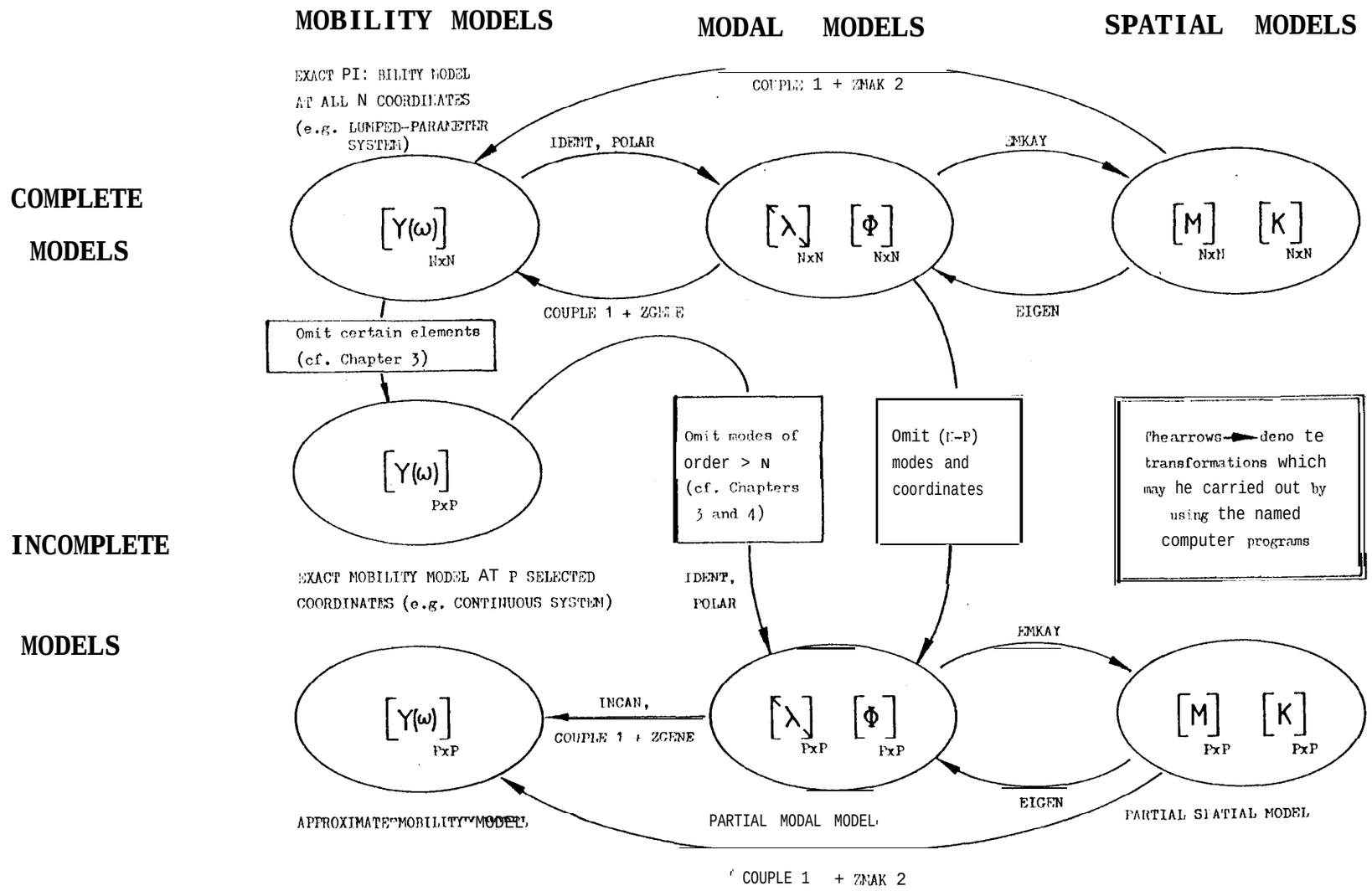

Figure 1.10 Mobility, Modal and Spatial Models

Figure 1.11 Construction of Nyquist Plots of Frequency Response

(a) $1/(1-(\omega/\omega_r)^2+i\eta_r)$

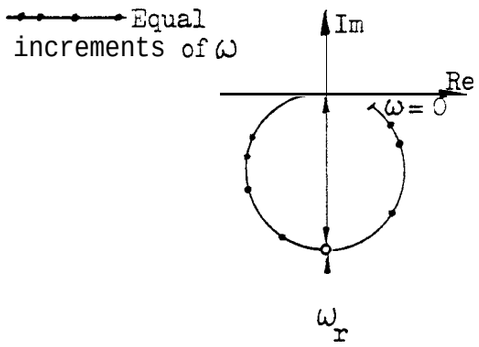

(b) $(C_r e^{i\theta_r})/(1-(\omega/\omega_r)^2+i\eta_r)$

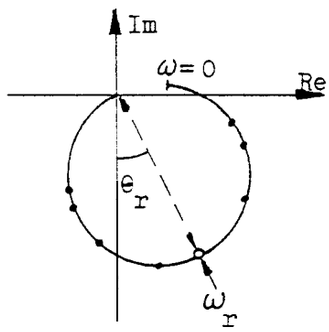

(c) $D_r + (C_r e^{i\theta_r})/(1-(\omega/\omega_r)^2+i\eta_r)$

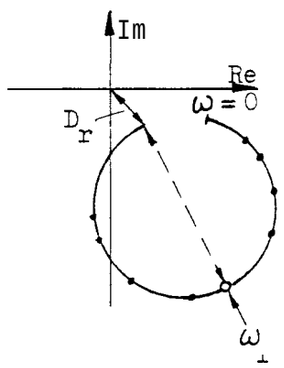

(d) $\sum_{r=1}^{N}(C_r e^{i\theta_r})/(1-(\omega/\omega_r)^2+i\eta_r)$

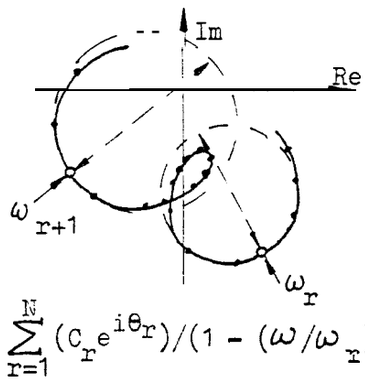

Figure 1.12 Types of Frequency Response Curve

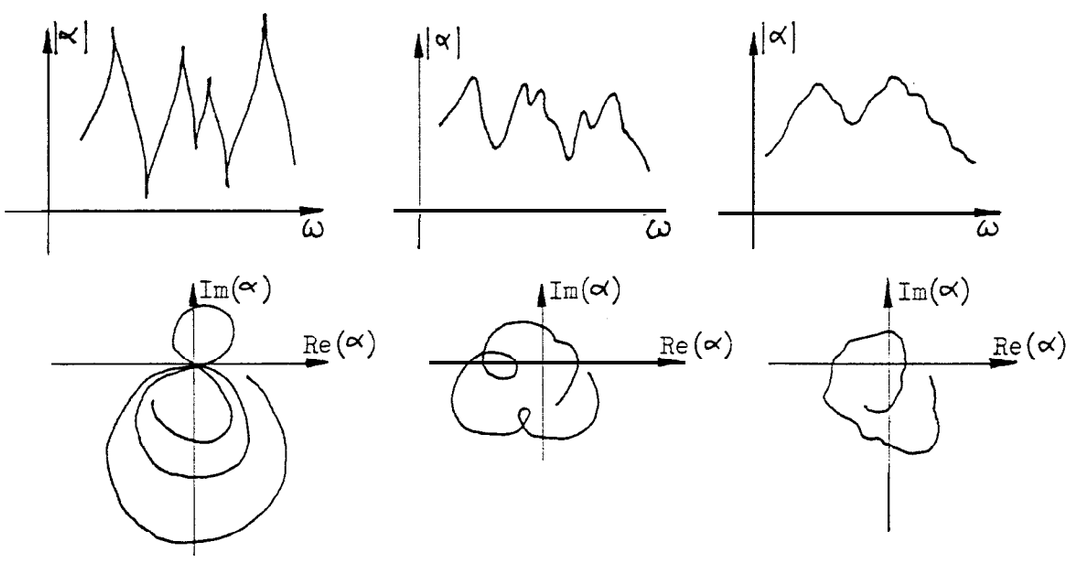

(a) Lightly Damped (b) Loosely-Coupled Modes (c) Tightly-Coupled Modes

2. IDENTIFICATION OF MODAL DATA AND CONSTRUCTION OF TEE SPATIAL MODEL

The objective of the techniques developed in this Chapter is the extraction of the modal model from a structure's frequency responses and the subsequent construction of a spatial model of the structure. Since consideration is restricted to lightly damped systems it is easy to identify the natural frequencies which constitute the eigenvalue matrix $\left[\lambda_r^2\right]$ from any of the curves that make up the response surface of section 1.2.2. The mode shape matrix $\left[\Phi\right]$ is obtained from the modal constants which are formed by consideration of one curve of the response surface at a time in section 2.1. The inter-relationships of modal constants which enable a reduction in the amount of measurement and analysis are treated in section 2.2 and the final 2ssembly of the spatial model is the subject of section 2.3.

2.1 Modal Analysis of One Frequency Response Curve

The number of mod21 constants that can be computed is finite, although there are theoretically an infinite number of modes which contribute to one frequency response curve of a continuous system which has an infinite number of degrees of freedom. Thus in this general case, analysis can provide only incomplete modal representation. However, it is desirable to establish a method of identification of all the nodal constants of 2 system with 2 finite number of degrees of freedom as 2 preliminary.

2.1.1 Complete Modal Representation

Fundamentals of Identification

This is the case where 2 frequency response curve contains contributions from a finite number of modes, N, andis to be analysed into N sets of modal constants. If damping is initially ignored as 2 secondary effect, there is the edvantage of 2 very simple computation yielding reel modal constants.

The key relationships are developed from the equation:

$$\alpha_{jk}(\omega) = \sum_{r=1}^{N} \frac{r^{A}jk}{\omega_r^2 - \omega^2} \qquad (2.1)$$

This may be recognised as equation (1.20) with loss factor η_r set to zero.

We can select N discrete values of $d_{jk}(W)$, say at frequencies $\Omega_1, \Omega_2, \ldots\ldots \Omega_N$ and write:

$$\begin{Bmatrix} \alpha_{jk}(\Omega_1) \\ \alpha_{jk}(\Omega_2) \\ \vdots \\ \alpha_{jk}(\Omega_N) \end{Bmatrix} = \begin{bmatrix} 1/(\omega_1^2-\Omega_1^2) & 1/(\omega_2^2-\Omega_1^2) & \ldots & 1/(\omega_N^2-\Omega_1^2) \\ & & & \\ 1/(\omega_1^2-\Omega_N^2) & \ldots & \ldots & 1/(\omega_N^2-\Omega_N^2) \end{bmatrix} \begin{Bmatrix} 1^{A}jk \\ 2^{A}jk \\ \vdots \\ N^{A}jk \end{Bmatrix}$$

or

$$\{\alpha_{jk}(\omega)\}_{Nx1} = [\Omega]_{NxN} \{A_{jk}\}_{Nx1} \qquad (2.2)$$

An alternative form of this equation arises when the measured data are expressed in inertance form, convenient because acceleration and force are the usual measurands when piezoelectric transducers are used. Using the substitution:

$$I_{jk}(\omega) = -\omega^2 \alpha_{jk}(\omega) \qquad (2.3)$$

equation (2.2) can be rewritten:

$$\begin{Bmatrix} I_{jk}(\Omega_1) \\ I_{jk}(\Omega_2) \\ \vdots \\ I_{jk}(\Omega_N) \end{Bmatrix} = \begin{bmatrix} 1/(1-\omega_1^2/\Omega_1^2) & 1/(1-\omega_2^2/\Omega_1^2) & \ldots & 1/(1-\omega_N^2/\Omega_1^2) \\ & & & \\ 1/(1-\omega_1^2/\Omega_N^2) & \ldots & \ldots & 1/(1-\omega_N^2/\Omega_N^2) \end{bmatrix} \begin{Bmatrix} 1^{A}jk \\ 2^{A}jk \\ \vdots \\ N^{A}jk \end{Bmatrix}$$

or

$$\{I_{jk}(\omega)\}_{Nx1} = [R]_{NxN} \{A_{jk}\}_{Nx1} \qquad (2.4)$$

The natural frequencies $\omega_1, \omega_2 \ldots\ldots\ldots \omega_N$ are obtained from the resonances of the frequency response curve. It is prudent to check by examining other curves belonging to the same response surface that no natural frequency is missed because the point of excitation or response is a node.

The related matrices $[\Omega]$ and $[R]$ contain terms which are functions only of the natural frequencies 2nd the selected response frequencies. The terms are real and of either sign and either matrix is easy to invert. Their relationship may be expressed:

$$[R] = -[\omega^2][\Omega] \qquad (2.5)$$

where $[\omega^2]$ is a diagonal matrix with elements Ω_1^2, Ω_2^2, Ω_N^2 based on the selected response frequencies. The matrix $[R]$ is slightly more convenient to calculate since it involves frequency ratios and, therefore, needs no terms in 2π when data is obtained in Hertz.

The modal constantscan be identified by using either of the equations:

$$\{A_{jk}\} = [\Omega]^{-1}\{\alpha_{jk}(\omega)\} \qquad (2.6)$$

or

$$\{A_{jk}\} = [R]^{-1}\{I_{jk}(\omega)\} \qquad (2.7)$$

The selection of response data points is considered in some detail in section 2.1.2 following but it may be said here that good results are usually obtained if 2s many as possible of those points are anti-resonances. Certainly it is wise to avoid data points near resonance since they are liable to error in the receptance value because of the unaccounted effect of damping 2nd because there would be en exceptionally large element in the matrix $[\Omega]$ whi ch would tend to make it ill-conditioned. Intuitively, also, one would seek to minimise the range of the numerical value of the matrix elements by having the frequencies interspersed $\ldots\ldots \omega_R, \Omega_R, \omega_{R+1}, \Omega_{R+1}$, etc.

As en example, consider the identification of 2 point response of an undamped 5- degree of freedom system (that of section 3.2). The

data used in the identification of the modal constants by analytical, digital means are indicated in Figure 2.1 as a clot of logarithmic modulus of mobility against logarithmic frequency. The segments between the discontinuities at resonance and antirescnance are labelled + or - according to the phase angle (+ or -90°).

There is a striking parallel with the graphical, analogue method of analysis developed by Salter [6] in which a skeleton of mass- and spring-lines of slopes + and - 20dB/decade respectively is sketched onto a measured frequency response plot as shown in Figure 2.2. While the corresponding values of mass and stiffness are not directly the modal mass and modal stiffness properties, they are related to them and one set can be calculated from the other.

The data used in identification of a transfer response are shown in Figure 2.3 in which it may be seen that in the absence of antiresonances between the resonances at ω_2 and ω_4, response frequencies Ω_3 and Ω_4 are set at local minima. Thus, in all, three non-zero responses are used. The corresponding Salter skeleton is seen in Figure 2.4 in which a change of slope from -20 to -40 dB/decade occurs at ω_3 and a further change to -60 dB/decade is seen at ω_4. The slope relaxes by +20 dB/decade at the last antiresonacce, then plunges again to maximum steepness above the final resonance. It is a satter of sone importance that the general level of the point skeleton in Figure 2.2 is roughly constant but that of the transfer skeleton has a very clear and rapid diminution at high frequencies.

The identified modal constants have signs which are the same as those on the low frequency side of resonance in Figures 2.1 and i.3. Thus the modal constants of the point resaonse are all positive and those of the transfer response are of both signs. Plainly, when all nodal contributions are summed as in equation (2.1) the effect of negative terms is to reduce the level of response. Again, transfer responses are seen to have lower levels than point responses.

Damning

Although damping has been omitted from the identification process so far it cannot be ignored altogether. Salter indicates that the skeleton should have its vertical limbs adjusted in length according to the resonant amplitude of the response curve and then be clothed by a curve whose sharpness is inversely related tc the amount cf damping which Salter expresses in terms of Q, the inverse of the loss factor η. This process is analogous to the techniques used by Gerasimov (76) in the modelling of the complete human body starting from the skeleton. Eis subjects ranged from unidentified murder victims to Ivan the Terrible. The important advantage of the identification process of equation (2.3) is that it establishes the modal constants upon which the structure's mass and stiffness parameters depend without any error due to the caprices of damping which is 2 limitation of the polar response circle fitting routines reviewed in Chapter 1.

It is convenient to include a loss factor as a secondary correction if necessary. The simplest approach is found by considering equation (1.18) for the condition $\omega = \omega_r$. In this case the series for $\alpha_{jk}(\omega_r)$ is dominated by the r^{th} term and there is a resonance peek whose amplitude has negligible contribution from the other modes. The equation is:

$$\hat{\alpha}_{jk}(\omega_r) = \frac{{}_r A_{jk}}{i \eta_r \omega_r^2} \qquad (2.8)$$

from which the loss factor is obtained:

$$\eta_r = \frac{\left| {}_r A_{jk} \right|}{\left| \hat{\alpha}_{jk}(\omega_r) \right| \omega_r^2} \qquad (2.9)$$

This formulation is given by Ewins (77) who develops it further to obtain the loss factor in terms of measured responses at two near-resonance frequencies. The iterative method used by Hemingway (66) already referred to in section 1 is also relevant but is more complex than that presented in equation (2.8) and seems to give no advantage for loss factors less than 0.01.

The Accuracy of Modal Constants

(a) Errors in Matrix inversion

The central calculation of identification is the inversion of the $[R]$ matrix, a process potentially subject to error. The inversion of this matrix may be summarised here under three headings.

(i) Estimate of Lost Digits

This has received attention from several authors. Strang (78) defines the condition number, C, of a matrix $[A]$ which indicates the likelihood of error in the calculation of $_{L}A_{1}^{-1}$.

For a symmetric positive definite matrix

$$C = \lambda_N/\lambda_1 = \lambda_{max}/\lambda_{min} = \text{ratio of eigenvalues}$$

one may quote Strang:

"The usual rule of thumb, experimentally verified, is that the computer can lose log C decimal places to the roundoff errors in Gaussian elimination."

Flannelly (79) obtains this result although his development includes a step which is inadmissible according to Albasiny* (80). The matrix $[R]$ is not symmetric and therefore not positive definite either. It has complex eigenvalues. Strang deals with this general case by defining the condition number as the product of the norm of the matrix 2nd the norm of its inverse. However, it was thought to be simpler (2nd equally valid) to calculate the complex eigenvalues of $[R]$ 2nd then to compare the moduli of the largest 2nd smallest. N-mode identification cf sever21 sets of data were carried out with N = 2, 3, 4, 5. The eigenvalues when plotted on an Argand diagram were either on the real axis or symmetrical about it with relatively small imaginary components. The ratio cf moduli of largest eigenvalue to smallest indicated that the number of digits lost in the process of

---

* an error pointed out by Ms B. Hillary.

inversion tight be 2s high 2s 2 or 3. Since the computers used handled more than 6 significant figures it was thought that at least 4 significant figures would be retained in the inversion and that this source of error was not inportant.

(ii) The Determinant and Norm of Matrix $[R]$

These properties of a matrix are defined in Appendix A5 in section A5.3. They were calculated in the course of a large number of inversions. The calculated determinants varied between 2×10^{-4} and 1×10^{3} and norms between 1×10^{-5} and 0.95. No correlation was observed between errors in inversion and the values of the corresponding determinant or nom.

(ii+) The Product of Matrix $[R]$ and its Inverse

A direct check on the accuracy of inversion of 2 oatrix can be obtained by multiplying the original matrix by its calculated inverse and comparing with the unit matrix by examining the off-diagonal terms which ideally should be zero.

This was done for three typical sets of data and gave results which indicated that there was little error in the inversion of this type of matrix. The largest off-diagonal term in any of the 5 mode calculations was 1×10^{-5}.

It should be noted that the matrix inversion routine used was MATIN1 adapted by Sainsbury [21] from the CERN Library routine for solving a system of equations by Jordan's method with partial pivoting. Strang [78] points out that roundoff error comes from two sources: first the natural sensitivity of the problem, which is measured by the condition number; and then the actual errors committed in solving it. These errors are minimised by partial pivoting.

We may say in conclusion that matrix inversion is not 2 significant source of error in these idectificatioc calculations.

(b) Errors in Input Data Levels

The r^{th} modal constant is the product of the r^{th} row of the matrix $[R]^{-1}$ and the column of measured inertance $\{I\}$.

$$A_r = R_{r1} I_1 + R_{r2} I_2 + \ldots\ldots R_{rN} I_N \qquad (2.10)$$

where 3_{ri} is the i^{th} element of the r^{th} row of $[R]^{-1}$ and the notation for inertances and modai constants is simplified by dropping the jk suffix:

$$I_r \equiv I_{jk}(\Omega_r) , \qquad A_r \equiv {}_rA_{jk}$$

Generally, the numerical values of the elements of the rows of $[R]^{-1}$ become smaller as i increases. Thus the errors of I_1 are more significant than those of I_N in contributing to the error in the value of A_1. Since it is usual for measured data to be more accurate at lower frequencies, this feature is likely to be of advantage when identification is based on such data. The advantage of using antiresonance frequencies giving zero values to all I_r except one is also apparent.

Eardenberg [65] suggested that the least squares estimate of $\{A\}$ would be given by linear regression:

$$\{A\} = \left([R]^T [R]\right)^{-1} [R]^T \{I\} \qquad (2.11)$$

improving the accuracy of the modal constants by increasing the number of measured inertances included in the calculation. This pseudoinverse approach is valid for the complete modal representation of this section but is not valid for the more usual incomplete modal representation to be discussed in section 2.1.2. Thus the situation remains that the modal constants' accuracy depends on that of the selected input data. If 2 particular data point selected for inclusion in the identification calculations turns out to be significantly in error it may be detected by graphical comparison of the original data with the smooth curve regenerated from the mod21 constants by use of equation (1.20) for a suitable range of specified values of ω. The regenerated smooth curve must pass through the selected measured data points and should fit to 211 the others also. Gross errors can be avoided by making this comparison.

Comparison of Modelled Response with Original Data

Graphical Presentation

If the frequency response data to be presented cover e wide range of frequency, it is usual to have the abscissa, the frequency scale, logarithmic. The only exceptions occur when the range is to be extended down to zero frequency or a very narrow range in the region of one resonance, for example, is to be plotted. Cf logarithmic ranges one-, two- and three-decade ranges are encountered with two decades being the commonest.

When consideration is given to the scale to be used for the ordinate then more choice is apparent. The vertical scale may be logarithmic or linear and any 0f the three response quantities, receptance, mobility or inertance may be chosen. An example of each type is given in Figure 2.5(a) to (f) in which a regenerated curve approximates to original data for the point response at the tip of a beam. The linear plots (a), (b) and (c) all have most points close to the frequency axis with only the resonance peaks clearly delineated. The divergence between the regenerated and original data is most marked in the case of the inertance curve at high frequency, being virtually invisible on the high frequency end of the receptance curve. In contrast, the inertance values at low frequencies are very small and uninformative. kntiresonances are not clearly indicated in any of the linear plots.

The plots (d), (e) and (f) with logarithmic ordinate expressed in decibels* all show resonances as do the linear plots, but they also give equally clear indication of antiresonances. The three presentations differ in the general trend of the plot, that for receptance falling

---

* Decibels here are defined in control engineer's rather than acoustician's terms:

$$\text{Number of decibels (dB)} = 20 \log_{10} \left(\frac{\text{modulus of measured response}}{\text{reference response}} \right)$$

where the reference response is the appropriate SI unit e.g. 1(m/s)/N for mobility.

with increase of frequency, the mobility plot being approximately constant While the inertance plot rises. Thus the mobility plot fits best inside a rectangular frame. It also has the advantage of symmetry since the mass lines and stiffness lines have opposite slopes of equal magnitude, 20dB/decade, as seen in Figure 2.3.

The discrepancy between regenerated and original data is equally apparent at the high frequency end of all the logarithmic ordinate plots since the divergence expressed in dB is the same for receptance, mobility or inertance. On balance, therefore, the most useful presentation of frequency response data is of logarithmic mobility v. logarithmic frequency.

Visual Comparison of Plots

It is desirable to attempt to quantify the tolerance implicit in the visual comparison of regenerated with original data. Let us assume that the plot is on an A4 page and has horizontally 2 decades of frequency in 240mm and vertically 100 dB in 150mm. Let us also suppose that a discrepancy of 0.5mm is noticeable but one smaller is not.

The minimum resolution horizontally is thus 2 x 0.5/240 = 0.00417 decades, which can be interpreted by considering the following:

1 decade	= frequency ratio	10	:1
0.5 decade	= " "	$\sqrt{10}$: 1 =	3.16 : 1
0.00417 decade	= " "	$10^{0.00417}$: 1 =	1.0096 : 1

1.0096 : 1 is very close to 1%

The minimum vertical resolution is 100 x 0.5/150 = .333 dB which corresponds to 4%.

In the regions of resonance *or* antiresonance the response curves are very steep and it may be that amplitude errors much greater than 4% will not be noticeable. In such regions, however, the frequencies of

resonance or antiresonance are most clear. Thus if data for identification were gathered directly from a plot such as Figure 2.1 it should be expected that the frequencies would be accurate within 1% and the measured level, away from resonance, be accurate within 4%. In most of the work reported in this thesis, the data selected for identification were chosen from a digital printout with an accuracy in both frequency and response of 4 significant figures and mobility graphs were used in comparison to avoid gross errors of modelling and not as sources of data in the first place. A final comment: if a pair of curves being compared coincide at antiresonances as well as resonances the discrepancies in between do not seem significant whereas a failure to match antiresonances is very noticeable even though the absoiute value of the divergence might be very small.

Program IDENT

This program was written by the author in the computer language DYNAMIC FOCAL appropriate to the Solartron JX 3381 Program Controlled Frequency Response Analyser incorporating a PDP8e minicomputer. This equipment is interfaced to peripheral devices, an XY graph plotter, a highspeed tape punch (HSP) and a highspeed tape reader (ESR).

The flow chart of the main segment of the program is shown as AppendixA2. Details of minor segments are omitted since they are conventional. The central calculation is that of equation (2.7) involving the inversion of the $[R]$ matrix and the establishment of modal constants in terms of measured inertances. If desired, the loss factor of a lightly damped system may be estimated by using ecuation (2.9).

The program incorporates sections for printout (listing), punching of tape or plotting of frequency response data obtained either as a result of identification cr from an external source tape, Such taped data may be input and output in a variety of formats. The data can be coded in terms of receptance, mobility or inertance v. frequency for

input or output. The inertance data output in a special code by the Solartron 1172 Transfer Function Analyser can be directly input to IDENT. Identified modal constants can be stored on tape also. Graphs can be plotted in any of the forms of Figure 2.5 and with a linear frequency axis.

The 'standard' way of using the program is: first, to plot the frequency response corresponding to a set of measured data read from paper tape; second, to carry out the identification calculation and third, to regenerate the response and compare it with the original by plotting it on the same graph - using ink of a different colour. If the comparison is not sufficiently close another selection of response data may be made and the second two steps repeated.

This version of IDENT has been used by members of the Dynamics Group in the Mechanical Engineering Department of Imperial College since 1976 and has proved useful, not least for the graph plotting facilities incorporated. A similar program with the same name has recently been developed by M. Ktorides for use with the main-frame CDC computer and its associated graphics facility. Once data have been entered the new program is much faster in calculation and plotting than the laboratory-based minicomputer version.

2.1.2 Incomplete Modal Representation

In the majority of practical cases vibration data are acquired by measurement over limited frequency ranges on structures which, being continuous, have an infinite number of degrees of freedom and a correspondingly infinite number of resonance modes. Thus it is impossible to carry out complete modal analysis with contributions from all modes. In the general case, an N-node representation can be used to approximate to a greater-than-Z-mode set of data. In this section some consideration is given to the quite large errors involved in the approximation. A graphical approach is used initially in which N-mode regenerated responses

are compared with the original complete response data. If a discrepancy is visible on a mobility plot,it is quite large, as was discussed in the previous section.

It is important to note that with incomplete modal representation there can be no unique solutions for eauations (2.6) or (2.7). Even with error-free inversion and error-free receptance or inertance data, the values of the modal constants depend on the selection of response data. For this reason a least squares or pseudo-inverse approach, using many sets of response data instead of only N will not converge to give an ideal set of modal constants. Nevertheless, such modal data as may be obtained can be evaluated and put to good use as will be shown in the following sections.

Much of the following discussion is based upon graphs of the frequency responses from the matrix of mobilities of the tip of a simple freely-supported beam - the Long Beam specified in Chapter 4 and experimentally investigated in Chapters 6 and 7. The matrix involves two coordinates X and 6 and corresponding stimuli, force F and moment M.

$$[Y] = \begin{bmatrix} (\dot{X}/F) & (\dot{X}/M) \\ (\dot{\theta}/F) & (\dot{\theta}/M) \end{bmatrix}$$

The response data of this matrix to be treated as 'measured' were obtained from closed form calculations based on the Bishop and Johnson Tables [5]. Such error-free data incorporating 211 the modes were then identified and an E-mode approximate response calculated using IDENT.

The Effect of the Number of Modes Represented

This effect is illustrated in Figure 2.6 in which the continuous system is represented by 2-,3-,4-and 5-mode approximations successively. Since the first mode of the freely supported body is at zero frequency, it is not plotted. The arrows on the Figure indicate the response data used in identifications - not antiresonances but corresponding to

mid-amplitude responses just below resonance. The two sets of curves coincide at these Points, of course. Consequently, the antiresonances do not coincide, although the error decreases as the number of modes increases. Above the last mode represented the regenerated curve is always asymptotic to a mass line at -20 dB/decade. The fit of the two curves is quite good up to the last resonance included, but not beyond.

The Accuracy of Modal Constants

if all the modes could be represented, then, given an error-free matrix inversion and error-free inertance data, an accurate set of modal constants could be obtained by using equation (2.7). This is impracticable for continuous structures in general but in the special case of .the ideal beam, Bishop & Johnson[5] provide tabuiated data from which the infinite-series modal constants may be calculated. These data are mode-shapes typified by the vector $\{\phi\}_r$. Modal constants are obtained by appropriate use of equation (1.19) or, for the modes at zero frequency, from rigid-body inertia terms. Figure 2.7 shows a comparison between the summation of the first five of these 'infinite-series' modes and the closed form responses which are equivalent to the complete summation. The mismatch of antiresonances becomes greater as frequency increases. In contrast, the comparison of the five mode identification based on antiresonances with closed-form data is shown as Figure 2.6. The curve fit here is of better appearance because the antiresonances, being selected data, catch accurately. Thus the better curve fit is given by less accurate data. It is appropriate here to recall the ultimate objective of this Chapter - the spatial model. This is to be found using equation (1.12) from mode shape data which are related to the infinite-series nodal constents.

We should direct our investigations of curve-fitting with the fundamental criterion that the infinite-series constants are correct and we should adopt a strategy which allows as close an approach to them as possible.

It is observed from Figures 2.7 and 2.8 that discrepancies are most marked for the rotationai response ($\dot{\theta}/M$). These can be explained with reference to Figure 2.9 which shows the mobility contributions for each rode separately, each one having a characteristic response as specified in Figure 2.10 xith the curve fitted to three asymptotes. In the case of the translational point response ($\dot{X}/F$), successive mode3 have nobilities which decline with increasing frequency, following the -20 dB/decade mass line. The intermediate cross responses ($\dot{X}/M$) and ($\dot{\theta}/F$) share the same values since the mobility matrix is symmetrical and they decline at the lesser slope of -10 dB/decade. Finally, the point rotational response ($\dot{\theta}/M$) has mobility contributions which are constant with frequency, thus maximising the low-frequency effect of high-frequency modes. Since ($\dot{\theta}/M$) represents the most difficult case, it is the focus of attention in the following sections.

The Contributions of Lox- and High-Frecuency Nodes

Let us designate the modes that have natural frequencies within the measured range as 'low' and those of higher frequency outside the range as 'high'. Accordingly, designate the inertance contribution from low modes as I_L and that from high modes as I_H. Thu3 the 'measured' inertance selected for identification calculation is given by:

$$\{I\} = \{I_L\} + \{I_H\} \qquad (2.12)$$

Accordingly, the modal constants $\{A\}$ have two components; given by:

$$\{A\} = \{A_C\} + \{A_E\} \quad (2.13)$$

where suffix C = Correct and E = Erroneous

and $$\{A_C\} = [R]^{-1} \{I_L\} \quad (2.14)$$

$$\{A_E\} = [R]^{-1} \{I_H\} \quad (2.15)$$

We wish to select response frequencies so as to maximise $\{A_C\}$ and minimise $\{A_E\}$, which is seen from equations (2.14) and (2.15) to be equivalent to maximising $\{I_L\}$ with respect to $\{I_E\}$. The 'shape' of the $[R]^{-1}$ matrix also has a significant effect.

The Shape of the $[\bar{a}]^{-1}$ Matrix

It is instructive to look at results in which the effect of selection of ideal, error-free response data upon identification accuracy is investigated. The regenerated and original curves for $(\dot{e}/M)$ for two cases are shown here in Figure 2.11.

The response data of set D1 were chosen to have mid-range mobility modulus and $+90^{\circ}$ phase. The identification curve-fit in Figure 2.11(a) is seen to be reasonable, showing divergence from the true curve only at higher frequencies.

The response data of set D2 are substantially the same as those for 31 with the difference that the response at 5C.l Hz is omitted and that at 1030 Hz added. The regenerated curve based on identified modal constants does indeed match the selected date points in amplitude and phase but is otherwise catastrophically wrong. All the identified modal constants have the wrong sign es indicated by the signs in Figure 2.11(b).

The reason for this dram-tic failure can be found by studying $\{I_L\}$, $\{I_E\}$ and $[R]^{-1}$, which are presented for each set in Table 2.1. The data for set 31 shows in the $\{A_E\}$ column an error which increases greatly with node number. This indicates the general trend for the nodal constants of higher nodes to be exaggerated because they are increasingly influenced by the high frequency oat-of-rage nodes. Another comparison of Figures 2.7 and 2.8 at this juncture confirms the trend. The response regenerated from some of the infinite-series constants is lower than the true curve at higher frequencies.

The reasonably good results for the 31 set were obtained despite the very large errors in the last two rows of $\{I\}$, as seen explicitly in $\{I, _3$. This happens because the right hand columns of $[R]^{-1}$ have elements which are small compared with those in the left hand columns, and this results in the $\{A\}$ values being substantially dependent on the more accurate low frequency data of $\{I\}$. The elements of the first row of $[R]^{-1}$ have a range about 10^4 : 1 and those of the last row about 50 :1.

When the 32 data of Table 2.1(b) are ccnsidered,it is seen that the $\{A\}$ constants are all of the wrong sign and magnitude. The $\{I\}$ data on which these constants are based are very similar to those of set D1 but feature a very large error in the last row. The $[R]^{-1}$ matrix, however, is remarkably different froa its D1 equivalent in that the range of values in any row is reduced and the largest values are not always in the left hand columns. The first row has range 100: 1 and the last 1 : 10. Thus $\{A\}$ has a greater dependence on the lower elesents of $\{I\}$ corresponding to the erroneous high frequency data. The difference in 'shape' of the D2 matrix arises principally because the frequencies ω_1 ..... ω_N, Ω_1 ..... Ω_N are not uniformly alternated.

Table 2.1 The $[R]^{-1}$ Matrix, Inertances and Modal Constants

(a) **Set D1**

$$[R]^{-1} = \begin{bmatrix} 1.49 & -0.48 & -.009 & -.0004 & -.00004 \\ 2.06 & -2.18 & .123 & .0038 & .00035 \\ 4.91 & -4.09 & -.978 & .149 & .0085 \\ 7.80 & -6.36 & -1.09 & -.468 & .125 \\ 24.8 & -20.1 & -3.26 & -.899 & -.490 \end{bmatrix}$$

A	A_C	A_E	I	I_L	I_H
.690	.700	-.010	-.882	-.564	-.319
5.13	5.04	.09	-3.92	-3.11	-.801
16.3	14.4	1.9	-11.5	-4.82	-6.71
40.5	28.3	12.2	-40.2	-4.32	-35.9
165	46.4	119	-71.1	44.1	-115

(b) **Set D2**

$$[R]^{-1} = \begin{bmatrix} .897 & .068 & .019 & .008 & .008 \\ -.635 & .472 & .093 & .035 & .034 \\ -.131 & -.324 & .317 & .074 & .064 \\ -.044 & -.076 & -.207 & .227 & .099 \\ -.026 & -.043 & -.076 & -.169 & .314 \end{bmatrix}$$

A	A_C	A_E	I	I_L	I_H
-5.58	.700	6.28	-.882	-.564	-.319
-23.3	5.04	28.4	-11.5	-4.82	-6.71
-37.0	14.4	51.4	-40.2	-4.32	-35.9
-42.5	28.3	70.6	-71.1	44.1	-115
-96.8	46.4	143	-357	170	-528

Equation: $\{A\} = \{A_C\} + \{A_E\} = [R]^{-1}\{I\} = [R]^{-1}(\{I_L\} + \{I_E\})$

The most significant differecce between the 'good' set D1 and the 'bad' set 32 therefore lies in the different 'shapes' of the $[R]^{-1}$ matrices. This is an extreme example of erroneous identification. The gross error would be detected in the norm.1 use of the IDENT program at the stage when regenerated data are compared with original data. The remedy is to rake another selection of response data and repeat the calculation. Since the process is fast, such a trial and error method is not onerous, especially if a mainframe computer and cathode ray tube graphics are available. Some guidance in the selection of data is developed in the next section.

Reducing the Influence of High Frequency Modes

The 'high' and 'low' response contributions are plotted separately in Figure 2.12 for the rotational mobility $(\dot{\theta}/M)$. These can be regarded as suitable summations of the individual modal contributions of Figure 2.9(c). The figures for nobilities $(\dot{\theta}/F)$ and $(\dot{X}/F)$ corresponding to Figure 2.12 are not shown. They are similar, but as the Figure 2.5 curves indicate, have a much smaller contribution from the high frequency nodes. In Figure 2.12 the equation

$$I_L = -I_H \qquad (2.11)$$

is solved at the marked points of intersection to the left of the indicated antiresonances of I_L. These points are the true antiresonances of the complete response. Thus at frequencies a little higher than these true astiresonances the moduli of I_H are much greater than those of I_L and the error colu{n} is potentially large. However, if $[R]^{-1}$ is 'well-shaped' in having its left columns much larger than its right, and the first row of $\{I\}$ corresponds to an accurate low frequency data point, such as I_1, then the resultant calculation of $\{A\}$ reed not be too inaccurate. The experienced vibration engineer when comparing measured and predicted levels of vibration is disturbed by discrepancies of orders of magnitude but often accepts divergences of

tens of percent or a few dB as reasonable. He requires much closer agreement between resonance frequencies, though.

Returning to Figure 2.12, one sees that errors would be reduced by choosing response frequencies a little lower than the true antiresonances. When experimental data are used, and I_H and I_L are not separable, it is difficult to judge 'a little lower'. A sensible strategy, then, is to choose one non-zero response at low frequency well away from resonance and then select (B-l) antiresonances to complet$\{I\}$. At anti-resonances, both I_L and I_H are quite small and the error is not greater than the true value. This calculation is least subject to rounding or experimental errors of the selected response data. The effect of variations of one response data point in the region of antiresonance upon the calculated modal constants is the subject of the next section.

Sensitivitv of Modal Constants to Variations of One Response Antiresonance

Calculations were made using error-free response data consisting of one low frequency non-zero response, (L-2) antiresonances and one response varied around the remaining antiresonance. Graphs of error in modal constant expressed in decibels plotted against linear frequency are shown in Figure 2.13. The effect of changes cf the response data point near the third antiresonance of $(\dot{e}/M)$ is shown in Figure 2.13(a). The trend is for the errors in the fourth and fifth modal constants $_4A_{22}$ and $\$22$ to decrease slightly with the increase in this response frequency and for $_3h_{22}$, $_2A_{22}$, and $_1A_{22}$ (much less in error anyway) to increase.

Greater sensitivity is shown in Figure 2.13(b) where the fourth response point is perturbed. In this case only $_5A_{22}$ increases with decrease in this response frequency. A similar pattern is observed for $(\dot{X}/F)$ constants $\{A_{11}\}$ in Figure 2.13(c), although 211 the errors are relatively small when compared with those of $\{A_{22}\}$, the rotational

modal constants. Graphs of this type are given further consideration in section 2.1.3 in connection with the effect of residuals.

The Identification of an Isolated Mode

The tendency of the modal constants nearest the end of the frequency range included in identificaticc to have enhanced valueshas been noted above. If three modes are isolated a 3-mode identification calculation based on one non-zero response and two antiresonances can be carried out. The middle modal constant will have a value reasonably close to its infinite-series value while the outside two will have enhanced values. This situation is sketched in Figure 2.14. it is possible to identify an N-mode response by a series of overlapping 3-mode 'windows', retaining all the 'middle' constants and the lowest and highest. The resulting ensemble of constants produces an acceptably good regenerated curve-fit. The 'window' method is incorporated in program IDENT. The author has not experienced a situation where the 'window' method had advantages over the direct method but, since it involves only 3 x 3 matrices, a hand-calculator could be used. Interestingly, Flannelly (81) has developed a method of checking measured data using resonances, anti-resonances and a hand-calculator. This method is useful for on-site evaluation of results obtained with complex test equipment, but does require all the resonances and antiresonances rather than the few in a limited range of frequency.

Identification of Small Modal Constants

so far, the examples discussed have bees tip responses of 2 beam in which all modes are represented. The resonance frequencies are well spaced and the modal constants are similar in magnitude. In a more general case it is likely that the point of response will be quite close to a node of one of the modes and consequently will have a small response at that particular resonance. In such 2 case, that modal constant will be small and have 2 relatively large error. This error is unlikely to

cause a mismatch of regenerated curve tc original data but say well be very significant if it is used in the determining of a node shape vector. This relationship of modal parameters is discussed in section 2.2.

In the case of a small isolated mode, the nodal constant is related to the ratio of the modal resonance frequency ω_R to the adjacent anti-resonance frequency ω_{AR}. To express this in simple mathematics, consider that the local response is dominated by modes of lower frequency which have an effectively constant inertance, A_L, in the range of interest. Thus the inertance is given by:

$$I = A_L + \frac{A_R}{(1-\omega_R^2/\omega^2)} \tag{2.12}$$

The local resonance occurs when:

$$\omega = \omega_R \tag{2.13}$$

and antiresonance when:

$$A_L = \frac{-A_R}{(1-\omega_R^2/\omega_{AR}^2)} \tag{2.14}$$

which leads to:

$$\frac{A_R}{A_L} = \left(\frac{\omega_R}{\omega_{AR}}\right)^2 - 1 \tag{2.15}$$

The relationship between nodal constant and R/AR ratio is tabulated in Table 2.2.

Table 2.2 Small Modal Constant v. R/AR Ratio

R/AR Ratio	0.95	0.98	0.99	1.01	1.02	1.05
Modal Constant Ratio	-.1	-.04	-.02	+.02	+.04	+ .1

It follows that 2 small mode will have an antiresonance very close to its resonance so that its effect will simply put a small local kink in the response curve and have nc long range effects.

2.1.3 Residuals

The idea of an isolated mode can usefully be extended to the consideration of an isolated group of modes. Suppose that the N nodes represented in equation (1 .20) were such a group, filling the frequency range of interest but there were also other nodes out of this range at lower frequencies and at higher frequencies. At the lower **frequencies** the inequality

$$\omega_r << \omega \tag{2.16}$$

would hold and in the range of interest the L lower nodes would be approximated by:

$$\sum_{r=1}^{L} \frac{r^A_{jk}}{-\omega^2} = \frac{S_{jk}}{-\omega^2} \tag{2.17}$$

Conversely at higher frequencies we have:

$$\omega_r >> \omega \tag{2.18}$$

and the H higher nodes are approximated by:

$$\sum_{r=N+L}^{H} \frac{r^A_{jk}}{\omega_r^2} = R_{jk} \tag{2.19}$$

The term $S_{jk}/-\omega^2$ corresponds to a residual nass which accounts for out-of-range low frequency terns. S_{jk} has dinension 1/mass and unit l/kg., This unit tight **in** future be known as **'samm'.**

The term R_{jk} corresponds to a residual compliance accounting for the out of range high frequency terms. R_{jk} has dimensions l/stiffness and units m/N.

Now equation **(1.20)** can be rewritten:

$$\alpha_{jk}(\omega) = -\frac{S_{jk}}{\omega^2} + \sum_{r=1}^{N} \left(\frac{r^A_{jk}}{\omega_r^2(1 - \omega^2/\omega_r^2 + i\eta_r)} \right) + R_{jk} \tag{2.20}$$

Low Frequency Residuals

It is possible to take account of low frequency residuals by including en arbitrary resonance frequency, lower than the range of interest, in identification calculations. In very many cases, the lightly damped structures which we are specifically considering are components rather than assemblies 2nd they are small enough to be freely supported. In these cases, the low frequency response is dominated by the rigid body mode which resonates at zero frequency and the identification calculations in program IDENT work without modification with $\omega_1 = 0$. When consideration is given later (in section 2.2) to mode shapes involving related points on the response surface the rigid body modes are 2 source of difficulty which can usually be resolved with separate analysis.

High Frequency Residuals

Though in many practical cases only one low frequency resonance frequency (zero) need be considered, there is no such simplification in the case of high frequency residuals since for a practical continuous structure there is no bound to the number of modes. Representation of such modes is necessarily approximate. Equation (2.19) provides the key. To identify a high frequency residual simply declare an extra mode at en arbitrary high frequency out of the range of interest 2nd carry out the calculation using IDENT in the normal way. The residual stiffness, for example, would be given by:

$$K_{res} = 1/R_{jk} = \omega_N^2/A_{jk} \qquad (2.21)$$

The choice of ω_N, the residual 'resonance' frequency has some influence on the accuracy of the mod21 constants within the range of interest, as we shell now see.

Sensitivity of Modal Constants to Residual 'Resonance' Frequency

Further calculations were done for elements of the mobility matrix of the tip of the Long Beam. Modal constants were calculated in several 6-mode identifications with the same selected respcnse data based on anti-resonances but with variation in the nominal 6^{th} resonance frequency. The correct and target values for the modal constants were taken, as before, to be the 'infinite-series' values. The deviation from these values expressed in dB is plotted against log ω_6 in Figure 2.15. comparison with Figure 2.13 shows immediately that the addition of the high frequency residual term has the effect of greatly reducing the error in the $(\dot{e}/M)$ rotational nodal constants $\{A_{22}\}$.

The graphs in Figure 2.15 start at 1146 Hz, the true 6^{th} natural frequency of the Long Beam. It is interesting tc see that there is an optimum value of ω_6 which gives least error for each modal constant. Each respcnse has a limited range of frequency in which the errors are all small, although no two error lines pass through zero at the same frequency. In practice it would be possible to gauge the best choice of ω_6 by the best curve fit - a trial and error process which might be difficult because small errors would not be easy to discriminate. Another feature of the curves of Figure 2.15 is important: they all become asymptotic to horizontal lines at the higher frequencies at values which, in the case of $(\dot{e}/M)$, have less error than the true resonance at 1146 Hz. Thus if a high enough value of ω_6 is chosen a definite set of modal constants will be established. Using equation (2.21) the high frequency residual can be consistently expressed as a residual stiffness.

Yet another feature of the curves of Figure 2.15 is of interest. Equivalent curves in (a), (b) and (c) share the same curvature (within the limits of graphical tolerances) although they cross zero at different points. For example, the $_5A_{12}$ curve car be laid into ace-to-ore

correspondence with both the $_5A_{22}$ and the $_5A_{11}$ curves. Attempts to provide 2n amlytical expression of this similarity have revealed that the relationship is riot exact but a good approximation, which does not seem to have immediate application.

Other calculations have shown that if the selected response data were not based on antiresonances then there was no improvement in the accuracy of nodal constants resulting fron the inclusion of a high-frequency residual term.

Residuals of Transfer Responses

Low frequency residuals, in particular rigid body nodes, exist 2nd are important. When Figures 2.3 and 2.4 are reviewed the fell-off of the response at high frequencies, usually steeper than -20 dB/decade, indicates that high frequency residuals are small enough to be neglected. Asimilar conclusion is reached when it is remembered that transfer modal constants tend to alternate in sign 2nd therefore tend to sum to zero. This is also indicated in the bird's-eye view of the response surface shown 2s Figure 1.5.

Visualisation of High Frequency Residual

Assuming that the low-frequency residual S_{jk}/ω^2 can be represented by a zero-frequency node we may write for the point response receptance:

$$\frac{X_j}{F_j} = \alpha_{jj}(\omega) = \sum_{r=1}^{N} \left| \frac{r^A_{jj}}{\omega_r^2(1 - \omega^2/\omega_r^2 + i\eta_r)} \right| + R_{jj} \qquad (2.22)$$

Remembering equation (2.21) we can visualise the high frequency residue1 2s a spring:

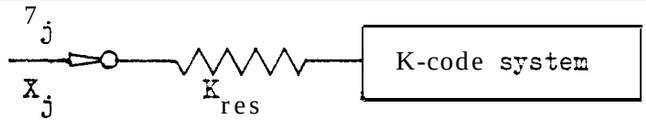

Figure 2.16 Visualisation of High Frequency Residual

2.2 Modal Analysis of Related Frequency Response Curves

The response surface of Figure 1.2 shows a group of related frequency response curves which share resonances and are related spatially (i.e. along the Z axis) by smooth curves which are recognised as mode shapes at resonances. These relationships are further explored in the following sections.

2.2.1 Graphical Representation of Mode Shapes

The r^{th} mode is characterised by a mode shape vector $\{\phi\}_r$ which expresses the mode shape in terms of the generalised coordinates. The first three bending modes of a simple beam are shown in Figure 2.17 as smooth curves, appropriate to a continuous sys ten. In a practical case such shapes have to be indicated by a discrete number of coordinates. In Figure 1.2 , for example, twenty-one displacement coordinates define the mode shape curves. The second bending mode, defined in terms of ten displacement coordinates is shown as Figure 2.18(d). Part (b) of that Figure shows the same shape in terms of five displacement and five rotational coordinates. It will be remembered that the coupling of two beams, at its simplest, requires one coordinate of displacement and one of rotation at the mating beam tips: the butt connection of two beams cannot be satisf ac tori1y described in displacement terms alone. Each of the parts of Figure 2.18 contains ten items of mode shape data - each could serve as the basis of an interpolated smooth curve which would make a gooc approximation to the second curve in Figure 2.17.

The scaling of these graphs deserves a little consideration. Let us assume a horizontal scale factor along the length of the beam in Z direction of 1 mm/m. The vertical displacements may be scaled as d mm/unit. Thus when the elements $_r\phi_i$ of the mode shape vector $\{\phi\}_r$ correspond to displacements we write:

$$ryi = {}_r\phi_i \, d \qquad (2.22)$$

However, when ${}_r\phi_i$ correspond torotations the angles are given by:

$$ {}_r\theta_i = \arctan({}_r\phi_i \; d/l) \qquad (2.23) $$

usually evaluated in degrees for plotting with adjustable set scuare or drawing head.

In the case of Figure 2.18(b) and the mode shape Figures of Chapters 4 and 7 the odd-numbered elements of $\{\phi\}_r$ are plotted as displacement points and the even-numbered elements as angled lines.

2.2.2 Derivation of Modal Constants

Each of the coordinates of an N degree-of-freedom system nay have (in principle) an input force and each will mare a displacement response. Such 2 system will have 2 complete receptance matrix $[\alpha]_{N\times N}$ of which $\alpha_{jk}(\omega)$ as defined in equation (1.18) is 2 typical element. For each resonance mode there is 2 matrix $[A]$ containing all the modal constants of that mode. Their inter-relationship can be developed by extending equation **(1.17)** to include all j and k:

$$ \{\phi\}_r\{\phi\}_r^T = \begin{Bmatrix} {}_r\phi_1 \\ {}_r\phi_2 \\ \vdots \\ {}_r\phi_N \end{Bmatrix} \{ {}_r\phi_1 \; {}_r\phi_2 \cdots {}_r\phi_N \} = \begin{bmatrix} {}_r\phi_1^2 & \cdots & {}_r\phi_1\,{}_r\phi_2 & \cdots & {}_r\phi_1\,{}_r\phi_N \\ & {}_r\phi_2^2 & & & \\ & & \ddots & & \\ {}_r\phi_N\,{}_r\phi_1 & & & & {}_r\phi_N^2 \end{bmatrix} $$

$$ = \begin{bmatrix} {}_rA_{11} & \cdots & {}_rA_{12} & \cdots & {}_rA_{1N} \\ & & {}_rA_{22} & & \\ & & & \ddots & \\ {}_rA_{N1} & & & & {}_rA_{NN} \end{bmatrix} = [A]_r \qquad (2.24) $$

This equation can Se used in the calculation of mode shape data $\{\phi\}_r$ from the identified modal constants $[A]_r$. It is not necessary to know all the elenents of $[A]_r$ in order to find all the elements of $\{\phi\}_r$; **one** row or column will suffice.

For example, if the j^{th} column of $[A]_r$ has been established by identifying the frequency response curves obtained at all N coordinates when force was input at coordinate j we can write:

$$ {}_rA_{jj} = ({}_r\phi_j)^2 \text{ , hence } {}_r\phi_j = \pm({}_rA_{jj})^{\frac{1}{2}} \qquad (2.25) $$

$$ {}_rA_{jk} = {}_r\phi_j\,{}_r\phi_k \text{, hence } {}_r\phi_k = {}_rA_{jk}/{}_r\phi_j $$

$$ = {}_rA_{jk}/({}_rA_{jj})^{\frac{1}{2}} \qquad (2.26) $$

Equation (2.26) can be applied for k = 1, (j-1) and k = (j+1), N giving eventually all the data for $\{\phi\}_r$. Subsequently, the complete matrix of nodal constants ${}_{t-l}A_r$ can be calculated from $\{\phi\}_r$ using equation (2.24).

To consider one specific modal constant:

$$ {}_rA_{jk} = {}_r\phi_j\,{}_r\phi_k = \frac{{}_rA_{ji}}{({}_rA_{ii})^{\frac{1}{2}}}\,\frac{{}_rA_{ki}}{({}_rA_{ii})^{\frac{1}{2}}} = \frac{{}_rA_{ji}\,{}_rA_{ki}}{{}_rA_{ii}} \qquad (2.27) $$

Thus the modal constants of the response at coordinate j arising from force at coordinate k can be derived from the nodal constants of responses at i, j and k arising from force input at a different coordinate, i.

Applications of Derivation Relationships

(i) Single Point Excitation

The possibility of determining a complete mode shape vector $\{\phi\}_r$ from measurements of response obtained sith a single coordinate of excitation has been exploited by several investigators, including Flannelly etal. [71, 79], Goyder [12] and Potter & Richardson [82] and nay now be regarded as a standard technique. The derivation of one row or column of $[A]_r$ involves identification of one point response and (N-1) transfer responses. It is to be expected in practice that sone transfer measurements relating to points on a structure remote from each other or otherwise poorly coupled (by proximity to a node, for example) will give nodal constants of small value which have proportionately large errors.

Richardson 2nd Kniskern [83] have responded to these difficulties by proposing a method which allows the inclusion of data from sever21 columns or rows of the modalconstant matrix, in other words by using more than one excitation point.

(ii) Multipoint Excitation

A method of acquiring reliable data is to obtain the point nodal constants corresponding to the main diagonal of C^{A}_{lr} by identifying the point responses obtained at each coordinate is turn. It will be remembered that point responses always fehture antiresonances 2nd have levels of response which tend tc be maintained, rather than fell off, at higher frequencies. These features enhance the likelihood of obtaining accurate modal constants. The numerical value of the elements of the mode shape matr$[\Phi]$ are simply obtained from the square roots of the corresponding modal constants 2s in equation (2.25). These square roots are indeterminate in sign and thus it is necessary to obtain the signs by other means. This is done most readily by measuring the transfer responses associated with force input at one coordinate which is not a node of any mode and finding the signs of the nod21 constants from the phase information, 2s shown earlier in Figure 2.3.

(iii) Point Response at Inaccessible Locations

Sone points on structures are accessible for attachment of accelerometers but not accessible for force input which recuires not only the force transducer but also alignment of the shaker and push rod. The inside of a small dianeter bearing housing would typify such an inaccessible location. The point mobility is required, perhaps, in order to predict the effect of the support upon the dynamics of 2 rotating shaft.

Designate the inaccessible location 2s coordinate A and 2 nearby accessible location as coordinate B. The mobility matrix relating A and B is:

$$[Y] = \begin{bmatrix} Y_{AA} & Y_{AB} \\ Y_{BA} & Y_{BB} \end{bmatrix} \qquad (2.28)$$

The elements of the second column, Y_{AB} and Y_{BB}, with force input at Bcan be measured. The nodal constents, r^{A}_{AB} and r^{A}_{BB}, can be identified and then r^{A}_{AA} found using equation:

$$r^{A}_{AA} = r^{A}_{AB}{}^{2} / r^{A}_{BB} \qquad (2.29)$$

The response Y_{AA} can then be reconstituted by summing modal contributions using an equation similar to (1.16).

(iv) Improvement of Rotational Measured Data

in Chapter 5 some practical difficulties associated with the measurement of rotation21 mobilities are recorded. The mobility matrix for the tip of 2 beam can be written:

$$[Y] = \begin{bmatrix} (\dot{X}/F) & (\dot{X}/M) \\ (\dot{\theta}/F) & (\dot{\theta}/M) \end{bmatrix} \qquad (2.30)$$

The parameter $(\dot{\theta}/M)$ is difficult to measure accurately, not least because of the difficulty of producing an input moment, M. As is reported in 2 published paper [84], which is included 2s Appendix A6, inaccuracies of $(\dot{\theta}/M)$ were compensated for by deriving the modal constants of that parameter from those of $(\dot{X}/F)$ 2nd $(\dot{\theta}/F)$ which are amenable to reasonably accurate measurement. An extension of this -use of modal modelling to simplify rotational measurements is included 2s section 5.2.2.

Residuals 2nd Derivation

It must now be pointed out that high frequency residuals do not derive. Derivation is possible because it is an expression of the properties of a mode shape. If 2 mode shape is

known and a particular amplitude of one elerent of that shape is known then the amplitudes of all elements are determined. The high frequency residual is an approximation to the combined effects of a number of nodes which can be expressed in term of 2 modal constant of a fictitious node at an assumed 'resonance' frequency. There is no residual rode shape. Consequently, residual terms for Y_{AA} cannot be derived from Y_{AB}, Y_{BB} measurements. At this juncture it seems 2s if the use of 2 high frequency residual and derivation, two rost useful devices in nod21 identification, nullify each other. Fortunately; there is 2 workable solution to the problem. The representation of a high frequency residual 2s a spring introduced in section 2.1.3 proves to be 2 valuable contrivance. It will be discussed in section 2.3.

Similar comments apply in general tolow frequency residuals in those cases where the effects cf several modes of different frequencies are included. The commonest case encountered in this study of lightly damped structures is of freely supported components. Their low frequency residuals correspond to rigid body modes at zero frequency, to be dealt with in the next section.

2.2.3 Rigid Body Modes

A freely-supported body has six rigid body modes. Three of these are tramlational 2nd three rotational. Each has a mode shape which is orthogonal tc all the others. Since they all have the safe resonance frequency, zero, they can combine. A general rigid body motion is thus a combination of rigid body modes. As in the case of the bending modes shown in Figure 2.17 the individual rigid body nodes have definite shapes which relate to specific coordinates and permit derivation. It is very easy to excite rigid body motion featuring more than one code. In such a case derivation is not simple 2nd can only work when the modes are separated. It is a feature cl t h e identificaticc calculations based on equation (2.7) which are used in program IDENT that $[R]$ is singular if two resonance frequencies are the same. Consequently IDENT can identify only one

set of modal constants at zero frequency - most usually corresponding to a combination of modes - and these must be separated before $[\Phi]$, the mode shape matrix, can be evaluated. Numerical examples of the separation of rigid body modes are given in Chapters 4 and 7 in connection with the motion of beams in two dimensions, a simple case which can be discussed here.

Separation of Rigid Body Modes

Consider the tip response of a beam as shown in Figure 2.19:

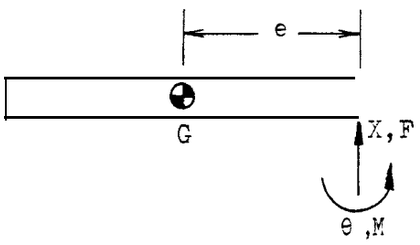

Inertence Matrix

$$[I(\omega)] = \begin{bmatrix} (\ddot{X}/F) & (\ddot{X}/M) \\ (\ddot{\theta}/F) & (\ddot{\theta}/M) \end{bmatrix} \qquad (2.31)$$

Figure 2.19 Rigid Body Tip Responses of a Free-Free Beam

We wish to find the nodal constants of the rigid body mode ${}_0[A]$. This process is facilitated by use of equation (2.4). Firstly set $\omega_1 = 0$ and observe that the first column of $[R]$ has each element unity. Then observe that the remaining elements of the first row of ${}_C^R{}_1$ tend to zero es Ω_1, the first excitation frequency, tends to zero. Thus we get:

$$I_{jk}\ (0) = {}_oA_{jk} \qquad (2.32)$$

where the prefix 0 denotes the first mode (at zero frequency). The elements of ${}_0[A]$ can thus be found from consideration cf zero frequency inertances which relate steady accelerations to steady forces.

There are two rigid body nodes excited by the input force F which does not pass through the centroid G and consequently produces rotation about G as well as translation of G. Thus:

$$F.\ e = I_G\ \ddot{\theta} \qquad (2.33)$$

$$F = m\ddot{X}_T \qquad (2.34)$$

where $\ddot{X}_T$ is the translational component of $\ddot{X}$.

The rotational component $\ddot{X}_R$ is giver by:

$$\ddot{X}_R = e\ddot{\theta} = e^2F/I_G \tag{2.35}$$

using equation (2.33).

Combining (2.34) and (2.75) acd rearranging:

$$\ddot{X}/F = (\ddot{X}_T + \ddot{X}_R)/F = 1/m + e^2/I_G = {}_oA_{11} \tag{2.36}$$

and from (2.33):

$$\ddot{\theta}/F = e/I_G = {}_oA_{21} \tag{2.57}$$

The applied moment M excites only the rotational rigid body node:

$$M = I_G\ddot{\theta} \tag{2.38}$$

Thus:

$$\ddot{\theta}/M = 1/I_G = {}_oA_{22} \tag{2.39}$$

and, using (2.35) again:

$$\ddot{X}_R/M = e/I_G = {}_oA_{12} \tag{2.40}$$

The complete matrix of nodal constants is:

$${}_o[A] = \begin{vmatrix} {}_oA_{11} & {}_oA_{12} \\ {}_oA_{21} & {}_oA_{22} \end{vmatrix} = \begin{bmatrix} (1/m + e^2/I_G) & e/I_G \\ e/I_G & 1/I_G \end{bmatrix} \tag{2.41}$$

The simplest derivation fomula in which $(\ddot{\theta}/M)$ is obtained in terms of $(\ddot{X}/F)$ and $(\ddot{\theta}/F)$ does not hold since:

$${}_oA_{22} \neq {}_oA_{21}{}^2/{}_oA_{11} \tag{2.42}$$

This happens because the two rigid body nodes which excited by F are not separated. When the separation is carried out by calculating the Pass of the free body and simply subtracting its reciprocal we may write:

$${}_o[A]_T = \frac{1}{m}\begin{bmatrix} 1 & 0 \\ 0 & 0 \end{bmatrix} = \frac{1}{m}\begin{Bmatrix} 1 \\ 0 \end{Bmatrix}\{\,1 \quad 0\,\} \tag{2.43}$$

arid $${}_o[A]_R = \frac{1}{I_G}\begin{bmatrix} e^2 & e \\ e & 1 \end{bmatrix} = \frac{1}{I_G}\begin{Bmatrix} e \\ 1 \end{Bmatrix}\{\,e \quad 1\,\} \tag{2.44}$$

where $${}_o[A] = {}_o[A]_T + {}_o[A]_R \tag{2.45}$$

Now that the sets of nodal constants have been separated, useful derivation relationships do hold:

$$ {}_{o}A_{22T} = {}_{o}A_{21T}^{2} / {}_{o}A_{11T} \qquad (2.46) $$

$$ {}_{o}A_{22R} = {}_{o}A_{21R}^{2} I \, {}_{o}A_{11R} \qquad (2.47) $$

When selected curves from the response surface of a freely supported body are identified it is the total matrix ${}_{0}[\mathbf{A}]$ which is obtained, and in the general case it might be quite difficult to separate the nodal constants of the several rigid body codes. The relationships involved in rigid body notion have been developed and are presented as Appendix A3.

2.2.4 Consistency

it is usually possible to collect more date from the response surface than is strictly necessary for identifying the modal constants of the systen. Such 'redundant' data can be used to make second estimates of constants and will help to avoid gross errors. Let us *assume* that one column and the leading diagonal of a nobility matrix have been measured: the method which is likely to give the best data for identification as discussed in section 2.2.2. There will have been N points of excitation used. The first step to obtaining a consistent model is to check that the resonance frequencies measured at different points do coincide or if not, estimate a best value using simple averaging. It is important that the identification calculations for the different point responses are all carried out with the same set cf nominal resonance frequencies.

It is to be expected that the point modal constants should be accurately evaluated. Extra data will be available from a set of transfer responses which will give second estimates for the point nodal constants using the derivation relationships developed is section 2.2.2. In some cases, particularly Mere rotations are concerned, the derived

values of point modal constants are nearer their true values than the directly identified set. The values ultimately adapted for the matrices of modal constants $[A]_r$ should certainly be adjusted so that they consistently conform to the derivation relationships of equation (2.27).

The data contained in the N matrices designated $[A]_r$ can be reccced and be contained in cae matrix $[\Phi]_{NxN}$. The resonance frequencies will be listed (squared) in the diagonal matrix $[\omega_r^2]_{NxN}$. These two consistent matrices form the basis of the spatial model.

2.3 Construction of the Spatial Model

2.3.1 The Spatial Model without Residuals

The construction is simply done by using equations (1.12):

$$[M] = [\Phi]^{-T}[\Phi]^{-1}$$

$$[K + iH] = [\Phi]^{-T}[\lambda_r^2][\Phi]^{-1}$$

The latter can be modified for the undamped case:

$$[K] = [\Phi]^{-T}[\omega_r^2][\Phi]^{-1} \qquad (2.48)$$

This calculation is carried out using the program EMKAY written by the author in FORTRAN for use on a nain frame computer and in FOCAL for use with the PDP8 minicomputer in the laboratory. The central feature of the program is the standard matrix inversion routine MATIN1, already mentioned in section 2.1.1(iii). The remainder of the program is concerned with the input, handling, multiplication and output of matrix arrays. The data input consists of N, then N resonance frequencies expressed in Hz, then $[\Phi]$ entered by columns. The printed output includes $[\Phi]$ (for checking) $[\Phi]^{-1}$, $[\Phi]^{-T}$, $[M]$, ΣM, $[K]$ and ΣK, where ΣM, for example, is the summation of all the elements of matrix $[M]$.

A significant problem was encountered by Maleci [85] when he first used identified measured data in the construction of a spatial model. The test piece was an aluminium I girder loaded by point masses and its point 2nd transfer responses were identified by use of program IDENT,

which, as remarked earlier, can handle only one zero frequency resonance.

Accordingly, Maleci entered ϕ values based on the square roots of the rigid body nodal constants in the first column of $[\Phi]$. Program EMMAY produced mass and stiffness matrices which were not meaningful in themelves but which would successfully regenerate the response data on which they were based in the frequency region 50 to 1000 Hz. Below 50 Hz the regenerated curve did not fit the original data. The summation ΣM also bore no relation to the mass of the beam.

A second attempt was made, this tine with the rigid body nodes separated by the technique based on knowiedge of the total mass as discussed in the previous section. Thus the first two columns of $[\Phi]$ corresponded to rigid body modes and since that matrix had to be square (because it needed to be inverted) the measured data of the highest frequency node included in the first calculation was omitted.

The *results this* tire were very encouraging in that the total mass ΣM was *now close* to the measured mass of the beam and its added masses. Furthermore, the regenerated frequency response matched the original data in the low frequency region. This experience highlights the necessity of separating the different zero frequency modes.

A demonstration of the feasibility of the proposed method of spatial modelling using ideal data of several simple N-degree-of-freedom systems is reported in Chapter 3 and a similar exercise identifying an ideal continuous structure is the subject of Chapter 4. The separation of rigid body modes is denocstrsted in Chapter 4 and also in Chapter 7.

2.3.2 The Spatial Model with Residuals

Residual Stiffness

We saw in section 2.1.3 that the addition of high frequency residuals could make a significant improvement in the accuracy of identification. It is thus desirable tc include their beneficial effects in the spatial model. There is a major difficulty, indicated in section

2.2.2, that residuals do not derive. This means that they cannot be incorporated in a consistent mode shape matrix $[\Phi]$. However they can be incorporated in the form of residual springs attached one to each spatial coordinate. Each spring represents the high-frequency residual of the point at which it is attached as sketched in Figure 2.16. Transfer residuals are negligible, as discussed in section 2.2.2. Thus residuals can be incorporated into the spatial model by a method which is in concept non-mathematical.

In Figure 2.20(a) the spatial model as generated by program EMKAY in terms of mass and stiffness matrices is represented as having N accessible generalised coordinates and containing beneath its surface the spring and mass elements distributed in an unspecified manner. As we will see the spatial model of an incomplete system features off-diagonal and some negative masses which cannot be represented by a simple mass-spring chain.

Figure 2.20(b) shows the array of springs which contain the high frequency residual data; each, of course, has two terminals and thus the array now has 2N generalised coordinates, as does the final assembly of spatial model and extra springs shown as Figure 2.20(c). Only the new coordinates $q_{N+1}, q_{N+2} \ldots q_{2N}$ are now to be regarded as accessible although all coordinates will have to be included in the revised matrix formulations.

The partitioned mass and stiffness matrices for system A can be written in terms of 2N coordinates:

$$\begin{Bmatrix} Q_1 \\ \vdots \\ Q_N \\ \hline Q_{N+1} \\ \vdots \\ Q_{2N} \end{Bmatrix}_A = \left[\begin{array}{c|c} K_s & 0 \\ N\times N & N\times N \\ \hline 0 & 0 \\ N\times N & N\times N \end{array}\right] \begin{Bmatrix} q_1 \\ \vdots \\ q_N \\ \hline q_{N+1} \\ \vdots \\ q_{2N} \end{Bmatrix}_A + \left[\begin{array}{c|c} M_s & 0 \\ N\times N & N\times N \\ \hline 0 & 0 \\ N\times N & N\times N \end{array}\right] \begin{Bmatrix} \ddot{q}_1 \\ \vdots \\ \ddot{q}_N \\ \hline \ddot{q}_{N+1} \\ \vdots \\ \ddot{q}_{2N} \end{Bmatrix}_A \qquad (2.49)$$

System B is a set of springs with no intenal connections and can be written:

$$\begin{Bmatrix} Q_1 \\ \vdots \\ Q_N \\ \hline Q_{N+1} \\ \vdots \\ Q_{2N} \end{Bmatrix}_B = \left[\begin{array}{c|c} K_r & -K_r \\ NxN & NxN \\ \hline -K_r & K_r \\ NxN & NxN \end{array}\right] \begin{Bmatrix} q_1 \\ \vdots \\ q_N \\ \hline q_{N+} \\ \vdots \\ q_{2N} \end{Bmatrix}_B \qquad (2.50)$$

System C has the same mass matrix as system A and its stiffness matrix is the sum of those for A and 3.

$$\left[M_c\right]_{2Nx2N} = \left[\begin{array}{c|c} M_s & 0 \\ \hline 0 & 0 \end{array}\right] \qquad (2.51)$$

$$\left[K_c\right]_{2Nx2N} = \left[\begin{array}{c|c} K_s+K_r & -K_r \\ \hline -K_r & K_r \end{array}\right]$$

The two matrices $\left[M_c\right]$ and $\left[K_c\right]$ constitute the spatial model with residuals and in most cases the quadrupling of number of elements associated with doubling the size of each matrix will not cause any difficulty. Should there be any problem it is possible to retain N x N matrices, as seen below.

Residual Flexibility

The equation of motion for steady-state sinusoidal excitation of system C is: $\{\ddot{q}\} = \left[K_c\right]\{q\} - \omega^2 \left[M_c\right]\{q\}$ (2.52)

$$\text{or} \quad \begin{Bmatrix} Q_1 \\ \vdots \\ Q_N \\ \hline Q_{N+1} \\ \vdots \\ Q_{2N} \end{Bmatrix} = \left[\begin{array}{c|c} K_s+K_r & -K_r \\ \hline -K_r & K_r \end{array}\right] - \omega^2 \left[\begin{array}{c|c} M_s & 0 \\ \hline 0 & 0 \end{array}\right] \begin{Bmatrix} q_1 \\ \vdots \\ q_N \\ \hline q_{N+1} \\ \vdots \\ q_{2N} \end{Bmatrix}$$

We are looking for a relationship between the forces and displacements of the accessible coordinates $q_{N+1}, q_{N+2} \cdots\cdots q_{2N}$.

Expand the partitioned matrices:

$$\begin{Bmatrix} Q_1 \\ \vdots \\ Q_N \end{Bmatrix} = \left[K_s - \omega^2 M_s\right] \begin{Bmatrix} q_1 \\ \vdots \\ q_N \end{Bmatrix} + \left[K_r\right] \begin{Bmatrix} q_1 \\ \vdots \\ q_N \end{Bmatrix} - \left[K_r\right] \begin{Bmatrix} q_{N+1} \\ \vdots \\ q_{2N} \end{Bmatrix} \quad (2.53)$$

$$\begin{Bmatrix} Q_{N+1} \\ \vdots \\ Q_{2N} \end{Bmatrix} = -\left[K_r\right] \begin{Bmatrix} q_1 \\ \vdots \\ q_N \end{Bmatrix} + \left[K_r\right] \begin{Bmatrix} q_{N+1} \\ \vdots \\ q_{2N} \end{Bmatrix} \quad (2.54)$$

Adding (2.53) tc (2.54) we get:

$$\begin{Bmatrix} Q_1 \\ \vdots \\ Q_N \end{Bmatrix} + \begin{Bmatrix} Q_{N+1} \\ \vdots \\ Q_{2N} \end{Bmatrix} = \left[K_s - \omega^2 M_s\right] \begin{Bmatrix} q_1 \\ \vdots \\ q_N \end{Bmatrix} \quad (2.55)$$

Hence $$\begin{Bmatrix} q_1 \\ \vdots \\ q_N \end{Bmatrix} = \left[K_s - \omega^2 M_s\right]^{-1} \left(\begin{Bmatrix} Q_1 \\ \vdots \\ Q_N \end{Bmatrix} + \begin{Bmatrix} Q_{N+1} \\ \vdots \\ Q_{2N} \end{Bmatrix} \right) \quad (2.56)$$

Substitution in (2.54) yields:

$$\begin{Bmatrix} Q_{N+1} \\ \vdots \\ Q_{2N} \end{Bmatrix} = -\left[K_r\right] \left[K_s - \omega^2 M_s\right]^{-1} \left(\begin{Bmatrix} Q_1 \\ \vdots \\ Q_N \end{Bmatrix} + \begin{Bmatrix} Q_{N+1} \\ \vdots \\ Q_{2N} \end{Bmatrix} \right) + \left[K_r\right] \begin{Bmatrix} q_{N+1} \\ \vdots \\ q_{2N} \end{Bmatrix} \quad (2.57)$$

Thus, rearranging:

$$\begin{Bmatrix} q_{N+1} \\ \vdots \\ q_{2N} \end{Bmatrix} = \left[\left[K_r\right]^{-1} + \left[K_s - \omega^2 M_s\right]^{-1} \right] \begin{Bmatrix} Q_{N+1} \\ \vdots \\ Q_{2N} \end{Bmatrix} + \left[K_s - \omega^2 M_s\right]^{-1} \begin{Bmatrix} Q_1 \\ \vdots \\ Q_N \end{Bmatrix} \quad (2.58)$$

Since the terminals 1 to N are iaeccessible there can be no external force input on then.

'Therefore $$\begin{Bmatrix} Q_1 \\ \vdots \\ Q_N \end{Bmatrix} = 0 \quad (2.59)$$

and $$\begin{Bmatrix} q_{N+1} \\ \vdots \\ q_{2N} \end{Bmatrix} = \left[\left[C_r\right] + \left[K_s - \omega^2 M_s\right]^{-1} \right] \begin{Bmatrix} Q_{N+1} \\ \vdots \\ Q_{2N} \end{Bmatrix} \quad (2.60)$$

The diagonal matrix $\left[C_r\right]$ represects residual flexibility.

The receptsnce matrix is:

$$\underset{NxN}{[\alpha]} = \underset{NxN}{[C_r]} + \underset{NxN}{[K_s - \omega^2 M_s]^{-1}} \qquad (2.61)$$

which has the sane frequencies of resonance es the system without residuals. The antiresonances will be somewhat modified.

The residual stiffness and residual flexibility methods are compared in Chapter 4.

2.4 CONCLUSIONS: IDENTIFICATION OF MODAL DATA AND CONSTRUCTION OF SPATIAL MODEL

(1) Modal constants which represent one frequency response curve can be found with reasonable accuracy.

(2) The modal identification calculations for each curve should incorporate $(N+1)$ resonance frequencies, the first N corresponding to true resonances and the $(N+1)^{th}$ being set at a nominal frequency about a decade or more above the N^{th} resonance.

(3) The $(N+1)$ items of response data should have frequencies interspersed with the resonance frequencies and coincide with anti-resonances or (in the case of some segments of transfer response curves) with local minima.

(4) A spring element to be used as a representation of high-frequency residual effects should be calculated from the $(N+1)^{th}$ modal constant of each point response.

(5) If there is more than one rigid body mode the modal constants at zero frequency should be separated into parts corresponding to each mode.

(6) The two methods of using modal constants of related frequency response curves to evaluate the elements of the mode shape matrix $[\Phi]$:

(i) Identify 1 point and $(N-1)$ transfer response curves all obtained by excitation at one station. The elements of $[\Phi]$ can then be found from one column of the modal constant matrix.

(ii) Identify the N point response curves obtained by excitation at each station in turn. The numerical values of each column of $[\Phi]$ then can be found by taking the square root of the main diagonal elements of $_r[A]$ for each r in turn. The signs of $[\Phi]$ elements are obtained from the responses at all stations arising from excitation at one - as in (i).

It is to be expected that method (ii) would normally give more accurate results.

(7) The bases of the spatial model are the NxN matrices $[\Phi]$ and $[\omega_r^2]$ as established above in 2 and 6.

(8) The high-frequency residuals of point responses can be incorporated as springs joined to the spatial model at its coordinates. The free ends of the springs become the new coordinates.

(9) The high frequency residuals of transfer responses are small enough to be neglected.

(10 All the above calculations can be carried out using programs IDENT and EMKAY and a hand calculator.

Figure 2.1 Identification of a Point Response

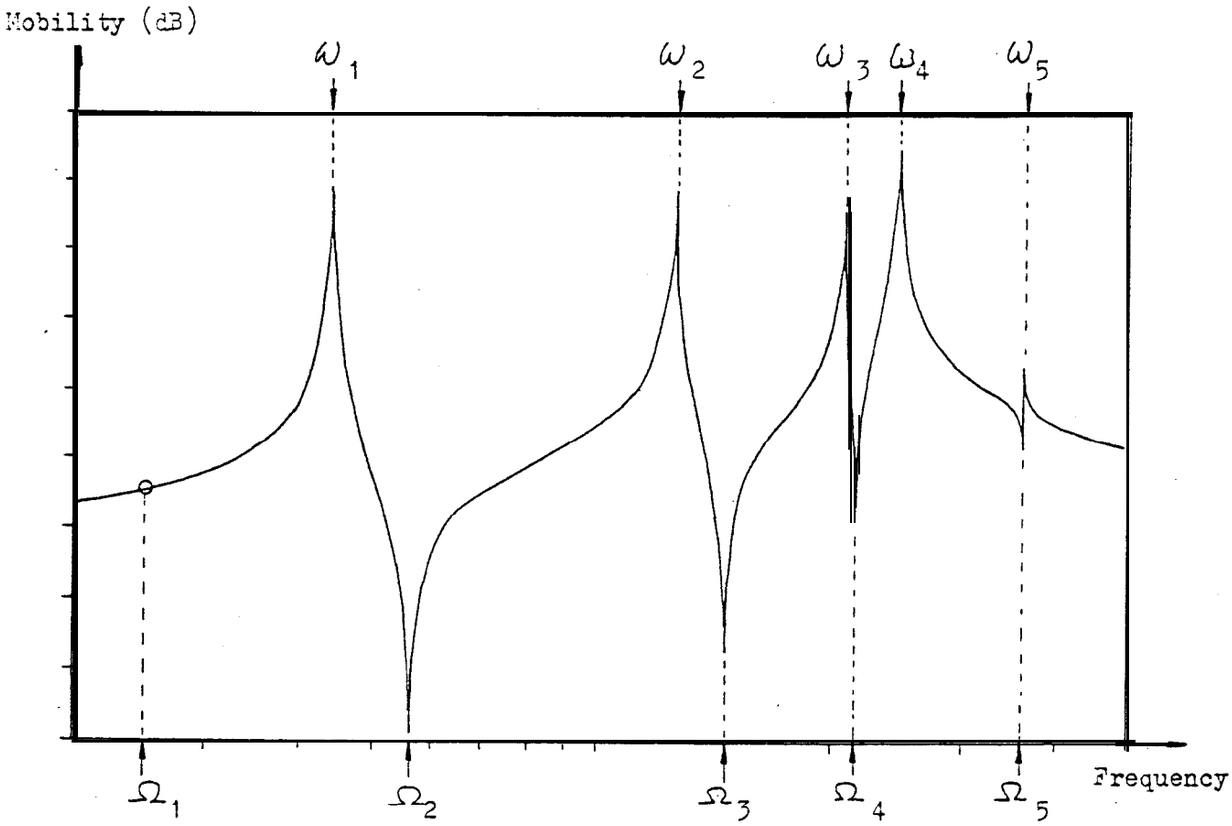

Figure 2.2 Salter Skeleton of a Point Response

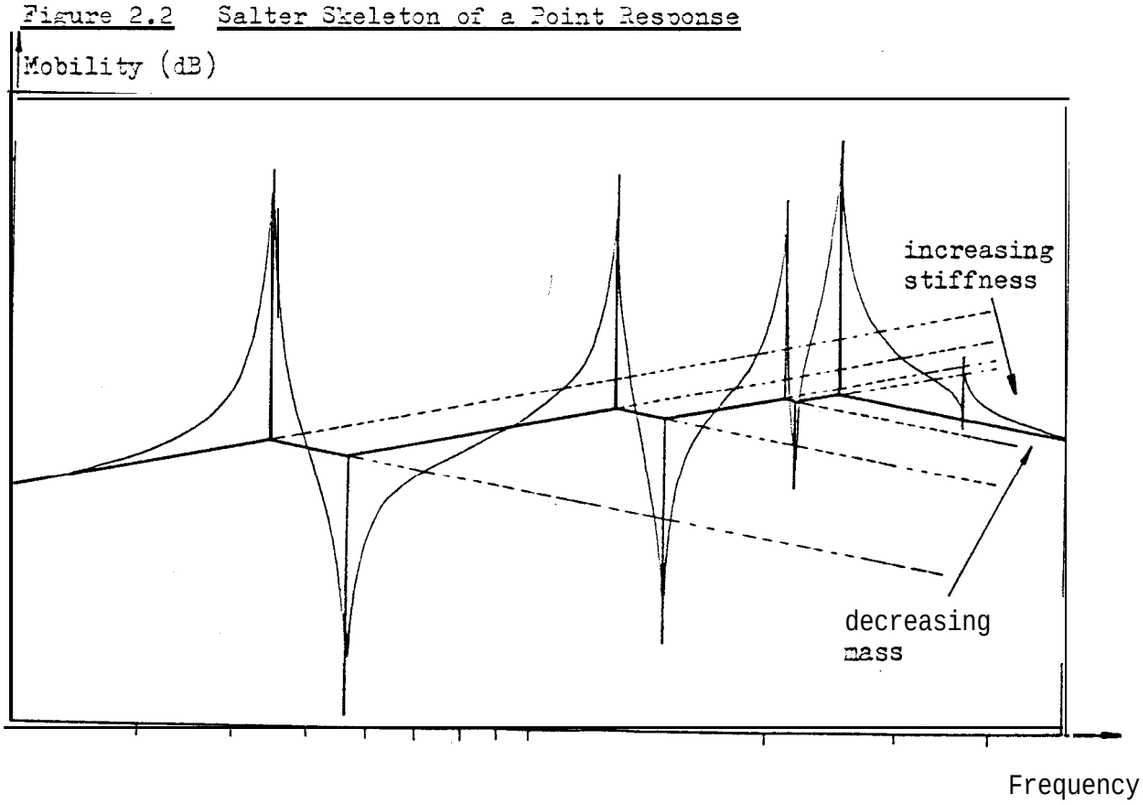

Fi ure 2. Identification of a Transfer Response

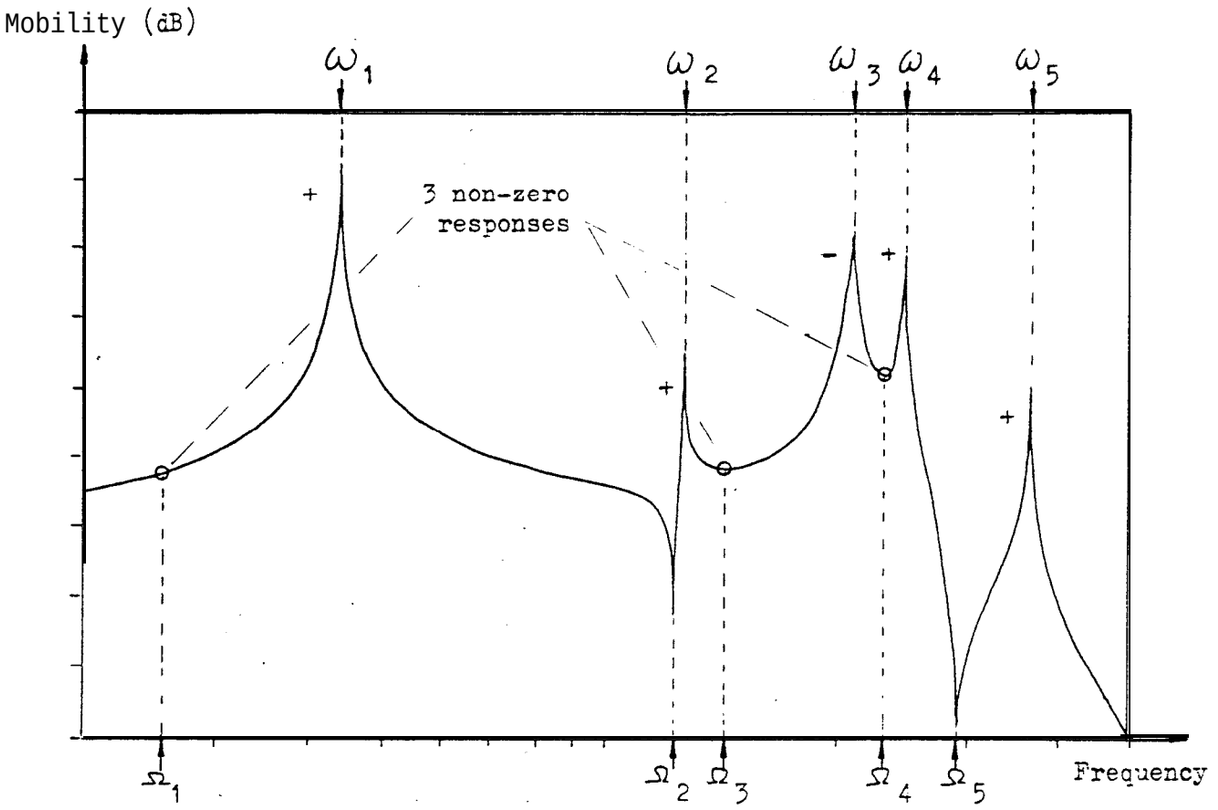

Figure 2.4 Salter Skeleton of a Transfer Response

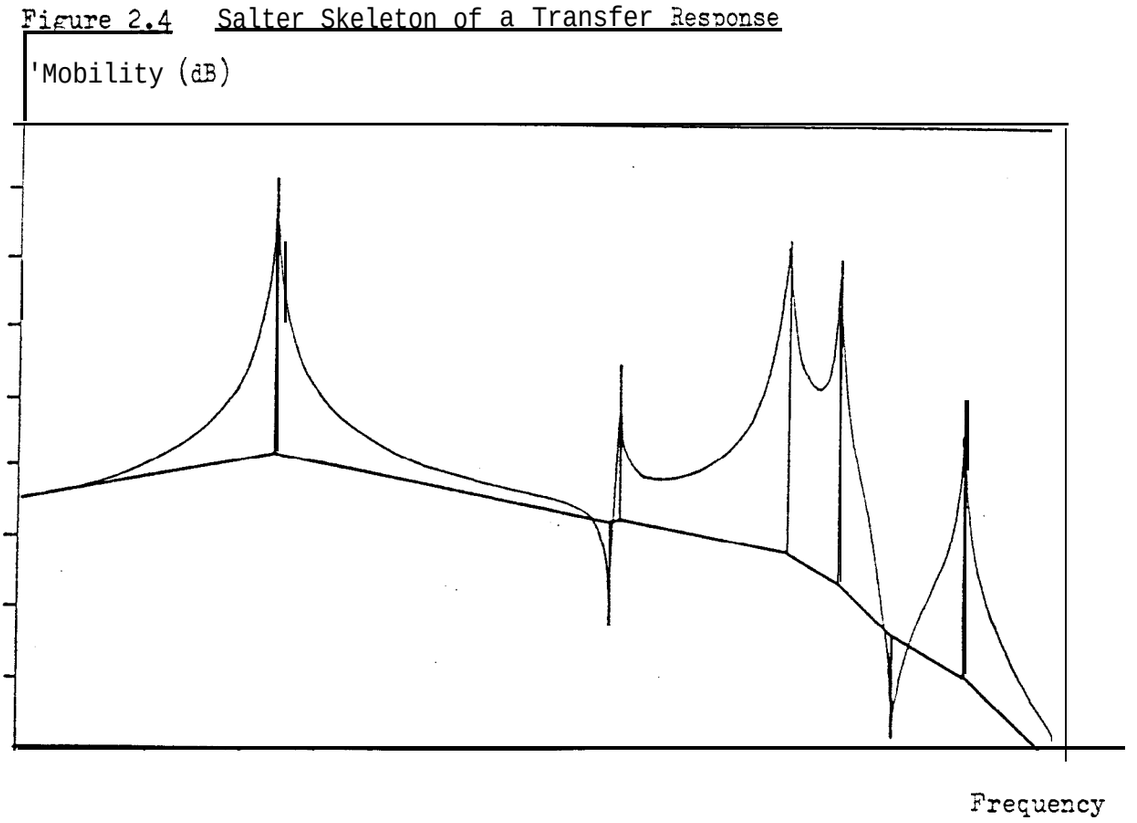

Figure 2. Identification of a Transfer Response

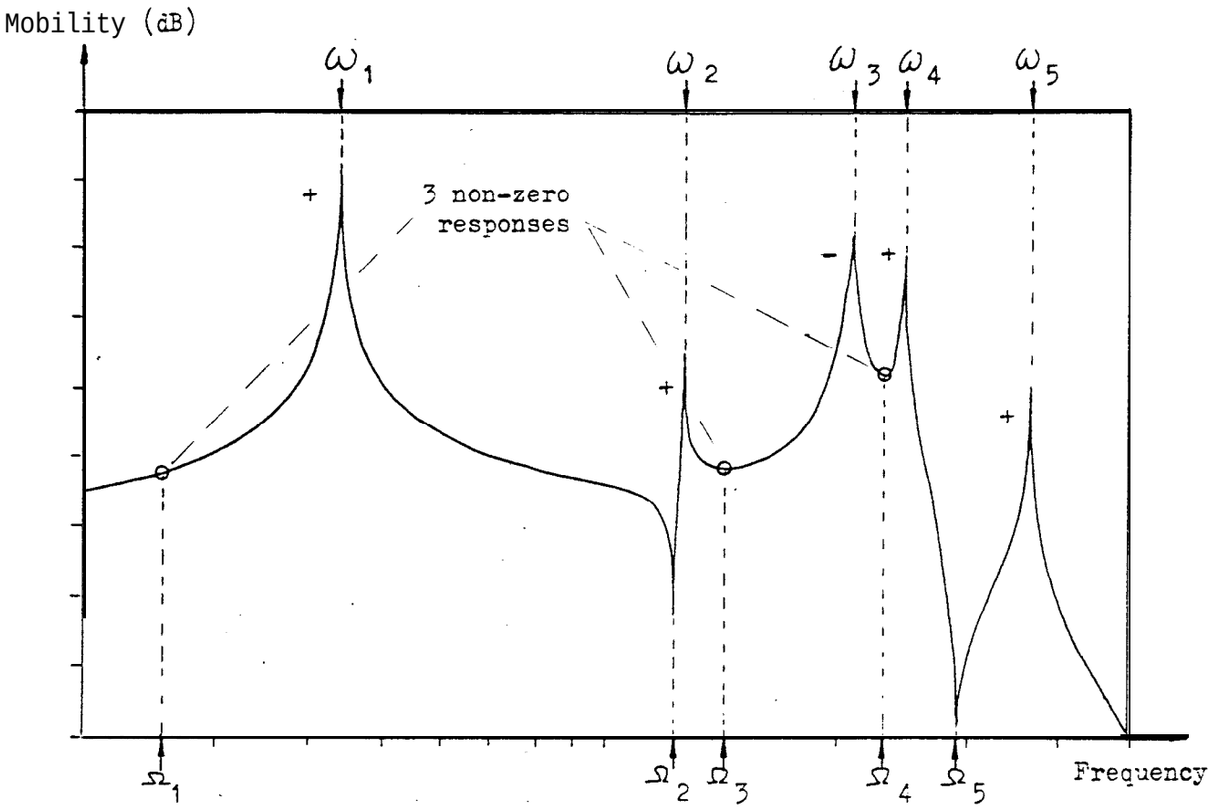

Figure 2.4 Salter Skeleton of a Transfer Response

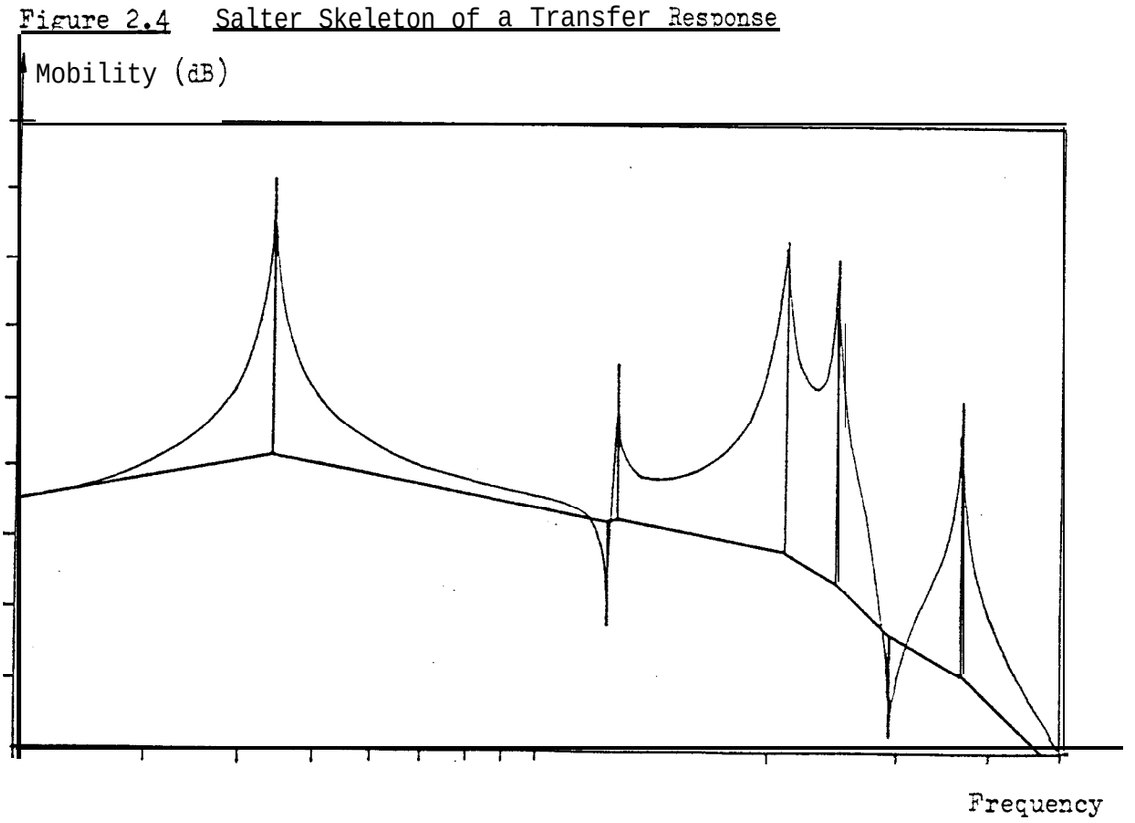

Figure 2.5 Frequency Responses

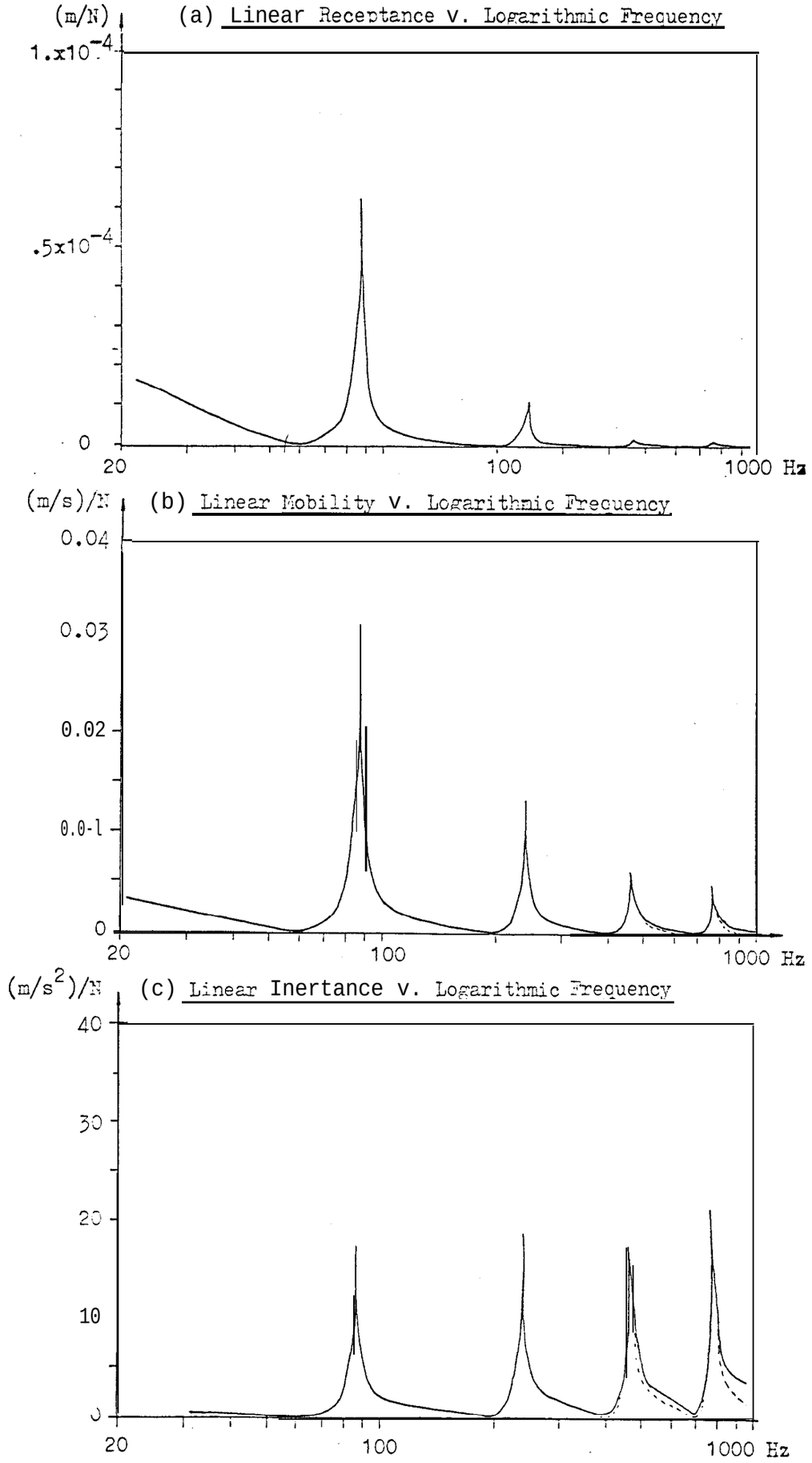

Figure 2.5 (continued) Frequency Responses

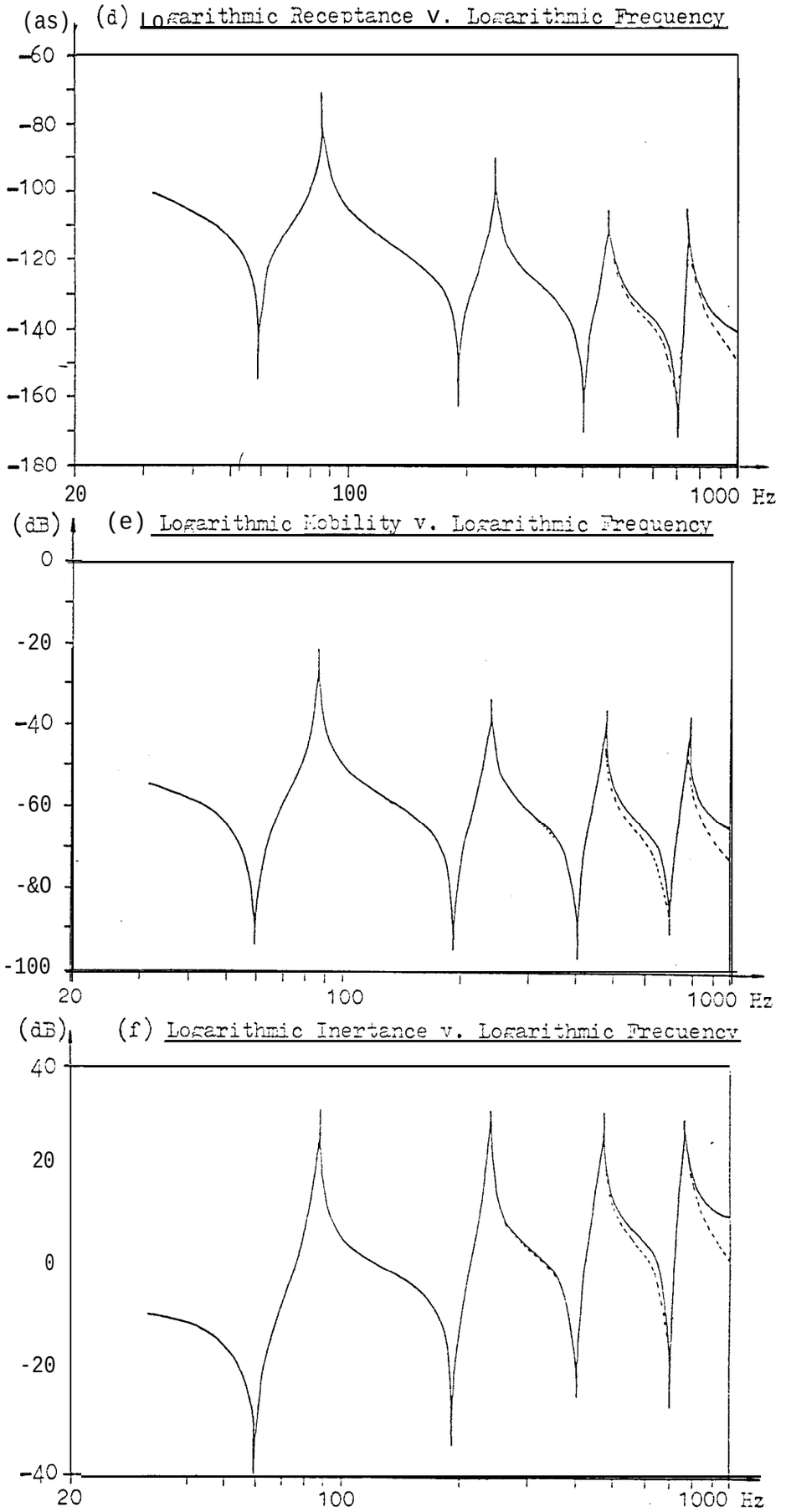

Figure 2.6 Point Response ($\dot{X}/F$) at Tip of Beam
Comparison of Regenerated Curve with Original Data

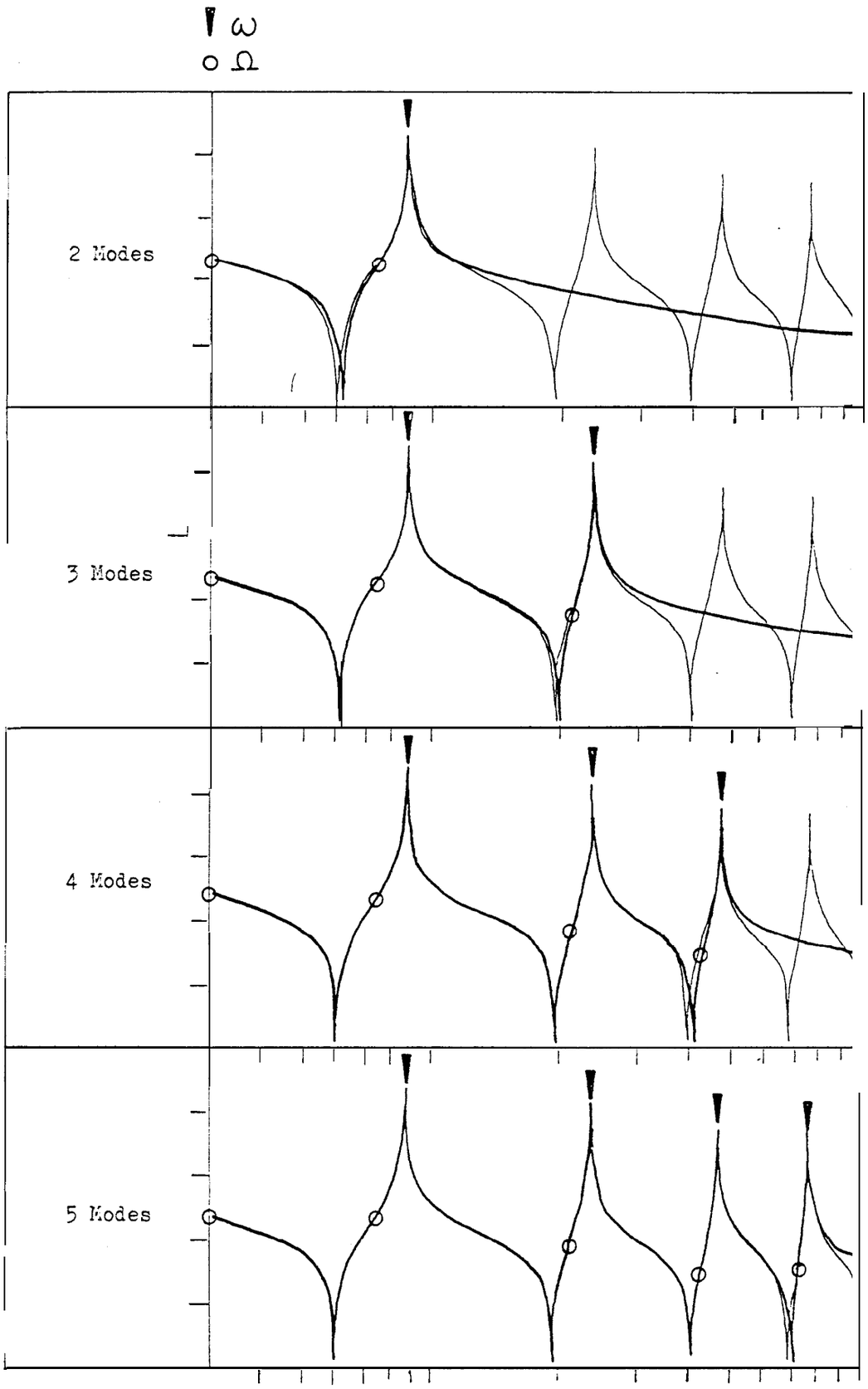

Figure 2.7 Responses Calculated from First Five Terms of Infinite Series

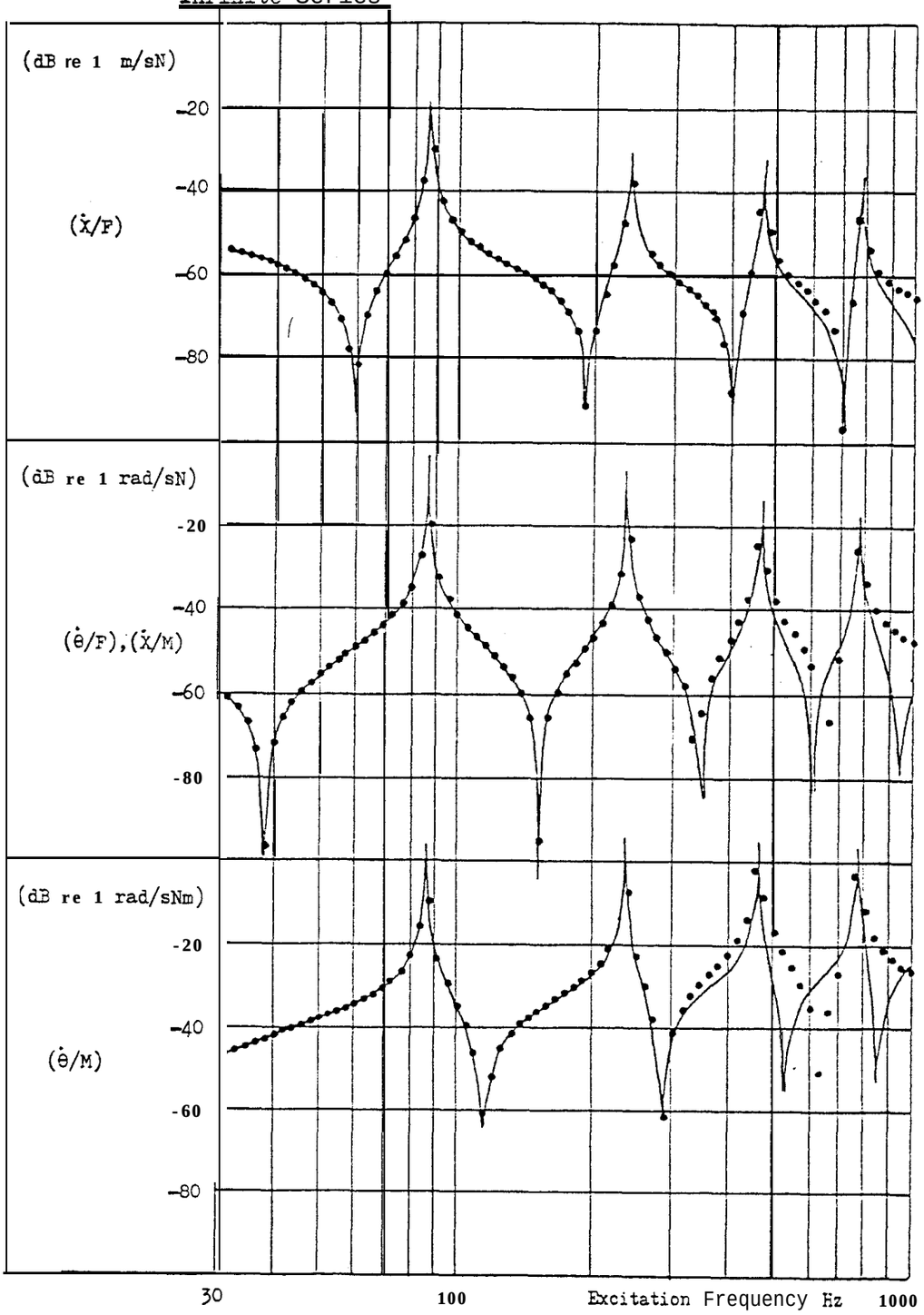

2.7

Figure 2.8 Responses Calculated from Modal Constants based on Anti Resonances

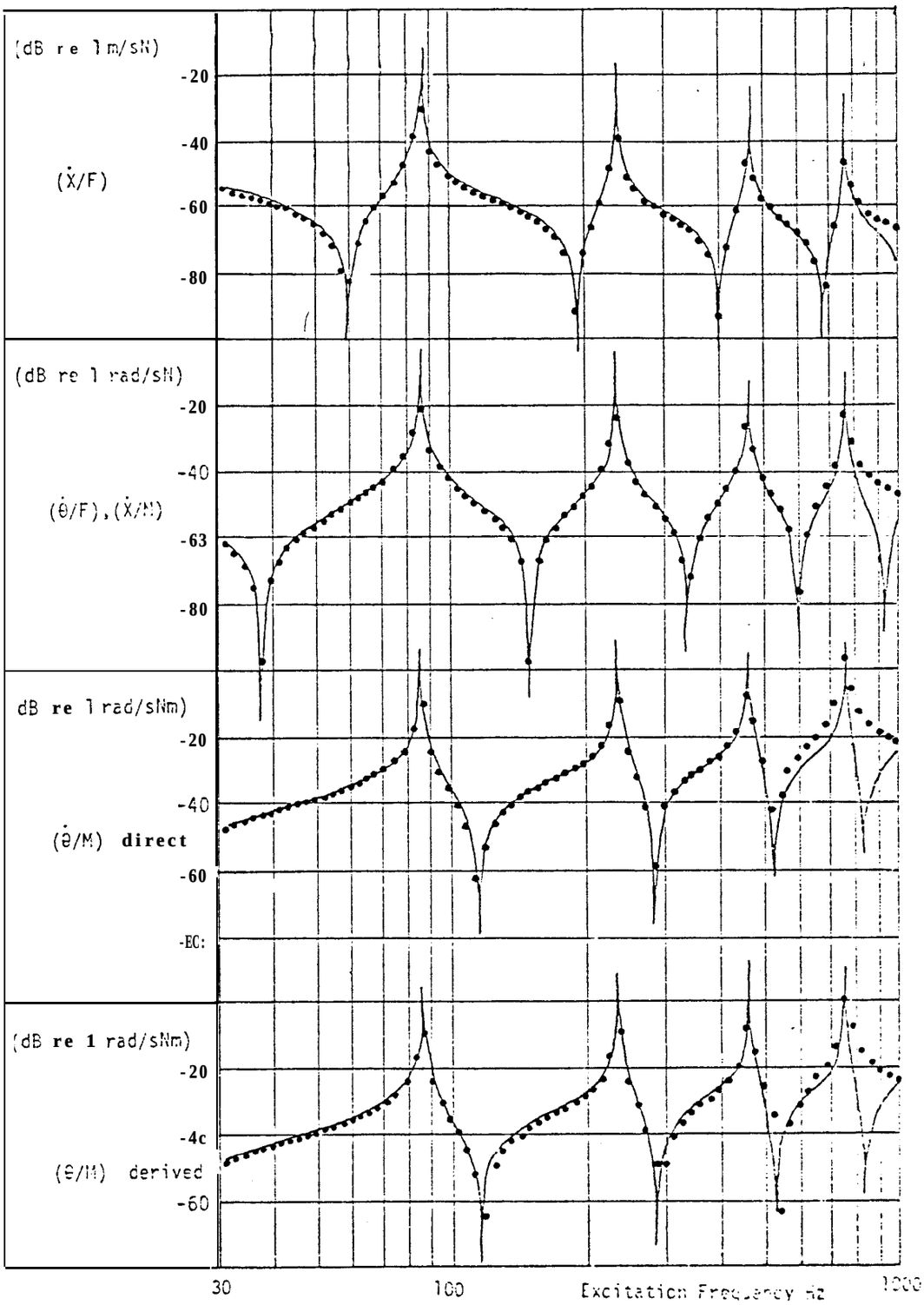

Figure 2.9 Components of Nobilities at Tip of Freely Supported Beam

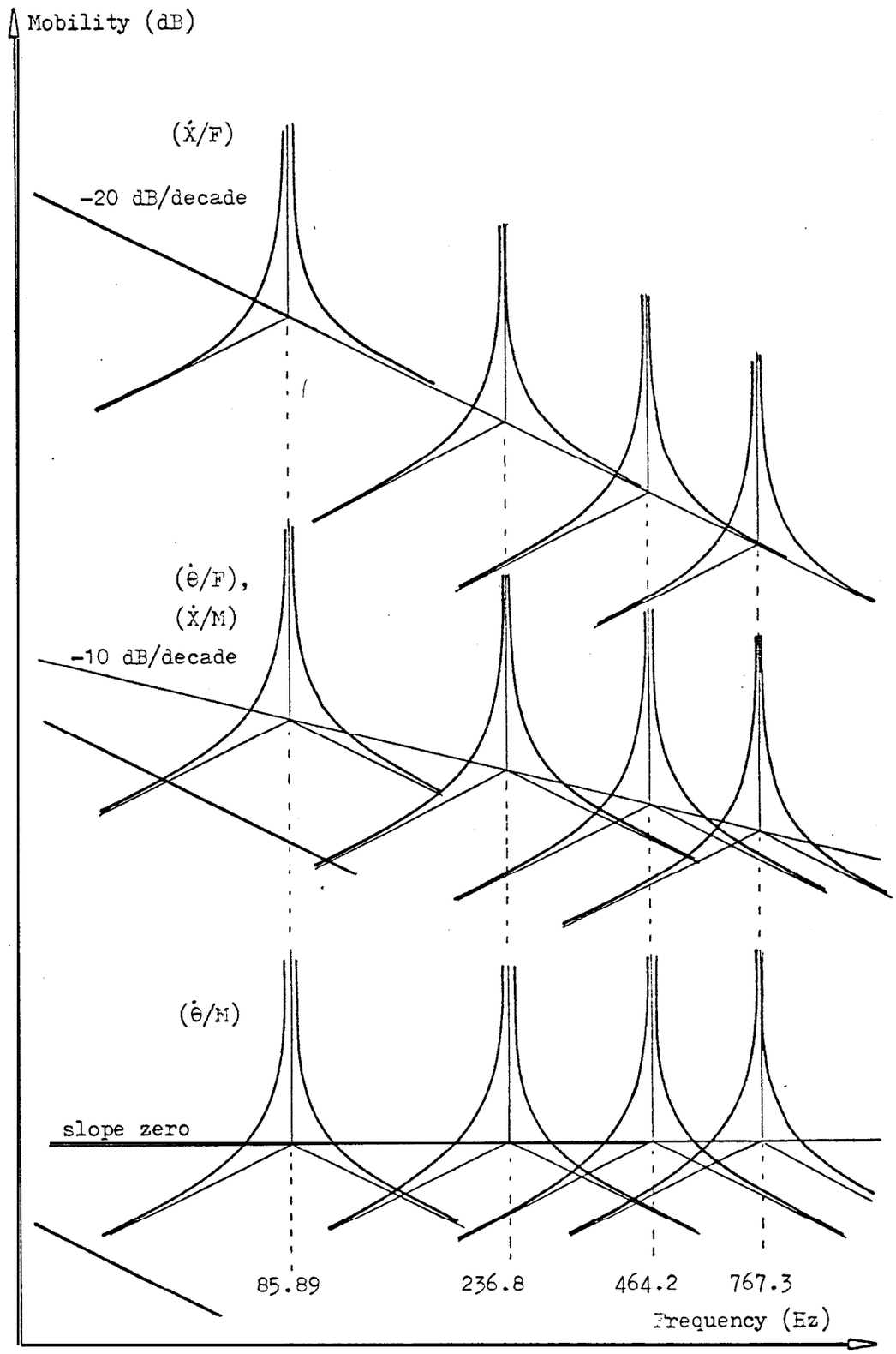

Figure 2.10 The Frequency Response of an Isolated Node

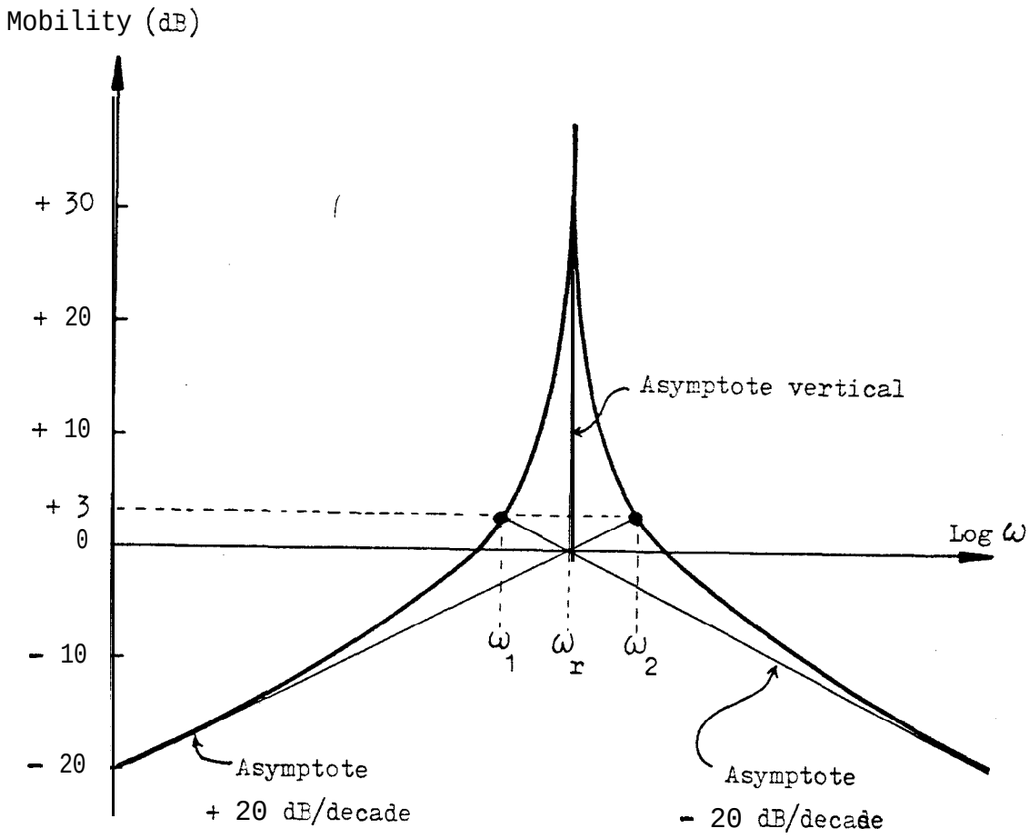

0 dB corresponds to $A_r/2\pi f_r = A_r/\omega_r$

Note $\omega_1 = \omega_r / \sqrt{2}$

$\omega_2 = \omega_r \times \sqrt{2}$

Figure 2.11 Showing the Effect of Selection of Data Points upon Identification

Resonances at 0, 85.9, 237, $64, 767 Hz

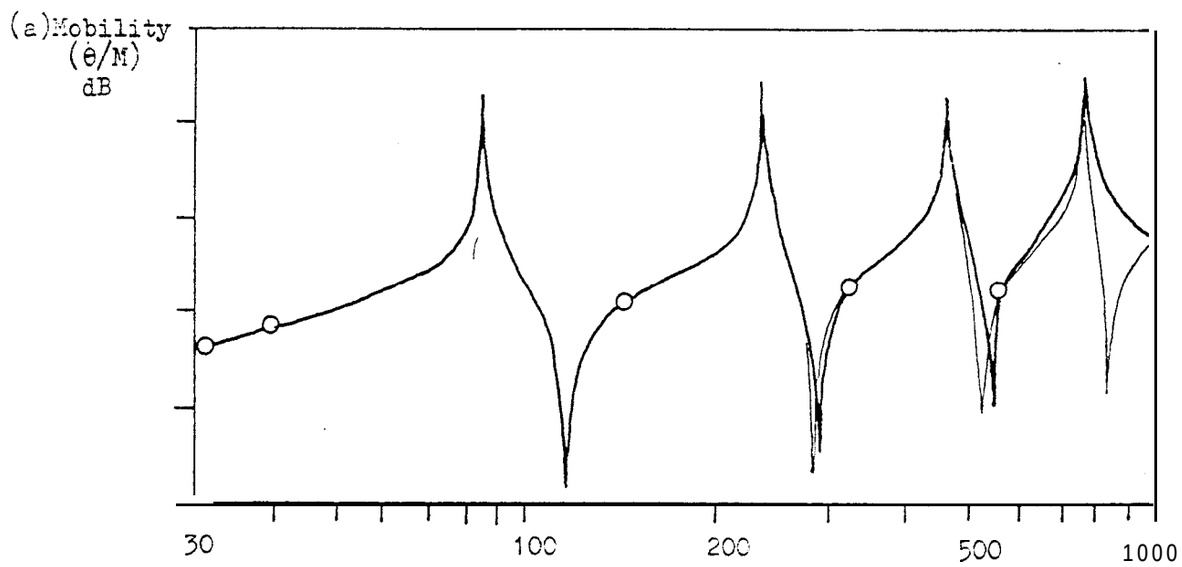

Set 31 Selected response data at 31.6, 50.1, 144.5, 331, 575 Hz

—— true curve

——— regenerated curve based on identified modal constants

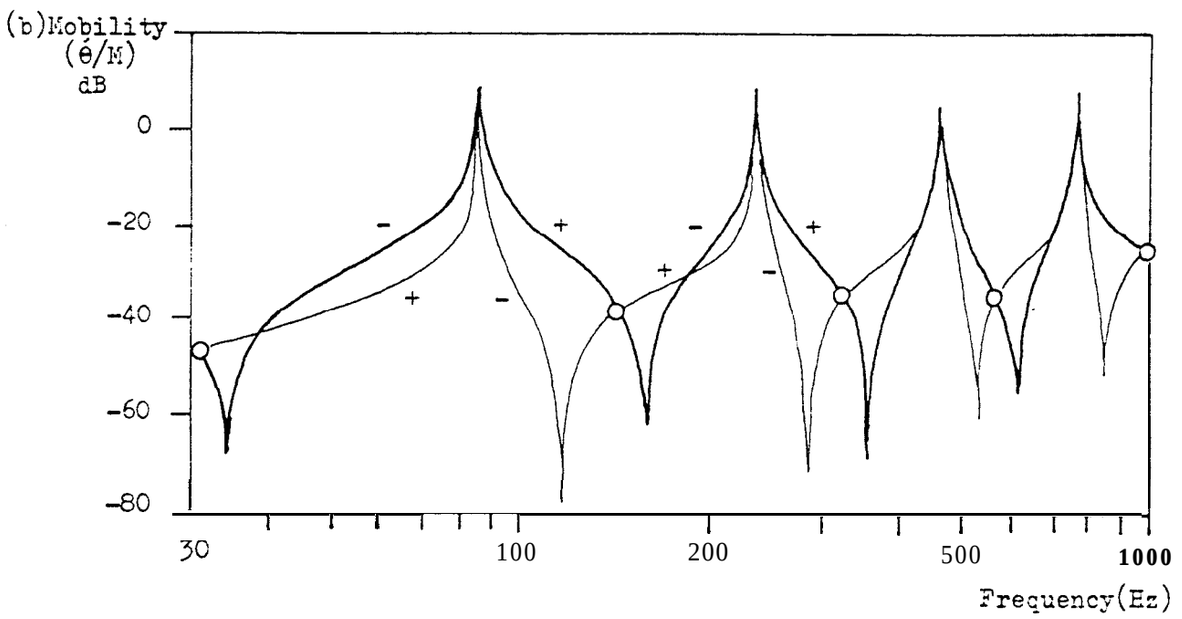

Set D2 Selected response data at 31.6, 144.5, 331, 575, 1000 Hz

Segments marked + have phase angle $+90^{\circ}$

Segments marked - have phase angle -90°

Figure 2.12 High and Low Frequency Contributions to Mobility ($\dot{\theta}/M$)

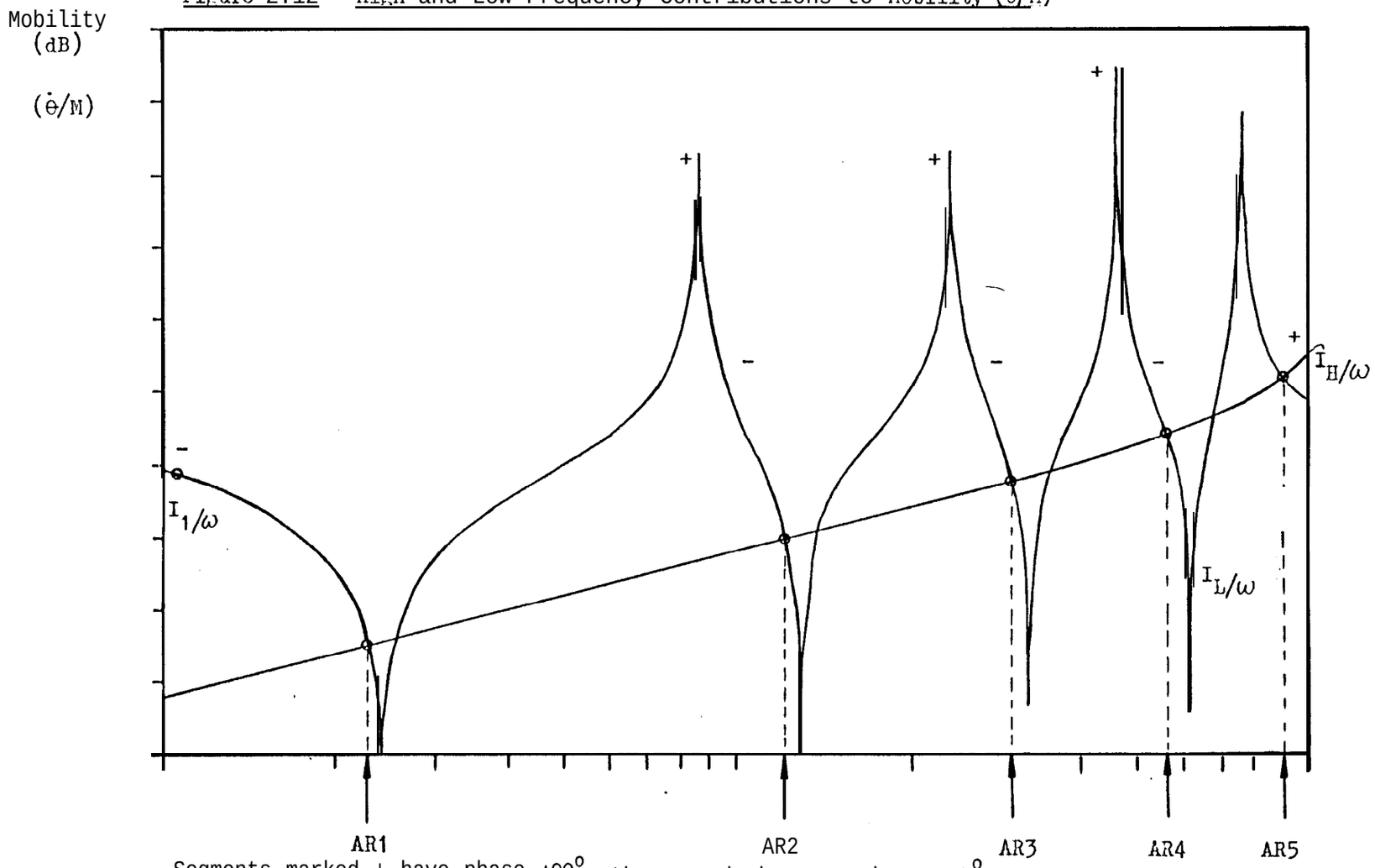

Segments marked + have phase $+90^{o}$, those marked − have phase -90^{o}

Figure 2.13 Sensitivity of Modal Constants to Variations Around One Antiresonance

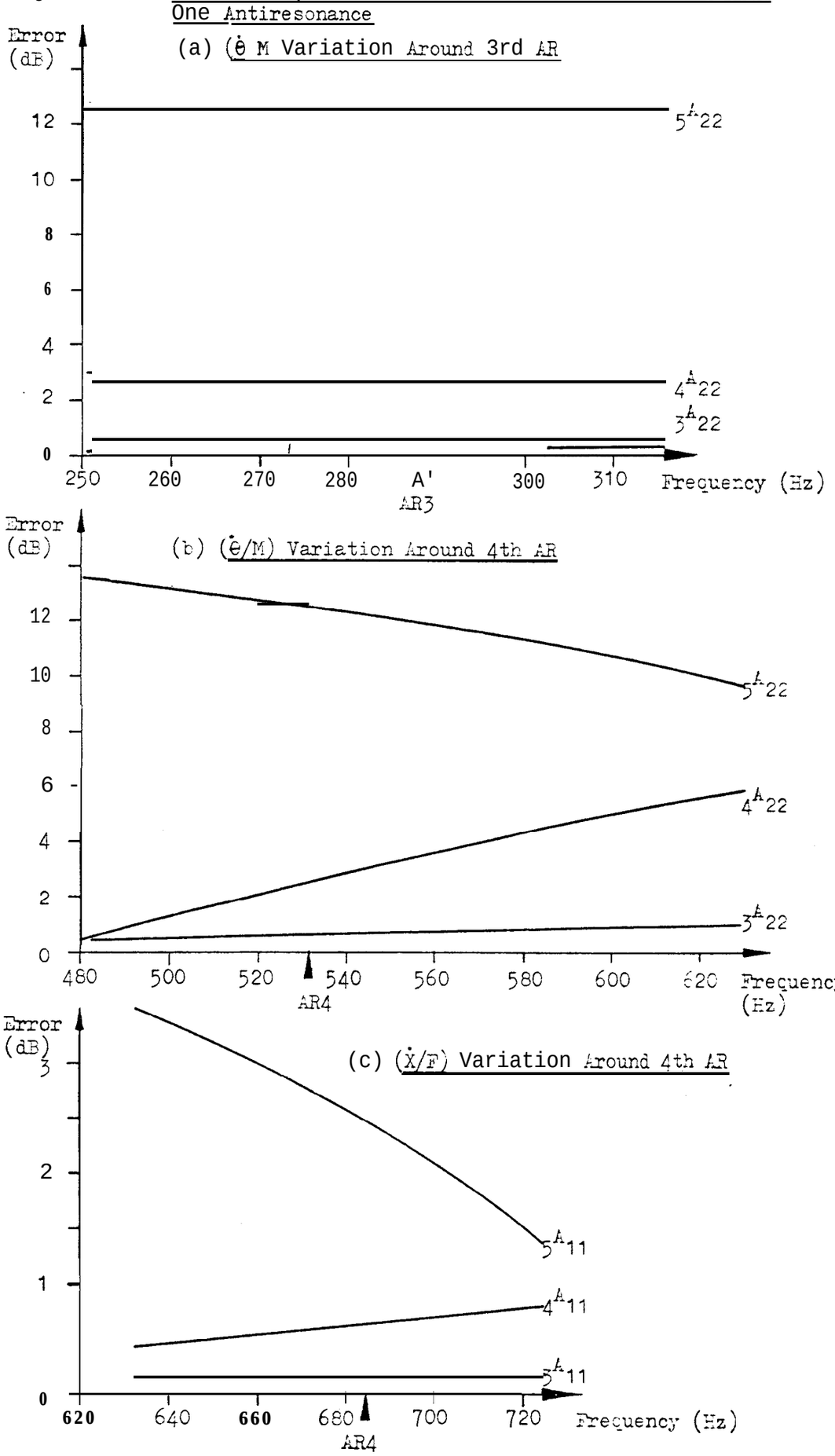

Figure 2.14 The Identification of an Isolated Mode

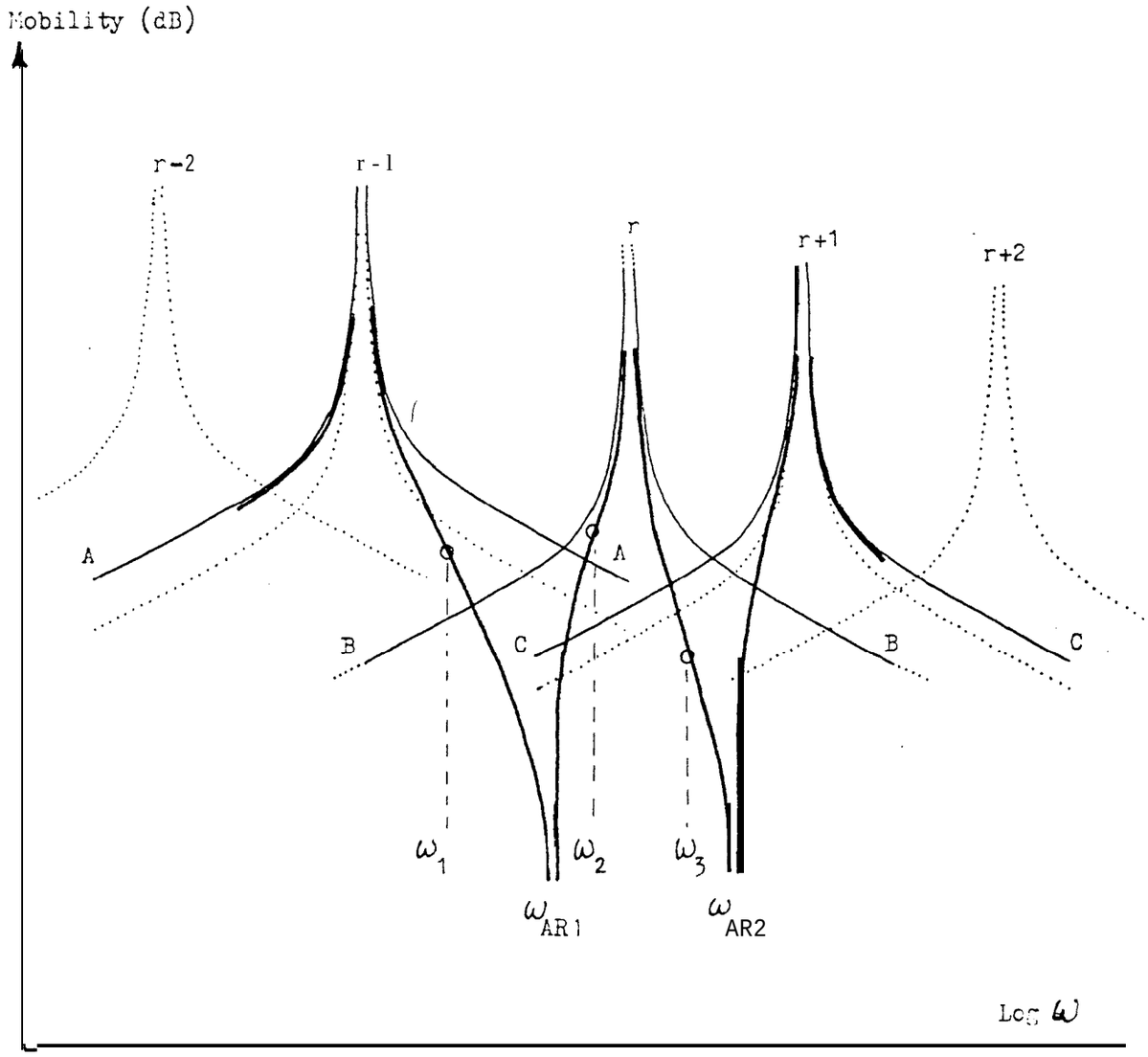

..... True responses of individual modes

——— Responses of modes identified in 3-mode calculation

——— Measured responses = true resultant of all modal contributions

Curve A - Response of mode at ω_r, raised to include effects of modes at ω_{r-2} and below

Curve B - Response of mode at ω_r maintained at true value

Curve C - Response of mode at ω_{r+1} raised to include effects of nodes at ω_{r+2} and above

Figure 2.15 Sensitivity of Modal Constants to Residual 'Resonance' Frequency

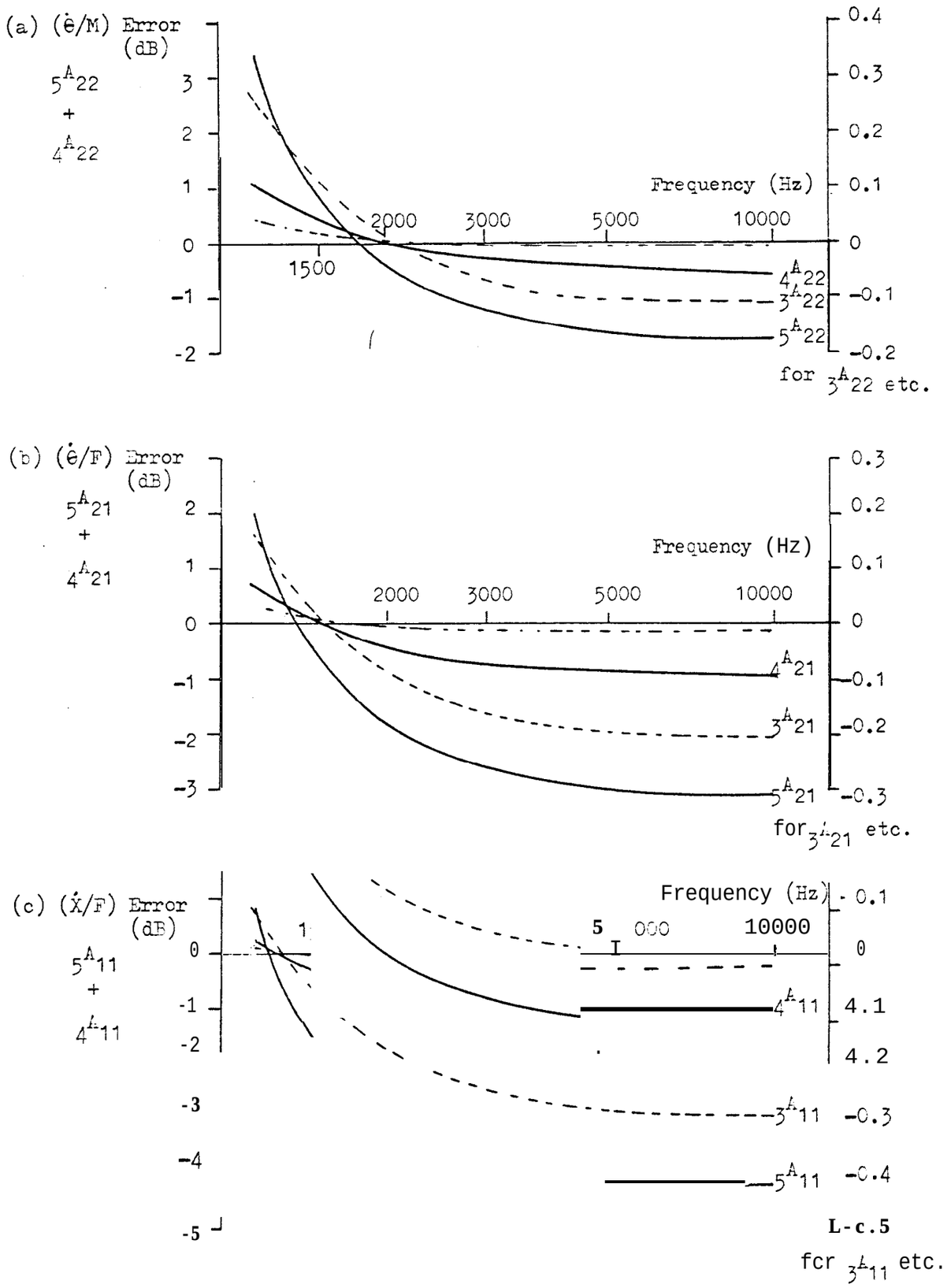

Figure 2.17 Bending Modes of a Free-Free Beam

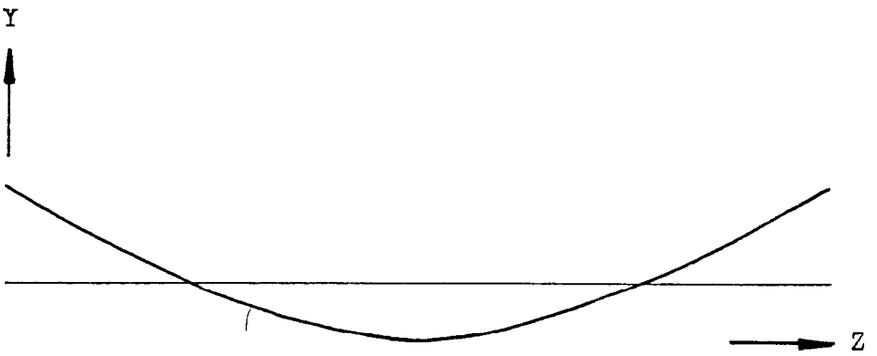

1 st Bending Node

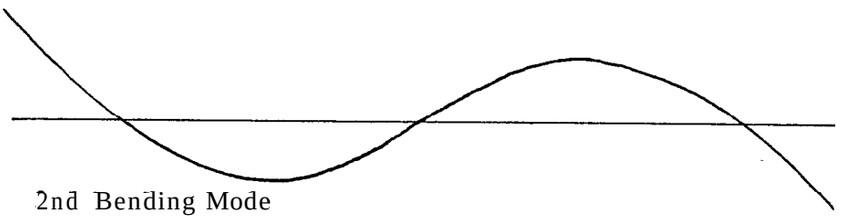

2nd Bending Mode

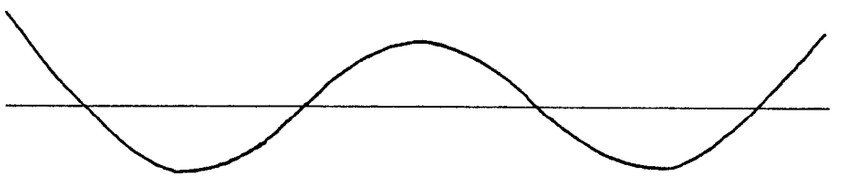

3rd Bending Mode

Figure 2.16 Discretized Representation of a Kode Shape

$$\{\phi_r\} = \begin{Bmatrix} {}_r\phi_1 \\ {}_r\phi_2 \\ \vdots \\ {}_r\phi_N \end{Bmatrix} \text{ throughout}$$

Scale → 1 mm/m

↑ d mm/unit

(a) In Terms of Displacement Coordinates

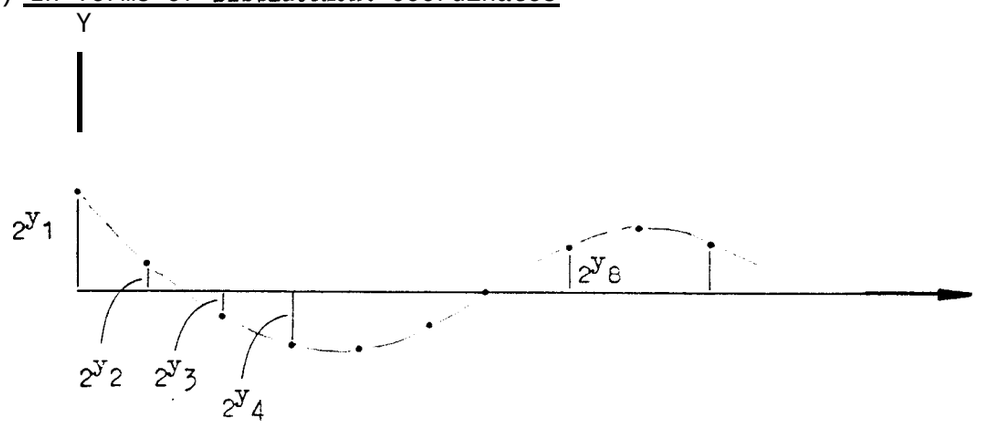

$${}_r y_i = {}_r\phi_i \, d \qquad \text{for all } i$$

(b) In Terms of Rotation and Displacement Coordinates

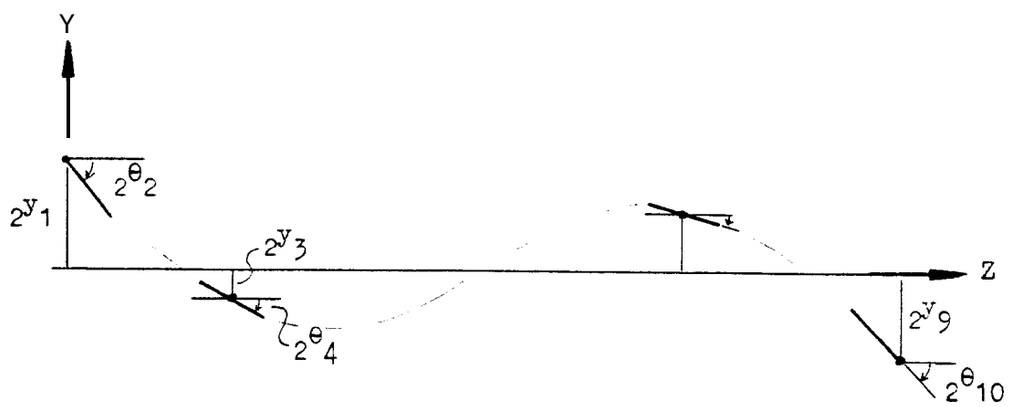

$${}_r y_i = {}_r\phi_i \, d \qquad \text{for } i \text{ odd}$$

$${}_r\theta_i = \arctan({}_r\phi_i \, d/l) \qquad \text{for } i \text{ even}$$

Figure 2.20 Addition of Residual Springs to the Spatial Model

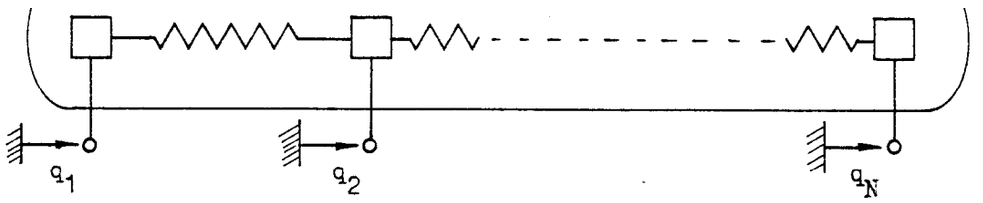

(a) Representation of N x N Spatial Model

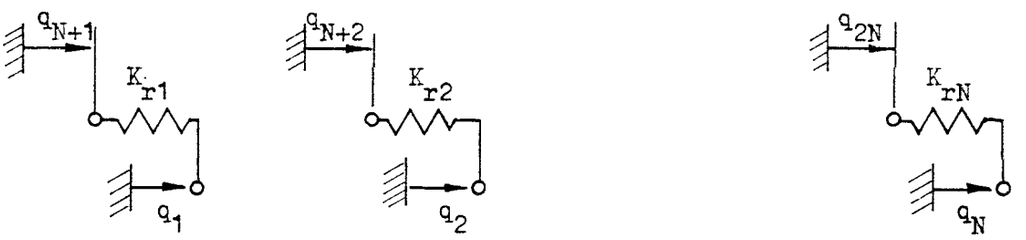

(b) Representation of High Frequency Residuals

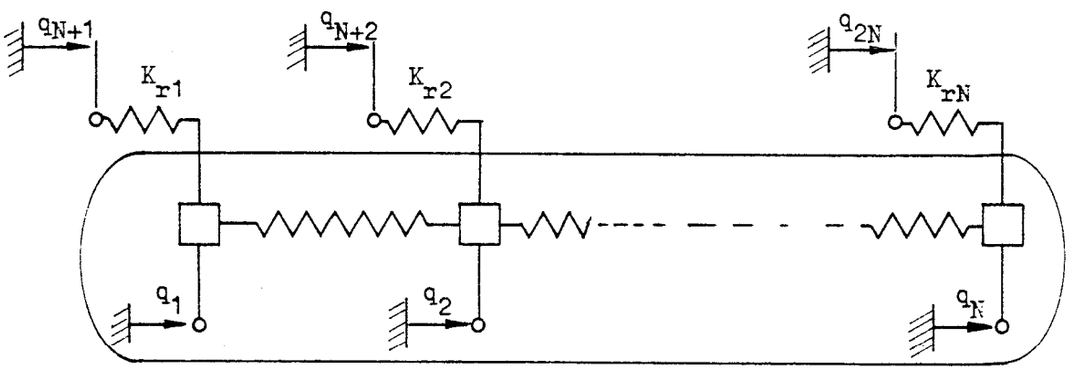

(c) Representation of 2N x 2N Spatial Model with High Frequency Residuals

3. SPATIAL MODELS OF IDEAL MASS-SPRING SYSTEMS

3.1 Introduction to Lumped-Parameter Systems

The modal identification techniques developed in Chapter 2 are applied in this Chapter to ideal undamped systems consisting of simple mass-spring chains, grounded and ungrounded, in order to investigate the feasibility of the spatial modelling techniques of Chapter 2.

3.1.1 Properties of Simple Mass-Spring Chains

A typical mass-spring chain is sketched in Figure 3.1. The inertia of this system is in the form of lumped rigid masses, each capable of motion in the horizontal direction measured by its numbered generalised coordinate. The kinetic energy of the system can be expressed in terms of the masses and their velocities.

$$T = \tfrac{1}{2} \{\dot{q}\}^T [M] \{\dot{q}\} \qquad (3.1)$$

In this case the generalised coordinates coincide with the spatial coordinates with the result that the mass matrix is diagonal.

The elastic properties of the system are represented by massless springs whose deformation and stored energy are expressed in terms of the differences of the relevant pairs of coordinates.

$$V = \tfrac{1}{2} \{q\}^T [K] \{q\} \qquad (3.2)$$

The matrix $[K]$ is not diagonal because the potential energy expressions each involve two coordinates.

The property of the simple mass-spring chain which is of most importance in this study is that the number of degrees of freedom, N, is finite and so a complete spatial model is feasible. Indeed, it exists in the form of the matrices $[M]$ and $[K]$. There are, for this system, N modes of vibration and N corresponding natural frequencies.

3.1.2 The Generation of Frequency Response Data

The frequency response data of the system can be generated by repeated use of equation (1.20) for successive stimulus frequencies. The program COUPLE1 [21] has a 'module' ZMAK2 designed for the purpose of producing response data using this equation for a systen specified in terms of matrices of mass, stiffness and damping properties. Such data may be regarded as 'error-free' because it is not subject to the unknown random and systematic disturbances which occur when practical measurements are made on physical structures.

3.1.3 The Calculation of Modal Data

Modal data may be obtained directly from the mass and stiffness matrices by use of the computer program EIGEN written in Fortran. It calls the Numerical Algorithm Group NAG5 eigenvalue subroutine F02AEF which employs Eouseholder's method and the QL algorithm. The input data required by the subroutine are N, the order of the matrices, and matrices [A] and $[B]$ of the following equation:

$$[A - \lambda B]\{x\} = 0 \qquad (3.3)$$

in which $[A]$ is real symmetric and $[B]$ is real symmetric positive definite.

When the hysteretic damping matrix $[H]$ is set to zero in equation (1.2) we get:

$$[K - \omega^2 M]\{q\} = 0 \qquad (3.4)$$

which corresponds to (3.4) when $[K]$ is substituted for $[A]$, $[M]$ for $[B]$ and ω^2 for λ.

The subroutine F02AEF produces output data λ_1 to λ_N, a set of eigenvalues, and corresponding eigenvectors $\{\phi\}_1$ to $\{\phi\}_N$ which are normalised according to the equation:

$$\{\phi\}_r^T [B] \{\phi\}_r = 1 \qquad (3.5)$$

which, conveniently, is equivalent to equation (1.8).

The mode shape data are thus obtained directly. The natural frequencies are obtained from the eigenvalues by using the equation:

$$f_r = (\mathrm{Abs}(\lambda_r))^{\frac{1}{2}}/2\pi \qquad (3.6)$$

Program EIGEN is used to read N, $[M]$ and $[K]$ and then print them and the calculated λ_r, f_r and $\{\phi\}_r$ for $r=1,N$. The method of calculation ensures that the mode shape matrix $[\Phi]$ obeys the crthogonality equation (1.8).

3.1.4 The Objectives of the Investigation

Having produced an ensemble of frequency responses it is intended to demonstrate in this Chapter that such data can firstly be identified by means of accurate curve fit procedures and then the modal data be assembled into a structural model which should closely resemble the prototype, since the model should be 'complete' in that all N modes are represented and in that all N coordinates are included.

An 'incomplete' rode1 is then to be constructed starting from the same N-mode response data, this time with the assumption that only (N-1) modes lie in the 'measured' range. High frequency residuals are not considered in this Chapter. In order for $[\Phi]$, the mode shape matrix, to be square it is further assumed that one coordinate is inaccessible and that no data involving that coordinate are available. The appearance and properties of this incomplete model are investigated.

Lastly, the usefulness and accuracy of both complete and incomplete spatial models in the prediction of the effects of parameter changes is to be noted.

3.2 Complete Models

3.2.1 Introduction

Three different mass-spring chains are considered. The first as shown in Figure 3.1 is designated AGS, asymmetrical grounded system. The asymmetry is apparent in the diagram. The mass at station 2 is

bigger than any other and the stiffness between coordinates 3 and 4 is similarly enhanced. The matrices $[M]$ and $[K]$ are symmetric about the main diagonal, however.

The second, designated SGS, is a symmetrical grounded system. All five masses and all six springs are equal, both outermost springs being grounded as shown in Figure 3.3.

The third is designated SFS, symmetrical free system, shown in Figure 3.4. This is semi-definite since a finite force will produce an infinite displacement at zero frequency; the properties of a rigid body mode. In this case the stiffness matrix $[K]$ can be evaluated but not inverted.

Each of these systems has five modes and all are represented in the following identification calculations and all five coordinates are retained in the spatial models which are thus complete.

3.2.2 AGS Asymmetrical Grounded System of 5 Degrees of Freedom

The properties of this system are shown in Figure 3.1. There is a sketch of the basic configuration and the corresponding mass and stiffness matrices. The modal properties obtained directly by use of program EIGEN are also shown in the form of natural frequencies and corresponding mode shapes, adapting the device usual in representation of longitudinal vibrations of indicating modal deflections at right angles to the actual motion.

Frequency response datawerethen generated using program COUPLE1 as specified in section 3.1.2. Each of the five coordinates was specified in terms of output velocity for input force input at each of the five coordinates in turn. Thus for each frequency of the computed sweep a 5 x 5 matrix of mobility responses, $[Y]$, was calculated, and printed out in decibels truncated to 4 figures. Results were obtained for about 100 frequencies in the range 25 to 400 Hz.

Nodal Identification

The data obtained above were regarded as 'measured'. The point responses $(\dot{X}_1/F_1)$, $(\dot{X}_2/F_2)$, $(\dot{X}_3/F_3)$, $(\dot{X}_4/F_4)$ and $(\dot{X}_5/F_5)$ together with the transfer responses $(\dot{X}_2/F_1)$, $(\dot{X}_3/F_1)$, $(\dot{X}_4/F_1)$ and $(\dot{X}_5/F_1)$, corresponding to the leading diagonal and first column of the mobility matrix $[Y]$, were examined in detail and, for each curve, 5 sets of response data were noted for use in the program IDENT. In each case, the response at 25 Hz was used and the remaining 4 sets of data corresponded as nearly as possible to antiresonances (AR) in the case of the point mobilities or, in the cage of the transfer mobilities, were a mixture of antiresonances or minima (Kin), as appropriate.

Sketches of the 5 responses of the first column and the data selected are shown in Figures 3.2. The + and - signs adjacent to segments of the response curves indicate whether the phase angle of the mobility is $+ 90^{\circ}$ (spring-like) or $- 90^{\circ}$ (mass-like). The sign to the left of each resonance peak of the point response is always positive but an irregular sequence of signs is obtained for each transfer response, as already indicated in connection with the Salter skeleton in section 2.1, Figure 2.3.

The array of modal constants corresponding to the first column of $[Y]$ is shown as Table 3.1(a). The constants $_rA_{11}$ corresponding to the point mobility Y_{11} are all positive while those corresponding to transfer responses feature some negative values. Table 3.1(b) shows the point modal constants derived from the transfer constants by use of equation (2.26).

Directly identified point modal constants are shown in Table 3.1(c) and the values agree well with thederivedvalues of Table 3.1(b) except for the 5th mode where the uncertainty in the very small value of $_5A_{11}$ leads to errors in derivation. The direct values are in this case more accurate.

The mode shape matrix can be found from the array of point modal constants by the Method (ii) of section 2.4(6) since the signs to be given to the square roots of the elements of Table 3.1(c) can be obtained from the array of Table 3.1(a) or the corresponding frequency responses of Figure 3.2(f).

Table 3.1(d) constitutes the matrix of mode shapes, $[\Phi]$, found from measured data. It may be compared directly with Table 3.1(e) which contains the modeshapes calculated by EIGEN. The differences in sign of the second and fifth columns are of no significance in subsequent calculation, though the 'modal constant' signs of Table 3.1(d) are to be preferred as having meaning while those from EIGEN are arbitrary. The numerical values being corn-pared in these two Tables are very closely similar.

At this stage we have found the resonance frequencies needed for the diagonal matrix $[\omega_r^2]$ and the mode shape matrix $[\Phi]$, accurate to 4 significant figures. Such accuracy might reasonably be attained in a practical measurement using the best equipment available.

The summation of all the elements of $[M]$ gives $\Sigma M = 5.90884$ kg which is a reasonable approximation to the true value of 6 kg. Similarly, $\Sigma K = 1.00209 \times 10^6$ X/m is very close to the true value 1.00 x 106 N/m.

Construction of the Spatial Model

Mass and stiffness matrices were calculated according to equation (1.12) using program EMKAY on the PDP8 mini-computer. The results are shown in Table 3.2(a).

It can be seen that these matrices resemble closely the prototype matrices of Figure 3.1. The largest off-diagonal element of $[M]$ is -0.0137 which is 0.6% of the largest element of the leading diagonal. The largest element of $[K]$ corresponding in position to a zero of the

original matrix is 0.184×10^5 which is 0.06% of the largest element of the leading diagonal.

In each case the presence of small elements in the modelled matrix corresponding to zeroes of the original matrix can be attributed to errors arising from the rounding to 4 significant figures.

A check was carried out by using the 6 significant figures of the EIGEN mode shape data output as direct input to EIGAY. In this case, the largest off-diagonal element of $[M]_{L^{-1}}$ was 1.67×10^{-6} which can be attributed to rounding errors in the processes of matrix inversion and multiplication. The $[K]_{C^{-1}}$ matrix was similarly accurate. These matrices are shown in Table 3.2(b).

Error Sensitivity of Complete Model

Small perturbations were made in one element of each of the 4 digit spatial model matrices of Table 3.2(a). The consequent effects on the resonance frequencies were evaluated using program EIGEN. The results are shown in Table 3.3. The largest effect of 1% change in one mass element on resonance frequency is -.15% whereas a similar stiffness change caused a 4% shift in resonance frequency.

The calculations are evidently much more sensitive to errors in stiffness values than for mass values.

3.2.3 (SGS) Symmetrical Grounded System of 5 Degrees of Freedom

The properties of this system are incorporated in Figure 3.3. A most significant consequence of the symmetry of the system is to be noted. Coordinate 3 is a node of both the second and the fourth mode and in the third mode coordinates 2 and 4 are nodes.

Calculations were made using COUPLE1 and the resulting frequency response data were selected and identified by methods akin to those of section 3.2.2. As in that case, the spatial model constructed from the identified mode shape data was similar to the prototype.

3.2.4 (SFS) Symmetrical Free System of 5 Degrees of Freedom

This system has a specification and properties shown in Figure 3.4. The middle coordinate, 3, is a node of the second and fourth modes, because of symmetry. The first mode is a rigid body mode at zero frequency.

As before, modal identification based on generated frequency responses gave data for the spatial model which were similar to the original specified by the $[M]$ and $[K]$ matrices of Figure 3.4.

3.2.5 Discussion of Modelling with Complete Data

The accuracy of the check calculation mentioned in section 3.2.2 using 6-figure data demonstrated that the method of producing mass and stiffness matrices from a mode shape matrix and the corresponding set of resonance frequencies is capable of giving accurate results and indicates that the process is numerically well-conditioned.

In all the cases considered in this section there are only a finite number (5) of modes and all are represented. In these circumstances program IDENT can be expected to yield accurate modal constants and enable response data to be regenerated which will coincide with the original data at all frequencies.

We have shown that point modal constants can be derived from transfer measurements. This feature is of great value if point measurements are difficult - as in the case of the rotational measurements reported in Chapter 6. The redundant data in this case here reported were used as a check on consistency.

However, it is likely that point measurements will generally be more accurate than transfer measurements so that the calculation of mode shape matrix elements from point modal constants is to be recommended. The necessary signs are readily obtained by inspection of transfer response plots.

3.2.6 Conclusions

(1) Spatial models involving mass and stiffness matrices related to defined coordinates can be calculated from frequency response data.

(2) One method requires data corresponding to force input at one coordinate and response measured at all coordinates and subsequent calculation of point and transfer modal constants.

(3) A second method, generally to be preferred, requires numerical data for point responses at each coordinate, together with plots of transfer responses corresponding to excitation at one coordinate.

(4) The total mass of each system is closely approximated by the summation of the elements of the mass matrix. Similarly, the total stiffness is given by the summation of the elements of the stiffness matrix.

3.3 Incomplete Models

3.3.1 Introduction

In measuring continuous structures which 'have an infinite number of natural frequencies, it is practicable to get data for only a limited number of low frequency modes. The data obtained are thus truncated, by exclusion of resonances above a certain limit of frequency.

An approximation to this situation was made in this investigation by limiting the range of response data to 250 Hz, thereby excluding the highest resonance frequency. The truncated data do, of course, still include the effect of the highest mode but the modelling process has to be confined to 4 degrees of freedom. In order to retain simple calculations with square matrices, the number of coordinates was also reduced to 4, in this case by the arbitrary omission of the 5th variable coordinate.

3.3.2 AGS Asymmetrical Grounded System of 4 Degrees of Freedom

Identification

The mobility matrix wasnextreduced to size 4 x 4 and accordingly the data for the point responses $(\dot{X}_1/F_1)$,$(\dot{X}_2/F_2)$,$(\dot{X}_3/F_3)$ and $(\dot{X}_4/F_4)$ and the transfers $(\dot{X}_2/F_1)$, $(\dot{X}_3/F_1)$ and $(\dot{X}_4/F_1)$ were input in turn to program IDENT. The data selected corresponded in each case to the first four response frequencies used previously in the 'complete' calculations of section 3.2.2.

The modal constants corresponding to the first column of the mobility matrix are shown in Table 3.4(a) and close comparison shows that they are quite similar to the corresponding values in Table 3.1(a). Similarly, the derived point modal constants in Table 3.4(b) compare closely with those of Table 3.1(b). The directly-identified values of Table 3.4(c) when compared with those of Table 3.1(c) are generally somewhat larger. The approximations of this process were discussed in section 2.1.2.

Generation of Approximate Response Data

The modal constants found above were used to regenerate the frequency response curves and a selection of the results is shown as dashed lines in Figure 3.5. The dashes coincide with the original response curves except in the high frequency region around the omitted 5th mode,thus indicating a good approximation at the lower frequencies.

Mass and Stiffness Matrices

The identified point modal constants were used as before in the calculation of numerical values of the mode shape matrix presented as Table 3.4(d) whose signs are the same array as those of Table 3.4(a).

This mode shape matrix with data of 4 significant figures was used in program EMKAY to give the mass and stiffness matrices of Table 3.5.

The mass matrix [M] has off-diagonal elements of similar numerical value to those on the leading diagonal. Some of the off-diagonal elements have negative values. The matrix is not at all similar to the original diagonal matrix or to the 5 x 5 approximation in Table 3.2(a) and it is not easily interpretable in physical terms. It is, however, of interest to note that the sum of all the elements of [M] is close to the total mass of the system (6.000 kg).

Similar comments apply to the stiffness matrix [K] which also has a total sum similar to that of the original stiffness matrix (1 x 106 N/m). A description of some of the characteristics of these matrices based on truncated data is given in Appendix A4.

Mode Shapes

The first test of the validity of these strange matrices was made by using them as input to the program EIGEN and thus calculating associated mode shapes and frequencies which are presented in comparison with the original values of Figure 3.6 case (b). When all 6 figures of [M], [K] data were retained, natural frequencies (eigenvalues) were obtained coinciding with the original values to 4 figures.

However, a second calculation in which the matrix elements were rounded to 4 figures before input to EIGEN gave significant errors of frequency - case (c) of Figure 3.6 - although the mode shapes were not markedly different from the 6-figure values. As one might expect, if EIGEN is given data of sufficient accuracy (e.g. 6 figures) it simply returns the natural frequency and mode shape data that were input to EMKAY in the first place.

It can be seen that the node shapes of the first two modes are indistinguishable fron the original except, of course, in the omission of coordinate 5. The third and fourth codes show some divergence from the original in the region of coordinates 3 and 4 although coordinates 1 & 2 are accurately defined, within the limits of the sketch dimensions.

Error Sensitivity of the Incomplete Model

As before, for the complete AGS model, small perturbations were made in one element of $[M]$ and of $[K]$ for the incomplete spatial model. The effect of such changes on natural frequencies are shown in Table 3.6. The 1% increment in an element of the mass matrix gave at worst -.4% shift in one natural frequency, showing slightly more sensitivity than before. The 1.2% change in one stiffness element caused at worst a 23% error in natural frequency.

Thus, as before, a greater sensitivity to errors in stiffness than in mass is shown, leading to the observation that once the spatial model has been established in terms of S-figure EIGEN output all 6 figures should be retained even if the original data were only of 3or 4 figure accuracy.

3.3.3 AGS Symmetrical Grounded System of 4 Degrees of Freedom Identification

The response data used in section 3.2 were truncated and used in a manner similar to that of the previous section in a series of calculations using program IDENT.

The directly-identified modal constants of the first column of the mobility matrix are shown in Table 3.7(a) and the point values derived from them are shown in Table 3.7(b). This latter Table can be compared with Table 3.7(c) of the point modal constants directly identified.

It is apparent that the consistency of these data is very poor. Suspicion of numerical error also arises because of the negative values agpearing in Table 3.7(c) which should all be positive because they correspond to point modal constants which are squares of mode shape vector elements. Comparison with the complete data of section 3.2.4 (not presented here) shows great divergence in values expected to be comparable, especially for the higher modes and for transfers between remote coordinates.

No further calculations were done with these data, but the reasons for their poor accuracy are discussed in section 3.3.5, below.

3.3.4 (SFS) Symmetrical Free System of 4 Degrees of Freedom Identification

The complete data of section 3.2.3 were truncated in a similar way to that of the incomplete AGS model of section 3.3.2 and used in IDENT calculations, resulting in the soda1 constants shown in Tables 3.8. Point modal constants derived from the elements of Table 3.8(a) are shown in Table 3.8(b) which should be compared with the directly identified values of Table 3.8(c). The correlaticc is reasonable although the negative sign of $_2A_{33}$ is anomalous and indicates a likelihood of error.

The comparison of Table 3.8(a) with the corresponding data for the complete 5-degree-of-freedom model shows quite good agreement with divergences increasing with mode number and range of transfer; i.e. left to right and downwards in the Tables, as found for the AGS system of section 3.3.2.

It can be seen from the mode shapes of Figure3.4 that the constants $_2A_{33}$ and $_4A_{33}$ should be zero as a result of the symmetry of the system. They are correctly found in the set of derived values of Table 3.8(b) but are non-zero in the identified data of Table 3.8(c). It is thus clear from this case that directly identified data is not always more accurate than derived data. Accordingly, 2 mode shape matrix was calculated for each case (Tables 3.&(d) and (e)).

Mass and Stiffness Matrices

The two alternative mode shape matrices were used in two runs of program EMMAY to give corresponding mass and stiffness matrices presented as Table 3.9(a) based on identified data and Table 3.9(b) based on derived data.

As found for the incomplete AGS model, the mass and stiffness matrices are not easy to interpret physically.

The summation of mass elements is 5.000 kg and that of stiffness elements is zero. The values obtained by EMKAY are quite close to these values. It should be observed that the stiffness summation of order 10^2 is negligible compared with the order of magnitude (10^7) of some of the matrix elements (especially when data have been truncated to 4 significant figures).

Mode Shapes

The results of EIGEN calculations using $[M]$, $[K]$ matrices of the previous section are shown in Figure 3.7; being calculations to 6 significant figures they agree with the mode shape matrices of Tables 3.8(d) and (e). It is apparent that in this case the results based on derived data are slightly more accurate than those based on directly identified data.

3.395 Discussion of Modelling with Incomplete Data

The incomplete model can be used to predict frequency responses which are of good accuracy up to the highest resonance frequency included, but, of course, are inaccurate in the region of omitted resonances at high frequencies.

Predicted mode shapes are of reasonable accuracy, but distortion occurs affecting those coordinates nearest to the coordinate omitted.

A study of Figure 3.3 showing the mode shapes of the Symmetrical Grounded System reveals the reason for the failure indicated by the lack of consistency of Table 3.7. In the second and fourth modes the centre coordinate 3 had no motion and for the third rode coordinates 2 and 4 were zero. Such 2 large amount of null data led to identifications of great inaccuracy. In practice, the siting of accelerometers at nodes should be avoided. If such a placement were discovered, 2 re-siting

involving movement of the attachment point by a small distance would solve the problem.

The usefulness of derivation as a check on consistency is seen when the results of section 3.3.4 sre considered. In this case of the Symmetrical Free System, coordinate 3 in the centre was et 2 node of the second and fourth modes. This led to a small inaccuracy of the directly-identified point model constants which could, to a certain extent, be corrected by using the derived constants.

3.3.6 Conclusions

(1) The spatial model besed on incomplete data does not readily provide a direct physical interpretation of the system's configuration.

(2) The model gives genereted frequency responses of acceptable accuracy.

(3) The node1 gives good prediction cf eigenvelues (nature1 frequencies) provided 6 figure data is retained for the mass and stiffness metrices.

(4) The mode shape data obtained ere slightly distorted at higher frequencies and at coordinates near the omitted coordinate(s).

(5) The method of calculation ensures that the mode shape vectors, however, are orthogonal.

(6) The use of redundant data provides a useful check of consistency - it is possible for derived data to be more accurate than directly identified data.

(7) If response data are measured at a point which is a node for one or more modes, then the approximate model will be inaccurate. Steps should be taken to check for this condition and, if encountered, to correct for it by reselection of coordinates.

(8) Once again, even though the mass and stiffness matrices have no ready physical interpretation, the overall summations $[M]$ and $[K]$ are close to the known true values of the corresponding prototype system.

3.4 Parameter Changes in Incomplete Models

Any change in the mass or stiffness properties of 2 system such as we are considering will produce corresponding changes in natural frequencies and mode shapes. To be of value, the approximate spatial model should give reasonably accurate predictions of frequencies and mode shapes when it undergoes modifications corresponding to those affecting the original system. Predicted frequency responses may also be compared.

Program EIGEN was used to calculate the natural frequencies and mode shapes of both the complete system of 5 degrees of freedom and the truncated-data model of 4 degrees of freedom. Corresponding elements in the matrices were changed by equal amounts.

Frequency responses were computed 2s before, using program COUPLE1 with module ZMAX2. The input data were the incomplete 4 x 4 mass and stiffness matrices. The desired responses were computed in the range 20 to 500 Hz. Although only certain selected responses are reported on, below any of the 16 elements of the mobility matrix could have been calculated from the spatial model. This shows a significant advantage of the spatial model when compared with modal identification alone which enables regeneration of only those responses which have been directly identified.

3.4.1 Chanee of Mass

AGS Mass Change in Asymmetrical Grounded System

The change made was the addition of 2 further 3 kg to the 2 kg mass at coordinete X_3, the second variable coordinete. The mass matrix became:

$$[M] = \begin{vmatrix} 1 & 0 & 0 & 0 & 0 \\ & \underline{2} & 0 & 0 & 0 \\ & & 1 & 0 & 0 \\ & & & 1 & 0 \\ \text{symmetric} & & & & 0 \end{vmatrix} \text{ kg} \quad \text{(changed element underlined)}$$

A similar addition of 3 kg was made to the m_{22} element of the 4DF mass matrix of Table 3.5.

These mass matrices together with the appropriate unchanged stiffness matrices were input to EIGEN giving the results shown in Figure 3.8 in which one sees excellent prediction of frequencies which have been substantially altered and mode shapes which match 2s well as the CD? approximations of the unchanged system of Figure 3.6.

Response calculations using COUPLE1 2re presented for comparison in Figure 3.9 in which it can be seen that the 4DF approximation diverges from the 'complete' response only in the region of the 5th mode.

These results show very satisfactory behaviour of the approximate spatial model.

SFS Mass Change of Symmetrical Free Srs tem

In order to save time, computations for this system were restricted to use of program EIGEN, thus no frequency responses were obtained.

The mass matrix for the complete model was modified by the addition of 4 kg at coordinate 2 2nd it thus became identical with that of AGS above. Both ' identified' and 'derived' matrices of the 4DF approximation were modified.

The results of the EIGEN calcula tion with appropriate unchanged stiffness matrices are summarised in Figure 3.10. The identified oodel, (b), is marginally better at natural frequency prediction, giving 2 maximum error of 0.3% for the fourth mode for which the 'derived code1 (c), has an error of 1.5%. It does seen, however, that the derived ncdei gave mode shapes slightly nearer to the correct ones.

It is apparent that the eigenvalue routine called by EIGEN has difficulty with the frequencies of the lowest free node which shouid be zero in all cases. in case (a) the computed value was 0.000016 Hz which was rounded to zero in the Figure.

3.4.2 Change of Stiffness

3.4.2.1 Stiffness Change of Asymmetrical Grounded System

A change of stiffness between coordinates 3 and 4 was made by reducing the corresponding spring from 2 MN/m to 1 MN/m. Four elements of the stiffness matrix were thus altered; the revised 5DF matrix being:

$$[K] = \begin{bmatrix} 2 & -1 & 0 & 0 & 0 \\ & 2 & -1 & 0 & 0 \\ & & \underline{2} & \underline{-1} & 0 \\ & & & \underline{2} & -1 \\ \text{symmetric} & & & & 1 \end{bmatrix} \text{ MN/m} \quad \text{(changed elements underlined)}$$

Similar modifications were made to the 4 x 4 incomplete stiffness matrix.

The results of the two EIGEN calculations using these modified matrices are shown 2s Figure 3.11. The mode shapes seem to be of similar accuracy to those for the mass change but the predicted frequencies are significantly less close, especially for the second mode in which the error is 4.4%. One nay note that this mode involves the greatest difference in displacement between coordinates 3 2nd 4.

Corresponding calculations of frequency response involving the coordinates 3 and 4 are shown 2s Figure 3.12. The response in the region of the first and third modes is reasonably accurate in both frequency 2nd ievel; the fourth somewhat less so 2nd the second mode is the least well predicted. One of the pair of antiresonances is omitted in Figure 3.12(b), the transfer response Y_{34}, just above the erroneous second mode. in this case the low-amplitude response is of poor accuracy. An examination of the signs associated with modal constents shows that the sign of the third mod21 constant is wrong.

Stiffness Change of Symmetrical Free System

For this system, a change of stiffness was made between coordinates 2 and 3 by increasing the corresponding spring stiffness by 1 MN/m. The revised complete stiffness matrix is:

$$[K] = \begin{bmatrix} 1 & -1 & 0 & 0 & 0 \\ & \underline{3} & \underline{-2} & 0 & 0 \\ & & \underline{3} & -1 & 0 \\ & & & 2 & -1 \\ \text{symmetric} & & & & 1 \end{bmatrix} \quad \text{MN/m} \quad \text{(changed elements underlined)}$$

The EIGEN results are shown as Figure 3.13 in which the 'derived' model clearly gives better mode shapes and closer frequencies than does the 'identified' model. In either case, hoverer, the frequency of the fourth mode is seriously in error.

The reason for the relatively poor performance of the stiffness matrix may be discovered by studying the equation (1.12) by which it is formulated. It involves the squares of the natural frequencies. If these are erroneous or, as in the incomplete model, omitted, there are substantial effects on the stiffness matrix which is thus inherently more prone than the mass matrix to ill-conditioning.

3.4.3 Discussion of Prediction using Incomplete Models

In the most favourable circumstances, the incomplete model gives extremely good prediction. in section 3.3.2 it was established that the Asymmetrical Grounded System, which had no nodes at measurement coordinates, led to an accurate model. It was found in section 3.4.1 that the effects of a change of mass distribution in this system were very accurately predicted. The same model coped adequately, but less precisely, with changes in the stiffness matrix although it may be argued that the results are acceptable.

Study of the Symmetrical Free System led to two incomplete models which are a little inaccurate because of the node that appeared at 2 measurement -point in the original second and fourth modes. Thus its

prediction of the effects of change of mass are worse than was the case for the Asymmetrical Grounded System. The change of stiffness predictions are somewhat worse again. Nevertheless, it is felt that even in this relatively unfavourable case, the spatial model was useful in that reasonable first estimates of the effects of changes could be made with a minimum of computational effort.

The truncated frequency response data could, of course, have been used directly, frequency by frequency, in impedance coupling calculations of the effects of parameter changes. The prediction of frequency response by this relatively time-consuming method will be accurate. Resonance frequencies would have to be found by interpolation and no mode shape data would be directly available.

3.4.4 Conclusions

(1) Very accurate predictions of the effects of change of mass at a specified coordinate can be made.

(2) The prediction of stiffness change effects is less accurate but still useful.

(3) A truncated model based on data involving a node at a measurement point gives less accurate predictions.

3.5 CONCLUSIONS: SPATIAL MODELS OF MASS-SPRING SYSTEMS

(1) The method of constructing a spatial model from frequency response data is feasible and usually the calculations are weii-conditioned.

(2) Complete spatial models incorporating all coordinates and all modes are accurate within the rounding errors of the computation.

(3) The spatial model cansupplydata for 211 coordinates Of response and stimulus.

(4) If the measured frequency range is limited and a mode is excluded it is feasible still to construct a spatial model using square matrices Obtained by reducing the number of coordinates to match the number of modes.

(5) The spatial model based on incomplete data is not capable of physical interpretation but the total sums of the matrix elements are 2 good approximation to the total mass 2nd stiffness of the original system.

(6) It is necessary to retain all the significant figures (usually 6) in the incomplete spatial model even though it is based on data with 4 or fewer significant figures. Rounding errors lead to relatively large discrepancies in predicted frequencies.

(7) The loss of information arising from response coordinates being sited at nodes leads to considerable inaccuracy -even computational failure.

(8) The incomplete spatial model gives excellent prediction of the effects on frequency response of large changes of mass elements. The prediction of the effects of stiffness changes is less accurate but is 2 useful indication of trends.

Figure 3.10 AGS Properties of Asymmetrical Grounded System

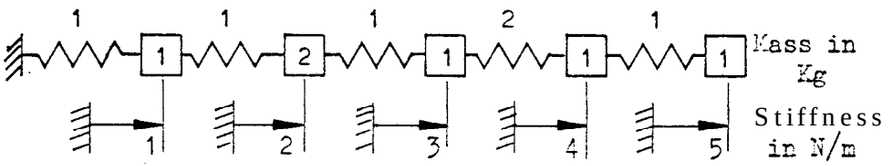

Matrices related to ungrounded coordinates)

$$[M] = \begin{bmatrix} 1 & & & & \\ & 2 & & & \\ & & 1 & & \\ & & & 1 & \\ & & & & 1 \end{bmatrix} \text{Kg}, \quad [K] = 10^6 \begin{bmatrix} 2 & -1 & 0 & 0 & 0 \\ & 2 & -1 & 0 & 0 \\ & & 3 & -2 & 0 \\ & & & 3 & -1 \\ \text{Symmetric} & & & & 1 \end{bmatrix} \text{N/m}$$

Resonance Frequencies 2nd Mode Shapes

Output of Program EIGEN with input matrices above.

Mode	Frequency (Hz)
1	43.83
	124.8
3	208.4
4	247.2
5	362.3

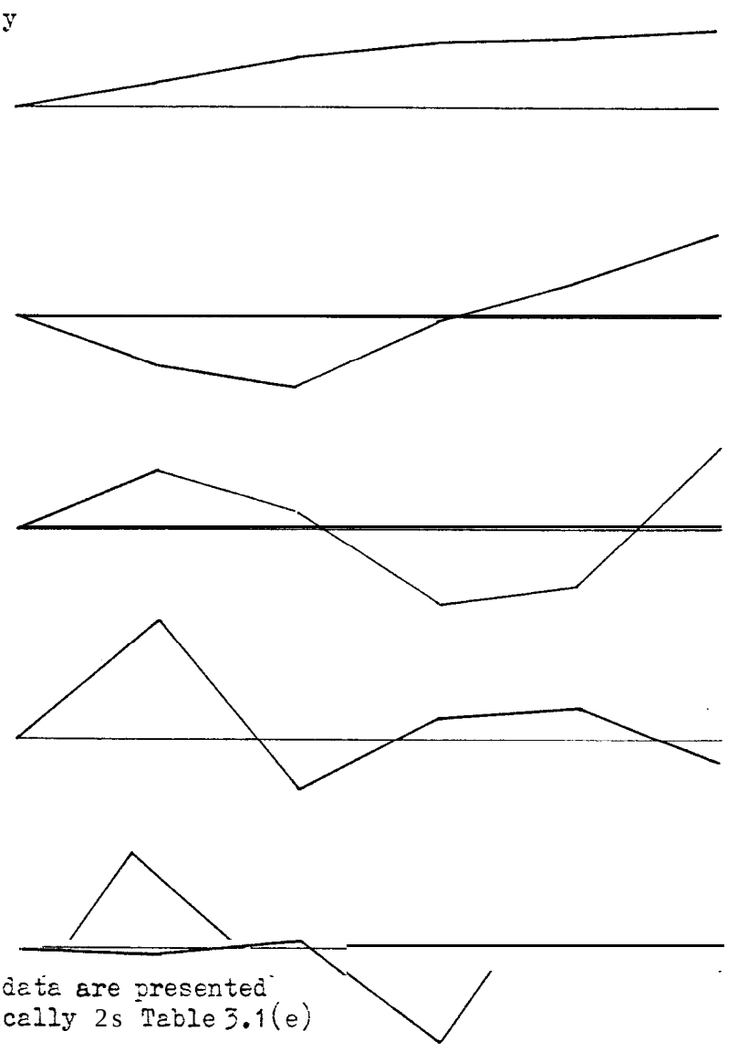

These data are presented numerically 2s Table 3.1(e)

Figure 3.2 0_{AGS} Identification

Resonances at **43.83, 124.8, 208.4, 247.2, 362.3** Hz

	Frequency Response	Selected Data			
		Freq.(Hz)	Mod.(dB)	Phase	Type
(a) $(\dot{X}_1/F_1)$	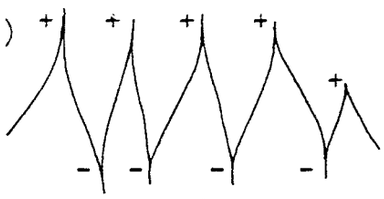	25.00	**-74.40**	90	
		56.13	**-110.4**	90	AR
		147.2	-88.20	90	AR
		216.5	-83.73	-90	AR
		350.9	**-61.93**	-90	AR
(b) $(\dot{X}_2/F_1)$	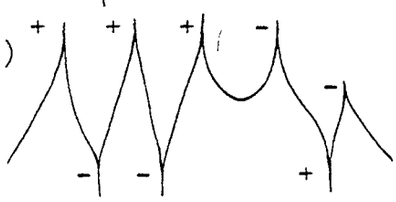	**25.00**	**-73.17**	90	
		78.04	**-109.3**	90	AR
		203.0	-82.30	-90	AR
		216.5	**-57.26**	-90	Min
		350.9	-81.30	90	AR
(c) $(\dot{X}_3/F_1)$	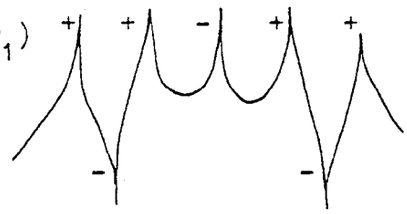	25.00	-72.48	90	
		121.3	**-89.95**	-90	AR
		142.5	**-70.76**	-90	Min
		230.9	-57.78	90	Min
		298.7	**-100.9**	90	AR
(d) $(\dot{X}_4/F_1)$	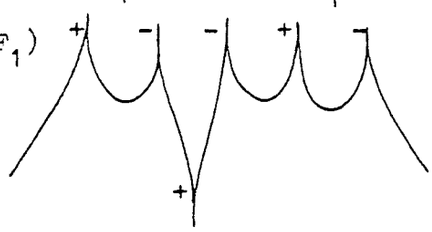	**25.00**	**-72.26**	90	
		85.38	**-68.61**	-90	Min
		156.9	**-94.43**	90	AR
		230.9	**-55.87**	90	Min
		329.0	**-79.85**	-90	Min
(e) $(\dot{X}_5/F_1)$	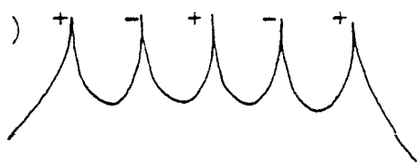	25.00	**-72.05**	90	
		78.04	-65.98	-90	Min
		167.4	**-63.84**	90	Min
		230.9	**-57.74**	-90	Min
		329.0	**-90.15**	90	Min

(f) Sign Array

Mode	1	2	3	4	5
	+	+	+	+	+
	+	+	+	-	-
	+	+		+	+
	+	-	-	+	-
	+	-	+	-	+

Figure 3.3 (SGS) Properties of Symmetrical Grounded Systen

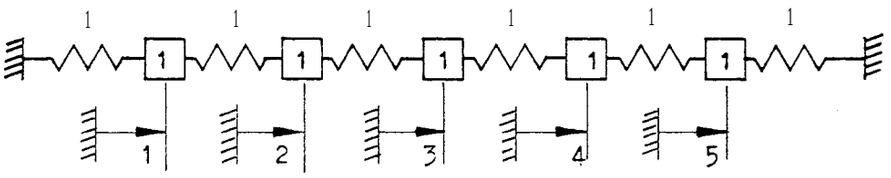

Mass in Kg

Stiffness in MN/m

Matrices (related to ungrounded coordinates)

$$[M] = \begin{vmatrix} 1 & & & & \\ & 1 & & & \\ & & 1 & & \\ & & & 1 & \\ & & & & 1 \end{vmatrix} \text{ Kg}, \quad [K] = 10^6 \begin{vmatrix} 2 & -1 & 0 & 0 & 0 \\ & 2 & -1 & 0 & 0 \\ & & 2 & -1 & 0 \\ & & & 2 & -1 \\ \text{Symmetric} & & & & 2 \end{vmatrix} \text{ N/m}$$

Resonance Frequencies and Mode Shapes

Mode	Frequency (Hz)	
1	82.36	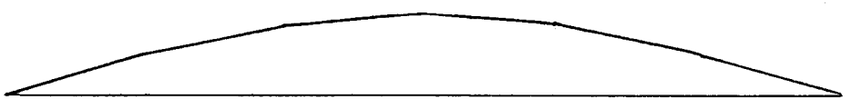
2	159.2	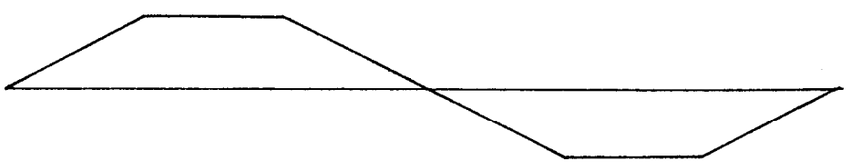
3	225.1	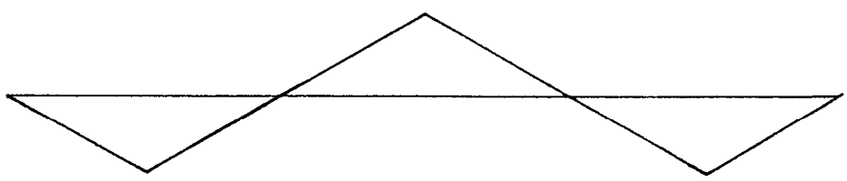
4	275.7	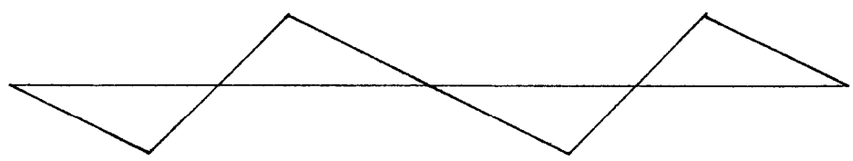
5	307.5	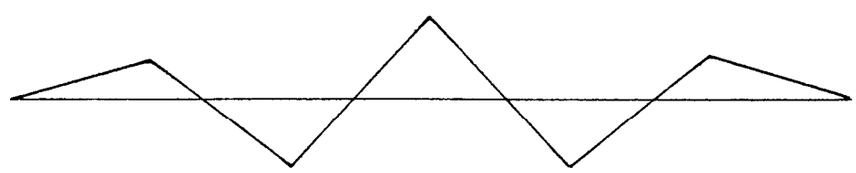

Figure 3.4 (SFS) Properties of Symmetrical Free System

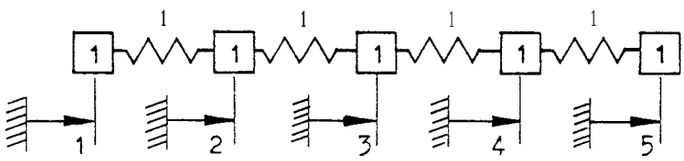

Matrices

$$[M] = \begin{bmatrix} 1 & & & & \\ & 1 & & & \\ & & 1 & & \\ & & & 1 & \\ & & & & 1 \end{bmatrix} \quad K_g \,, \quad [K] = \begin{bmatrix} 1 & & & & \\ & & & & \\ & & & & \\ & & & & \\ S_{\text{Symmetric}} & & & & \end{bmatrix}$$

Resonance Frequencies and Mode Shapes

Mode	Frequency (Hz)
1	0
2	98.36
3	187.1
4	257.5
5	302.7

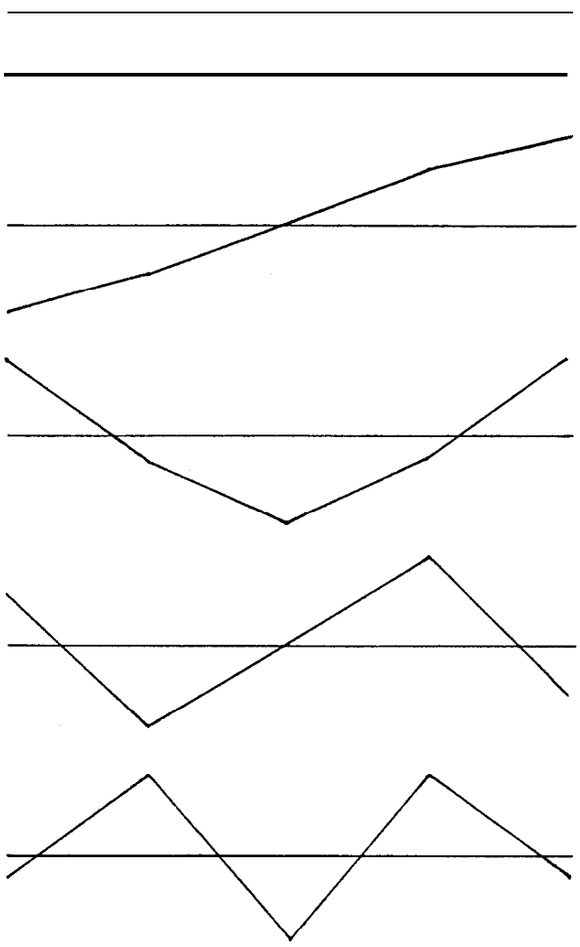

Figure 3.5 (AGS) Frequency Responses of Models

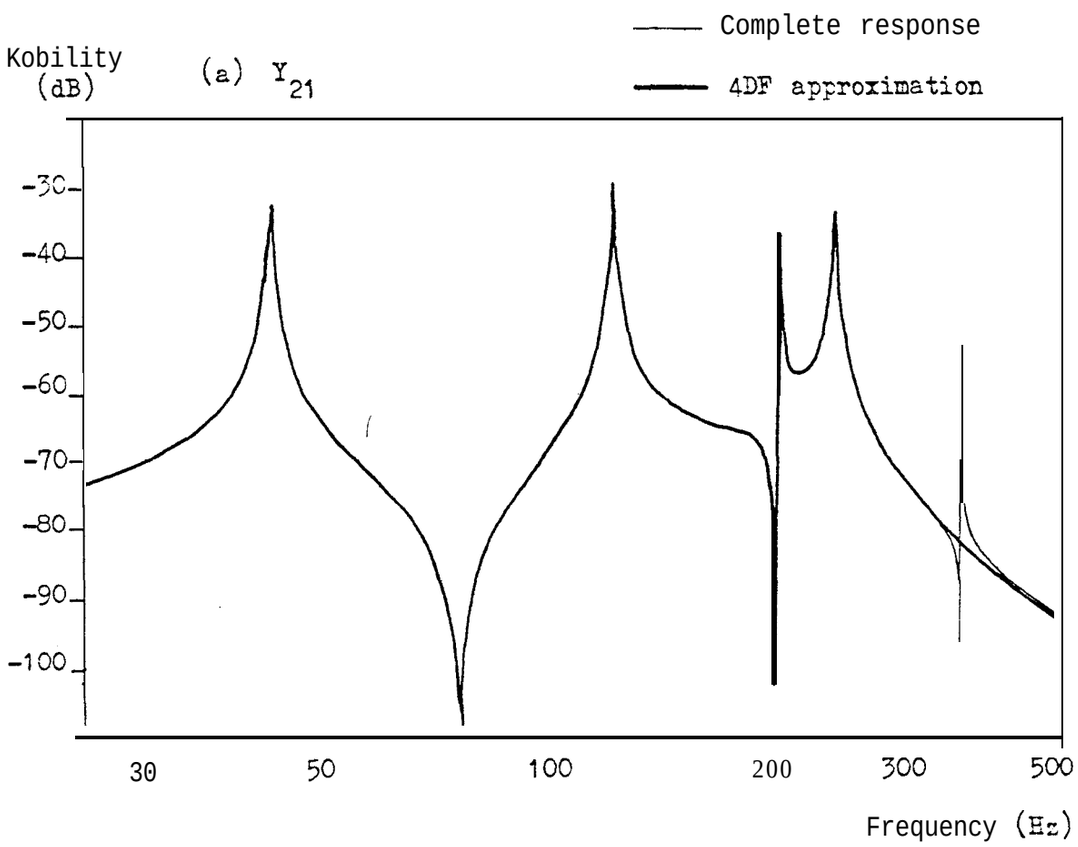

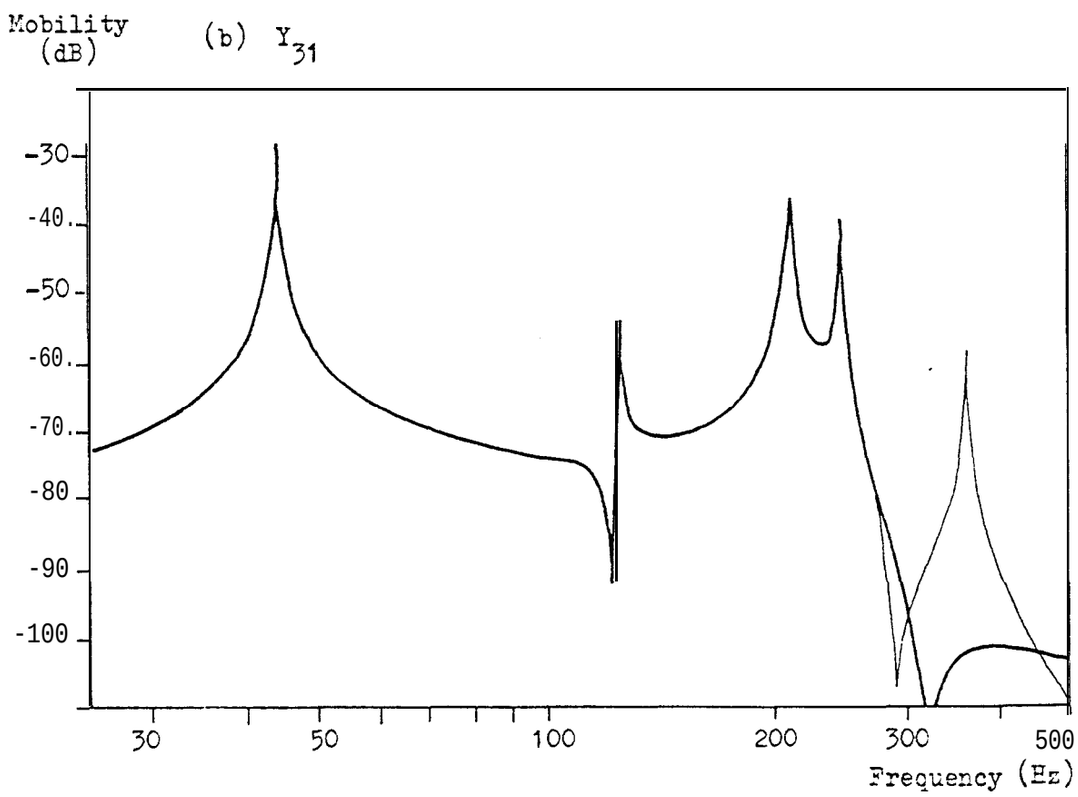

Figure 3.5 (AGS) Frequency Responses of Models

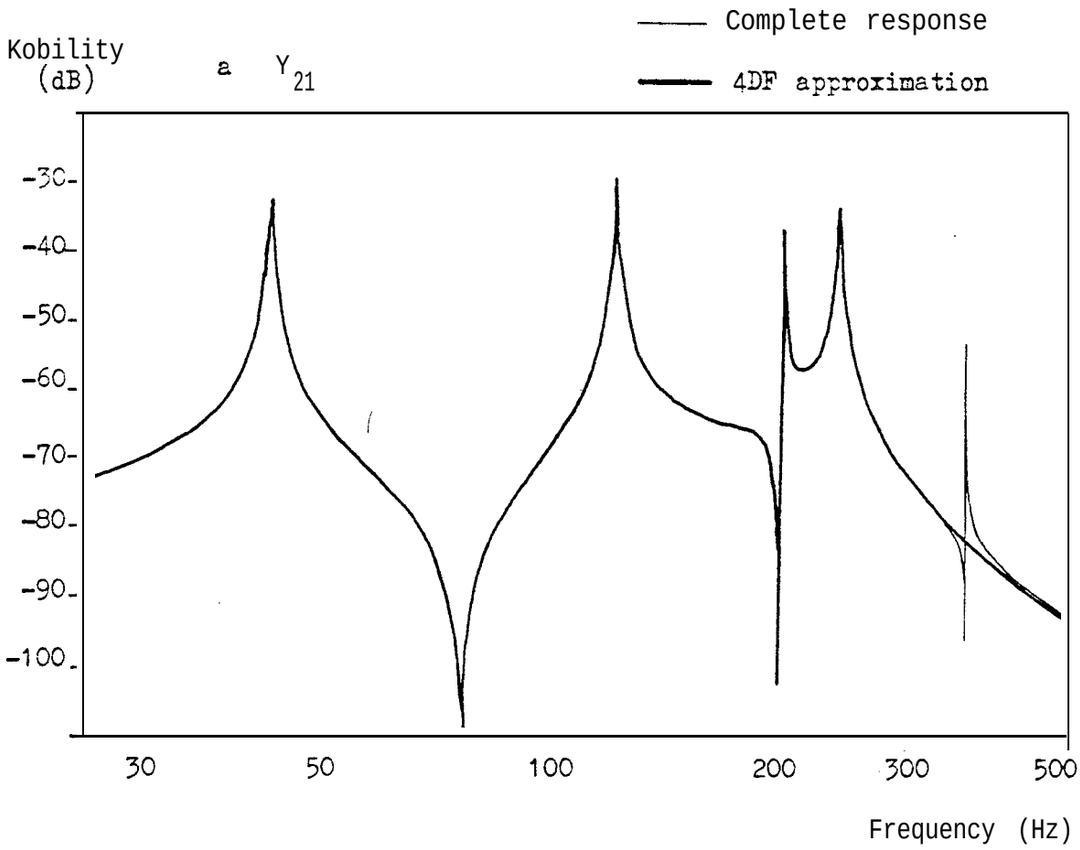

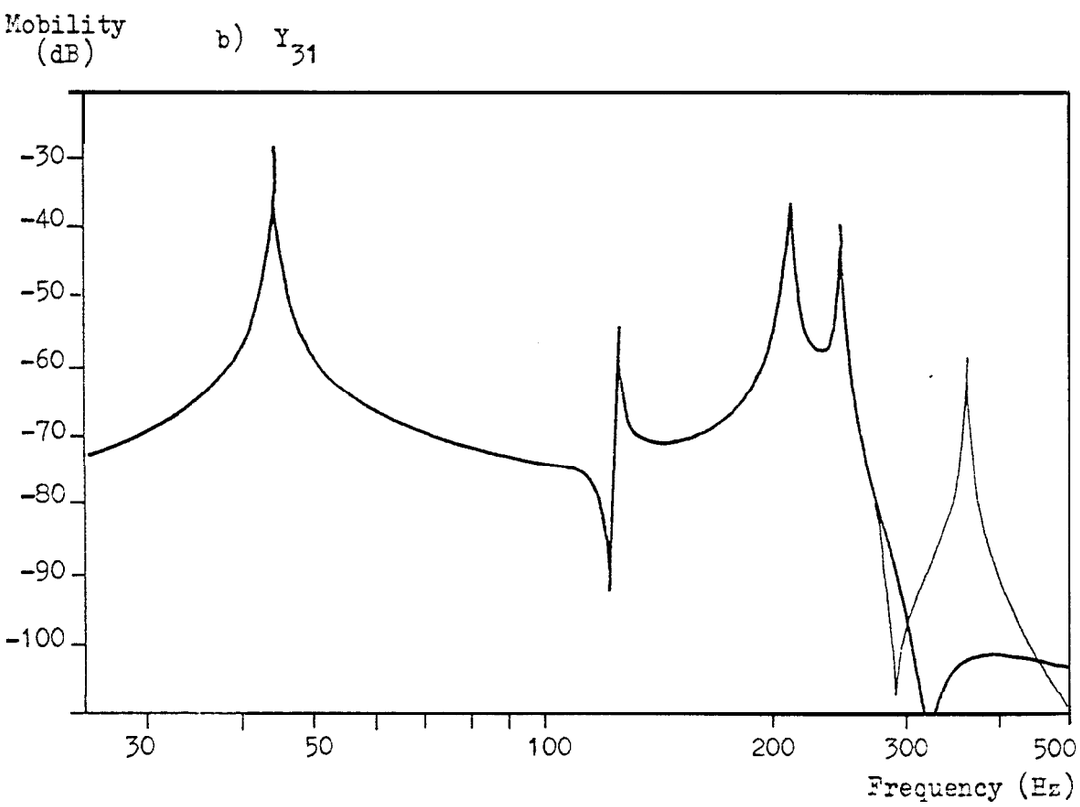

Figure 7.5 (AGS) Frequency Responses of Models (cont'd)

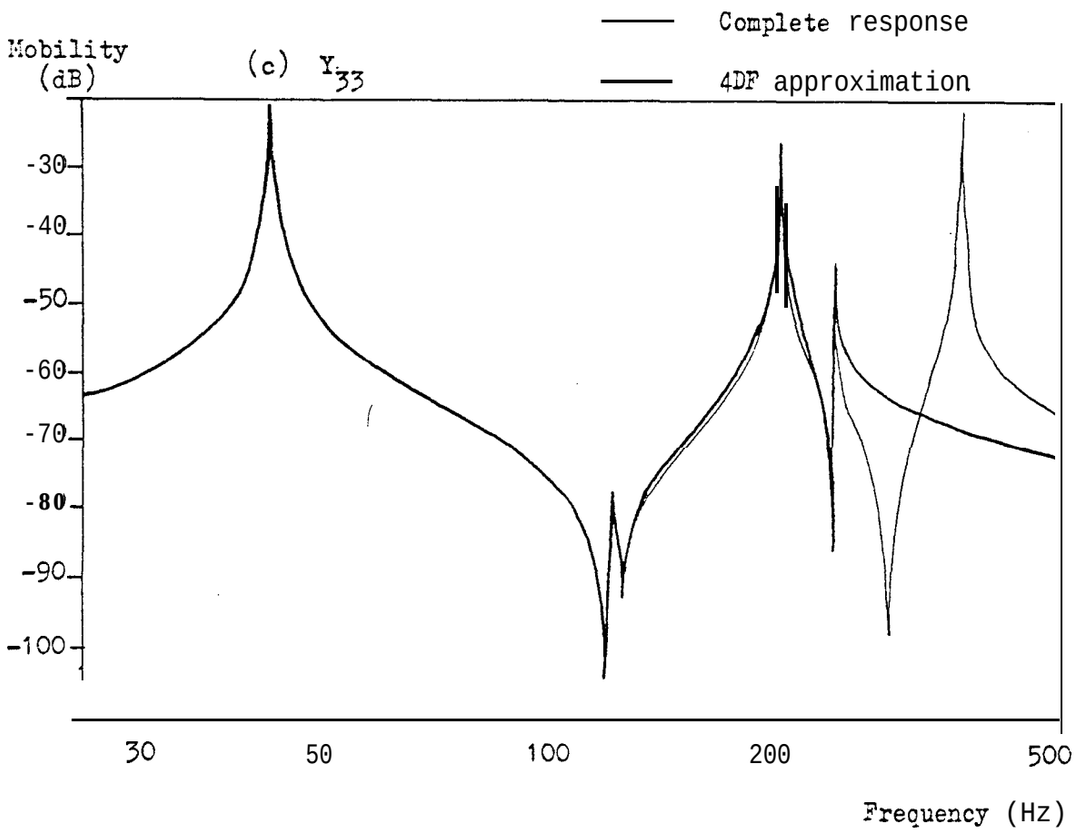

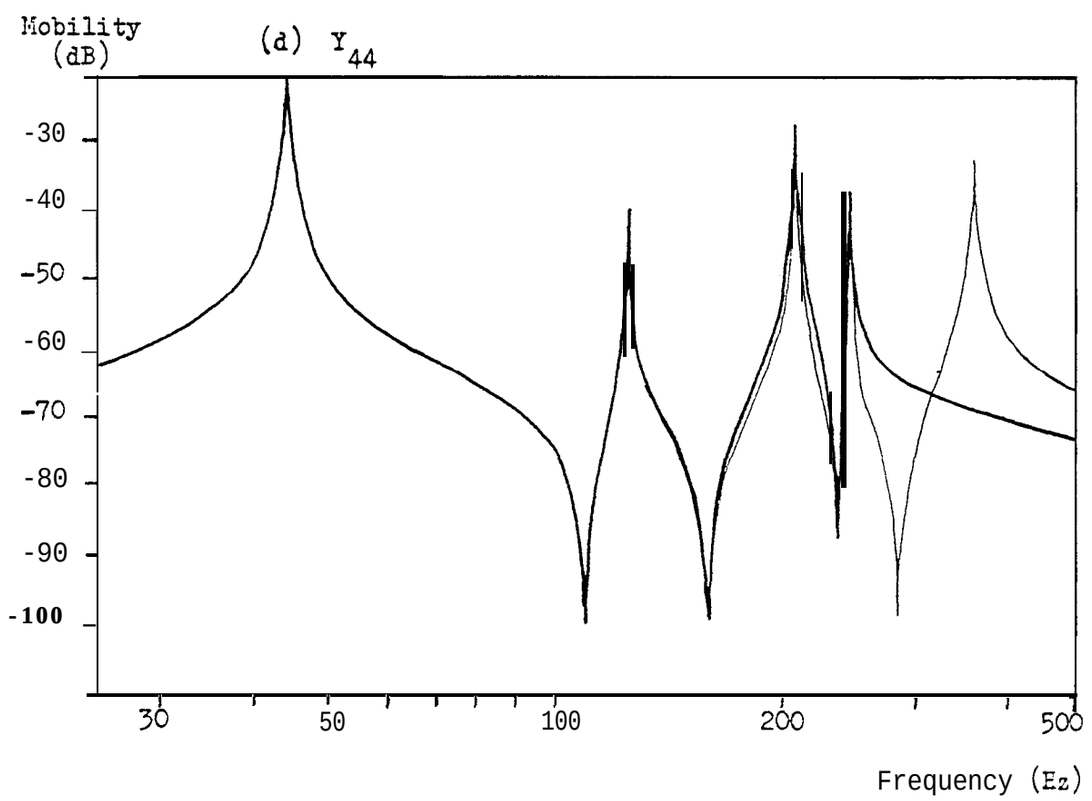

Figure 3.6 AGS Predicted Nodal Properties

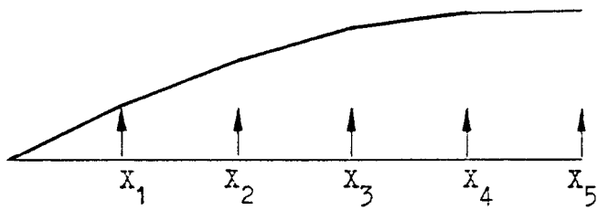

Mode 1

(a) 43.83 Hz

(b) 43.8'3 'Hz

(c) 42.32 Ez

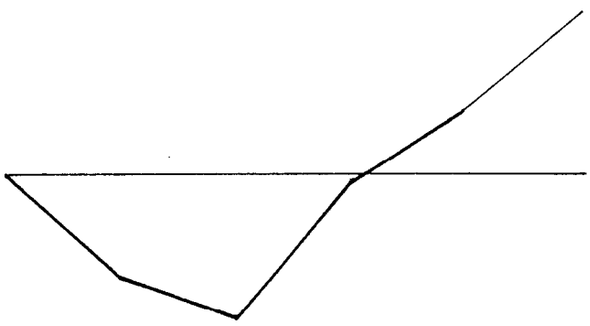

Mode 2

(a) 124.8 Hz

(b) **124.8** Hz

(c) 124.8 Hz

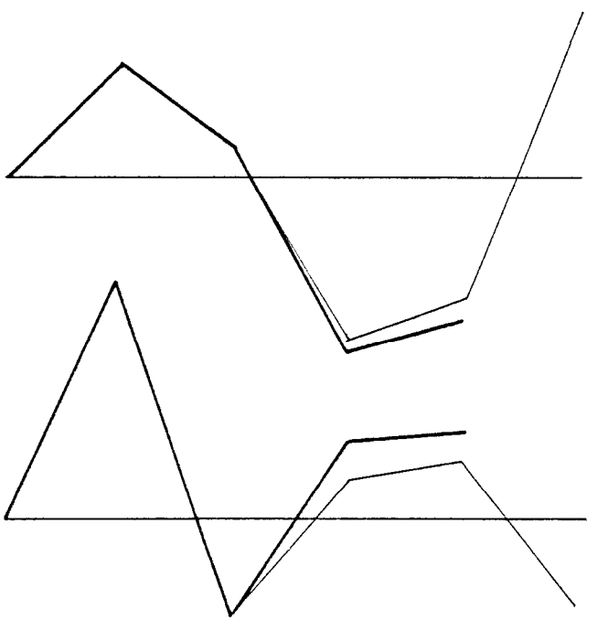

Mode 3

(a) 208.4 Hz

(b) 208.4 Hz

(c) 207.8 Hz

Mode 4

(a) **247.2** Hz

(b) **247.2** Hz

(c) **247.1** Ez

(a) —— Complete Model of 5 DF

(b) —— Incomplete Model of 4 DF (6 figure calculations)

(c) " " " II (4 " ")

Figure 3.7 (SFS) Predicted Modal Properties

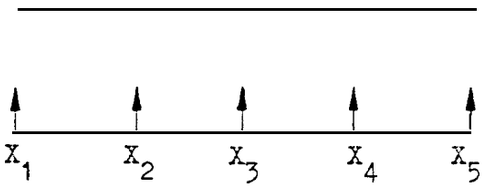

Mode 1

(a) 0 Hz
(b) 0.18 Hz
(c) 0.12 Hz

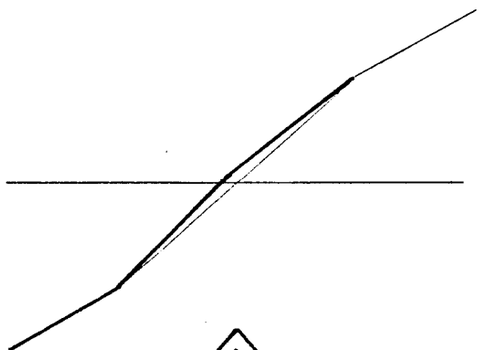

Mode 2

(a) 98.36 Hz
(b) 98.36 Hz
(c) 98.36 Hz

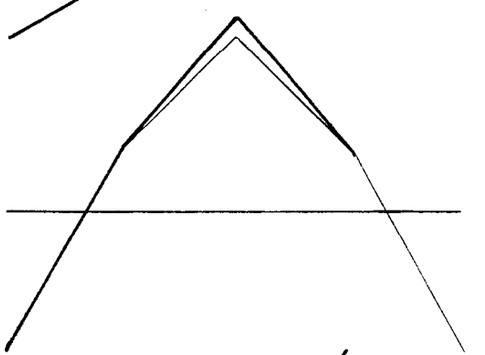

Mode

(e) 187.1 Hz
(b) 187.1 Hz
(c) 187.1 Hz

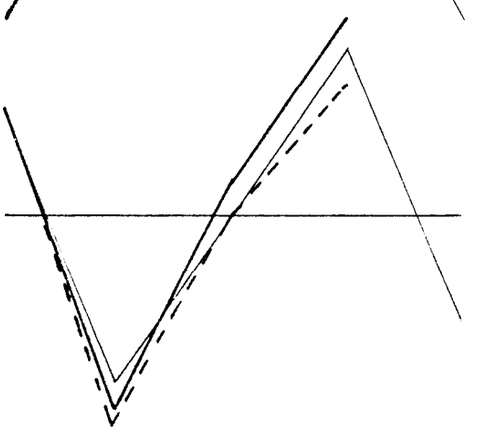

Mode A

(a) 257.5 Hz
(b) 257.5 Hz
(c) 257.5 Hz

(a) ——— Complete Model of 5 DF
(b) ——— Incomplete Model of 4 DF - identified Data
(c) -- — " " " " - Derived Data

Figure 3.8 (AGS) Change of Mass - Predicted Modal Properties

Mass at X_2 changed from 2 to 5 kg

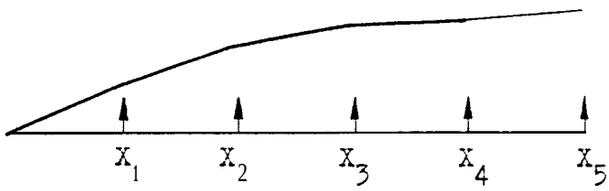

Mode 1

(a) 37.28 Hz
(b) 37.28 Hz
(c) 43.83 Hz

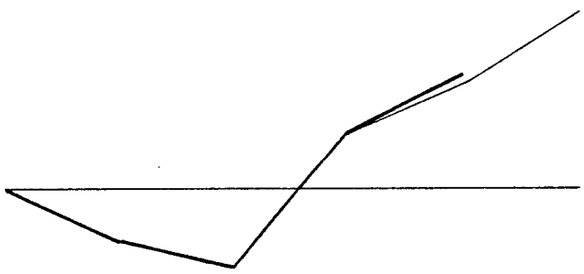

Mode 2

(a) 100.3 Hz
(b) 100.3 Hz
(c) 124.8 Hz

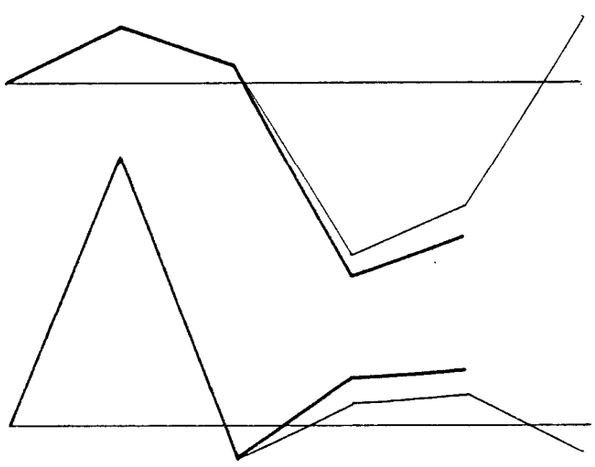

Mode 3

(a) 206.1 Hz
(b) 206.1 Hz
(c) 207.8 Hz

Mode 4

(a) 232.1 Hz
(b) 232.0 Hz
(c) 247.2 Hz

(a) ——— Complete Model of 5 DF
(b) ——— Incomplete Model of 4 DF
(c) Original System (Figure 3.6)

Figure 3.9 (AGS) Change of Mass - Frequency Response

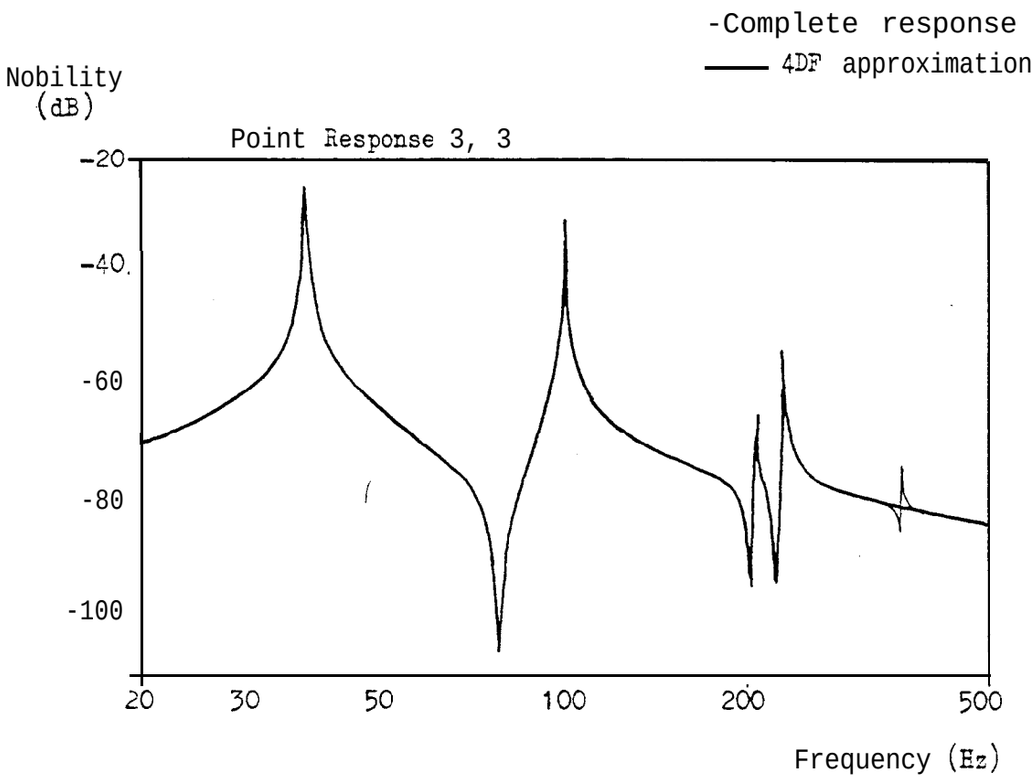

Figure 3.12 (AGS) Change of Stiffness - Frequency Response

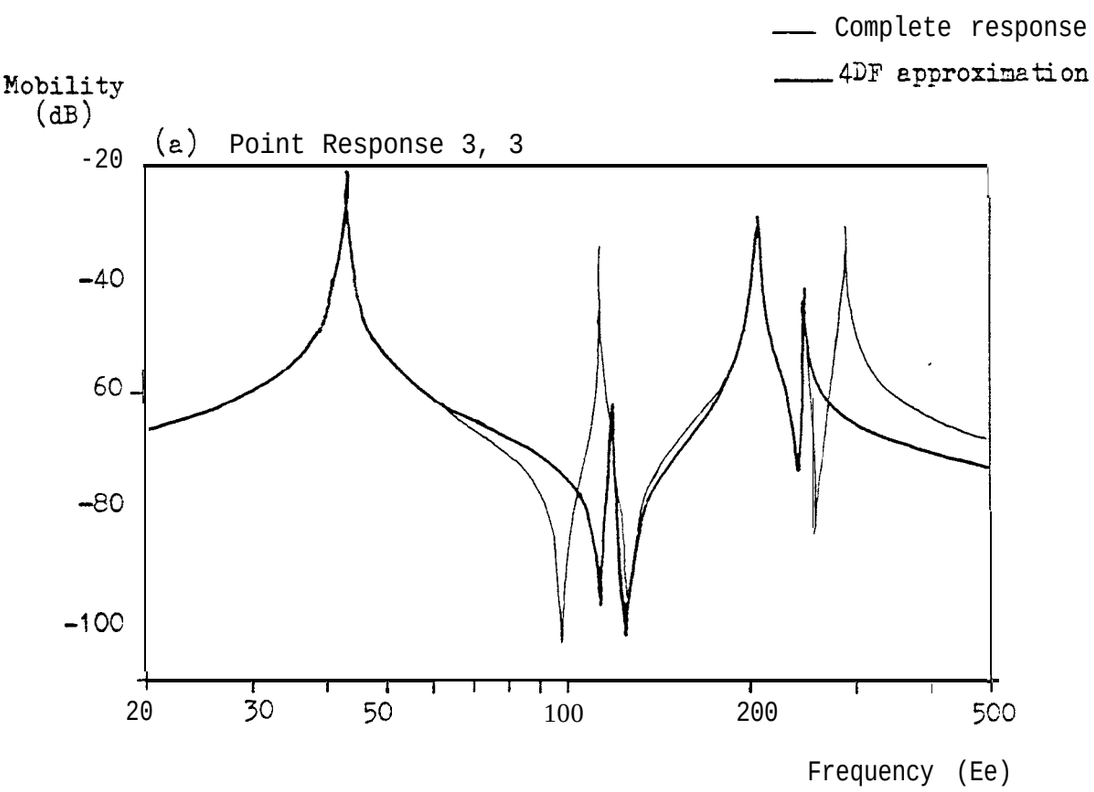

Figure 3.12 (cont'd) (AGS) Change of Stiffness - Frequency Responses

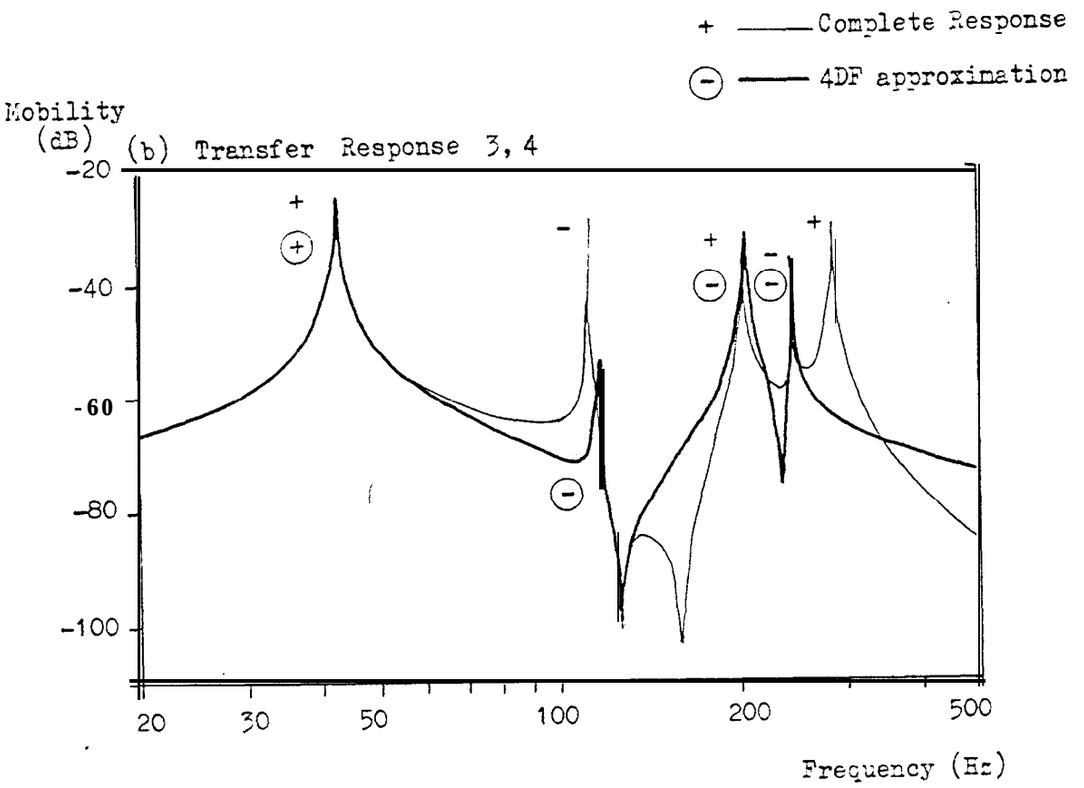

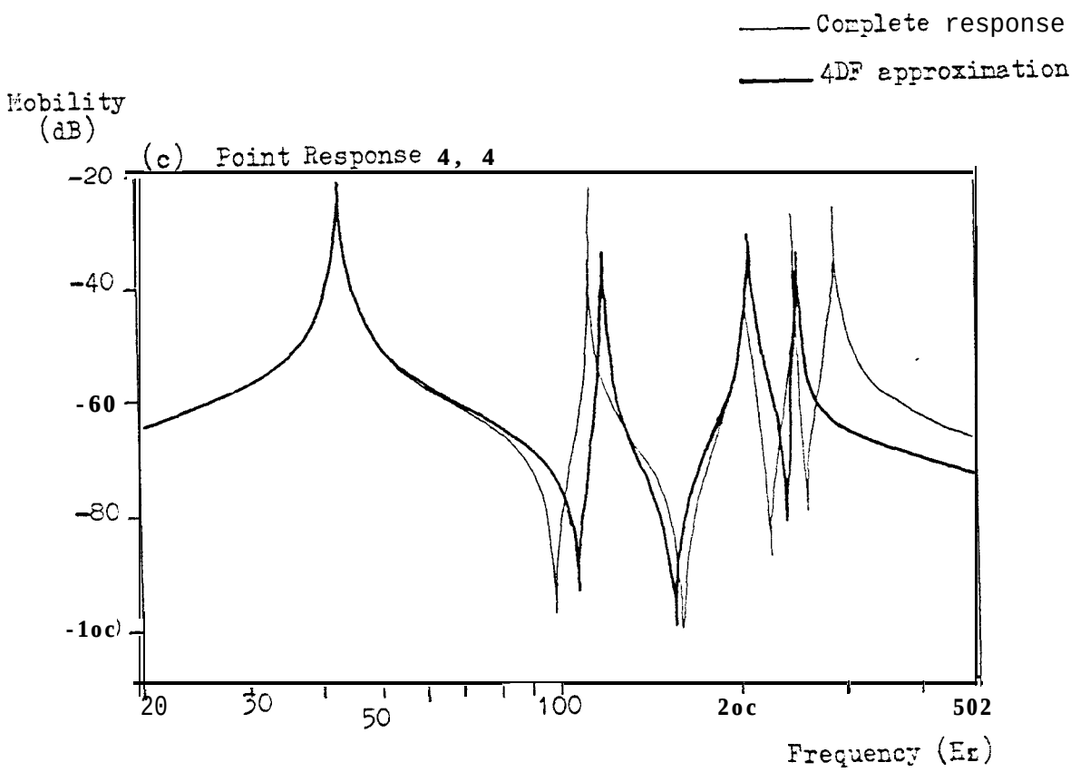

Figure 3.10 SRS Change of Mass - Predicted Modal Properties

Mass at X2 changed from 1 to 5 kg

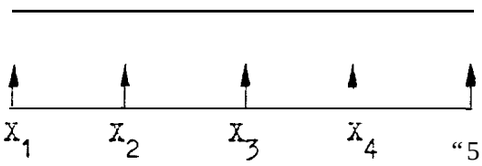

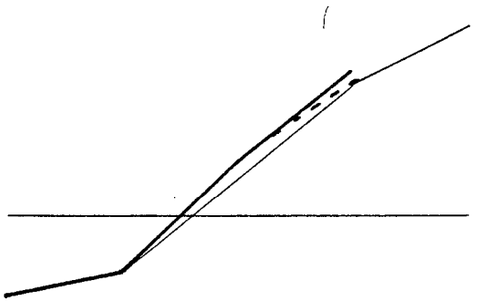

Mode 1

(a) 0 Hz
(b) 0.13 Hz
(c) 0.09 Hz
(d) 0 Hz

Mode 2

(a) 84.09 Hz
(b) 84.16 Hz
(c) 84.25 Hz
(d) 91.36 Hz

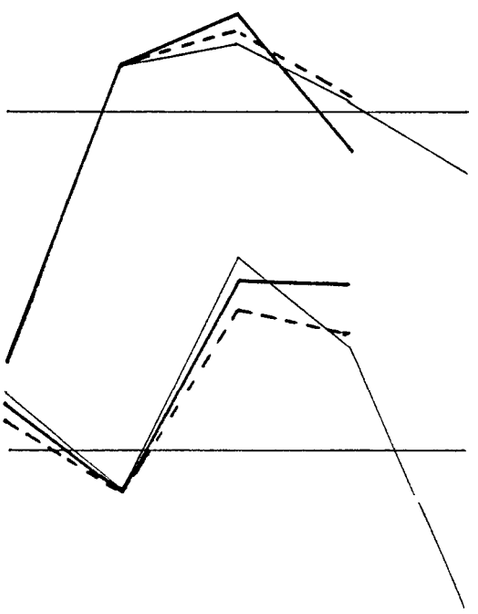

Mode 3

(a) 173.2 Hz
(b) 172.7 Hz
(c) 171.1 Hz
(d) 187.1 Hz

Mode 4

(i) 205.3 Hz
(b) 204.6 Hz
(c) 202.3 Hz
(d) 257.5 Hz

(a) ——— Complete Model of 5 DF
(b) ——— Incomplete Model of 4 DF - Identified Data
(c) -- - " " " " - Derived 3ata
(d) Original System (Figure 3.7

Figure 3.11 ACS Change of Stiffness - Predicted Modal Properties

Stiffness between X_3 and X_4 changed from 2×10^6 to 1×10^6 N/m

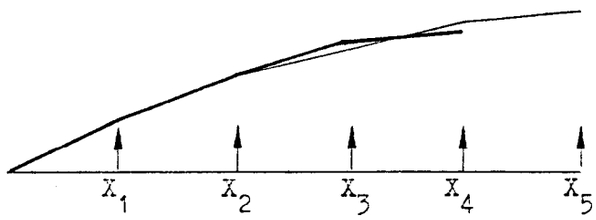

Lode 1

(a) **42.95** Hz
(b) **43.31** Hz
(c) **43.83** Hz

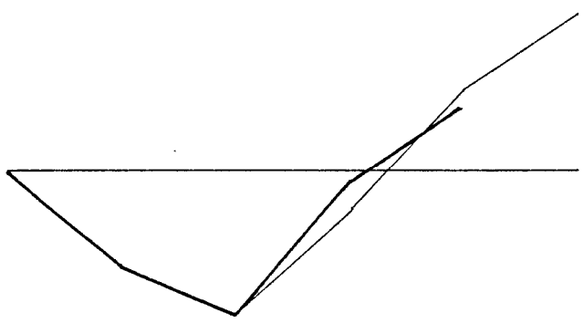

Mode 2

(a) 113.8 Hz
(b) 118.0 Hz
(c) 124.8 Hz

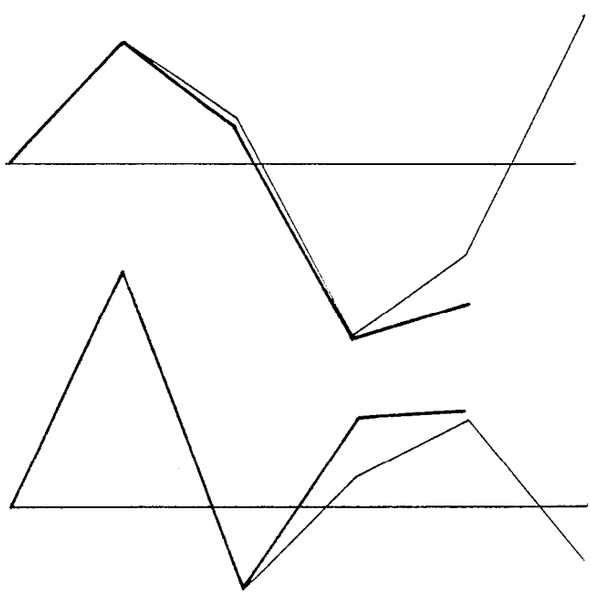

Mode 3

(a) **205.9** Hz
(b) **207.4** Hz
(c) **208.4** Hz

Mode 4

(a) 246.5 Hz
(5) 247.1 Hz
(c) 247.2 Hz

(a) —— Complete Model of 5 DF
(b) —— Incomplete Model of 4 DF
(c) Original System (Figure **3.6**)

Figure .13 (SFS) Change of Stiffness - Predicted Modal Properties

Stiffness between X2 and X_3 changed from 1 x 10^6 to 2 x 10^6 N/m

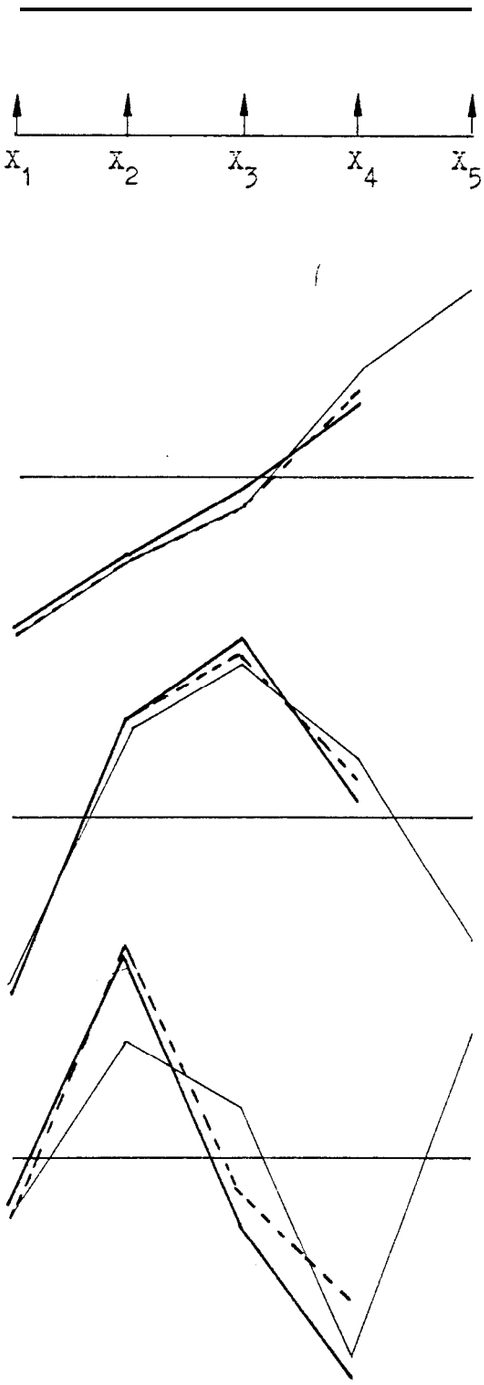

Mode 1

(a) 0 Hz
(b) 0.22 Hz
(c) 0.5 Hz
(d) 0 Hz

Mode 2

(a) **107.3** Hz
(b) 111.0 Hz
(c) 109.8 Hz
(d) 98.36 Hz

Mode 3

(a) 194.1 Hz
(b) 196.7 Hz
(c) 194.7 Hz
(d) 187.1 Hz

Mode 4

(a) 265.0 Hz
(b) 294.6 Hz
(c) 287.6 Hz
(d) 257.5 Hz

(a) —— Complete iiodel of 5 DF
(b) —— Incomplete Model of 4 DF - Identi_fied Data
(c) - - - - " " " " - Derived 3 ata
(d) Original Systen (Figure **3.7**)

Table 3.1 AGS Development of Mode Shape Matrix

(a) Point and Transfer Modal Constants

Mode	1	2	3	4	5
A_{11}	+0.0316	+0.1290	+0.1549	+0.6825	+0.00057
A_{21}	+0.0608	+0.1779	+0.0449	**-0.2801**	**-0.0021**
"3,	+0.0808	+0.0084	**-0.2202**	+0.1125	+0.0177
A_{41}	+0. **0877**	-0.0790	-0.1637	+0. **1739**	-0.0186
"51	+0.0948	**-0.2055**	+0.2296	**-0.1226**	+0.0048

(b) Point Mod Constants (derived from (a))

A_{11}	**0.0310**	**0.1290**	**0.1549**	0.6825	0.00057
A_{22d}	0.1171	0.2453	0.0130	0.1150	0.0078
A_{33d}	**0.2069**	**0.0006**	0.3130	0.0185	0.5516
A_{44d}	0.2437	0.0484	0.1730	0.0443	0.6091
A_{55d}	0.2848	0.3274	0.3403	0.0220	0.0406

Using $X_{1.} = \phi_{i1}^2/A_{11}$ for i = 2,5

(c) Point Modal Constants (directly identified)

A_1,	**0.0316**	0.1290	3.1549	0.6825	0.00057
A_{22}	0.1166	0.2466	0.0129	0.1162	**0.0072**
A_{33}	0.2063	0.0006	0.3096	0.0185	**0.5516**
A44	C.2432	0.0486	0.1720	0.0443	**0.4921**
"55	0.2849	0.3277	0.3370	0.0217	**0.0281**

(d) Mode Shape Matrix (from (c))

Frequency (Hz)	**43.83**	**124.8**	208.4	**247.2**	362.3
$\sqrt{A_{11}}$	+0.1778	+0.3592	**+o. 3936**	+0.8261	+0.0239
$\sqrt{A_{22}}$	+0.3419	+0.4966	+0.1136	-0.3409	-0.0849
$\sqrt{A_{33}}$	+O. 4542	10.0245	-0.5564	+O. 1360	**+0. 6812**
$\sqrt{A_{44}}$	+O. 4932	-0.2205	-0.4147	+0. 2104	-0.7015
$\sqrt{A_{55}}$	+o. 5338	**-0.5725**	**10.5805**	-0.1473	+0.1676

(e) Mode Shape Matrix (EIGEN calculation from data of Figure 3.1)

ϕ_1	**To.1777**	-0.3589	+0.3952	+0.8263	**-0.0266**
ϕ_2	+0.3419	-0.4970	+0.1130	**-0.3408**	+0.0847
ϕ_3	+0.4543	**-0.0236**	**-0.5566**	+0.1363	-0.6817
ϕ_4	**10.4333**	+0.2204	**-0.4144**	+0.2104	+0.7015
ϕ_5	+0.533 7	+0.5727	+0.5803	-0.1490	**-0.1677**

Table **3.2** 66 Spatial Model

(a) Matrices Based on 4-Digit Data

Output of program ENKAY with input of Table 3.1 (d)

$$[M] = \begin{bmatrix} 1.00145 & -.000422 & .000524 & -.002274 & -.003541 \\ & 2.00086 & .000009 & .000445 & -.413661 \\ & & 1.00107 & -.000017 & -.008488 \\ & & & .999892 & -.009858 \\ \text{Symmetric} & & & & .979498 \end{bmatrix}$$

$\sum M = 5.90884$ kg

$$[K] = 10^6 \begin{bmatrix} 2.00280 & -1.00186 & .000417 & .000798 & -.001560 \\ & 2.00409 & -1.0043 & .018381 & -.015569 \\ & & 3.03256 & -1.99161 & -.007289 \\ & & & 3.01923 & -1.00028 \\ \text{Symmetric} & & & & .979275 \end{bmatrix}$$

$\sum K = 10^6(1.00209)$ N/m

(b) Matrices Based on 6-Digit Data

$$[M] = \begin{bmatrix} 1.00000 & 0 & 0 & 0 & 0 \\ & 1.99999 & 0 & .000002 & 0 \\ & & .999998 & 0 & 0 \\ & & & .999999 & 0 \\ \text{Symmetric} & & & & .999999 \end{bmatrix}$$

$\sum M = 6.00000$ kg

$$[K] = 10^6 \begin{bmatrix} 2.00001 & -1.00000 & .000002 & 0 & -.000001 \\ & 2.00000 & -.999997 & -.000002 & 0. \\ & & 2.99999 & -1.99999 & -.000001 \\ & & & 2.99999 & -1.00000 \\ \text{Symmetric} & & & & 1.00000 \end{bmatrix}$$

$\sum K = 10^6(1.00000)$

(Numbers $< 10^{-6}$ recorded as 0)

Table 3.3 (AGS) Sensitivity to Error

% Change of Matrix Element		% Change in Natural Frequency				
δM_{33}	δK_{33}	1	2	3	4	5
+1	C	-.1	0	-.15	-.01	-.22
0	+1	+ 4	0	+ .3	+.01	+ .1

based on L-digit matrices of Table 3.2(a)

Table 3.4 (AGS) Development of Incomplete Mode Shape Matrix

(a) Point and Transfer Modal Constants

Mode	1	2	3	4
A_{11}	+0.0316	+0.1290	+0.1550	+0.6827
A_{21}	+o. 0608	r0.1778	+0.0449	-c. 2806
A_{31}	+0.0808	+o. 0084	-0.2182	i0.1158
A_{41}	+0. 0876	-0.0792	-0.1657	+0.1703

(b) Point Modal Constants (derived from (a))

A_{11}	0.0316	0.1290	0.1550	0. 6827
A_{22d}	0.1170	0.2451	0.0130	0.1153
A_{33d}	0.2066	0.0005	0.3072	0.0196
A_{44d}	0.2428	0.0486	0.1771	0.0425

(c) Point Modal Constants (directly identified)

A_{11}	0.0316	0.1290	0.1550	0.6827
A_{22}	0.1169	0.2470	0.0129	0.1174
A_{33}	C. 2073	0.0007	0.3907	0.0704
A_{44}	0.2446	0.0521	0.2414	0.0945

(d) Mode Shape Matrix (from (c))

Frequency (Hz)	43.83	124.8	208.4	247.2
$\sqrt{A_{11}}$	50.1778	+0. 3592	+0.3937	+0.8263
$\sqrt{A_{22}}$	+0.3419	+c. 4970	10.1136	-0.3426
$\sqrt{A_{33}}$	+0.4553	+0.0265	-0.6251	+0.2653
$\sqrt{A_{44}}$	+0.4946	-0.2263	-0.4913	+0.3074

Table 3.5 (AGS) Incomplete Spatial Model

Output of program EMMAY with input data of Table 3.3(d)

Mass Matrix

$$[M] = \begin{bmatrix} 1.00913 & -.0370472 & .0508781 & -.161160 \\ & 2.95191 & -3.75324 & 4.10214 \\ & & 16.5135 & -16.4969 \\ \text{Symmetric} & & & 18.1315 \end{bmatrix}$$

$$\sum M = 6.01533 \text{ kg}$$

Stiffness Matrix

$$[K] = 10^6 \begin{bmatrix} 2.00809 & -.917324 & -.196748 & .1\,10257 \\ & 2.42306 & -3.71277 & [illegible] \\ & & 16.4797 & -12.8267 \\ \text{Symmetric} & & & 10.6290 \end{bmatrix}$$

$$\sum K = 10^6(1.00411) \text{ N/m}$$

Table 3.6 (AGS)$_0$ IncompleteModel- Sensitivity to Error

% Change of Matrix Element		% Change in Natural Frequency			
δM_{33}	δK_{33}	1	2	3	4
+1	0	-.2	-.4	-.02	-.2
0	+1.2	+23	+.4	+2.3	+.33

Table 3.7 SGS Incomplete Model

(a) Point and 'i'ransfer Modal Constants

Mode	1	2	3	4
A_{11}	+0.0835	co. 2526	+0.3466	+0.2859
A_{21}	+0.1364	+0.1896	**-0.0726**	+0.0465
A_{31}	+0.1710	+0.0058	**-0.2942**	**-0.0061**
A_{41}	+0.1365	-0.3236	-0.0398	+0.5371

(b) Point Modal Constants (derived from (a))

A11	0.0835	0.2526	0.3466	0.2859
A_{22d}	0.2228	0.1423	**0.0152**	0.0076
A_{33d}	0.3502	0.0901	**0.2497**	0.0001
A_{44d}	0.2231	0.4146	**0.0046**	**1.009**

(c) PointModal Constants (directly identified)

A_{22}	0.2667	G. 3905	**0.0322**	-0 . 2310
A_{33}	0.4747	-0.000 7	-0.8348	0 . 0135
A_{44}	0.2667	0.3905	0.0022	-3.2310
A_{11}	0.0835	**0.2526**	0.3466	0.2859

Table 3.8 (SFS) Development of Incomplete Mode Shape Matrix

(a) Point and Transfer Modal Constants

Mode	1	2	3	4
A_{11}	+0.1999	+0.3596	+0.2606	+0.1513
A_{22}	+0.1999	+C. 2204	-0.1029	**-0.2918**
A_{33}	+0.1996	-0. 0003	-0.3063	+0.0036
A_{44}	+o. 2002	-0.2228	-0.1024	+0.1805

(b) Point Modal Constants (derived from (a))

A_{11}	0.1999	0.3596	0.2606	**0.1513**
A_{22d}	0.1999	0.1351	0.0406	**0.5628**
A_{33d}	0.1943	0	0.3600	**0**
A44d	0.2005	0.138c	0.0402	**0.2153**

(c) Point Modal Constants (directly identified)

A_{11}	0.1999	0.3596	0.2506	**C.1513**
A_{22}	0.1998	0.1384	C.0409	0.5125
A_{33}	0.1988	-0.0011	**G.4532**	0.0115
A_{44}	0.1998	0.1384	0.0409	0.5125

(d) Mode Shape Matrix (f rom (b))

Frequency (Hz)	0	9S.36	187.1	**257.5**
$\sqrt{A_{11}}$	+0.4471	+0.5997	+0.5105	+0.3890
$\sqrt{A_{22d}}$	+0.4471	+0.3676	**-0.2075**	-0.7502
$\sqrt{A_{33d}}$	+0.4464	- 0	-0.6000	+ 0
$\sqrt{A_{44d}}$	+0.4478	-0.3715	**-0.2005**	+0.4640

(e) Mode Shape Matrix (from (c))

$\sqrt{A_{11}}$	+0.4471	+0.5997	+0.5105	+0.3890
$\sqrt{A_{22}}$	+0.4470	+0.3720	-0.2022	-0.7159
$\sqrt{A_{33}}$	+0.4459	-0.0332*	-0.6732	+0.1072
$\sqrt{A_{44}}$	+0.4470	-0.3720	**-0.2022**	+0.7159

* $0.0332 = (0.0011)^2$; the negative sign of $_2A_{33}$ being ignored

Table 3.9 (SFS) Spatial Models

(a) Matrices based on Identified Data

Output of Program EMKAY with input data of Table 3.7(e)

$$[M_I] = \begin{bmatrix} 1.82173 & & & \\ & 5.59552 & -6.15616 & 5.83441 \\ & & 9.14045 & -7.62927 \\ \text{Symmetric} & & 1.92693 & 2.50795 & -2.43695 & 7.85446 \end{bmatrix}$$

$\sum M_I$ = 4.99465 kg

$$[K_I] = 10^6 \begin{bmatrix} 1.56285 & -2.42406 & 2.19513 & -1.32886 \\ & 5.42721 & -6.15406 & 3.13632 \\ & & 9.28160 & -5.30353 \\ \text{Symmetric} & & & 3.48432 \end{bmatrix}$$

$\sum K_I$ = 10^6(.000039) ≃ 0

(b) Matrices based on Derived Data

Output of program EMKAY with input data of Table 3.7(d)

$$[M_D] = \begin{bmatrix} 1.28540 & -.864188 & 1.46454 & -1.26469 \\ & & & \\ \text{Symmetric} & 3.80948 & -4.75875 & 8.66676 & -6.76359 & 4.21094 & 7.17739 \end{bmatrix}$$

$\sum M_D$ = **4.98757** kg

$$[K_D] = 10^6 \begin{bmatrix} 1.20894 & & & \text{82} \\ & 5.09308 & -6.04828 & 2.7773333 \\ & & 9.96815 & -5.3405454 \\ \text{Symmetric} & & & 3.3636767 \\ & -1.83595 & 1.44463 & -.814082 \end{bmatrix}$$

$\sum K_D$ = 10^6(.000048) ≃ 0

4. SPATIAL MODELS OF IDEAL UNIFORM BEAMS

4.1 Introduction to Continuous Sys tems

The development of the modelling techniques of Chapters 2 and 3 is here taken a step nearer to application to real physical systems. 'tie consider in this Chapter the identification of spatial models of continuous systems which have unlimited numbers of degrees of freedom and resonances. Thus the spatial models must be incomplete but the compensation afforded by the use of high frequency residuals can be investigated. The response data upon which the model is basedars again to be error-free, being generated for an ideal structure.

4.1.1 Properties of Beams

A beam is a simple structure which has physical existence and also has dynamic properties capable of being computed accurately. It is continuous and has an unlimited number of modes which are fairly evenly distributed in frequency. A suitable test of a method of modelling would be the prediction of the vibration properties of a beam constructed by the joining of two smaller beams. This is a process which could be checked since the properties of the coupled beam could be predicted with as much accuracy as those of the constituent beams which differ from it and each other only in length. The simplest coupling would be a butt joint of two beams of equal section. Such a joint would transmit force and torque and thus at least would require two coordinates, one translational and one rotational, to describe it. It must be that in many practical structures vibrations are transmitted by torque coupling at joints, but it is not a phenomenon which has had extensive study.

4.1.2 Objectives of the Investigation

Accepting the desirability of using both linear and angular coordinates at a junction, it is a natural extension to use a mixture of such coordinates as the generalised coordinates with reference to which a spatial model could be constructed. As was demonstrated in section 2.2.1, a mode shape can equally well be represented by N/2 translational and N/2 rotational coordinates as by the more conventional N translational coordinates. It would be interesting to see if a spatial model based on such mixed coordinates would be meaningful.

A modelling exercise based on error-free response data from ideal beams could reveal systematic errors and numerical ill-conditioning and also indicate if the addition of high frequency residuals by the methods developed in section 2.3 improves the results.

4.1.3 The Short and Long Beams

These were specified first in terms of their natural frequencies. It was decided that the range of frequencies used in the theoretical investigation should correspond to what would be reasonably measurable in practice. This was taken to be the two decades from 20 Hz to 2 kHz. The vibration properties of standard steel rectangular bar are plotted in Figure 4.1 as length versus frequency for depth of section and mode number as parameters. Stock of section 31.75 mm x 25.4 mm (1¼" x 1") was chosen. A 'Long' beam of 1.4 m vibrating free-free would have resonances at 0, 86, 237, 464, 767, 1150, 1600 and 2130 Hz and thus conveniently have six modes in the range and six coordinates, three translational and three rotational, to describe its mode shapes and to act as its spatial model coordinates. Similarly a 'Short' beam of 0.65 m would have resonances at 0, 395, 1100 and 2150 Hz and thus have four modes dominating the response in the range of interest. The two beams connected at a butt joint would be constituent parts of a 'Coupled' beam

of length 2.05 m and which would have resonances at 0, 40, **110, 217, 358, 535, 746, 994,** etc. Hz.

Plainly, since the Long Beam was to be coupled to the Short Beam, each needed two of its coordinates at one end. It was then reasonable to site two further coordinates et the other end of each beam. Four coordinates sufficed for the Short Beam; the Long Beam had two stili to allocate. A location 0.4 m from one end was chosen, which would be as far as possible from any node of the modes whose frequencies lay in the chosen range.

The specification of the Long Beam and its nobility matrix is shown as Figure 4.2(a) and the corresponding data for the short beam are in Figure 4.2(b).

4.1.4 Generation of Frequency Response Data

Response data were calculated using program COUPLE1 with module ZFLAX1 appropriate to an undamped Bernoulli-Euler beam. For each of the three beams a NxN matrix of mobility terms was calculated for 101 frequencies spaced logarithmically between 20 and 2CO0 Hz. These were, within rounding limits, error-free and were to be treated as 'measured' data in the following modelling process. These original data were designated T for 'Theoretical'.

4.2 ST Modelling Without High Frequency Residuals

All the data in this sectionare designated ST for 'Spatial Theoretical'. In later sections STR for 'Spatial Theoretical with Residual', SM for 'Spatial Measured' and SMR for 'Spatial Measured with Residual' will be encountered. It is hoped that the code will help to clarify comparisons and avoid confusion of similar, but different, data.

4.2.1 $_0^{ST}$ Identification of Modal Constants for Short and Long Beam

The modal constants needed for establishment of the moduli of elements of mode shape matrix $[\Phi]$ were to be found from the point responses on the main diagonal of the mobility matrix. The mode shape signswere to be obtained from the transfer responses of one column of that matrix and in each case this column was chosen to be the first corresponding to translational excitation of each beam tip. The tip of a free-free beam, of *course, can* never be a node and so tip excitation must stinulate all possible modes.

The identification of the Short Bean is illustrated by Figure 4.3. The point response Y_{11} is sketched as Figure 4.3(a) and all the data used in 4-mode IDENT calculations are listed. The resultant modal constants, $_rA_{11}$, of the first three nodes are presented in Table 4.1, together with the $_rA_{22}$ series whose calculation is not shown. The sign array for the Short Beam is presented at Figure4.3(e)*and* it was obtained by inspection of the transfer responses sketched in Figures 4.3(a) to (d). The data at 20 Hz are dominated by the rigid body mode and thus the signs of those data indicates the signs of the zero frequency modal constants.

Similar information for the Long beam S-node IDENT calculations is presented as Figure 4.4. It is to be noted that all the identifications of Point responses for both Long and Short Beams were done using antiresonances and the response at 20 Hz. Because of the symmetry at the tips of the Long Beam it is to be noted that $_rA_{55}$, and $_rA_{66}$ are identical with $_rA_{11}$ and $_rA_{22}$ arid thus are not recorded in Table 4.4., which contains data for the first five modes.

4.2.2 Separation of Rigid Body Modes

The rigid body motion of the beam is confined to one place and is described by two rather than three coordinates. This is the simple case exemplified in section 2.2.3. One rigid body mode, the translational, is completely specified in terms of the mass of the beam. The modal constants for this node cre given simply by the equation:

$$ {}_1A_{iiT} = 1/m \text{ for } i \text{ odd} $$
$$ {}_1A_{iiT} = 0 \text{ for } i \text{ even} \qquad (4.1) $$

remembering that even numbered coordinates are rotational.

The modal constants; for the rotational mode are obtained from the total zero-frequency constants as obtained by use of program IDENT by subtracting the translational component:

$$ {}_1A_{iiR} = {}_1A_{ii} - {}_1A_{iiT} \text{ for all } i \qquad (4.2) $$

The first two columns of the square matrix of point nodal constants correspond now to the two zero frequency modes. This matrix for the Short Beam is shown in Table 4.1(c) and that for the Long Beam in Table 4.4(c)

4.2.3 Spatial Models of Short and Long Seams

The mode shape matrix $[\Phi]$ has elements which have numerical values equal to the square roots of the corresponding elements in the matrix of point modal constants. The sips of the $[\Phi]$ elements are those found from the transfer plots sketched in Figures 4.3 and 4.4 for the bending modes and from the thumb-nail sketches of the rigid body modes which appear at the bottom of Tables 4.1 and 4.4.

The elements of the diagonal matrix $[\omega_r^2]$ are based on the natural frequencies, which of course were established for the IDENT calculations.

Application of equation (1.12) by program EIGAY with the input data of Table 4.1(d) produced the spatial model for the Short Beam in the form of the mass and stiffness matrices of Table 4.2. Similarly, for the Long Beam, the modal data of Table 4.4(d) were transformed into the spatial model of Table 4.5. The matrices are all fully populated.

These spatial models require careful examination. It must be remembered that odd numbered coordinates have translations or applied forces and even numbered coordinates are associated with rotations and applied torques. Thus the elements of the $[M]$ and $[X]$ matrices with exclusively odd numbered suffixes may be designated M_{trans} and K_{trans}, respectively. Their summations are meaningful as can be seen, for example, in Table 4.5 which shows $\sum M_{trans}$ close tc the true value in Table 4.4(b), whereas the total summations over all coordinates gives meaningless results. it is tempting to think that M_{rot} and K_{rot}, being the elements of $[M]$ and [X-j which are exclusively even-numbered, thus relating rotational quantities, will have summations capable of interpretation. Unfortunately, this is not so, because the inertia terms are not simple scalars as masses are but they are dependent on the position of the rotation coordinate with respect to the applied torque coordinate.

The values of $\sum M_{trans}$ and $\sum K_{trans}$ serve as a check on the spatial model. Another check can be made by using the spatial model matrices as inputs to program EIGEN in order to find the mode shapes and frequencies. The results of such a calculation for the Short Beam are shown in Table 4.3. The mode shapes are very well determined but the two rigid body modes have indicated frequencies of 3.50×10^{-5} and 0.625 Hz rather than the correct frequency of C Hz. This tendency to indicate small finite frequencies rather than zero frequency was previously commented on in section 3.4.1 in connection with the eigenralues of an exactly defined Symmetrical Free System and may be regarded as a

feature of the F02AEF subroutine used in EIGEN. It has also been observed that these errors in deter&nation of would-be zero values are a function of the particular computer used for the calculation and the size of fioeting point numbers which are handled. The DEC10 mainframe computer at Middlesex Polytechnic gives less accurate prediction of zero eigen values than does the CDC6600 computer at Imperial College, using identical program. The DEC10 has a limit about $10^{\pm 50}$ for a floating point number whereas the CDC6600 has $10^{\pm 250}$.

4.2.4 Spatial Yodel of the Coupled Beam

The two beams constituting the Coupled Beam are joined at twc coordinates, one translational and one rotational. Thus the spatial model of the Coupled Sean is formed by joining together the spatial models of the Long and Short Beams using the natrix method of coupling of substructures which was introduced in section 1.4. The last two coordinates of the Long Beam matrices coincide with the first two of the Short Beam. This joining is presented in sketch form in Table 4.6(a) and the mass and stiffness matrices of the Coupled Beam are shown in Tables 4.6(b) asd (c) in which the overlap is seen to be confined to a 2 x 2 submatrix associated with the joint coordinates.

Natural Frecuencies

These data were first assessed by using them with program EIGEN to predict the natural frequencies of the Coupled Dem. The results are shown in Table 4.6(d) in which it may be seen that there are two codes at low frequencies which can perhaps be interpreted as rigid body modes, remembering that the EIGEN routines are not capable of indicating zero frequency exactly. The other frequencies are between 2.4% and 13.7% in error, this being always positive.

(ST) Error Sensitivity of Spatial Model

The sensitivity of this spatial model to error was indicated by the effect of a small change of one nain diagonal element of the stiffness matrix upon the predicted natural frequencies as listed in Table 4.6(e). The shift of frequency was negligible for the eighth node but increased with decreasing mode number to +62% for the first bending code. The shift of the second 'rigid body' code is enormous and clearly anomalous.

This result indicates extreme sensitivity of the natural frequencies (eigenvalues) to perturbations of the stiffness matrix and confirms the idea thrt 211 significant figures of the spatial model matrices should be retained, even though data of fewer significant figures were used in their calculation. This concept is contrary to the advice, given to students using calculators when tackling more elementary problems, to retain only 2s many significant figures in solutions 2s were in the problem input data. However, since spatial model calculations are impracticable without computers which can handle data with many or few significant figures with equal facility, there is no need to round off the elements of spatial model matrix elements in order to make manual calculations easier to record. The spatial model matrices should be regarded 2s an intermediate stage and fin21 results, such as predicted frequency responses, should be rounded.

(ST) Coupling at One Coordinate

It was asserted in section 4.1.1 that the coupling of beans et 2 joint required two coordinates at the joint. This assertion is verified by the results presented in Table 4.6(f) which shows the nine natural frequencies predicted for the Coupled Beam constructed by joining the Long and Short Beams at one coordinate (the translational) only. The frequencies listed bear no relationship with the true values.

Mode Shapes

Program EIGEN produces mode shape data as a column $\{\phi\}_r$ for each value of r, the mode number. The odd-numbered elements of $\{\phi\}_r$ are presented es points corresponding to translations and the even-numbered elements as sloping lines corresponding to rotations in Figure 4.5 and subsequent mode shape diagrams. The continuous lines on these diegrams show the ideal shapes of the modes, based on Bishop and Johnson'-s Tables. (5)

The ST data in Figure 4.5(a) and (b) clearly relate to rigid body modes since they are collinear. The mode at 0.478 Hz should ideally have zero slope. The other rigid body mode which has a negative eigenvalue (hence the indication of imaginary frequency 0.236j Hz) is quite close to the ideal rotational rigid body mode.

The first three bending modes are quite accurately indicated by the ST data, the worst error being for the third bending mode at the tips, the translations being too large although the rotations are accurate. The next three bending modes shox rather more divergence from the ideal with inaccuracy increasing with frequency. This trend was explained in Chapter 2 as the increasing influence of modes whose resonances are outside the frequency range of the simple spatial model.

Frecuency Responses

The frequency responses of 64 responses could be generated for the spatial model of the Coupled Beam represented by 8 x 8 matrices. A selection, corresponding to response and excitation at the tip and at the point of junction of Long and Short Beams, is shown in Figure 4.6, in which the thinner continuous curves correspond to the true 'T' frequency response cf an ideal 2.05 m beam. In each of the diagrams six modelled resonances corresponding to the bending modes may be observed. Each shows a simple asymptotic approach to a mass-line at frequencies above 800 Hz. Discrepancies of resonances and antiresonance frequency are clear but the general level of all the responses is correct. The

junction cross response of Figure 4.6(d) has a correct alternation of antiresonances and non-zero minima between resonances. Figure 4.6(f) for the rotational response Y_{66} has the second bending node making a negligible contribution to the model response although it puts a small kink into the ideal curve. The reverse is true for the fifth bending mode.

4.2.5 (ST) Conclusions: Modelling Without High Frequency Residuals

The ST spatial node1 of the Coupled Bear: has been comprehensively matched against the ideal in (a) natural frequencies, (b) node shapes arid (c) frecuencv response. it can be given an over211 rating as 'fair'. In summary:

(1) The construction of an incomplete spatial model of a continuous system is feasible.

(2) The spatial model can be based on a mixture of translational and rotational coordinates.

(3) The total summation of the elements of the spatial model matrices is not meaningful but summations of elements exclusively translational in nature do correspond to the total mass and the total stiffness of the structure.

(5) Each spatial node1 matrix is in effect substantially perturbed by the coupling process. The fair approximation to ideal behaviour given by the spatial node1 of the Coupled Beam indicates that the process is v&id.

(6) The range of frequencies for which the N x N spatial model gives valid predictions has an upper bound corresponding to the N^{th} mode.

(7) ?he spa tial model without high frequency residuals shows increasing error in node shape as the modal frecuencv rises.

(8) The high frequency trend of the predicted frequency respccse beyond the range of validity is mass-like.

4.3 STR Modelling With High Frequency Residuals

In Chapter 2 we saw that the incorporation of 2 high frequency residual term could make a significant improvement in the curve fitting of one response 2nd that such a residual could be reyesented 2s 2 spring. When several related curves were identified 2nd the spatial model constructed the high frequency residuals of point responses could readily be accommodated as springs and those of transfer responses could be neglected. in this present Chapter we seek to identify the response *curves once* more, this time making provision for calculation of the high frequency residuals.

4.3.1 STR Calculation of High Frequency Residual Terms

The identification calculations were carried cut using the same response data as were used formerly in section 4.2.1. The highest frequencies, however, were altered to 10000 Hz in the case of the Short Beam 2nd 5000 Hz for the Long, these being convenient round figures about a decade above the highest true resonance in each case. The residual stiffnesses were calculated from the N^{th} modal constant and N^{th} 'resonance' frequency according to equation (2.21) and are presented 2s part (b) of Tables 4.7 and 4.9 for Short and Long Beams respectively.

4.3.2 STR Spatial Models of Short and Lona Seam

The renainder of Tables 4.7 and 4.9 is devoted to the development of the data for the respective $[\Phi]$ end $[\omega_r^2]$ matrices by the same methods as were used for the ST node1 in Tables 4.1 and 4.4. The mode shape matrices for the STR model can be seen to differ from those cf the ST models in that the numerical values of the $\{\phi\}_r$ elements of STR become smaller than those of ST as r increases. This is the effect of the high frequency residuals which remove the need for cods-1 constants to be exaggerated in order to approximate the out-of-range modes.

The spatial models of the Short and Long Beams were calculated using program EMKAY and are listed in Tables 4.8 and 4.10, together with the diagonal matrices of residual stiffnesses.

0ST4. Residual Stiffness Model

The 2N x 2N matrices which constitute the spatial models with residual stiffness were discussed in section 2.3.2 and are specified in equation (2.5) and are composed of submatrices which can be found from the data of Tables 4.8 and 4.10. Since the nass matrices have zeroes on the nain diagonal they have zero determinants and are therefore singular. Thus they are not positive definite and consequently cannot be used unmodified to calculate eigenvalues and mode shapes using program EIGEN. The summations of ΣM_{trans} and ΣK_{trans} for the expanded matrices give the same results as before, however.

0ST3 Residual Flexibility Model

The alternative approach for inclusion of high frequency residuals that was discussed in section 2.3.2 involves several steps which entail computer file manipulation.

(i) Use program COUPLE1 with nodule ZMAK2 with input data $[M]$, $[K]$ to generate a matrix of linear receptances for each frequency of the sweep and store that data on file.

(ii) Use a special short program ADFLEX with input data $[C_{res}]$ and add that data, frequency by frequency, to that of (i) above and store on file.

(iii) Use program COUPLE1 with nodule ZFILE to process the receptance data into the desired final output format, usually nobility in logarithmic form.

This node1 was tested by going through steps (i) and (ii) using data for the Short Beam. Ultimately, a 4 x 4 receptance matrix was obtained for each of 101 frequencies. The method. involves considerable file manipulation, done by control cards in this particular case, and the

procedures were tedious. The results were compared with those prepared by the residual stiffness method using 8 x 8 matrices. The two sets were not identical but were nearly so, the largest discrepancy being 0.1%. The residual flexibility node1 was seen to work but offered no advantage and was therefore not further used.

4.3.3 STR Spatial Model of the Coupled Beam (Residual Stiffness Model)

The *Long* Beam with residual stiffness has a representation with 12 coordinates, numbers 7 to 12 being available for external connections. In the case of the Coupled beam coordinate 11 is used for translational coupling and coordinate 12 for rotational coupling. Continuing sith system coordinates those for the Short beam are numbers 11 to 18. Coordinates 11 tc 14 are available for external connections, numbers 15 to 18 are inaccessible.

The spatial model of the Coupled Beam is specified in Table 4.11 firstly as a sketch with labelled coordinates in 4.11(a) and then in terns of the two subsystems, the Long bear! in 4.11(b) and the Short bean in 4.11(c).

The complete 18 x 18 matrix of the Coupled Bean does not have to be specified, since the frequency response of the system can be generated by use of program COUPLE1 and nodule ZMAX2 with two subsystem using the computer to do the necessary coupling calculations. It will be remembered that the complete 8 x 8 matrix for the ST Coupled Bean was specified although the frequency response calculations could equally well have been done using program COUPLE1 to assemble the system matrices. In that case, however, the system matrices could be used with program EIGEN for the direct calculation of natural frequencies and mode shapes, an option not available for the STR matrices above because of the singularity of the mass matrices.

STR Natural Frequencies

The spatial model with residual springs can be modified so that the natural frequencies can be calculated using EIGEN. The modification involves removing all the coordinates which do cot designate mass points. In this example the springs attached at coordinates 7,8,9, 10, 13 and 14 shown in Table 4.11 are omitted altogether, and each pair of springs connected at junction coordinates 11 and 12 is replaced by an equivalent single spring representing the series connection of the two residual springs. The resultant system has 10 coordinates, each at a mass point, and the mass matrix is non-singular. The natural frequencies predicted by program EIGEN are j0.329, 0.465, 40.20, 110.2, 215.1, 361.1, 535.2, 740.4, 1040 and 1456 Hz, the latter two being anomalous since the model has at the outset only 8 external coordinates arid 8 valid modes. The mode shape vectors output by EIGEN do not correspond to the external coordinates and are thus not directly useful.

STR Frequency Responses

The frequency responses of selected parameters, at the tip and at the junction, were generated and plotted in Figure 4.7. The spatial model has eight external coordinates and has eight true resonance modes, two of which are rigid body codes. There are six bending modes, therefore, which are predicted. This covers the frequency range up to 750 Hz. The model makes no valid prediction at higher frequencies.

The modelling of the two tip responses is excellent. Slight discrepancies are observed for Y_{77} at the antiresonances about 190 Hz and 700 Hz. None are apparent for Y_{88}. Mismatch of antiresonances is apparent for the tip cross response Y_{78} but they are cct serious errors. Slightly core substantial errors are to be seen for the junction responses. The junction cross response $Y_{,\ ,\ 2}$ has the nodal constant for the fifth bending mode at 535.2 Hz a little too large, evidently, although it has the correct sign. The point translational response $Y_{11,11}$ at the junction has its antiresonances slightly astray, a feature of no great

significance. Lastly $Y_{12,12}$ shows good agreement with the exception of a contribution of the fifth bending mode showing its resonances, whereas the true response has a negligible resonance for that mode as can be deduced from the near horizontal slope of the shape of that mode seen in Figure 4.8.

Another feature is apparent in all the responses of Figure 4.7; there are two indicated resonances, at 1040 and 1456 Hz, of which more will be said below. Also, the final trend of all the curves at high frequency is upwards towards a swing-line. This is, as expected, an effect of the residual spring.

STR$_0$ Mode Shapes

At first sight the calculation of mode shapes seems to present a problem, again because EIGEN is inapplicable to the external coordinates. Modal identification, using program IDENT is the solution. Accordingly, response data were selected for the eight responses at external coordinates (7 to14) to excitation et coordinate 7, the bean tip. Eight runs of IDENT were sade giving data from which the mode shape natrix could be calculated. No tabular data are presented; the results are plotted as translational points and rotational slopes in Figure 4.8.

Onemaycomment first on the rigid body modes; their predicted shapes are accurate within the tolerances of the graph. Their indicated frequencies are very low, well below the range of interest. The first three bending modes exhibit slight discrepancies in mode shape, slight errors of displacement perhaps being more noticeable. The fourth bending rode at 361.2 Hz has a perceptible slope error at coordinate 12. The fifth bending mode at 535.2 Hzshows significant errors at some inboard coordinates; 9 having only 60% of its true value and 11 about 125%. Thisfact help to explain tie relatively poor fit of the frequency responses $Y_{11,12}$ and $Y_{12,12}$ in the vicinity of that mode, which has already received comment. The sixth bending mode, whose frequency marks the upper-limit of the range of validity of this spatial nodel, shows marked angular discrepancies at coordinates 10 and 12 and an error in the tip displacement, coordinate 14.

The modal data for the indicated resonances et 1040 2nd 1456 Hz are compared with the true mode shapes in Figure 4.8(g) and (h j. Their anomalous nature is very clear since the nodal data appears to be incoherent. The inboard slopes and displacements tight conceivably be fitted to plausible curves but the slopes fcr the beam tips must be wrong sinctne trend to higher slopes at the tip as the nodal frequency rises is inexorable. This particular spatial model has, fron the outset, eight coordinates and eight modes and can give valid data only up to the eighth resonance frequency. Thus such anomalous modes could be detected and excluded in the general case when true frequency response data are not available for comparison.

The major results for both ST and STR modelling are summarised iri Figure 4.9.

4.3.4 (STR) Conclusions: Modelling With High Frequency Residuals

The innovationOf representation of point residuals by spring elements is simple, easy to visualise, and produces a remarkable improvement in the fin21 predictions from 'fair' to 'excellent'.

(1) The ST3 frequency responses in comparison to the ST responses 2re 'focussed' since the mismatch between model 2nd prototype is very small.

(2) Natural frequencies, found by using EIGEN with a modified spatial model, are accurate within 1% everywhere.

(3) Mode shapes, found by using program IDENT, are mostly accurate, the exceptions being at inboard coordinates near rotational nodes, which are slightly in error.

(4) The residual stiffness model involving 2N x 2N matrices to incorporate residue1 springs is much easier to manipulate th2.n the equivalent residual flexibility model involving program ADFLEX and much file manipulation.

(5) The high *frequency* trend of the predicted frequency response beyond the range of validity is springlike.

(6) There ere two anomalous high frequency modes easily detected and discarded because they have strange 'mode shapes' and because they lie *beyond* the valid range of frequency bounded by the I!th mode.

4.4 CONCLUSIONS: SPATIAL MODELS OF IDEAL UNIFORM BEAMS

(1) The construction of 2 useful spatial model of a continuous system is feasible.

(2) The spatial model can be b-tilt with respect to 2 mixture of translational and rotational coordinates.

(3) Elements of the spatial model exclusively relating translational quantities have meaningful summations.

(4) The spatial model accurately predicts the effect of the substantial perturbation involved in coupling two substructures,

(5) Beams connected et 2 butt joint must have two coordinates of coupling.

(6) The overall process of modelling and coupling is numerically well-conditioned.

(7) The frequency response predicted by an X-node spatial model is valid up to but not beyond the N^{th} mode.

(8) The innovatory addition of springs tc the spatial model to represent high frequency residuals of point responses makes 2 most significant improvement in the accuracy of the model.

(9) This addition of spring elements is most easily achieved by increasing the size of the matrices tc 2N x 2N, the 'residual stiffness' model.

(10) The mass matrices resulting from (9) are singular, and the spatial model has to be reduced so that EIGEN can be used to calculate the natural frequencies. Close frequency sweeps using program COUPLE1 with the full model will give responses, program IDENT will then give mode shapes.

(11) The residual-spring method produces two high frequency anomalous modes which affect the response in the region beyond the range of validity.

NOTE

The CONCLUSIONS of Chapters 2, 3 and 4 taken together constitute a summary of theoretical tools which can be used in the latter part of the thesis, Chapters 5, 6 end 7 which are concerned with experimental neasuresents and the application of the techniques of identification of spatial models of lightly damped systems.

Figure 4.1 Natural Frequencies of Beams as Functions of Length and Depth

From Bishop & Johnson Tables p. 17 :-

$\lambda_r = (\omega_r^2 A\rho/EI)^{\frac{1}{4}}$ $\quad \therefore \omega_r = \lambda_r^2 (EI/A\rho)^{\frac{1}{2}}$

But for rectangular beam :-

$I = d.h^3/12$, $\quad A = d.h \quad \therefore (EI/A\rho)^{\frac{1}{2}} = h(E/12\rho)^{\frac{1}{2}}$

B & J p. 36 :- $(\lambda_r.l)^2 = 22.373$

$\therefore \quad f_1 = \omega_1/2\pi = 22.373\ h\ (E/12\rho)^{\frac{1}{2}}/2\pi l^2$

For steel :- $E = 0.206 \times 10^{12}$ N/m·, $\rho = 0.7740 \times 10^4$ kg/m^3

$\therefore \quad f_1 = 5303\ h/l^2$ Hz

r is mode number

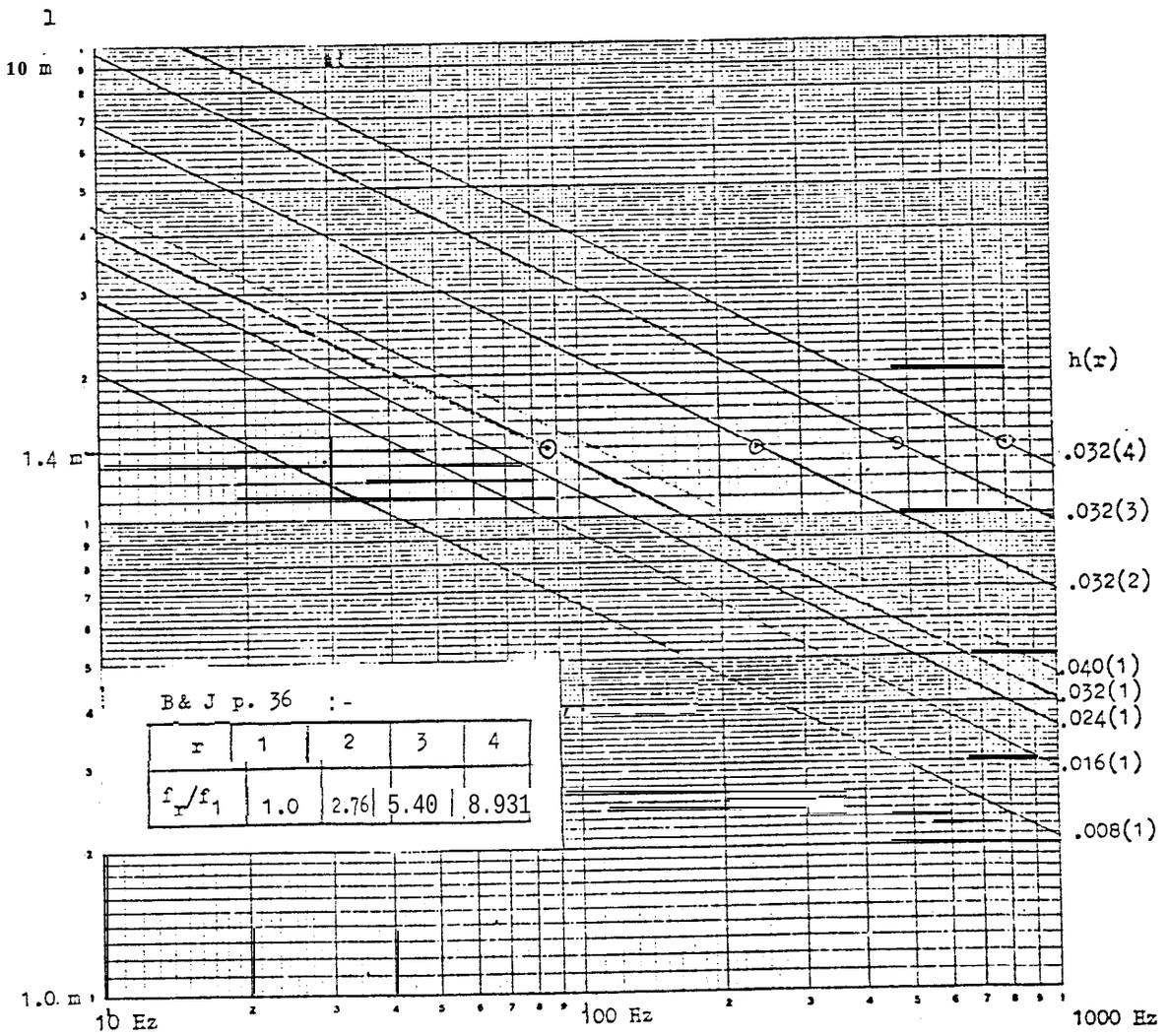

B& J p. 36 :-

r	1	2	3	4
f_r/f_1	1.0	2.76	5.40	8.931

Figure 4.2 Specification of Coordinates and Mobilities

(a) Long Beam

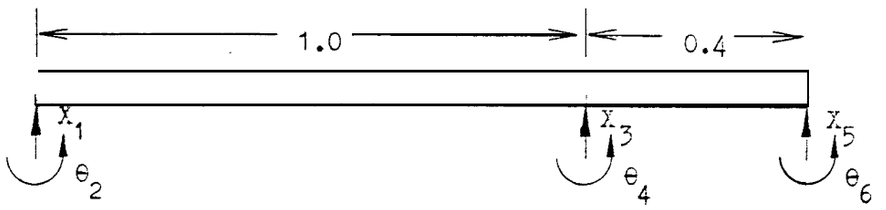

$$\begin{Bmatrix} \dot{X}_1 \\ \dot{\theta}_2 \\ \dot{X}_3 \\ \dot{\theta}_4 \\ \dot{X}_5 \\ \dot{\theta}_6 \end{Bmatrix}_L = \begin{bmatrix} Y_{11} & Y_{12} & Y_{13} & Y_{14} & Y_{15} & Y_{16} \\ Y_{21} & Y_{22} & Y_{23} & Y_{24} & Y_{25} & Y_{26} \\ Y_{31} & Y_{32} & Y_{33} & Y_{34} & Y_{35} & Y_{36} \\ Y_{41} & Y_{41} & Y_{43} & Y_{44} & Y_{45} & Y_{46} \\ Y_{51} & Y_{52} & Y_{53} & Y_{54} & Y_{55} & Y_{56} \\ Y_{61} & Y_{62} & Y_{63} & Y_{64} & Y_{65} & Y_{66} \end{bmatrix}_L \begin{Bmatrix} F_1 \\ M_2 \\ F_3 \\ M_4 \\ F_5 \\ M_6 \end{Bmatrix}_L \quad \text{or} \quad \{\dot{X}\}_L = [Y]_L \{F\}_L$$

$$[Y]_L = \begin{bmatrix} (\dot{X}_1/F_1) & (\dot{X}_1/M_2) & (\dot{X}_1/F_3) & (\dot{X}_1/M_4) & (\dot{X}_1/F_5) & (\dot{X}_1/M_6) \\ (\dot{\theta}_2/F_1) & (\dot{\theta}_2/M_2) & (\dot{\theta}_2/F_3) & (\dot{\theta}_2/M_4) & (\dot{\theta}_2/F_5) & (\dot{\theta}_2/M_6) \\ (\dot{X}_3/F_1) & (\dot{X}_3/M_2) & (\dot{X}_3/F_3) & (\dot{X}_3/M_4) & (\dot{X}_3/F_5) & (\dot{X}_3/M_6) \\ (\dot{\theta}_4/F_1) & (\dot{\theta}_4/M_2) & (\dot{\theta}_4/F_3) & (\dot{\theta}_4/M_4) & (\dot{\theta}_4/F_5) & (\dot{\theta}_4/M_6) \\ (\dot{X}_5/F_1) & (\dot{X}_5/M_2) & (\dot{X}_5/F_3) & (\dot{X}_5/M_4) & (\dot{X}_5/F_5) & (\dot{X}_5/M_6) \\ (\dot{\theta}_6/F_1) & (\dot{\theta}_6/M_2) & (\dot{\theta}_6/F_3) & (\dot{\theta}_6/M_4) & (\dot{\theta}_6/F_5) & (\dot{\theta}_6/M_6) \end{bmatrix}_L$$

Figure 4.2 (continued) Specification of Coordinates and Mobilities

(b) Short Beam

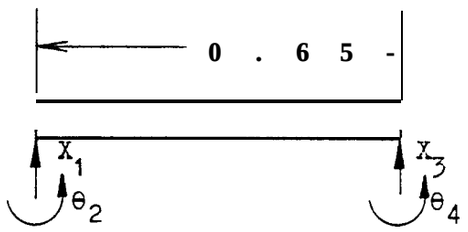

$$\begin{Bmatrix} \dot{X}_1 \\ \dot{\theta}_2 \\ \dot{X}_3 \\ \dot{\theta}_4 \end{Bmatrix}_S = \begin{bmatrix} Y_{11} & Y_{12} & Y_{13} & Y_{14} \\ Y_{21} & Y_{22} & Y_{23} & Y_{24} \\ Y_{31} & Y_{32} & Y_{33} & Y_{34} \\ Y_{41} & Y_{42} & Y_{43} & Y_{44} \end{bmatrix} \begin{Bmatrix} F_1 \\ M_2 \\ F_3 \\ M_4 \end{Bmatrix}_I \quad \text{or} \quad \{\dot{X}\}_S = [Y]_S \{F\}_S$$

$$[Y]_S = \begin{bmatrix} (\dot{X}_1/F_1) & (\dot{X}_1/M_2) & (\dot{X}_1/F_3) & (\dot{X}_1/M_4) \\ (\dot{\theta}_2/F_1) & (\dot{\theta}_2/M_2) & (\dot{\theta}_2/F_3) & (\dot{\theta}_2/M_4) \\ (\dot{X}_3/F_1) & (\dot{X}_3/M_2) & (\dot{X}_3/F_3) & (\dot{X}_3/M_4) \\ (\dot{\theta}_4/F_1) & (\dot{\theta}_4/M_2) & (\dot{\theta}_4/F_3) & (\dot{\theta}_4/M_4) \end{bmatrix}_S$$

Figure 4.3 Identification of Short Beam

Resonances at 0, 398.5, 1099, 2154

Frequency Response

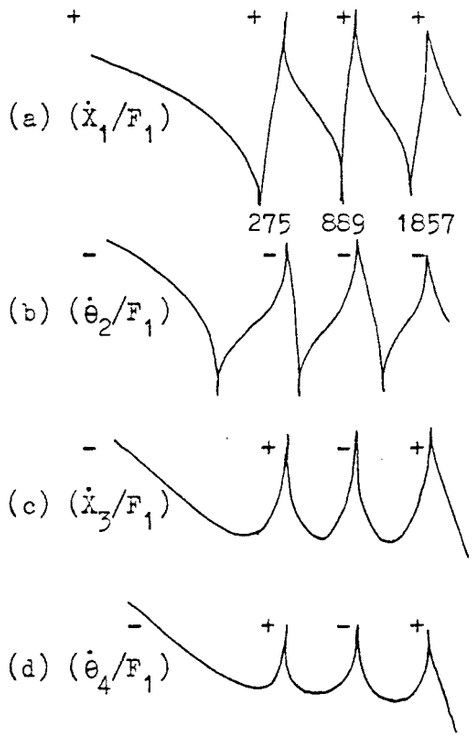

Selected Date

Frequency(Hz)	IN	Phase	Type
20.00	.9829	0	
274.6	0	0	AR
889.3	0	0	AR
1857	0	0	AR
20.00	-2.25	0	
20.00	-.4951	0	
20.00	-2.290	0	

(e) Sip Array

Mode	1	2	3	4
Frequency(Hz)	0	398.5	1099	2154
	+	+	+	+
	-	-	-	-
	-	+	-	+
	-	+	-	+

Figure .4 Identification of Long Beam

Resonances at 0, E5.91, **236.8, 464.2, 767.4, 1146**

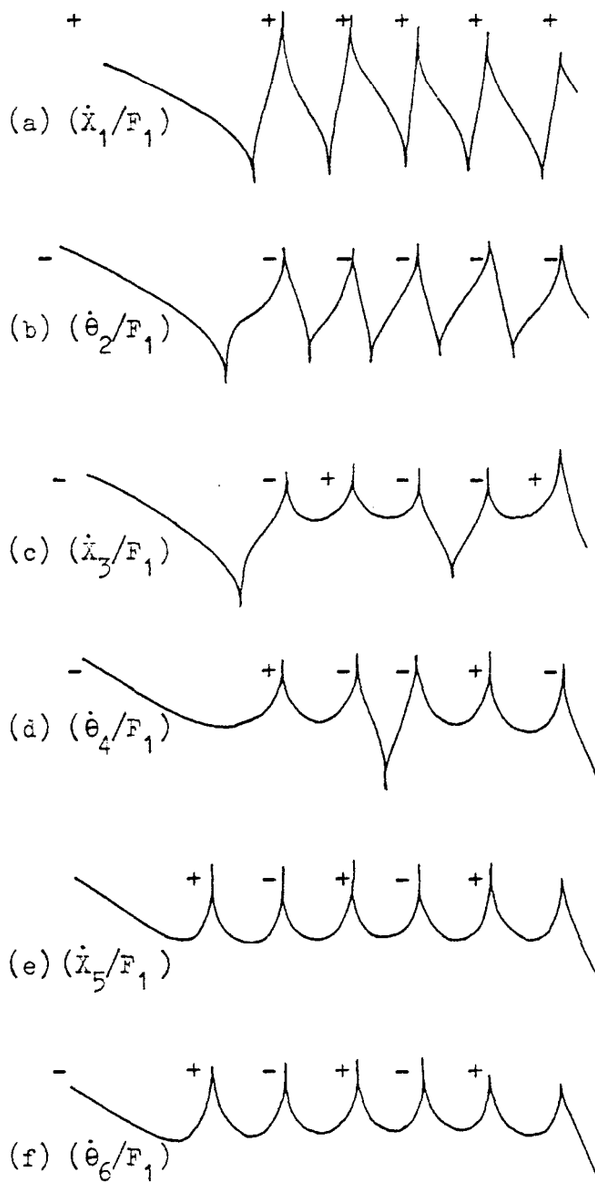

	Frequency(Hz)	IN	Phase	Type
	20.00	.4267	**0**	
	59.20	0	0	AR
	191.7	0	0	AR
	400.3	0	0	AR
	684.5	0	0	AR
	1045	0	0	AR
(b)	**20.00**	-.3694	**0**	
(c)	**20.00**	-.02854	**0**	
(d)	50.00	-.5489	0	
(e)	**20.00**	-.2524	**0**	
(f)	**29.00**	-.5636	0	

(g) Sign Array

Mode	1	2	3	4	5	6
Frequency(Hz)	0	85.89	236.8	464.2	767.4	1146
	+	+	+	+	+	+
	-	-	-	-	-	-
	-	-	+	-	-	+
	-	+	-	-	+	-
	-	+	-	+	-	+
	-	+	-	+	-	+

Figure 4.5 (ST) Predicted Modal Data for Coupled Beam

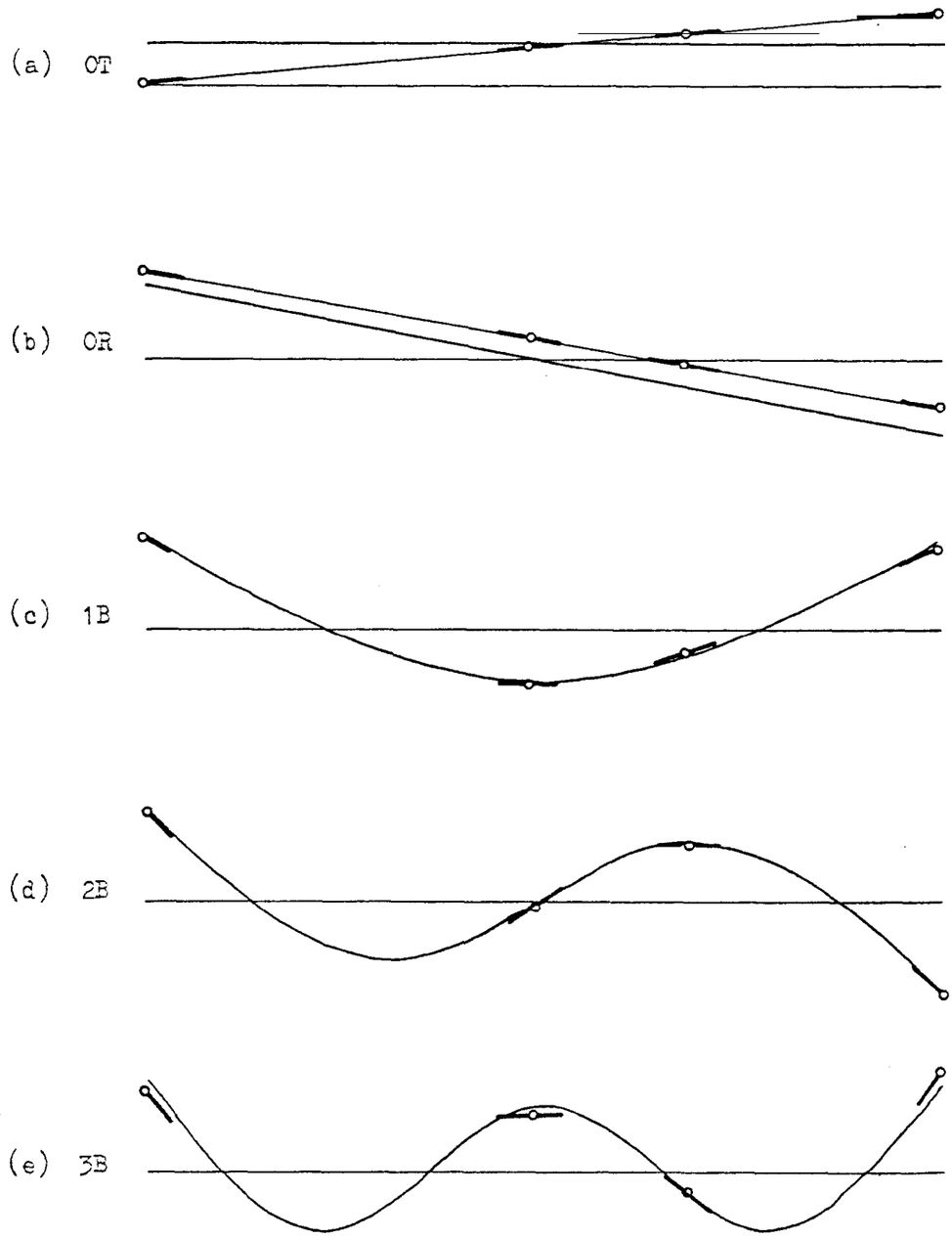

Frequency (True Frequency) (Hz)

(a) j 0.23 (0) (b) 0.48 (0)

(c) 42.47 (40.07) (d) 123.1 (110.4) (e) 221.7 (216.5)

Figure 4.5 (ST) Predicted Modal Data for Coupled Beam (cont'd)

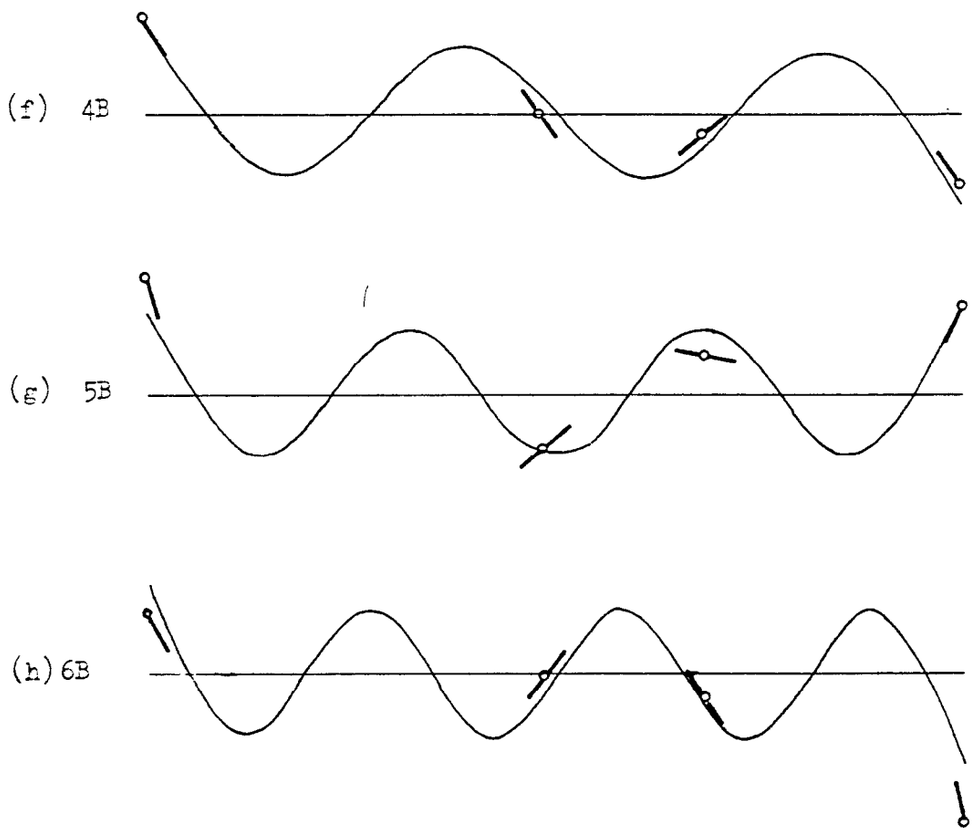

Frequency True Frequency) (Hz)

(f) 370.6 (357.9) (g) 608.0 (534.7) (h) 601.2 (746.8)

Key (a) Rigid Body Translation 0T

(b) Rigid Body Rotation 0R

(c) 1st Bending Mode 1B

(d) 2nd Bending Mode 2B

etc.

Figure 4.6 S[T] Frequency Responses of Coupled Sean

(a) Tip Response 1, 1

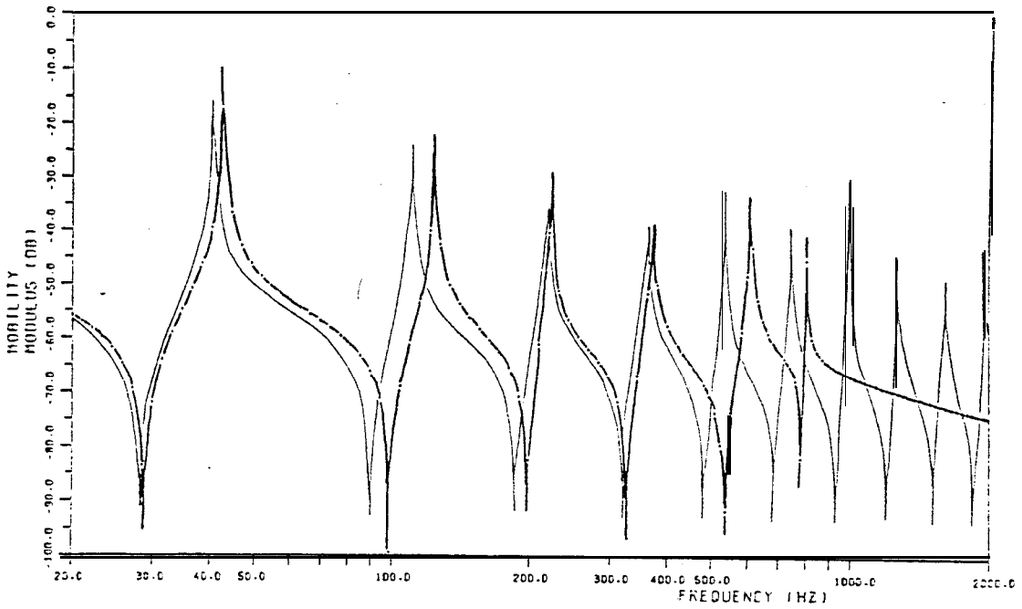

Spatial Model

Ideal

(b) Tip Response 2, 2

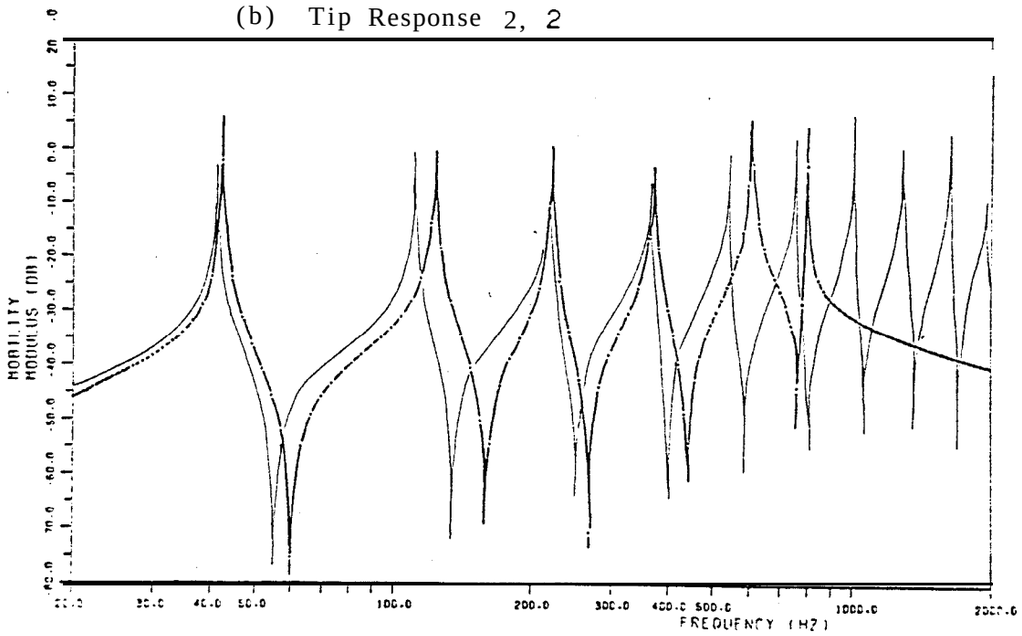

Figure 4.6 (ST) Frequency Responses of Coupled Beam (cont'd)

(c) Tip Cross Response 1, 2

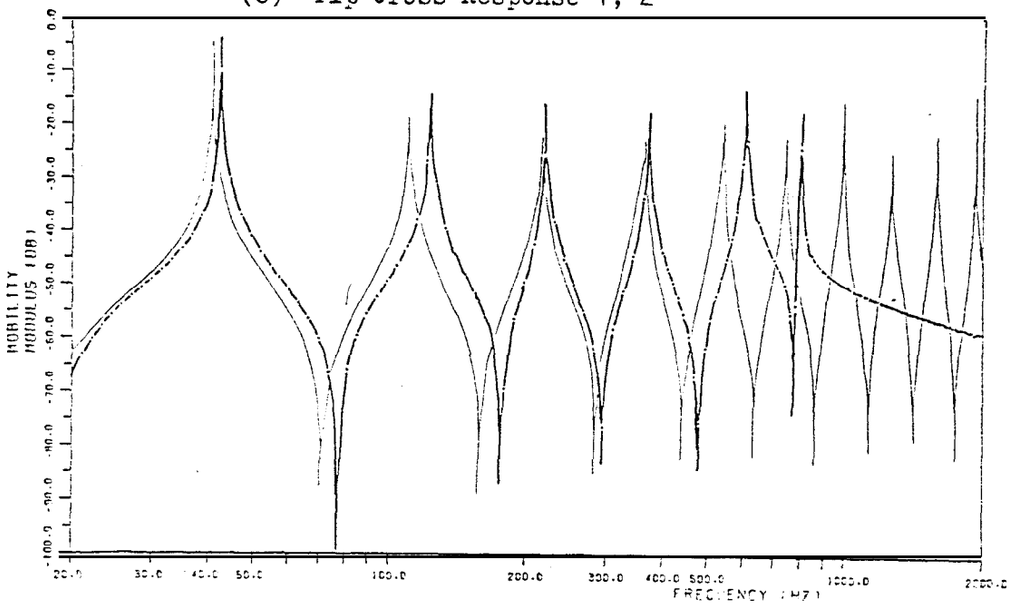

Spatial Model

Ideal

(d) Junction Cross Response 5, 6

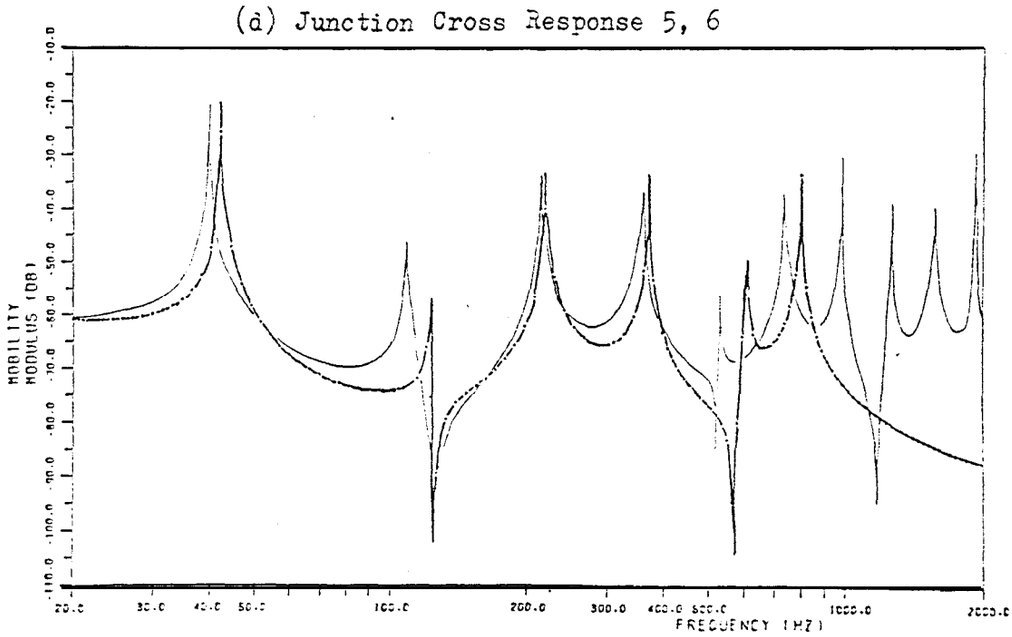

Figure 4.6 (ST) Frequency Responses of Coupled Beam (cont'd)

(e) Junction Response 5, 5

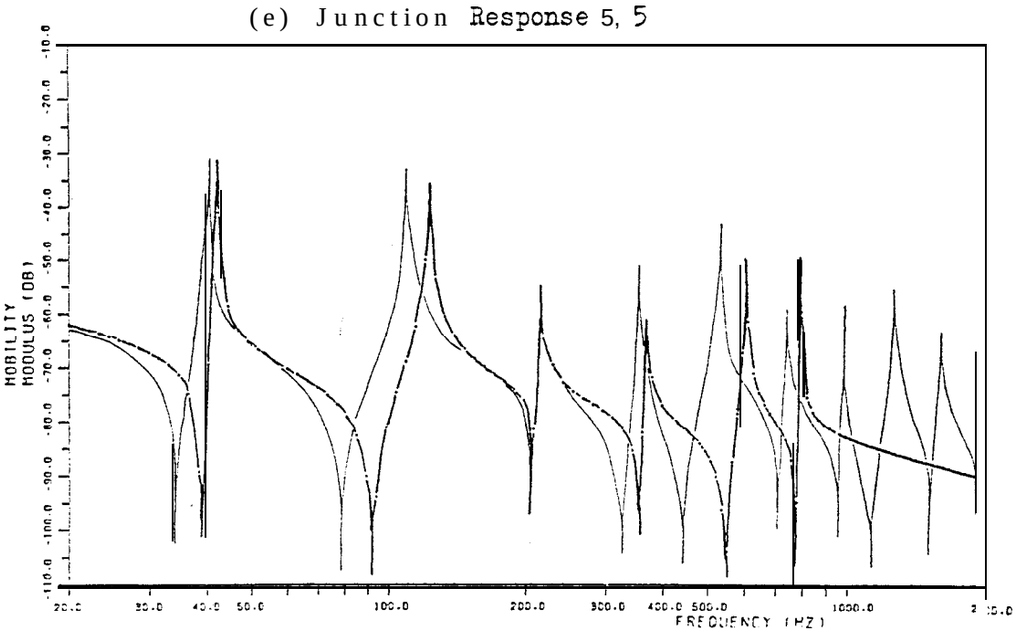

Spatial Model

Ideal

(f) Junction Response 6, 6

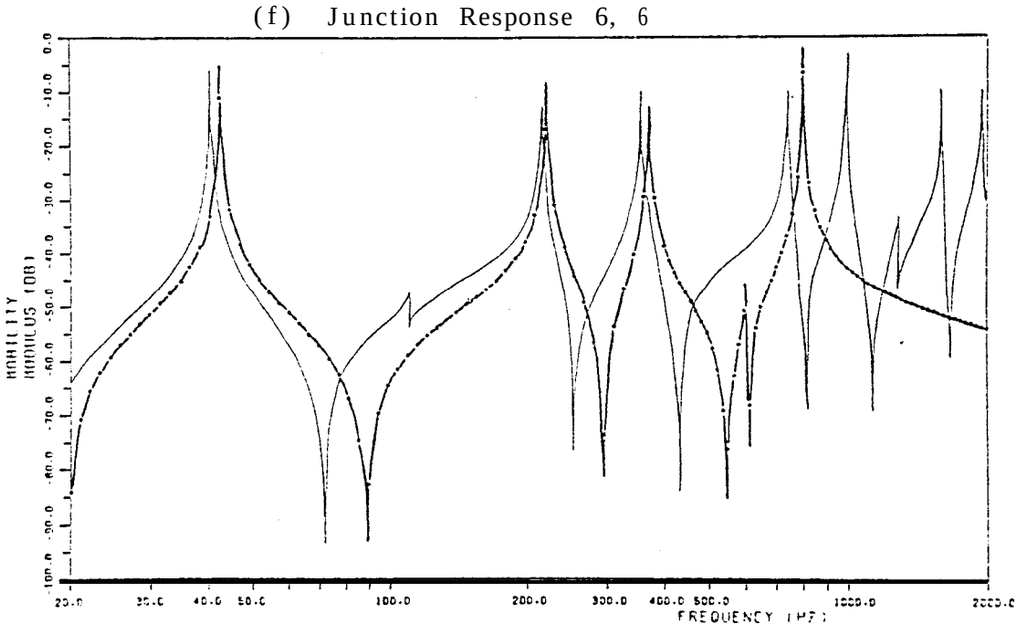

Figure 4.7 (STR) Frequency Responses of Coupled Beam

(a) Tip Response 7, 7

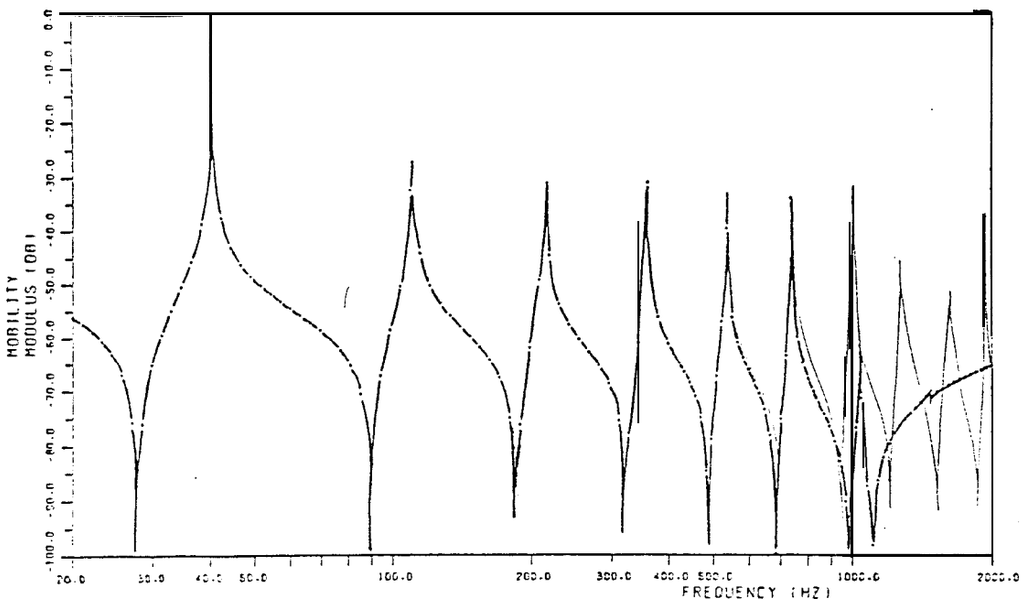

Spatial Model

Ideal

(b) Tip Response 8, 8

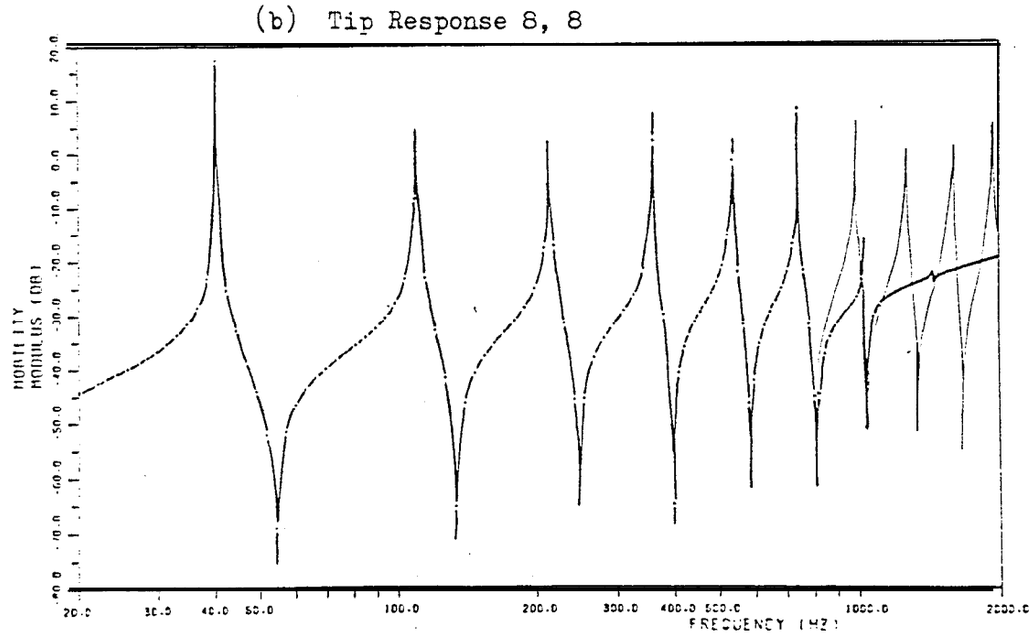

Figure 4.7 (STR) Frequency Responses of Coupled Beam (cont'd)

(c)Tip Cross Response 7, 8

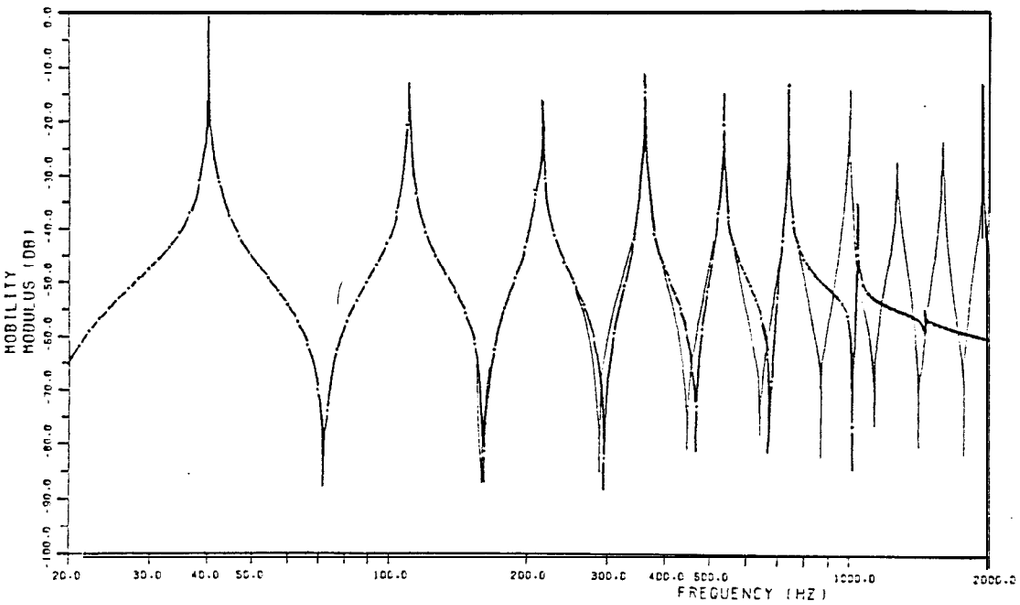

Spatial Model

Ideal

(d) Junction Cross Response 11, 12

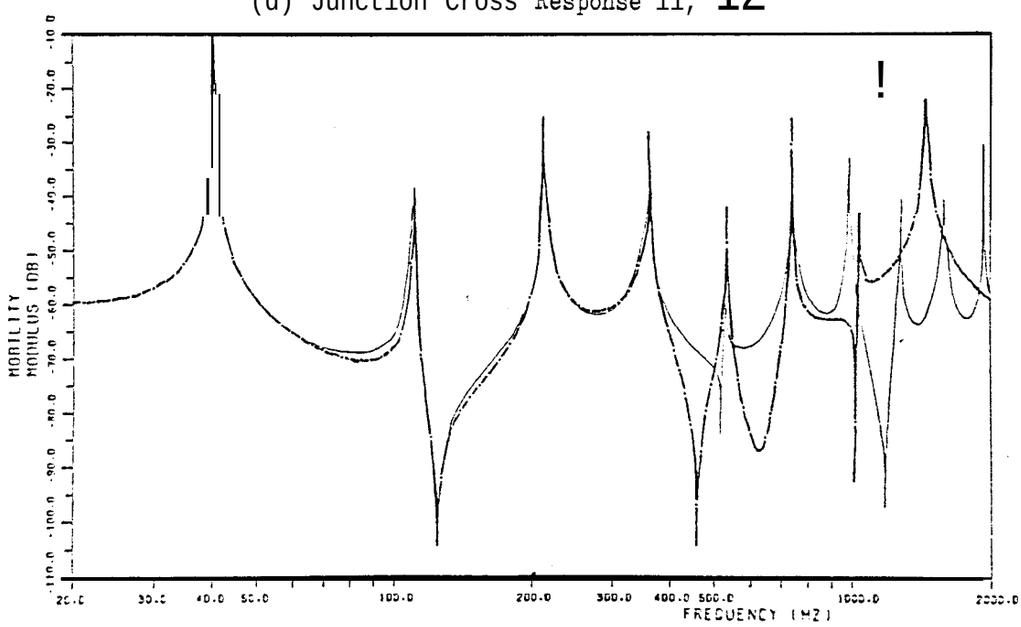

Figure . 7 (STR) Frequency Responses of Coupled Bear (cont'd

(e) Junction Response 11, 11

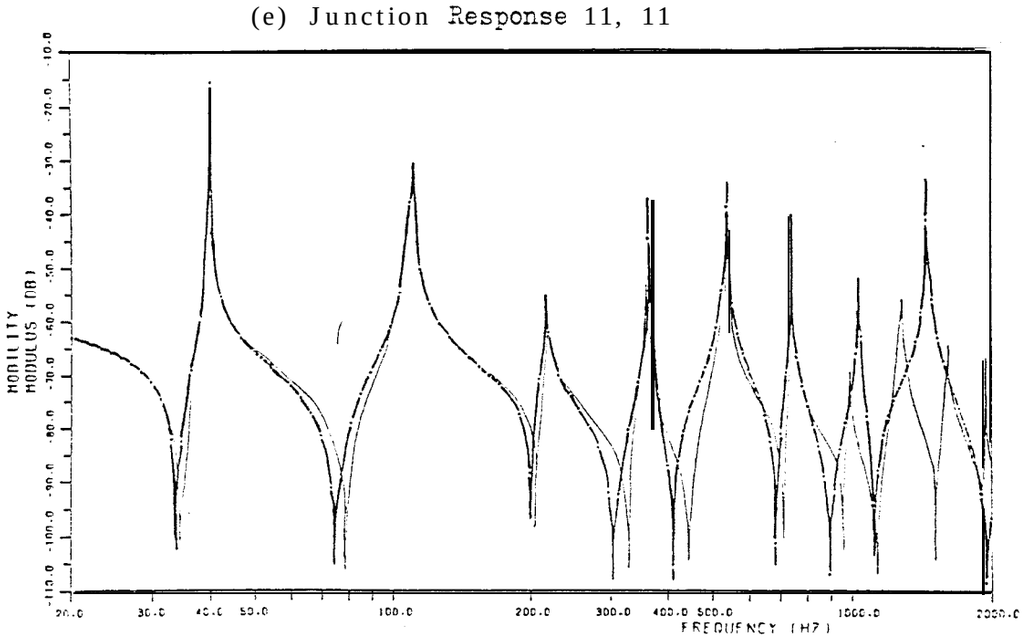

Spatial Model

Ideal

(f) Junction Response 12, 12

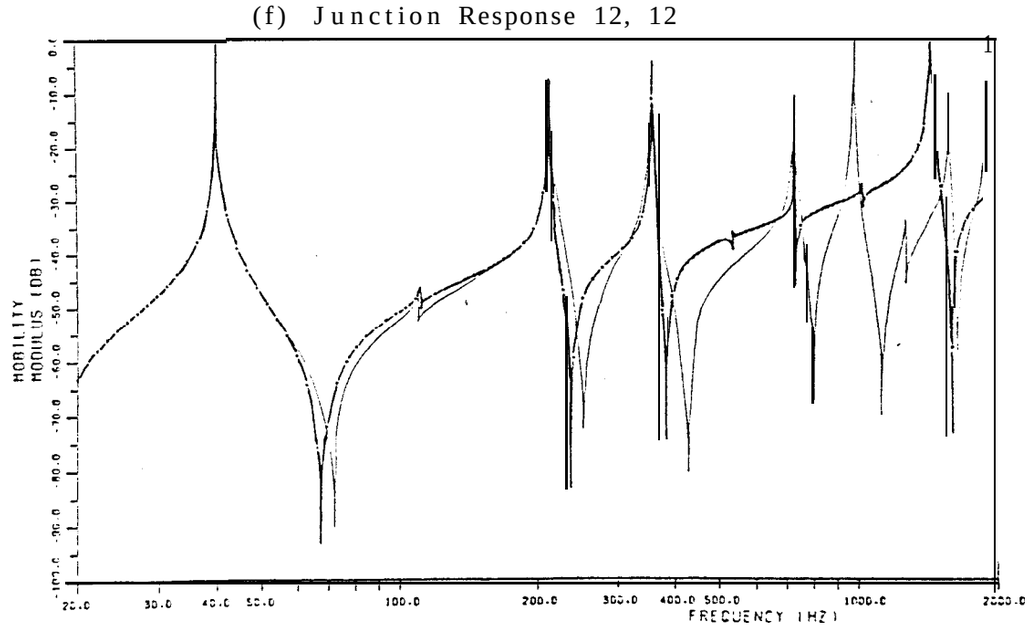

Figure 4.8 (STR) Predicted Modal Data for Coupled Beam

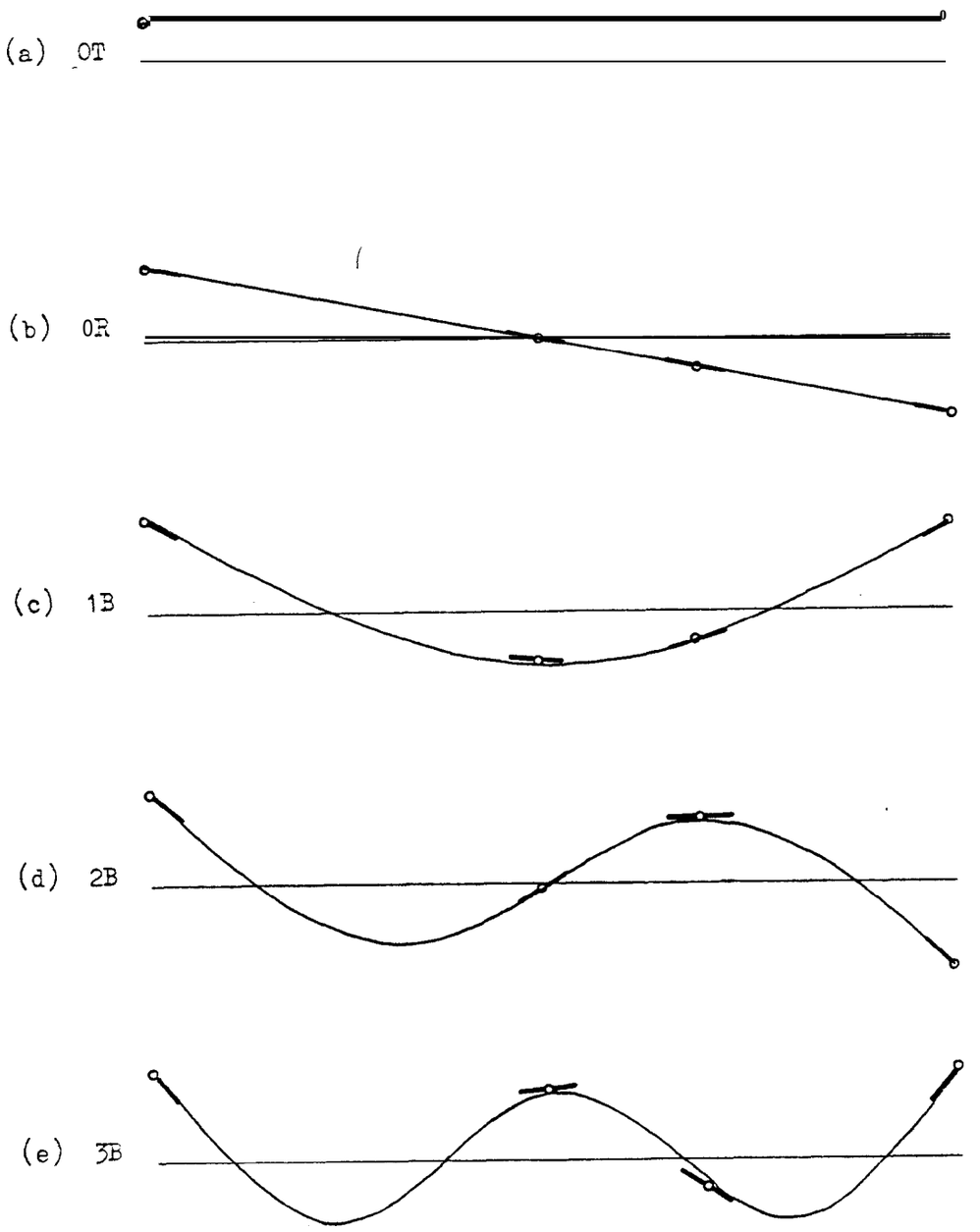

Frequency (True Frequency) (Hz)

(a) j0.239 (0) (b) 0.465 (0)

(c) 40.20 (40.07) (d) 110.23 (110.4) (e) 215.1 (216.5)

Figure 4.8 (STR) Predicted Modal Data for Coupled Beam (cont'd)

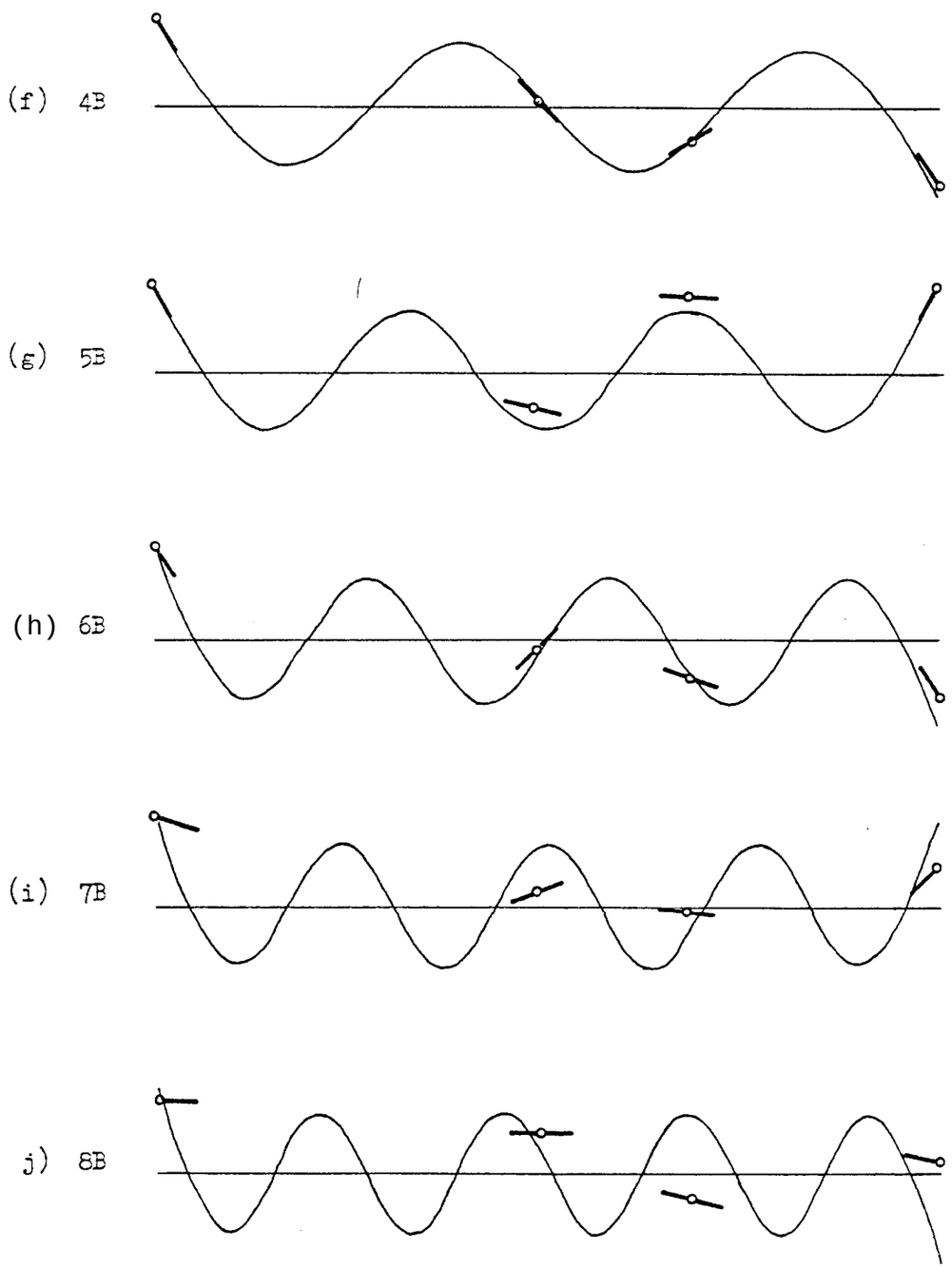

Frequency True Frequency Hz

(f) 361.1 (357.9) (g) 535.2 (534.7) (h) 740.4 (746.6)

(i) 1040.2 (994.1) (j) 1455.6 (1277) - both anomalous

Figure 4.9 (ST) (STR) Spatial Models of Coupled Beam Coordinates and Natural Frequencies

(a) Ideal Beam

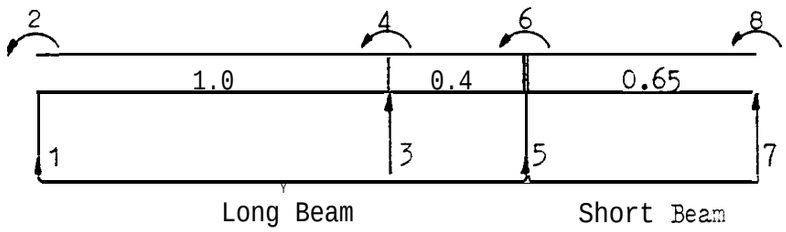

(b) Natural Frequencies (Hz)

0 0 40.07 110.4 216.5 357.9 534.7 746.8 etc.

(b) (ST) Spatial Model - Theoretical Data

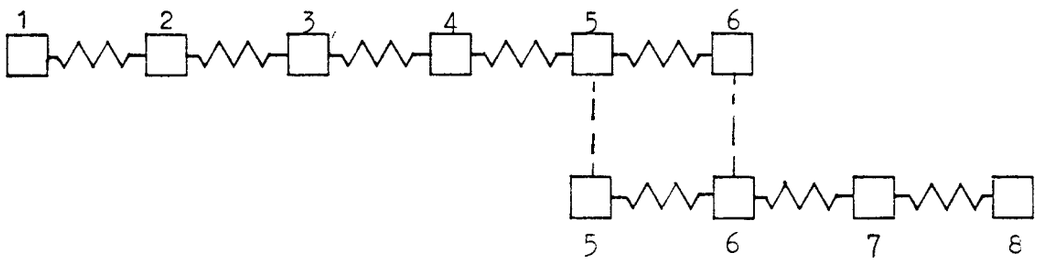

Tip Coordinates 1,2 Junction Coordinates 5,6

Natural Frecuencies (Hz) - Error (%)

j.23	.48	42.47	123.1	221.7	370.6	608.0	801.2
		(+6.0)	(+11)	(+2.4)	(+3.5)	(+13.7)	(+7.3)

(c) (STR) Spatial Model with Residuals - Theoretical Data

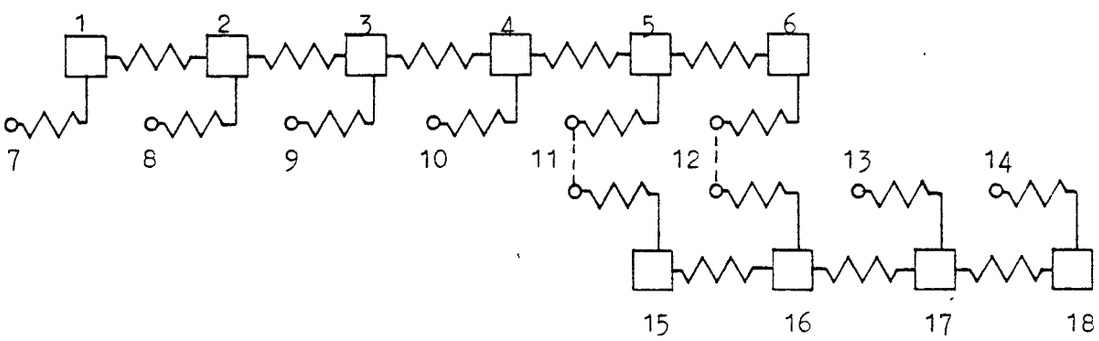

Tip Coordinates 7,8 Junction Coordinates 11,12

Natural Frequencies (Hz) - Error (%)

j.329	.465	40.20	110.2	215.1	361.1	535.2	740.4
		(+.3)	(+.1)	(-.7)	(+.9)	(+.1)	(-.9)

plus 1040, 1456 (anomalous)

Table 4.1 (ST) Development of Mode Shape Matrix for Short Beam

(a) Modal Constants

Output of program IDENT.

Mode	1	2	3
Frequency (Hz)	0	398.5	1099
A_{ii}	.9859	.9910	1.038
A_{22}	7.000	51.51	173.1

(b) Separation of Rigid Body Modes

T - Translational R - Rotational

$m = 4.057$ kg , $1/m = .2465$ kg^{-1}

$_1A_{11T} = .2465$	$_1A_{11R} = .9859 - .2465 = .7394$
$_1A_{22T} = 0$	$_1A_{22R} = 7.000$

where $_1A_{iiT} = 1/m$ for i odd

$_1A_{iiT} = 0$ for i even

$_1A_{iiR} = {}_1A_{ii} - {}_1A_{iiT}$ for all i

(c) Matrix of Point Modal Constants

Because of symmetry $A_{ij} = A_{11}, A_{44} = A_{22}$

Frequency (Hz)	0(T)	0(R)	398.5	1099
A_{11}	.2465	.7394	.9910	1.038
A_{22}	0	7.020	51.51	173.1
A_{33}	.2465	.7394	.9910	1.038
a_{44}	0	7.000	51.51	173.1

(d) Mode Shape Matrix

Frequency (Hz)	0(T)	0(R)	398.5	1099
$\sqrt{A_{11}}$	+.4965	+.8599	+.9955	+1.019
$\sqrt{A_{22}}$	+ 0	-2,646	-7.177	-13. 16
$\sqrt{A_{33}}$	+.4965	-.8599	+.9955	-1.019
$\sqrt{A_{44}}$	+ 0	-2.646	+7.177	-13.16

The signs in the lasttwo columns were found from the plotted and identified short beam transfer responses Figure 4.3. The signs in the first tuc columns were found from the rigid body mode shapes below:

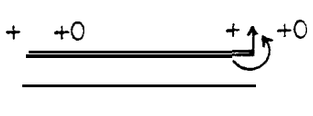

Translation

Rotation

Table 4.2 (ST) Spatial Model of Short Beam

Output of program EMKAY with input data from Table 4.2.1.

Mass Matrix

$$[M_S] = \begin{bmatrix} 1.62039 & .193443 & .407904 & -.0878957 \\ & .0303468 & .0878957 & -.0183839 \\ & & 1.62039 & -.193443 \\ \text{Symmetric} & & & .0303468 \end{bmatrix}$$

$$\Sigma M = 4.08052 \text{ kg}$$

But $\Sigma M_{trans} = 4.056588$ kg

Stiffness Matrix

$$[K_S] = 10^5 \begin{bmatrix} 11\,1.2320 & 3.65028 & -11.2320 & 3.65020 \\ & 1.49352 & -3.65020 & .881989 \\ & & 11.2320 & -3.65020 \\ \text{Symmetric} & & & 1.49052 \end{bmatrix}$$

$$\Sigma K = 10^5(4.74498) \text{ N/m}$$

But $\Sigma K_{trans} = 0$

Table 4.3 (ST) Modal Properties of the Short Beam Predicted from its Spatial Model

Output of program EIGEN with input $[M_s]$ $[K_S]$ of Table 4.2.

Natural Frequencies (Hz)	3.50E-5	.625	398.5	1098
Matrix	.497	.860	-.995	-1.02
	1			
	.497	.860	.995	-1.02
Mode Shape	1.2E-8	-2.65	-7.18	13.16
	1.2E-8	-2.65	7.18	13.16

Compare with Table 4.1(d)

Table 4.4 (ST) Development of Mode Shape Matrix for Long Beam

(a) Modal Constants

Output of program IDENT.

Mode	1	2	3	4	5
Frequency (Hz)	0	85.91	236.8	464.2	767.4
A_{11}	.4577	.4581	.4636	.4736	.5082
A_{22}	.7000	5.061	14.83	31.77	68.58
A_{33}	.1774	.0233	.1959	.1081	.0043
A_{44}	.7003	2.619	.2827	7.629	35.58

(b) Separation of Rigid Body Modes

$m = 8.74$ kg , $1/m = .1144$ kg^{-1}

$1^{A}_{11T} = .1144$	$1^{A}_{11R} = .4577 - .1144 = .3433$
$1^{A}_{22T} = 0$	$1^{A}_{22R} = .7000$
$1^{A}_{33T} = .1144$	$1^{A}_{33R} = .1774 - .1144 = .0630$
$1^{A}_{44T} = 0$	$1^{A}_{44R} = .7003$

Using equations of Table 4.1 (b).

Table 4.4 continued $_{0}^{ST}$

(c) Matrix of Point Modal Constants

Because of Symmetry $A_{55} = A_{11}$, $A_{66} = A_{22}$

Frequency (Hz)	0(T)	0(R)	**85.91**	236.8	464.2	767.4
A_{11}	.1144	.3433	.4581	.4636	.4736	.5082
A_{22}	0	.7000	**5.061**	14.83	31.77	68.58
A_{33}	.1144	.0630	.0233	.1959	.1081	.0043
A_{44}	**0**	.7003	**2.619**	.2827	7.629	35.58
A_{55}	.1144	.3433	.4581	.4636	.4736	.5082
A_{66}	**0**	.7000	**5.061**	14.83	31.77	68.58

(d) Mode Shape Matrix

Frequency (Hz)	0(T)	0(R)	**85.91**	236.8	464.2	767.4
$\sqrt{A_{11}}$	+.3382	+.5859	+.6768	+.6809	+. 6862	+.7129
$\sqrt{A_{22}}$	+ 0	-.8367	**-2.250**	-3.851	-5.636	-8.281
$\sqrt{A_{33}}$	+. 3382	-.2510	-.1526	+.4426	-.3288	-.0656
$\sqrt{A_{44}}$	+ 0	-.8367	+1.618	-.5317	-2.762	+5.965
$\sqrt{A_{55}}$	+.3382	-.5859	+.6768	-.6809	+.6882	-.7129
$\sqrt{A_{66}}$	**+ 0**	-.8367	+2.250	-3.851	+5.636	-8.281

The signs in the last four columns were found from the plotted long beam transfer responses, Figure 4.4.

The signs in the first two columns were found from the rigid body mode shapes sketched below.

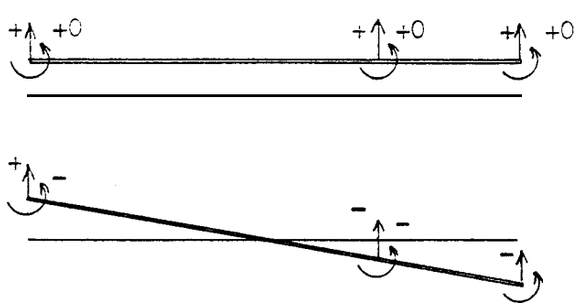

Table 4.5 (ST) Spatial Model of Long Beam

Output of program ENKAY with input data from Table 4.2.4(d)

Mass Matrix

$$[M_L] = \begin{bmatrix} 2.42399 & .431632 & -5.60223 & -1.16026 & 6.22342 & -1.54614 \\ & .100957 & -1.66088 & -.350506 & 1.86052 & -.461354 \\ & & 45.5975 & 10.0147 & -50.8450 & 12.5811 \\ & & & 2.36038 & -11.8349 & 2.91720 \\ & & & & 61.1720 & -14.8899 \\ \text{Symmetric} & & & & & 3.65802 \end{bmatrix}$$

$$\Sigma M = 6.66408 \text{ kg}$$

But $$\Sigma M_{trans} = 8.74287 \text{ kg}$$

Stiffness Matrix

$$[K_L] = 10^5 \begin{bmatrix} 3.20505 & 1.56869 & 18.1014 & 5.10643 & -21.3065 & 5.05890 \\ & .969344 & 2.49452 & 1.32806 & -4.06322 & .898019 \\ & & & & & \\ & & & 30.3421 & -167.092 & 40.3183 \\ & & & & 960.216 & -234.495 \\ \text{Symmetric} & & 920.808 & 161.986 & -938.909 & 57.77035 \\ & & & & & 229.436 \end{bmatrix}$$

$$\Sigma K = 10^5(174.104) \text{ N/m}$$

But $$\Sigma K_{trans} = 10^5(.00085) \simeq c \text{ N/m}$$

Table 4.6 Spatial Model of Coupled Beam

(a) Coordinates

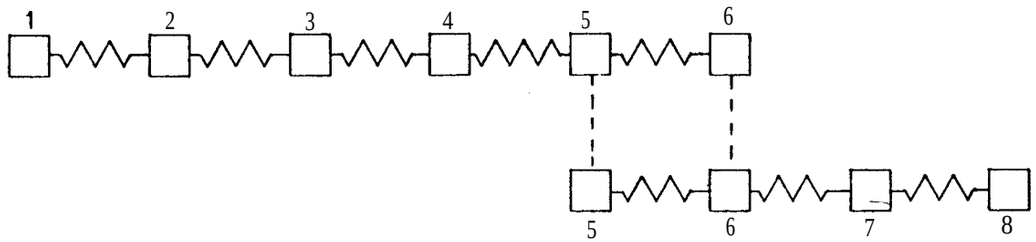

Tip Coordinates 1, 2

Junction Coordinates 5, 6

(b) Mass Matrix

$$[M_C] =$$

2.42099	.431632	-5.60223	-1.16026	6.22342	-1.54614	0	0
	.100957	-1.66083	-.350506	1.86032	-. 461354	0	0
		45.5975	10.0147	-50.8450	12.5811	0	0
			2.36030	-11.8349	2.91720	0	0
				62.7924	-14.6965	.407904	-.087896
					3.68837	.087896	-.0183839
						1.62039	-. 193443
Symmetric							.0303468

Table 4.6 continued

(c) Stiffness Matrix

$$[K_C] = 10^5 \begin{bmatrix} 3.20505 & 1.56869 & 18.1014 & 5.10643 & -21.3465 & 5.05890 & 0 & 0 \\ & .969344 & 2.49452 & 1.32806 & -4.06322 & .898019 & 0 & 0 \\ & & 920.808 & 161.986 & -938.909 & 229.436 & 0 & 0 \\ & & & 30.3421 & -167.092 & 40.3183 & 0 & 0 \\ & & & & 971.448 & -230.845 & -11.2320 & 3.65020 \\ & & & & & 59.1940 & -3.65020 & .881969 \\ & & & & & & 11.2320 & -3.65020 \\ \text{Symmetric} & & & & & & & 1.49052 \end{bmatrix}$$

(d) Predicted Natural Frequencies (Hz) (Error %)

.23i	.48	42.47	123.1	221.7	370.6	607.8	801.2
		(+ 6)	(+11.5)	(+2.4)	(+3.5)	(+13.7)	(+7.3)

(e) Predicted Natural Frequencies (Hz) for +2% Change in K_{55} (% difference from (d))

.023i	37.36	68.85	148.0	224.6	372.1	610.7	802.1
(-90)	(+7700)	(+62)	(+20)	(+1.3)	(+0.4)	(+0.5)	(+0.1)

f) Predicted Natural Frequencies (Hz) for Coupling at One Coordinate Only

0.22i	0.33i	0.95	74.14	206.0	330.5	448.8	721.6	1006

Data for (d), (e) and (f) output by program EIGEN

Table 4.7 $\underset{0}{\text{STR}}$ Development of Mode Shape Matrix for Short Beam

(a) Modal Constants

Output of program IDENT

Mode	1	2	3	4(residual)
Frequency (Hz)	0	398.5	1099	10000
A_{11}	.9859	.9587	.7772	**89.23**
A_{22}	**7.000**	**49.83**	**129.6**	**26235**

(b) Residual Stiffness

$$K_{rsi} = \omega_4^2 / {}_4A_{ii} = (2\pi \times 10000)^2 / {}_4A_{ii}$$

$K_{rs1} = 442.478 \times 10^5$, $K_{rs2} = 1.50489 \times 10^5$

(c) Separation of Rigid Body Modes

${}_1A_{11T} = .2465$ ${}_1A_{22T} = 0$	${}_1A_{11R} = .9859 - .2465 = .7394$ ${}_1A_{22R} = 7.003$

Using equations of Table 4.1(b)

(d) Matrix of Point Modal Constants

Because of symmetry $A_{33} = A_{11}$, $A_{44} = A_{22}$

Frequency (Hz)	C(T)	c(3)	398.5	1099
A_{11}	.2465	.7394	.9587	.7772
A_{22}	0	7.000	49.83	129.6
A_{33}	.2465	.7394	.9587	.7772
A_{44}	**0**	**7.000**	49.83	**129.6**

(e) Mode Shape Matrix

Frequency (Hz)	0(T)	0(R)	398.5	1099
$\sqrt{A_{11}}$	+.4965	+.8599	+.9791	+.8816
$\sqrt{A_{22}}$	+ 0	**-2.645**	**-7.059**	-11.38
$\sqrt{A_{33}}$	**i.4965**	-.8599	i.9791	-.8816
$\sqrt{A_{44}}$	+ 0	-2.646	+7.059	-11.38

Signs as for Table 4.7(d)

Table 4.8 (STR) Spatial Model of Short Beam

Output of program EMMAY with input data from Table 4.7(e)

Mass Matrix

$$[M_{SR}] = \begin{bmatrix} 1.62852 & .196059 & .399772 & -.0852701 \\ & .0313537 & .0852701 & -.0177016 \\ & & 1.62852 & -.196059 \\ \text{Symmetric} & & & .0313537 \end{bmatrix}$$

$$\sum M_{trans} = 4.056554 \text{ kg}$$

Stiffness Matrix

$$[K_{SR}] = 10^5 \begin{bmatrix} 15.0251 & 4.88288 & -15.0251 & 4.88288 \\ & 1.90138 & -4.88288 & 1.27231 \\ & & 15.0251 & -4.88288 \\ \text{Symmetric} & & & 1.90138 \end{bmatrix}$$

$$\sum K_{trans} = 0$$

Residual Stiffness Matrix

from Table 4.7(b)

Because of symmetry $K_{rs3} = K_{rs1}$, $K_{rs4} = K_{rs2}$

$$[K_{rs}] = 10^5 \begin{bmatrix} 442.478 & & & \\ & 1.50489 & & \\ & & 442.478 & \\ & & & 1.50489 \end{bmatrix}$$

Table 4.9 (STR) Development of ModeShape Matrix for Long Beam

(a) Modal Constants

output of program IDENT

Mode	1	2	3	4	5	6(residual)
Frequency (3)	0	85.91	236.8	464.2	767.4	5000
A_{11}	.4578	.4558	.4450	.3995	.2872	**54.88**
A_{22}	.7008	**5.000**	**14.24**	**26.82**	38.79	**8590**
A_{33}	.1775	.0232	.1881	.0918	.0012	**13.75**
A_{44}	.7005	**2.603**	.2505	**6.123**	18.85	2006

(b) Residual Stiffnesses

$$K_{rli} = \omega_6^2 / {}_6A_{ii} = (2\pi \times 5000)^2 / {}_6A_{ii}$$

$K_{rl1} = 179.824 \times 10^5$ N/m	$K_{rl2} = 1.14903 \times 10^5$ N/m
$K_{rl3} = 717.875 \times 10^5$ N/m	$K_{rl4} = 4.91884 \times 10^5$ N/m

(c) Separation of Rigid Body Modes

${}_1A_{11T} = .1144$	${}_1A_{11R} = .4578 - .1144 = .3434$
${}_1A_{22T} = G$	${}_1A_{22R} = .7008$
${}_1A_{33T} = .1144$	${}_1A_{33R} = .1775 - .1184 = .0631$
${}_1A_{44T} = 0$	${}_1A_{44R} = .7005$

Using equations of Table 4.1(b)

Table 4.9 continued

(d) Matrix of Point Modal Constants

Because of symmetry $A_{55} = A_{11}$, $A_{66} = A_{22}$

Frequency (Hz	C(T	C(R)	85.91	236.8	464.2	767.4
A_{11}	.1144	.3434	.4558	.4450	.3995	.2872
A_{22}	0	.7008	5.040	14.24	26.82	38.79
A_{33}	.1144	.0631	.0232	.1881	.0918	.0012
A_{44}	0 /	.7005	2.603	.2505	6.123	18.85
A_{55}	.1144	.3434	.4558	.4450	.3995	.2872
A_{66}	0	.7008	5.040	14.24	26.82	3E.79

(e) Mode Shape Matrix

Frequency (Hz)	O(T)	O(R)	85.91	236.8	464.2	767.4
$\sqrt{A_{11}}$	+.3382	+.5860	+.6751	t.6671	+.6321	+.5359
$\sqrt{A_{22}}$	+ 0	-.8371	-2.245	-3.773	-5.179	-6.228
$\sqrt{A_{33}}$	+.3382	-.2512	-.1523	1.4337	-.3030	-.0346
$\sqrt{A_{44}}$	+ 0	-.8370	+1.613	-.5005	-2.474	+4.342
$\sqrt{A_{55}}$	+.3382	-.5860	+.6751	-.6671	+.6321	-.5359
$\sqrt{A_{66}}$	+ G	-.8371	is.245	-3.773	15.179	-6.228

Signs as for Table 4.4(d)

Table 4.10 STR Spatial Model of Long Beam

Output of program EMKAY with input data from Table 4.9(e)

Mass Matrix

$$[M_{LR}] = \begin{bmatrix} 2.40190 & & & & & \\ & .0985572 & -1.53284 & -.326770 & 1.72166 & -.425818 \\ & .425694 & -5.27879 & -1.10783 & 5.88821 & -1.43869 \\ & & 45.1140 & & & \\ & & & 2.37033 & -11.7661 & 2.88845 \\ & & & & 60.3773 & -14.6433 \\ \text{Symmetric} & & & & & 3.58592 \\ & & & 9.94157 & -50.1846 & 12.3780 \end{bmatrix}$$

$$\sum M_{trans} = (8.74284 \text{ kg}$$

Stiffness Matrix

$$[K_{LR}] = 10^5 \begin{bmatrix} 3.96883 & 1.94368 & 31.0199 & 7.60471 & -34.9888 & 8.41565 \\ & 1.15510 & 8.72279 & 2.53812 & -10.6665 & 2.51707 \\ & & 1271.70 & 220.634 & -1302.72 & 322.719 \\ & & & 40.5604 & -228.239 & 55.7966 \\ & & & & 1337.71 & -331.134 \\ \text{Symmetric} & & & & & 82.5475 \end{bmatrix}$$

$$\sum K_{trans} = 10^5(.00103) \simeq 0$$

Residual Stiffness Matrix

from Table 4.9(b)

Because of symmetry $K_{r15} = K_{r11}$, $K_{r16} = K_{r12}$

$$[K_{r1}] = 10^5 \begin{bmatrix} 179.824 & & & & & \\ & 1.14903 & & & & \\ & & 717.875 & & & \\ & & & 4.91884 & & \\ & & & & 179.824 & \\ & & & & & 1.14943 \end{bmatrix}$$

Table 4.11 (STR) Spatial Model of Coupled Beam

(a) Coordinates

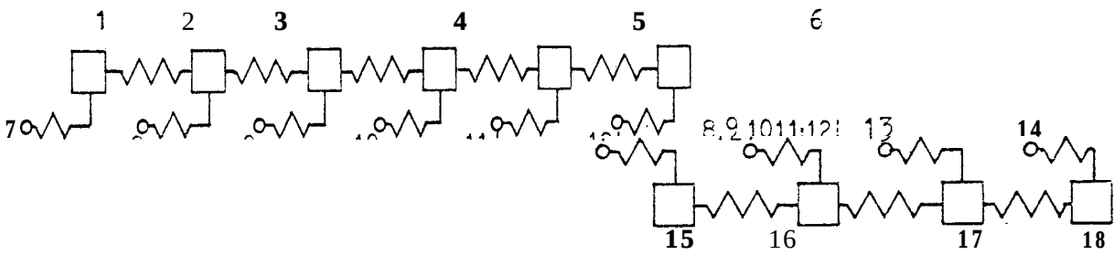

Tip Coordinates 7, 8 Junction Coordinates 11, 12

(b) Subsystem 1 Long Beam

$$[M_1] = \begin{bmatrix} M_{LR} & \\ 6x6 & \\ & 0 \\ & 6x6 \end{bmatrix}, \quad [K_1] = \begin{bmatrix} K_{LR}+K_{rl} & -K_{rl} \\ 6x6 & 6x6 \\ -K_{rl} & K_{rl} \\ 6x6 & 6x6 \end{bmatrix}$$

submatrices from Table 4.10

(c) Subsystem 2 Short Beam

$$[M_2] = \begin{bmatrix} 0 & 0 \\ 4x4 & 4x4 \\ 0 & M_{SR} \\ 4x4 & 4x4 \end{bmatrix}, \quad [K_2] = \begin{bmatrix} K_{rs} & -K_{rs} \\ 4x4 & 4x4 \\ K_{rs} & K_{SR}+K_{rs} \\ 4x4 & 4x4 \end{bmatrix}$$

submatrices from Table 4.8

(d) Predicted Natural Frequencies (Hz) (Error %)

j0.239	0.465	40.20	110.2	215.1	361.1	535.2	740.4
		(+.3)	(+.1)	(-.7)	(+.9)	(+.1)	(-.9)

plus 1040 , 1456 (anomalous) , output by program EIGEN

(e) Reduced Spatial Model for EIGEN Calculation

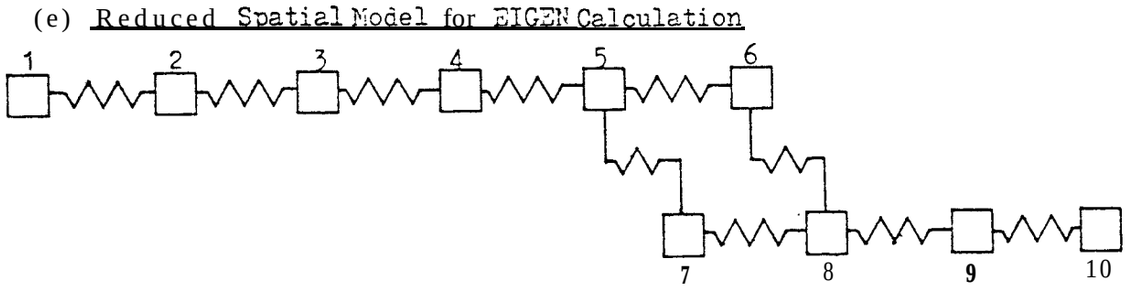

5. MEASUREMENT OF MOBILITY PARAMETERS

The theoretical tools necessary for the identification of spatial models were developed in Chepters 2, 3 and 4, the conclusions of which summarise the techniques available for use. This Chapter is concerned with the development of experimental tools for use in the modelling of physical structures. There is aemphasis on the measurement of rotational mobilities including the use of the derivation relationship of Chapter 2 to reduce the effects of errors. The errors of measurement arising from certain properties of accelerometers are also discussed, and renedies prescribed./

5.1 Established Mobility Measurement Techniques

5.1.1 Available Test Equipment

The available techniques for acquiring measured mobility data have been briefly discussed in Chapter 1. In the subsequent Chapters it was shown that successful identification of spatial models was founded on accurate values of frequencies, particularly antiresonances, and of response levels, especially of rigid body modes. While it is possible to get good measurements using transient techniques there is always difficulty in establishing within close tolerances the responses at low levels such as antiresonances and the low frequency rigid body nodes. The tine taken for tests to be carried out is not the most important criterion as it might be in commercial vibration investigations, SC for both these reasons stezdp-state sinusoidal testing is to be recommended.

The digital transfer function analyser (DTFA) equipments for steady state sinusoidal testing have the advantages of performing well at low levels and of quickly producing data that is easy to visualise and easy to check, thus facilitating the development process during which unfamiliar results have to be assessed. Two system based on DTFA principles were available in the Dynamics Section of Imperial College

Mechanical Engineering Department. These were both manufactured by Solartron Ltd.

The larger apparatus, the JX 3381 Programmable Frequency Response Analyser, consists of a JM 1600 Transfer Function Analyser with high frequency extension unit JX 1639 interfaced with a PDP8e minicomputer manufactured bytne Digital Equipment Company. Thesystem is controlled by programming the minicomputer via 2 teletypewriter, using the high level conversation21 language DYNAMIC FOCAL. The minicomputer is also interfaced with peripheral equipment, 2 high speed tape reader, high speed tape punch and an XY graph plotter. Electronic signals originating in the TFA oscillator are amplified in a power amplifier and applied to an electromechanical shaker which applies force to the test structure. Signals from piezoelectric force gauges and accelerometers mounted on the structure are taken through charge amplifiers before being input sequentially tc the TFA Correlator which has ten input channels available. A block diagram of the whole systen is shown 2s Figure 5.1.

The smaller apparatus is transportable 2nd consists mainly of the microprocessor-controlled 1172 TFA which is nore compact than the JM 1600 + JX 1639. It has only two input channels, sufficient for one input force 2nd one input acceleration. Linear or logarithmic frequency sweeps can be programmed by touch buttons. The output level of the oscilletor has to be preset 2nd there is no provision for the setting of limits on oscillator voltage, force level or response level which is a feature of the nore versatile JX 3381. The measured data can be output in the form of the level of either input channel with respect to the initial oscillator sign21 or the ratio of inputs. These data can be expressed in Cartesian or polar form and in the latter case the modulus may be linear or logarithmic. They are displayed digitally, together with the frequency, 2nd they may be stored on tape or printed by use of the attached peripheral devices. Data stored on tape can, if necessary, be processed after the test by using the PDP8 computer and its peripherals.

The shaker can be floor- or table-mounted or supported on pivots by a crane so that it can be aligned to apply force in any direction to the structure under test. This structure will have accelerometers mounted et specified coordinates for detection of response and will have one force gauge to which a push-rod is connected. The push-rod, typically 2 steel wire1mm diameter, 25 mm long, allows transmission of axial force without imposition of significant rotational restraint. In many cases the test structure is to be freely supported. Such 2 free support is obtained to a good approximation by use of soft rubber cords.

Mobility testing in general has been comprehensively described by Ewins [4] who has also written a handbook [86] for the JX 3311 mini-computer controlled facility. Silva [9] has provided 2 description of both sets of Solartroc equipment available in the Imperial College Dynamics Section together with 2 discussion of measurement and calibration procedures. An earlier work by Sainsbury [31] gives details of multidirectional nobility measurement methods. These are based on the use of 2 single shaker together with an 'exciting block' on to which accelerometers could be connected and through which forces and torques could be applied to the test structure. This Chapter is principally concerned with the development of exciting block techniques for multi-direction21 measurements on smaller structures than Sainsbury tested.

5.1.2 Foint and Transfer Translational Measurements

The standard FOCAL program MOB2 [86] is used for making point and transfer translational measurements using the mini-computer controlled system introduced in the previous section. It features mass-cancellation for point measurements. The basic configuration 2nd mathematical relationships are outlined in Figure 5.2. As many response transducers can be used as are desired up to the channel selector limit (10).

Similar inertance data can be obtained by using the 1172 DTFA but in that case mass cancellation has to be done by processing taped data after the test run is complete. Program IDENT has a facility for reading a 1172 coded tepe, de-coding it 2nd carrying out mass-cancellation. if desired the data so transformed can be output on tape, printed or plotted. With either equipment, it is not possible to cancel completely the effects of the added mass of the transfer accelerometer(s) so it is always desirable to choose as small a transducer as possible to fulfil such a rôle.

5.1.3 Point Translational and Rotational Measurements

The point mobility matrix involving translation and rotation can be found by attaching an exciting block equipped with two accelerometers to the test structure and then carrying out two identical frequency sweeps for excitation at two different points on the block. The tests are controlled by the JX 3381 system mini-computer with the standard FOCAL program PM2/1. The test configurations and mathematical relationships are presented in Figure 5.3. The inertial effects of the exciting block and its attachments are cancelled in the processing of the data, the equation having a similar form to the simpler one-dinecsional mass-cancellation of program MOB2.

5.2 Development of Rotational Mobility Measurement

The design of exciting blocks is here considered, progressive modificatioos being made in the light of experience obtained in the measurements on beams reported in Chapter 6. The derivation relationships of the modal model reported in Chapter 2 are applied to simplify the process so that the four elements of the point mobility matrix can be determined from measurements of only two.

5.2.1 Design of Exciting Blocks

The bases of the exciting block method were laid by Sainsbury (31) who developed four relatively large blocks and used them for tests on engine foundations and other massive structures, including the 135 kg assembly later used by the author in the cantilever tests on a turbine blade reported in section 7.2. Owing to a lack of communication, the author began his series with Block Mark 4 which now has the extra identification 'G' to distinguish it from Sainsbury's block of the same mark number.

The blocks described are all designed for use with program PM2/1 asd therefore to provide points of attachment for two accelerometers of standard 'general-purpose' size typified by the Endevco 233E equidistant from the datum point. There also has to be provision for two mounting positions for the force gauge, the Bruel and Kjaer 8200 type.

Block Mark 4G

This block was designed with the intention of being as small and as light as possible consistent with the outline specification above. The material used was dural and as can be seen fron Figure 5.4, the transducers are separated by 25 mm between centres, as close as is practicable without interference of their projecting electrical connections. In the first position of the force gauge the input excitation passes through the datum point P, in the second position there is an offset of 50 mm and a corresponding input torque. The height of the block was chosen to permit the mounting of transducers for the input of horizontal force and the neasurenect of horizontal acceleration, features which have not been used. The width of the bloc-4 was set at 25 mm to match (nearly) the width of the first test structures, the Long and Short Beams of Chapter 6. The block was intended to be attached to the test structure by means of adhesive - usually 'Plastic Padding', sometimes strain gauge adhesive.

Block Mark 4G is equivalent to a beam 96 mm long and 32 mm deep and;! es can be deduced from the data of Figure 5.1 will have its first bending node of vibration at about 18 kHz, well above the maximum intended to be used. It was, therefcre, expected to be adequately stiff despite the reduction in natural frequency expected when the block was loaded by the mass of the acceleromaters.

Program PM2/1 calls for the inertial properties of the block + accelerometers including the location of the centroid, G, and the mass moment of inertia about it, I_G, as well as the total mass, m. These quantities could be estimated theoretically but they were also checked experimentally. The location of the certrcid was found for each block systes by balancing about two axes. Subsequently, the block was supported by a bifilar suspension so that the period of small oscillations could be measured and the result related to the length of the cords by the formula:

$$k^2 = \frac{I_G}{m} = \frac{T^2}{L}\left|\frac{gl^2}{16\pi^2}\right| \qquad (5.1)$$

where k = radius of gyration
T = period of oscillation
L = length of support cords
g = 9.81 m/s^2
l = distance of separation of cords = length of block

The 'best' value was obtained from the slope of the graph of T^2 against L.

This block was used for the tests at a point on the Long beam reported in section 6.2.1. These results were poor, especially for the rotational quantity ($\dot{\theta}/M$). The rotational insut 2nd output signals were estimated in section 5.3.1 and found to be very small in comparison with their translational equivalents. Accordingly, a new design was sought which would increase rotational signals.

Block Mark 5

This block is specified in Figure 5.5. The accelerometer offset, s, is doubled to 50 mm and the two force gauge locations set to be $\pm$50 mm also, this arrangement being possible because the transducers could be mounted back to back and share a comon mounting stud. The 'skirts' of the block were set at 6 mm in order to give it adequate stiffness. The block at 30 mm was slightly wider than the test bean. Block Mark 5 was used extensively in measuring the four nobility parameters of the beams. *hs* before, the rotstional quantities were obtained less accurately than the translational with $(\dot{e}/M)$ generally being poor, especially at low frequencies. Two factors were significant:

(2) The transverse sensitivity of the accelerometers gave rise to signals comparable to the small difference Signals associated with θ measurement shown in the tests of section 6.2.2 and 5.3.2; 2nd

(b) There was direct interference between the force gauge and the 2cceleroneter when the transducers shared a comon mounting stud.

The first factor could be minimised by selecting accelerometers with a transverse sensitivity about 1%. The second factor was to be corrected by producing a new design of block.

Block Mark 6

The chief feature of this design is the offset between the lines of action of the input force et $\pm$ 50 mm and axes of the accelerometers at $\pm$ 44 mm. The 'skirts' have been omitted as Figure 5.6 shows, but adequate stiffness is maintained by the top-section having increased depth. This block was used in the tests on Long and Short Beam reported in section 6.3.1 and summarised in the paper by Ewins & Gleeson [84]. Modal modelling and derivation developed for this purpose in section 5.2.2 were used as one method of reducing the effects of $(\dot{e}/M)$ errors. The principal source of these errors was identified as base strain sensitivity in accelerometers. The experimental evidence for this conclusion is tabulated in section 5.3.3. Thus ultimately Block Mark 6 with

appropriate transducers is a satisfactory device for use in rotational mobility measurement. The later designs of exciting block have the same basic features bat they were designed for specific applications.

Block Mark 7

The tests on the turbine blade resorted in section 7.2 were made using the two part block shown in Figure 5.7. Part B being a cube of side 30 mm was machined tc fit closely over the fir tree root of the blade. Part A was 2 beam with locations provided for two accelerometers and one force gauge 2s usual. There was a slot 30 mm by 2 mm deep milled in pert A so that it could be attached tc part 3 in a variety of configurations for the stimulation of different responses.

Block Mark 8

The idea of the two part block was extended in this design sc that several interchangeable components could be used according to the shape of the test piece. The basic beam, part A, has a shallow central notch, as seen in Figure 5.8. A second part of the beam - 2 'foot' shaped to the test structure, could then be inserted 2nd secured by adhesive. One minor defect of Block Mark 6 when used with beams is that the measurement point P cannot be sited at the end of 2 Sear but has to be 2 few millimetres inboard. The 'end foot' for use with Block Mark 8 does allow P to be placed exactly at the end of the test beer;. There is also a 'mid foot' for use on a flat surface.

There would be no difficulty and little expense in designing special feet for particular test structures. Three Blocks of the Mark 8 pattern were used in the tests cf section 7.1 which mark the culmination of this phase of the work.

appropriate transducers is a satisfactory device for use in rotational mobility measurement. The later designs of exciting block have the same basic features but they were designed for specific applications.

Block Mark

The tests on the turbine blade resorted in section 7.2 were made using the two part block shown in Figure 5.7. Part B being a cube of side 30 mm was machined to fit closely over the fir tree root of the blade. Part A was a beam with locations provided for two accelerometers and one force gauge as usual. There was a slot 30 mm by 2 mm deep milled in part A so that it could be attached to part B in a variety of configurations for the stimulation of different responses.

Block Mark 8

The idea of the trio part block was extended in this design so that several interchangeable components could be used according to the shape of the test piece. The basic beam, part A, has a shallow central notch, as seen in Figure 5.8. A second part of the beam - a 'foot' shaped to the test structure, could then be inserted and secured by adhesive. One minor defect of Block Mark 6 when used with beams is that the measurement point P cannot be sited at the end of a beam but has to be a few millimetres inboard. The 'end foot' for use with Block Mark 8 does allow P to be placed exactly at the end of the test beam. There is also a 'mid foot' for use on a flat surface.

There would be no difficulty and little expense in designing special feet for particular test structures. Three Blocks of the Mark 8 pattern were used in the tests of section 7.1 which mark the culmination of this phase of the work.

5.2.2 Use of Modal Modelling

The mobility matrix involving translation 2nd rotation et a point cm be measured by use of an exciting block with two accelerometers 2nd carrying out two tests with different input force considerations as was noted in section 5.1.3. If the parameters of the 2 x 2 matrix are expressed in modal terms their inter-relationship offers the possibility of simplifying the necessary measurements. The concept was mentioned briefly in section 2.2.2(iv) and is here treated nore fully.

The derivation relationship of equation (2.24) lead to the observatioo that all the elements cf a square matrix of related modal constants can be found from knowledge of one row or one column. In the particular case we are considering here it is qnacticable tc measure 2nd identify response data for the first row or first column of the point mobility matrix. If two accelerometers are used it is possible to measure $\ddot{X}$ and $\ddot{\theta}$ and thus one run with force input along the X coordinate will give the data corresponding tc the first column of the matrix. Conversely, it is also possible to measure $\ddot{X}$ with one accelercseter but to provide two excitation patterns involving force and moment and thus give the data of the first row of the matrix. Either method has the advantage that the exclusively rotational quantity $(\dot{\theta}/M)$ does not have to be measured directly.

The Two-Accelerometer Method of Measuring the Point Mobility Matrix

This method is summarised in, Figure 5.9. The input from the shaker is applied through the force gauge tc the middle of the exciting block, 2nd the resultant angular and translational motion can be deduced from the indications of the symmetrically placed 2cceieroneters. If the mini-computer-controlled system is used only one test run needs to be made using program MOB2, three input channels being required.

The Solartron 11'72 equipment can also be used effectively, but two runs are necessary because only two input channels are available. Since this equipment is sost conveniently used to search for the resonances

and antiresonances which are different for each accelerometer/force gauge combination there is no significant resulting handicap because of the change in electrical connection. No change in the mechanical configuration of the system is needed throughout.

The symmetrical mounting of the accelerometers and the central position of the force input result in a minimal base strain effect (discussed below in section 5.3.3). The errors due to transverse inputs (discussed in section 5.3.2) are likely to have more effect than in the Single-Accelerometer method, although this is unlikely to be significant if accelerometers with low transverse sensitivity are chosen.

It should be noted that this method of testing will give no rotational information if the test piece is symmetrical about the X axis through the centre of the exciting block. This situation is not often encountered although it is possible that the rotational signals for certain test pieces might be rather small.

The Single-Accelerometer Method of Measuring the Point Mobility Matrix

The arrangements for each of the two test runs necessary are indicated in Figure 5.10. The measurements can be made using program MOB2 with the JX 3381 system but it is particularly suited to the 1172 equipment since only two channels are required. The use of only one accelerometer simplifies the precautions needed to minimise accelerometer transverse response (section 5.3.2) but increases the risk of inaccurate measurement of antiresonances since these are frequencies at which the force input is a maximum. They are thus also frequencies of maximum strain in the exciting block which can give rise to errors in the accelerometer output if it has significant base strain sensitivity (section 5.3.3). In many applications, it might be possible to avoid base strain effects altogether by mounting the accelerometer on the test piece itself rather than on the exciting block, as shown in Figure 5.10(c).

A feature of the single-accelerometer method of test is the obligation to change the mechanical configuration of the system between Run 1 and Run 2 by moving the force gauge and realigning the shaker.

Processing the Measured Data

The equations:

$$\left.\begin{aligned} Y_{XX} &= (Y_A + Y_B)/2 \\ Y_{eX} &= (Y_A - Y_B)/2s \end{aligned}\right\} \quad \text{(i) of Figure 5.9} \qquad (5.2)$$

and

$$\left.\begin{aligned} Y_{XX} &= (Y_1 + Y_2)/2 \\ Y_{Xe} &= (Y_1 - Y_2)/2e \end{aligned}\right\} \quad \text{(iv) of Figure 5.10}$$

are very similar. The first pair (5.2) will suit both methods provided that e is interpreted as the offset of the force gauge from the line through the test point P in the 'single-accelerometer' method and as the offset of both accelerometers in the 'two-accelerometer' method.

Identification

The measured data for Y_{XX} and Y_{eX} (or Y_{Xe}) must be converted to modal form before that for Y_{ee} can be derived. The identification process is most accurate when the response data used in the calculation are based on antiresonances (section 2.1.2). However, since Y_{XX}, Y_{Xe} or Y_{eX} are not measured directly* their antiresonances are not known. It is, therefore, sensible to carry out the identification calculations directly on the measured quantities Y_1, Y_2 of equation (5.2) whose antiresonances can be observed experimentally.

The following development shows that equation (5.2) and the derivation of Y_{ee} can be carried out mode by mode:

Define
$$R_r = (1 - \omega_r^2/\omega^2) \qquad (5.3)$$

where ω_r is the resonance frequency for which the modal constant for Y_1 is $_rA_1$.

---

* but see section 7.1 where direct indication was contrived by modification of program MOB2.

Thus, at a particular frequency :

$$Y_1 = \sum_{r=1}^{n} {}_rA_1/R_r \quad ; \quad Y_2 = \sum_{r=1}^{n} {}_rA_2/R_r \tag{5.4}$$

It must be remembered that the resonance frequencies ω_r and consequently the values of R_r are the same for Y_1, Y_2, Y_{xx}, Y_{xe}.

so for the point translational mobility:

$$\begin{aligned} Y_{xx} = \tfrac{1}{2}(Y_1 + Y_2) &= \tfrac{1}{2}\left\{{}_1A_1/R_1 + {}_2A_1/R_2 + {}_3A_1/R_3 + \ldots\ldots\ldots\right\} \\ &+ \tfrac{1}{2}\left\{{}_1A_2/R_1 + {}_2A_2/R_2 + {}_3A_2/R_3 + \ldots\ldots\ldots\right\} \\ &= \tfrac{1}{2}\left\{({}_1A_1 + {}_1A_2)/R_1 + ({}_2A_1 + {}_2A_2)/R_2 + \ldots\ldots\right\} \\ &= \sum_{r=1}^{n} {}_rA_{xx}/R_r \end{aligned} \tag{5.5}$$

where $${}_rA_{xx} = ({}_rA_1 + {}_rA_2)/2 \tag{5.6}$$

Similarly $$Y_{xe} = \sum_{r=1}^{n} {}_rA_{xe}/a_r \tag{5.7}$$

where $${}_rA_{xe} = ({}_rA_1 - {}_rA_2)/2e \tag{5.8}$$

and derived $$Y_{ee} = \sum_{r=1}^{n} {}_rA_{ee}/R_r \tag{5.9}$$

where $${}_rA_{ee} = ({}_rA_{xe})^2/{}_rA_{xx} \tag{5.10}$$

In the case of rigid-body motion ($\omega_1 = 0$) the derivation equation for ${}_1A_{ee}$ requires special development, as indicated in section 2.2.3.

Inertia Cancellation

The mobility parameters Y_{xx}, Y_{xe}, Y_{ex} and Y_{ee} as determined above are properties of a complete system, C, which consists of the test piece, A, to which is coupled the exciting block, 3. The system C will have resonance frequencies different to those of the test piece alone. The effects of the block must be removed by inertia cancellation.

The basic relationships can be expressed in terms of impedance $[Z]$:

$$[Z_C] = [Z_A] + [Z_B] \quad (5.11)$$

Therefore $$[Z_A] = [Z_C] - [Z_B] = [Y_C]^{-1} - [Z_B] \quad (5.12)$$

Then $$[Y_A] = [Z_A]^{-1} \quad (5.13)$$

At the end of the identification/derivation process the mobility parameters from which the elements of $Y_{C_{ij}}$ can be calculated at any frequency will be available. The appropriate impedance matrix for the exciting block, $[Z_B]$, may be found from measurement or calculation of its inertial properties. It is not necessary to assume that the block is infinitely stiff, although such an assumption will normally be justified. Compensation for the effects of block flexibility is possible by using, frequency by frequency, the dynamic properties of the block considered as a beam in program COUPLE1, but the calculations are cumbersome and best avoided.

Program INCAN

This program for use with the PDP8/e minicomputer system has been developed to carry out full inertia cancellation and other calculations outlined above. It will accept as input data the inertia parameters of the exciting block, together with the data for $[Y_C]$ in modal form or in the form of a series of values constituting a frequency response. The output data for $[Y_A]$ can be plotted on a graph, listed or punched on to paper tape. Where the data for $[Y_C]$ is in modal form, the program enables searches for resonances and antiresonances of the test piece alone to be made.

Program INCAN shares several 'groups' or subroutines with program IDENT, particularly those concerned with input, output and transformation of data. It calculates the 2 x 2 point mobility matrix and also the determinant and norm* of that matrix at each frequency. The norm is a

---

* Norms are classified in Appendix A5.

well-conditioned indicator of the singularity of the matrix of a freely-supported body which occurs when the frequency is a cantilever frequency*. A flow chart of the main segment of INCAN is presented in Appendix X2.

5.3 Errors in the Measurement of Rotational Mobility

Conventional accelerometers are sensitive to translational accelerations and so measurements of rotation can only be made by determining the difference between the outputs of two accelerometers. The following sections are concerned with the overall low level of rotational, as compared to translational, acceleration components; with the errors due to transverse sensitivity, and with the errors arising from base strain effects.

The nature of the problem can be illustrated by reference to Figure 5.11 which shows the measured nobilities at a point 0.4 m along the 1.4 m Long beam, one of the test pieces featured in Chapter 6. The point translational response ($\dot{X}/F$) is shown compared with the ideal in Figure 5.1 I(a). The agreement is quite close. On the other hand, Figure 5.11(b) illustrating the rotational mobility ($\dot{\theta}/M$) shows good agreement only near resonances, and poor agreenent elsewhere, the measured data shoving systematic rather than random error. The cross responses ($\dot{x}/M$) and ($\dot{\theta}/F$) which are not shown were of intermediate accuracy.

5.3.1 Low Excitation and Response

An estimate of the relative sizes of rotational and translational quantities can be made by considering the geometry of the test configuration fcr measurement of the point mobility matrix shown as Figure 5.3.

---

* The prediction of Cantilever frequencies is summarised in section 7.2

The magnitude of the input torque F.e applied by the shaker is restricted by the relatively short lever arm of effective length e. The rotational acceleration response is controlled in its turn by the distance s from each accelerometer tc the reference point, P.

$$(\ddot{\theta}/M) = \{(a_A - a_B)/2s\}/F.e \qquad (5.14)$$

whereas the translational acceleration response is given by:

$$(\ddot{X}/F) = \{(a_A + a_B)/2\}/F \qquad (5.15)$$

The ratio of rotational to translational quantities can be written:

$$R/T = \frac{(a_A - a_B)}{(a_A + a_B)} = s.e \frac{(\ddot{\theta}/M)}{(\ddot{X}/F)} \qquad (5.16)$$

The responses $(\ddot{\theta}/M)$ and $(\ddot{X}/F)$ have resonances et the same frequencies but otherwise have different frequency response characteristics. The r a t i o tends to infinity in the vicinity of antiresonances of $(\ddot{X}/F)$ 2nd to zero at antiresonances of $(\ddot{\theta}/M)$. Away fror these singularities the ratio is generally quite small. Worst-case values are found for low frequency vibrations dominated by rig-id body modes. In such 2 frequency range the R/T ratio is fairly constant 2s frequency varies and is determined by the effective (mass moment of inertia)/(mass) ratio.

Example 1 Tip of Short (0.65 m) beam at 25 Ez:

$R/T = 17.1 \times 10^{-3} \simeq 1:60$

Example 2 Point 0.4 m along Long (1.4 m) beam

$R/T = 7.07 \times 10^{-3} \simeq 1:140$

The lower ratio indicated fcr the second example can be explained in terns of the larger mass moment of inertia of the longer beam 2nd the smaller rotational response which results when the excitation is towards the centroid rather than et the tip of the been. This type of test piece then may be considered tc give rise to a rotational signal about 1% of the translational signal. Signals of the order of 1 to 6% of the translational signal can arise from transverse sensitivity of accelero-meters, a source of error discussed in section 5.3.2.

5.3.2 *Transverse* Sensitivity of Xcceleroneters

The 'transverse' or 'cross' sensitivity of piezoelectric accelerometer arises because of unavoidable misalignment in manufacture which has the effect that the axis of maximum sensitivity of the sensing element has a small component, T_N, *in* a direction perpendicular to the geometricaxisof the transducer. The situation is sketched in Figure 5.12(a) in which theangle β is greatly exaggerated for clarity. T_N usually lies between 1% and 6%, the corresponding values of β being in the range 0.6° to 3.4°.

As the accelerometer is rotated through angle θ about its main axis, the vector of maximum sensitivity describes 2 cone shown in plan and in elevation as Figures 5.12(b) and (c). If there is constant transverse excitation along the axis XX^1 the apparent transverse sensitivity, T_A, of the aoceleroreter varies in magnitude as θ is varied:

$$T_A = T_N \cos \theta \qquad (5.17)$$

where $$T_N = \tan \beta \qquad (5.18)$$

This gives rise to the double-circle polar response shown as Figure 5.12(d). From this it is clear that if the acceleroneter can be aligned so that its direction of maximum cross-sensitivity is orthogonal to the direction of excitation then there will be no error signal caused by this ezcitatior.

In order to assess the possibility of rotational measurement accuracy being impaired by the transverse sensitivity limitations of the transducers, some evaluations of $(\dot{e}/M_\theta)$were made using the established method with program PM2/1 of section 5.1.5. The only quantity varied in these tests was acceleroneter orientation. The results showed marked differences in systematic error and thus established transverse sensibility of accelerometers as a major source of this type of error. The subsequent investigation reported here was an attempt to minimise errors caused by transverse sensitivity.

Proposed Method for Reduction of Transverse-Sensitivity Errors

The two accelerometers mounted on the exciting block should be arranged with their directions of maximum positive transverse sensitivity parallel to each other so that any transverse excitation produces an error signal in one accelerometer which is in phase with that in the other, thus producing the minimum error in the difference quantity $(a_A - a_B)$ upon which rotational measurements depend. The sum quantity $(a_A + a_B)$ will be subject to an increased error which will, however, be negligible in proportion since $(a_A + a_B)$ is typically two orders of magnitude greater than $(a_A - a_B)$, 2s shown in section 5.3.1.

If transverse excitation occurs in only one direction which can be identified then the parallel directions of maximum transverse sensitivity should be at right angles to this. The proposed arrangement is shown in Figure 5.13.

The directions of maximum transverse sensitivity with respect to the accelerometer body, where not specified by the manufacturer, can be found by oeasurenent of transverse response.

Measurement of Polar Response of Accelerometers subject to Transverse Excitation

Elaborate apparatus has been developed by manufacturers for the measurement of accelerometer transverse sensitivity [87][88][89][90] In order to obtain data quickly, a single nodificatioo was made to the standard laboratory calibration syster based on 2 cylindrical steel 10 kg mass. The arrangements are sketched in Figure 5.14 in which it can be seen that the accelerometer mounted on a subsidiary block could be excited at right angles to its main axis of sensitivity and could be secured at any angle about that axis. Zero angle corresponded to alignment of the accelerometer electrical connector with the axis of excitation. The angle θ was incremented by 45° between measurements; a complete polar plot thus being obtained with eight readings.

Polar Responses of Accelerometers

Examples of the polar response of a Birchall accelerometer of nominal transverse sensitivity 6% are shown 2s Figures 5.15, 5.16 2nd 5.17. The first two Figures show clearly two lobes of similar magnitude with 2 minimum response direction orientated at 13° to the datum. The third, resulting from a re-test, is not clear, having only one dominant lobe.

When an Endevco accelerometer of nominal transverse sensitivity 2% was similarly tested the resultant polar response shown as Figure 5.18 is single-lobed with no clear orientation. The indicated transverse response is about 9%, larger than anticipated. There is no clear indication of a direction of minimum sensitivity.

Discussion of Polar Response Measurement

The anomalous results obtained for the Endevco accelerometer and the re-tested Birchall accelerometer indicate that the excitation received by the transducers was riot entirely transverse, the simple rig of Figure 5.14 perhaps allowing some rotational input in 'rocking-' of the 10 kg mass. This effect would be frequency dependent 2s Figure 5.15, showing Birchall raw data, indicates. The differences between Figures 5.15 2nd 5.17 for the same accelerometer in different tests indicate that 2 significant variable factor was not controlled when the 2pparatus was set up. Thus further analysis was carried out.

The Effect of Misalignment upon Transverse Sensitivity

The concepts of Figure 5.11 are modified in Figure 5.19 to include the misalignment of the geometric axis of the accelerometer with respect to the normal to the XX^1 direction of excitation. Thus the cone swept out by the vector of maximum sensitivity itself has an angle α measured from the Z axis. The projection of the circle of Figure 5.11(b) upon the XY plane becomes an ellipse as shown in Figure 5.19(a). Point Q traverses this ellipse as the angle e is varied and the projection of OQ on the XX^1 axis has a greater negative maximum than positive giving a polar diagram with unequal lobes as in Figure 5.19(c). The apparent transverse sensitivity is given by:

$$I_A = (T_N \cos \theta - \tan\alpha) \cos\alpha \qquad (5.19)$$

which degenerates into equation (5.17) when α is set to zero. It can be seen that if $\alpha > 0$ the polar response will be asymmetrical and if $\alpha \geq \beta$ this response will show no phase reversal. It is evident that the angle α was not effectively kept constant in the foregoing tests. Since polar plots which indicate the direction of minimum transverse sensitivity are only to be obtained when $\alpha << \beta$ and β for an accelerometer with 2% transverse sensitivity is only 1.15' it is evident that care must be taken to keep α very small. In practice the angle α depends on the alignment of the exciting block with the test structure and in turn on the alignment of the accelerometer to the exciting block. Particular care must therefore be taken if a hole is tapped for stud mounting of the accelerometer.

Analogue Computer Simulation of Polar Response Model

Equation (5.13) can be rewritten:

$$T_A = T_N \cos\alpha \cos\theta - \sin\alpha \qquad (5.20)$$

T_N andd are to be specified and θ is to run through all values 0 to 2π. It is convenient to make $\theta = \omega t$, a continuously increasing angle, so that sin ω tandcosωt can be generated by a simple oscillator circuit.

Since the polar response of T_A versus θ is required, write:

$$X = T_A \cos \theta = (T_N \cos \alpha) \cos^2 \theta - (\sin \alpha) \cos \theta$$
$$Y = T_A \sin \theta = (T_N \cos \alpha) \cos \theta \sin \theta - (\sin \alpha) \sin \theta \quad (5.21)$$

writing $T_N \cos \alpha = A$ and $\sin \alpha = B$ we get

$$\left.\begin{aligned} X &= A \cos^2 \omega t - B \cos \omega t \\ Y &= A \cos \omega t \sin \omega t - B \sin \omega t \end{aligned}\right\} \quad (5.22)$$

An analogue computer was programmed as shown in Figure 5.20 to simulate equations (5.22) and theoretical plots of polar response for various values of α are shown as Figure 5.21 for which $T_N = 6\%$, corresponding to the nominal transverse sensitivity of the Birchall accelerometer and Figure 5.22 for which $T_N = 2\%$ as for the Endevco transducer. Clearly these plots have the same essential nature as the puzzling plots of Figures 5.17 and 5.18 and thus indicate that mechanical misalignment of even 1° or 2° of the axis of sensitivity from the normal to the excitation direction is sufficient to produce a gross anomaly. Paradoxically, the better transducer is more sensitive to disturbance, although it is less sensitive to transverse excitation.

Evaluation of Proposed Method of Reducing Transverse Sensitivity Errors

The polar measurements made on the two Birchall accelerometers yielded clear indications of their axes of minimum sensitivity. Accordingly they were mounted on the top of Block Mark 5 and oriented so that these axes were coincident with the long axis of the block. The result of a measurement of $(\dot{e}/K)$ is shown as Figure 5.23. There is still evidence of systematic error, especially in the region below the first resonance. There is a slight improvement in the fit to the theoretical response between the first resonance and the second antiresonance immediately following but the overall accuracy is not satisfactory,

Mobility Measurements using Accelerometers of Low Transverse Sensitivity

The Birchall accelerometers used in the test reported above were removed 2nd replaced by two of Endevco manufacture. Since their axes of maximum transverse sensitivity were unknown for reasons which have been explained above they were connected tc the exciting block with random orientation. The result for the difficult ($\dot{e}/M$) measurement is shown as Figure 5.24 which is scarcely more accurate than those seen before but the inaccuracy is of a random rather than systematic nature. Such errors may potentially be reduced by averaging the results of several tests.

Conclusion: Transverse Sensitivity of Accelerometers

The response of accelerometers to transverse excitation is a source of error in rotational measurements which can best be reduced by using accelerometers of the lowest transverse sensitivity available, taking care over their alignment and reducing transverse inputs if possible.

5.3.3 Base Strain Effects in iccelerometers

Introduction

As a result of the investigation reported in section 5.3.2 accelerometers of very low transverse sensitivity (< 2%) were specified for any further measurements of rotational nobilities using exciting blocks.

Early experience of applying the 'single-accelerometer' method of section 5.2.2 was encouraging, the first tests being carried out on a 0.65 m beam of rectangular section - the Short bean. This showed a generally good comparison between theoretical and measured data although with 0.43 dB (5%) discrepancy in the rigid body low frequency response which was treated as insignificant. A later test on 2 1.4 m beam - 'the Long Beam -of the same section to that used earlier gave similar results but with a larger discrepancy of 2 dB (25%) at low frequencies. The next test piece used was a rectangular frame foned by welding

together two 0.65 m and two 1.4 m beams, and when this was the subject of a 'single-accelerometer' measurement, the error at low frequencies was 4 dB (60%). In each case, the measured response was higher than that predicted theoretically. The trend to larger errors for bigger test pieces was disquieting since it was intuitively thought that errors should reduce as the exciting block became smaller in comparison with the test item.

Test Configuration

In order to obtain more data about the discrepancies described above, the exciting block (Hark 6) was attached to the Long Beam with accelerometers and force gauge located as shown in Figure 5.25. This was a standard 'single-acceleroneter' set-up with the addition of a second accelerometer (3) attached to the beam by means of a mounting stud, itself stuck to the beam with 'Plastic Padding' adhesive. This adhesive was also used to secure the exciting block to the beam. Accelerometer (A) was attached to the top of the block so that the accelerometers shared a common axis. The method of attachment of accelerometer A was changed during the course of the tests reported below.

Tests on Endevco Accelerometers

Accelerometer A Screwed to Block

Accelerometer A was attached to the top of the block by means of a grub screw, its base being directly in contact with the block surface. Accelerometer B was connected to the test beam as indicated in Figure 5.25. Both transducers were Endevco Type 233E.

Mobility tests were carried out using program MOB2 with the beam supported 'free-free' on rubbers and excited by a shaker via a push rod for a range of frequencies between 10 and 1000 Hz. The data obtained were processed and it was found that the mobility measurements made with the accelerometer mounted directly on the beam (B) were quite accurate

whereas those for the accelerometer on the block (A) were in error, most noticeably at low frequencies where the rigid-body motion dominated. Subsequently, attention was paid to the ratic of the outputs of the two accelerometers, which quantity was available as a 'transmissibility' from the standard version of MOB2. The transmissibility $(\ddot{X}_A/\ddot{X}_B)$ was recorded for a number of different excitation configurations indicated in Figure 5.25.

Complete frequency responses of $(\ddot{X}_A/\ddot{X}_B)$ are presented in Figure 5.26. The response of the system at 31.62 Hz is dominated by the rigid body mode, and it was taken as a typical point of the low frequency region. Varying tests were carried out at this frequency. Figure 5.27 is based on data obtained in these tests and it shows tine dependence of the output ratic (which is essentially a measure of error in the reading of accelerometer A) upon the distance e, the offset of the force gauge from the accelerometer axis.

Figure 5.26(a) is typical of several frequency responses showing the error of accelercneter A. It has the feature that the error is zero at 84, 230, 440 and 770 Hz which are resonance frequencies of the block/beam combination. The largest errors occur in the regions around 60, 190, 400 and 660 Ez, which are regions of antiresorance of the inertance $(\ddot{X}/F)$ of the combination, Between a resonance and the nezt highest antiresonance the ratio is approximately constant, and has its largest value below the first antiresonance, in the region dominated by the rigid body mode. The apparent mass, $(F/\ddot{X})$, fcr the tip of the test beam is shown es Figure 5.28. Its similarity to Figure 5.26(a) is very close, and leads tc the supposition that the error is directly related to the apparent mass of the test object.

The error Plotted in Figure 5.26(a) is positive except In regions of antiresonance. This means that it is the accelerometer mounted on the block which generally has 2 higher reading.

Figure 5.27 shows the dependence of the error upon the offset of the force gauge, 2nd it indicates an approximately linear dependence, the error being greater than unity (0 dB) for both positive and negative offset. Itwas not possible tc carry out 2 test with zero offset but it is reasonable to infer from this Figure that in that case the error would be very small. The error is unlikely to be associated with tramverse sensitivity of the 2cceleroneters. In the test configurations used transverse inputs were likely tc be small 2nd the accelerometers were specially chosen because they had a transverse sensitivity of less than 1.5%. The error is very unlikely to arise because of flexibility in the 'Plastic Padding' adhesive. J.M.M. Silva reports[91] that the adhesive is more rigid than a bolt.

Accelerometer A Mounted on Isolating Stud

The grub screw used for the tests of the previous section was removed and replaced by an isolating stud attached to the topof the block with Philips strain gauge cement. A full frequency sweep test gave the results shown in Figure 5.26(b). This shows substantial reduction in error when compared with Figure 5.26(e). The large errors at 190 Hz and 660 Hz are not significant since these are frequencies of antiresonance fcr which the acceleration levels are very small. Examination of the actual mobilities (2s distinct fror their ratio) shows that the frequencies of antiresonance are found accurately using either accelerometer.

Accelerometer A Screwed to Modified Block

In order to isolate the base of accelerometer A from surface strain the block was modified by cutting a circular groove of inside diameter 14 mm and outside diameter 16 mm at the centre of the top surface cf the block. The accelerometer was secured at the centre of the 'moat' by using the same grub screw 2s had previously been used in the first section. The groove was initially cut to a depth of 2 mm ant the results

ofa full frequency sweep made with the block in this condition are shown in Figure 5.26(c). These results make it clear that the 2 mm groove reduces the error in accelerometer A indication considerably. The results shown in Figure 5.26(c) are not as good, however, 2s those of Figure 5.28(b). The depth of groove was increased to 4 mm 2nd the results of a subsecuent frequency sweep are shown in Figure 5.26(d) which is comparable to Figure 5.26(b) and may be regarded as satisfactory.

Tests on Bruel & Kjaer Accelerometers

The series cf tests/ using block Mark 6 attached to the 1.4 m beam were repeated when B & K 'delta shear' accelerometers of type $366 became available.

A full frequency sweep showed that the error for the 3 & K transducers was very much smaller than that for the Endevcos, having maxima of about + 1 dB at antiresonances (maximum values of apparent mass) and typical values around + 0.2 dB. This result is presented 2s Figure 5.29(a). Another sweep was made with the mounting Gf accelerometer changed from 2 grub screw to an isolating stud attached to the top of the block at point A with strain gauge cement. The result of this test is shown in Figure 5.29(b) which is not significantly different to Figure 5.29(a).

Further sweep tests were carried out with the block modified by the cutting of the'moat'. None of the results was appreciably different to those of Figure 5.29(a). It say be concluded that the use of an isolating stud or modification of the block by cutting 2 groove make no difference to the performance of B & K accelerometers of this type.

The foregoing observations lead to the suspicion that the errors associated with the accelerometer mounted on the exciting block are attributable to the effects of strain in the top surface of the block. The following development converts suspicion into conviction.

ofa full frequency sweep made with the block in this condition are shown in Figure 5.26(c). These results make it clear that the 2 mm groove reduces the error in accelerometer A indication considerably. The results shown In Figure 5.26(c) are not 2s good, however, 2s those of Figure 5.28(b). The depth of groove was increased to 4 mm 2nd the results of a subsequent frequency sweep are shown in Figure 5.26(d) which is comparable to Figure 5.26(b) and may be regarded as satisfactory.

Tests on Bruel & Kjaer Accelerometers

The series cf tests/ using block Mark 6 attached to the 1.4 m beam were repeated when B & 6 'delta shear' accelerometers of type 4366 became available.

A full frequency sweep showed that the error for the 3 & K transducers was very much smaller than that for the Endevcos, having maxima of about + 1 dB at antiresonances (maximum values Of apparent mass) and typical values around + 0.2 dB. This result is presented es Figure 5.29(a). Another sweep was maae with the mounting of accelerometer changed from 2 grub screw to an isolating stud attached to the top of the block at point A with strain gauge cement. The result of this test is shown in Figure 5.29(b) which is not significantly different to Figure 5.29(a).

Further sweep tests were carried out with the block modified by the cutting of the 'moat'. None of the results was appreciably different to those of Figure 5.29(a). It say be concluded that the use of an isolating stud or modification of the block by cutting a groove make no difference to the performance of B & K accelerometers of this type.

The foregoing observations lead to the suspicion that the errors associated with the accelerometer mounted on the exciting block are attributable to the effects of strain in the top surface of the block. The following development converts suspicion into conviction.

Rigid Body Motion

Consider the rigid body motion of the block/beam combination sketched in Figure 5.30. The equations of motion for the test piece are:

$$F_P = m_A \ddot{X} \tag{5.23}$$

and

$$M_P = I_2 \ddot{\theta} \tag{5.24}$$

where m_A is the apparent mass of the test piece as measured at point P.

The equations of motion for the exciting block are:

$$F_Q - F_P = m_1 \ddot{X} \tag{5.25}$$

$$= F_P \, m_1/m_A \quad \text{(using 5.23)}$$

and

$$eF_Q - M_P = I_1 \ddot{\theta} \tag{5.26}$$

$$= M_P \, I_1/I_2 \quad \text{(using 5.24)}$$

Thus

$$F_Q = F_P(1 + m_1/m_A) = m_A \ddot{X} (1 + m_1/m_A) \tag{5.27}$$

and

$$eF_Q = M_P(1 + I_1/I_2) \tag{5.28}$$

If the exciting block is small compared to the test piece:

$$F_Q \simeq m_A \ddot{X} \tag{5.29}$$

$$eF_Q \simeq M_P \tag{5.x}$$

Apparent Mass at Tip of Beam

For measurements at the tip of a slender beer of length 2L:

$$I_2 = m_2 L^2/3 \tag{5.31}$$

$$1/m_A' = 1/m_2 + L^2/I_2 = 1/m2 + 3/m_2 = 4/m_2 \tag{5.32}$$

Therefore

$$m_A = m_2/4 \tag{5.33}$$

Bending

The bending moment applied to the block is approximated by eF_d. Since the block has a complex shape it is not easy to predict exactly how much strain is caused by this moment. Bounds can be set, however, by considering cantilever beams of rectangular section whose depths correspond to tie smaller and larger dimensions of the block. See Figure 5.31.

It is reasonable to suppose that the strain caused by the moments M_P and eF_Q at point A on the exciting block will lie between the two values of strain caused by the moment eF_Q et the corresponding points A on the cantilever beams of different thickness.

For the cactilever:

$$\text{Stress at A} = \sigma_A = eF_Q\, y/I \qquad (5.34)$$

where y is the distance of the point A from the neutral axis.

The corresponding strain is given by:

$$\varepsilon_A = \sigma_A/E = eF_Q\, y/E\ I \qquad (5.35)$$

where E is Young's modulus of elasticity.

Substituting for F_Q using equation (1):

$$\varepsilon_A/\ddot{X} \simeq e\ y\ m_A/E\ i = C\ e\ m_A \qquad (5.36)$$

Estimates of Strain at Accelerometer Mounting Position

For test piece consisting of 1.4 m bear! of mass 8.74 kg, m_A = 2.175 kg. Block is aluminium so take E = 70 x 10^9 N/m^2, e = 0.05 m for worst case.

For bloc4 of depth, d = 0.02 m	For block of depth, d = 0.046 m
I = second moment of area	
= b d^3/12 = 1.6 x 10^{-8} 2 4	I = 1.35 x10^{-7} m^4
b = 0.024 m	b = 0.024 m
y = C.01 9	y = 0.023 El
$\varepsilon_A/\ddot{X} \simeq \frac{0.05 \times 0.01 \times 2.185}{70 \times 10^9 \times 1.6 \times 10^{-8}}$	$\varepsilon_A/\ddot{X} \simeq \frac{0.05 \times 0.023 \times 2.185}{70 \times 10^9 \times 1.95 \times 10^{-7}}$
= 0.98 strain/(m/s^2)	= 0.18 strain/(m/s^2)
= 9.6 strain/'g'	= 1.8 strain/'g'

Base Strain Sensitivity

The base strain sensitivity of the Endevco accelerometers is quoted 2s 25 equivalent 'g' at 250 μ strain (Type 233E compression type). The Endevco company do warn [29] that this sensitivity is not a linear function of strain. However, in order to make an initial estimate of error tie may take the base strain sensitivity tc be C. 1equivalent 'g'/ μstrain.

Supposethatan input force produces an acceleration of 1g at point A, then the resultant strain at A will lie between 1.8 and 9.6 μstrain. Such strain will give rise to error signals between 0.18 and 0.96 equivalent g i.e. between 18% and 96% or 1.4 dB arid 5.8 dB. Since this is the order of magnitude of the errors observed when Endevco accelerometers were used with block Mark 6 it is reasonable to assume that the effects of base strain were the dominant source of error.

The quoted base strain sensitivity of tie 'delta shear' B & K accelerometers of Type 4366 is 0.0006 'g'/ μstrain which is about 160th of the Endevco figure. The error calculated assuming use of B & K delta snear accelerometers will thus lie between 0.01 dB and 0.05 dB, when the apparent mass is about 2 kg.

Conclusions: Base Strain Effects in Accelerometers

From the observations above we may conclude that the error for Endevco accelerometers is associated with the accelerometer which is mounted on the block end, moreover, is a function of the offset of the force gauge (or the moment transmitted through the block) and of the apparent mass of the test object.

It has been shown that there is a relationship between the strain/acceleration ratio at point A and the offset of the force gauge and the apparent mass of the test object:

$$\varepsilon/\ddot{X} \simeq C\, e\, m_A$$

Thus, for accelerometers with large base strain sensitivity, an acceleration $\ddot{X}$ will be associated with 2 base strain which in its turn gives rise to a signal output which is 2 significant fraction of the correct output arising directly from acceleration. The errors observed lie between the estizates made. it is to be noted particularly that the effect of base strain is independent of force level and of frequency 2s far 2s the block itself is concerned. The intuitive idea that a block is rigid at frequencies well below its first antiresonance is not

relevmt; base strain errors would be present at zero frequency.

The effects of base strain can be mitigated in the case of the Endevco type 233B accelerometers by use of an isolating stud or by reducing the strain at the mounting point by cutting a 4 mm groove in the top surface of the exciting block.

The effects of base strain can be avoided by the use of B & K accelerometers or eny others with a low bese strain sensitivity.

Such eccelercneters should be selected for any tests involving exciting blocks or for direct attachment to a test- object for which surf&ice strain at the mounting point is likely.

5.4 CONCLUSIONS: MEASUREMENT OF MOBILITY PARAMETERS

Several developments were reported in this Chapter. They featured exciting block design, simplification of testing by use of nodal modelling and consideration of sources of error.

(1) The small exciting blocks, Mark6, 7 and 8 were satisfactory. The latter two are made more versatile for being composed of two sections, one to mate with the test object, the other to provide a rigid beam for input of torque and measurement of rotational response.

(2) The use of the modal modelling and derivation relationships of Chapter 2 enables rotational measurement to be simplified sufficiently for use with a measuring system restricted to two response channels, such as the Solartron **1172** equipment. These relationships also enable the pure rotational quantity ($\ddot{\theta}/M$) to be determined with improved accuracy, especially where the two-accelerometer method is employed. This avoids to a certain extent the effects of errors due to accelerometer defects.

(3) It is unfortunate that some accelerometers which are excellent in having very low transverse sensitivity prove to be very susceptible to base strain, especially when the 'single accelerometer' method is used. There are now available accelerometers which have got low transverse sensitivity and low base strain sensitivity and their use would minimise the errors attributable to the transducers.

(4) Where nodal modelling is used it is convenient to model the exciting block/test structure combination as a whole and to determine the properties of the test structure alone by cancelling the mass of the block and its attached accelerometers at the final stage of data processing.

(5) Program INCAN facilitates the identification calculations necessary to carry out the steps of section (4) above.

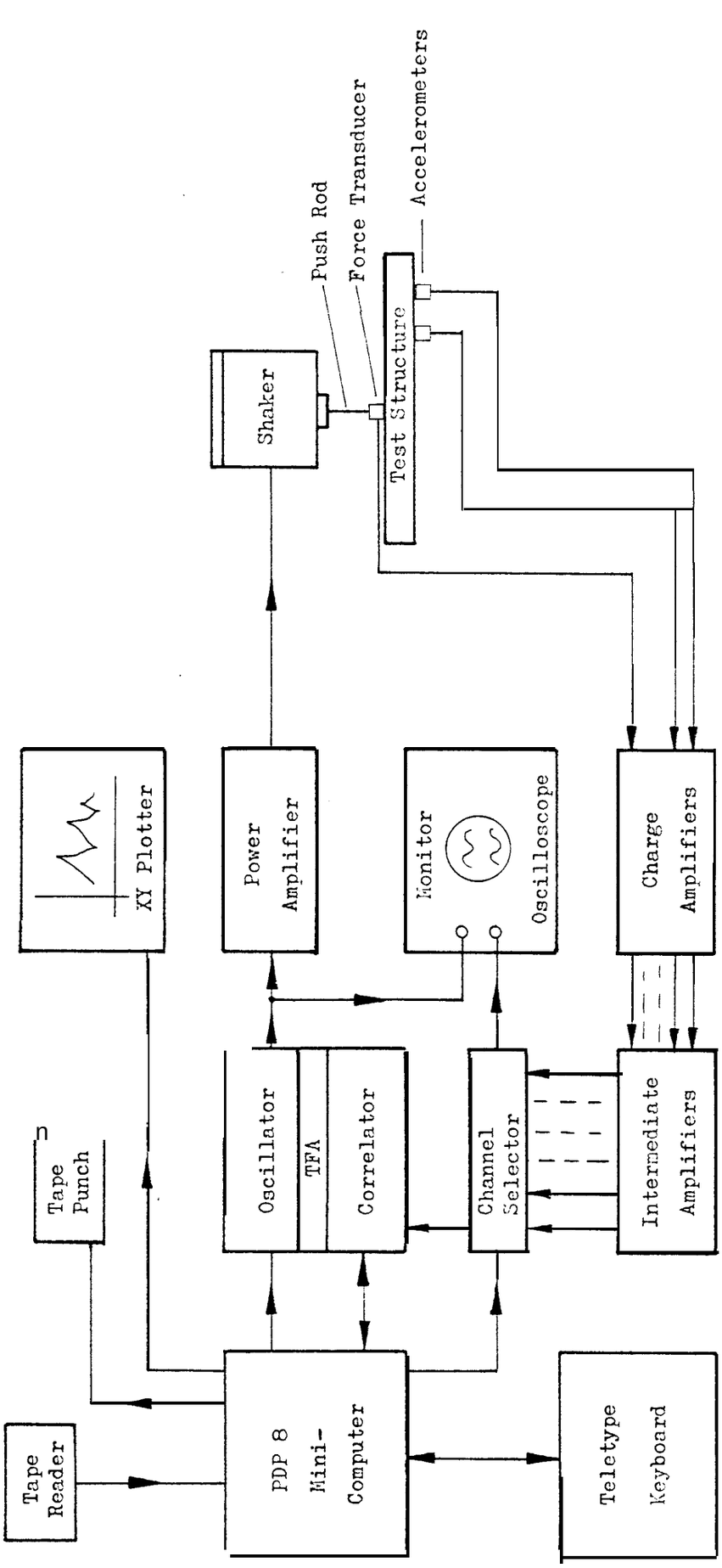

Figure 5.1 Block Diagram of Computer-Controlled Mobility Measurement System

Figure 5.2 Measurement of Point and Transfer Mobilities

Program MCB 2

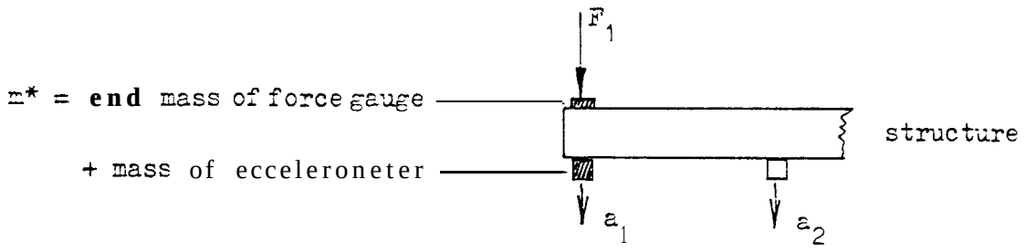

$\dot{X}_1 = Y_{11} F_1$ $\quad \dot{X}_2 = Y_{21} F_1$

$\therefore \; Y_{11} = (\dot{X}_1/F_1)$ $\quad Y_{21} = (\dot{X}_2/F_1)$

Mass Cancellation

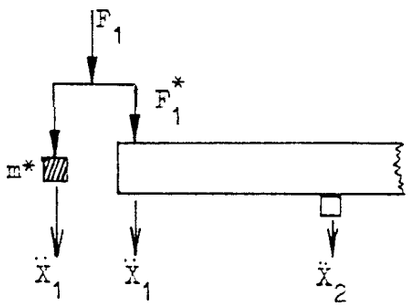

The force which affects the structure is $F_1^* = F_1 - m^* \ddot{X}_1$

Thus $\dot{X}_1 = Y_{11} F_1^* = Y_{11} (F_1 - m^* \ddot{X}_1)$

and $(\dot{X}_1/F_1) = Y_{11} (1 - m^* (\ddot{X}_1/F_1))$

giving $Y_{11} = (\dot{X}_1/F_1) (1 - m^* (\ddot{X}_1/F_1))^{-1}$

It is not known how much force input at coordinate 1 is needed to accelerate the transducer at coordinate 2. Consequently it is not possible to cancel the effective inertia of that accelerometer.

In general, mass cancellation can be carried out only for point quantities. It is sensible, therefore, to use accelerometers of low mass.

Figure 5.3 Measurement of Point Rotational 2nd Translational Mobilities

Program PM2/1

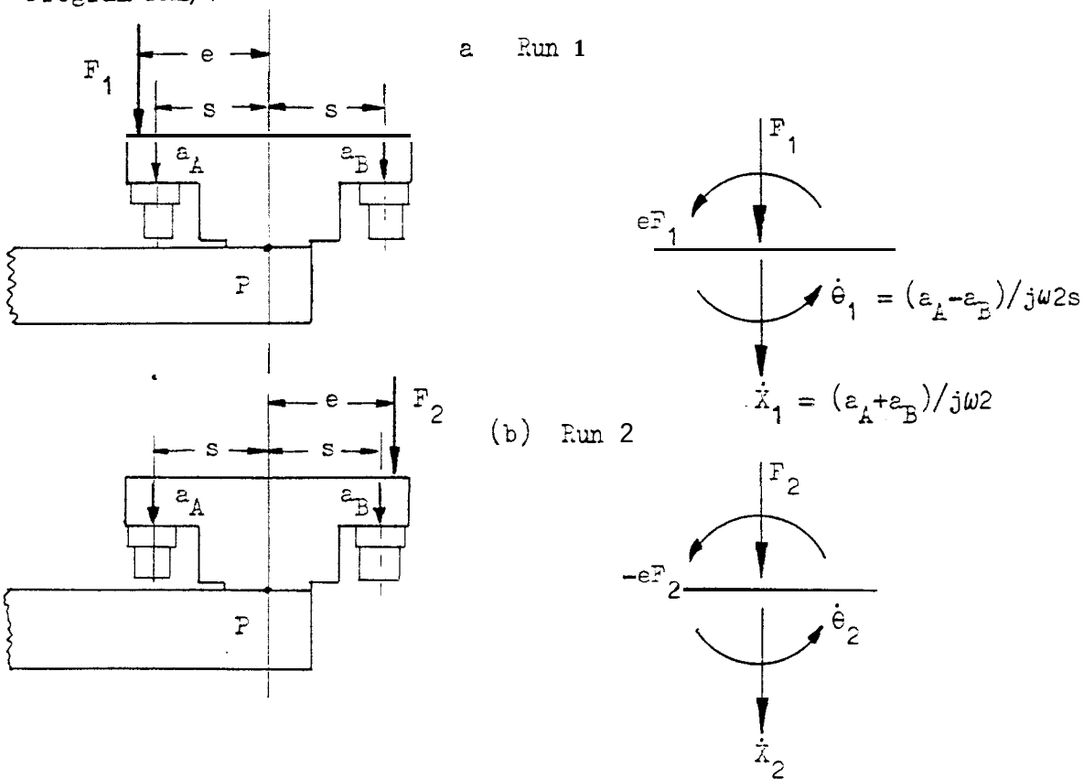

Thus

$$\begin{bmatrix} \dot{X}_1 & \dot{X}_2 \\ \dot{\theta}_1 & \dot{\theta}_2 \end{bmatrix} = \begin{bmatrix} Y_{xx} & Y_{x\theta} \\ Y_{\theta x} & Y_{\theta\theta} \end{bmatrix} \begin{bmatrix} F_1 & F_2 \\ eF_1 & -eF_2 \end{bmatrix}$$

2nd

$$\begin{bmatrix} Y_{xx} & Y_{x\theta} \\ Y_{\theta x} & Y_{\theta\theta} \end{bmatrix} = \begin{bmatrix} (\dot{X}/F)_1 & (\dot{X}/F)_2 \\ (\dot{\theta}/F)_1 & (\dot{\theta}/F)_2 \end{bmatrix} \begin{bmatrix} 1 & 1 \\ e & -e \end{bmatrix}^{-1}$$

and correcting for exciting block inertia:

$$\begin{bmatrix} Y_{xx} & Y_{x\theta} \\ Y_{\theta x} & Y_{\theta\theta} \end{bmatrix} = \begin{bmatrix} (\dot{X}/F)_1 & (\dot{X}/F)_2 \\ (\dot{\theta}/F)_1 & (\dot{\theta}/F)_2 \end{bmatrix} \left(\begin{bmatrix} 1 & 1 \\ e & -e \end{bmatrix} - \begin{bmatrix} m & 0 \\ 0 & I_p \end{bmatrix} \begin{bmatrix} (\ddot{X}/F)_1 & (\ddot{X}/F)_2 \\ (\ddot{\theta}/F)_1 & (\ddot{\theta}/F)_2 \end{bmatrix} \right)^{-1}$$

Figure 5.4 Exciting Block Mark 4G

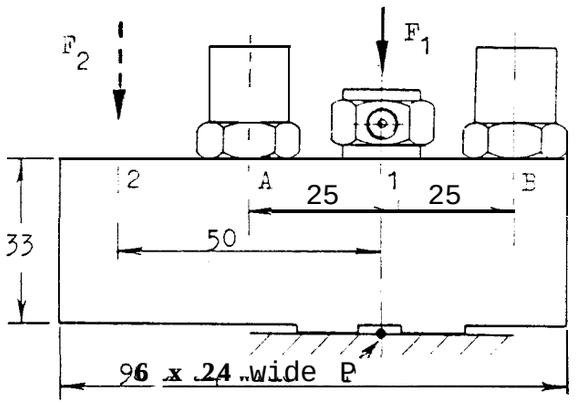

2, A, 1, B are holes drilled and tapped 10/32 UNF

A and B for Endevco 233E Accelerometers

1 and 2 for B & K 8200 Force Gauge

Figure 5.5 Exciting Block Mark 5

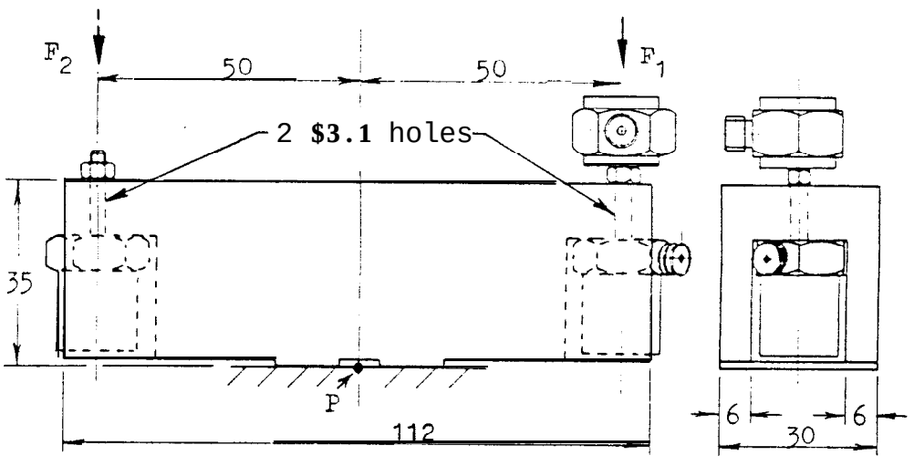

Figure 5.6 Exciting Block Mark 6

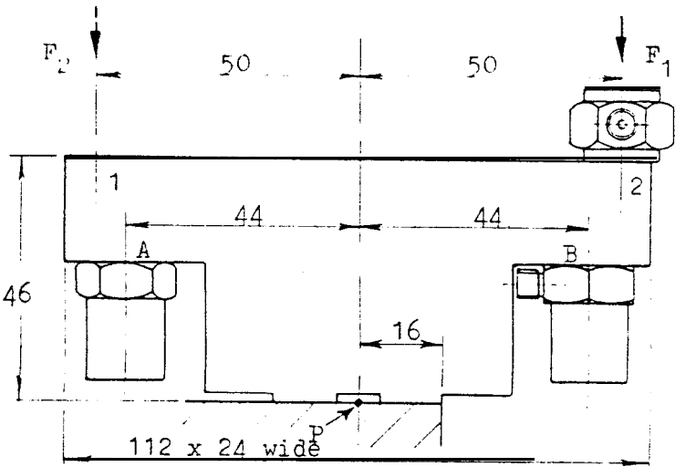

Scale 3:4 All dimensions in mm Block Material DURAL throughout

Figure 5.7 Exciting Block Mark 7

Scale 3:4 All dimensions in mm

Material DURAL

Block 7A

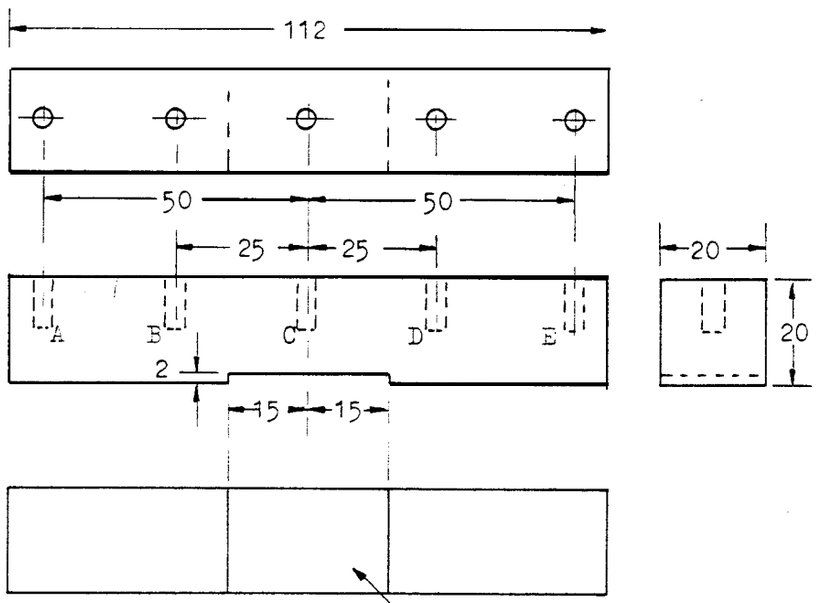

Holes 6, B, C, D, E
all drilled and tapped
10/32 UNF, depth 14 mm

Notch 2mm deep 30 mm wide
to fit over Block 7B

Block 7B

Material DURAL

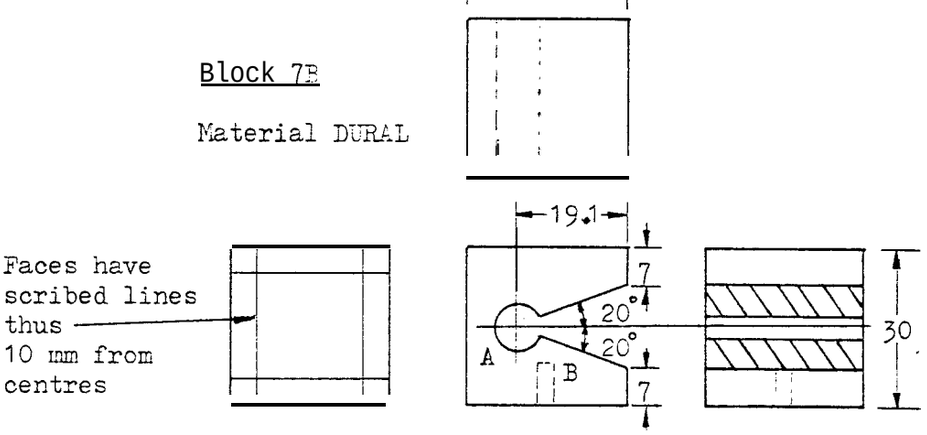

Faces have
scribed lines
thus
10 mm from
centres

Hole A 9.53mm diameter

Hole B drilled and tapped
10/32 UNF, depth 9 mm

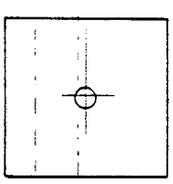

Figure 5.8 Exciting Block Mark 8

Scale 3:4 All dimensions in mm

Material DURAL

Block 8A

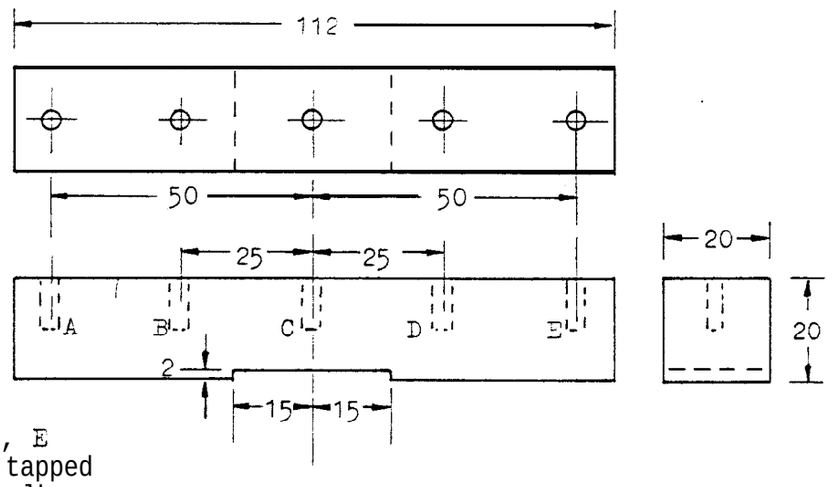

Boles A, B, C, D, E
all drilled and tapped
10/32 UNF, dapth lb mm

Block 8B

End Foot

Block 8C

Kid Foot

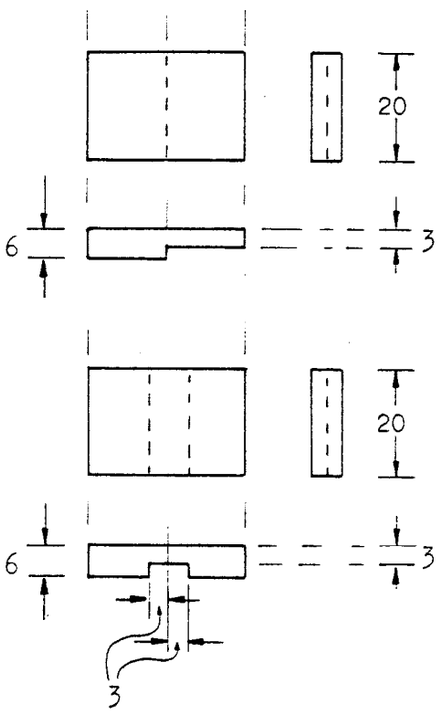

Note: Block Mark 8A is identical with Block Mark 7A

Figure 5.9 The Two-Accelerometer Method of Measuring the Point Mobility Matrix - Measurement of Y_{xx}, Y_{ex}

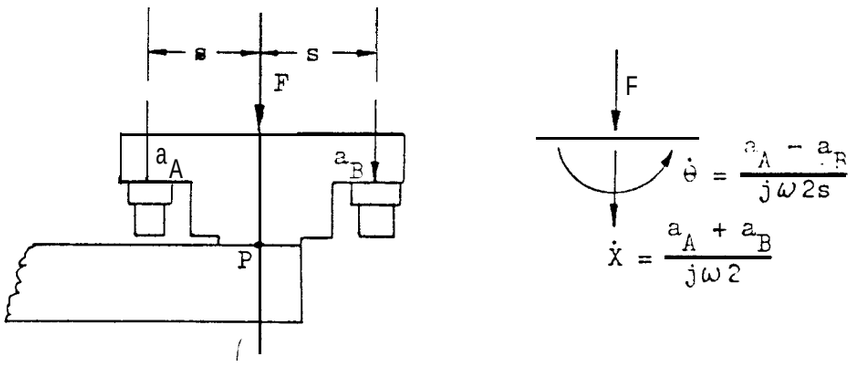

$$Y_{xx} = (\dot{X}/F) = \{(a_A/F) + (a_B/F)\}/j\omega 2 = (Y_A + Y_B)/2$$

$$Y_{ex} = (\dot{\theta}/F) = \{(a_A/F) - (a_B/F)\}/j\omega 2s = (Y_A - Y_B)/2s \qquad \text{(i)}$$

Data Required

s = Offset of each accelerometer from measurement point, P

ISF(A), ISF(B) = Inertance Scale Factors for two accelerometers, one force gauge

where (a/F) = ISF x (V_a/V_F)

and V = voltage output from the charge amplifier connected to an accelerometer or to the force gauge

Procedure (a) Using Solartron 1172

1. Measure (V_A/V_F) v.ω. Compute $Y_A = (a_A/F)/j\omega$ using ISF(A)
2. Change electrical input to other accelerometer channel.
3. Measure (V_B/V_F) v.ω. Compute $Y_B = (a_B/F)/j\omega$ using ISF(B)

(b) Using Program MOB2

1. YA' Y_B v.ω can be obtained directly in one run

Figure 5.10 The Sir&e-kcceierometer Method of Measuring the Point Mobility Matrix - Measurement of Y_{xx}, Y_{xe}

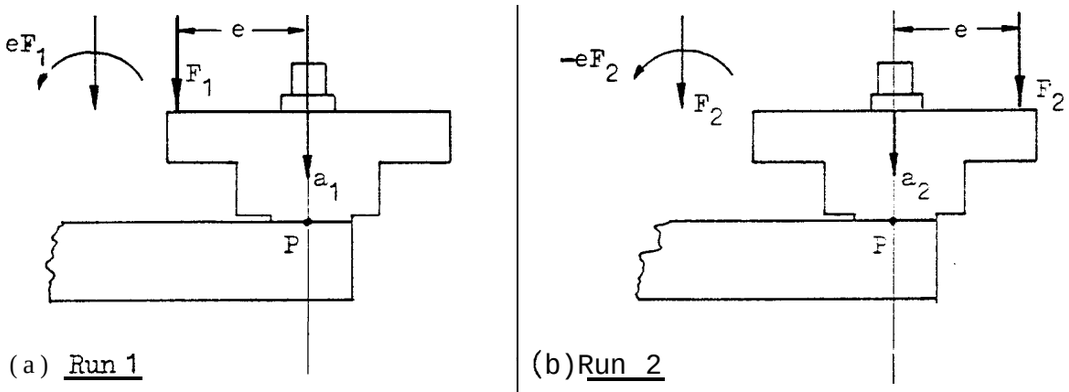

(a) Run 1

$\dot{X}_1 = (\dot{X}/F)\, F_1 + (\dot{X}/M)eF_1$

$Y_1 = (\dot{X}_1/F_1) = Y_{xx} + e\, Y_{xe}$ (ii)

$= (a_1/F_1)/j\omega$

(b) Run 2

$\dot{X}_2 = (\dot{X}/F)F_2 - (\dot{X}/M)eF_2$

$Y_2 = (\dot{X}_2/F_2) = Y_{xx} - e\, Y_{xe}$ (iii)

$= (a_2/F_2)/j\omega$

Combining (ii) and (iii) gives :

$Y_{xx} = (Y_1 + Y_2)/2$

$Y_{xe} = (Y_1 - Y_2)/2e$

Data Required

e = Offset of force gauge from measurement point, P

ISF = Inertance Scale Factor

Procedure

1. Set up Run 1 configuration. Measure (V_a/V_F) v.ω. Compute Y_1 v.ω
2. Move force gauge. Re-align shaker for Run 2 configuration.
3. Measure (V_a/V_F) v.ω. Compute Y_2 v.ω.

(c) Alternative Position For Accelerometer

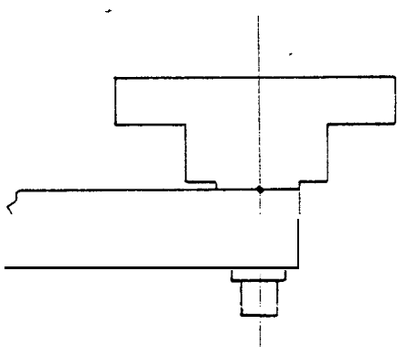

Note : Equations (iv) have similar form to equations (i) of Figure 5.9 so the same Program will serve fcr either set cf calculations.

Figure 5.11 Measured Nobilities at a Point on the Long Beam

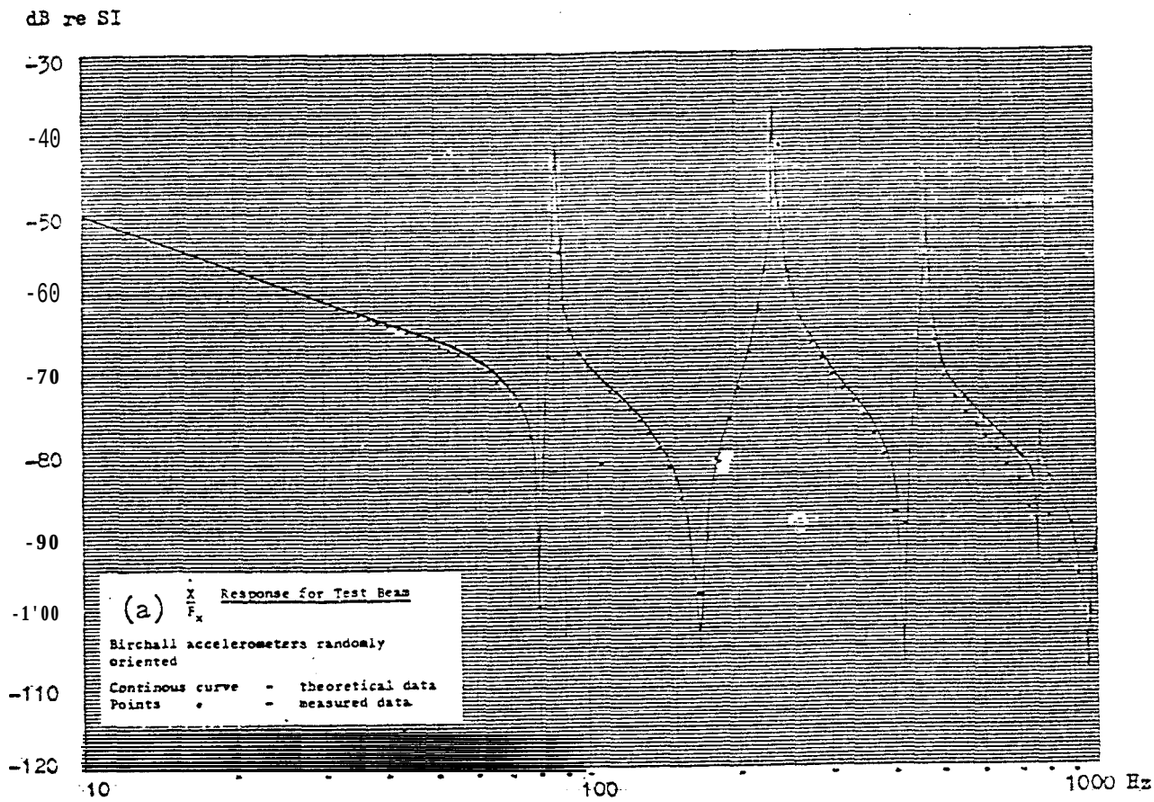

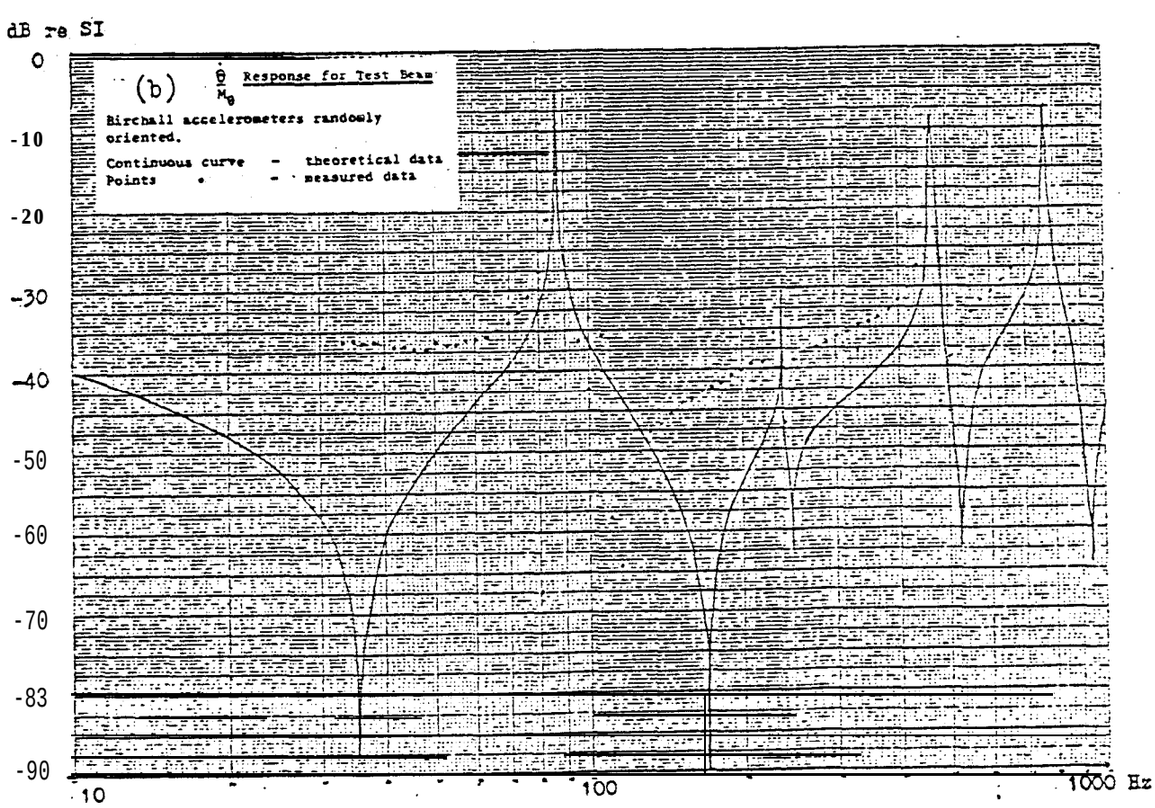

Figure 5.12 Illustration of Transverse Sensitivity

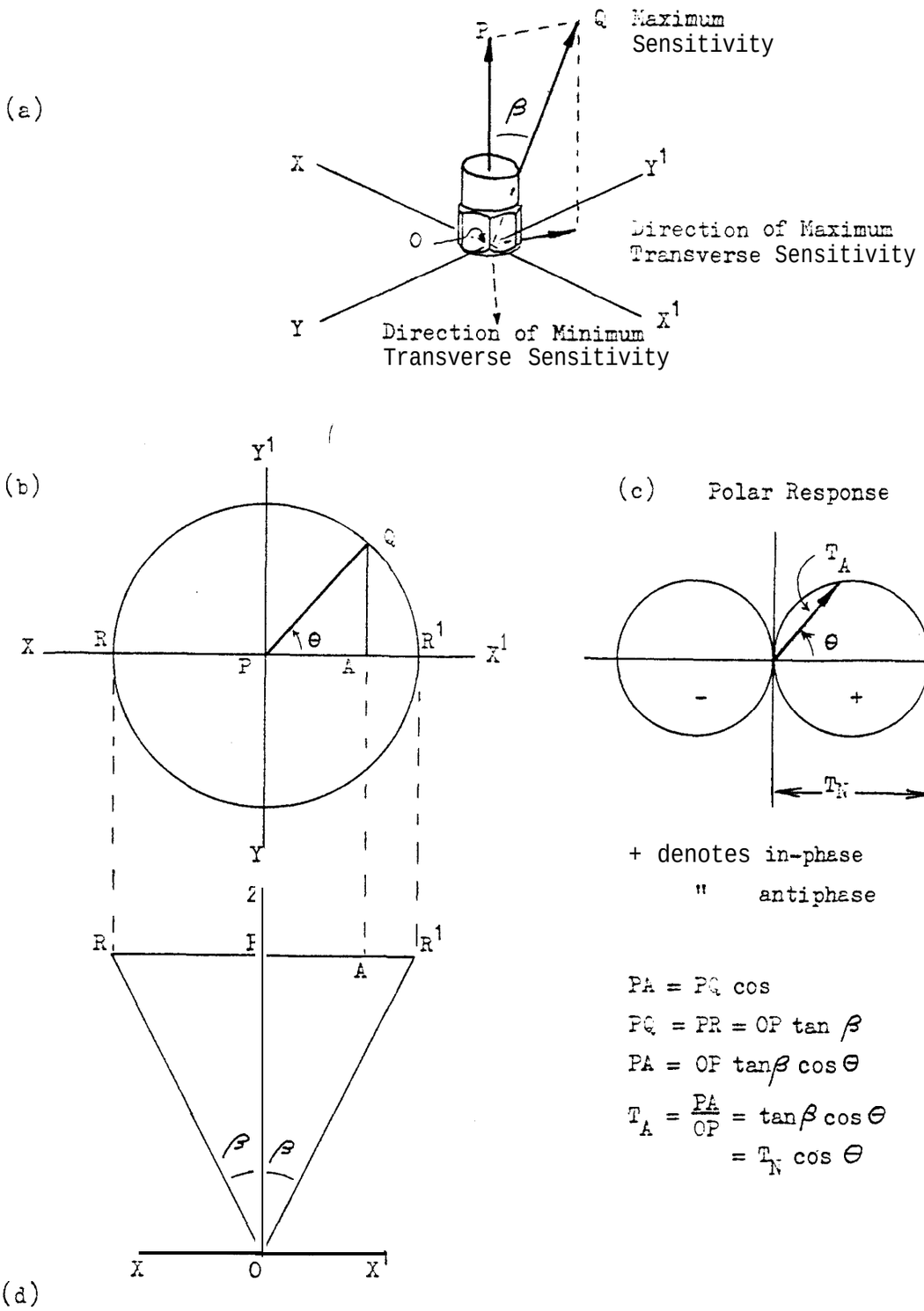

Figure 5.13 Proposed Arrangement to Minimise Transverse Sensitivit Errors

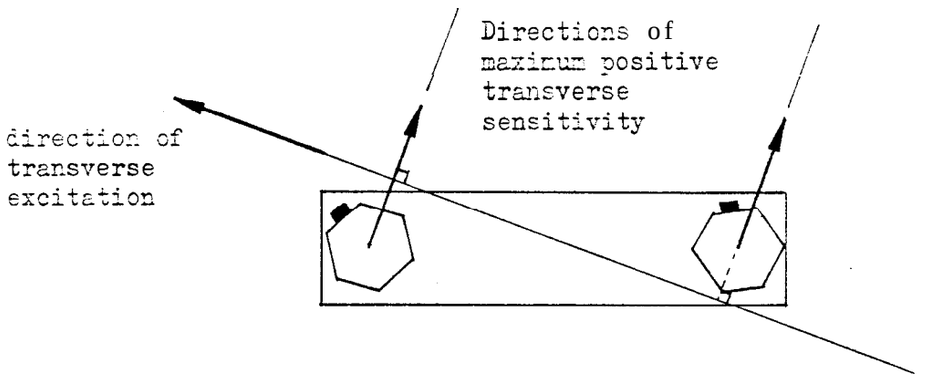

Figure 5.14 Arrangement of Test Equipment for Transverse Sensitivity Measurement

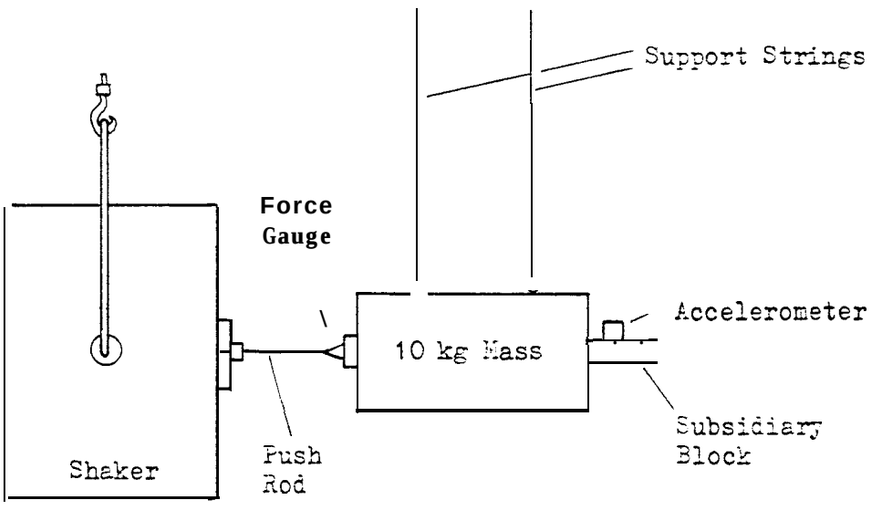

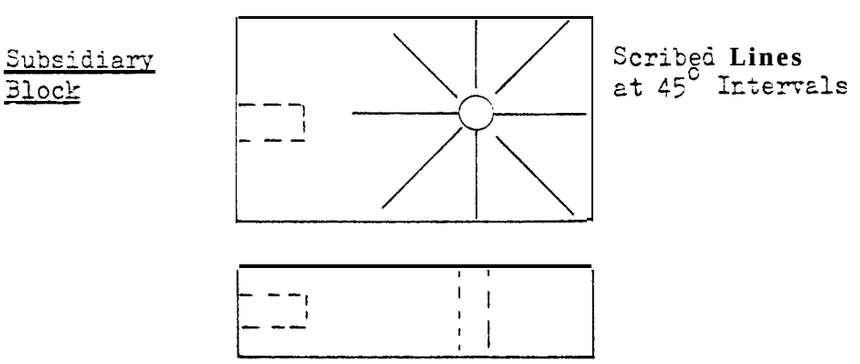

Figure 5.15 Measured Polar Response of Birchall Accelerometer

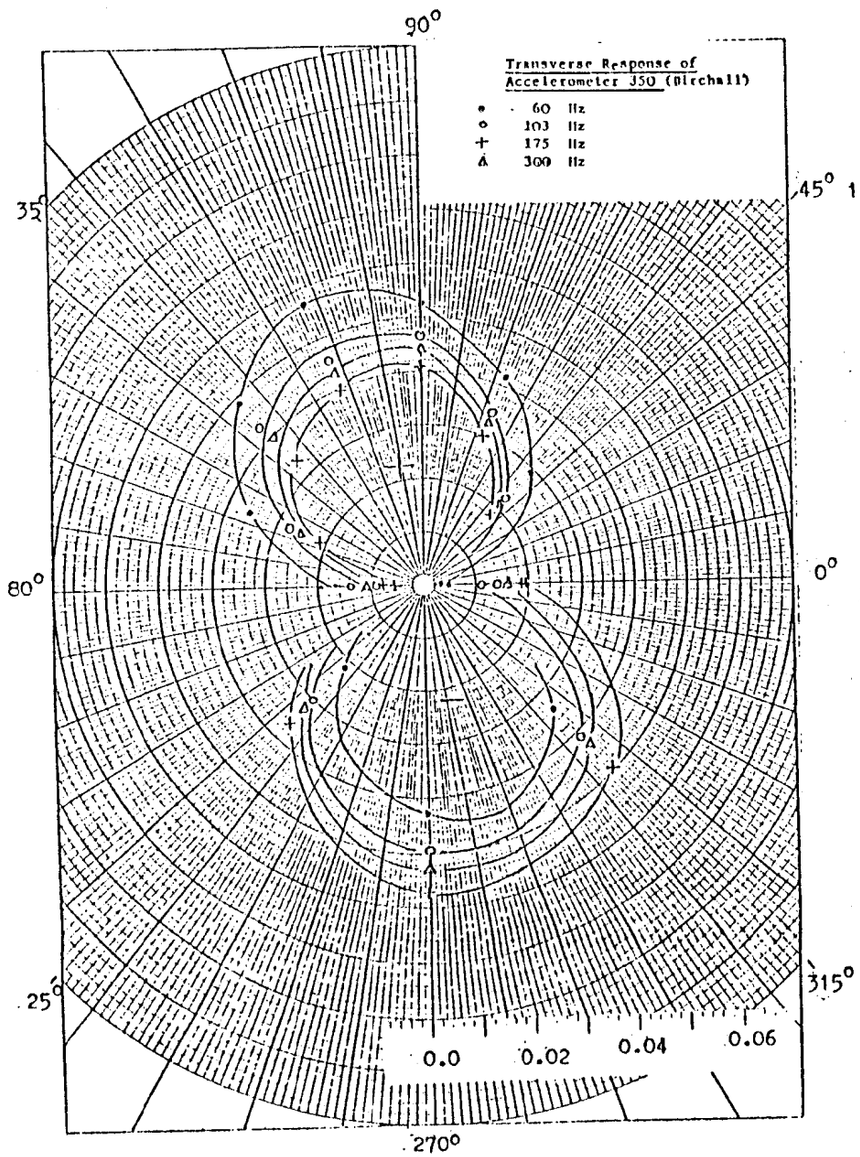

Figure 5.16 Modelled Polar Response of Birchall Accelerometer

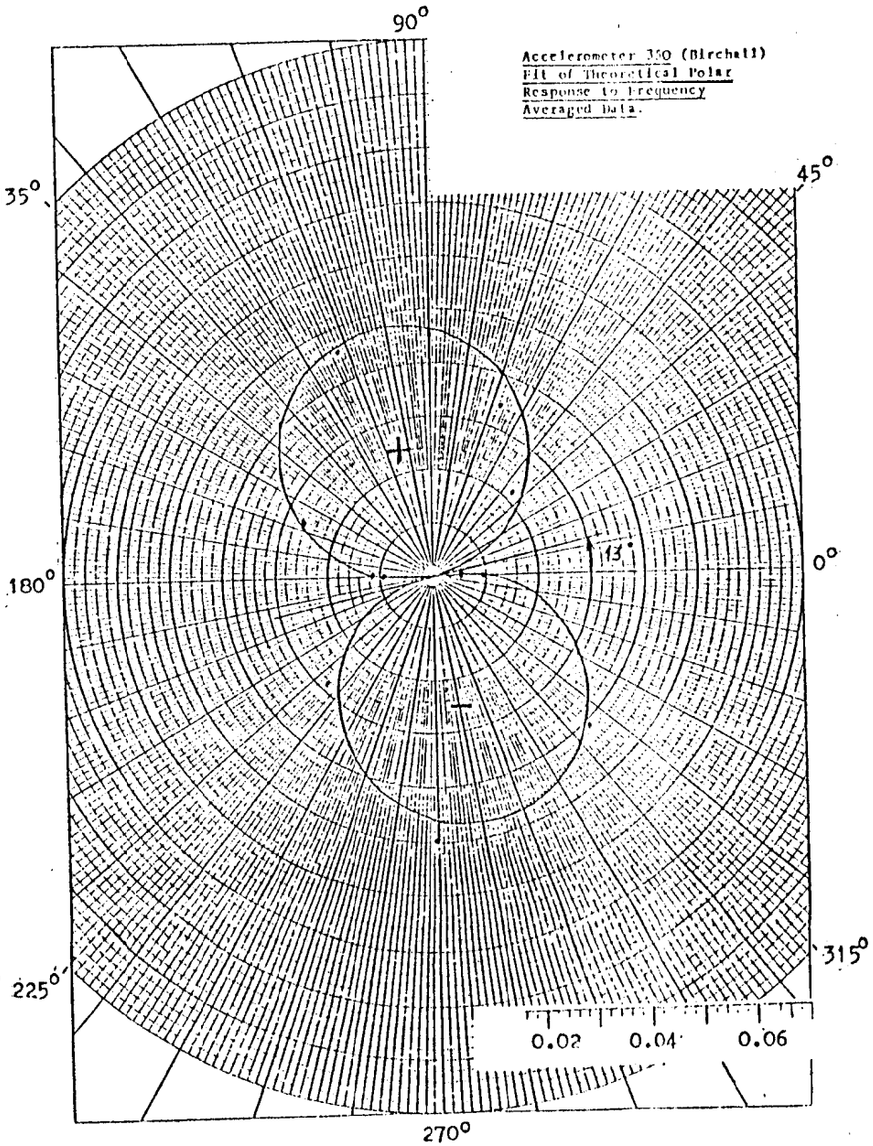

Figure 5.17 Re-measured Polar Response of Birchall Accelerometer

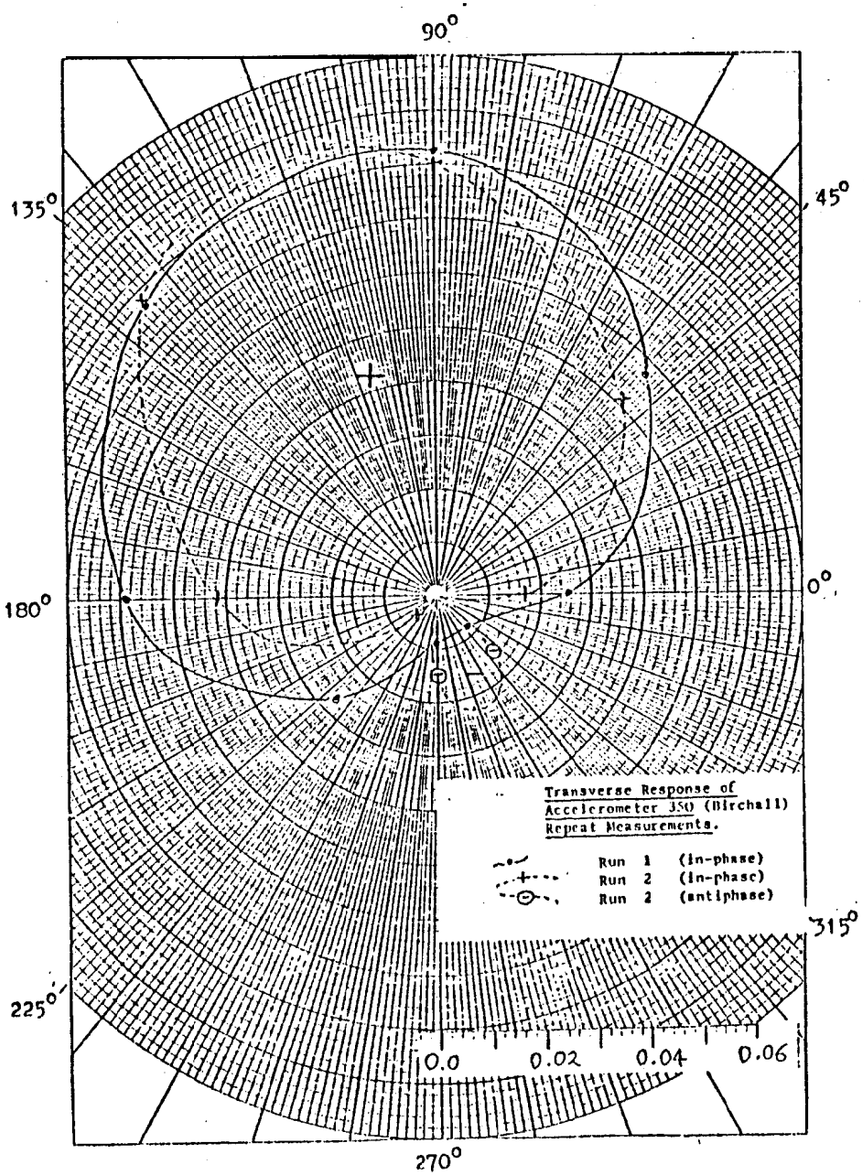

Figure 5.18 Polar Response of Endevco Accelerometer

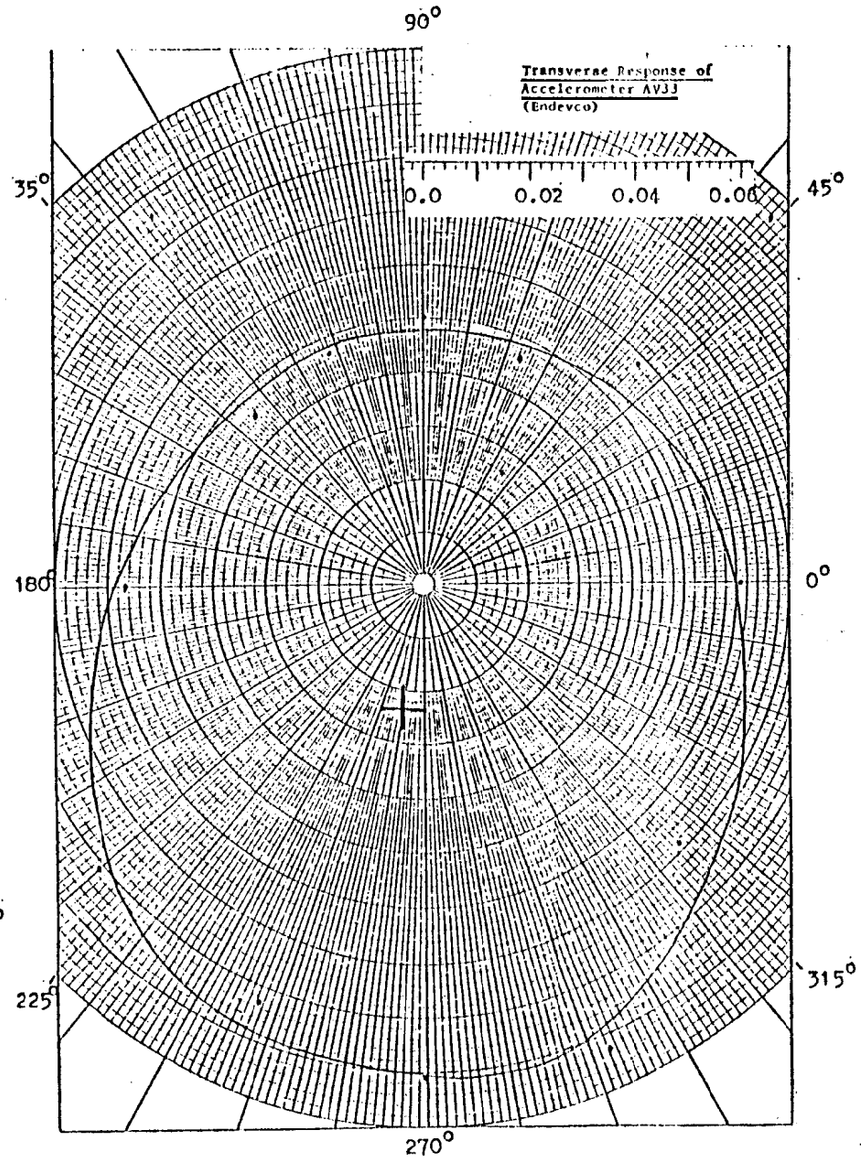

Figure 5.19 Illustration of Transverse Sensitivity with Misaligned Geometric Axis

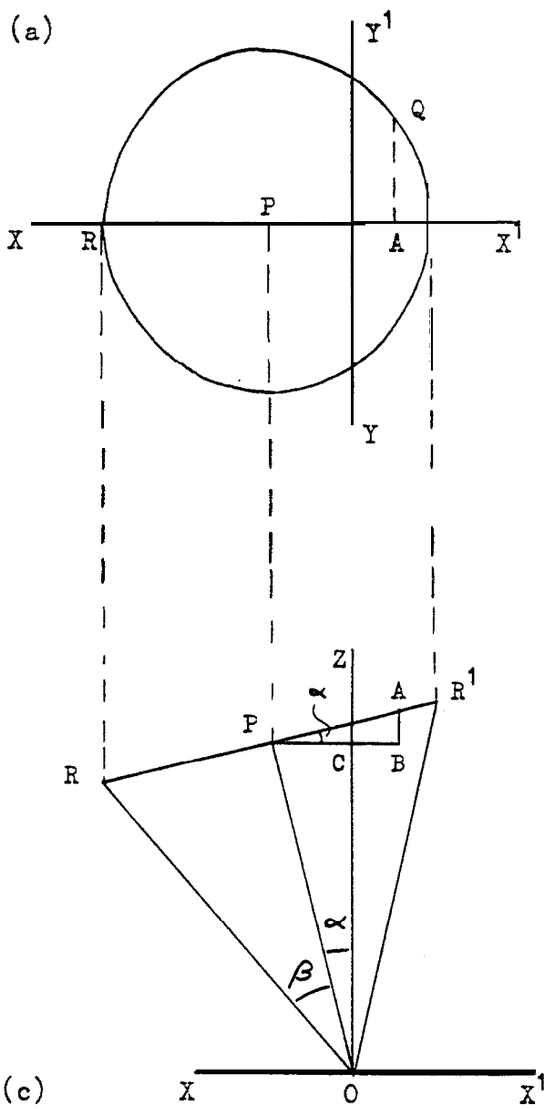

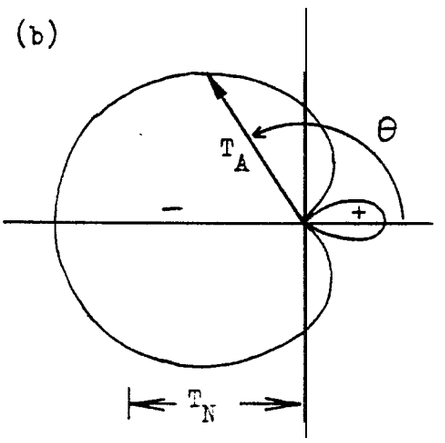

\+ denotes in-phase

" antiphase

$$CE = PB - PC$$
$$= PA\cos\alpha - OP\sin\alpha$$
$$= OP\tan\beta\cos\theta\cos\alpha - OP\sin\alpha$$
$$= OF\cos\alpha(\tan\beta\cos\theta - \tan\alpha)$$

$$TA = \frac{CB}{OP} = \cos\alpha(\tan\beta\cos\theta - \tan\&)$$
$$= \cos\alpha(T_N\cos\theta - \tan\alpha)$$

Figure 5.20 Circuit for Analogue Computer Simulation of Transverse Responses

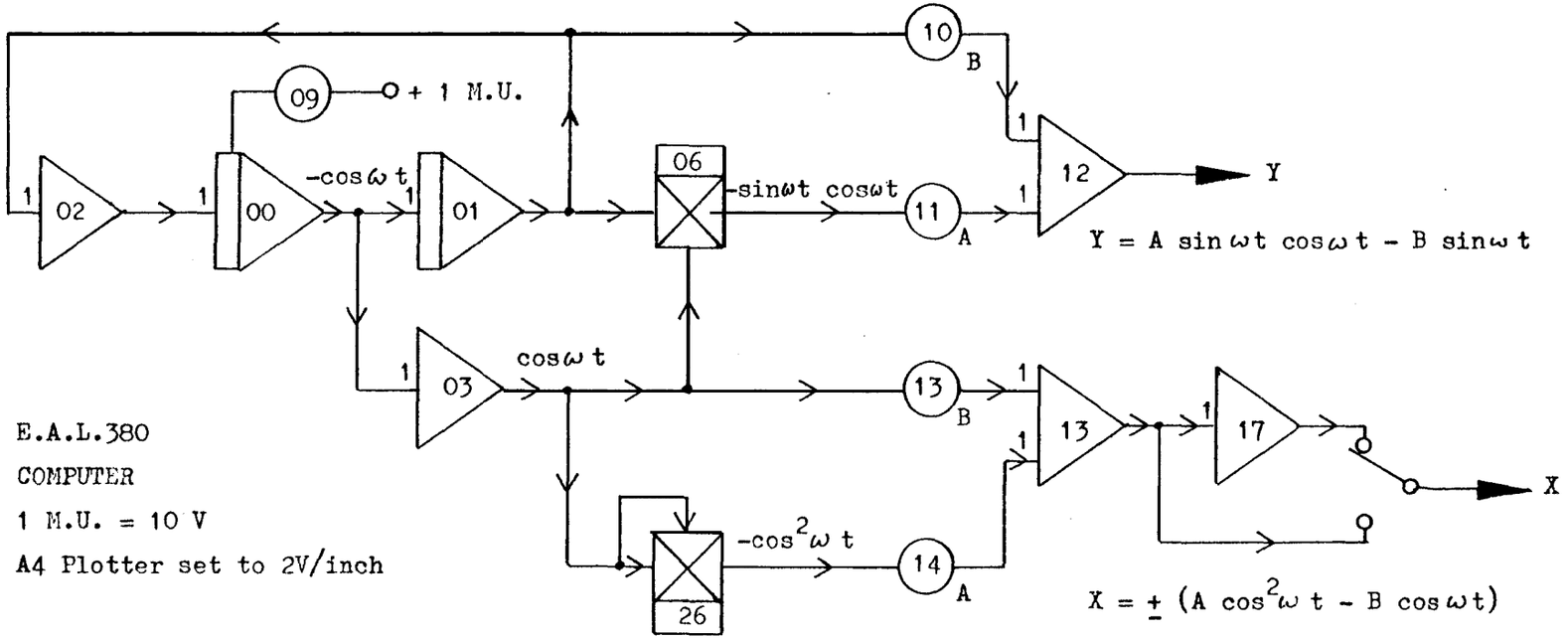

Potentiometer List

09	1.00	1.00	1.00	1.00	
10	0	0.15	0.30	0.45	B
11	0.2	0.2	0.6	0.6	A
13	0	0.15	0.30	0.45	B
14	0.2	0.2	0.6	0.6	A
α	0°	0.86°	1.72°	2.58°	
T_N	0.02	0.02	0.06	0.06	

the sign change of X
is needed to convert

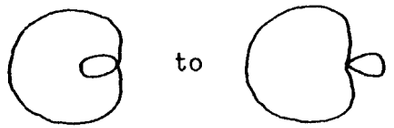

Figure 5.21 Analogue Computer Simulation of Birchall Polar Response

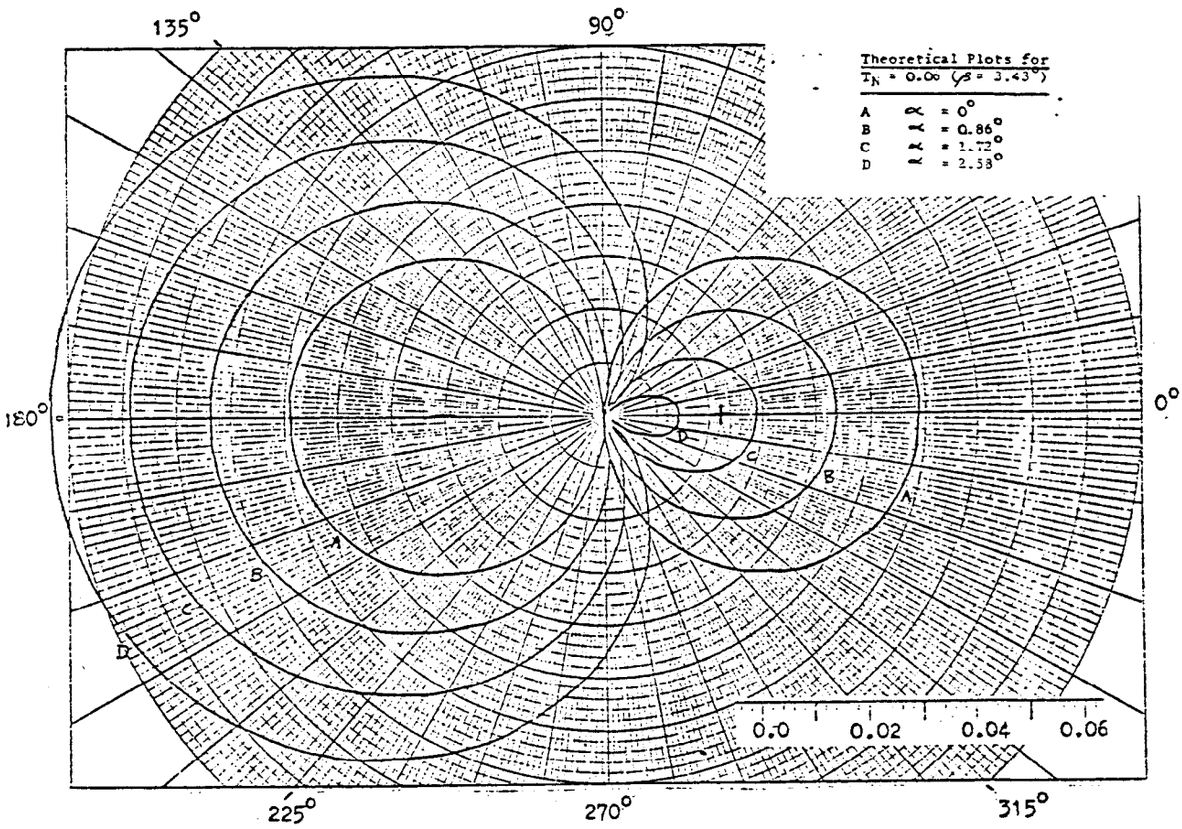

Figure 5.22 Analogue Computer Simulation of Endevco Polar Response.

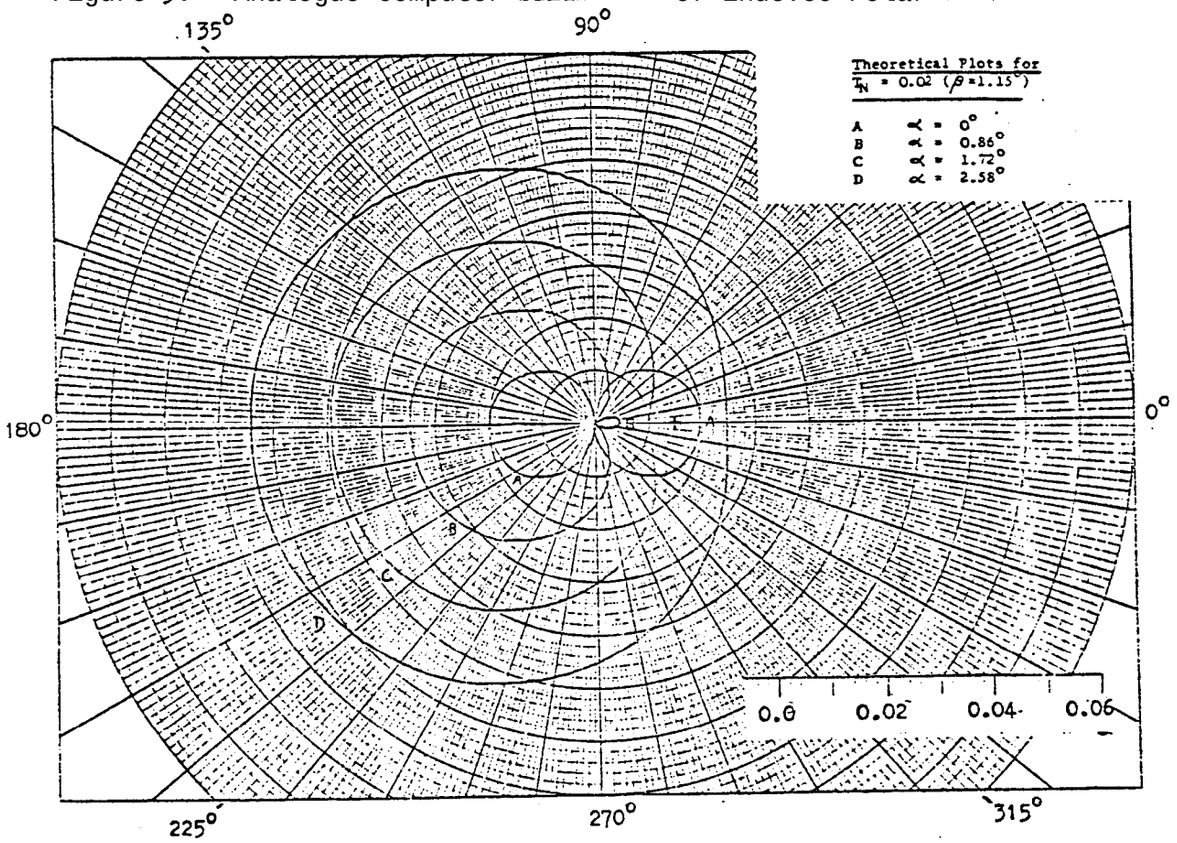

Figure 5.23 Measured Rotational Mobility of a Point on the Long Bear; Birchall Accelerometers with Selected Orientation

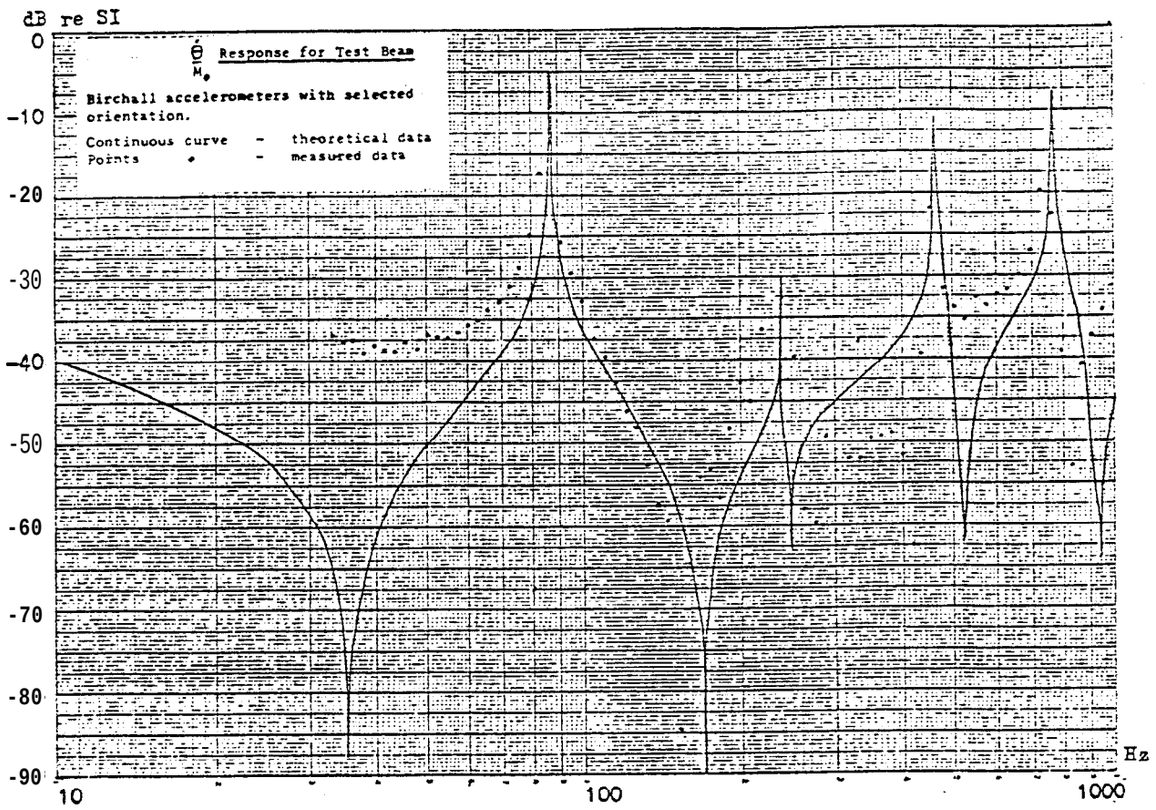

Figure 5.24 Measured Rotational Mobility of a Point on the Long Beam Endevco Accelerometers with Random Orientation

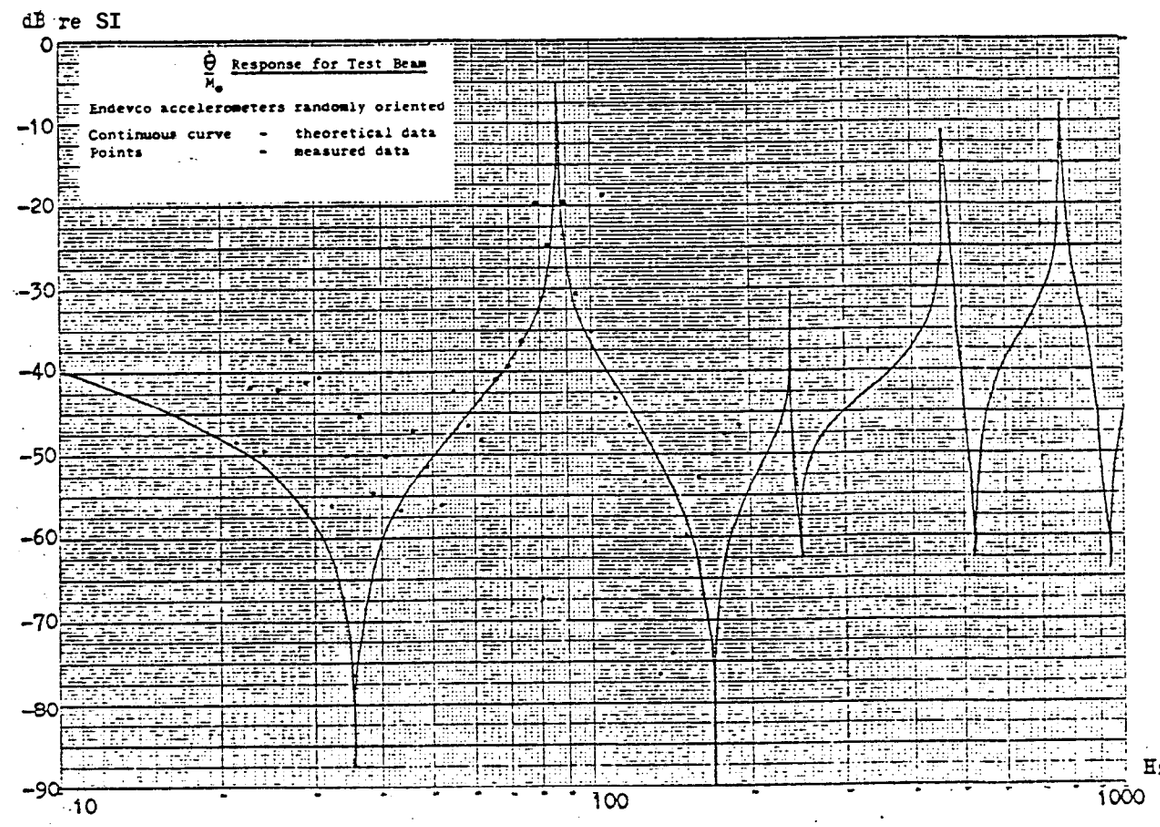

Figure 5.25 Base Strain Test Configurations

A, B - Accelerometers

e - Offset of Force Gauge from axis of Accelerometers

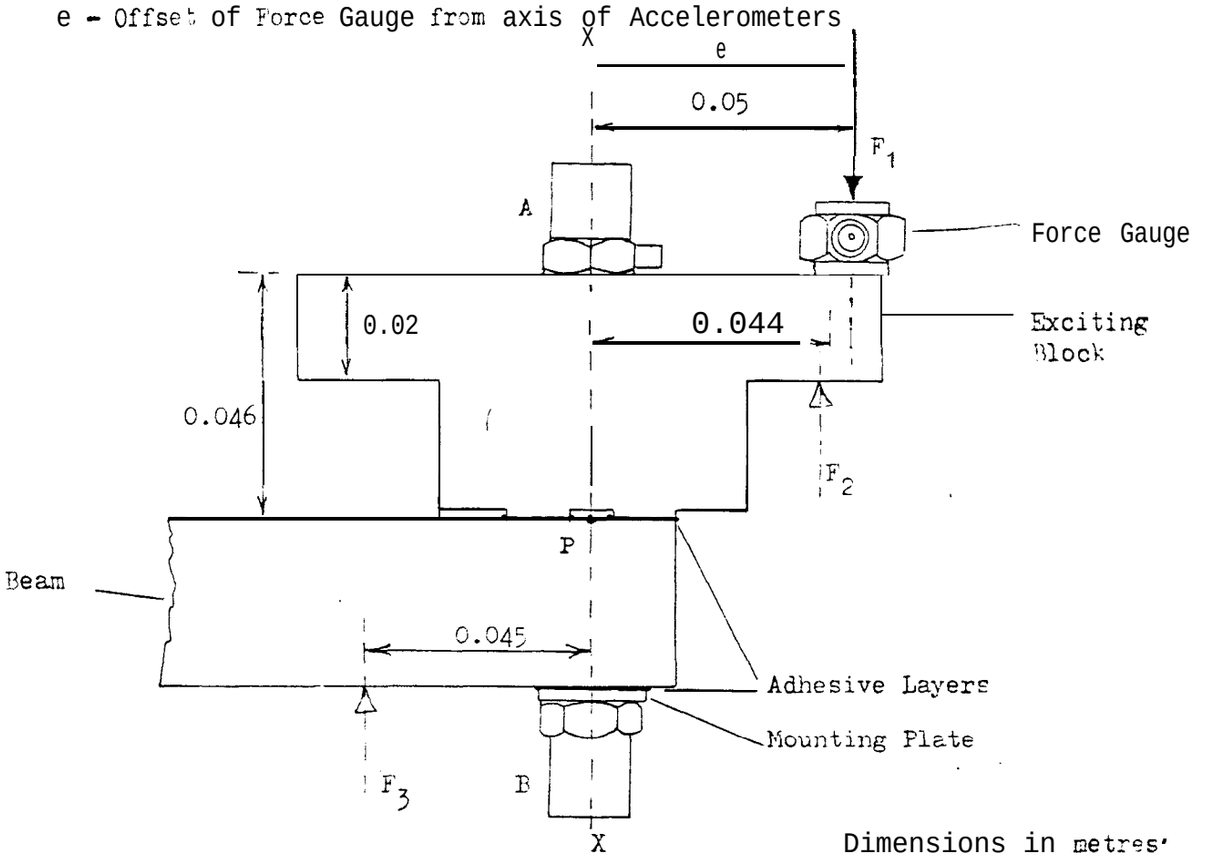

Configuration 1 - Force applied to top surface of block

" 2 - " " underneath bloc!;

" 3 - " " to beam

Force Gauge - Bruel & Kjaer Type 8200, No. 364411

Accelerometers - B 1 " " " 4366 " 549165 'delta shear'

- B 2 " " " " " 547501 " "

- E 1 Endevco Type 233E No. CE58 'single ended compression'

- E 2 " " " " CE93 " "

Figure 5.26

(a) Ratio of Outputs of Endevco Accelerometers
Accelerometer A screwed directly to Block

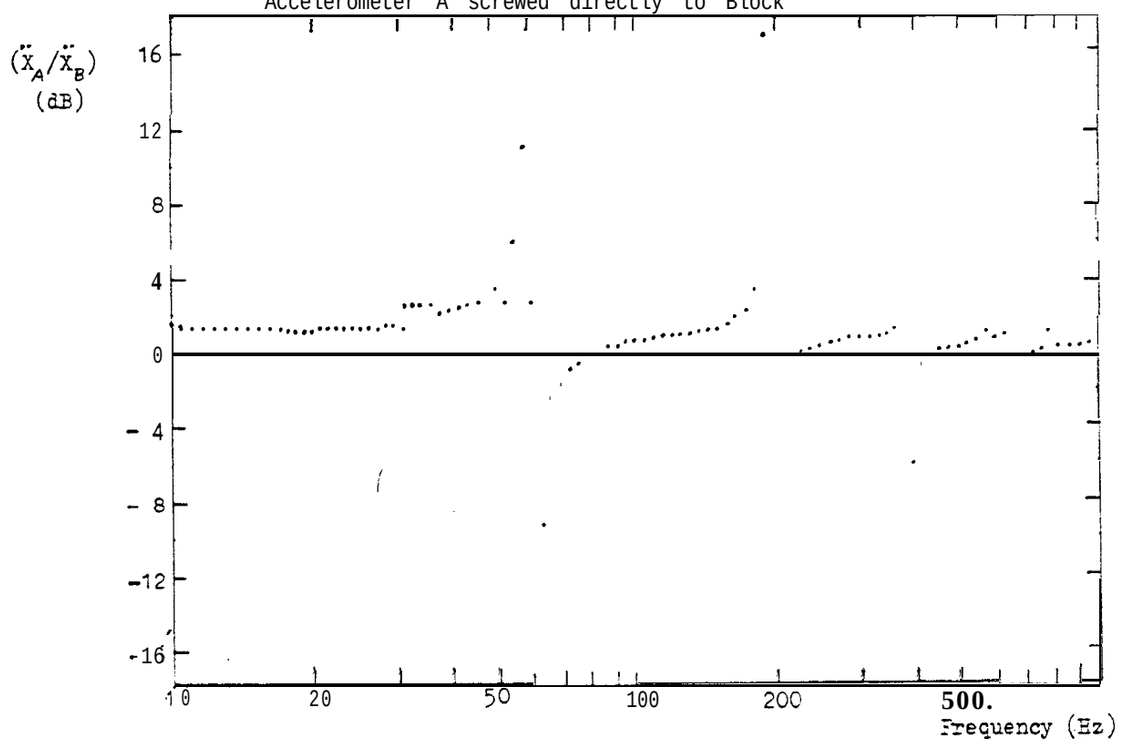

(b) Ratio of Outputs of Endevco Accelerometers
Accelerometer A screwed to Isolating Stud

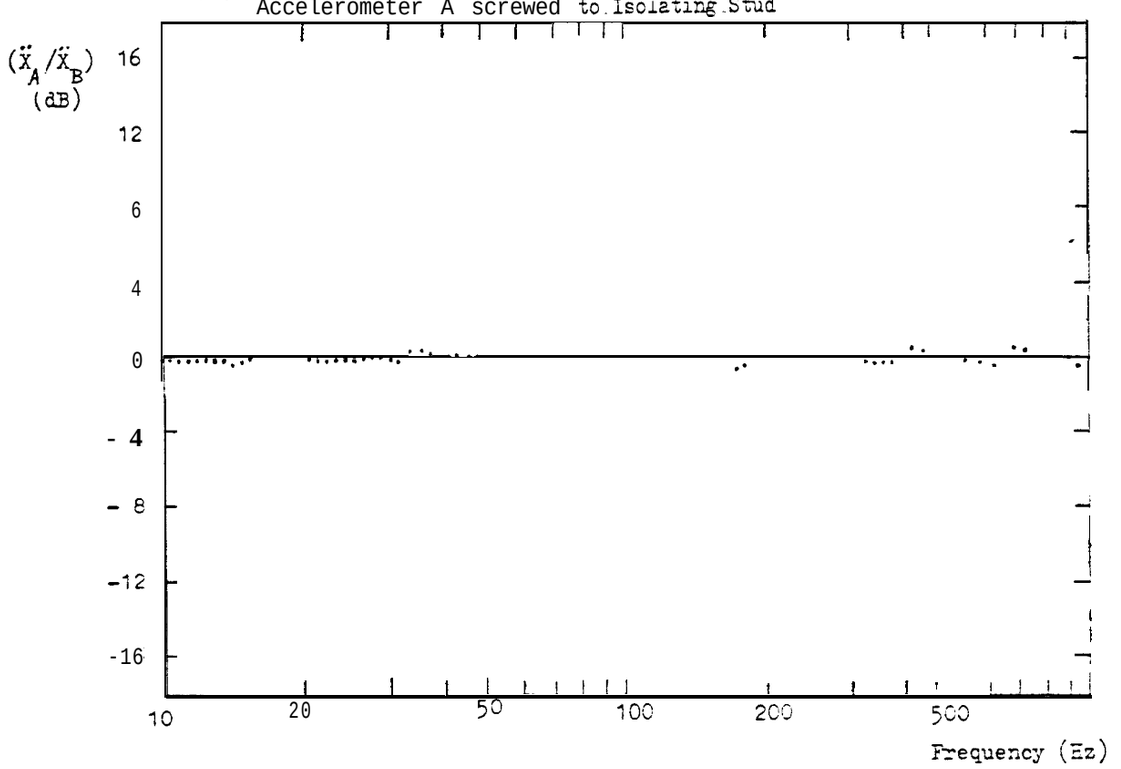

Figure 5.26 cont'd

(c) Ratio of Outputs of Endevco Accelerometers
Block Modified by Groove of Depth 2 mm

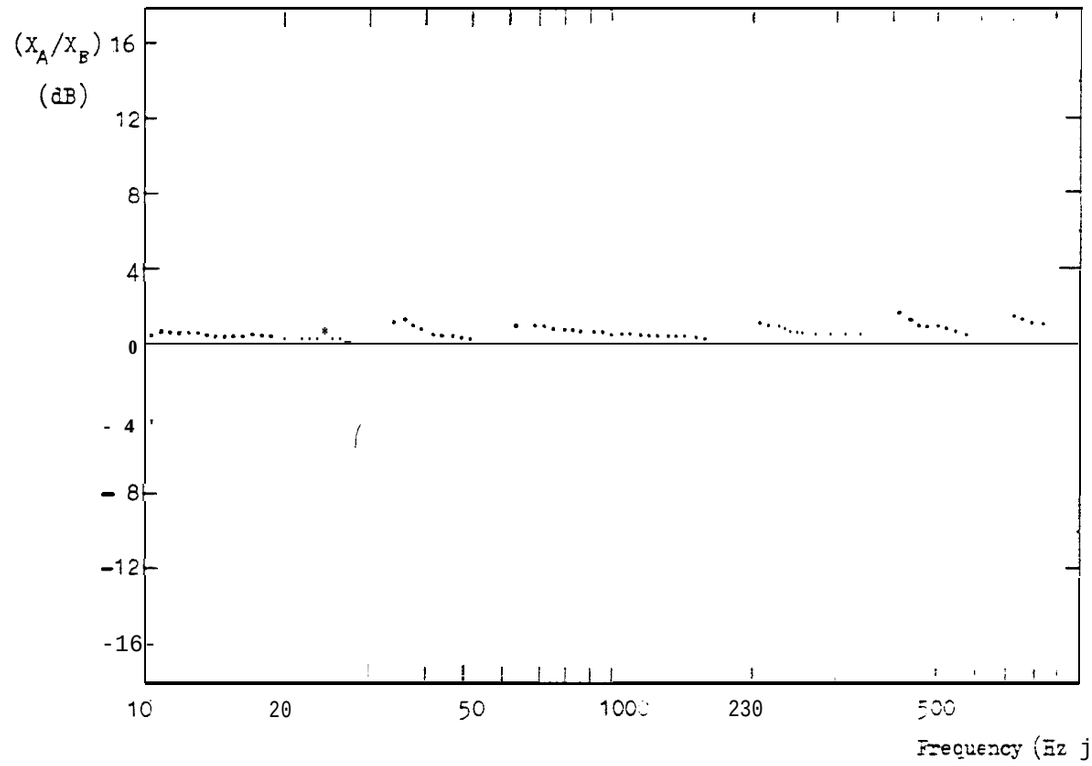

(d) Ratio of Outputs of Endevco Accelerometers
Block Modified by Groove of Depth 4mm

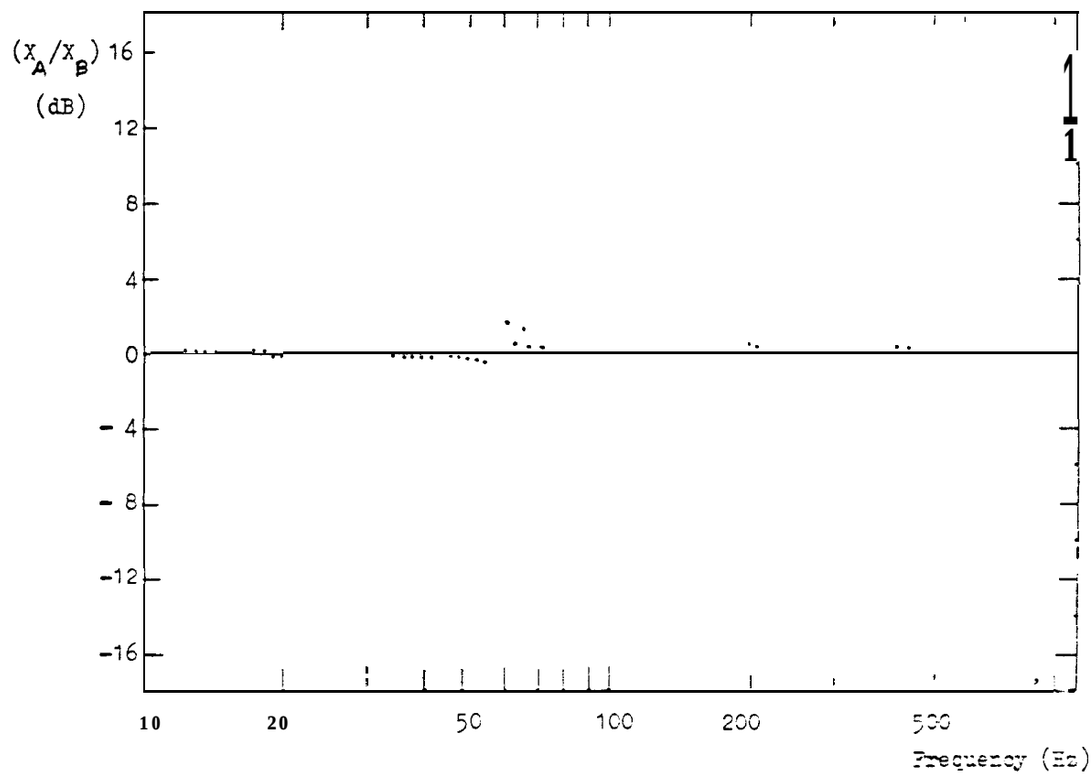

Figure 5.27 Ratio of Accelerometer Outputs as a Function of Force Gauge Offset

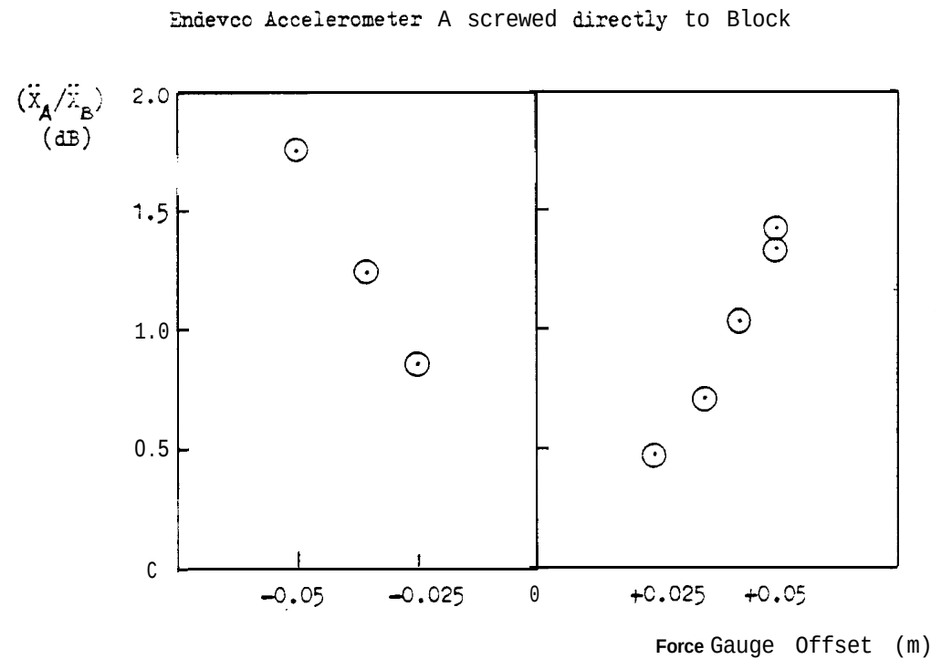

Figure 5.28 Apparent Mass at Tip of Beam

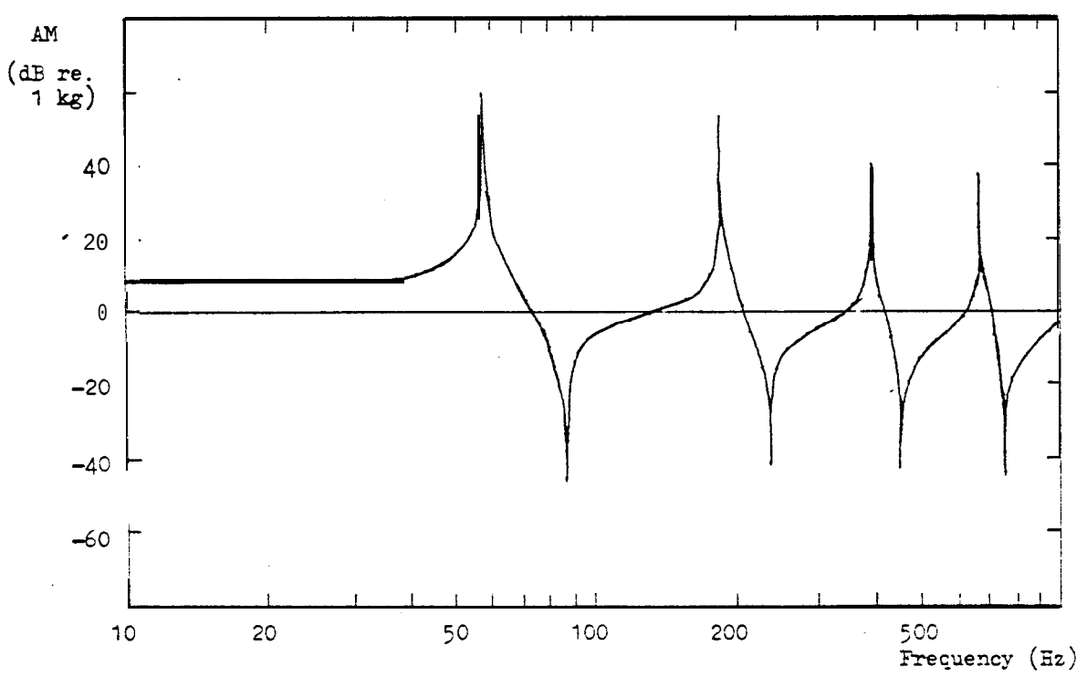

Figure 5.29

(a) Ratio of Outputs of Bruel & Kjaer Accelerometers
Accelerometer A screwed directly to Block

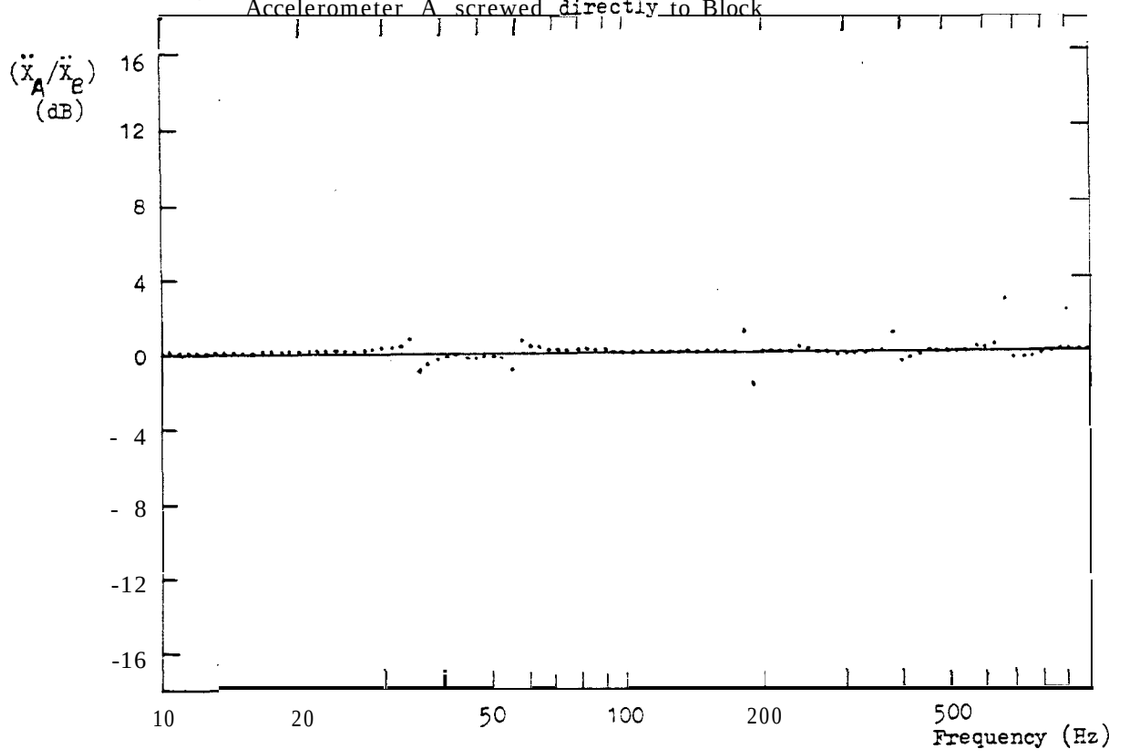

(b) Ratio of Outputs of Bruel & Kjaer Accelerometers
Accelerometer A screwed to Isolating Stud

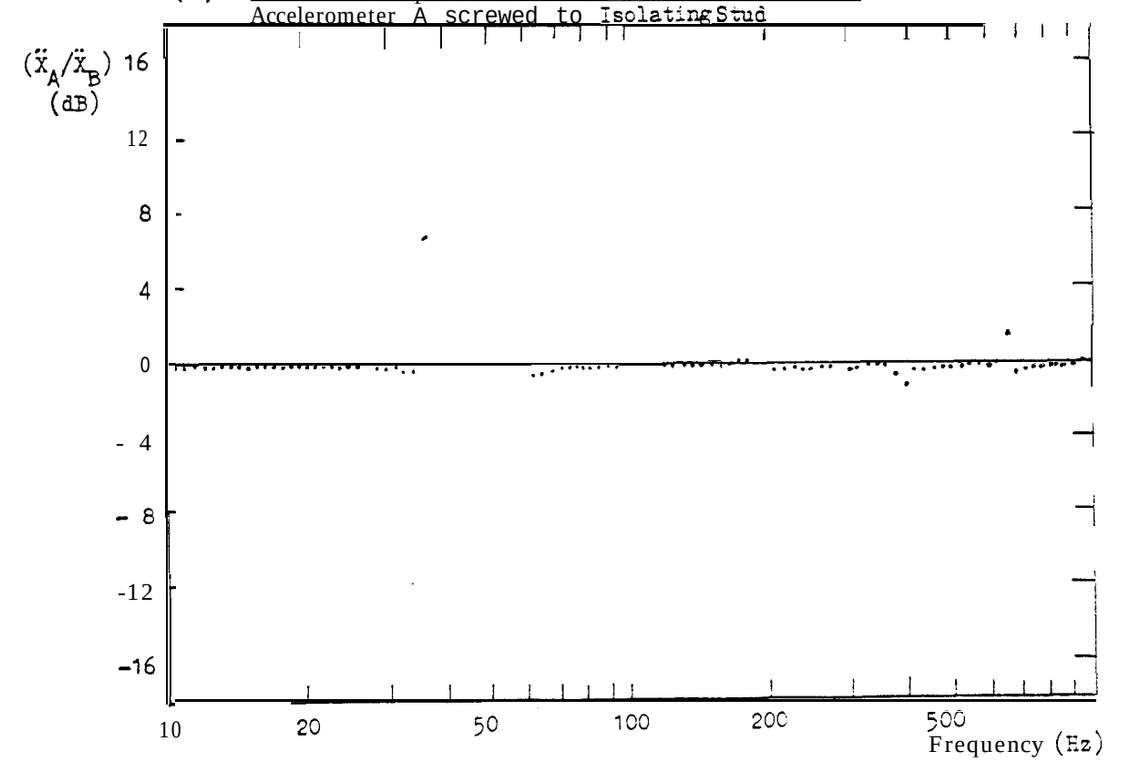

Figure 5.30 Free Body Diagrams of Exciting Block and Beam

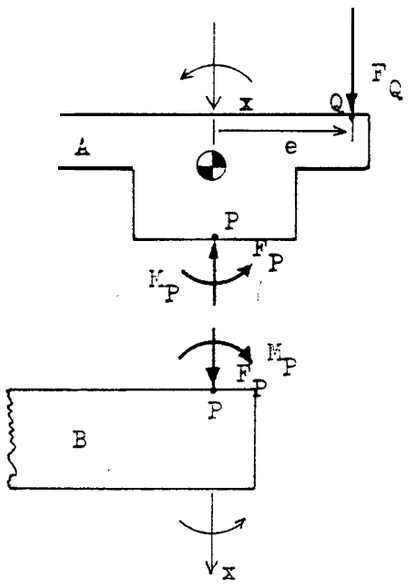

Exciting Block

Mass m_1

Centroidal Moment of Inertia I_1

Test Piece

Mass m_2

Centroidal Moment of Inertia I_2

Figure 5.31 Strain in the Exciting Block

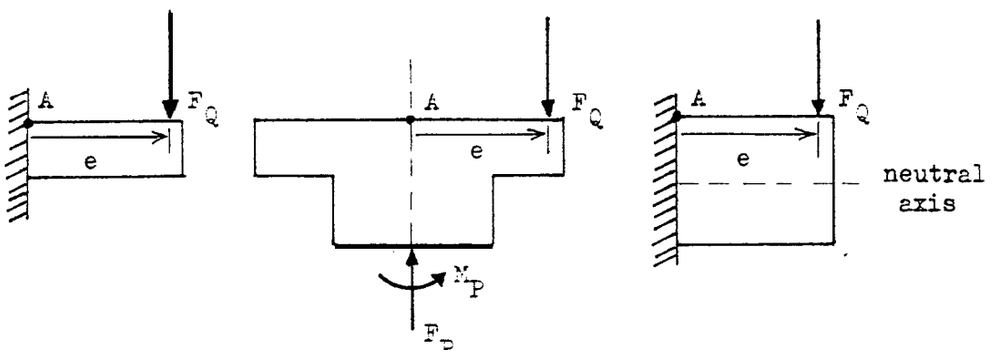

6. MEASUREMENT OF MULTI-DIRECTIONAL MOBILITIES ON BEAMS

The measurements reported in this Chapter were made on uniform steel beam of rectangular section, test pieces for which precise predictions of nobility properties could be made using, for example, program COUPLE1 and nodule ZFLAX1. The specification of the beams is discussed in section 6.1. The measurements reported in section 6.2 generally reveal discrepancies between the parameter ($\dot{e}/\dot{K}$) obtained from measurements and calculated theoretically. As sources of error were identified, the information was used tc evolve block design from Mark 4G and Mark5-which have serious defects-to Mark 6 which ultimately is shown to be satisfactory. Section 6.3 is mainly concerned with the application of the modal modelling and derivation techniques of section 5.2.2 to measurements nade using the final exciting block, Hark 6.

6.1 Specification of Test Beams

The material used for the test beams was steel, chosen for its availability and also because, being very lightly damped, it would offer a wide dynamic range of response and thus tax the measurement process Several factors were considered in deciding upon the dimensions of two beams. The beam were to have their dynamic properties as substructures measured and then the properties of a coupled beam structure consisting of the two beams joined end to end were to be predicted end compared with the actual properties.

Therewere frequency constraints to be imposed in order to keep within the range in which accuratemeasurenects could be reliably expected. This range had a lower bound of 50 Hz (mains frequency) and an upper one of about 1000 Hz above which transducers and drive rods carbegin to cause problems. Thus the decade 83 to 800 Hz was selected 2s the 'central' frequency range.

The beams were to be tested in a free-free configuration; this having boundary conditions which can be cost closely achieved in an experiment. The longer of the two beams was chosen with a section of 25.4 mm x 31.75 mm (1" x 1¼") and a length of 1.4 m. Figure 4.1 shows the relationship between length of beam and natural frequency for rectangular steel beams of various depths and it can be seen that the Long Beam bending in its stiffer plane has four natural frequencies in the 'central' range, at 85.91, 236.8, 464.2 and 767.4 Hz. The Short Beam was chosen to have the same cross-section and length of 0.65 m. This beam has its first two natural frequencies at 396.5 and 1099 Hz, deliberately chosen so as not to coincide with those of the Long Beam.

Dimensional Tolerances

The limit of measurement of mobility using the Solartron mini-computer-controlled equipment was 1% (≏ 0.1 dB) and it was decided to investigate the dimensional tolerances of the beams necessary for this order of accuracy to be achieved. A special Fortran computer program was written to investigate the limits which were frequency-dependent and not easy to analyse and it was found that a 0.02% change in length, l, caused a maximum mobility error of 0.11 dB and a 0.03% change of thickness an error of 0.1 dB. Thus the beams were specified:

$w = 25.4 \pm 0.1$ mm
$h = 31.75 \pm 0.01$ mm
} within nominal tolerances of bar stock

$l_L = 1400 \pm 0.2$ mm for the Long Beam

$l_S = 650 \pm 0.1$ mm for the Short Beam

The natural frequency is independent of the width, w, of the beam.

6.2 Development of Exciting Block Design via Tests on Beams

6.2.1 Use 0f Exciting Block Mark 4G

This small exciting block, whose dimensions are given in Figure 5.4, was attached by adhesive to a point on the Long Beam 0.4 m fror one end. This pointwas chosen because it was not a node of any mode in the frequency range up to1000 Hz. Itwasfairlyclosetoa rotation antinode and a displacement node of the fourth node at 767.4 Hz. Reference tc the theoretical data presented as continuous lines on Figure 6.1 shows that the ($\dot{X}/F$) response has a relatively small (but far fron zero) resonance and the ($\dot{\theta}/M$) response a relatively large resonance at this frequency. The point mobility matrix data presented as dots on this Figure were obtained by using the standard method involving program PM2/1 . The force was input centrally for Run 1 and offset 0.05 m fpr Run 2.

These data have interesting characteristics. The fit of point translational data ($\dot{X}/F$) is excellent showing very little scatter throughout the rage 10 to 1000 Hz. The cross-nobilities ($\dot{\theta}/F$) and ($\dot{X}/M$) are reasonably accurate around the first resonance at 86 Hz and above the second at 237 Ez. The values at low frequencies are seriously in error, showing a resonance at about 17 Hz which could be attributed to the suspensioo rubbers. The deviation Iron the rigid body mass line below 50 Ez averages 6 dB - an error of 100%. The fit of the measured rotational quantity ($\dot{\theta}/M$) is ever, worse, showing error throughout the frequency range and averaging +20 dB (1000%) in the region dominated by rigid body motion.

The poorness of this measurement was considered is section 5.3.1 and attributed to the low rotational signal levels. Accordingly it was decided to increase the torque input by using two shakers in a push-pull configuration. Block Mark 4G was modified by the addition of an auxiliary block and the apparatus set up as shown in Figure 6.2. The twin-

shaker equipment was that used by Sainsbury [31] andwas available in the laboratory. The results obtained using this equipment show a slight improvement in the parameter ($\dot{x}/M$) but rather worse accuracy f o r ($\dot{\theta}/M$)As commented upon in section 5.2.1 Block Mark 4G evidently has too small 2 lever am to give sufficient rotationai signal.

6.2.2 Use of Exciting Block Mark 5

The salient feature of Block Mark 5 (Figure 5.5) is that both input force and output acceleration have values of $\pm$ 0.05 m, the force transducer sharing a common axis and common mounting stud uith one or other accelerometer. Experiments with this block showed that the orientation of the accelerometers about their nominal axes of sensitivity was a variable affecting accuracy. Accelerometers with low transverse sensitivity were specified subsequently.

Two different methods of arranging that accelerometer 2nd force gauge sharing a common axis are sketched in Figure 6.3. Experience obtained in measurements on the Long been indicated that such commonality wasa source of systematic error whose magnitude was altered if the systen of block and transducers was dismantled and they? reassembled.

A series of tests on the Short Beam gave useful information. Emphasis was laid on the rotational response ($\dot{\theta}/M$) which could be measured with the exciting bloc% attached at the end but et right angles to the beam, so that excitation parallel to the long axis would induce transverse vibrations. Four configurations of transducer positions are shown in Figure 6.4. The mobility parameters measured using Configuration (a) are snown in Figure 5.5. The translational response ($\dot{x}/F$) which should be a simple mass line appears to have a resonance about 900 Hz and is otherwise about +5 dB in error. The ideal cross response is zero

(at $-\infty$/on the dB scale), there being no interaction between applied torque and longitudinal displacement for this symmetrical combination of bear.? and block. As can be seen the neasured cross response is mainly in the range -60 to -80 dB. The rotational nobility ($\dot{e}/F$) is also grossly in error by about 20 dB in the low frequency region.

The function of progran PM2/1 is to acquire nobility data for each accelerometer with respect to the force gauge and then to process these data to give the rotational and translational parameters based on the sums and differences as shown in Figure 5.2. A calculation was done to 'invert' the procedure, starting with ideal mobility data for the beam and then calculating the mobilities that would be observed at accelerometer locations on an added exciting block. The resultant frecuency response curves are shown as Figure 6.6. At low frequencies the two accelerometers indicate a small difference which vanishes at 100 Hz, the first antiresonance frecuency of ($\dot{e}/F$), the frecuency at which the accelerometer signals are ecual. One accelerometer experiences an antiresonance with a change of phase at 330 Hz so that although both accelerometers indicate a resonance at 400 Hz the sum of their signals is small and finite and in this ideal case does not deviate from the mass line.

Direc t measurement was made of the individual mobility properties at the mounting points of the accelerometers using Configuration (a). The results shown as Figure 6.7 show systematic errors although the general shape of each curve is correct. it is most significant that the accelerometer with the greater error is mounted on the same side of the block as the force gauge. These data and others similar led to the conclusion reached in section 5.3. j that base strain sensitivity of accelerometers was a major source of systematic error. it can be seen fron Figure 6.4(a) that in Configuration (a) one accelerometer is inboard cf the force gauge and it is mounted on a surface which will be strained

when Force is applied. With this consideration in mind it can be seen in Figure 6.4(c) that the strain in the block has least effect on the accelerometer in Configuration (c). The results of mobility measurement using Configuration (c) are shown in Figure 6.6 and they are seen to be significantly better than those presented in Figure6.5. The mass line of $(\dot{X}/F)$ is mostly accurate; the *cross* responses are about 20 dB lower than *before* (noting the change of dB scale) and the $(\dot{e}/F)$ mobility is now about -3 dB in error at the low frequencies dominated by rigid body behaviour.

At this juncture it seemed that $(\dot{e}/F)$ would never be satisfactorily measured directly and stimulus was given to the development of the modal model derivation method of section 5.2.2 as a potential way of providing adequate $(\dot{e}/F)$ data indirectly.

Lastly, it should be mentioned that Block Mark 5 was used in measurements on various L-shaped assemblies of Long and Short Beams joined orthogonally at their tins. There were four different methods of connection. Two involved continucus contact at the joint, one using 'Plastic Padding' as adhesive and the other a welded joint. The other two methods had bolt fixings, in one case incorporating four 2BA cap-head bolts and the other a single $\frac{1}{2}$" BSF cap-head bolt. In the two cases of continuous contact the comparison of measured data with computed ideal data was quite close. In the case of bolt fixing, on the other hand, the measured results were very erratic and quite unrepeatable. The nature of joints and their effects upon coupling calculations were subsequently investigated by Silva [92].

Comments on Exciting Block Mark

This block was partially successful in that increased rotational input and response were obtained. It was apparent that sharing a common mounting axis for force gauge and accelerometer led to interference between the transducers. In all configurations there was some effect

of base strain sensitivity and in some the associated errors were excessive. it was found that the 'skirts' intended to stiffen the block made connection and alignment of the accelerometers when they were mounted under the block very awkward. However, in the light of experience gained with Block Mark 5, its satisfactory successor - Mark 6 - was designed.

6.3 Application of a Developed Exciting Block - Mark 6

6.3.1 Established Mobility Measurement Techniques Extended by Modal Modelling and Derivation

Data for point translational and rotational quantities were acquired in a conventional manner using exciting Block Mark 6 with the mini-computer-controlled system. Modal modelling using the identification and derivation techniques of Chapter 2 were used to smooth the data and to compensate for errors in the measurement of rotational quantities.

Measured Mobilities of Long and Short Beams

In order to measure the mobilities of the Long Beam the Mark 6 exciting block was attached by adhesive to the beam such that the test point, P, Was as close as possible (0.16 m) tc the tip. A B & K 8200 force transducer was used, together with two Endevco 233E accelerometers. Measurements were made at 76 discrete frequencies in the range 31.6 Hz to 1 OOC Hz, this being the upper three-quarters of a logarithmic sweep of 101 frequencies for the two decades from 50 Hz to 1000 Hz.

The resultant measured data are shown as dots on Figure 6.9 in which the continuous lines show the theoretical response for the beam tip, computed using closed-form receptance formulae.

The measured responses for $(\dot{X}/F)$, $(\dot{\theta}/F)$ and $(\dot{X}/M)$ show a little scatter but are accurate to within about 2 dB up tc 800 Hz. The $(\dot{\theta}/M)$ response is inaccurate below the first response arid shows an antiresonance at about 57 Hz whereas the theoretical antiresonance is well below 30 Hz. Above the first resonance at 86 Hz, however, the measured $(\dot{\theta}/M)$ response is reasonably accurate. The results of other tests 33 this

beam have very similar features.

A number cf corresponding tests were carried out on the Short Beam 2nd the results are shown in Figure 6.10. These show very good correlation between the measured date and the theoretic21 tia response for the $(\dot{X}/F)$, $(\dot{\theta}/F)$ and $(\dot{X}/M)$ mobilities. The biggest discrepancies are in the location of the antiresonances, but this is probably 2 result of the measurement point not being quite at the tip of the beam, but 0.016m inboard. (A theoretic21 calculation Was made for 2 point 0.016 m along a 0.65 beam. This showed antiresonances exactly coincident with those of the measured date. The resonances, of course, were uncharged and remained in close coincidence with the measured data points.) The $(\dot{\theta}/M)$ response is reasonably accurate above 200 Hz but has a considerable error of about +8 dB below that frequency.

In general, it can be seen that the two rotational responses $(\dot{\theta}/F)$ 2nd $(\dot{\theta}/M)$ are the more difficult to measure accurately and $(\dot{\theta}/H)$, which involves two rotational quantities, is unlikely to be accurate at frequencies below the first resonance. The $\ddot{\theta}$ data deaends, 2s has Been discussed, on the difference between the signals of the two accelerometers, which have therefore to be accurately matched and carefully calibrated. Any spurious response which has only 2 slight effect on the $\ddot{X}$ data (which depends on the sum of the accelerometer signals) will 'have a major effect on the $\ddot{\theta}$ value. In most cases it is also true tc say that the expected values of acceleration due to rotation are much smaller than those due to translation.

It is apparent that the low frequency discrepancies in the $(\dot{\theta}/M)$ response, which are larger for the Long Beam than the Short, arose because of the effects of base strain on the 2cceleroneter nearer the force gauge. At the time of these tests alternative accelerometers with lower base strain sensitivity which also had transverse sensitivity as low 2s 1% were not available. The techniques cf modal modelling and derivation were used to bypass the problem.

Analyses of the Coupled Beam

The mathematics of coupling substructures were noted in section 1.3.3 2nd were seen to involve the addition of impedance quantities. In the particular case here considered the 2 x 2 point mobility matrix for the junction point 1.4 m along the 2.05 m Coupled Beam, C, is to be found by use of the equation:

$$\left[Y_C\right] = \left[\left[Y_L\right]^{-1} + \left[Y_S\right]^{-1}\right]^{-1} \qquad (6.1)$$

where $\left[Y_L\right]$ and $\left[Y_S\right]$ are the 2 x 2 point mobility matrices for the tips of the Long and Short Beams respectively.

The calculation has to be carried at each frequency data point.

Coupled-Beam Analysis Using Raw Data

The measured data used for Figures 6.9 2nd 6.10 were combined, frequency by frequency, in a calculation of the mobility responses at the point of connection between the Long beam (1.4 m) 2nd the Short beam (0.65 m).

The result of this direct calculation is shown 2s Figure 6.11, together with the theoretical values cf the mobility at a point 0.65 m along a 2.05 m beam. The predicted results are extremely poor for all four nobility parameters except in the range 180 Hz to 400 Hz. Examination of the input data shows that this is the only frequency range for which the ($\dot{e}$/M) response of the Short Beam is accurate. The other seven mobility parameters have wider ranges of reasonable accuracy. Thus it is concluded that if any of the eight input mobility parameters is inaccurate at a particular frequency, then all the calculated mobilities of the combined structure will probably be wrong at that frequency.

Analyses of the Coupled Beam

The mathematics of *coupling* substructures were noted in section 1.3.3 and were seen to involve the addition of impedance quantities. In the particular case here considered the 2 x 2 point mobility matrix for the junction point 1.4 m along the 2.05 m Coupled Beam, C, is to be found by use of the equation:

$$\left[Y_C\right] = \left[\left[Y_L\right]^{-1} + \left[Y_S\right]^{-1}\right]^{-1} \qquad (6.1)$$

where $\left[Y_L\right]$ and $\left[Y_S\right]$ are the 2 x 2 point mobility matrices for the tips of the Long and Short Beams respectively,

The calculation has to be carried at each frequency data point.

Coupled-Beam Analysis Using Raw Data

The measured data used for Figures 6.9 and 6.10 were combined, frequency by frequency, in a calculation of the mobility responses at the point of connection between the Long beam (1.4 m) and the Short beam (0.65 m).

The result of this direct calculation is shown as Figure 6.11, together with the theoretical values of the mobility at a point *0.65 m* along a 2.05 m beam. The predicted results are extremely poor for <u>all four</u> nobility parameters except in the range 180 Hz to 400 Hz. Examination of the input data shows that this is the only frequency range for which the ($\dot{e}$/M) response of the Short Beam is accurate. The other seven mobility parameters have wider ranges of reasonable accuracy. Thus it is concluded that if <u>any</u> of the eight input mobility parameters is inaccurate at a particular frequency, then <u>all</u> the calculated mobilities of the combined structure will probably be wrong at that frequency.

The $(\dot{e}/M)$ responses were confirmed 2s the chief sources of error by another calculation in which the raw $(\dot{e}/M)$ data of both subsystem were replaced by theoretic21 $(\dot{e}/M)$ data. The result of this exercise is shown in Figure 6.12 which illustrates 2 considerable improvement in accuracy when compared with Figure 6.11 especially below 80 Hz. The overall accuracy, however, is still not acceptable since there are ranges where the scatter is considerable, (80 - 100 Hz; 120 - 140 Hz; 400 - 500 Hz, for example).

Improvement in the resultant coupled data could evidently be made first, by smoothing, and second, by improving the accuracy of the rotational mobilities $(\dot{e}/F)$ 2nd $(\dot{e}/M)$ for the tsc component subsystems.

Coupled Beam Analysis Using Smoothed Data

A major advantage of the identification process developed in Chapter 2 is that the frequency response regenerated fros modal data is smooth, having none of the small irregularities of directly-measured data. Accordingly, the measured data for the substructure beams were examined and data selected for use in an identification curve fit.

The raw date for the Long Beam were exe-iced 2nd five resonant frequencies (0, 86, 274, 457 and 758 Hz) estimated. Data measured et the N off-resonant frequencies of 31.6, 63.2, 120, 302 and 724 Hz were t&en 2nd used tc calculate modal constants from which the smoothed curves cf Figure 6.13 were calculated. These are seen to be quite similar to the raw data of Figure 6.1 C except above 758 Hz, the highest resonant frequency used. Above thet frequency, the curves approach the 20 dB/decade mobility line of a mass, because the dominant contribution is from the highest mode included in the identification which is mass-like above its resonant frequency.

In the case of the Short Beam, the resonance frequencies were estimated from the raw data to be G, 394 2nd 1100 Hz and data measured at 31.6, 209 and 603 Hz were used in the modal calculations giving the

results shown in Figure 6.14 which is recognizably a snoothed version of Figure 6.10. There is no high frequency discrepancy on this plot because the highest node use? is at a frequency higher then the range limit of 1000 Hz. In general, smoothing by modal identification gives acceptable accuracy provided that the number of modes identified is one more than the number of modes which lie within the frequency range of interest.

The snoothed date of Figure 6.13 and 6.14 were coupled using exactly the same process 2s before to produce a predicted set of responses for a 2.05 m beam. The results are presented in Figure 6.16 but although having less scatter, they are not otherwise any improvement in the unsmoothed results in Figure 6. 11.

However, there was one advantage in using smoothed data at this stage, and that was k - i the computation time which was considerably reduced since much less data needed to be handled. However, it should be said that inconsistencies may be built into the calculations if the related curves are smoothed independently; using different estimates of resonance frequencies, for example.

Derivation of Rotational Mobilities

The idea of deriving $(\dot{e}/M)$ data to avoid the inaccuracies of measurement was introduced in section 2.2.2 example (iv) and further developed in section 5.2.2. In this case the substructure beams were freely supported during the tests and thus have rigid body modes at zero frequency. It has to be remembered that the derivation relationships for this case must take account of the separation of rigid body modes as detailed in section 2.2.3 and demonstrated in Chapter 4.

The mobilities $(\dot{e}/F)$ and $(\dot{e}/M)$ can be derived from measurements of $(\dot{x}/F)$ and $(\dot{x}/M)$ using the modal identification techniques, without measuring rotations directly.

Calculations using the relationships between the modal constants developed above were carried out for both beams and the results are shown in Figures 6.16 and 6.17. In these, there are only three distinct responses presented since $(\dot{e}/F)$ is now automatically identical to $(\dot{X}/M)$ (since $_{r}A_{12} = {}_{r}A_{21}$).

When the derived $(\dot{e}/M)$ response of Figure 6.16 is compared with the smoothed $(\dot{e}/M)$ response of Figure 6.13, it is immediately apparent that the accuracy at low frequencies below the first resonance at 86 Hz, where the Figure 6.13 response is very poor, is now greatly improved and at higher frequencies up to 800 Hz, where Figure 6.13 was quite good, it is a little further improved.

Similar observations apply to the comparison of $(\dot{e}/M)$ responses of Figures 6.14 and 6.17 for the Short Beam. The accuracy of the Figure 6.17 curve is less than that of Figure 6.16 because fewer modes are included, but most significantly the $(\dot{e}/M)$ response is accurate around 30 Hz.

The conclusion of this section is that better $(\dot{e}/M)$ results may be obtained by identifying the $_{r}A_{11}$ and $_{r}A_{12}$ modal constants from $(\dot{X}/F)$ and $(\dot{X}/M)$ measurements and then calculating $_{r}A_{21}$ and $_{r}A_{22}$ than by trying to identify $_{r}A_{21}$ and $_{r}A_{22}$ directly from the inevitably less reliable $(\dot{e}/F)$ and $(\dot{e}/M)$ raw data.

Coupled Beam Analysis Using Derived Data

The four mobility responses for the Coupled Beam were again computed, this time using the derived $_{r}A_{21}$ and $_{r}A_{22}$ constants together with the identified $_{r}A_{11}$ and $_{r}A_{12}$ constants. Again, there are only three distinct responses presented in Figure 6.18 because $(\dot{e}/F)$ and $(\dot{X}/M)$ are taken as identical.

These coupled data are inaccurate above 800 Hz, the highest frequency for which the data for the Long beam is reliable. Below 800 Hz the fit of the smoothed and derived data to the curve calculated from closed-

form receptance formulae is much better than either of the previous examples shown in Figures 6.15 and 6.11. In particular, these results based on consistent data for both subsystem predict the low frequency resonance at 42 Hz which is absent from the earlier Coupled Beam results. The other 5 resonances are also indicated with reasonable accuracy for the mobility ($\dot{X}/F$), and this response has the right general shape and level up to 800 Hz. The ($\dot{e}/F$), ($\dot{X}/M$) responses maintain good shape up to 400 Hz, although the resonance at 120 Hz is only just noticeable. The 120 Hz resonance is missed altogether from the ($\dot{e}/M$) response but it should be noted that the corresponding theoretical resonance is very small.

The identification and derivation process is thus more accurate for low frequencies than for high which may be explained by the inherently greater accuracy of low frequency modal constants. The results were felt to be significant mainly because it had not been possible, at that time, to measure ($\dot{e}/M$) at all accurately at frequencies below the first resonance by any other method.

Conclusions

The extension of conventional multidirectional measurement techniques by modal modelling and derivation has proved valuable in the smoothing of the data in the reduction of time of computation and, most importantly, in the compensation of rotational errors most significantly arising from base strain effects in accelerometers. The results could be further improved if the measurement point could be sited exactly at the beam tip rather than at some small distance inboard. The success of the derivation method used prompted the development of simplified measurement techniques of section 5.2.2 which are evaluated in section 6.3.3 following.

6.3.2 Established Mobility Measurement Technique used with Accelerometers of Low Base Strain Sensitivity

When the relatively high bese strain sensitivity of Endevco 233E eccelerometers was revealed in section 5.3.3, replacements were sought which would have the same overall characteristics including low transverse sensitivity but also have low bese strain sensitivity. The Bruel & Kjaer 'Delta Shear' types fulfilled this specification and when they became available in the Dynamics Laboratory a test was carried out using the=: with Block Mark 6 on the Long beam with the same arrangements as used before 2nd reported above in section 6.3.1. The results obtained are shown as Figure 6.19. The cost remarkable feature tc be seen is the general accuracy of the low frequency ($\dot{e}/F$) mobilities, not previously obtained without nodal modelling and derivation. There are inaccuracies still, especially in the region of the ($\dot{\theta}/F$), ($\dot{x}/F$) antiresonance at 40 Hz. It is to be expected that further improvement would be obtained by arranging that the force transducer was mounted inboard of the accelerometers so thet the surface on which they are mounted experiences less strain. The cut ting of a 'moat' around an zcceleroneter wasshown in section 5.3.3 tc produce such an isolating effect.

6.3.3 Use of Simplified MobilitMeasurement Techniques

The two simplified mobility measurement techniques which were developed theoretically in section 5.2.2 were applied to the Long and Short Beams.

Single-Accelerometer Measurements

Short Beam

Measurements were nade using two runs of program MOB1 using one Endevco 233E scceleroneter et the centre of Block Mark 6 attached at the tip of the Short Beam. The data obtained were processed by using program INCAN whose output is plotted as Figure 6.20. These results are is good is

those using conventional methods and shown in Figure 6.17. The slight inaccuracy of the antiresonances of $(\dot{\theta}/M)$ are explicable because only three modes of the system were modelled. It is to be noted that the rigid body response of $(\dot{X}/F)$ below 100 Hz is slightly high.

Long Beam

The results measurement and processing as above data measured at the tip of the Long beam are shown as Figure 6.21. Once again the single Endevco accelerometer was used. Figure 6.21 may be compared with Figure 6.16 and seen to be similar except for a larger low frequency discrepancy in $(\dot{X}/F)$. This discrepancy is larger than that for the Short Beam already commented upon. Both are attributable to the effects of base strain.

When the Endevco accelerometer was replaced by a Delta Shear B & K accelerometer of type 4366 the result obtained was free of the $(\dot{X}/F)$ low frequency discrepancy, as expected. The other responses as can be seen in Figure 6.22 are disappointingly poor. Investigation of this anomaly revealed that one of the response frequencies used for identification was a frequency of unusually high base strain, thus causing a significant error in the value of $\dot{\theta}$ estimated at that frequency. The measurement was repeated using the same accelerometer transferred to the beam itself (location 3 of Figure 5.25). The results shown in Figure 6.23 are satisfactory.

Two-Accelerometer Measurements

A single run test was carried out using two Endevco accelerometers attached to the block at ± 0.05 m. Force was input through the centrally-mounted force gauge. After IMCAL processing, the results shown in Figure 6.24 were obtained. The parameters $(\dot{X}/F)$ and $(\dot{\theta}/F)$, $(\dot{X}/M)$ are satisfactorily modelled end there is no evidence of base strain effects. The derived $(\dot{\theta}/M)$ data are a little in error, to an extent similar to that seen previously in Figures 6.16 and 6.21.

Conclusions

Either of the methods outlined in section 5.2.2 for obtaining the point mobility matrix from measured data can give satisfactory results when compared with the established method involving two accelerometers and two runs.

The two-accelerometer method has the advantage of requiring only one run if used with the mini-computer controlled multichannel equipment and, in addition, it needs no mechanical alterations during the course of the measurements. In the comparatively rare event of the testing of a symmetrical structure which responds to an input force with translation but no rotation, the method cannot be applied.

The single-accelerometer method is effective and accurate provided that base strain effects are negligible. Correct selection of the accelerometers to be used and modification of the block make this a realizable objective. The method does require mechanical alterations to be made between the two test runs but has the advantage of requiring only one accelerometer and associated signal conditioning equipment and thus is less expensive to organise than the two-accelerometer method.

Both methods may be used in laboratories equipped for accurate measurement of frequency and response level but without on-line computer facilities since all the complex and tedious calculations can be done on an off-line computer.

6.4 CONCLUSIONS: MEASUREMENT OF MULTI-DIRECTIONAL MOBILITIES ON BEAMS

The tests reported in this Chapter were carried cut on real, physical structures as distinct from computer simulations. The structures - beams - are very simple test pieces for which accurate data of natural frequencies and mobility responses could be predicted theoretically. Thus it was possible to evaluate the measurements made in the light of ideal results.

In the course of the measurements on beams the error-producing effects of the transverse sensitivity and base strain sensitivity of accelerometers were discovered and methods were developed to mitigate their effects. The persistent difficulty of getting a sufficiently large rotational signal was addressed with some success in that the Mark 6 Block, while being smaller and lighter than the blocks developed by Sainsbury [31] could be used ultimately to give acceptable data either with the established multidirectional mobility measurement techniques or with the simplified versions developed in this thesis.

The measurements on the L-shaped assembly of the two beams, mentioned briefly in section 6.2.2, provided the information that as far as mobility measurements go the use of adhesive to secure the beams was dynamically equivalent to a weld; a piece of information used in the design of the two-part blocks Mark 7 and Mark 8 used in the investigations reported in Chapter 7.

Use was made of the theoretical developments of Chapter 2 and value found in the smoothing effects of a regenerated response based on identified data and in the derivation of the purely rotational response ($\dot{e}/M$) from translational and mixed translational/rotational data in which errors are usually small.

No mention has been made so far in Chapter 6 of the use of high frequency residuals. They could, of course, be used in the modelling of individual responses to give improved high frequency curve fitting,

but they cannot be derived and thus are inapplicable to the simplified methods of rotational mobility measurement and modelling.

From this point it is now possible to go forward and apply the developed theoretical and practical techniques of mobility measurement and modelling to the acquisition of more comprehensive data for beams needed for the construction of spatial models and to more complex structures whose responses cannot be predicted theoretically.

Figure 6.1 Mobility Properties at 0.4m Point of Lonn Beam Block Mark 4G

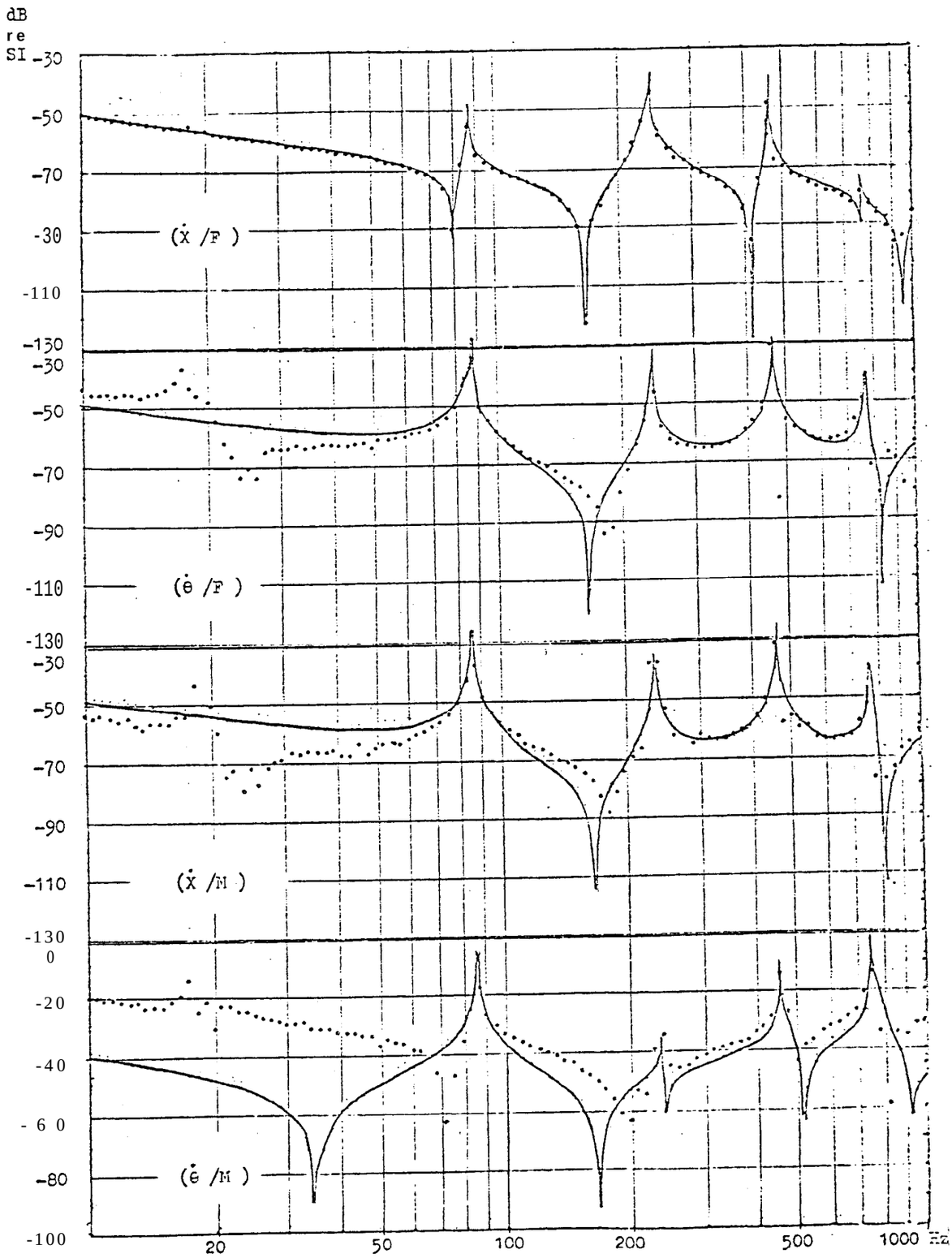

Figure 6.2 Arrangement of Plodified Block Mark 4G in Twin-Shaker Test

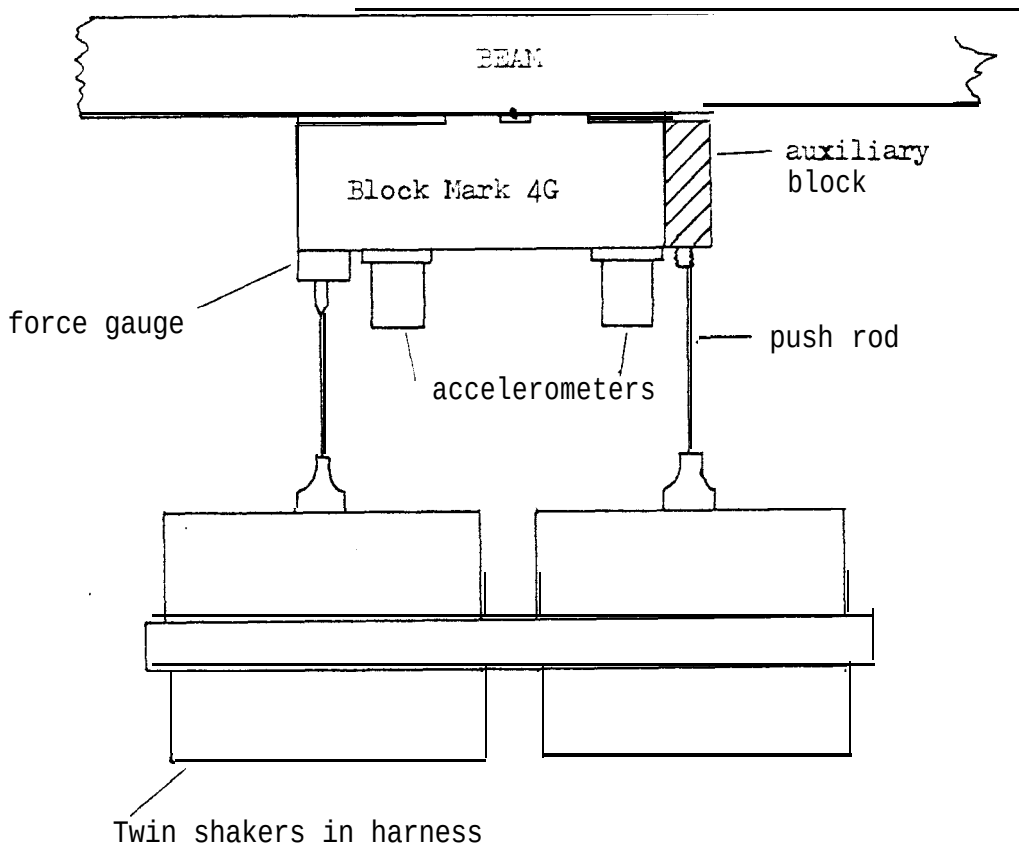

Figure 6.3 Block Mark 5 - Alternative Arrangements for Common Mounting Point

(a) Single Screw Fixing

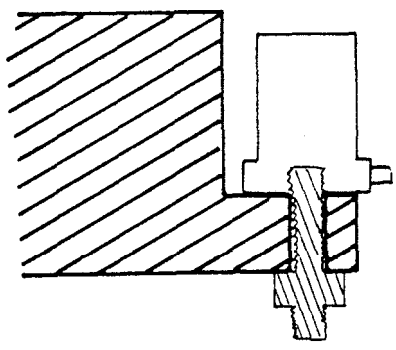

(b) Stud and Two Nuts

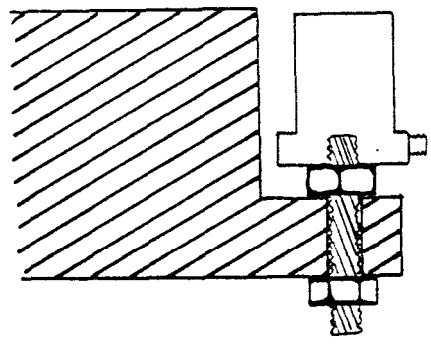

Both sketches show a section through the middle of the Block

Figure 6.4 Alternative Configurations of Transducers for Tests on Short i3ea.m

(a)

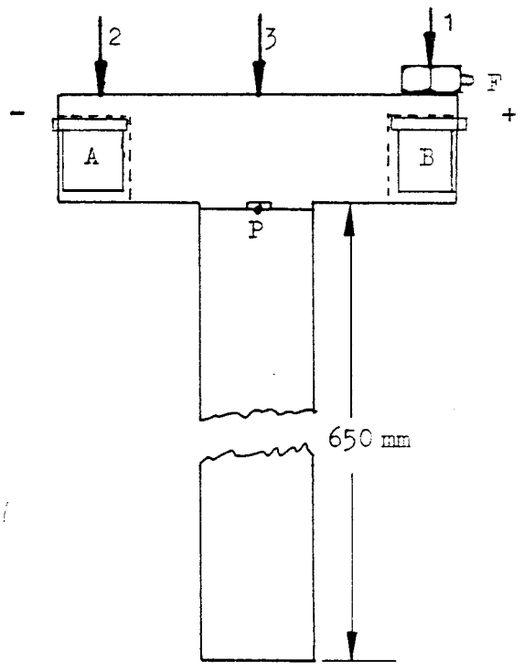

(b)

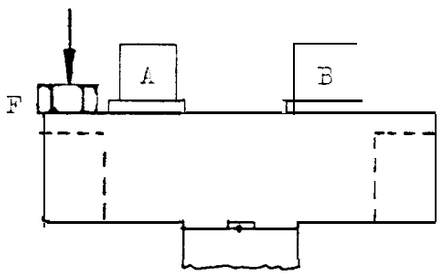

(c)

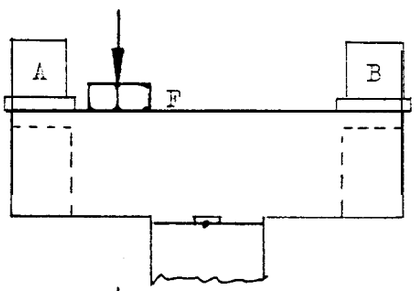

(d)

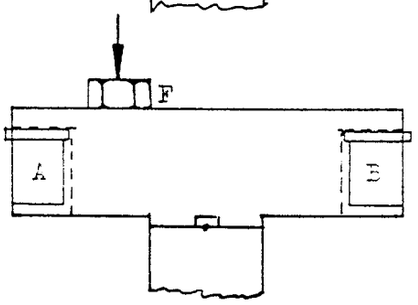

Figure 6.5 Mobility Properties at Tip of Short Beam, Configuration (a)

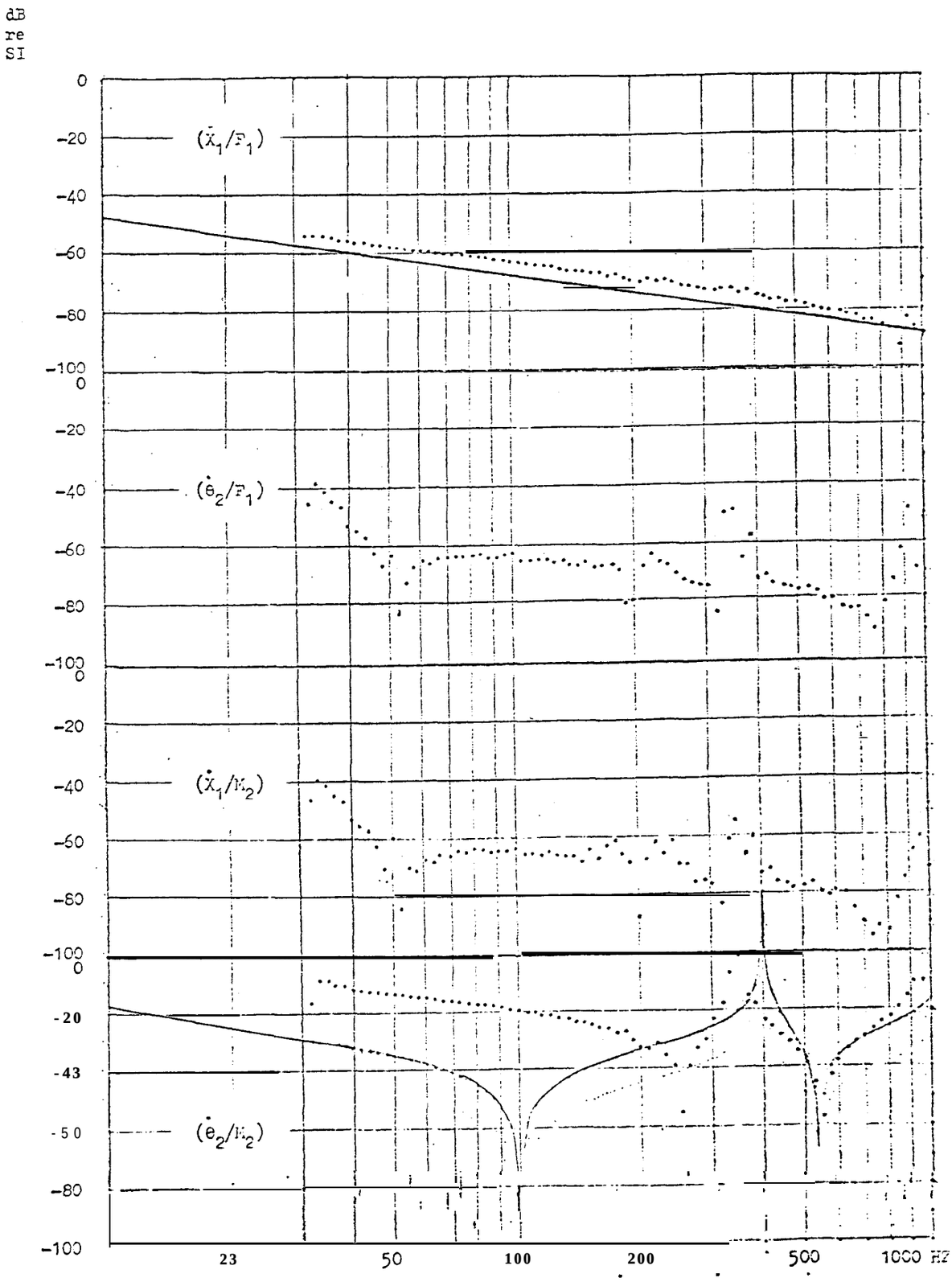

Figure 6.6 Theoretical Transfer Mobilities for Transducers in Configuration (a)

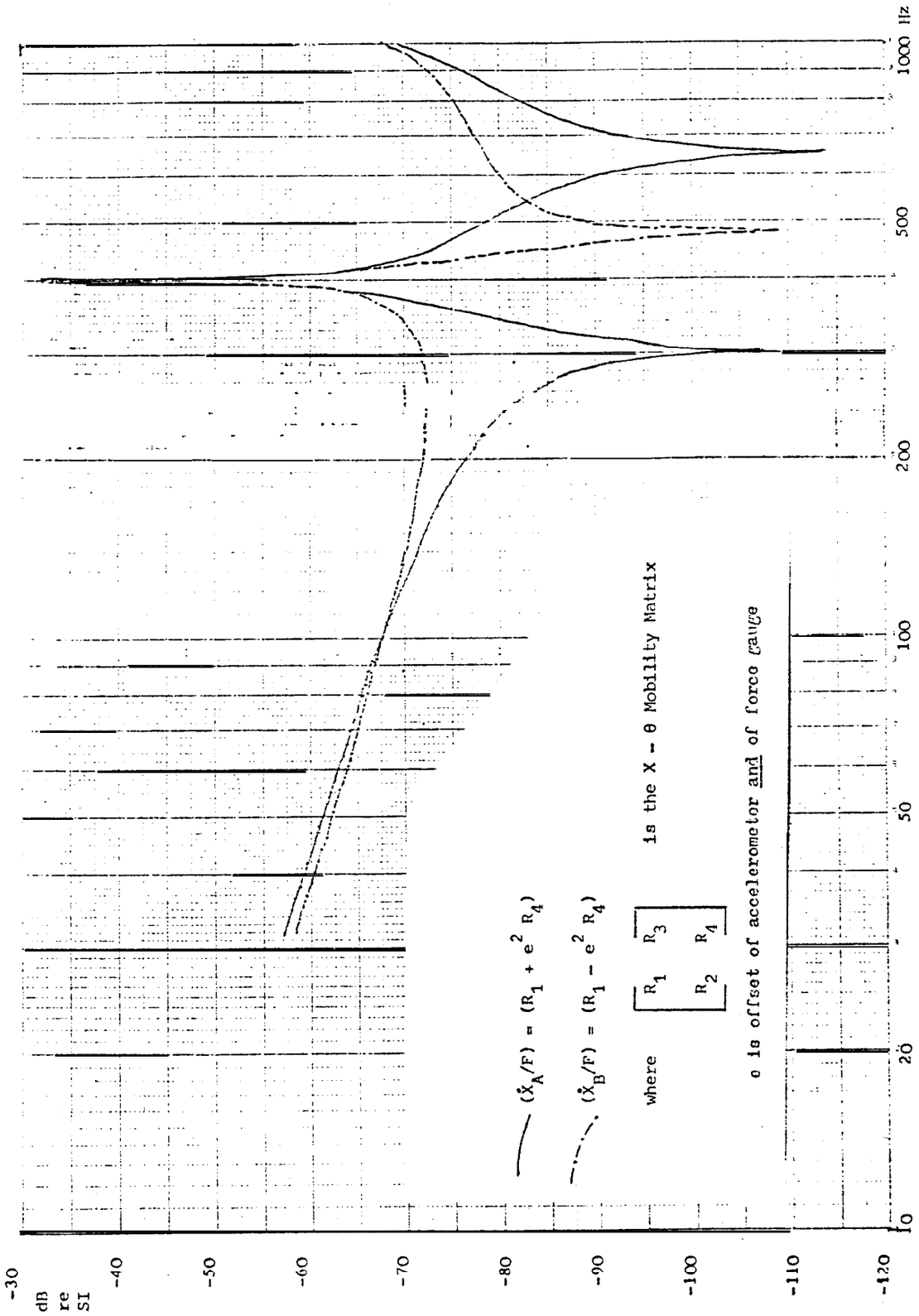

Figure 6.7 Measured Transfer Mobilities for Transducers in Configuration (a)

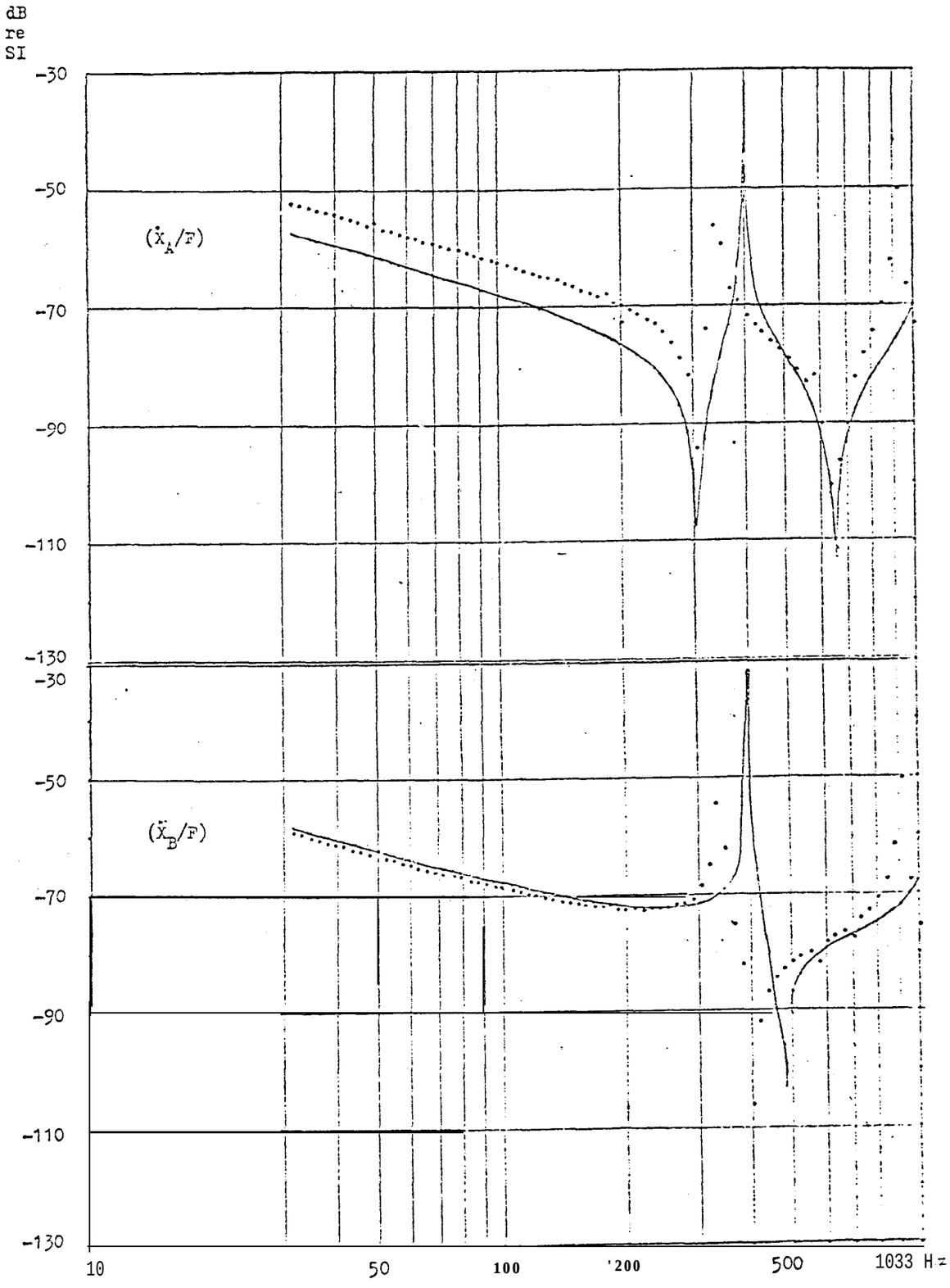

Figure 6.8 Mobility Properties at Tip of Short Beam, Configuration (c)

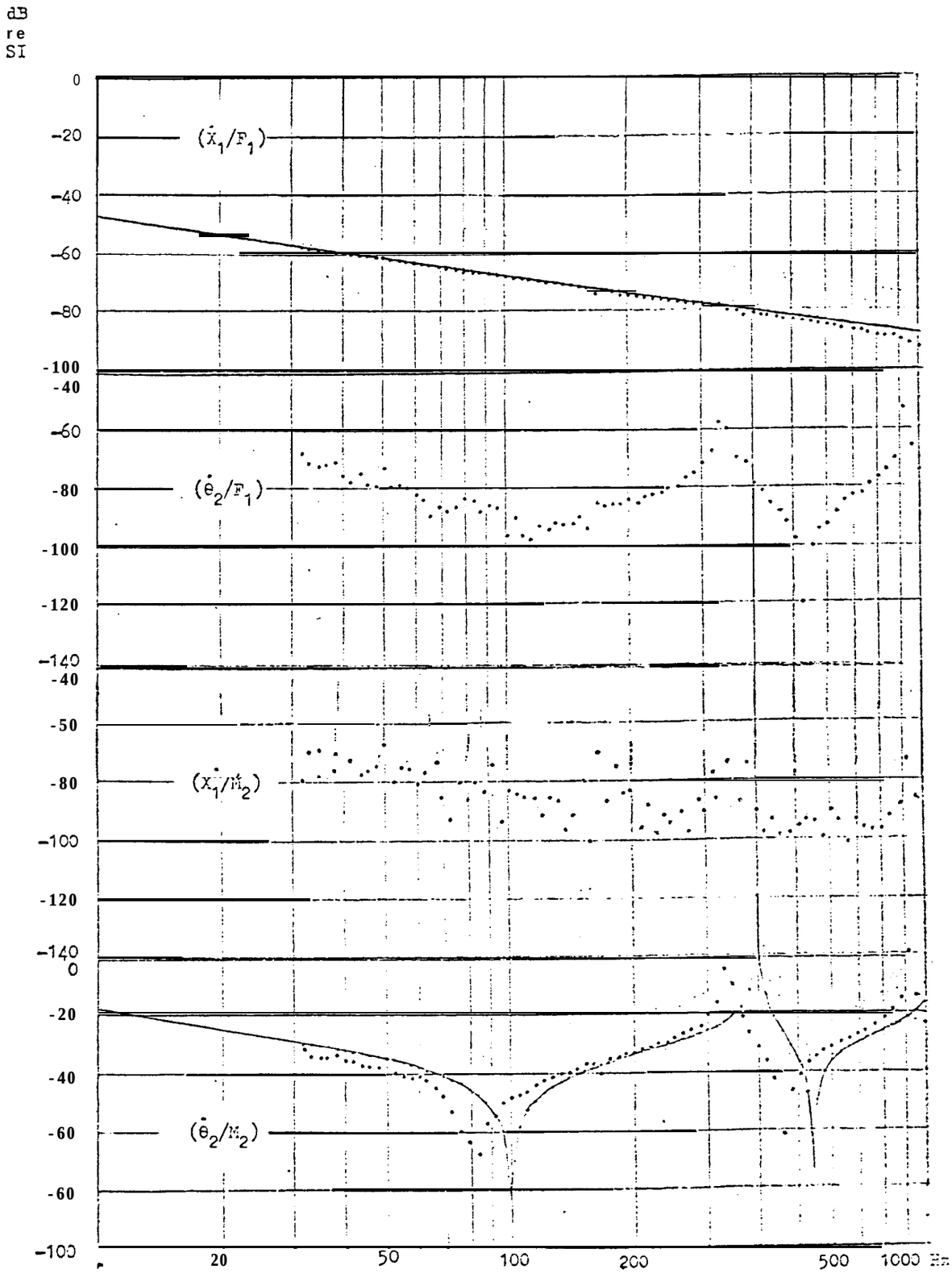

Note charge of scale of cross-mobility term

Figure 6.9 MOBILITY PROPERTIES OF THE LCNG BEAM: I

—— Theoretical . . . Direct Measurements

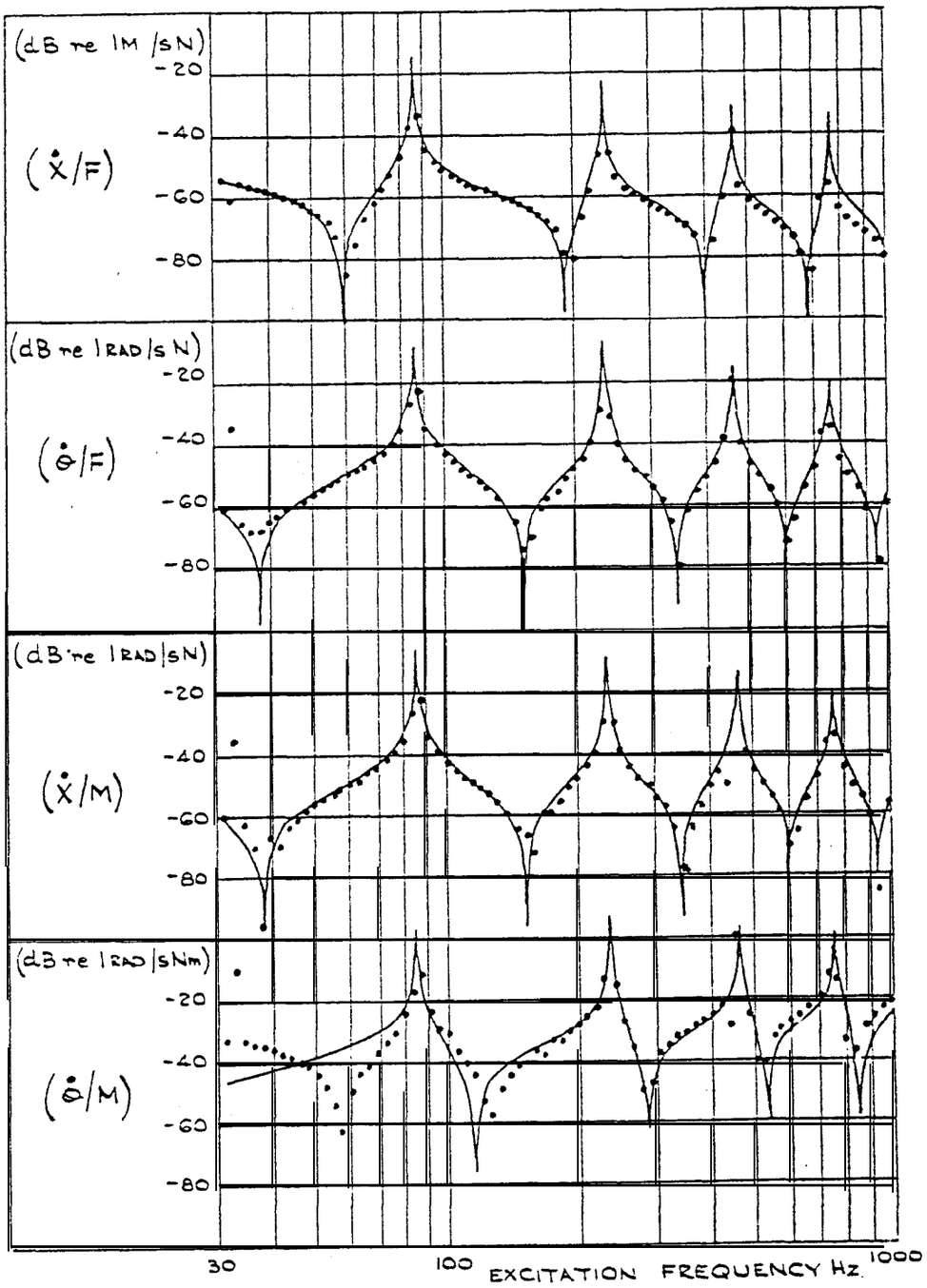

Figure 6.10 MOBILITY PROPERTIES OF THE SHORT BEAM: i

——— Theoretics1 . . . Direct Measurements

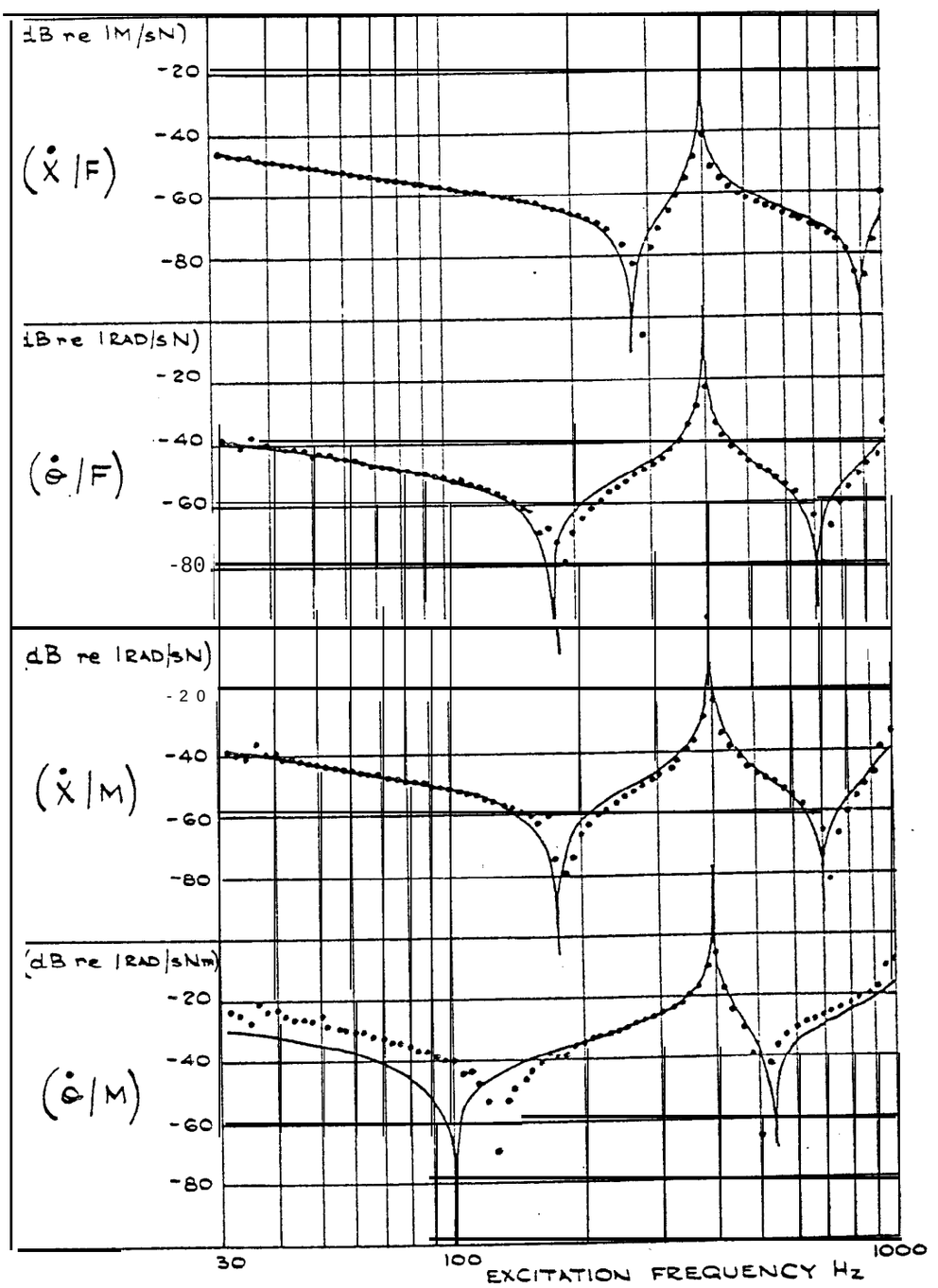

Figure 6.11 MOBILITY PROPERTIES OF THE COUPLED BEAM: I

—— Theoretical . . . predicted from direct measurements on component Seams

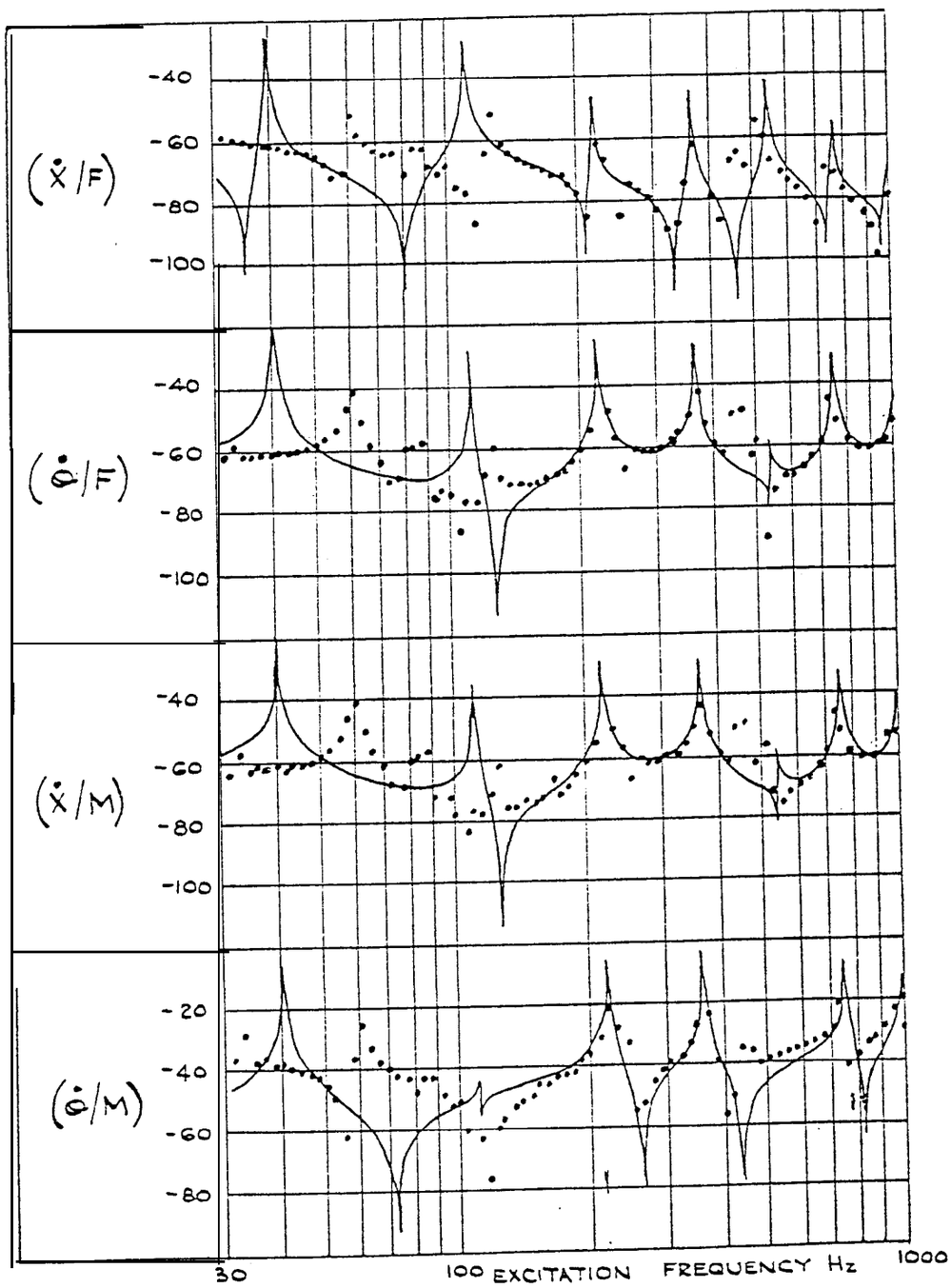

Figure 6.12 MOBILITY PROPERTIES OF THE COUPLED BEAM: II

——— Theoretical ... Predicted from direct measurements plus theoretical (β/M) data

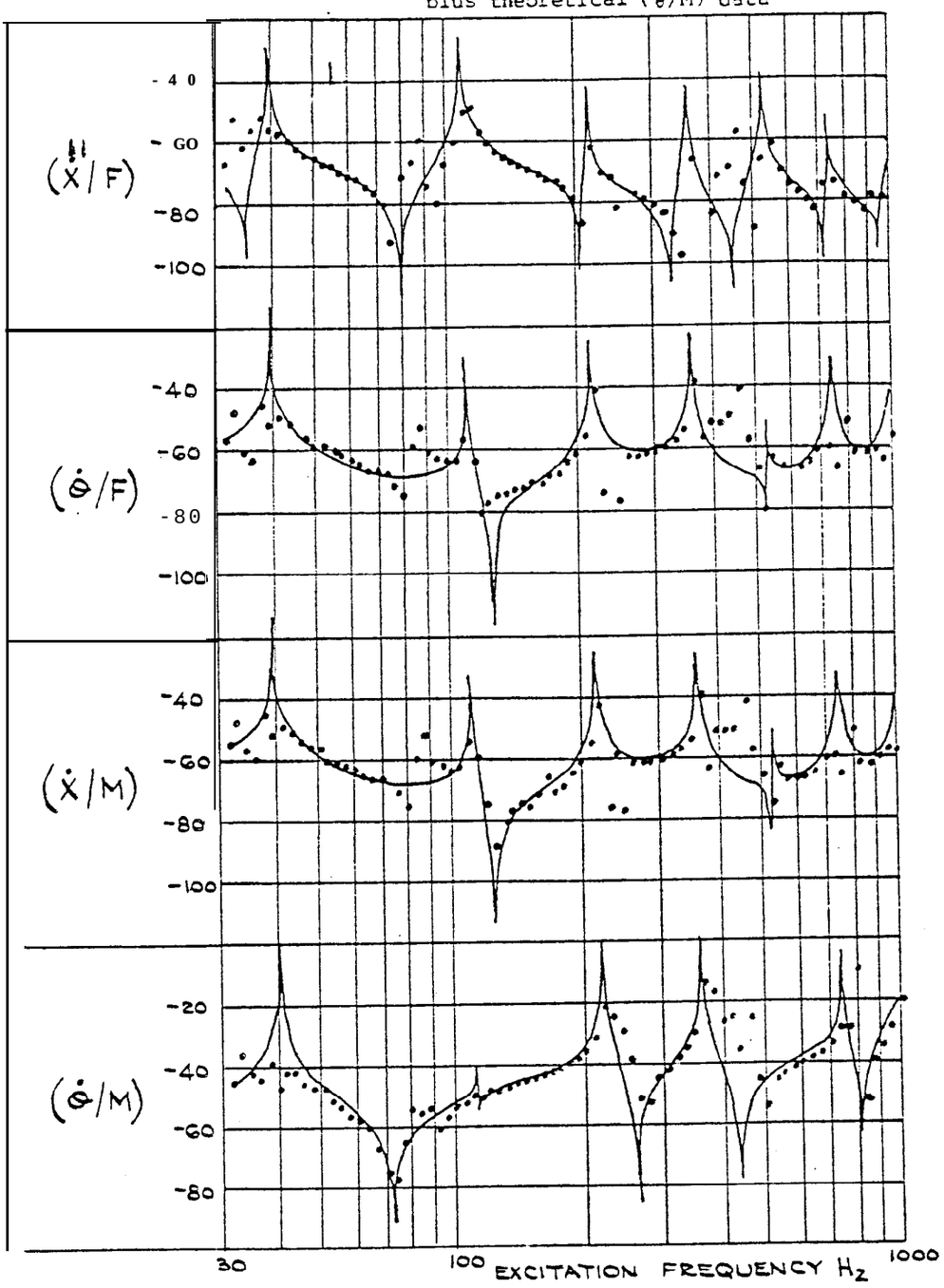

Figure 6.13 MOBILITY PROPERTIES OF THE JOINT BEAM II

——— Theoretical . . . Smoothed measurements

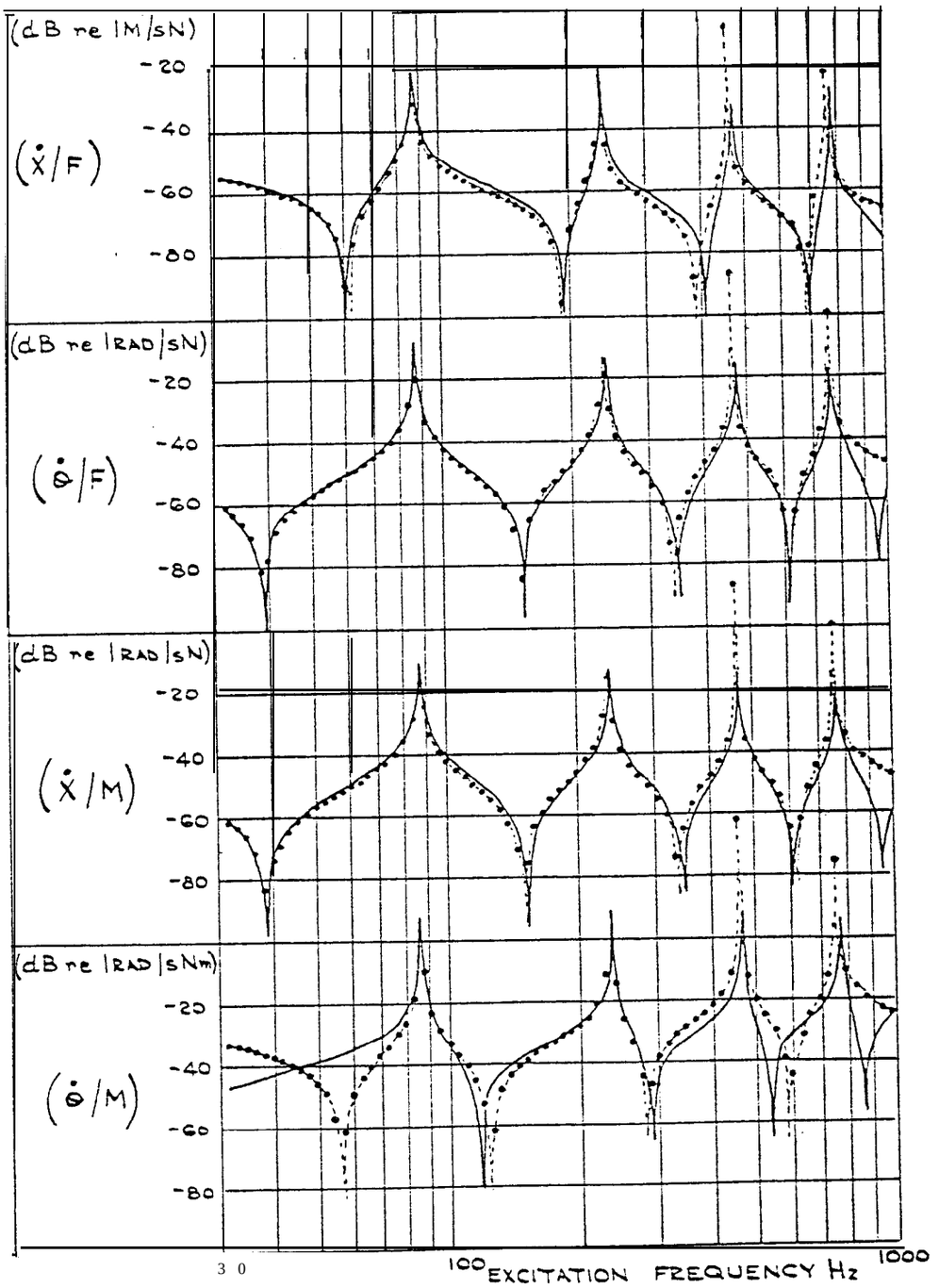

Figure 6.14 MOBILITY PROPERTIES OF THE SHORT BEAM: II

Theoretical . . . Smoothed measurements

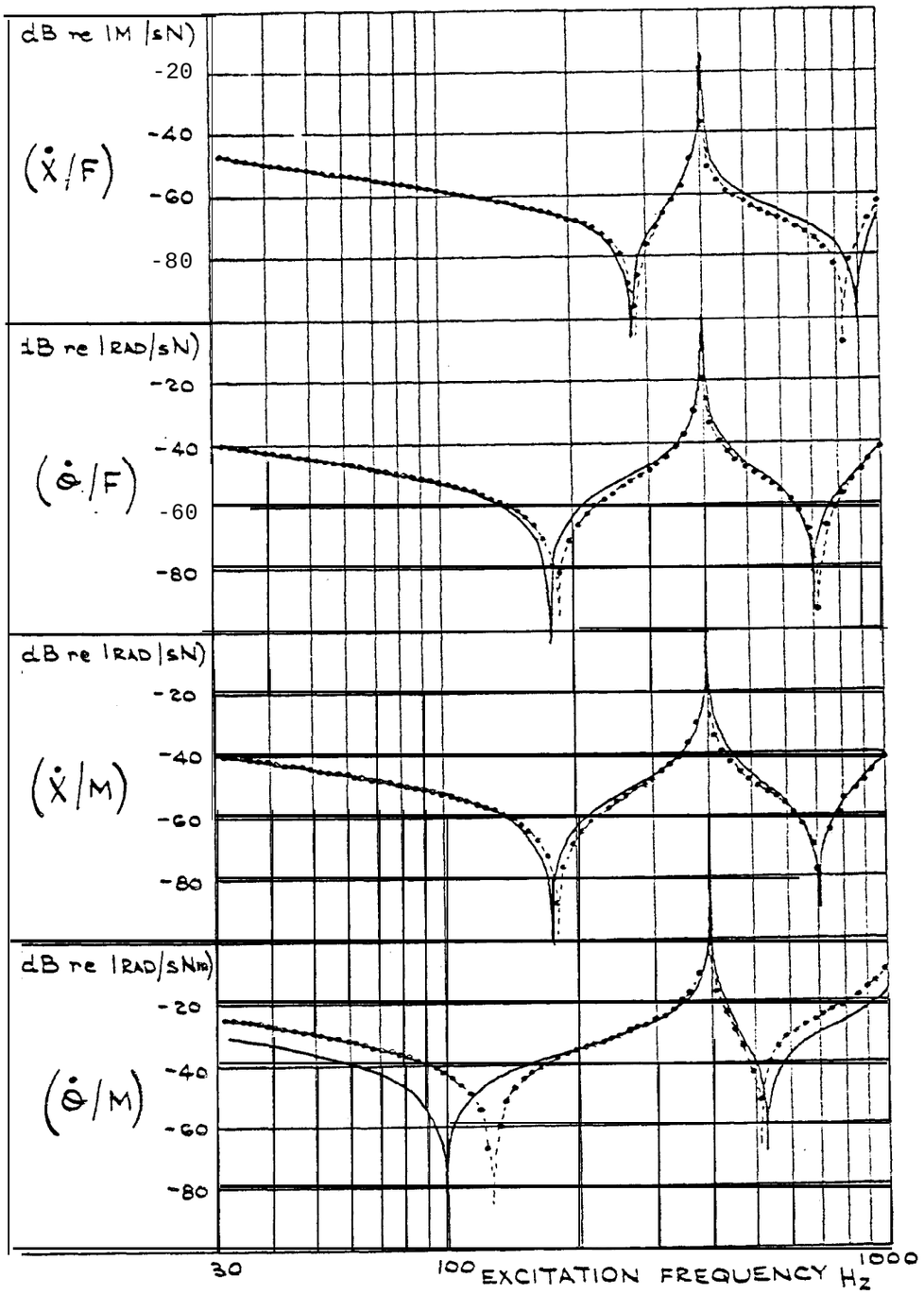

Figure 6.14 MOBILITY PROPERTIES OF THE SHORT-BEAM-II

Theoretical ... Smoothed measurements

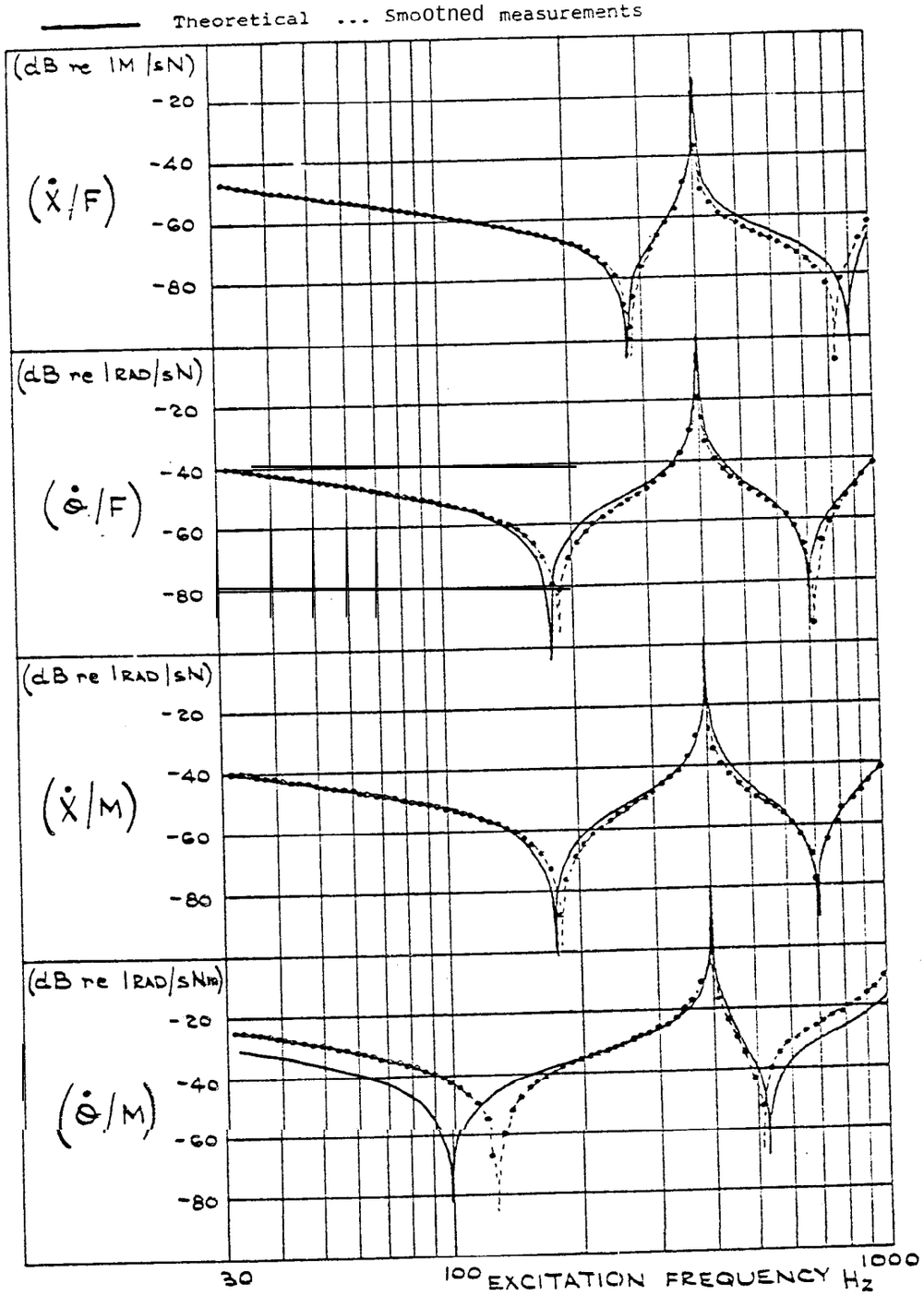

Figure 6.15 MOBILITY PROPERTIES OF THE COUPLED BEAM: III

——— Theoretical ... Predicted from smoothed measurements on component beams.

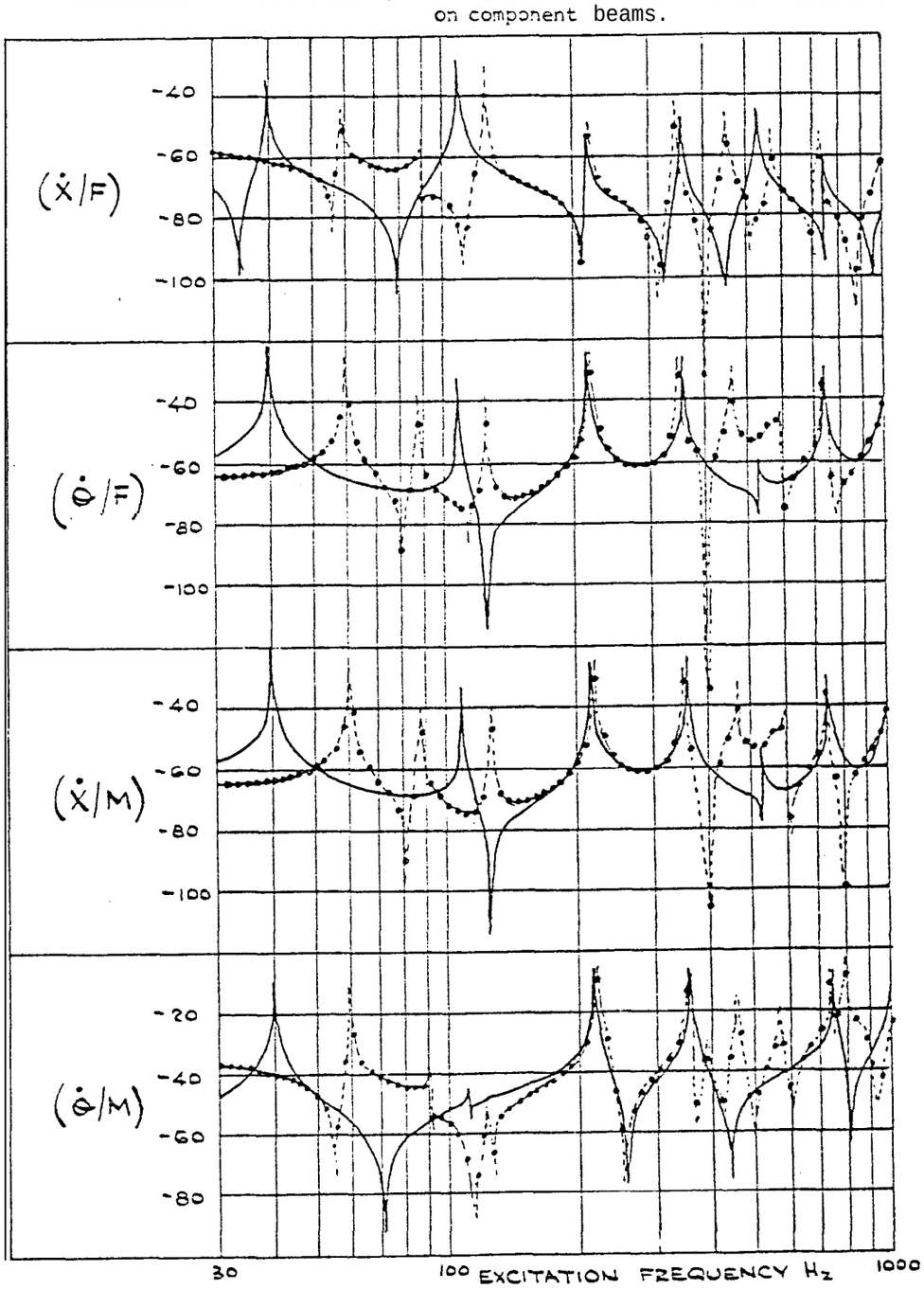

Figure 6.16 MOBILITY PROPERTIES OF THE LONG BEAM: I

——— Theoretical . . . Smoothed measurements for (X/F)(X/M)
Derived measurements for (θ/F)(θ/M)

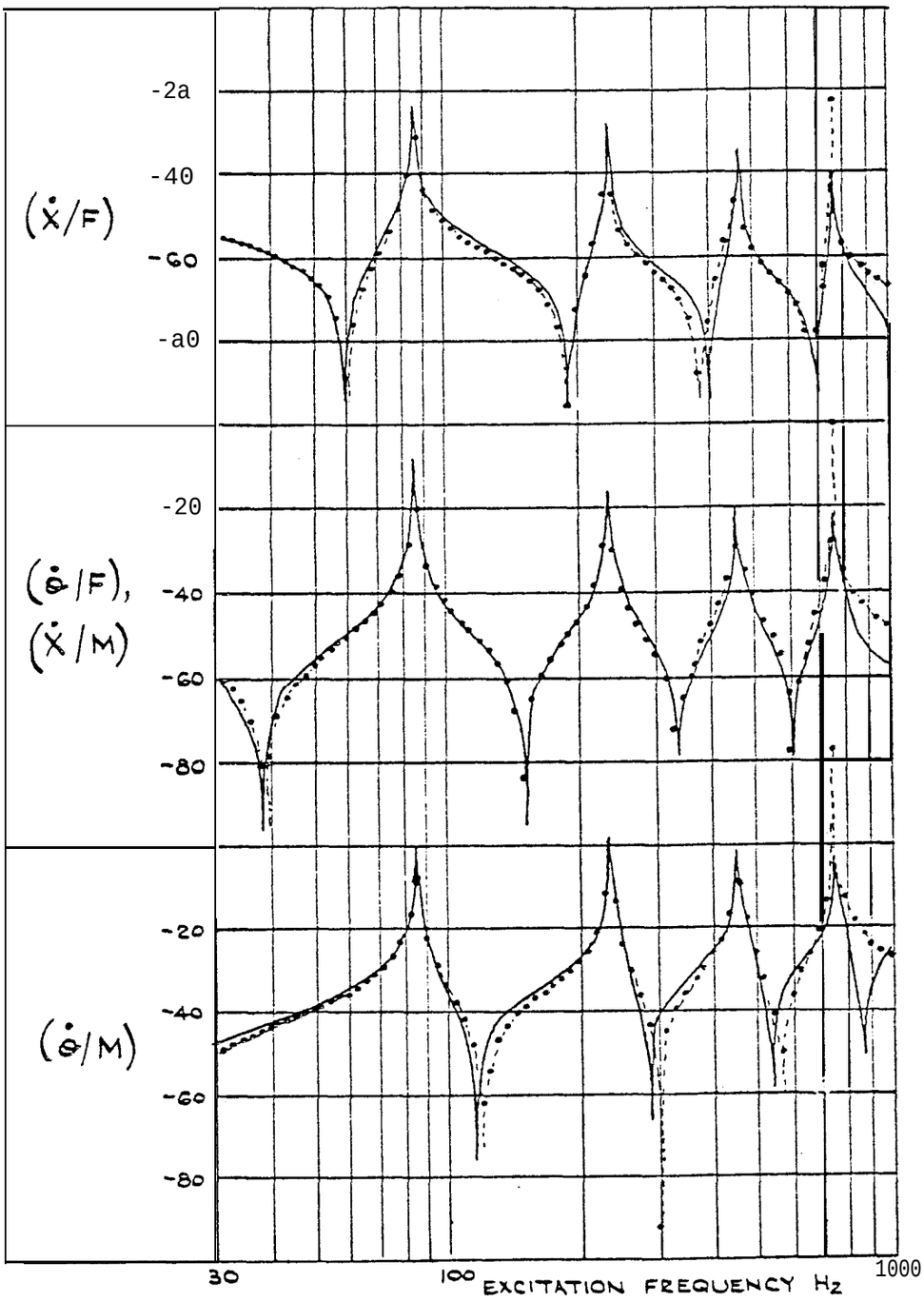

Figure 6.17 MOBILITY PROPERTIES OF THE SHORT BEAM: III

——— Theoretical ... Smoothed Measurements for $(\dot{X}/F)(\dot{X}/M)$
Derived measurements for $(\theta/F)(\theta/M)$

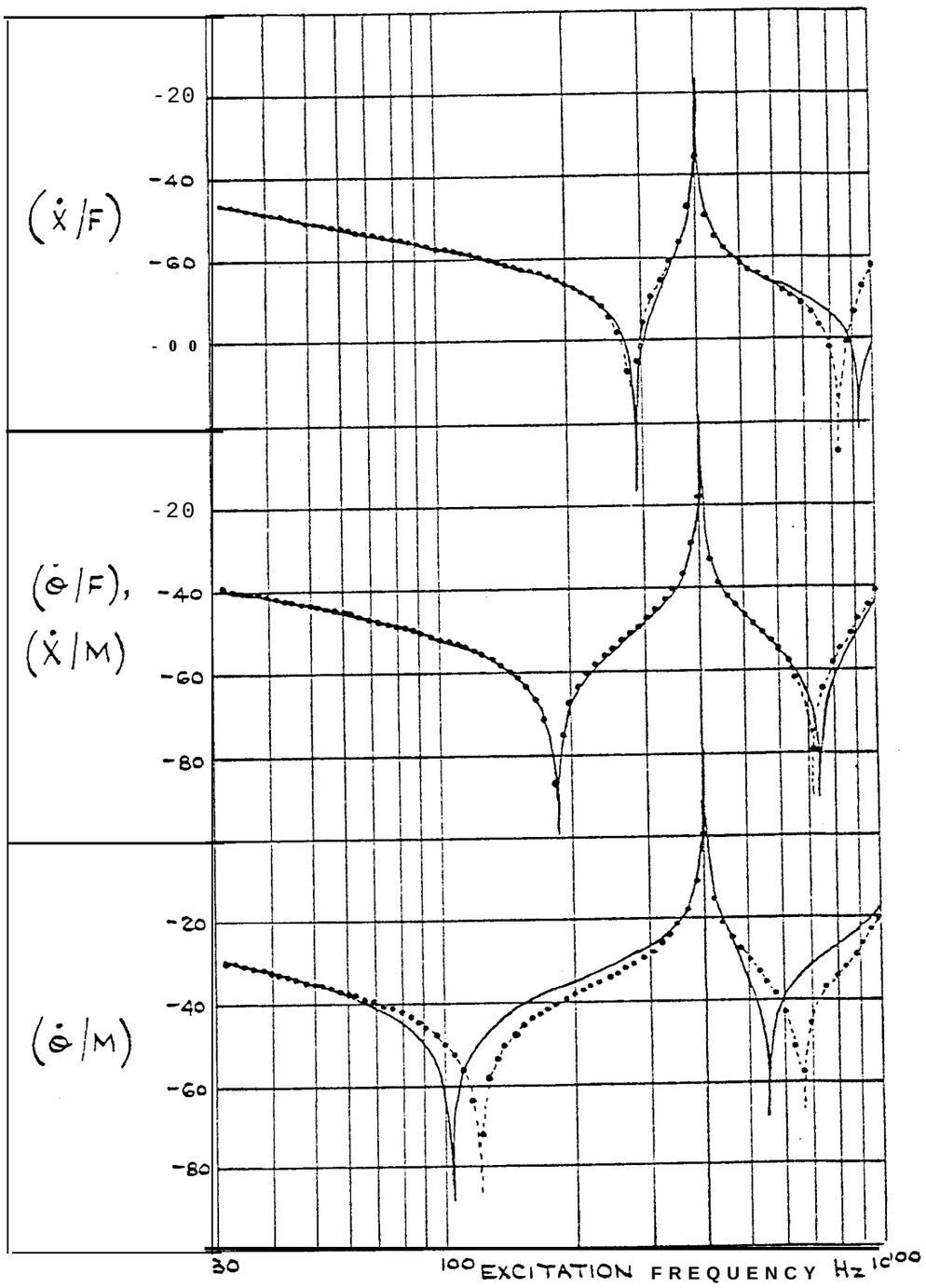

Figure 6.18 MOBILITY PROPERTIES OF THE COUPLED BEAM: IV

——— Theoretical . . . Predicted from Smoothed/derived measurements on component beams.

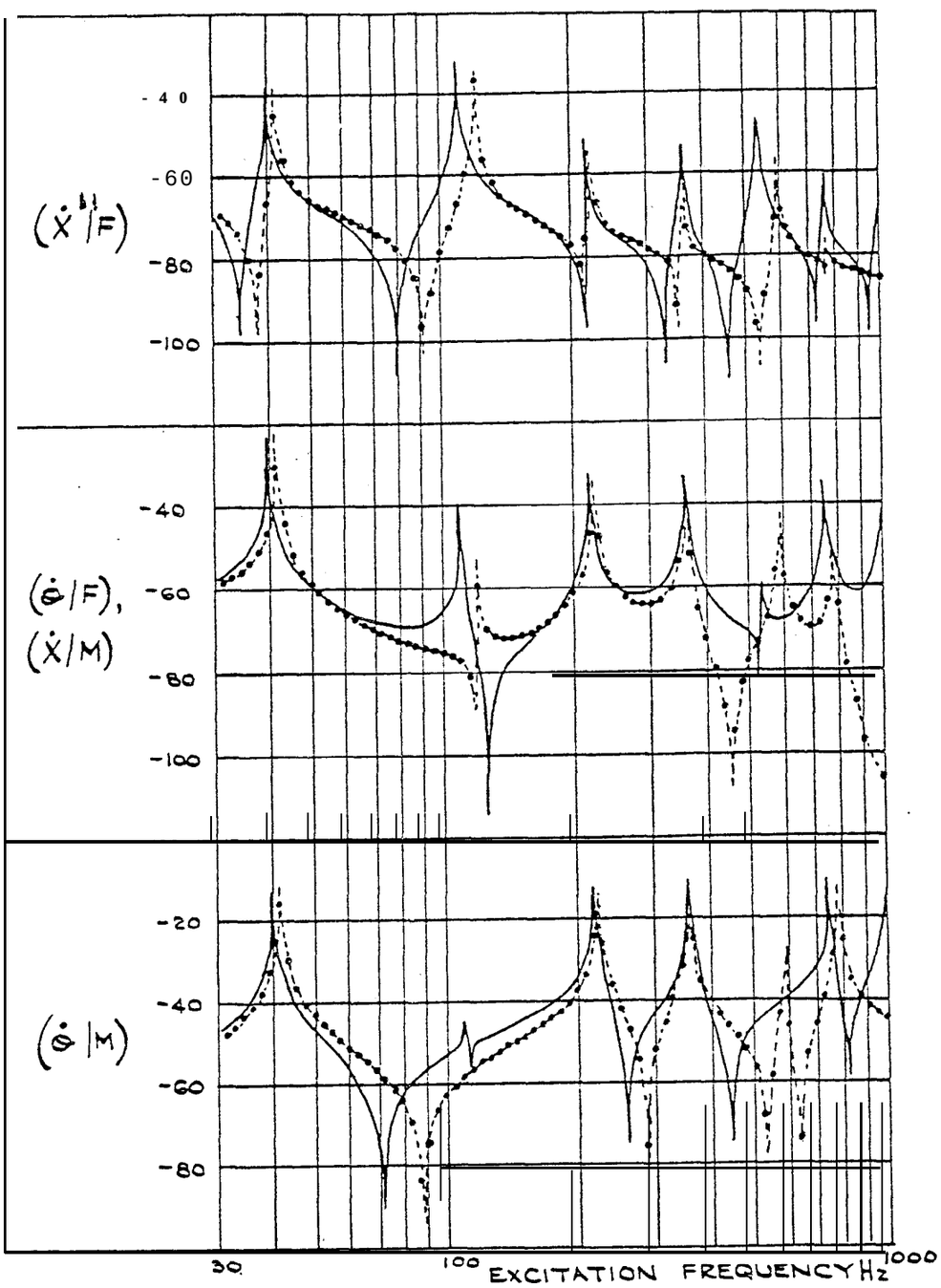

Figure 6.19 Mobility Properties at Tip of Long Beam
Two B. & K. Accelerometers

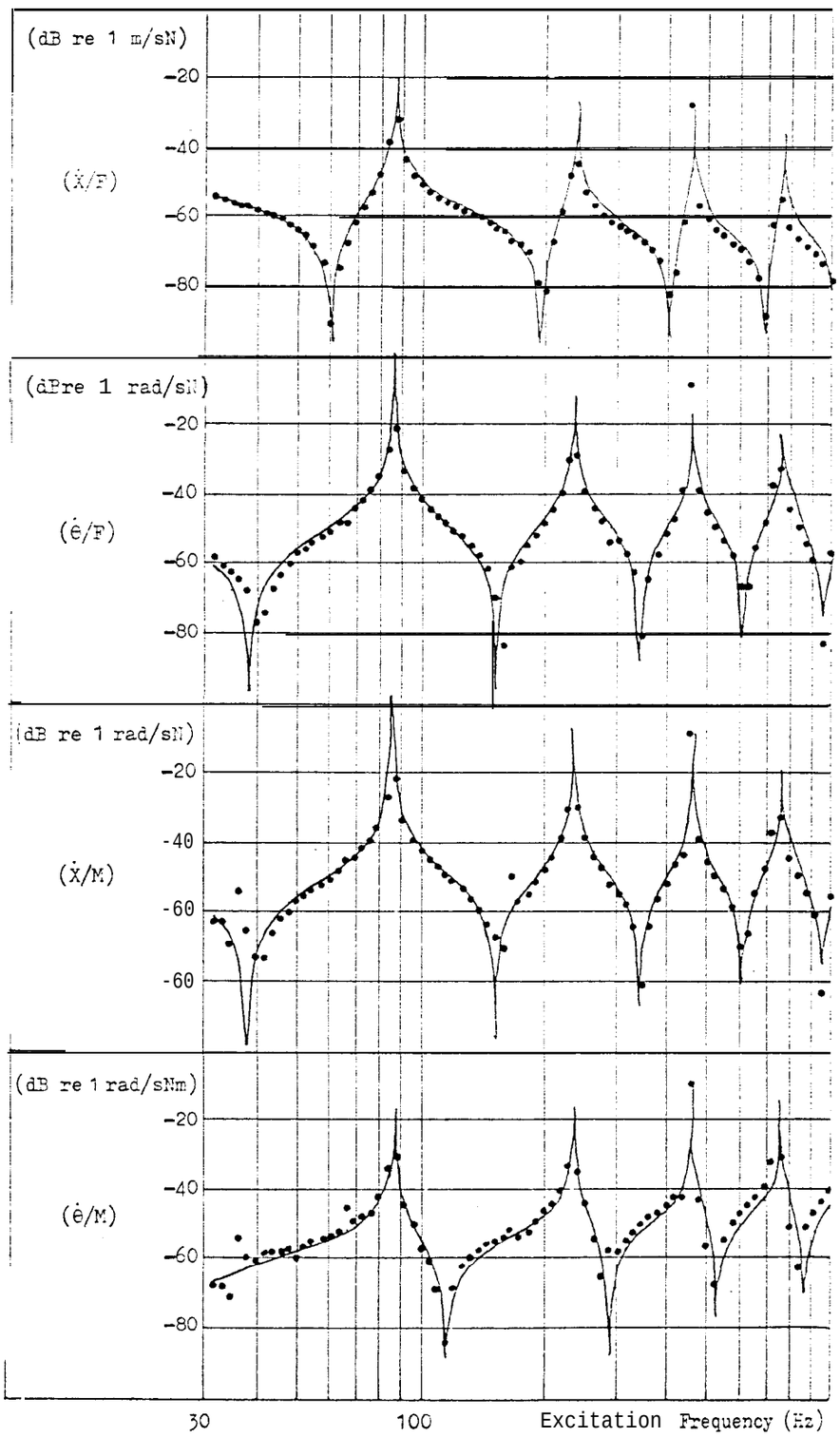

Figure 6.20 Mobility Properties at Tip of Short Beam
Single Endevco Accelerometer
$(\dot{e}/F),(\dot{e}/M)$ derived

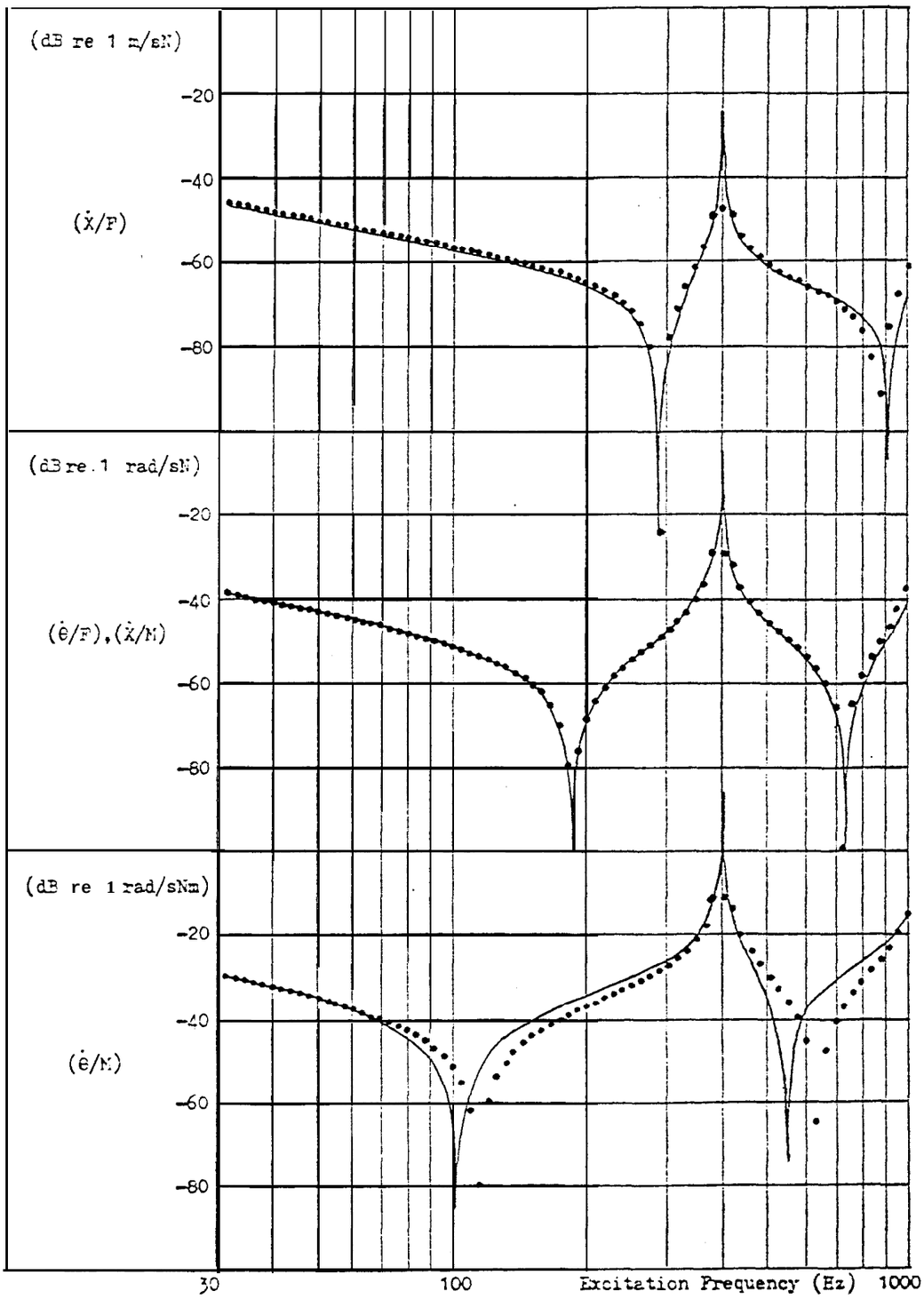

Figure 6.21 Mobility Properties at Tip of Long Beam
Single Endevco Accelerometer
$(\dot{e}/F)$,$(\dot{e}/M)$ derived

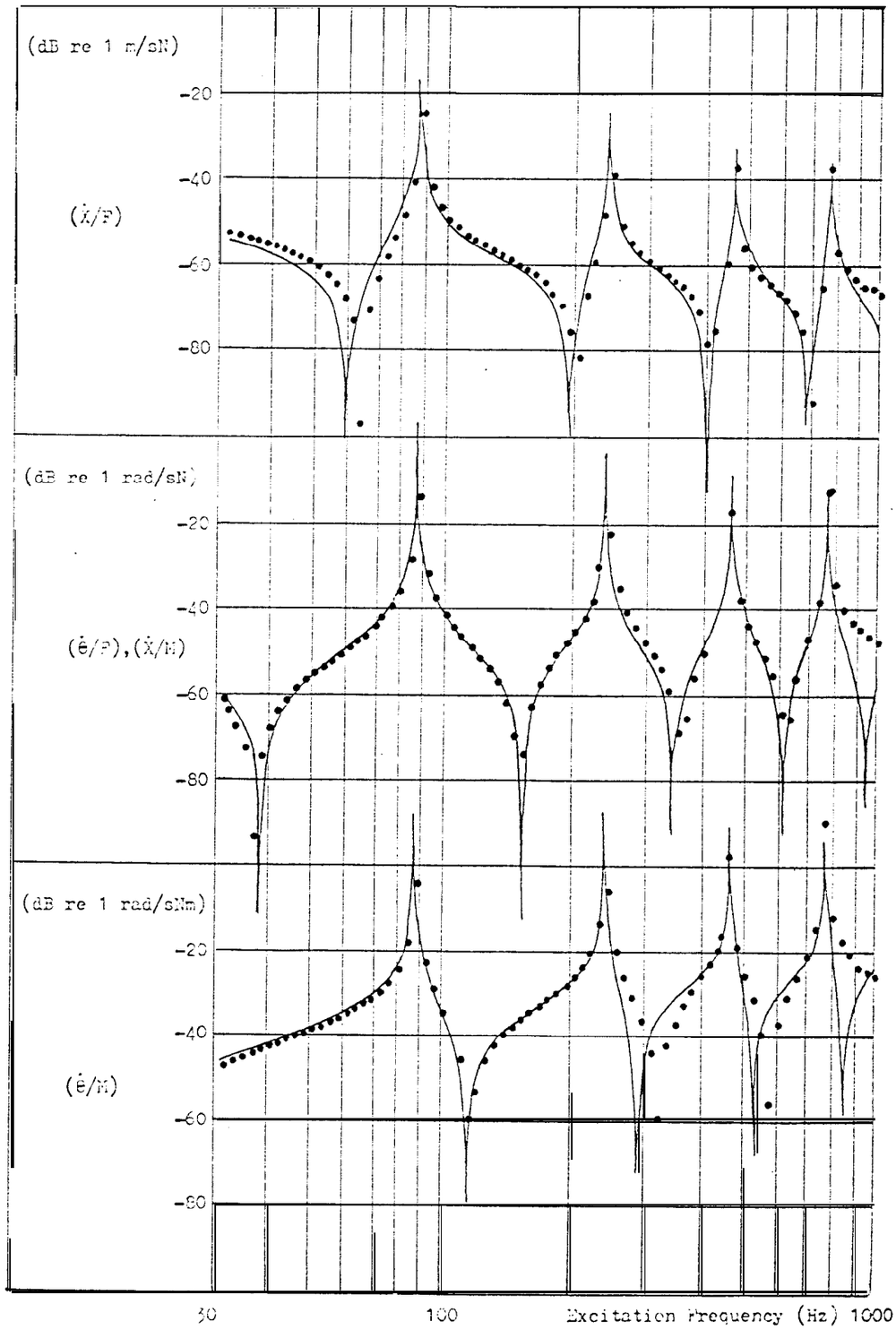

Figure 6.22 Mobility Properties at Tip of Long Beam
Single B.&K. Accelerometer on Block
$(\dot{e}/F), (\dot{e}/M)$ derived

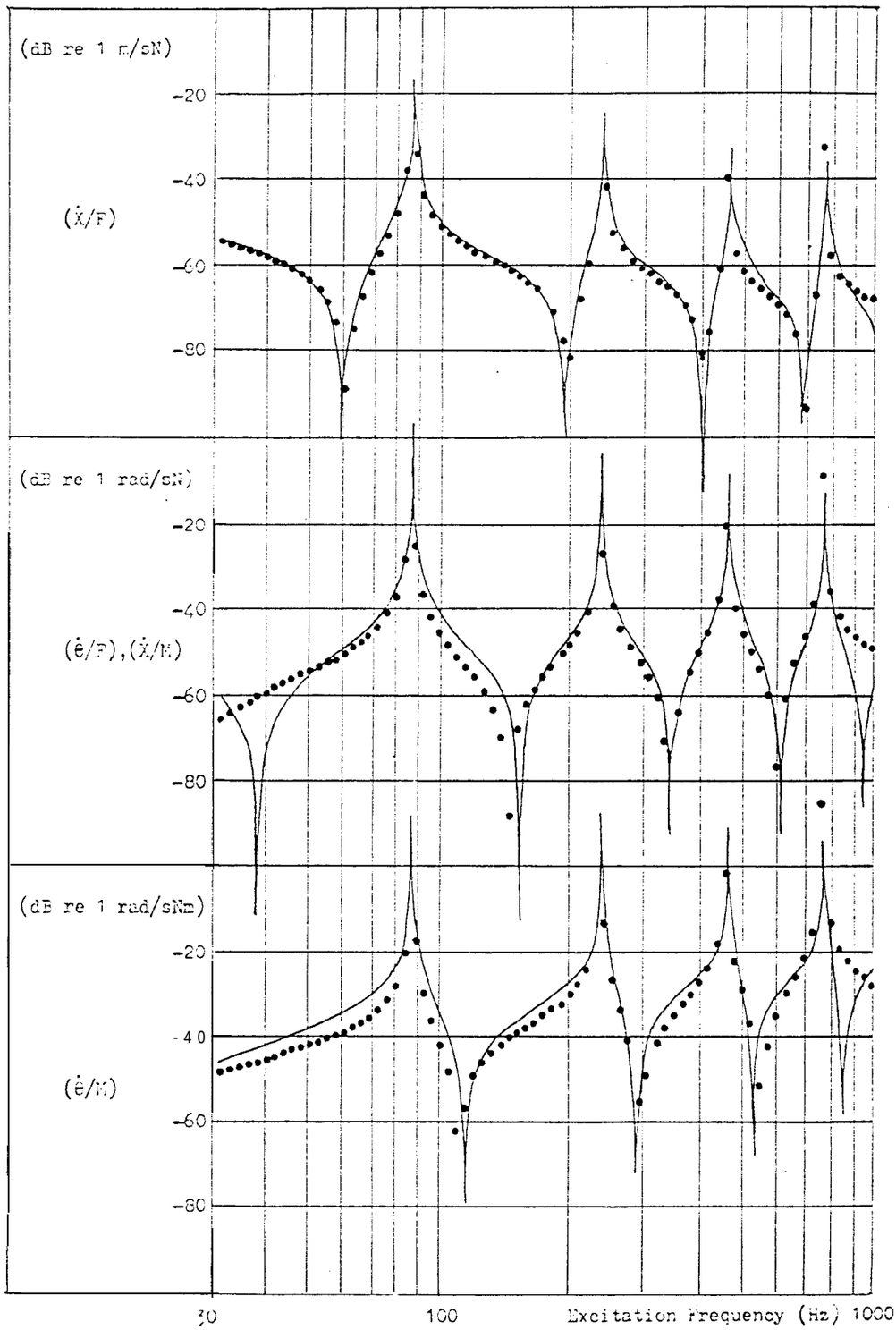

Figure 6.23 Mobility Properties at Tip of Long Bear
Single B. & K. kcceleroneter on Beam
$(\dot{e}/F), (\dot{\theta}/M)$ derived

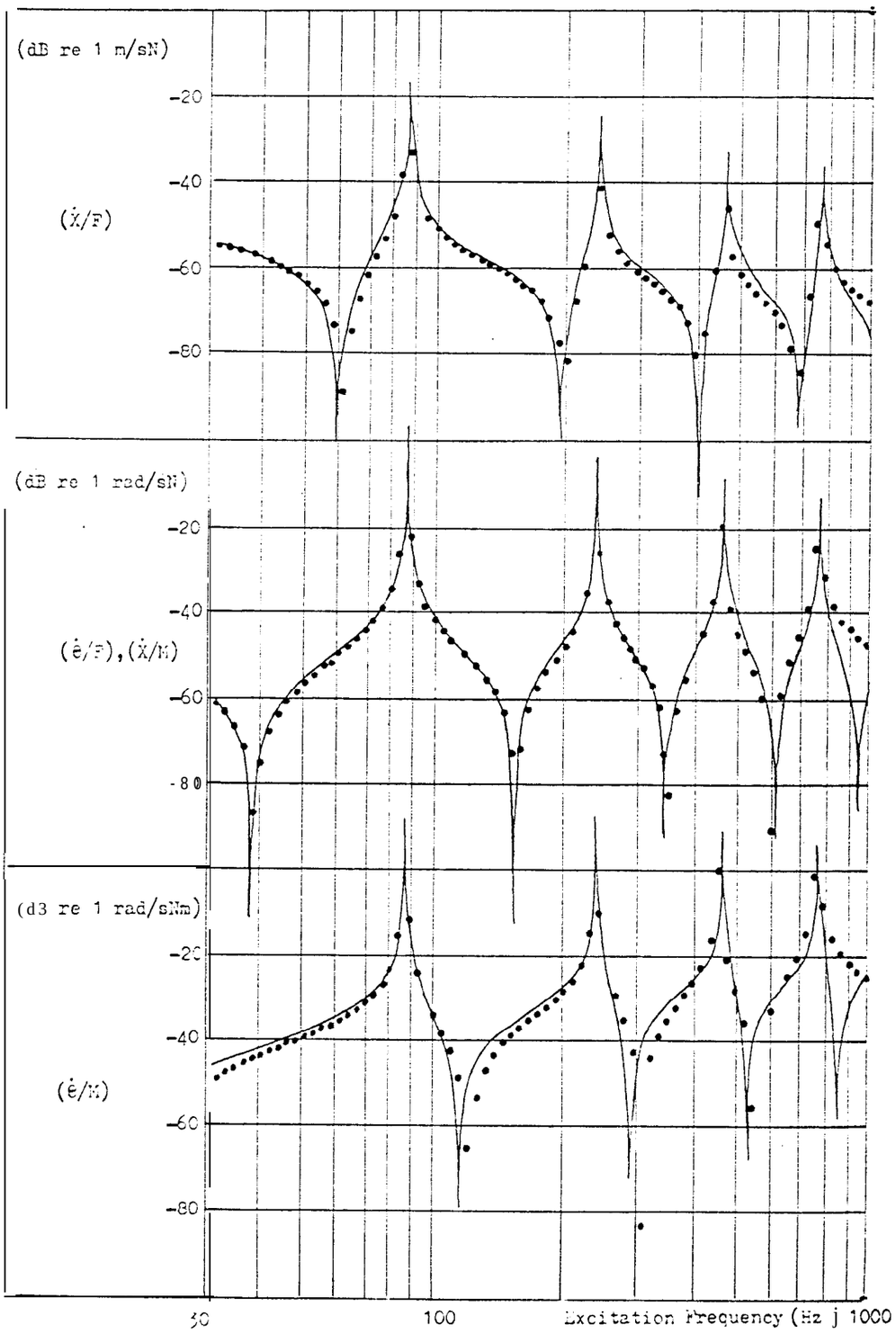

Figure 6.24 Mobility Properties at Tip of Lona Beam
Two Endevco Accelerometers: Single Run
(i/M), $(\dot{\theta}/M)$ derived

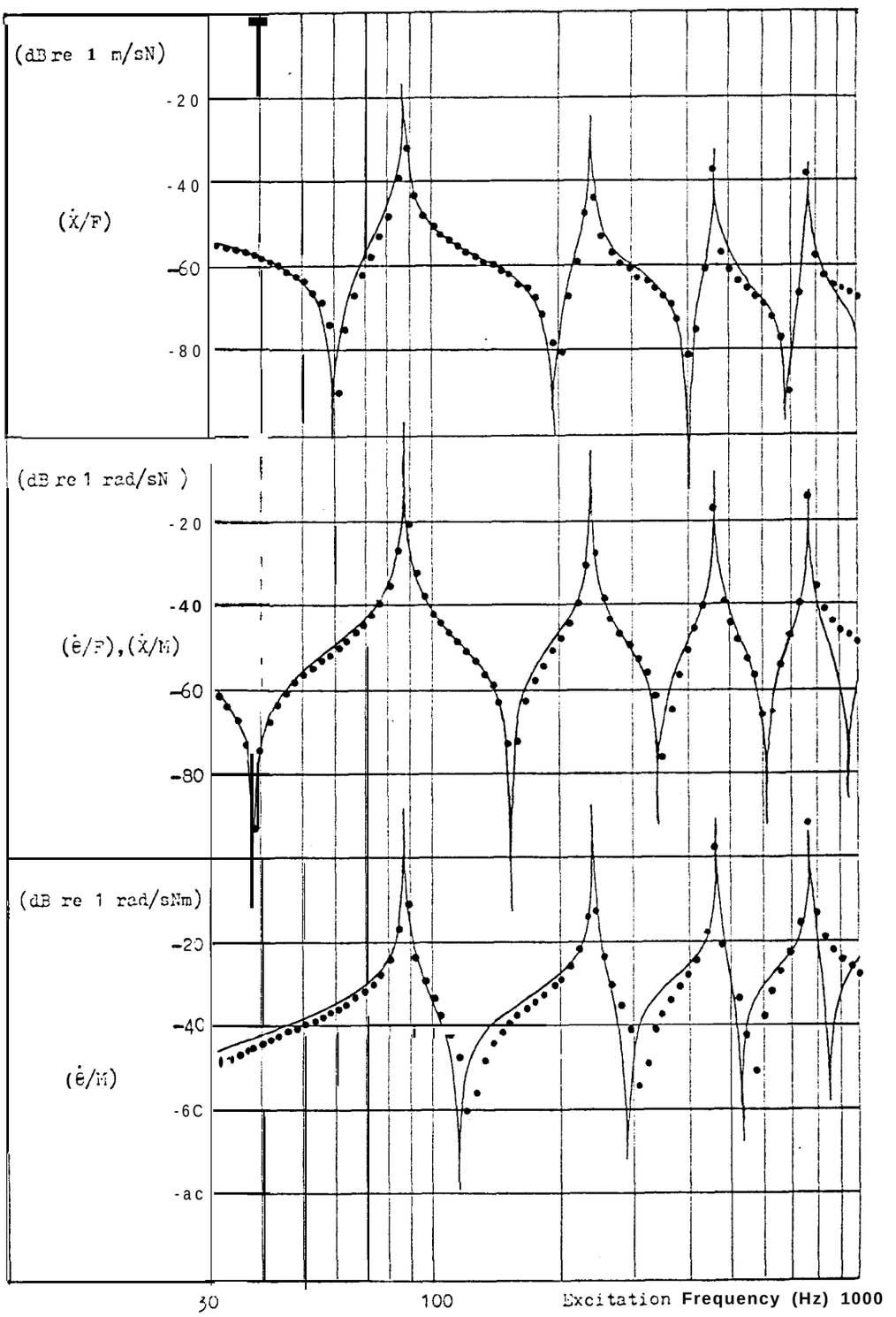

7. MEASURED-DATA MODELS USED FOR PREDICTION OF VIBRATION BEHAVIOUR

The investigations resorted in this chapter involve the application of the measurement techniques developed in Chapters 5 and 6 to physical structures - a pair of uniform steel beams and a turbine blade. The data accuired were used for making models using the theoretical methods established in Chapters 2, 3 and 4. In each case the model was used in an attempt to predict vibration properties which could be checked by other means.

7.1 Spatial Models of a Coupled Beam

7.1.1 Introduction

The sbjectives of this section involve application of the techniques of identification to frequency response data measured on physical structures and the subsequent construction and evaluation of spatial models of the structures. The structures chosen were the Long and Short Beams which had been used in Chapter 6 in the development of exciting block design. The validity of the models was to be tested by making a Coupled Beam by connecting the Long and Short Beam models as if at a butt joint and then predicting the vibration behaviour of the combination. A check could be made against ideal properties computed for the Coupled Beam, as in Chapter 4. The coordinate systems of Figure 4.2 could be used again. The frequency range was tc be PO to 2000 Hz, thus including six bending modes of the Long Beam and four of the Short Beam.

There were alternative methods for measuring the required data. The methods are summarised, for the Long Beam, In Figure 7.1. The first method would employ one exciting block, connected in turn tc the three points designated by translational coordinates. For each block location two runs, one for each of two force gauge positions, would be made. The program PM2/1 with two accelerometers on the block or the equivalent programs MOB2 and MCAN and a single accelerometer on the

the block (a method developed in Chapter 5) could Se used tc give ultimately the mass-cancelled point responses at all six coordinates. From these data the numerical values of the elements of the mode shape matrix $[\Phi]$ of the beam could be calculated. The signs of those elements, requiring transfer response information, could be found by the addition of an accelerometer mounted at a translational coordinate (for example, 3, in Figure 7.1(a) j and providing special program modifications to record its output during each of the six test runs. It would not be possible to compensate entirely for the additional mass of this accelerometer, but for a small accelerometer the error caused would probably be negligible.

A different approach could be adopted if the 'two accelerometer' method of Chapter 5 were applied. In that case three blocks, each with two accelerometers, could be attached to the beam and measurements made on the block/beam combination. Program MCB2, modified to give sum and difference data for each pair of accelerometers, could be used to make these measurements. The data obtained, including one column and the diagonal of the mobility matrix, would lead to a spatial model of the bean with blocks. Inertia cancellation could remove the effects of the blocks at this juncture.

Of the alternatives presented, the lest incorporated most of the measurements techniques developed in Chapter 5 and would depend on the theoretical techniques of Chapter 2. It would thus be a comprehensive test involving identification of spatial models for vibration analysis - a vindication, if successful, of the thesis. The third alternative was chosen.

7.1.2 Measurements on Long and Short Beams

A sketch of the test configurations of the Long Beam is shown in Figure 7.2 (a) and of the Short Beam in Pigure 7.2 (b). The test on the Long Beam required the use of three I-lark 8 exciting blocks, two with 'end feet' and one with a 'mid foot'. One force gauge was used together with six accelerometers, all connected via charge amplifiers to the Solartron JX3381 equipment.

The operational computer program MOB2 was modified as indicated in section7.1.1 2nd used first in the control of test on the Short Beam. The mobility parameter Y_{21} was monitored during the test and is shown as Figure 7.3. Coarse sweeps were made from 20 to 2000 Hz and then close sweeps in limited bands around, resonances and antiresonances. At each frequency, the four nobilities Y_{11}, Y_{21}, Y_{31} and Y_{41} in modulus (dB)/phase form were punched on to paper tape and printed. Only one run was made on the Short Beam which, having identical blocks and accelerometers at each end, was symmetrical.

The tests on the Long Beam were similar but since the beam with its blocks was asymmetrical a run had to be made with the force applied through the force gauge in each of the positions A, B and C successively. In each case, the point rotational parameter was monitored and six mobilities punched on tape at each frequency. The results were not printed at this stage, in order to save time. Towards the end of the testing a slight malfunction of the JX3381 system became apparent. It can be seen in Figure 7.4 that there are some anomalous points about 20 dB above the first antirescnance of Y_{65} between 40 and 50 Hz. A printout revealed that the faultwas associated with arbitrary changes of sign of the phase angle of responses $\dot{X}_5$ and $\dot{\theta}_6$. The smooth response

Y_{65} below the first antiresonance was about 10 dB higher than that of Y_{21}, which should be very similar. An adjustment cf data to correct this anomaly is noted in Table 7.4(a).

The raw rotational data obtained in these measurements do show some scatter at the higher frequencies but the low-frequency information is smooth. Thus the innovation of the direct calculation of rotational data during the frequency sweep may be judged to be successful.

Inertial Properties of Exciting Blocks

The inertial properties of the exciting blocks loaded by accelerometers are developed in Figure 7.5. Assuming that they are rigid, the three blocks attached to the Long Bees have 2 diagonal inertia matrix related to the beer coordinates at the neutral axis. This is $[I_L]$, specified in Table 7.5(b).

The corresponding matrix for the two blocks connected to the Short Beam is $[I_S]$, specified in Table 7.2(b).

Flexibility of Exciting Blocks

The Mark 8 Exciting Block is 2 beam which has 2 first bending mode at about 8 kHz, considerably above the 2 kHz upper limit of the tests. Eosever, since the accelerometers attached cause 2 reduction in resonance frequency the response of 2 block loaded with tip masses was calculated 2nd the results shown as Figure 7.6 2s 2 graph of inertance against frequency. The first antiresonance occurs about 3 kHz 2nd its effects begin to be visible at about 808 Hz. The highest response frequency used in the identification of the long beam was 760 Hz and that fcr the short beam was 1050 Hz (section 7.1.3). Since there was some scatter of the data obtained at these frequencies it was not thought necessary to make the small corrections for block flexibility but it is apparent that the blocks were only just stiff enough for the purposes of these

tests. Sainsbury [3] encountered similar difficulties and concluded that the local stiffness at the joint between the exciting block end the test structure was a significant but unpredictable factor. A useful rule of thumb might be to design a block with 2 first bending mode at 2 frequency about ten times greater then the highest measurement frequency to be used.

In cases where the block flexibility could not be neglected it might be thought possible to construct a spatial model of the block with 2 stiffness matrix as well as 2 mass matrix. This would require the addition of coordinates tc the block and to the system as 2 whole andwould thus necessitate tests at higher frequencies to include 2s many more modes as additional coordinates for spatial modelling to be done. It is herd to see the advantage in such a procedure. Better to have the block sufficiently rigid so that it needs oniy the coordinates of rotation 2nd translation at its centre 2nd the associated txo element inertia metrix $\begin{bmatrix} m & \\ & I_B \end{bmatrix}$.

7.1.3 Modelling Without High Frequency Residuals

The results of this section 2re design&ted, for ease of reference, as SM, signifying - Spatial, Measured.

(SM) Identification of Responses

The frequency responses obtained in the tests on the Short Beam with two attached exciting blocks revealed sharp resonances at 333, 780 and **1150** Hz and since the tests were made on a freely supported structure a zero-frequency resonance was assumed. Each response was plotted 2nd then response data points selected for use in program IDENT. Damping was assumed to be negligible. The data selected for calculation of the point modal constants of the Short Beam are shown in Figure 7.7 together with sketches of all the responses arising from force input at coordinate 1. The signs which characterise the mode shapes are shown

related to the responses and also presented in an array. The sign of the rigid body modal constant is determined from the phase angle of the quoted low frequency response (about 20 Hz). The signs for other modes then follow in sequence.

Similar treatment was given to the data measured for the Long Beam loaded with three exciting blocks, whose resonances were estimated as 0, 80, 219, 420, 655 and 800 Hz. The responses arising from input force at coordinate 1 are shown in Figure 7.8 which includes the associated array of mode shape signs. The data selected for calculation of the point modal constants are also shown. Further identification calculations were done for the responses Y_{33}, Y_{43}, Y_{55} and Y_{65}, the last of which caused a little difficulty because of the anomalous low frequency response already mentioned in section 7.1.2. Response data were regenerated from the modal constants determined in each calculation and plotted in comparison with the raw measured data. In some cases several selections of data were made before a sufficiently good curve fit was obtained.

7.3 Mode Shape Matrices

Program IDENT can provide only one modal constant for each resonance frequency. There are several potential rigid body modes at 0 Hz, of which two are significant in this instance, one translational and the other rotational. The modal constant identified for the mode at 0 Hz is the simple sum of the constant for translation and that for rotation. Since the transiational modal constant is the reciprocal of the mass of the tested system it is easy to calculate it and, by subtraction from the IDENT output, the rotational constant also. Part (b) of Tables 7.1 and 7.4 show this calculation for short and long beams respectively.

The derivation of the point rotational constants is shown in part (a) of these Tables and subsequently the matrix of point modal constants and the dependent matrix of mode shapes are shown in parts (c) and (d).

The array of signs for the bending modes were shown in Figures 7.7 and 7.8 and the signs for the rigid body modes were established in the thumb nail sketches at the bottom of the relevant Tables. The data of Tables 7.1 2nd 7.4 (d) are those needed for calculation of the spatial model, namely $[\omega_r]$ and $[\Phi]$.

6. Spatial Models of Short and Long Seams

The matrices established in the previous section were used as input to program EMMAY and the corresponding output is shown in Table 7.2(a) and 7.5(a). The sum of the translational elements m_{11}, m_{13}, m_{31} and m_{33} of the mass matrix $[M_{SB}]$ of the Short Seam with Blocks is equal to the mass of the bean with the blocks, 2nd the corresponding stiffness sum is zero as to be expected for a freely-supported system. Similar observations apply to the matrices M_{LB} 2nd K_{LB} for the Long Beam with Blocks.

The diagonal matrices of exciting block inertia terms as developed in Figure 7.5 are shown as part (b) of the Tables and simple subtraction provides the data of part (c) which constitutes the spatial models of the beams without blocks.

The first check made of these spatial models was to calculate mode shape information with program EIGEN. Table 7.3 (a) shows to three significant figures the modal properties of the Short Beam with Blocks. Ideally, these would exactly match those of Table 7.1(d), originally input to program EMMAY. The discrepancies are most marked for the two rigid body modes whose frequencies are low but not zero. The numeric21 values of mode shapes and frequencies for the two bending modes are accurately obtained. All the signs of the lest two columns have been altered, 2 netter of no significance. Evidently the calculations in program EIGEN are ill-conditioned for modes of zero frequency. Similar comments apply to the data for the Long Beam with Blocks as presented in Table 7.6(a).

Program EIGEN was used again, this time for prediction with spatial model matrices of the beams without blocks 2s input data. This calculation, whose results are in part (b), can be checked against the data for ideal beams in pert (c). Once again, there is inaccuracy in the rigid body mode shapes, being, at worst, 5.5% for the Short Beam translational mode 2nd 7.6% for the Long Beam rotationalmode. The indicated frequencies are very low but not zero.

The first bending mode of the Short Beam has 2 predicted frequency which is 0.4% high. The translational mode shape data are 3% high and those for rotation 33% **high.** Greater inaccuracy is shown, 2s expected, in the highest frequency mode, the estimated frequency being 112% higher than the true value of 1099 Ez.

The bending node resonwces found for the Long Beam are **85.67** (error + 0.9%), **243.2** (+ 2.7%), **475.1** (+ 2.39 and lastly **995.6** (+ 30%). **The node** shapedata are more accurate than those of the Short Beam.

These spatial models based on measured data were t&en as reasonable representations of the Long and Short Beans 2nd used in further calculations, specified below.

6.4 Spatial Model of Coupled Seem

The Coupled Beam consists of the Long Beam joined to the Short Beam attwo coordinetes, shown as **5 end** 6 **in** Figure **7.13** (a) for the ideal beam. The corresponding spatial model without residuals is shown 2s Figure **7.13** (b), **in** which the short bear coordinetes are 5, 6, 7 and 8. The corresponding partitioned matrices are found by simple addition:

$$\begin{bmatrix} M_C \end{bmatrix} = \begin{bmatrix} M_L \end{bmatrix} + \begin{bmatrix} M_S \end{bmatrix}$$

$$\begin{bmatrix} K_C \end{bmatrix} = \begin{bmatrix} K_L \end{bmatrix} + \begin{bmatrix} K_S \end{bmatrix}$$

and they are shown in Table **7.7.**

Three sets of predicted data were obtained in calculations with this spatial model:

1. Natural frequencies
2. Mode shapes
3. Frequency responses

For each of these sets comparison was made with corresponding data calculated for an ideal beam.

The frequencies are shown in Table 7.7 with the error of -36% in the first bending mode most apparent. The sixth bending mode has an indicated frequency 21% high and the second is 14% low. The third, fourth and fifth bending modes have errors less than 5%.

Mode shape data calculated using program EIGEN are presented in Figure 7.3 in comparison with those for an ideal continuous beam. Figures (a) and (b) clearly show rigid body modes, although there is a slight error of slope. The bending modes in Figures (c) to (h) show small deviations of slope or of location and the general trend is to greater inaccuracy at higher frequencies, particularly in the rotations. The mode shapes are, however, clearly distinguished from each ether.

The last and most stringent comparisons are to be seen in Figure 7.10 The frequency response of the beam, predicted using program COUPLE1 with module ZMAK2 to handle the spatial model matrices, is plotted as thick dotted lines. The thin lines in the background are the corresponding ideal responses. The inaccuracies of frequency, already commented upon, are evident in every graph. All plots are most accurate in the frequency range from 150 to 500 Hz and most have levels of response in this region which are satisfactory. The most obvious exception is the rotational junction response of Figure (e), which is 10 to 15 dB high, even in the favourable range of frequency. The junction cross response (f) shows a minimum rather than an anti-resonance just below the fifth non-zero resonance at 534 Hz. The limit of prediction is the sixth non-zero resonance, and beyond this point the

predicted response simply falls away as a mass line.

The forecasts made using this spatial model may be judged overall as 'fair'; reasonably accurate in the middle range of frequencies and levels but quite poor at the extremes.

7.1.4 Modelling with High Frequency Residuals

The results in this section are designated SMR - Spatial, Measured, with Residuals.

SMR Identification of Responses

The IDENT calculations including residuals were done using the same response data as had been used in section 7.1.3 but the highest resonance frequency was taken as 10 kHz *for the* Long Beam and 20 kHz for the Short Beam, arbitrarily chosen. Comparison plots were made using regenerated data and, as expected, they showed better fit at the higher frequencies.

SMR Mode Shape Matrices

The development of the mode shape matrices is shown in Tables **7.8 and 7.11** which follow the same pattern as the corresponding SM Tables **7.1** and 7.4. The one significant difference to be seen in the SMR Tables is the inclusion of calculations of point translational stiffness residuals from the modal constants of the fictitious high frequency modes. 'There is a limitation in this development which is that residual stiffnesses for the point rotational terms cannot be derived and thus the spatial model ultimately constructed has only half the number of residual springs that were used in the theoretical development of the STR model of Chapter 4.

(SMR) Spatial Models of Short and Long Beams

Program EMMAY was used 2s before to produce the natrices constituting the spatial models of the beams with blocks. Inertia cancellation removed the effects of the blocks. These natrices 2re listed in Tables 7.9 and 7.12 the residual stiffnesses being omitted at this stage.

Similar check calculations using program EIGEN were made giving the results in Tables 7.10 and 7.13. The numerical ill-conditioning nentioned previously affects the rigid body modes which should have zero frequency but do not.

Most significant for the Short Beam is the improved accuracy cf the natural frequencies predicted for the beam without blocks. The first bending node has a frequency error of only -0.2% and the second such node has only ace-sixth the error of the SM calculation - a mere 1%. The rigid body nodes are very similar to those of the SM calculations, and finally the second bending mode is less inaccurate than before.

For the Long Bean the bending mode frequencies are S6.66 (+ 0.9%), 242.6 (+ 2.4%), 465.1 (+ 1.9%) 2nd 767.6 (+ 0.02%). These 2re all an improvement whes compared with the SM series, especially in the last frequency, now almost exact, formerly 30% in error. The rode shape deta in the SMR list for the long bee-, is also somewhat improved.

(SMR) Spatial Model of Coupled Beam

A sketch of the SMR Coupled Beam model is shown as Table 7.14(a) in which residual springs are attached to the translational coordinates. The coordinates for the Long Eeam are numbered 1 to 9 in sequence, but those for the Short Beam have to be taken in the order 9, 10, 11, 6,12, 13. Spatial model matrices including residuals are presented in Table 7.14, which may be systematically related to the figure in part (a).No attenpt was oade to write the full matrix for the Coupled Beam because

it involved 13 coordicetes 2nd difficulty with the Short Beam because it would have to have its elements re-ordered. Since EIGEN could not be used directly, the mass matrix being singular, 2nd since COUPLE1+ module ZMAK2 could be used to assemble the spatial node1 fro-, the two convenient sub-systems for response calcula tions the full 13 coordinate matrix would be unnecessary, anyway.

The same criteria involving frequencies, rode shapes and response plots was used as before to evaluate the success of this spatial model. Different calculations had tc be used, however, since quick answers for natural frequencies using EIGEN required 2 reduced spatial model with co unattached springs, as shown in Table 7.14(e).

The natural frequencies found are significantly closer to the ideal values than for the spatial node1 without residuals. The worst error (for the first bending node) is 23% rather then 36%. The other bending modes have frecuencies within 5% of the ideal values. The frequencies indicated for the rigid body modes are very low. The EIGEN spatial model has nine modes corresponding to its nine coordinates, but only eight of those nodes are valid. The extra, anomalous, node is at 21'71 Hz. The mode shape data output by EIGEN are not directly useful because they do not refer to the external translational coordinates, at the remote ends of residual springs. The rigid body modes, however, will be indicated adequately by EIGEN since at very low frequencies the deflections of these residual springs will be negligble.

COUPLE1 was used tc generate frequency response and the sweep was carried to a frequency sufficiently high that the rising slope associated with a high frequency residual was established.

The response data produced for the tip 2nd junction coordinates had similar frequency sweeps, These results are assembled as Figure 7.11. The tip response Y_{77} is typical in having 2s 2 salient feature a very good agreement between 100 Hz and 600 Hz - significantly wider

than the range 150 to 500 Hz of the SM series and including all but the lowest of the bending nodes.

At the high end of the frequency spectrum above the sixth bending node and, incidentally, beyond the range of the prediction of this spatial model, the presence of the anomalous mode at 2171 Hz can be inferred from the antiresonance occurring between 1 kHz and 2 kHz in some of the plots - an exception being Y_{96} which has a minimum, also an indicator of the out-of-range resonance.

The fit of predicted response to the ideal is remarkably good for all the tip responses and for the translational junction response Y_{99}. The junction cross response is reasonably good but shows the same erroneous minimum around 500 Hz which was noted in the equivalent SM plot. Finally, the junction rotational response Y_{66} is marred only by having much too large a resonance at 105.4 and others a little too large at 522.6 and 74C.E Hz.

Mode shape data were not generally available, as has been said, from program EIGEN. Accordingly, modal constants were calculated using program IDENT on the frequency response data which have just been discussed. Moduli of node shape matrix elements were obtained as the square roots of these nodal constants and the signs needed established as usual from specially plotted transfer responses. The results are plotted as Figure 7.12 , The rigid body modes are shown clearly shown although there are small errors of slope.

The six bending modes are delineated by the points and slopes corresponding to translational and rotational coordinates. Generally, the translational data are better fitted than the rotational data and the goodness of fit is greater for lower frequency modes than for higher. Overall, the SMR mode shapes are a little better than those of the SM series. Finally, one may see in Figure 7.12(i) that the node at 2171 Hz has a shape which Sears no relation to the seventh (or any other) bending mode.

7.1.5 Discussion 2nd Conclusions

The objectives set out at the beginning of this section in 7.1.1 have been met to a substantial degree. The chosen measurement strategy proved to be successful, yielding smooth data, particularly for the rotational response of the form (θ/F). Such measurement difficulties 2s were encountered were capable of being overcome largely by use of redundant or rather duplicated data. The major results are charised in Figure 7.13 which may be compared with Figure 4.9.

The concept of the test piece consisting of beam plus exciting blocks (including accelerometers) proved to be simple and the cancelling of inertia effects of the blocks after the construction of the spatial model turned out to be simple 2nd sufficiently accurate, particularly in the case of the Long Beam in the more favourable case when residual terms were included. It is, however, evident that the Short Beam was less accurately modelled than the Long 2nd this chiefly because its model could only include two bending modes, the other two being needed for rigid body representation. Matching the number of modes to the number of coordinates is 2 restriction, not easily to be dismissed. In this case it is apparent that the upper frequency limit of rigidity of exciting blocks was reached 2nd inclusion of higher frequency modes for the Short Beam would have necessitated redesign of the blocks to be stiffer, possibly more massive 2nd probably more intrusive as the transducer system began to match the test piece in size.

The identification curve fits using program IDENT required some judgement in the selection of data and of the goodness of fit. The curve fits were successfully achieved, even for cross terms featuring minima rather than antiresonances. Since, at this stage in the thesis, curve fitting is regarded as an established process it was not thought necessary to include examples.

The processing of the modal constents in the various steps to the construction of the final spatial model have been carefully laid out in Tables 7.1 to 7.14. Each step is simple but there are a number of pitfalls to snare the unwary. Chief among these is the need to remember that the rigid body mode at zero frequency has a special derivation equation, usually ernressed in terms of the mass of the test piece. Extreme care is necessary also in the allocation of signs tc the transfer response graphs. It is easy to make an error in the phase angle of the rotational data in particular. In the final stage of the model including residuals, care must be taken to include the residual stiffnesses in the main diagonal of the fully populated segment of the matrix as well as in the extended matrix consisting only of terms on the diagonal.

Residual springs in this study could only be added to translational and not to rotational coordinates (whose modal constants were derived), thus reducing the potential icprcvement. Nevertheless, the addition of such residuals as were possible proved very effective in reducing error in the target frequency range encompassed by the six bending modes. It would be possible to -make measurements using program PM 2/1 which would yield the rotational responses of $(\dot{\theta}/M)$ form directly and for these identification usingafictitious high frequency mode would yield the desired residual terms, Such an experiment would involve more mechanical adjustment in the addition and removal of exciting blocks than in the experiment which was actually carried out. There would be some difficulty in the allocation of signs to the mode shape matrix, too.

The following points may be made:

1. The measurement technique involving simultaneous recording of vibration data on several channels was satisfactory.
2. The calculation steps required in the construction of the spatial model are easy to carry out systematically.

3. The SM model without residuals gives reasonably good predictions in the central range of frequencies but is poor at the extremes.

4. The addition of residuals to make the SMR model has the effect of adding an anomalous high frequency mode which is easily spotted and discounted.

5. The SMR model, despite including only half the potential number of residual terms, gives very good prediction of the rigid body modes and of the six bending modes of the coupled beam, which, in practice, would be most important to know.

Finally, the results of section 7.1 constitute a demonstration of measurements using techniques developed in Chapters 5 and 6, on real, albeit simple, physical structures. These measured data, identified by the theoretical techniques evaluated in Chapters 2, 3 and 4, give a spatial model which in a very compact way contains information which can be used in representations of the vibration behaviour of the substructures and of the complete assembly. The model matches up to very stringent criteria in prediction not only of resonance frequencies, a point at which many methods stop, but also of mode shapes and frequency responses.

Figure 7.1 Alternative Methods of Measuring Mobilities of Long Beam

(a) Using Program PM2/1 or equivalent 'Single Accelerometer' Method

Block at Coordinate 1

Force inputs A, B

Obtain: $\begin{bmatrix} Y_{11} & Y_{12} \\ Y_{21} & Y_{22} \end{bmatrix}$, $\begin{bmatrix} Y_{31}, & Y_{32} \end{bmatrix}$

Point Transfer

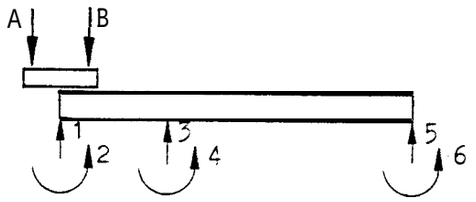

Block at Coordinate 3

Force inputs C, D

Obtain: $\begin{bmatrix} Y_{33} & Y_{34} \\ Y_{43} & Y_{44} \end{bmatrix}$

Point

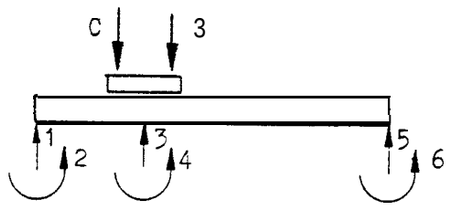

Block at Coordinate 5

Force inputs E, F

Obtain: $\begin{bmatrix} Y_{55} & Y_{56} \\ Y_{65} & Y_{66} \end{bmatrix}$, $\begin{bmatrix} Y_{35}, & Y_{36} \end{bmatrix}$

Point Transfer

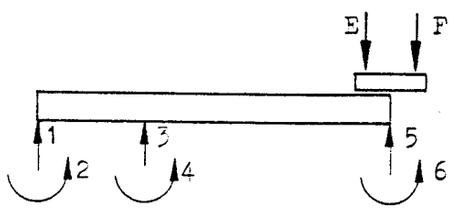

(b) Using 'Two Accelerometer' Method

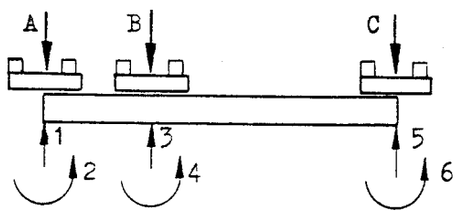

Force input A Obtain: $\begin{bmatrix} Y_{11}, & Y_{21}, & Y_{31}, & Y_{41} & Y_{51} & Y_{61} \end{bmatrix}$

Derive: $\begin{bmatrix} Y_{12}, & Y_{22} \end{bmatrix}$

Force input 3 Obtain: $\begin{bmatrix} Y_{33}, & Y_{43} \end{bmatrix}$

Derive: $\begin{bmatrix} Y_{34}, & Y_{44} \end{bmatrix}$

Force input C Obtain: $\begin{bmatrix} Y_{55}, & Y_{65} \end{bmatrix}$

Derive: $\begin{bmatrix} Y_{56}, & Y_{66} \end{bmatrix}$

Figure 7.2

(a) Long Beam Test Configuration

Scale 1:8

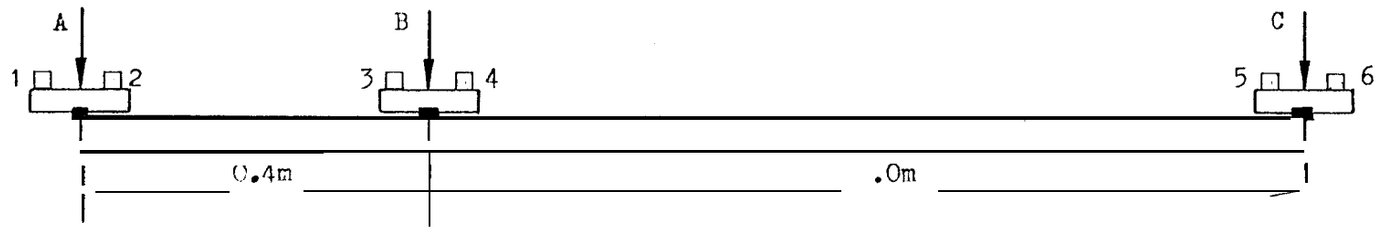

(b) Short Beam Test Configuration

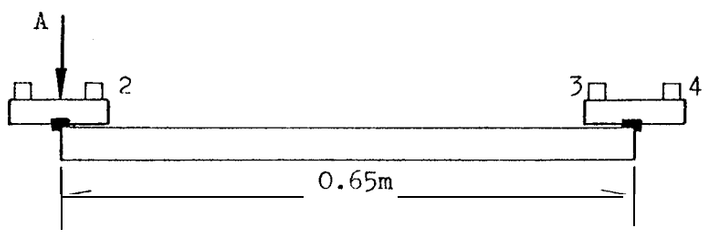

Transducer Details

All transducers manufactured by Bruel & Kjaer

Location	Transducer	Type	Number	I.S.F	Channel
A, B, C	Force Gauge	8200	615138	-	0
1	Accelerometer	4366	715608	0.819	1
2	"	"	715609	0.800	2
3	"	"	549165	0.851	3
4	"	"	574501	0.827	4
5	"	4367	614049	1.88	5
6	"	"	614055	2.09	6

Channels 0 to 5 standard rack mounted charge amplifiers

Channel 6 Channel 1 of Birchall Charge amplifier (SG 754)

Figure 7.3 Test on Short Beam : Raw Data (Y_{21})

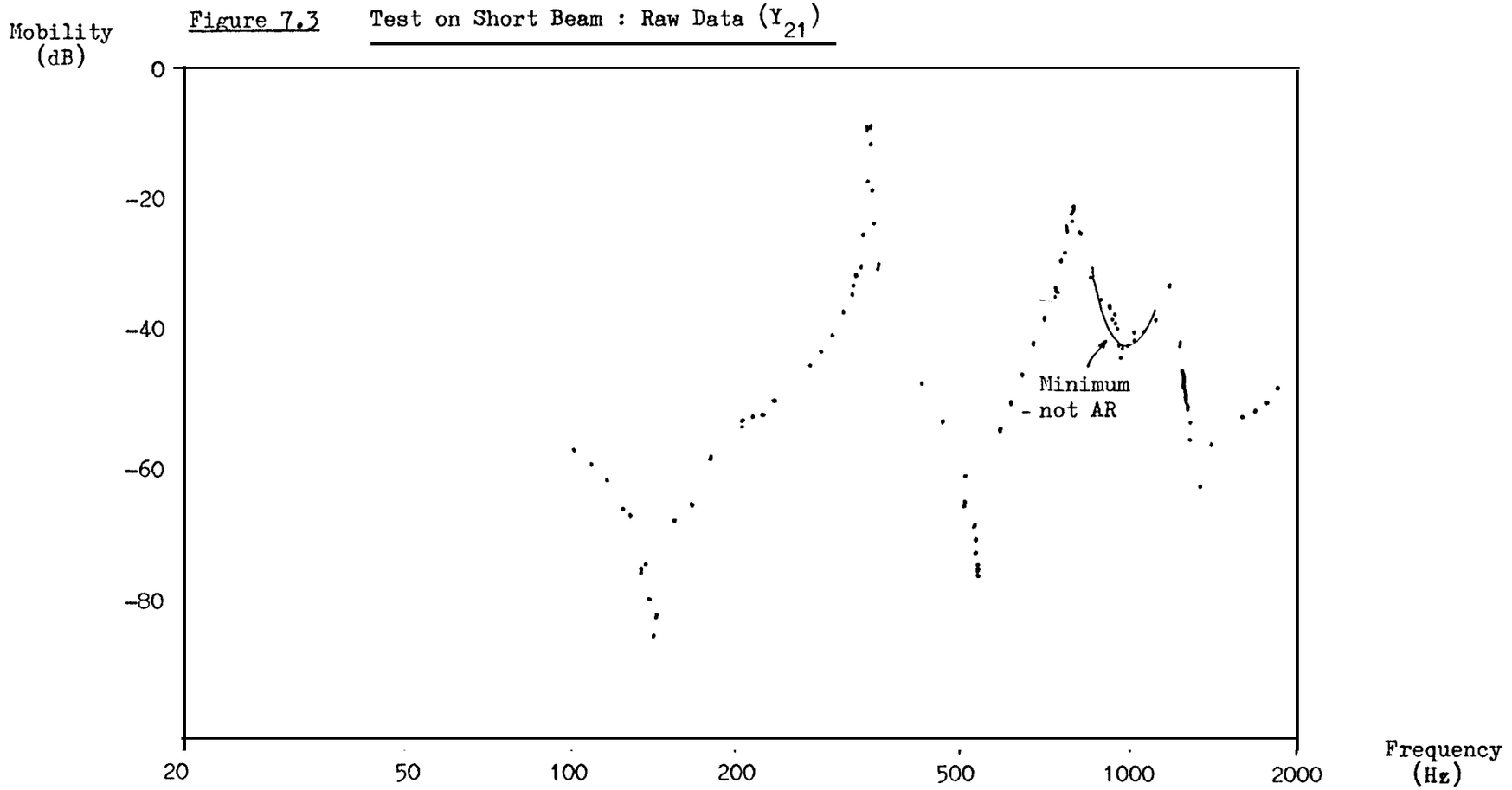

Figure 7.4 Tests on Long Beam - Raw Data

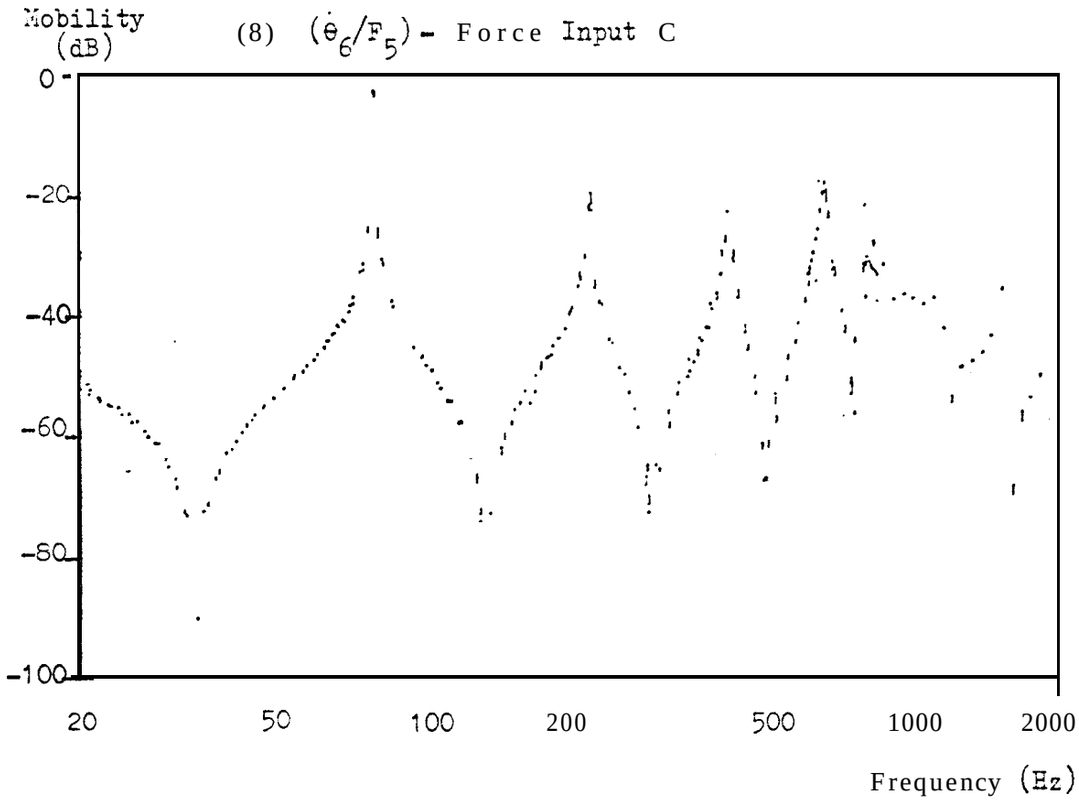

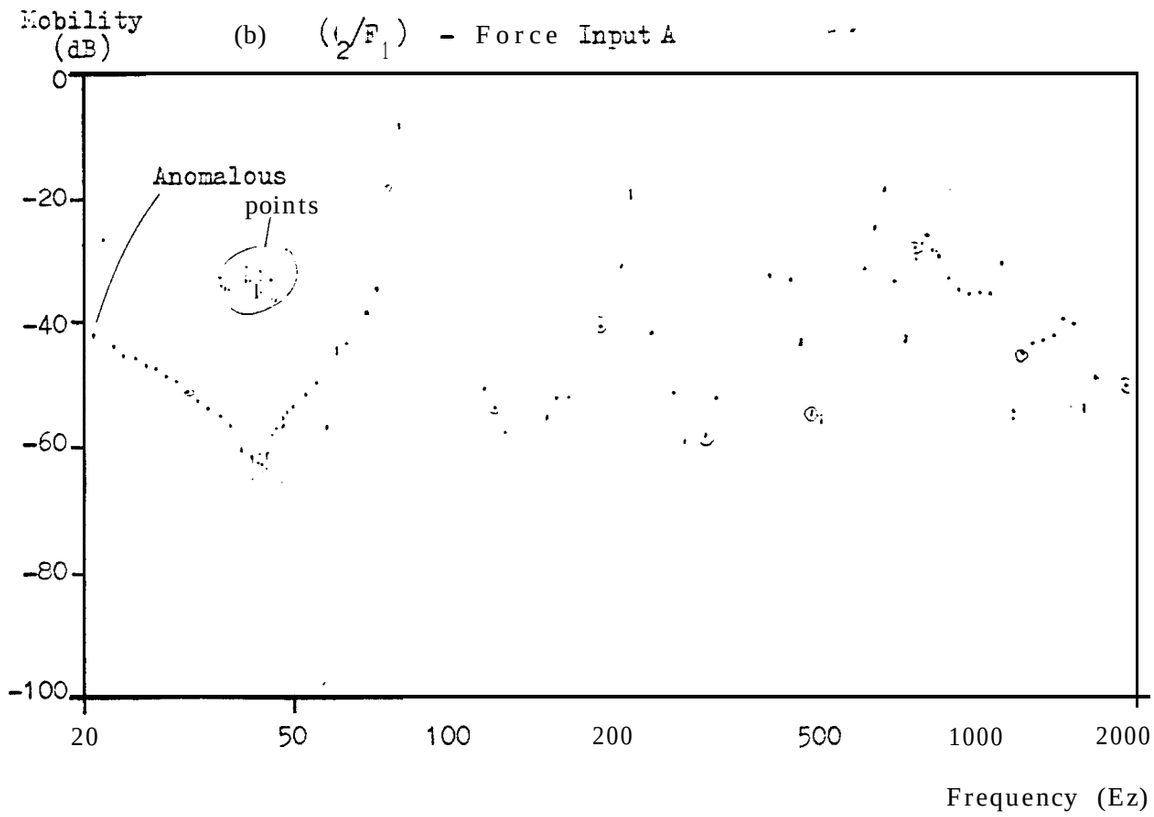

Figure 7.5 Inertial Effects of Exciting Block and Accelerometers

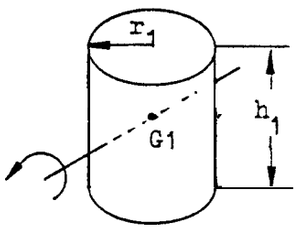

(2) Accelerometers - Assumed shape - cylinder

$I_G = m(r^2/4 + h^2/12)$

Type **4366** : $r_1 = 7.75$mm, $h_1 = 20$mm $m_1 = 29$ gm

$I_{G1} = 1.402 \times 10^{-6}$ kg m^2

Type **4367** : $r_2 = 6.75$mm, $h_2 = 16$ mm, $m_2 = 13.5$ gm

$I_{G2} = 0.4418 \times 10^{-6}$ kg m^2

(b) Exciting Block - Assumed shape - rectangular parallelipiped

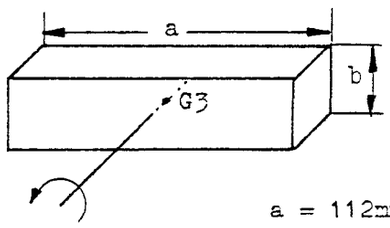

$I_G = m_B(a^2 + b^2)/12$

a = 112mm, b = 20mm, m_B = 0.124 kg

$I_{G3} = 1.338 \times 10^{-4}$ kg m^2

(c) Inertie of Exciting Block and Accelerometers w.r.t. Neutral Axis of Beam

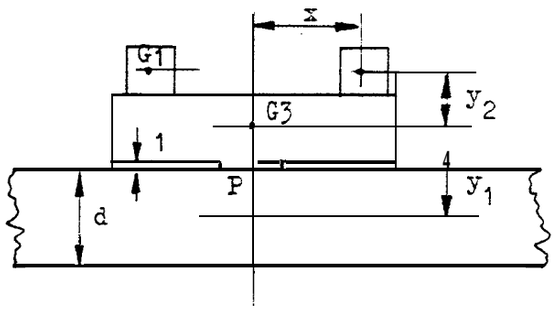

or

d = 32 mm
x = **50** mm
y_1 = **27** mm
y_2 = **20** mm **(4366)**
= 18 mm **($367)**

Inertia of Block about P = $I_{G3} + m_B y_1^2$

= 2.242×10^{-4} kg m^2

Inertia of **One** 4366 Accelerometer about P = $I_{G1} + m_1 (x^2 + \{y_1+y_2\}^2)$

= **1.38×10^{-4}** kg m^2

Inertiaof **One 4367** Accelerometer about P = $I_{G2} + m_2 (x^2 + \{y_1+y_2\}^2)$

= 5.75×10^{-5} kg m^2

Exciting Block plus Two Accelerometers

4366 : Mass = **0.182** Inertia about P = 5.00×10^{-4} **kg** m^2

4367 : Mass = 0.151 Inertia about P = 3.39×10^{-4} kg m^2

Figure 7.6 Computed Inertance of Exciting Block Mark 8

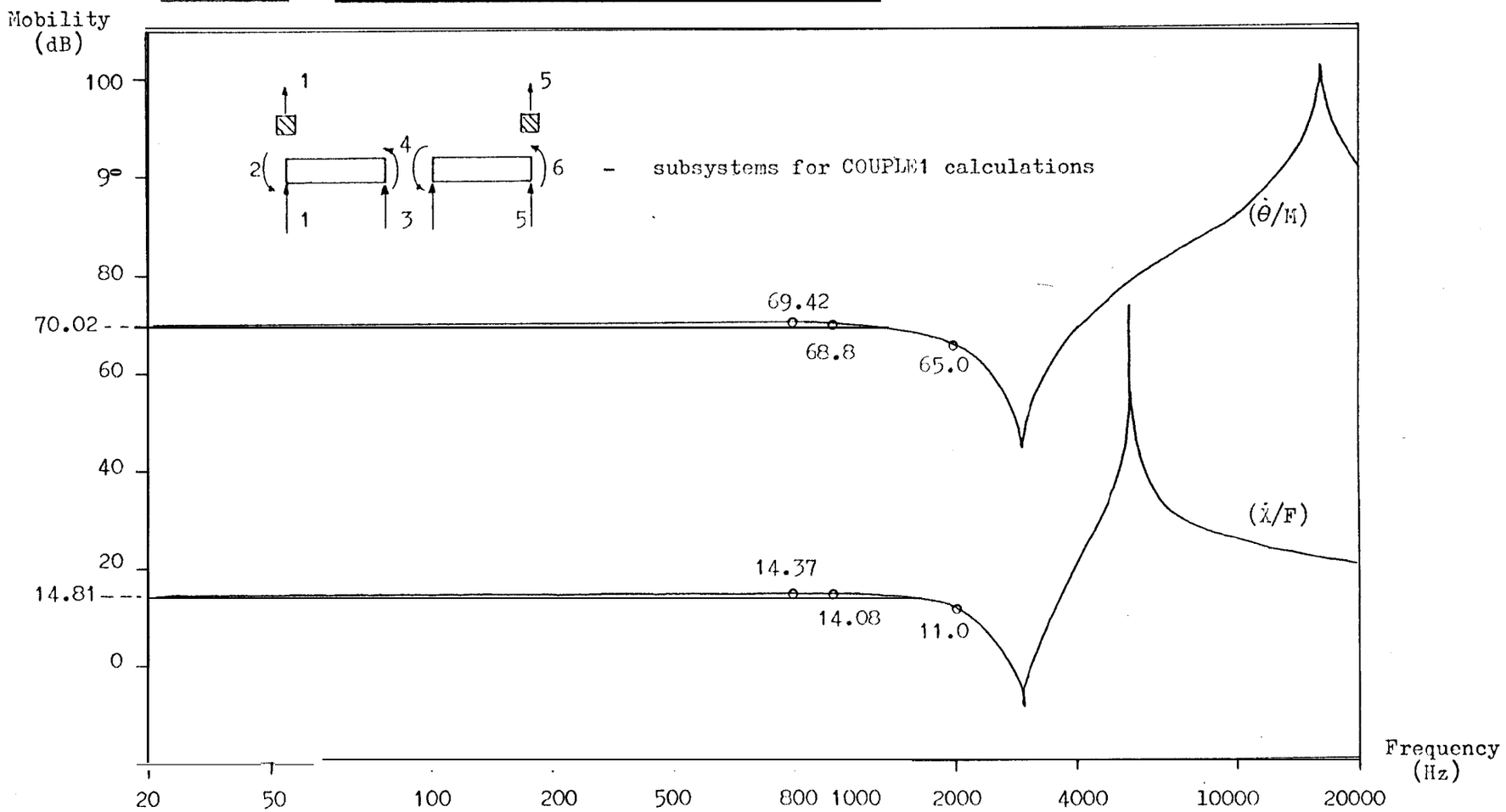

Figure 7.7 Identification of Short Beam with Blocks

Resonances at 0, 333, 780, 1150 He

(a) $(\dot{X}_1/F_1)$

Frequency Response

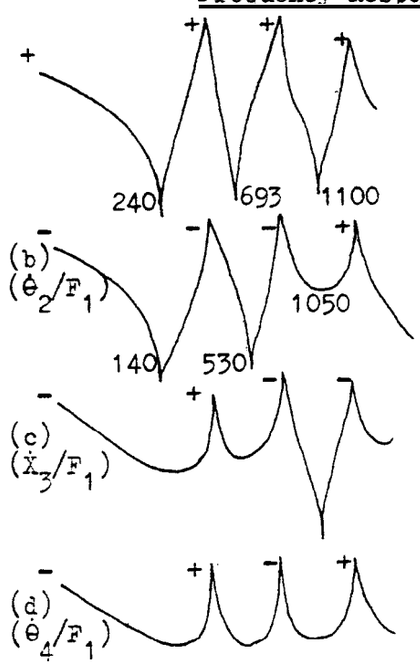

Selected Data

Frequency (Hz)	Mob(dB)	Phase (°)	Type
20	-44.05	-82	
240	-85	-90	AR
693	-84	-56	AR
1100	-75	-71	AR
20	-37	77	
140	-85	28	AR
530	-76	18	AR
1050	-39	95	Min
20	-51	105	
20	-37	78	

(e) Sign Array

Mode	1	2	3	4
Frequency	0	333	780	1150
	+	+	+	+
	-	-		+
	-	+		-
	-	+		+

Figure 7.8 Identification of Long Beam with Blocks

Resonances at 0, 80, 219, 420, 655, 800 Hz

Frequency Response

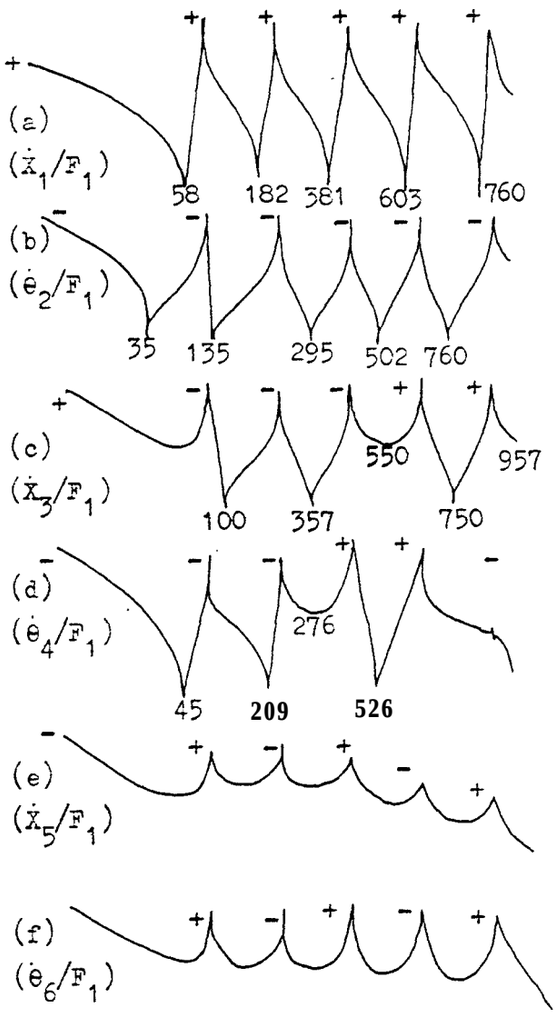

Selected Data

Freq.(Hz)	Mob(dB)	Phase(°)	Type
20.00	-48.89	-90.27	
57.68	an.57	83.72	AR
182.4	-96.27	62.22	AR
3El.l	-84.31	77.83	AR
603.98	-82.86	-26.81	AR
760.37	-66.89	-88.78	AR
20.00	-52.12	85.55	
34.76	-90.17	25.16	
135.00	-82.53	-55.72	
295.00	-75.69	-39.62	
502.37	-66.93	61.50	
760.37	-55.81	49.70	
20.00	-53.72	-91.02	
24.05	-52.66	102.97	
21.93	-54.56	84.76	
21.93	-43.42	-117.92	

(g) Sign Array

Mode	1	2	3	4	5
Frequency	0	80	219	420	655
	+	+	+	+	+
	-	-			-
	+	-			+
	-	-		+	+
	-	+		+	-
	-	+		+	-

Figure 7.9 (SM) Predicted Modal Data for Coupled Beam

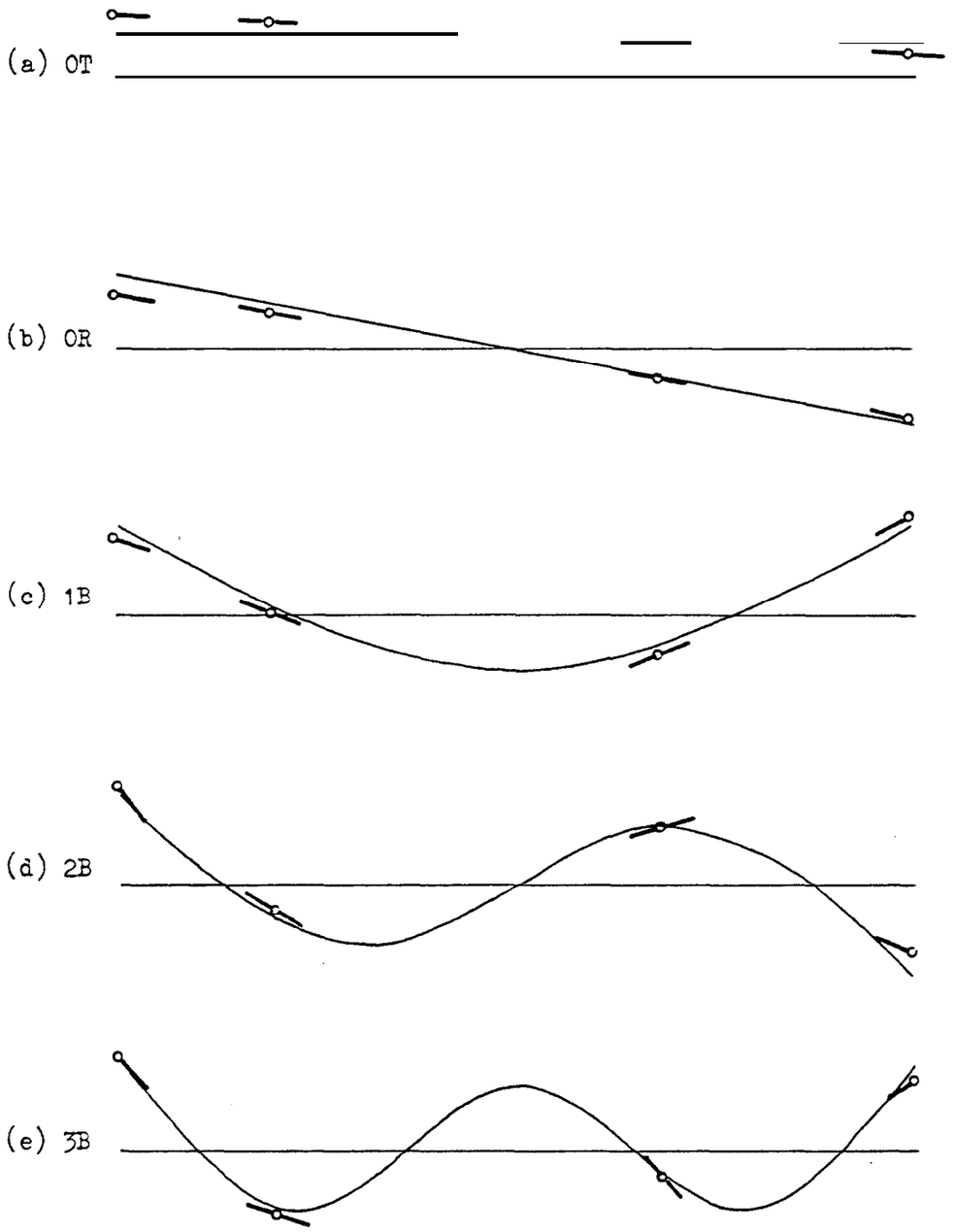

Frequency (True Frequency)(Hz)

(a) 0.122 (0) (b) j0.138 (0)

(c) 29.48 (40.07) (d) 96.46 (110.4) (e) 210.6 (216.5)

Figure 7.9 (SM) Predicted Modal Data for Coupled Beam (cont'd)

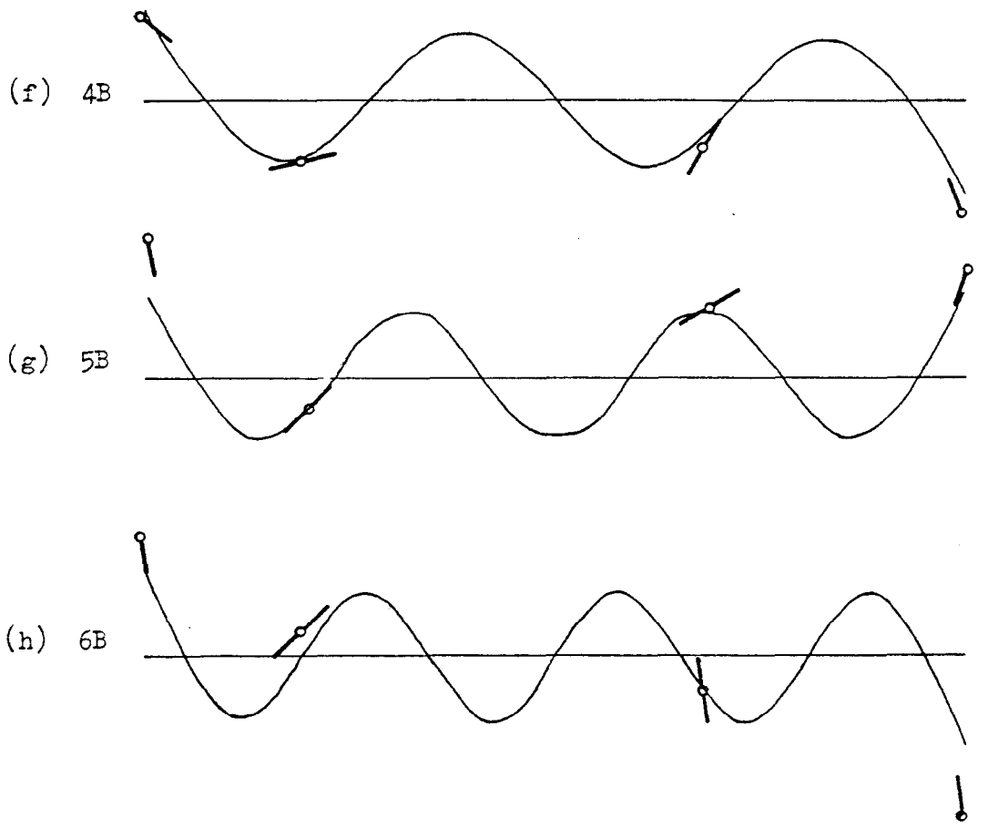

Frequency (True Frequency (Hz)

(f) 341.7 (357.9) (g) 523.4 (534.7) (h) 903.3 (746.8)

Key (a) Rigid Eody Translation CT

(b) Rigid Body Rotation OR

(c) 1st Bending Mode 1B

(d) 2nd Bending Mode 2B

etc.

Figure 7.10 Frequency Responses of Coupled Beam

(a) Tip Response 1 , 1

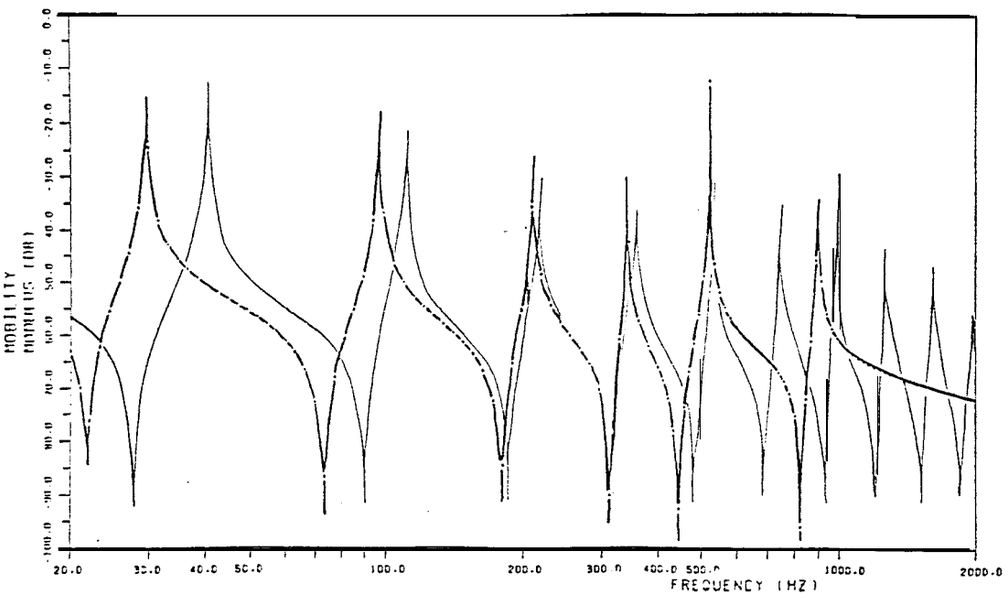

Spatial Model

Ideal

(b) Tip Response 2, 2

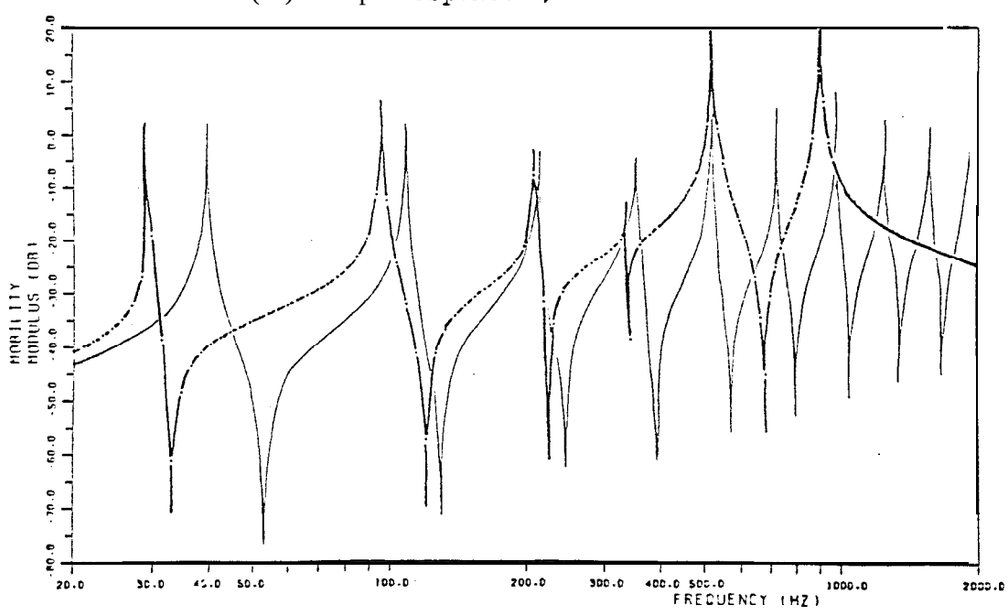

Figure 7.10 (cont'd) Precuency Responses of Coupled Beam

(c) Tip Cross Response 1, 2

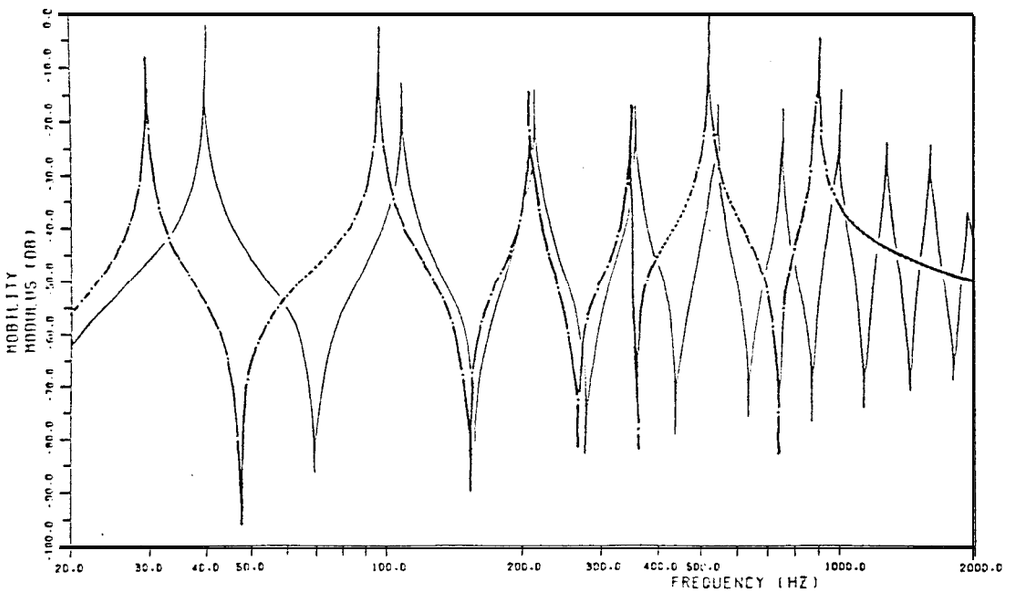

Spatial Model

Ideal

(d) Junction Cross Response 5,6

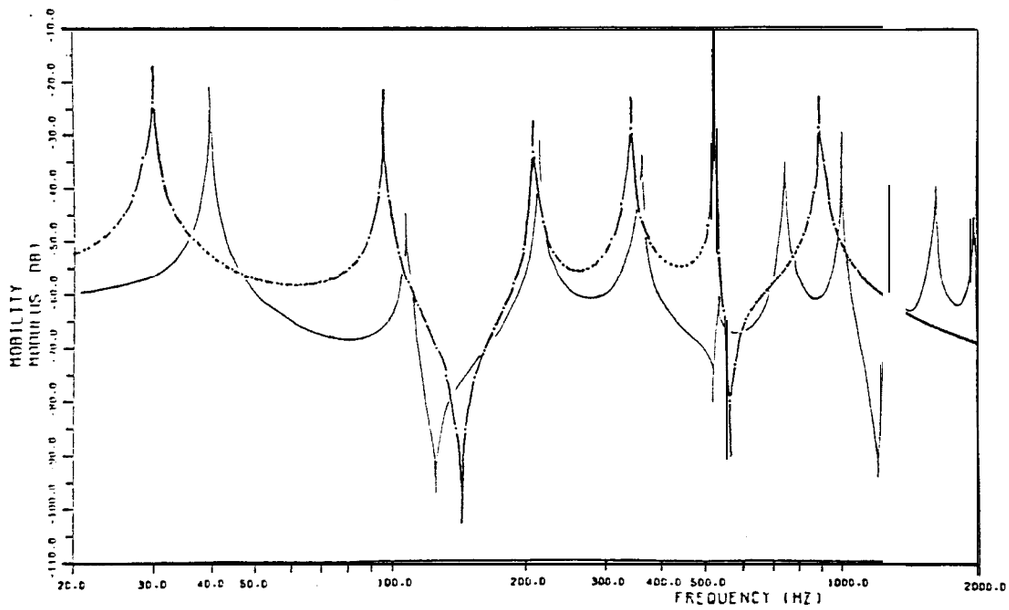

Figure 7.10 (SM) Frequency Responses of Cowled Beam (cont'd)

(e) Junction Response 5, 5

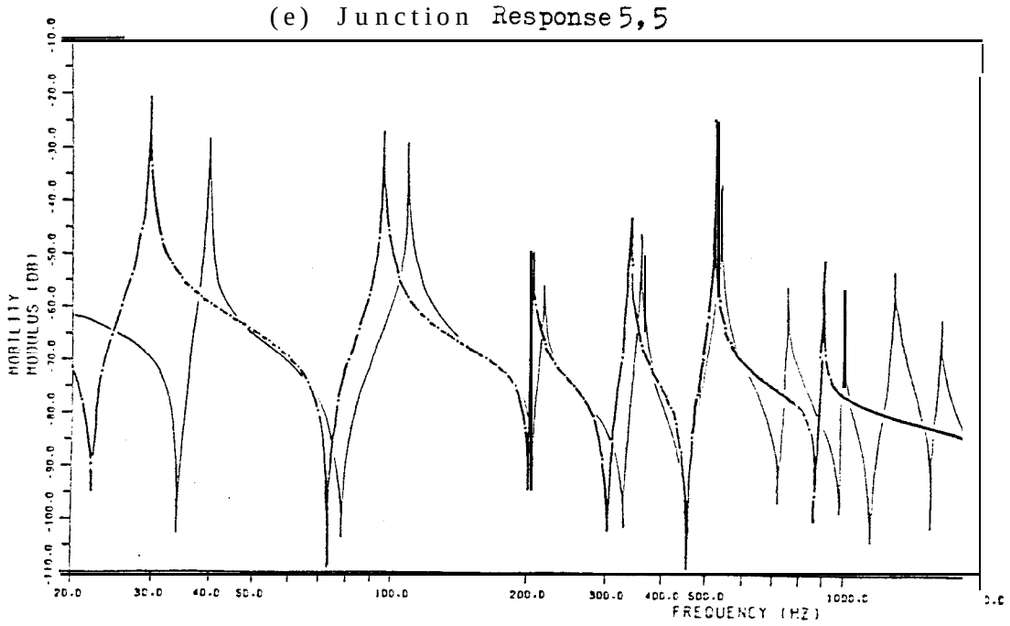

(f) Junction Response 6, 6

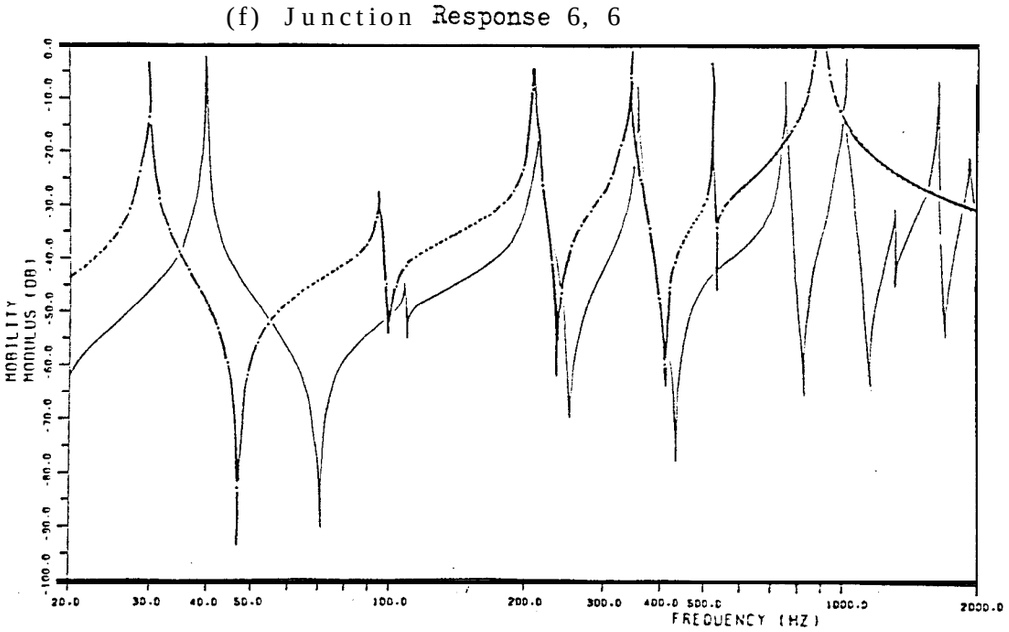

Figure 7.11 SMR Frequency Responses of Coupled Beam

(a) Tip Response 7, 7

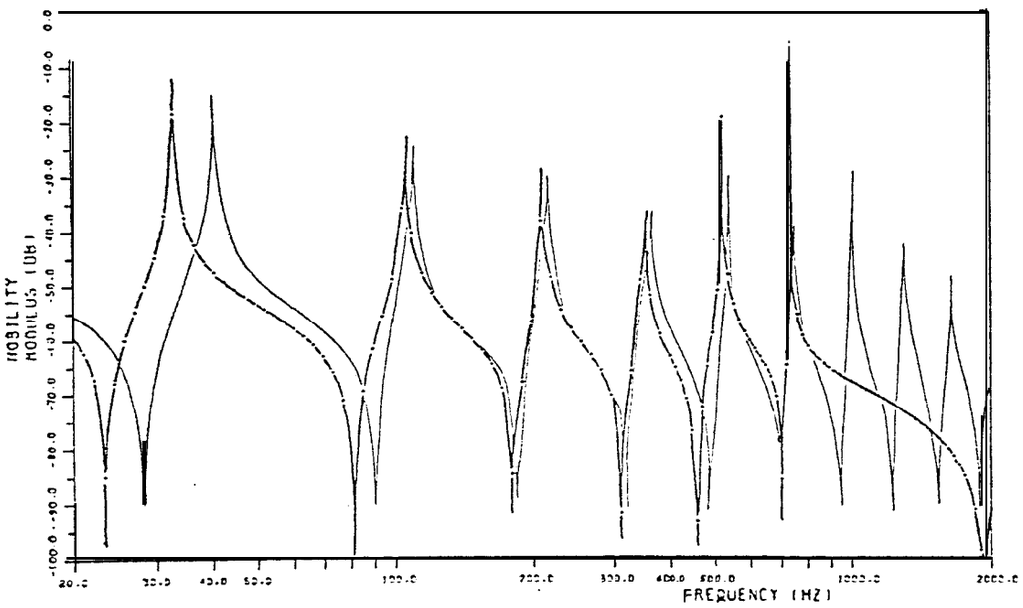

Spatial Model

Ideal

(b) Tip Response 2, 2

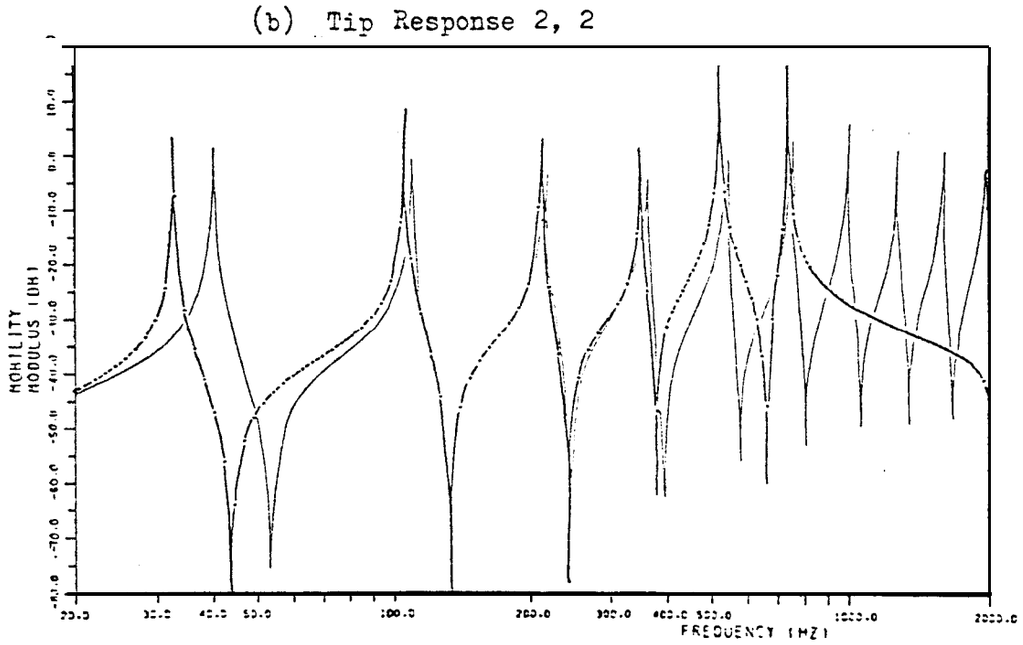

Figure 7.11 S_{0}^{MR} Frequency Responses of Coupled Beam (cont'd)

(c) Tip Cross Response 7, 2

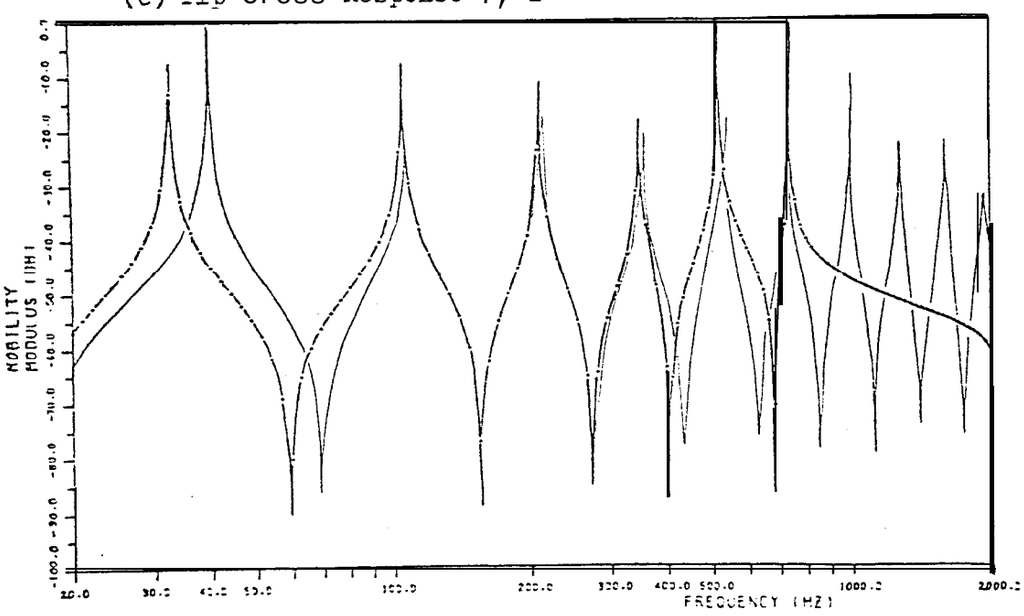

Spatial Model

Ideal

(d) Junction Cross Response 9, 6

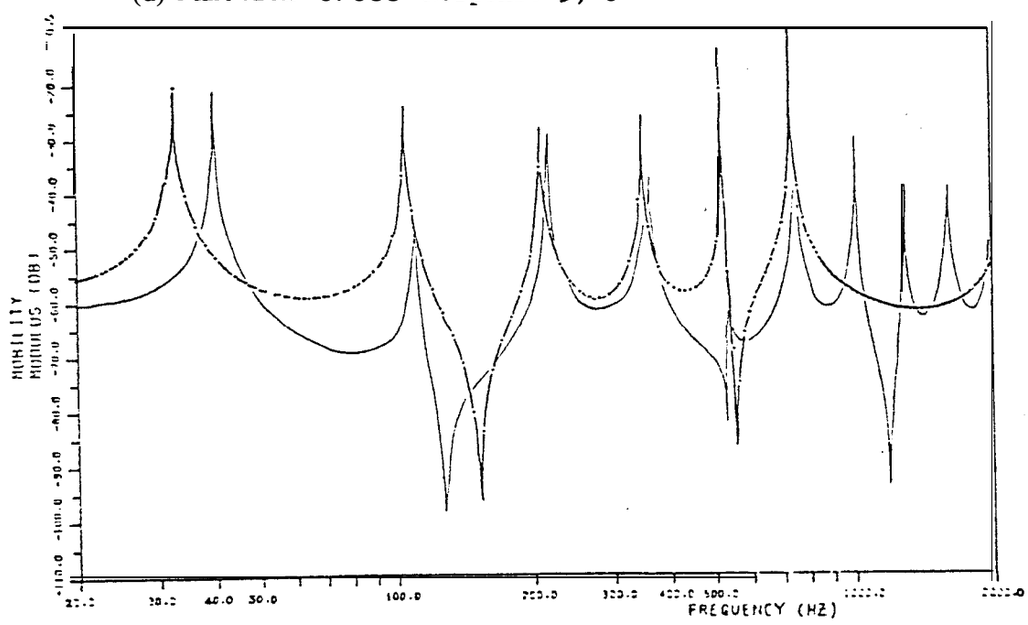

Figure 7.11 (SMR) Frequency Responses of Coupled Beam (cont'd)

(e) Junction Response 9, 9

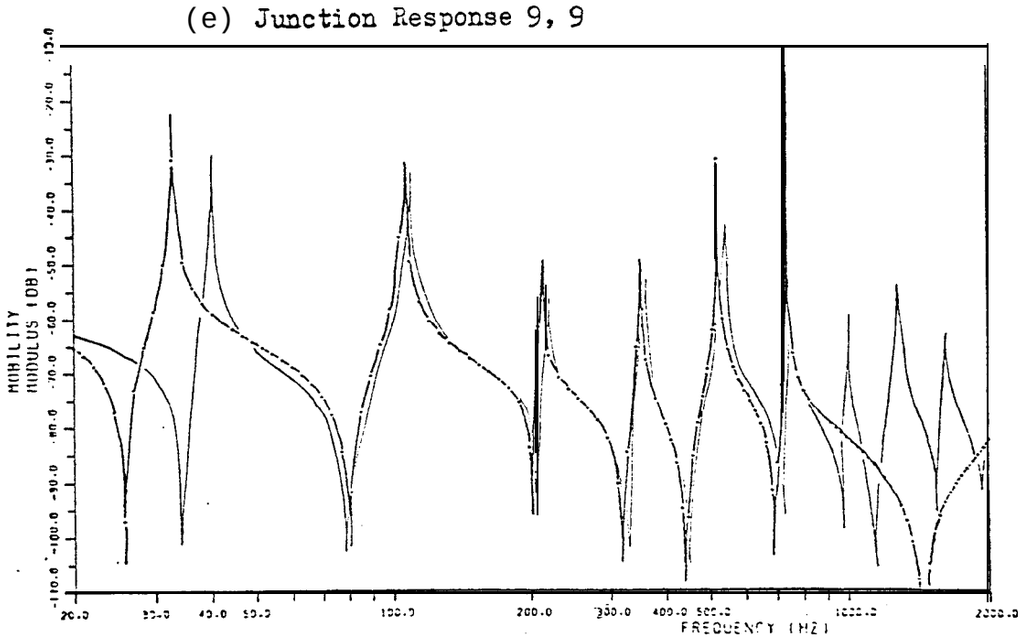

Spatial Model

Ideal

(f) Junction Response 6, 6

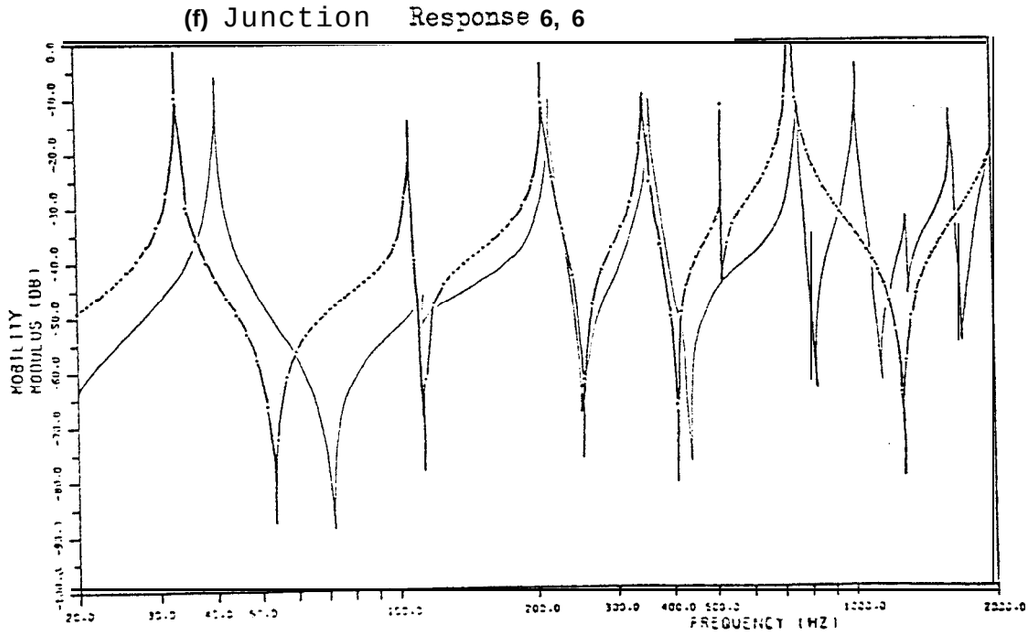

Figure 7.12 (SMR) Predicted Modal Data for Coupled Beam

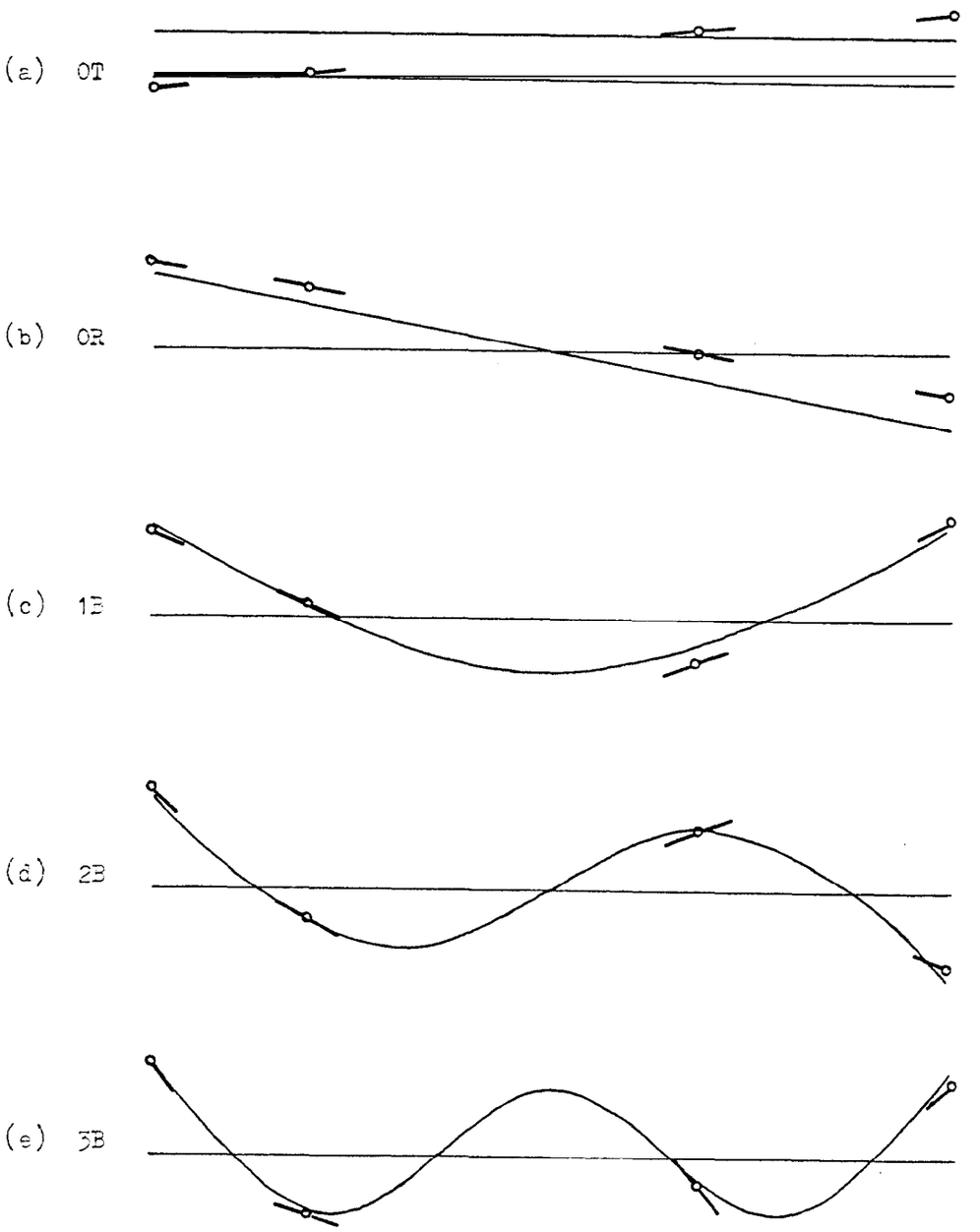

Frequency (True Frequency) (Hz)

(a) j0.82 (0) (b) 0.06 (0)

(c) 32.58 (40.07) (d) **105.42 (110.4)** (e) 210.87 **(216.5)**

Figure 7.12 SMR Predicted Modal Data for Coupled Beam (cont'd)

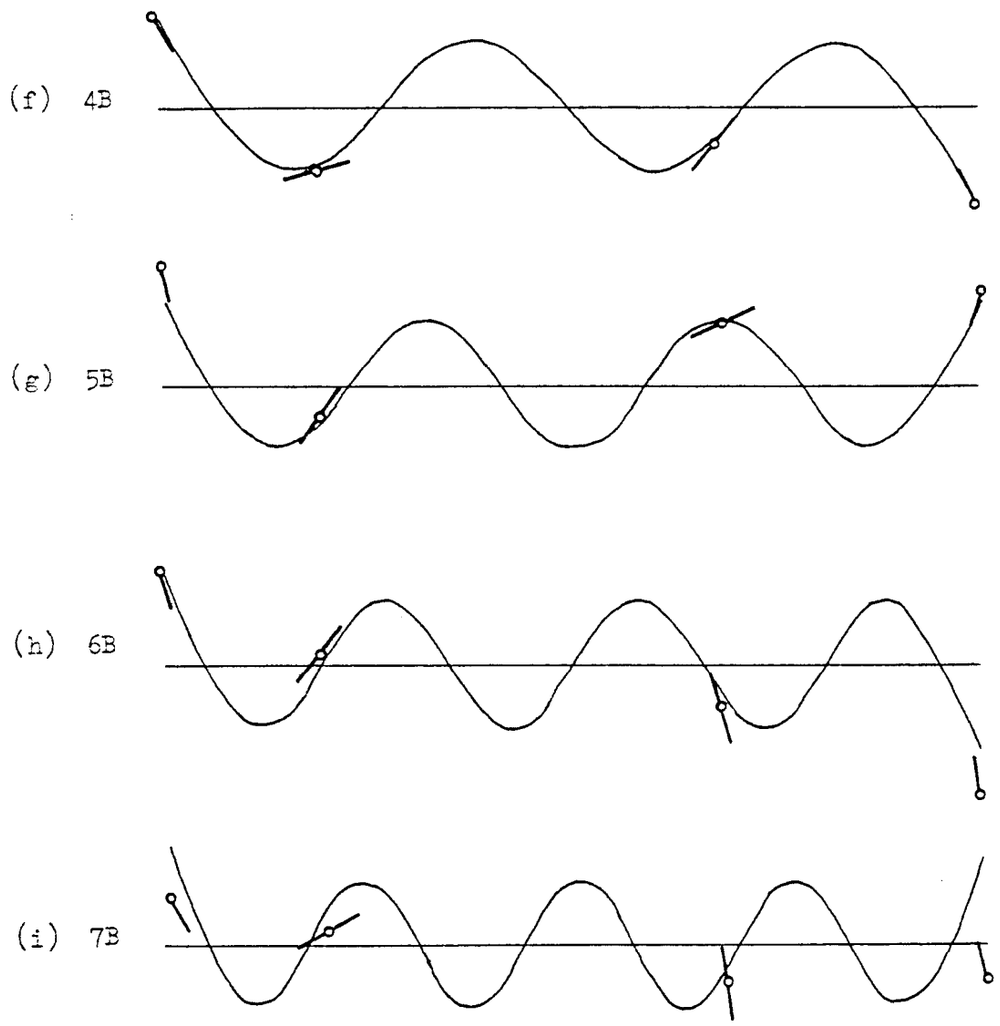

Frequency (True Frequency) (Hz)

(f) 350.32 (357.9) (g) 522.59 (534.7) (h) 740.77 (746.8)
(i) 2171.57 (994.1) - anomalous

Figure 7.13 (SM) (SMR) Spatial Models of Coupled Beams
Coordinates and Natural Frequencies

(a) ideal Beam

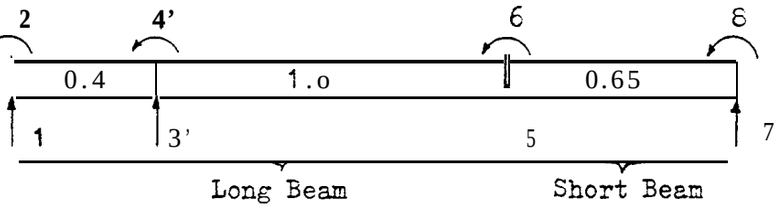

Natural Frequencies Hz

0	0	40.07	110.4	216.5	357.9	534.7	746.8	etc.

(b) (SM) Spatial Model - Measured Data

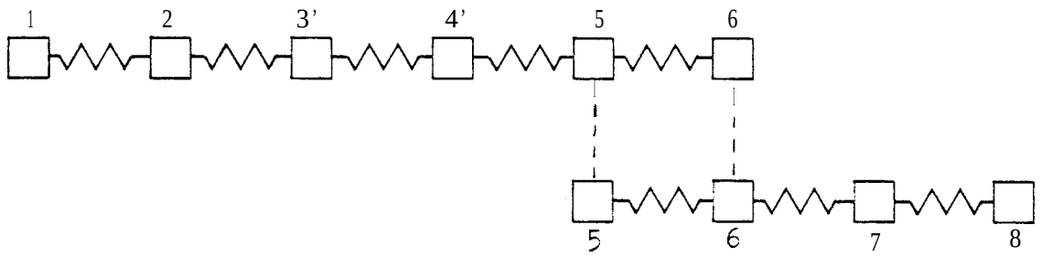

Tip Coordinates 1, 2 Junction Coordinates 5, 6

Natural Frequencies (Hz) - Error %

.121	-.138	29.48	96.46	210.6	341.7	523.4	903.3
		(-36)	(-14)	(-2.8)	(-4.8)	(-2.2)	(+21)

(c) (SMR) Spatial Model with Residuals - Measured Data

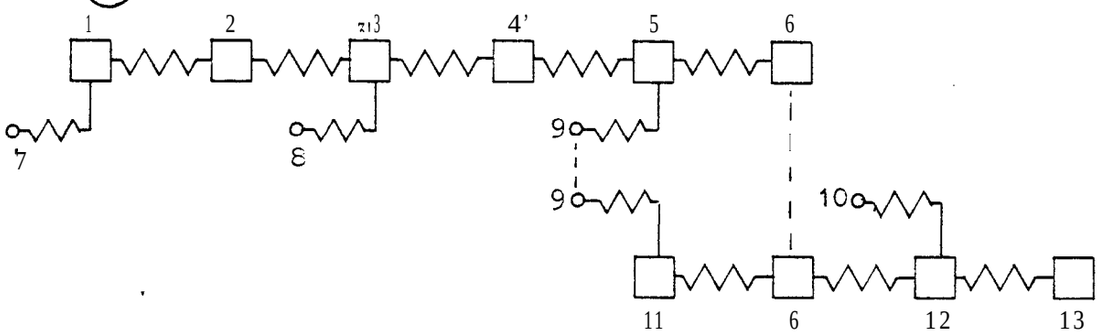

Tip Coordinates 7, 2 Junction Coordinates 9, 6

Natural Frequencies Hz - Error %

j0.82	0.06	32.58	105.42	210.87	35C.32	522.59	740.77
		(-23)	(-4.7)	(-2.7)	(-2.2)	(-2.3)	(-0.8)

plus 2171.57 (anomalous)

Table 7.1 (SM) Development of Mode Shape Matrix for Short Beam with Blocks

(a) Derivation of Rotational Modal Constants

Mode	1	2	3
Frequency (Hz)	0	333	780
A_{11}	.790815	.616797	.338670
A_{21}	-1.80585	-6.22252	-15.4156
$A_{22} = A_{21}^2/A_{11}$	5.77415*	62.7755	701.688

* $_rA_{jj} = {}_1A_{ij}^2/({}_1A_{ii} - 1/m)$ for i odd and j = i + 1

m = 4.06 (beam) + 2(.182) (blocks) = 4.424 kg
$l/n = .226040\ kg^{-1}$

(b) Separation of Rigid Body Modes - T=Translational, R=Rotational

$${}_1A_{11T} = 1/m = .226040\ ;\ {}_1A_{11R} = {}_1A_{11} - {}_1A_{11T} = .564775$$
$${}_1A_{22T} = 0\ ;\ {}_1A_{22R} = {}_1A_{22} - {}_1A_{22T} = 5.77415$$

(c) Matrix of Point Modal Constants

Because of symmetry of short beam with blocks $A_{33} = A_{11}$, $A_{44} = A_{22}$

Frequency (Hz)	0 (T)	0 (R)	333	780
A_{11}	.226040	.564775	.616797	.338670
A_{33}	.226040	.564775	.616797	.338670
A_{44}	0	5.77415	62.7755	701.688
A_{22}	0	5.77415	62.7755	701.688

(d) Mode Shape Matrix

Frequency (Hz)	0 (T)	0 (R)	333	780
$\sqrt{A_{11}}$	+.475437	+.751515	+.785364	+.581954
$\sqrt{A_{22}}$	+ 0	-2.40295	-7.92310	-26.4894
$\sqrt{A_{33}}$	+.475437	-.751515	+.785364	-.581954
$\sqrt{A_{44}}$	+ 0	-2.40295	+7.92310	-26.4894

The signs in the lest two columns were found from, the plotted and identified short beam transfer responses, Figure 7.1. The signs in the first two columns were found from the rigid body node shapes below.

Table 7.2 (SM) Spatial Models of Short Beam - Based on Measured Data

Output of program EMMAY with input data from Table 7.1

(a) Matrices for Short Beam with Blocks

$$[M_{SB}] = \begin{bmatrix} 1.62228 & .122198 & .589714 & -.0970625 \\ & .0155087 & .0970625 & -.0141900 \\ & & 1.62228 & -.122198 \\ \text{Symmetric} & & & .0155087 \end{bmatrix}$$

$$\sum M_{trans} = 4.424 \text{ kg}$$

$$[K_{SB}] = 10^5 \begin{bmatrix} 1.01210 & .316530 & -1.01210 & .316530 \\ & .273334 & -.316530 & -.0753462 \\ & & 1.01210 & -.316530 \\ \text{Symmetric} & & & .273334 \end{bmatrix}$$

$$\sum K_{trans} = 0$$

(b) Matrix of Exciting Block Inertia (from Figure 7.5)

$$[I_S] = \begin{bmatrix} .182 & & & \\ & 5.00\text{ E-4} & & \\ & & .182 & \\ & & & 5.00\text{ E-4} \end{bmatrix}$$

(c) Matrices for Short Beam without Blocks

$$[M_S] = [M_{SB}] - [I_S]$$

$$[M_S] = \begin{bmatrix} 1.44028 & .122198 & .589714 & -.0970625 \\ & .0150087 & .0970625 & -.0141900 \\ & & 1.44028 & -.122198 \\ \text{Symmetric} & & & .0150087 \end{bmatrix}$$

$$\sum M_{trans} = 4.06 \text{ kg}$$

$$[K_S] = [K_{SB}] \qquad \text{in (a) above}$$

Table 7.3 (SM) Modal Properties of the Short Beam Predicted from Spatial Models

(a) Short Beam with Blocks

Program EIGEN with input $\left[M_{SB}\right], \left[K_{SB}\right]$ of Table 7.2(a)

Natural Frequencies	.0163	.163	333	780
Node Shape Matrix	.456	.764	-.785	-.582
	.063	**-2.40**	**7.92**	**26.5**
	.494	-.739	-.785	.582
	.063	**-2.40**	**7.92**	26.5

(compare with Table 7.1(d))

(b) Short Beam without Blocks

Program EIGEN with input $\left[M_S\right], \left[K_S\right]$ of Table 7.2(c)

Natural Frequencies	.025	.185	400.1	2329
Mode Shape Matrix	.471	.861	**-1.03**	-2.37
	.081	**-2.70**	9.52	81.1
	.521	-.831	**-1.03**	**2.37**
	.081	-2.70	-9.52	81.1

(compare with (c) below)

(c) Ideal Short Beam

Natural Frequencies	0	0	**398.5**	1099
Mode Shape Matrix	.497	.860	1.00	1.02
	0	-2.65	-7.18	-13.2
	.497	-.860	1.00	-1.02
	0	-2.65	7.18	-13.2

Table 7.4 (SM) Development of Mode Shape Matrix for Long Beam with Blocks

(a) Derivation of Rotational Modal Constants

Mode	1	2	3	4	5
Frequency (Hz)	0	80	219	420	655
A_{11}	.432627	.391486	.371123	.298655	.262382
A21	-.441017	-1.31538	-2.37549	-4.26877	-10.1784
$A_{22} = A_{21}^2/A_{11}$	.599229*	**4.41963**	**15.2051**	**61.0149**	394.843
"33	.169413	.0306106	.196428	.071770	.0678318
A_{43}	-.199691	.251313	.0988312	-.651109	.637200
$A_{44} = A_{43}^2/A_{33}$	.649846*	**2.06328**	.049726	**5.90697**	**5.98574**
f55	.454949	.413042	• 413775	.391063	.472566
A_{65}	**1.07100**	**1.93318**	**3.14928**	**5.67542**	**15.0795**
$A_{66} = A_{65}^2/A_{55}$	**3.30656"**	**9.04795**	**23.9695**	**82.3662**	**481.184**

*Using : $_1A_{jj} = {}_1A_{ij}^2/({}_1A_{ii} - 1/m)$ for i odd and j = i + 1

where $1/m = .108050\ kg^{-1}$

$m = 8.74$ (bean) + 2(.182) + .151 (blocks) = 9.255 kg

$1/m = .108050\ kg^{-1}$

$_1A_{66} =$ **3.30656** is an order of magnitude greater than $_1A_{22}$, $_1A_{44}$, whereas, ideally, all three term have the same value. The plot of Y_{65} shows anomalous low frequency response about **10** dB high. It follows that $_1A_{65}$ is too big. In (b) below $_1A_{22}=_1A_{44}=_1A_{66}=(.599229+.649846)/2.$

(b) Separation of Rigid Body Modes

$_1A_{11T} = .108050$	$_1A_{11R} = .432627 - .108050 = .324577$
$_1A_{22T} = 0$	$_1A_{22R} = .624538$
$_1A_{33T} = .108050$	$_1A_{33R} = .169413 - .108050 = .061363$
$_1A_{44T} = 0$	$_1A_{44R} = .624538$
$_1A_{55T} = .108050$	$_1A_{55R} = .454949 - .108050 = .346899$
$_1A_{66T} = 0$	$_1A_{66R} = .624538$

Using , $A_{iiT} = 1/m$ for i odd

$= 0$ for i even

and $_1A_{iiR} = {}_1A_{ii} - {}_1A_{iiT}$ for all i

Table 7.4 continued

(c) Matrix of Point Modal Constants

Frequency(Hz)	0 (T)	0 (R)	60	219	420	655
A_{11}	.108050	.324577	.391486	.371123	.298655	.262382
A_{22}	0	.624538	4.41963	15.2051	61.0149	394.~43
A_{33}	.108050	.06 613630	● 0306106	.196428	.071770	.0678318
"44	0	.624538	2.06328	.049726	5.90697	5.98574
A_{55}	.108050	.346899	.413042	.413775	.391063	.472566
A_{66}	0	.624538	9.04795	**23.9695**	**82.3662**	481.184

(d) Kode Shape Matrix

Frequency(Hz)	0 (T)	0 (R)	80	219	420	655
$\sqrt{A_{11}}$	+.328710	+.569717	+.625688	+.609199	+.546493	+.512232
$\sqrt{A_{22}}$	+ 0	-.790277	-2.10229	-3.89937	-7.61120	-19.8707
$\sqrt{A_{33}}$	+.328710	+.247716	-.174959	-.443202	-.267899	+.260445
$\sqrt{A_{44}}$	+ 0	-.790277	-1.43641 36	-.222993	+2.43043	+2.44658
$\sqrt{A_{55}}$	+.328710	-.588981	+.642683	-.643253	+.625350	-.687434
$\sqrt{A_{66}}$	+ **0**	-.790277	+3.00798	-4.89587	+9.07558	**-21.9359**

The signs in the last four columns were found from the plotted and identified long bean transfer responses, Figure 7.8.

The signs in the first two columns were found fron the rigid body node shapes sketched below.

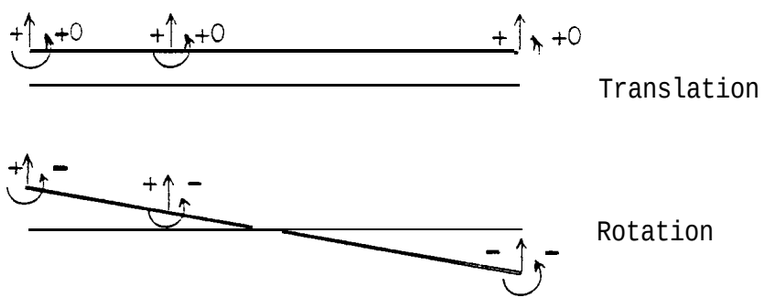

Table 7.5 Spatial Models of Long Beam - Based on Measured Data

Output of program EMKAY with input data from Table 7.4

(a) Matrices for Long Beam with Blocks

$$[M_{LB}] = \begin{bmatrix} 5.02113 & .654748 & -1.27187 & 1.70485 & 1.88910 & -.348653 \\ & .0984384 & -.242128 & .259411 & .296964 & -.0547216 \\ & & 3.01710 & -.584487 & -1.03067 & .182484 \\ & & & .772327 & .687852 & -.134620 \\ & & & & 2.04358 & -.225554 \\ \text{Symmetric} & & & & & .0360421 \end{bmatrix}$$

$\sum M_{trans}$ = 3.255 kg

$$[K_{LB}] = 10^5 \begin{bmatrix} 38.0273 & 5.19367 & -37.6849 & 11.7162 & -.342368 & -1.05300 \\ & .926648 & -5.31120 & 1.29737 & .117528 & -.232269 \\ & & 38.7745 & -10.4435 & -1.08957 & 1.55341 \\ & & & 4.78266 & -1.27267 & .0411795 \\ & & & & 1.43194 & -.500410 \\ \text{Symmetric} & & & & & .291845 \end{bmatrix}$$

$\sum K_{trans} = 10^5(.64 \times 10^{-5}) \simeq 0$

(b) Matrix of Exciting Block Inertias (from Figure 7.5

$$[I_L] = \begin{bmatrix} .182 & & & & & \\ & 5.00\text{ E-4} & & & & \\ & & .182 & & & \\ & & & 5.00\text{ E-4} & & \\ & & & & .151 & \\ & & & & & 3.39\text{ E-4} \end{bmatrix}$$

(c) Matrices for Long Beam without Blocks

$$[M_L] = [M_{LB}] - [I_L]$$

$$[M_L] = \begin{bmatrix} 4.83913 & .654748 & -1.27187 & 1.70485 & 1.88910 & -.348830 \\ & .0979384 & -.242128 & .259411 & .296964 & -.0547216 \\ & & 2.83510 & -.584487 & -1.03067 & .182484 \\ & & & .771827 & .687852 & -.134620 \\ & & & & 1.89258 & -.225554 \\ \text{Symmetric} & & & & & .0357031 \end{bmatrix}$$

$\sum M_{trans}$ = E.74 kg

$[K_L] = [K_{LB}]$ in (a) above

Table 7.6 (SI) Modal Properties of the Long Beam Predicted from Spatial Models

(a) Long Beam with Blocks

Program EIGEN with input $\left[M_{LB}\right], \left[K_{LB}\right]$ of Table 7.5(a)

Natural Frequencies	.133	.259	80	219	428	655
Mode Shape Matrix	.346	.559	.626	-.609	-.546	-.512
	-.024	-.790	-2.10	**3.90**	7.81	**19.9**
	.336	.237	-.175	-.443	.268	-.260
	-.024	-.790	-1.44	.223	**-2.43**	**-2.45**
	.310	-.599	.643	.643	-.625	.687
	-.024	-.790	**3.01**	4.90	-3.08	**21.9**

(compare with Table 7.4(d))

(b) Long Beam without Blocks

Program EIGEN with input $\left[M_L\right], \left[K_L\right]$ of Table 7.5 (c)

Natural Frequencies	.137	.274	86.67	243.2	475.1	**995.6**
Mode Shape Matrix	.354	.607	.695	-.732	-.798	**-1.14**
	-.022	-.844	-2.21	**3.75**	9.60	**31.5**
	.345	.263	-.163	.476	.336	-.312
	-.022	-.844	**-1.57**	.490	**-2.46**	**-3.36**
	.322	-.631	**0** 715	.761	-.831	1.49
	-.022	-.844	**3.20**	**4.84**	**-10.5**	**35.7**

(compare with (c) below)

(c) Ideal Long Bean!

Natural Frequencies	0	0	**85.91**	**236.8**	**464.2**	**767.4**
Mode Shape Matrix	.338	.586	.677	.681	.688	.713
	0	-.837	-2.25	-3.85	**-5.64**	-8.28
	.338	.251	-.153	-.443	-.329	.0656
	0	-.837	**-1.62**	-.532	**2.76**	**5.97**
	.338	-.586	.677	-.681	.689	-.713
	0	-.837	**2.25**	**-3.85**	**5.64**	-8.28

Table 7.7 Spatial Model of Coupled Beam

(a) Coordinates

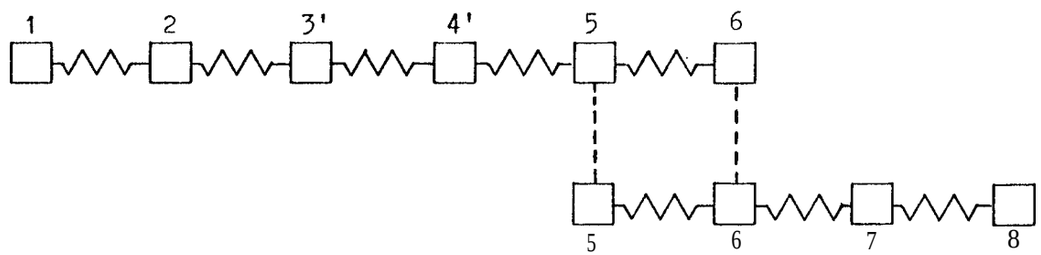

(b) Mass Matrix

$$[M_C] = \begin{bmatrix}
4.83913 & .654748 & -1.27187 & 1.70485 & 1.88910 & -.348830 & 0 & 0 \\
 & .097938 & -.242128 & .259411 & .296964 & -.054722 & 0 & 0 \\
 & & 2.83510 & -.584487 & -1.03067 & .182848 & 0 & 0 \\
 & & & .771827 & .687852 & -.134620 & 0 & 0 \\
 & & & & 3.33286 & -.103356 & .589714 & -.097063 \\
 & & & & & .050712 & .097063 & -.014190 \\
 & & & & & & 1.44028 & -.122198 \\
 & & & & & & & .015009
\end{bmatrix}$$

Symmetric

Table 7.7 continued

(c) Stiffness Matrix

$$\left[K_C\right] = 10^5 \begin{vmatrix} 38.0273 & 5.19367 & -37.6849 & 11.7162 & -.342368 & -1.05300 & 0 & 0 \\ & .926648 & -5.31120 & 1.29737 & .117528 & -.232269 & 0 & 0 \\ & & 38.7745 & -10.4435 & -1.08957 & 1.55341 & 0 & 0 \\ & & & 4.78266 & -1.27267 & .041180 & 0 & 0 \\ & & & & 2.44404 & -.183880 & -1.01210 & .316530 \\ & & & & & .565179 & -.316530 & -.075346 \\ & & & & & & 1.01210 & -.316530 \\ \text{Symmetric} & & & & & & & .273334 \end{vmatrix}$$

(d) Predicted Natural Frequencies (Hz) (Error %)

.121	-.138	29.48	96.46	21°.6	341.7	523.4	903.3
		(-36)	(-14)	(-2.8)	(-4.8)	(-2.2)	(+21)

Output of program EIGEN

Table 7.8 (SMR) Development of Mode Shape Matrix for Short Beam with Blocks

(a) Derivation of Rotational Modal Constants + Residual Stiffness

Mode	1	2	3	4 (residual
Frequency (Hz	0	333	780	20000
A_{11}	.790879	.602337	.282642	179.315
A_{21}	1.81023	6.01539	11.8064	
$A_{22} = A_{21}^2/A_{11}$	5.80153*	60.0742	493.172	

*${}_1A_{22} = {}_1A_{21}^2/({}_1A_{11} - 1/m)$ where $1/m = .226040$

(b) Residual Stiffness

$K_{rs1} = (2\pi \times 20000)^2/179.315 = 880.650 \times 10^5$ N/m

(c) Separation of Rigid Body Modes

${}_1A_{11T} = .226040$ ${}_1A_{22T} = 0$	${}_1A_{11R} = {}_1A_{11} - {}_1A_{11T} = .564839$ ${}_1A_{22R} = 5.80153$

(d) Matrix of Point Modal Constants

Because of symmetry: $A_{11} = A_{33}$, $A_{44} = A_{22}$, $K_{r3} = K_{r1}$

Frequency (Hz)	0 (T)	0 (R)	333	780
A_{11}	.226040	.564839	.602337	.282642
A_{22}	0	5.80153	60.0742	493.172
A_{33}	.226040	.564839	.602337	.282642
A_{44}	0	5.80153	60.0742	493.172

(e) Mode Shape Matrix

Frequency (Hz)	0 (T)	0 (R)	333	780
$\sqrt{A_{11}}$	+.475437	+.751558	+.776104	+.531641
$\sqrt{A_{22}}$	+ 0	-2.40864	-7.75075	-22.2675
$\sqrt{A_{33}}$	+.475437	-.751558	+.776104	-.531641
$\sqrt{A_{44}}$	+ 0	-2.40864	+7.75075	-22.2675

Signs as in Table 7.1.

Table 7.3 (SMR) Spatial Models of Short Beam

Output of program EMKAY with input data from Table 7.8 (e)

(a) Matrices for Short Beam with Blocks

$$[M_{SBR}] = \begin{bmatrix} 1 & 1.63133 & .125082 & .580669 & -.0964107 \\ & & .0161431 & .0964107 & -.0143586 \\ & & & 1.63133 & -.125082 \\ S & \text{Symme tric} & & & .0161431 \end{bmatrix}$$

$$\Sigma M_{trans} = 4.428 \text{ kg}$$

$$[K_{SBR}] = 10^5 \begin{bmatrix} 1.46705 & .457757 & -1.46705 & .45775? \\ & .325012 & -.457757 & -.0393478 \\ & & 1.46705 & -.457757 \\ \text{Symmetric} & & & .325012 \end{bmatrix}$$

$$\Sigma K_{trans} = 0$$

(b) Matrices for Short Beam without Blocks

$$[M_{SR}] = [M_{SBR}] - [I_S] \text{ (see Table 7.2(b))}$$

$$[M_{SR}] = \begin{bmatrix} 1.44933 & .125082 & .580669 & -.0964107 \\ & .0156431 & .0964107 & -.0143586 \\ & & 1.44933 & -.125082 \\ \text{Symmetric} & & & .0156431 \end{bmatrix}$$

$$\Sigma M_{tram} = 4.063 \text{kg}$$

$$[K_{SR}] = [K_{SBR}] \text{ in (a) above}$$

(c) Residual Stiffness Matrix

From Table 7. 8 (b).

$$[K_{rs}] = 10^5 \begin{bmatrix} 880.650 & & & \\ & 0 & & \\ & & 880.650 & \\ & & & 0 \end{bmatrix}$$

Table 7.10 SBR Modal Properties of the Short Beam Predicted from Spatial Models

(a) Short Beam with Blocks

Program EIGEN with input $[M_{SBR}]$, $[K_{SBR}]$ of Table 7.9(a)

Natural Frequencies: 1.4E-5, .125, 333, 780

Mode Shape Matrix:

$$\begin{bmatrix} .475 & .752 & -.776 & -.532 \\ 0 & -2.41 & 7.75 & 22.2 \\ .475 & -.752 & -.776 & .532 \\ 0 & -2.41 & -7.75 & 22.2 \end{bmatrix}$$

(compare with Table 7.1 (d))

(b) Short Seam without Blocks

Program EIGEN with input $[M_{SR}]$, $[K_{SR}]$ of Table 7.9(b)

Natural Frequencies: 2.0E-5, .155, 397.7, 1311

Mode Shape Matrix:

$$\begin{bmatrix} .496 & .846 & -1.010 & -1.212 \\ 0 & -2.71 & 9.26 & 38.36 \\ .496 & -.846 & -1,010 & 1.212 \\ 0 & -2.71 & -9.26 & 38.36 \end{bmatrix}$$

(compare with ideal, Table 7.3(c))

Table 7.11 SBR Development of Mode Shape Matrix for Long Beam with Blocks

(a) Derivation of Rotational Modal Constant + Residual Stiffness

Mode	1	2	3	4	5	6(residual)
Frequency (Hz)	0	80	219	420	655	10000
A_{11}	.432683	.390762	.365629	.284437	.229058	62.3506
A_{21}	-.441252	-1.30459	-2.22375	-3.34418	-4.38631	
$A_{22} = A_{21}^2/A_{11}$	.599764*	4.3554-E	13.5248	39.3182	83.9950	
A_{33}	.169495	.0303925	.184489	.0507017	.0320674	76.4577
A_{43}	-.199718	.251227	.0994088	-.641178	.683884	
$A_{44} = A_{43}^2/A_{33}$	.649154*	**2.07666**	.0535648	8.10839	**14.5848**	
A_{55}	.455071	.412029	.406801	.364028	.387669	101.485
A_{65}	1.07255	1.92052	2.97085	4.34011	8.83560	
$A_{66} = A_{65}^2/A_{55}$	3.31497@	8.95179	21.6960	51.7448	201.378	

*Using: $_1A_{jj} = {}_1A_{ij}^2/({}_1A_{ii} - 1/m)$ for i odd and j = i + 1
where, 1/m = .1 OS050 kg^{-1}

@ $_1A_{66}$ = **3.31497 is in** error because of the anomalous low frequency response of Y_{65} already commented upoo in Table 7.4(a).
In (b) below $_1A_{22} = {}_1A_{44} = {}_1A_{66} = (.599764 + .649154)/2 = .624459$

(b) Residual Stiffnesses

$$K_{ri} = \omega_6^2/{}_6A_{ii} = (2\pi \times 10000)^2/{}_6A_{ii}$$

K_{rl1} = 633.168 x 105 ; K_{rl3} = 516.543 x 10^5 ; K_{rl5} = **389.007 x** 10^5

(c) Separation of Rigid Body Modes

$_1A_{11T}$ =.108050	$_1A_{11R}$ = .432683 - .108050 = .324633
$_1A_{22T}$ = 0	$_1A_{22R}$ = .624459
$_1A_{33T}$ =. 108050	$_1A_{33R}$ = .169495 - .108050 = .461445
$_1A_{44T}$ = 0	$_1A_{44R}$ = .624459
$_1A_{55T}$ =. 108050	$_1A_{55R}$ = .455071 - .108050 = .347021
$_1A_{66T}$ = 0	$_1A_{66R}$ = .624459

Using: $_1A_{iiT}$ = 1/m for i odd
= 0 for i even
and : $_1A_{iiR} = {}_1A_{ii} - {}_1A_{iiT}$ for all i

Table 7.11 continued

(d) Matrix of Point Modal Constants

Frequency (Hz)	O (T)	O (R)	80	219	420	655
A_{11}	.108050	.324633	.390762	.365629	.284437	.229058
A_{22}	0	.624459	**4.35548**	**13.5248**	**39.3182**	**83.9950**
A_{33}	.108050	.061445	.0303925	.184489	.0507017	.0320674
A_{44}	0	.624459	2.07666	.0535648	**8.10639**	**14.5848**
A_{55}	.108050	.347021	.412029	.406801	.364028	.387669
A_{66}	0	.614459	**8.95179**	**21.6960**	**51.7448**	**201.376**

(e) Mode Shape Matrix

Frequency (Hz)	O (T)	O (R)	80	219	420	655
$\sqrt{A_{11}}$	+.328710	+.569766	+.625110	+.604673	+.533326	+.478600
$\sqrt{A_{22}}$	+ 0	-.790227	-2.08698	-3.67761	**-6.27042**	**-9.16488**
$\sqrt{A_{33}}$	+.328710	+.247881	-.174334	-.429522	-.225170	+.179074
$\sqrt{A_{44}}$	+ 0	-.790227	-1 .44106	-.231441	+2.84752	13.81901
$\sqrt{A_{55}}$	+.328710	-.589085	+.641895	-.637810	+.603347	-.622631
$\sqrt{A_{66}}$	+ 0	-.790227	+2.99195	-4.65790	+7.19339	-14.1908

Signs as in Table 7.4(a)

Table 7.12 Spatial Models of Long Beam

Output of program EMKAY with input data from Table 7.11(e)

(a) Matrices for Long Beam with Blocks

$$[M_{LBR}] = \begin{bmatrix} 17.4567 & 3.53401 & -10.8825 & 4.72573 & 3.25114 & -.649997 \\ & .744403 & -2.35505 & 1.00330 & .693001 & -.139267 \\ & & 9.91375 & -3.15513 & -2.45306 & .489490 \\ & & & 1.40910 & .839911 & -.174690 \\ & & & & 2.05329 & -.236663 \\ \text{Symmetric} & & & & & .0388722 \end{bmatrix}$$

$$\Sigma M_{trans} = 9.2549 \text{ kg}$$

$$[K_{LBR}] = 10^5 \begin{bmatrix} 186.627 & 38.8150 & -178.343 & 45.5929 & -8.28462 & .386041 \\ & 8.41497 & -37.1813 & 9.09710 & -1.63368 & .0288314 \\ & & 172.253 & -42.2925 & 6.08957 & .379347 \\ & & & 12.4297 & -3.30040 & .540303 \\ & & & & 2.19505 & -.765388 \\ \text{Symmetric} & & & & & .398771 \end{bmatrix}$$

$$\Sigma K_{trans} = 10^5(-1.05 \times 10^{-3}) \approx 0$$

(b) Matrices for Long Beam without Blocks

$$[M_{LR}] = [M_{LBR}] - [I_L] \qquad \text{(see Table 7.5 (b))}$$

$$[M_{LR}] = \begin{bmatrix} 17.2747 & 3.53401 & -10.8525 & 4.72573 & 3.25114 & -.649997 \\ & .743903 & -2.35505 & 1.00330 & .693001 & -.139267 \\ & & 9.73175 & -3.15513 & -2.45306 & .489490 \\ & & & 1.40860 & .839911 & -.174690 \\ & & & & 1.90229 & -.236663 \\ & & & & & .0385332 \end{bmatrix}$$

$$\Sigma M_{trans} = 8.7399 \text{ kg}$$

$$[K_{LR}] = [K_{LBR}] \text{ in (a above}$$

(c) Residual Stiffness Matrix

From Table 7.11 (b)

$$[K_{rl}] = 10^5 \begin{bmatrix} 633.168 & & & & & \\ & 0 & & & & \\ & & 516.343 & & & \\ & & & 0 & & \\ & & & & 389.007 & \\ & & & & & 0 \end{bmatrix}$$

Table 7.13 SMR Modal Properties of the Long Beam Predicted from Spatial Models

(a) Long Beam with Blocks

Program EIGEN with input $\left[M_{LBR}\right]$, $\left[K_{LBR}\right]$ of Table 7.12(a)

Natural Frequencies .188 .881 80 219 420 655

Mode Shape Matrix

-.104	.650	.625	-.605	-.533	-.479
.498	-.614	-2.09	3.68	6.27	9.16
.099	.400	-.174	.430	.225	-.179
.498	-.614	-1.44	.231	-2.85	-3.82
.626	-.250	.642	.638	-.603	.623
.498	-.613	2.99	4.66	-7.19	1.42

(compare with Table 7.11(d))

(b) Long Beam without Blocks

Program EIGEN with input $\left[M_{LR}\right]$, $\left[K_{LR}\right]$ of Table 7.12(b)

Natural Frequencies .191 .936 86.66 242.6 465.1 767.6

Mode Shape Matrix

-.108	.694	.694	-.732	-.761	-.775
.515	-.669	-2.21	3.92	7.62	11.43
.122	.422	-.163	.457	.275	-.168
.515	-.669	-1.57	.520	-2.93	-4.18
.648	-.286	.714	.759	-.779	1.03
.518	-.669	3.20	4.88	-8.13	18.2

(compare with Table 7.6(c))

Table 7.14 SMR Spatial Model of Coupled Beam

(a) Coordinates

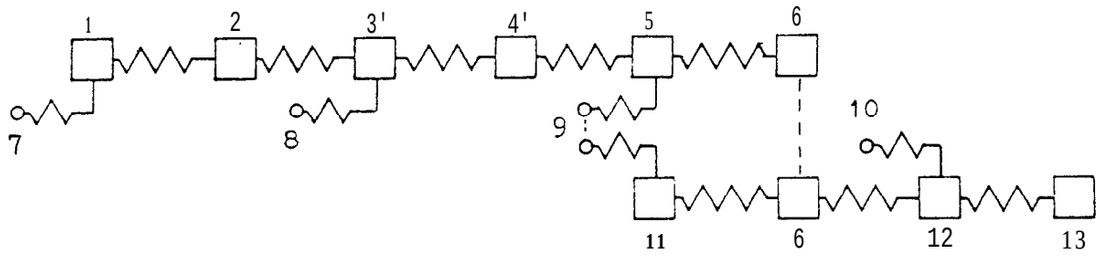

Tip Coordinates 7,2 Junction Coordinates 9,6

(b) Subsystem 1 Long Beam

$$[M_1] = \begin{bmatrix} M_{LR} & 0 \\ 6x6 & 6x3 \\ 0 & 0 \\ 3x6 & 3x3 \end{bmatrix}, \quad [K_1] = \begin{bmatrix} K_{LR}+K_{rl} & -K_{rl} \\ 6x6 & 6x3 \\ -K_{rl} & K_{rl} \\ 3x6 & 3x3 \end{bmatrix}$$

submatrices from Table 7.12

(c) Subsystem 2 Short Beam

$$[M_2] = \begin{bmatrix} 0 & 0 \\ 2x2 & 2x4 \\ 0 & M_{SR} \\ 4x2 & 4x4 \end{bmatrix}, \quad [K_2] = \begin{bmatrix} K_{rs} & -K_{rs} \\ 2x2 & 2x4 \\ -K_{rs} & K_{SR}+K_{rs} \\ 4x2 & 4x4 \end{bmatrix}$$

submatrices from Table 7.9

coordinate sequence 9, 10, 11, 6, 12, 13

(d) Predicted Resonance Frequencies Hz (Error %)

j0.82 0.06 32.58 105.4 210.9 350. [illegible] 522.6 740.8

(-23) (-4.7) (-2.7) (-2.;') (-2.3) (-0.8)

plus 2172 (anomalous) , output by program EIGEN

(e) Reduced Spatial Model for EIGEN Calculation

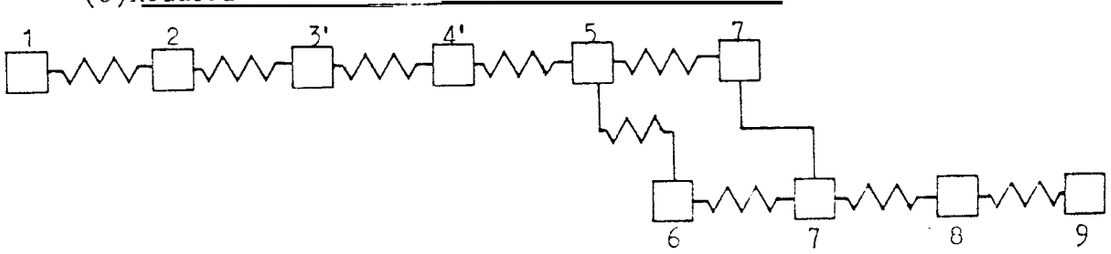

7.2 Modal Models of a Turbine Blade

7.2.1 Introduction

Following on the successful modelling of the simple structures of section 7.1 it was decided to apply the measuring and modelling techniques developed in the earlier chapters to a much more complicated test piece.

Much attention has been paid [93][94][95][96] to the behaviour of bladed discs which are tte dominant vibratory components of turbines. Aturbine blade is a challenging test component since it is very lightly damped (typical loss facto? 0.0001) and has a complex asymmetrical shape which makes analytical prediction of vibration behaviour very difficult. The objectives of the tests reported here were the measurement of translational and rotational properties of a freely supported blade, and subsequent construction of a partial modal model which could Se used to predict the effect of coupling the blade root tc ground, the first step being the estimation of cantilever frequencies. The blade used for testing is specified in Figure 7.14. Measurements and predictions were made wit'_ respect tc the 'fir-tree' mot and the coordinate system end matrices used are specified in Figure 7.15.

It is realised that the axes in Figure 7.15 are not principal axes of the blade, since that has about 30^0 of twist. Accordingly, a restriction of the analysis to only two dimensions at a time gives a relatively poor approximation to the blade properties which require three dimensions for adequate description. Nevertheless, it was thought worthwhile to evaluate the predictive powers of the experimental and theoretical techniques of this thesis when taken to the limit represented by such a complex component. It was decided to estimate the cantilever frequencies of the blade based on data measured for the free-free condition and check those frequencies by direct measurement.

7.2.2 Prediction of Cantilever Frequencies from Free-Free Measurements

Consider the NxN matrix of mobility terms relating to the coordinates of a free-free body which are to be grounded.

The relationship may be expressed:

$$\{\dot{X}\}_{Nx1} = [Y]_{NxN} \{F\}_{Nx1} \tag{7.1}$$

When the coordinates are grounded then the equation becomes:

$$[Y]\{F\} = \{0\} \tag{7.2}$$

This equation has a solution when $[Y]$ is singular, which implies:

$$|Y| = 0 \tag{7.3}$$

Each element of $[Y]$ is frequency dependent and solutions of equation (7.3) will be found at cantilever frequencies at which the velocities $\{\dot{X}\}$ are zero but the forces $\{F\}$ are not.

Let us take, for example, the ubiquitous Long Beam. Free-free data relating to its tip coordinates X, θ can be expressed In the form of a mobility matrix:

$$[Y] = \begin{bmatrix} Y_{11} & Y_{12} \\ Y_{21} & Y_{22} \end{bmatrix} = \begin{bmatrix} (\dot{X}/F) & (\dot{X}/M) \\ (\dot{\theta}/F) & (\dot{\theta}/M) \end{bmatrix} \tag{7.4}$$

Theoretical date, generated by *using* program COUPLD1, was used to calculate the determinant $|Y|$ for a range of frequencies:

$$|Y| = Y_{11} Y_{22} - Y_{12} Y_{21} \tag{7.5}$$

The numerical value of $|Y|$ has an extremely wide range so in Figure 7.16(a) it is expressed in logarithmic form as decibels v. logarithmic frequency. The first zero of this function is clearly located at 13.5 Hz, the first cantilever frequency. The second zero occurs at 84.6 Hz, closely followed by the first pole - which corresponds to the resonance at 85.9 Hz. Thereafter zeroes and poles are very nearly in coincidence, causing very little deformation of the general horizontal trend of the curve. A frequency sweep is thus very likely to miss any pole or zero other than the first unless the increments are very small. Plainly, the determinant is a function ill-conditioned for frequency

search purposes. A related function which has the same zeroes as the determinant is the Norm of the determinant as defined in the Appendix A5. In this example:

$$\text{Norm}\,|Y| = \frac{Y_{11}Y_{22} - Y_{12}Y_{21}}{(\sqrt{Y_{11}^2 + Y_{12}^2})(\sqrt{Y_{21}^2 + Y_{22}^2})} \qquad (7.6)$$

where $$-1 \leqslant \text{Norm}\,|Y| \leqslant +1 \qquad (7.7)$$

The norm so defined is a function with a maximum magnitude Of unity. It is plotted in Figure 7.16(b) for the Long Beam acd it can be seen to vary smoothly without discontinuity and in addition to indicating by its zeroes the cantilever and resonance frequencies of the beam, reveals antiresonances of various elements of the mobility matrix at those frequencies when it attains the value -1 . Clearly it is a function more suited to frequency searches than is the unmodified determinant $|Y|$.

7.2.3 Free-Free Measurements

Determination of the complete mobility matrix feature in Figure 7.15 can be done by using the techniques of Chapter 5 in several stages, measuring at each stage translation along one axis and rotation about another. Block Mark 7 was designed for the purpose and was made in two parts, as shown in Figure 5.7 and described in section 5.2.1. Block 7B could be attached to the blade root by using adhesive and subsequently Block 7A could be fixed to Block 7B in the appropriate attitude. The range of possible configurations is shown in Figure 7.17. It can be seen that the most significant mobility terms can be found by using configurations B2 and A1.

Tests using Two B & K Accelerometers

Tests were made using the two accelerometer method of obtaining rotational mobilities specified in section 5.2.2. The Solartron 1170 equipment was used and the physical arrangerents are shown in Figure 7.18(a). Since the 1170 has only two inputs, one of which is reserved in this application for the force gauge, two runs had to be made, one with the accelerometer in location 1 (+0.025 m) connected electrically, and the other with the lower accelerometer in location 2 (-0.025 m) corinected. There was no mechanical adjustment made between the two runs. The first two runs were made with Blocks in configuration B2. In this configuration the system centroid was found by simple balancing to be 0.01 m fro;! the origin at the centre of the 'fir-tree' root. The Blocks were then removed from the blade and reassembled in configuration A1, in which Block 72 had to be displaced fror the central axis of the blade in order for Block 7A to be attached without touching the blade.

Results - Configuration B2

The measured data plotted as dots in Figure 7.18 were obtained in a logarithmic 101-point sweep from 20C to 2000 Hz. Subsecuectly, close linear sweeps were made in order to establish accurately the frequencies cf resonance and antiresonance which were used 2s input data for curve-fitting using program IDENT. The smooth curves of Figure 7.18 show the results of 2 direct identification of five nodes including the rigid body mode 2nd the corresponding modal constants are listed in Table 7.16. Curves arising froa identification by the 'window' method are shown in Figure 7.19 and a high frequency residual node was added in a direct calculation tc get the curves of Figure 7.20. In each case, the response data used in identification is marked by arrows. It should be noted that the transfer characteristic, particularly noticeable in the

response of the lower accelerometer between 377 and 792 Hz and between 949 2nd 1486 Hz, is successfully modelled.

The three curve fits differ in minor ways. The five-mode curve of Figure 7.19 lies just below the data points between resonances but fits closely in the frequency range around 1400 Hz. In contrast, the 'window' curve of Figure 7.20 fits significantly less well in this range but is a little more accurate in off-resonance regions below 800 Hz. As might be expected the six-mode curve including a residual (Figure 7.21) has a superior fit at high frequency. However, since the low frequency response is of the greater interest 2nd since the residual terms cannot be useo in derivation the data selected for *further* processing *using* program INCAN were those of the direct five-node calculation of Figure 7.19.

Program INCAN has a two-fold purpose, first tc provide, frequency by frequency, the matrix of point and cross mobility terms fcr the designated point on the blade root, the inertia of the blocks and 2cceleroneters having been cancelled; and second, the norm of the determinant of this matrix. The norm has a value of zero et 2 predicted cantilever frequency. INCAN converts a partial nod21 model into an approximate mobility model.

The plot of the different mobility parameters 2s a function of frequency is shown 2s Figure 7.22 in which resonances occur at 357, 731 and 887 Hz. The parameter $(\dot{Y}/F_Y)$ is predominantly a mass line showing rigid body behaviour cost s trongly whereas the rotational mobility $(\dot{e}_x/F_y)$ has a trend which rises with frequency indicating large influence of high frequency modes.

The plot of the norm as a function of frequency is shown as Figure 7.23 which reveals no violent discontinuities. The curve crosses the zero line from below at 357, 731 2nd 887 Ez which have been established as resonance frequencies. The zero line is crossed from above at 111 .0 and 487.5 Hz and these may be taken as predicted cantilever frequencies.

Results - Configuration X1

The test procedure in this case was very similar to that for B2, above. The experimental connections are shown in Figure 7.18(b). A logarithmic frequency sweep was used as before to provide the plotted data points and then resonances and antiresonances determined by close linear sweeps. The measured data are presented as dots in Figures 7.24, 7.25 and 7.26 in which it can be seen that the rigid body modes are dominant. This observation is consistent with the expectation that the blade would be stiffer about the Y axis than it is about the X axis, since it has a larger section in X than in Y direction.

The results of a five mode IDENT curve fit are shown as smooth lines in Figure 7.24 and the corresponding modal constants are in Table 7.15. The response data points used for identification are marked by arrows and, save for the first point at 200 Hz, all coincide with anti-resonances. Mismatch between the raw data and the regenerated curves is apparent in off-resonance regions. The overall levels of these curves depend on the response data points which are not antiresonances. Thus the responses at 200 Hz are evidently not typical, since they do not lie on smooth curves which pass through most data points.

The 'window identification curves shown in Figure 7.25 do not suffer from the off-resonance discrepancy. Neither do the six mode identifications including a residual mode which are presented as Figure 7.26. However, since both of these identifications give problems of consistency, further calculations were done, as before, using the mode constants obtained in the direct five mode identification.

The frequency response of the mobility matrix of the blade without exciting blocks is shown in Figure 7.27 in which a minimum rather than an antiresonance occurs between the resonances at 396 and 778 Hz for the cross responses $(\dot{e}_y/F_x)$ and $(\dot{X}/F_y)$. The norm of this matrix is plotted over the same frequency range in Figure 7.28. The scatter of points around 800 Hz arose from singularity of the mobility matrix.

Cantilever frequencies are indicated at 112.2 and 402 Hz. The lower of these is remarkably close to the 111.0 Hz predicted from B2 measurements.

Review of 81 Results

The dominance of the rigid body modes is shown in the measured data of Figure 7.2-L and in the corresponding nod21 constents of Table 7.16. The modal constants of the nobility matrix of the blade/block combination are found by use of equations (5.2).

$$ {}_rA_{xx} = ({}_rA_1 + {}_rA_2)/2 $$
$$ {}_rA_{ex} = ({}_rA_1 - {}_rA_2)/2.EE $$
$$ {}_rA_{ee} = {}_rA_{ex}^2/{}_rA_{xx} $$

and for the rigid body node:

$$ {}_1A_{ee} = {}_1A_{ex}/EX \qquad \text{(i)} $$

or
$$ {}_1A'_{ee} = {}_1A_{ex}^2/({}_1A_{xx} - 1/m) \qquad \text{(ii)} $$

The rotational modal constants, being dependent on the difference between the nodal constants of runs1 and 2, are very sensitive to small errors in those constants. It was seen in the previous section that the level of rhe fitted curve depended on the non-antiresonance low frequency response point selected. A check on this sensitivity was made by calculating the cantilever frequencies predicted by INCAN for the sets of data contributing to Figures 7.24 7.25 and 7.26. The effect of substituting ${}_1A'_{ee}$ derived according to equation (ii) was also found.

The results are summarised in Table 7.17. The cantilever frequencies predicted have a very wide range and thus indicate that the calculations are ill-conditioned. The calculations of rows 3 2nd 5 may be compared. There 2re differences of -0.16% in ${}_1A_1$ 2nd 0.58% in ${}_1A_2$ which lead ultimately to 31% shift in estimated cantilever frequency.

The discrepancy between the values of ${}_1A_{ee}$ and ${}_1A'_{ee}$ calculated by different methods is also marked. This discrepancy is least in the case of rows 1 and 2 and accordingly, giving greatest weight to these data, a frequency of about 113 Hz remains the best estimate of the first cantilever frequency.

Conclusions - Tests on Freely Supported Blade

1. Measurements using the two-accelerometer method were successful in that they gave snooth data and consistent resonance frequencies.

2. Identification curve-fitting by direct and window methods was successful as was the inclusion of a residual high frequency mode.

3. The output of program INCAN indicated in the nobility responses of Figures 7.22 and 7.27 was plausible in that it showed the point translational terms dominated by rigid body (low frequency) modes and the point rotational terms, in contrast, dominated by high frequency modes. There were no data available for direct checking.

4. The plots of the norms of the mobility matrices were in each case smooth curves capable of interpretation.

5. The important difference between the signals output by accelerometers 1 and 2 was not sufficiently clearly established. Some part of the difficulty should be attributed to the necessity, when using the 1170 equipment, of gathering data in separate runs.

6. The best estimate of the first cantilever frequency is 113 Hz

7. The innovation of a two-part exciting block proved to be convenient and the data obtained gave no indication of lack of rigidity of the junction.

7.2.4 Cantilever Measurements

Direct measurements of the blade clamped to ground at its root were required as a check on the predictions of section 7.2.3. The connection to ground was simulated by mounting the blade in a suitable holder and then clamping that holder within a massive block which itself rested on the laboratory floor. In all cases the vibration of the blade was detected by means of a very small accelerometer (B & K Type 8303 - mass 3.5 gm) fixed to the blade tip. A variety of methods of clamping and excitation were investigated.

Tests with Tin Excitation

Conventional mobility tests were carried out, using a small shaker mounted on a retort stand. The output of the shaker was coupled via force gauge and push rod to the blade tip near the accelerometer. The experimental set-up is sketched in Figure 7.29(a).

(i) Root Held in Machined Block

The first tests were carried out using a steel block machined to accommodate the fir tree root. Data were acquired using the 1170 equipment and Figure 7.30 shows the variation of tip nobility, after mass cancellation, with frequency. The first three indicated *cantilever* frequencies are 128.9, 315.5 and 363.5 Hz. There appears to be a minor resonance around 230 Hz, and a scatter of points between 600 and 1000 Hz.

(iij Root Held In Zest Lead Block

Itwas surmised that the effective length of the free blade must have been shorter than that in the test just reported because, when assembled on to a disc, the blade would contact its neighbours at the tapered shoulder rather than at the root. Accordingly, a test -was devised in which this shoulder was clamped. A tapered lead block was cast and the blade was assembled into the massive block with its shoulders effectively clamped. The results of a mobility measurement are shown as Figure 7.31 which has cantilever frequencies indicated as 131, 310 end 380.5 iiz. The response between 200 and 50C Ez is quite different from that of Figure 7.30 and there is ccasiderable scatter above 700 Ez.

(iii) Root Held in Block 7B

If comparison with quoted data was not possible it was sensible to make measurements with the blade in a condition as near similar to that of the free-free tests. Block 7B was reconnected to the root in a central position and this 30 mm cube clamped within the large block. Test results are shown as Figure 7.32. The dominant first resonance is at 123.8 Ez and the next two occur at 259 and 306 Ez.

(iv) Summary

The measurements made with tip excitation show that the method of clamping has a considerable influence on the mobility of the blade and in particular its behaviour at high frequencies, The first cantilever frequency is consistently obtained in the range between 122 and 132 Ez which is above the predicted value of about 113 Ez of the free-free tests.

Tests with Root Excitation

The use of a short push rod in the tip excitation tests above tight have been a constraint which affected response. Transfer measurements in which the blade was excited at the root and response measured at the tip would remove this source of error. The blade held in Block 7B was clamped at the centre of the large block which itself was supported on rubber pads. A shaker was suspended above the large block and connected so that vertical notion was induced. The transfer nobility thus found is presented as Figure 7.33. A damped resonance is indicated at 25.8 Hz which, of course, is that of the rigid large block on its rubber mounts. The most significant information is that the next resonance, which is the first cantilever frequency of the blade, is at 130.7 Hz. Subsequent cantilever frequencies are indicated as 316.1 and 568.5 Hz.

Conclusions - Tests on Blade as Cantilever

The method of clamping does have an effect on the measured responses especially at frequencies above the first resonance. The results are summarised in Table 7.16. The first cantilever frequency was found to lie between 123 and 131Hz, somewhat above the value predicted from free-free data.

7.2.5 Discussion and Conclusions

The turbine blade proved to be a difficult test piece and the objectives of this investigation have only been partially net. The data measured in tests on the freely supported blade showed little scatter and the first stage of the mathematical modelling using program IDENT gave reasonable accuracy of fit to the measured data of the curve generated from nodal cocstacts. The fitting proved accurate even for the transfer characteristics. At this stage there was a partial modal model including five resonances related to two responses of the block/blade combination.

Program INCAN used the partial modal model as input to produce an approximate nobility model of the blade without the exciting block. The results were obtained as smooth curves of mobilities and of the norm of the mobility matrix. These were capable of interpretation in revealing predicted resonances 2nd cantilever frequencies. The consistency of the INCAN predictions, however, was shown to be dependent on the differences between the zero frequency modal constants determined in separate runs.

Thus, in conclusion, it can be said that program IDENT is effective in producing acceptable curve fits fror nodal constants but, for the turbine blade, further predictions based on the ideotified date are subject to numerical ill-conditioning.

Figure 7.14 Specification of Turbine Blade

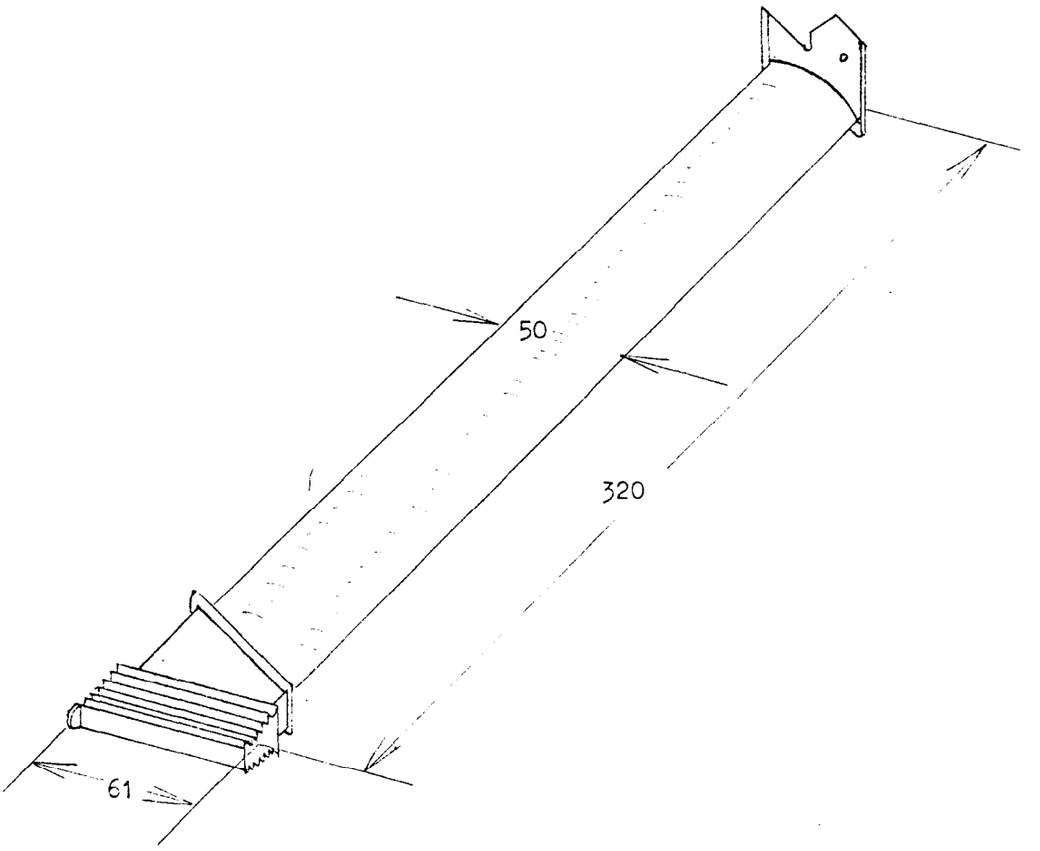

Detail: Full Scale

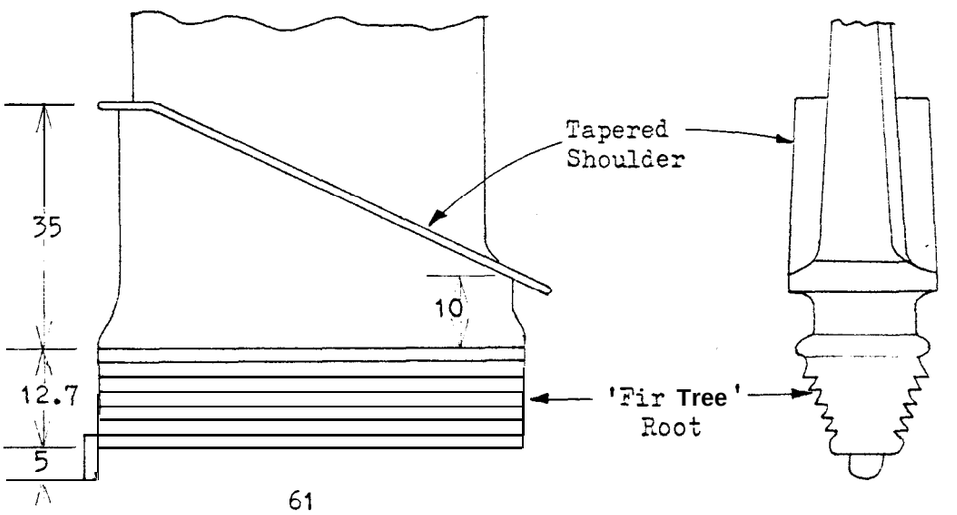

All Dimensions in mm

Figure 7.15 Turbine Blade: Coordinate System for ifobilities

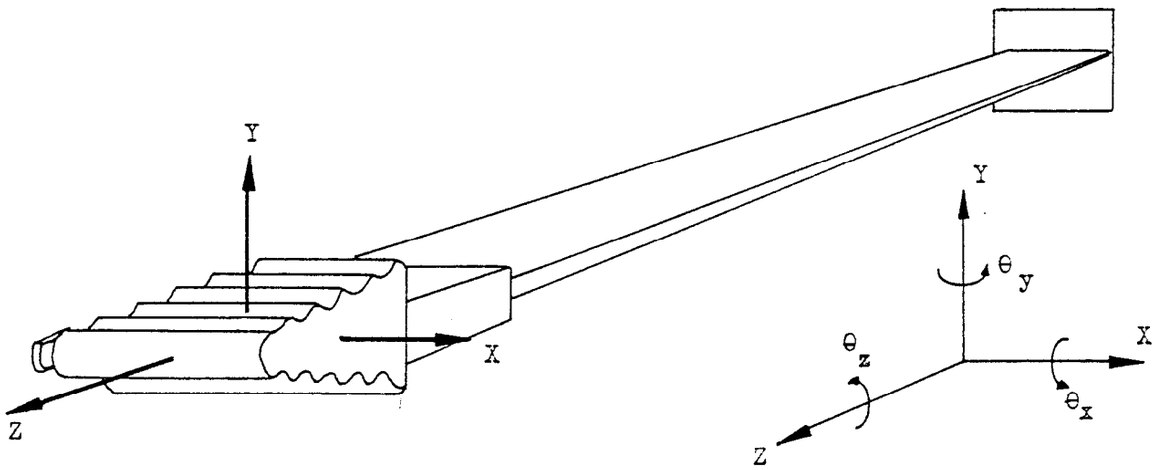

Origin at centre of 'fir-tree'

$$\begin{Bmatrix} \dot{X} \\ \dot{Y} \\ \dot{Z} \\ \dot{\theta}_x \\ \dot{\theta}_y \\ \dot{\theta}_z \end{Bmatrix} = \begin{bmatrix} (\dot{X}/F_x) & (\dot{X}/F_y) & (\dot{X}/F_z) & (\dot{X}/M_x) & (\dot{X}/M_y) & (\dot{X}/M_z) \\ (\dot{Y}/F_x) & (\dot{Y}/F_y) & (\dot{Y}/F_z) & (\dot{Y}/M_x) & (\dot{Y}/M_y) & (\dot{Y}/M_z) \\ (\dot{Z}/F_x) & (\dot{Z}/F_y) & (\dot{Z}/F_z) & (\dot{Z}/M_x) & (\dot{Z}/M_y) & (\dot{Z}/M_z) \\ (\dot{\theta}_x/F_x) & (\dot{\theta}_x/F_y) & (\dot{\theta}_x/F_z) & (\dot{\theta}_x/M_x) & (\dot{\theta}_x/M_y) & (\dot{\theta}_x/M_z) \\ (\dot{\theta}_y/F_x) & (\dot{\theta}_y/F_y) & (\dot{\theta}_y/F_z) & (\dot{\theta}_y/M_x) & (\dot{\theta}_y/M_y) & (\dot{\theta}_y/M_z) \\ (\dot{\theta}_z/F_x) & (\dot{\theta}_z/F_y) & (\dot{\theta}_z/F_z) & (\dot{\theta}_z/M_x) & (\dot{\theta}_z/M_y) & (\dot{\theta}_z/M_z) \end{bmatrix} \begin{Bmatrix} F_x \\ F_y \\ F_z \\ M_x \\ M_y \\ M_z \end{Bmatrix}$$

$$[Y] = \begin{bmatrix} Y_1 & Y_7 & Y_{13} & Y_{19} & Y_{25} & Y_{31} \\ Y_2 & Y_8 & Y_{14} & Y_{20} & Y_{26} & Y_{32} \\ Y_3 & Y_9 & Y_{15} & Y_{21} & Y_{27} & Y_{33} \\ Y_4 & Y_{10} & Y_{16} & Y_{22} & Y_{28} & Y_{34} \\ Y_5 & Y_{11} & Y_{17} & Y_{23} & Y_{29} & Y_{35} \\ Y_6 & Y_{12} & Y_{18} & Y_{24} & Y_{30} & Y_{36} \end{bmatrix}$$

If only the most significant terms are included:

$$\begin{Bmatrix} \dot{X} \\ \dot{Y} \\ \dot{\theta}_x \\ \dot{\theta}_y \end{Bmatrix} = \begin{vmatrix} Y_1 & Y_8^0 & Y_{20}^0 & Y_{25} \\ 0 & Y_8 & Y_{20} & 0 \\ 0 & Y_{10} & Y22 & 0 \\ Y_5 & 0 & 0 & Y_{29} \end{vmatrix} \begin{Bmatrix} F_x \\ F_y \\ M_x \\ M_y \end{Bmatrix}$$

Figure 7.16(a) Alternative Methods of Prediction of Cantilever Frequencies

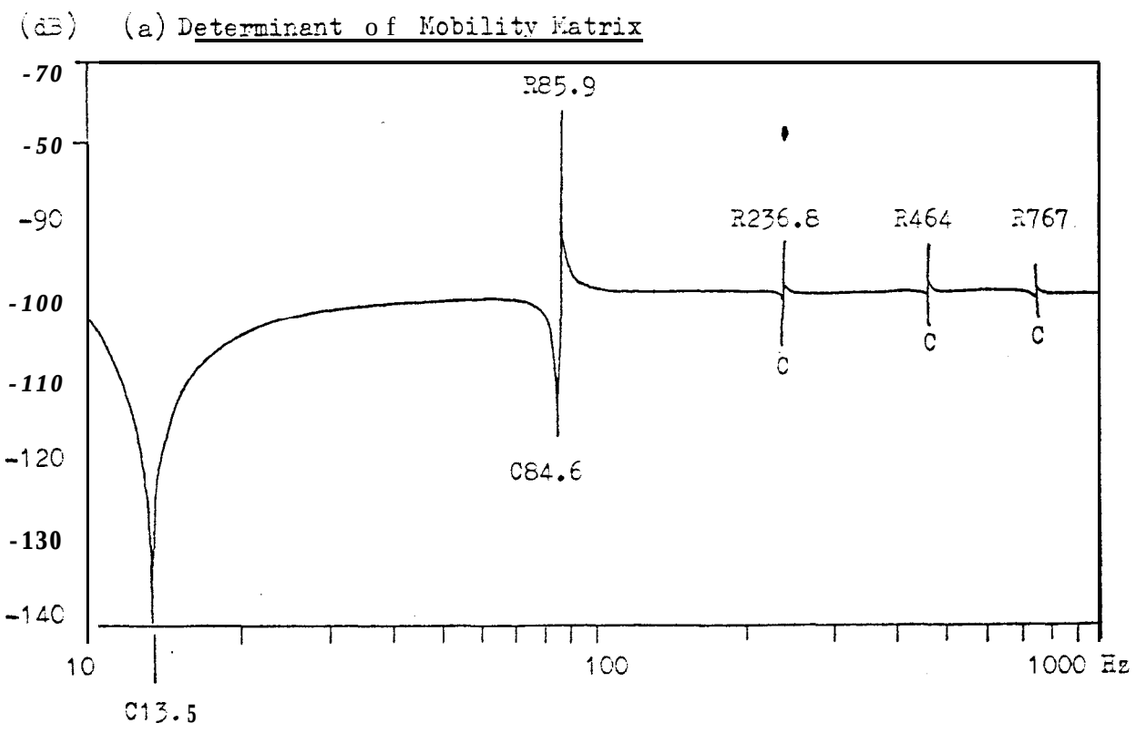

C - Cantilever frequency R - Free-free resonance frequency
AR - Antiresonance frequency

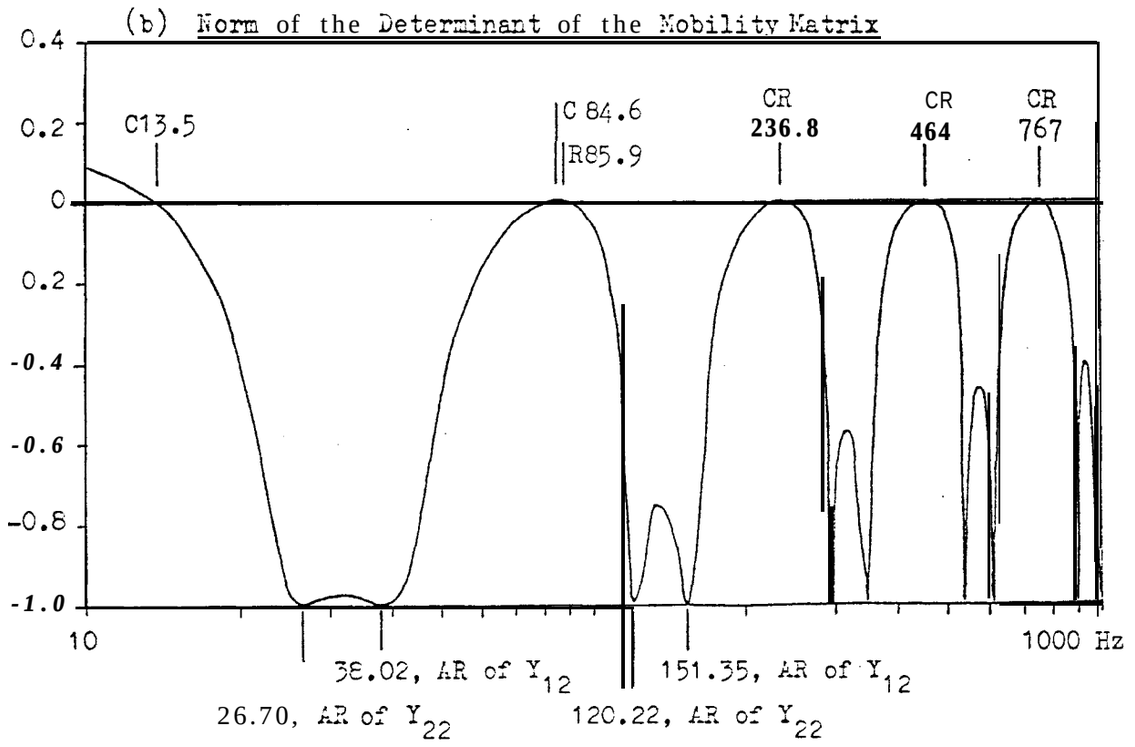

Data for Long Beam

Figure 7.17 Test Configurations

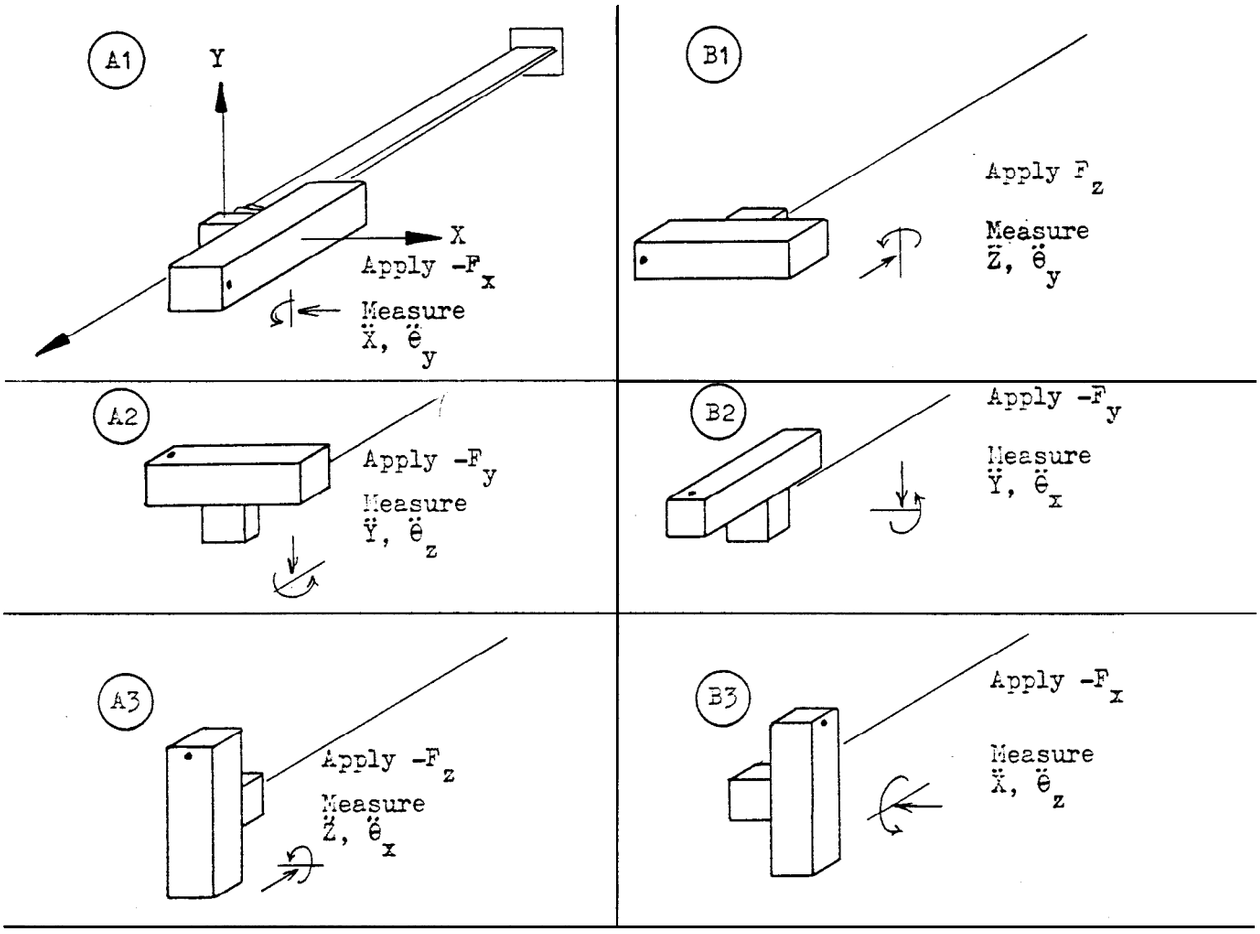

If F_y is input

either A1, X2, A3

or B1, 32, B3 will give all data for second columns of Y

Configuration 32 with Y excitation will give $(\dot{Y}/F_y)$, $(\dot{\theta}_x/F_y)$

i.e. Y_8, Y_{10}

Configuration A1 with X excitation will give $(\dot{X}/F_x)$, $(\dot{\theta}_y/F_x)$

i.e. Y_1, Y_5

Figure 7.18(a) Two Accelerometer Test - Configuration B2

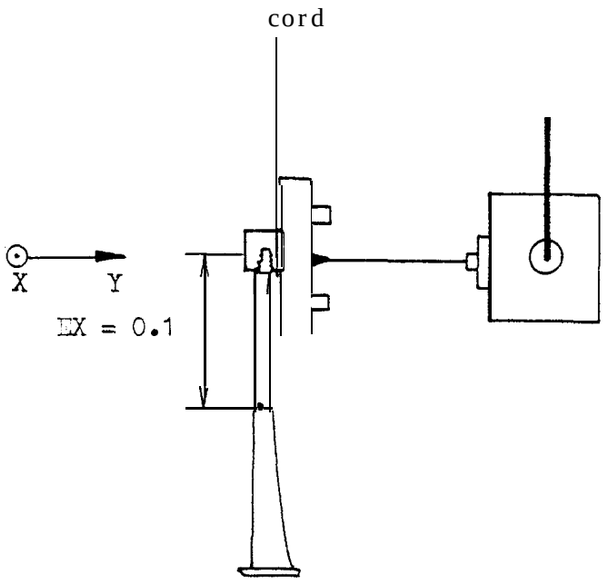

Figure 7.18(b Two-Accelerometer Test - Configuration A1

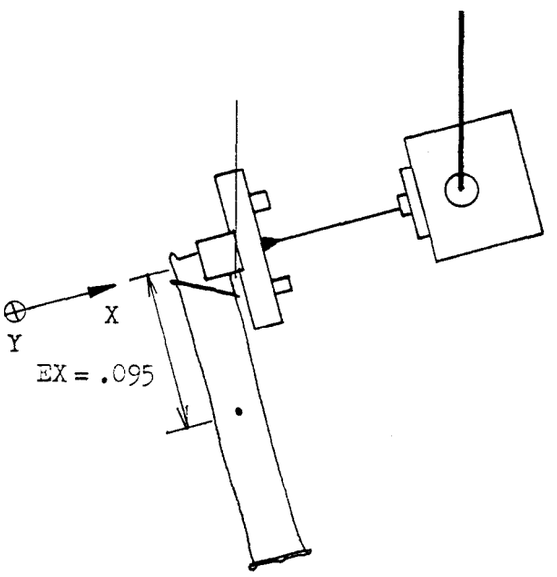

Figure 7.19 Direct Identification of B2 Data - 5 Modes

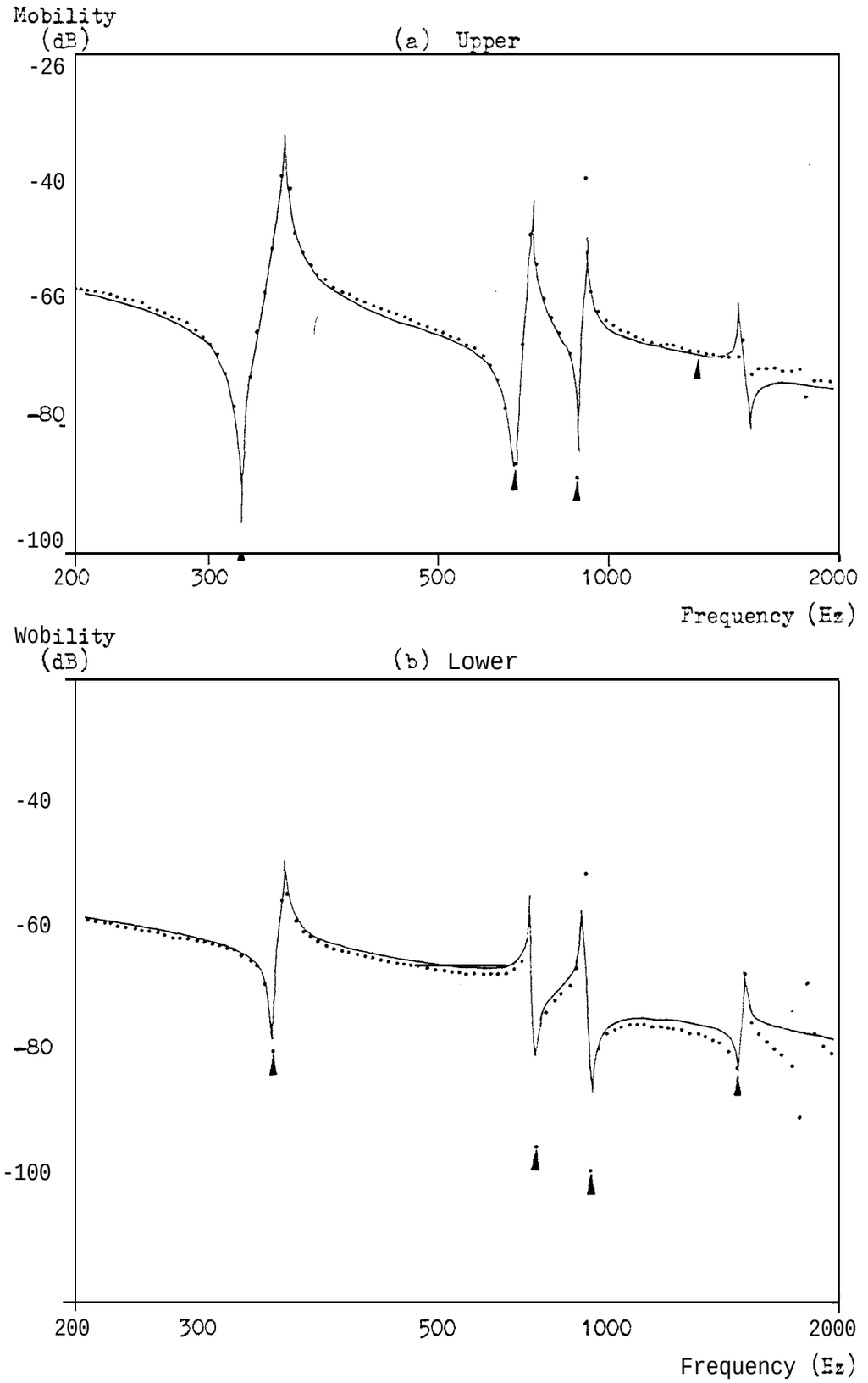

Figure 7.20 'Window' Identification of B2 3ata -5Modes

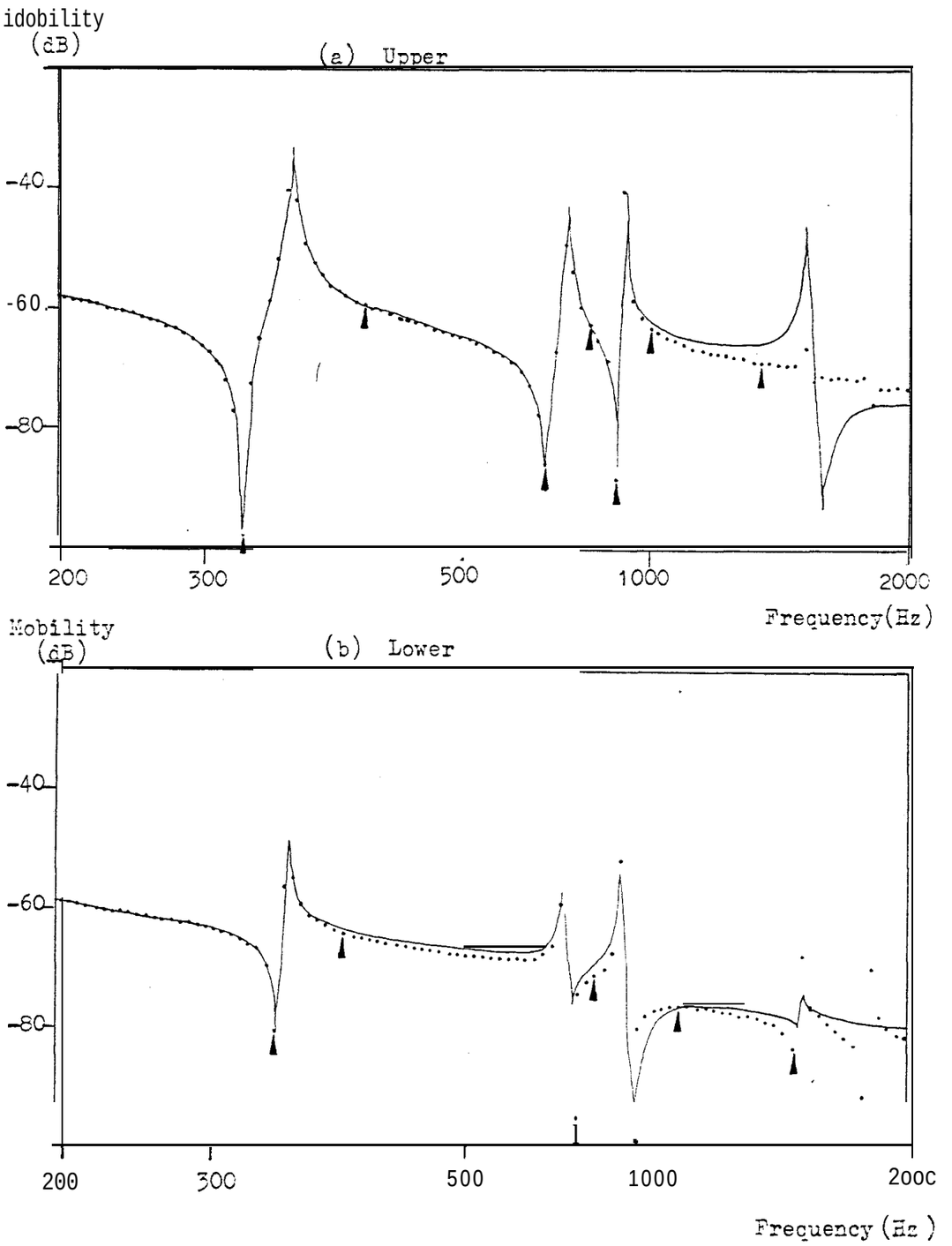

Figure 7.21 Direct Identification of 32 Data - 5 Modes + Residual

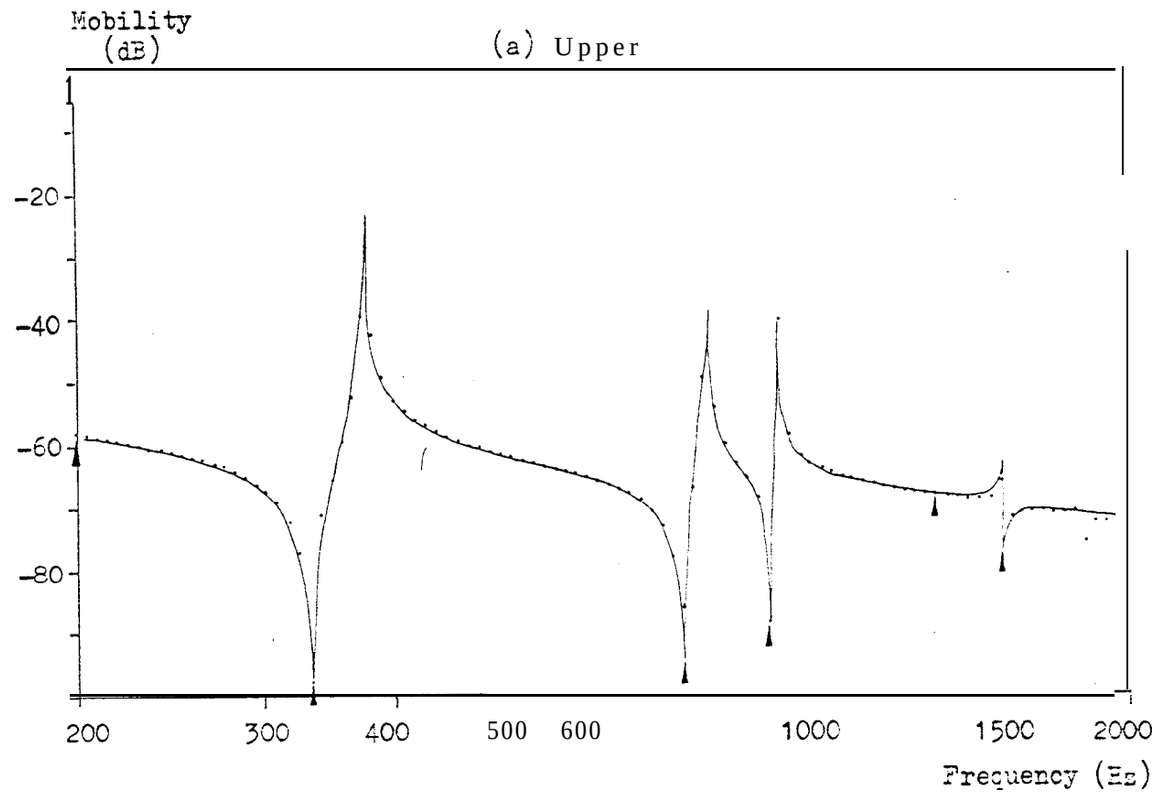

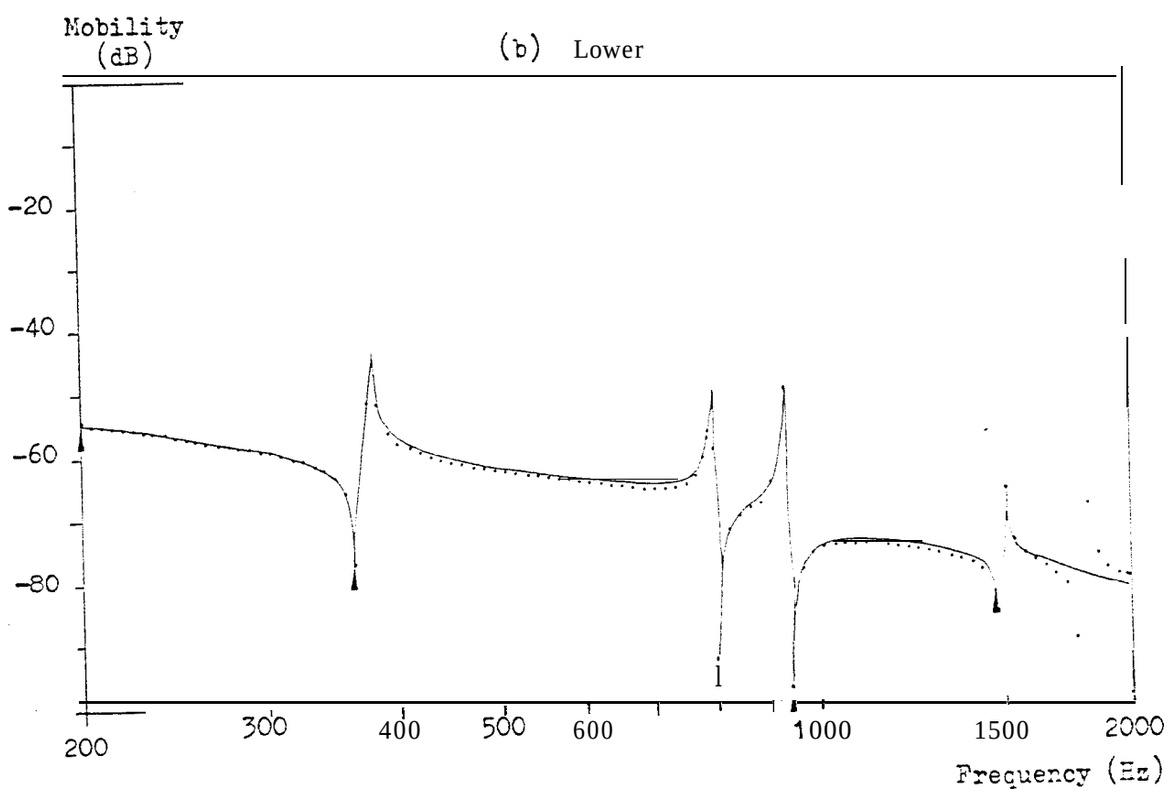

Figure 7.22 B2 Predicted Frequency Responses at Blade Root

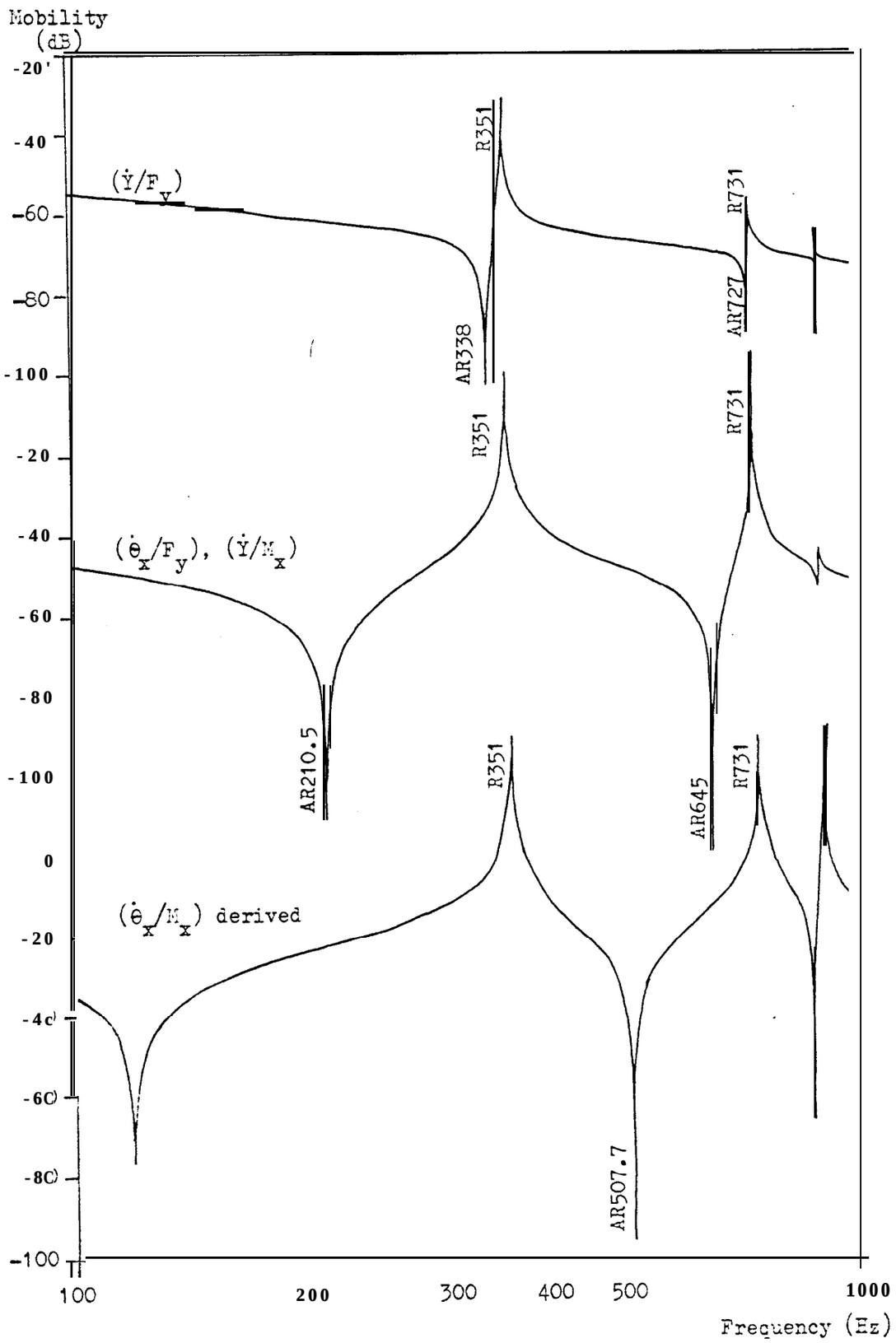

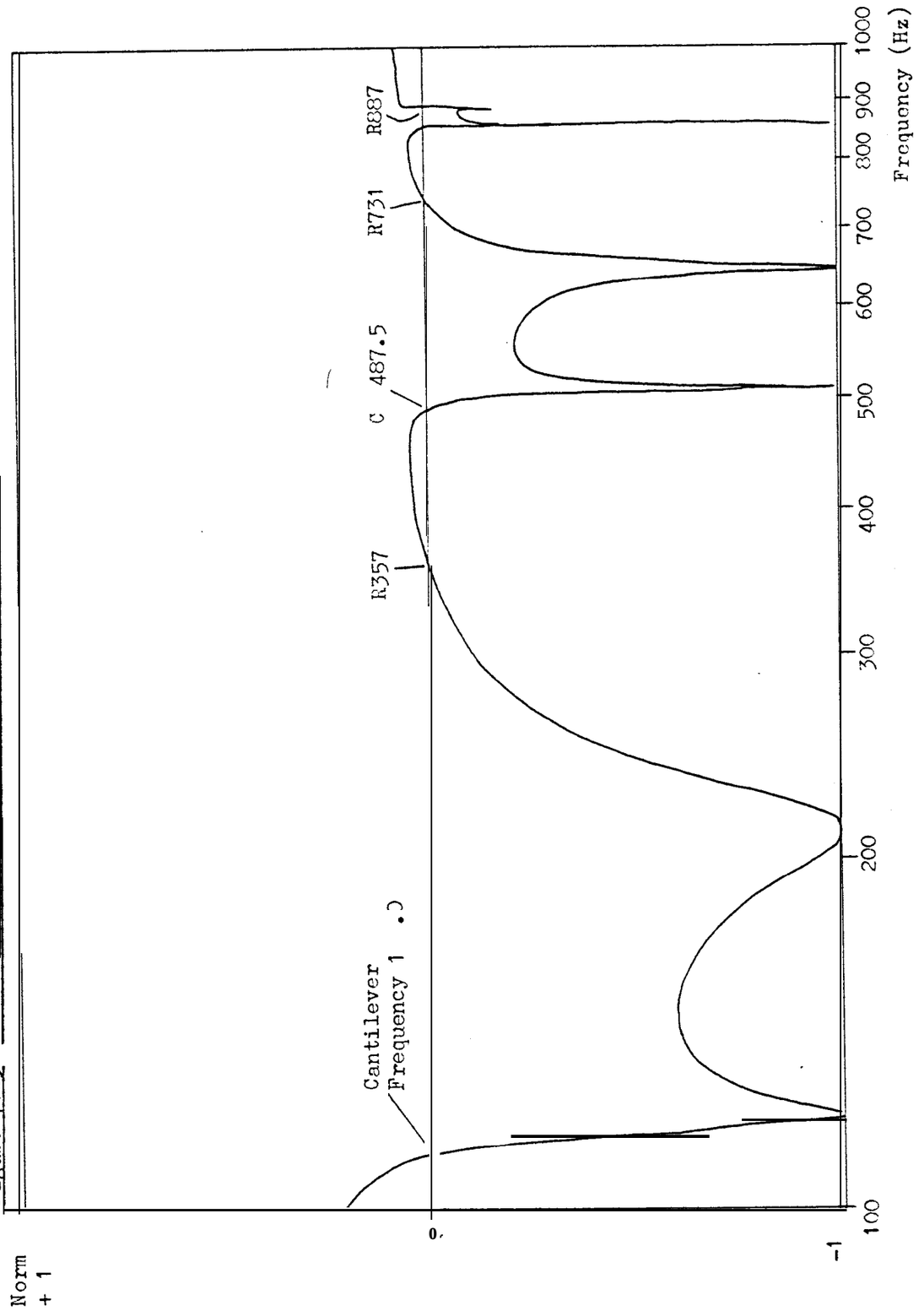

Figure 7.23 The Norm as a Function of Frequency - B2 Data

Figure 7.24 Direct Identification of A1 Data - 5 Modes.

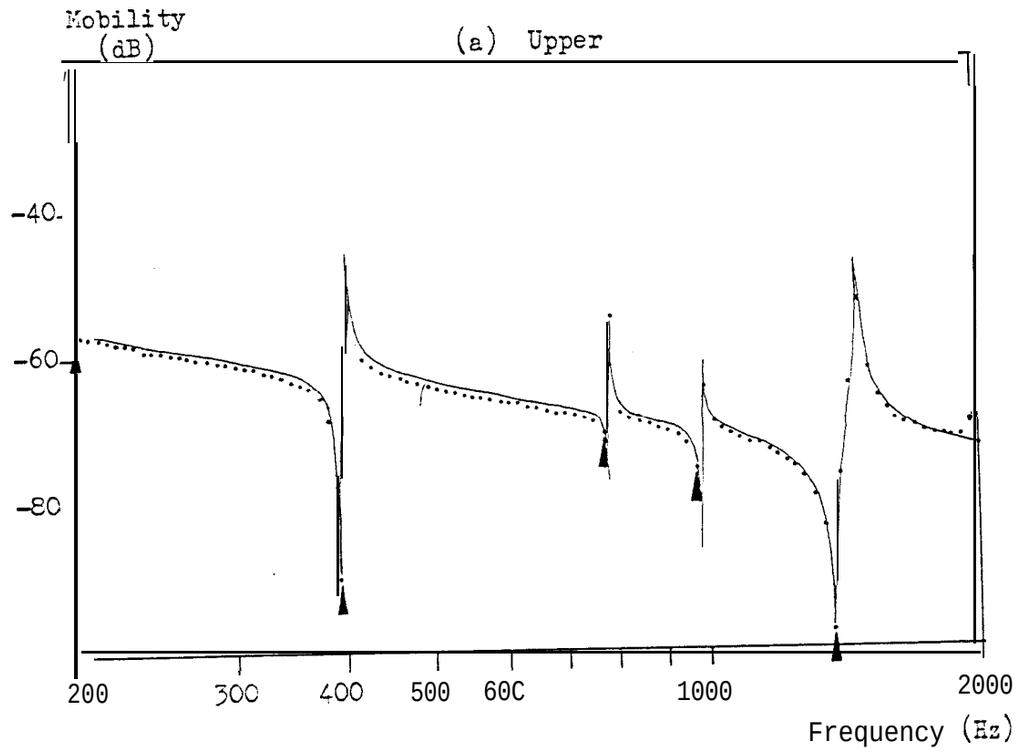

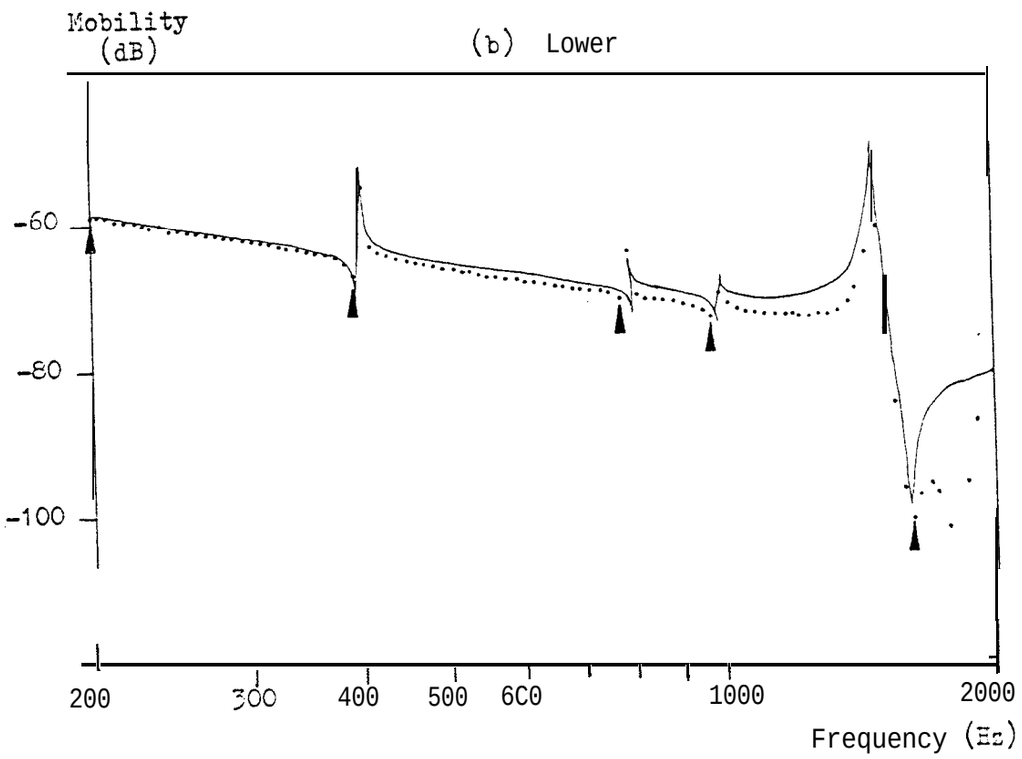

Figure 7.25 'Window' Identification of A1 Data - 5 Modes

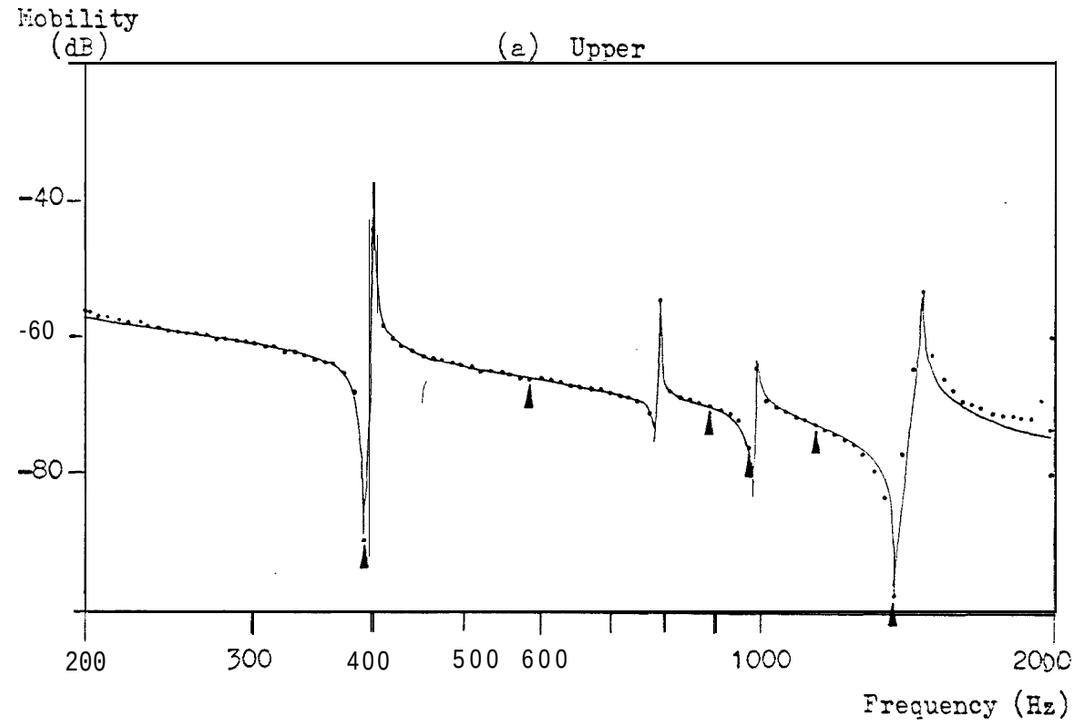

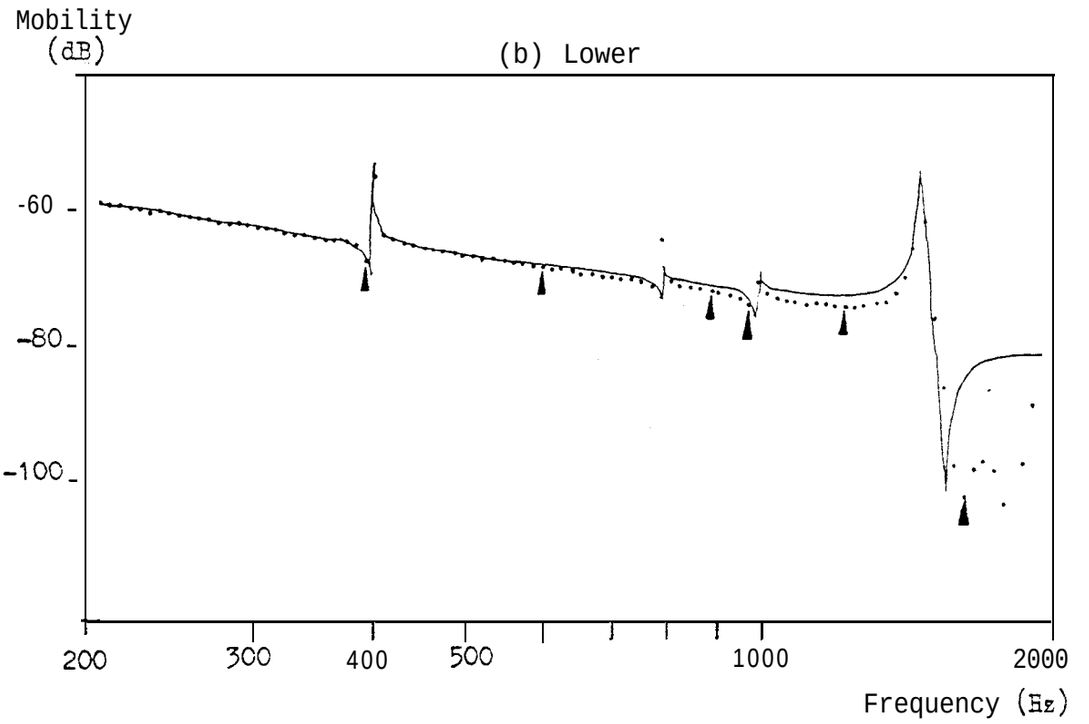

Figure 7.26 Direct Identification of Al Gata - 5 Modes + Residual

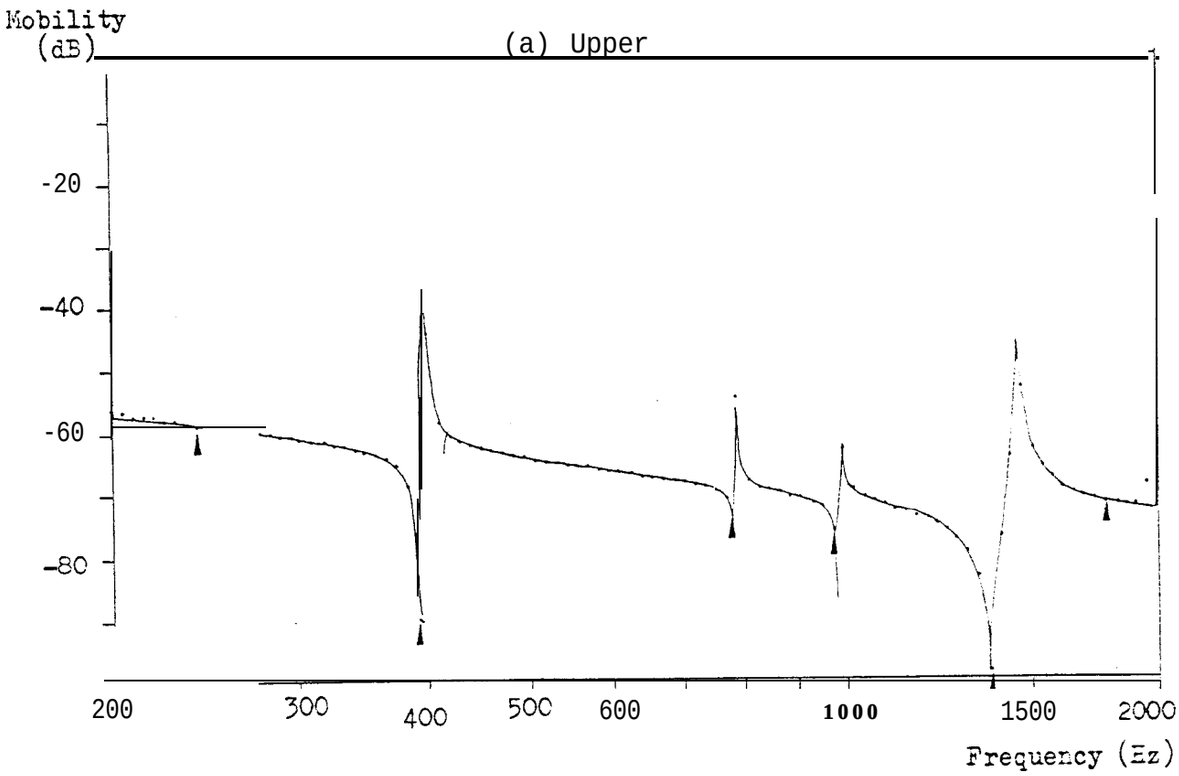

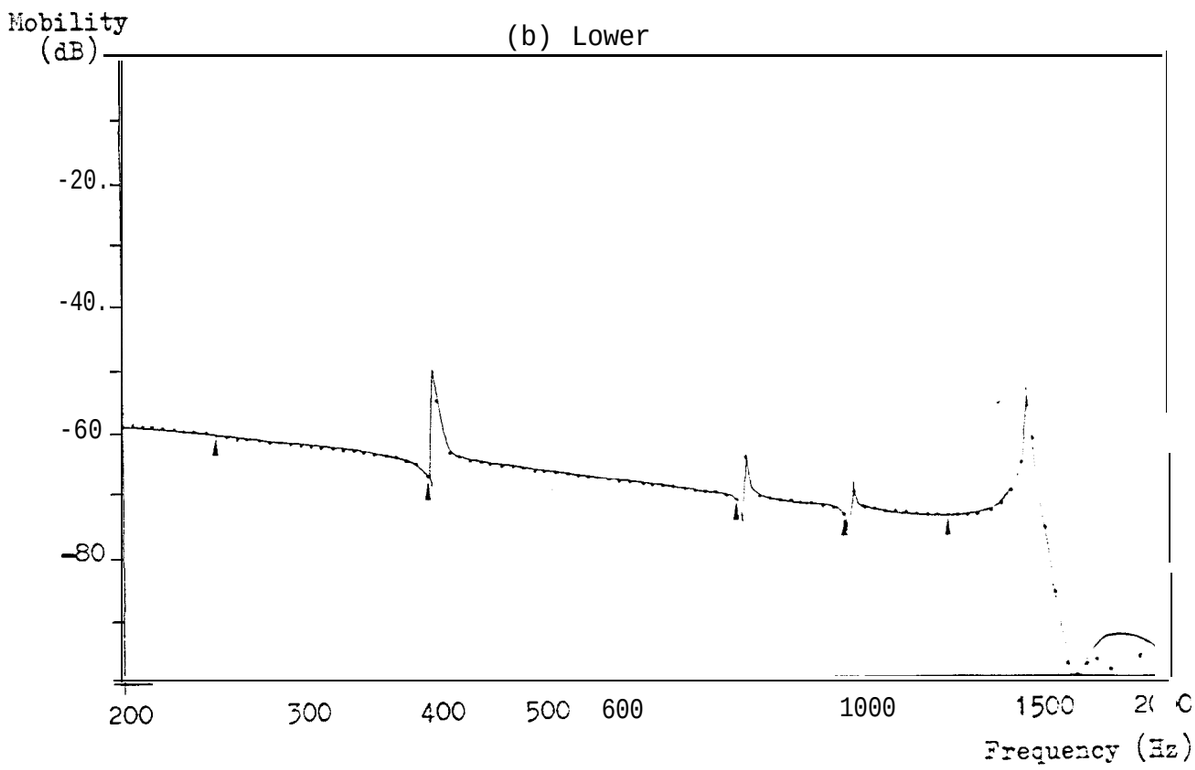

Figure 7.27 A1 Predicted Frequency Responses at Blade Root

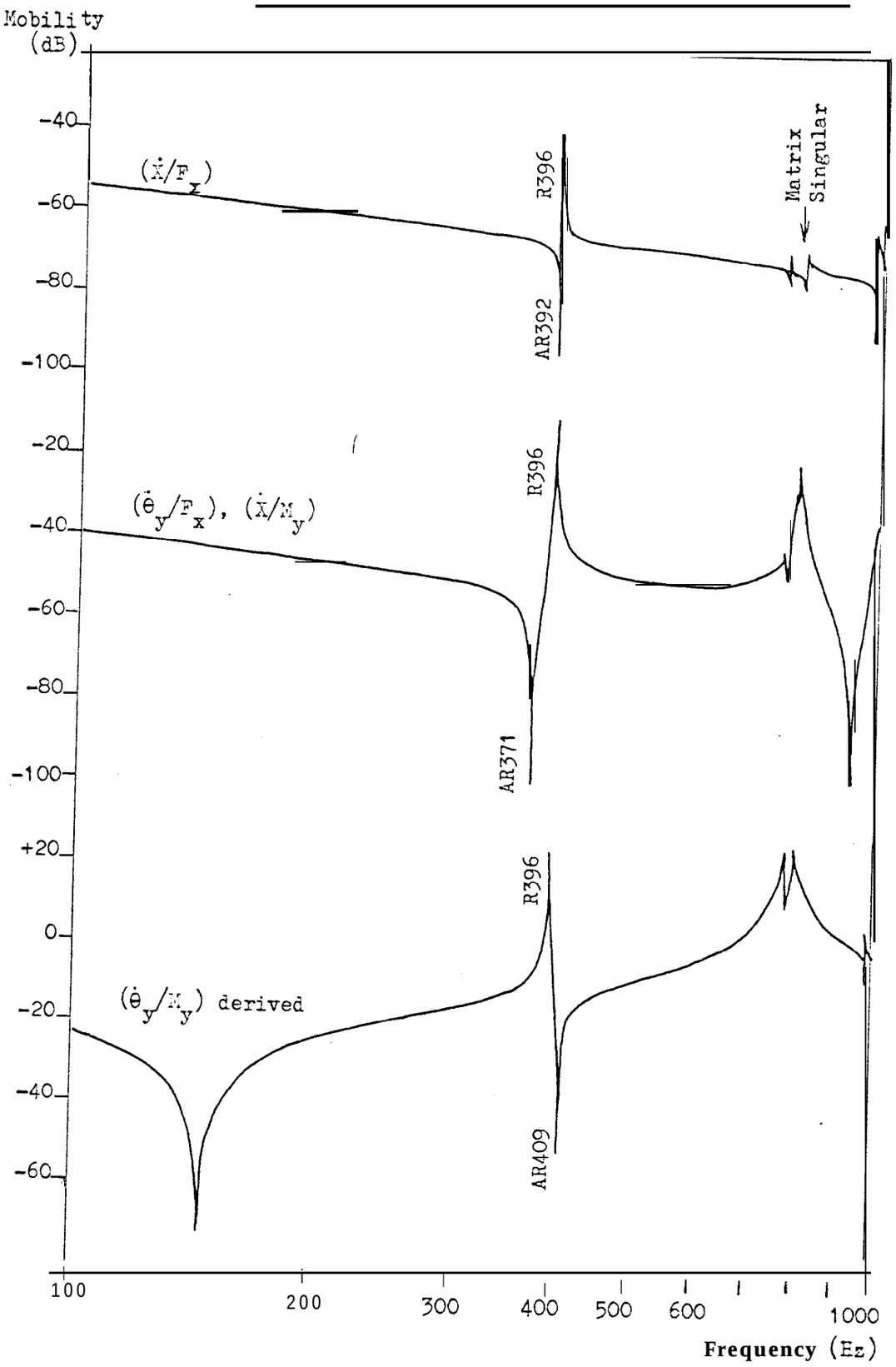

Figure 7.28 The Norm asa Function of Freauencs - Al Data

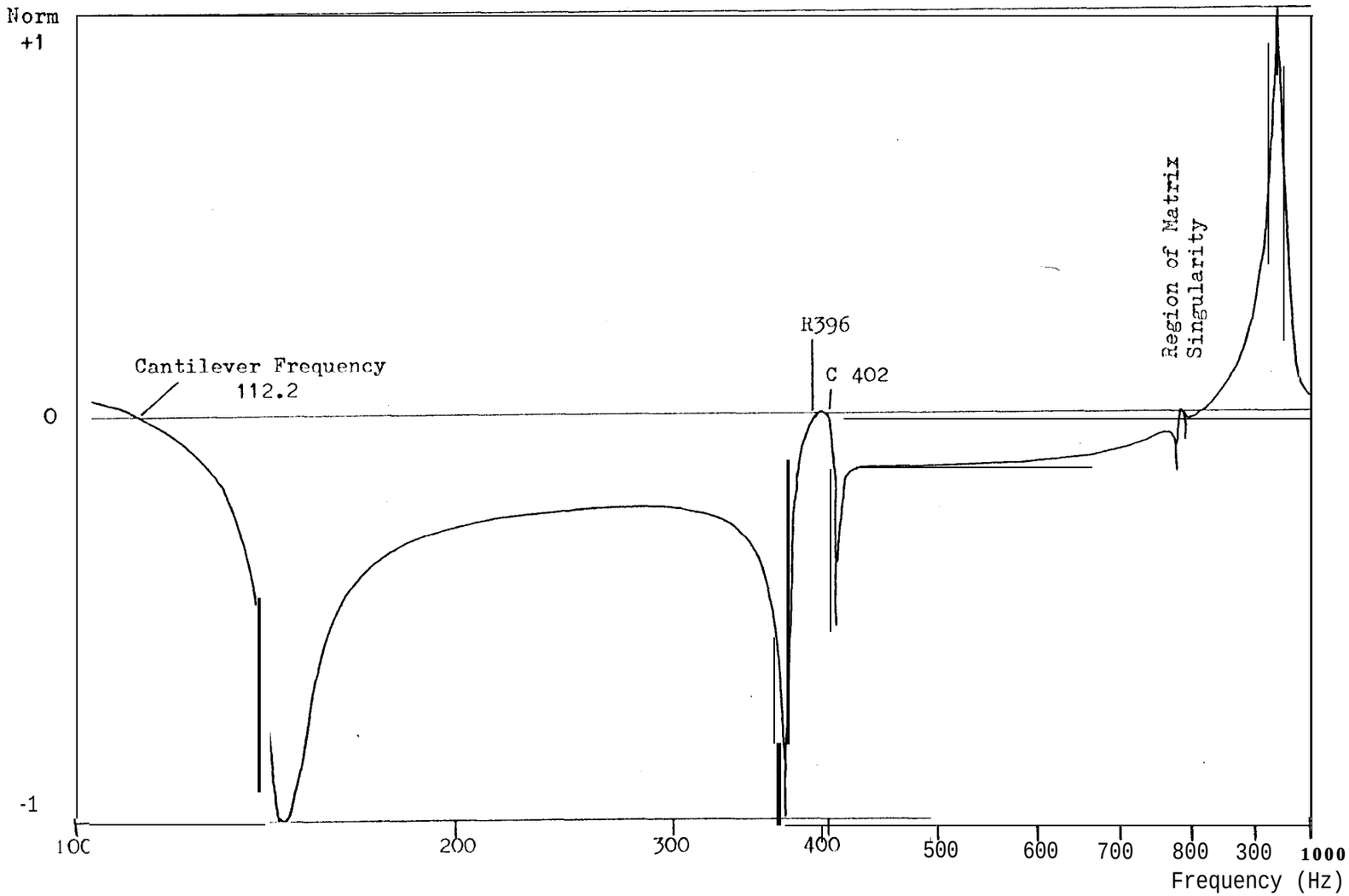

Figure 7.29 General Arrangement for Measurement of Cantilever Frequencies

(a) Tip Excitation

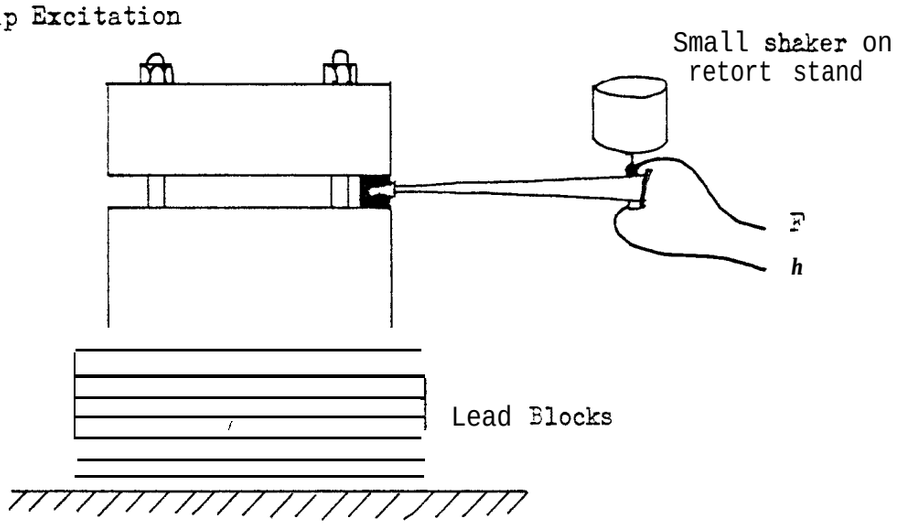

(b) Root Excitation

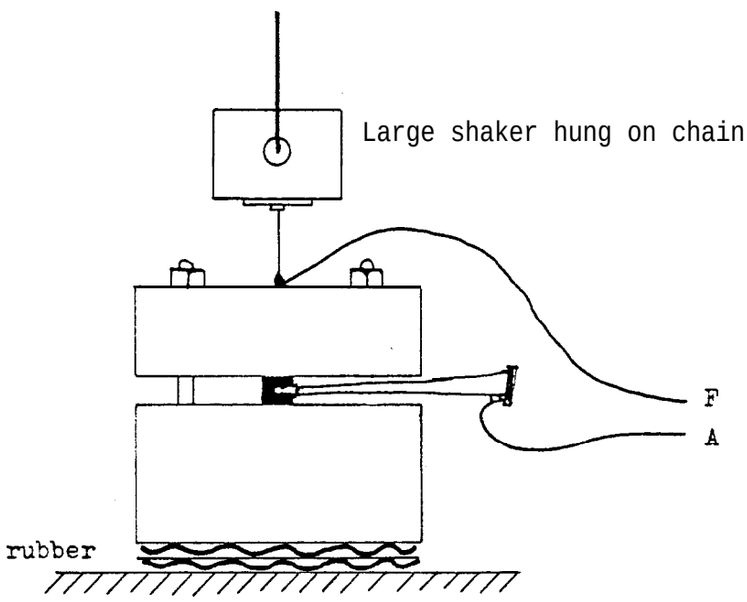

Figure 7.30 Frequency Response of 3lade Excited -at Tip Root field in Machined Block

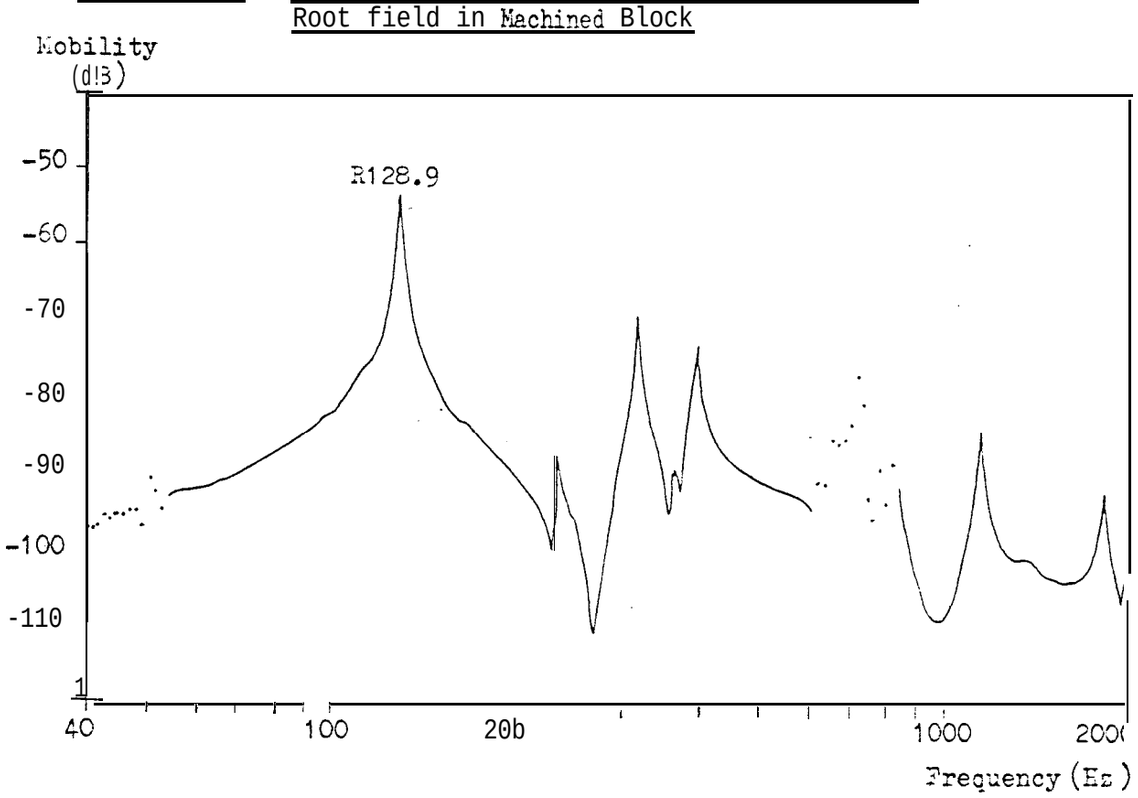

Figure 7.31 Frequency Response of Blade Excited et Tip Root Held in Tapered Leed Block

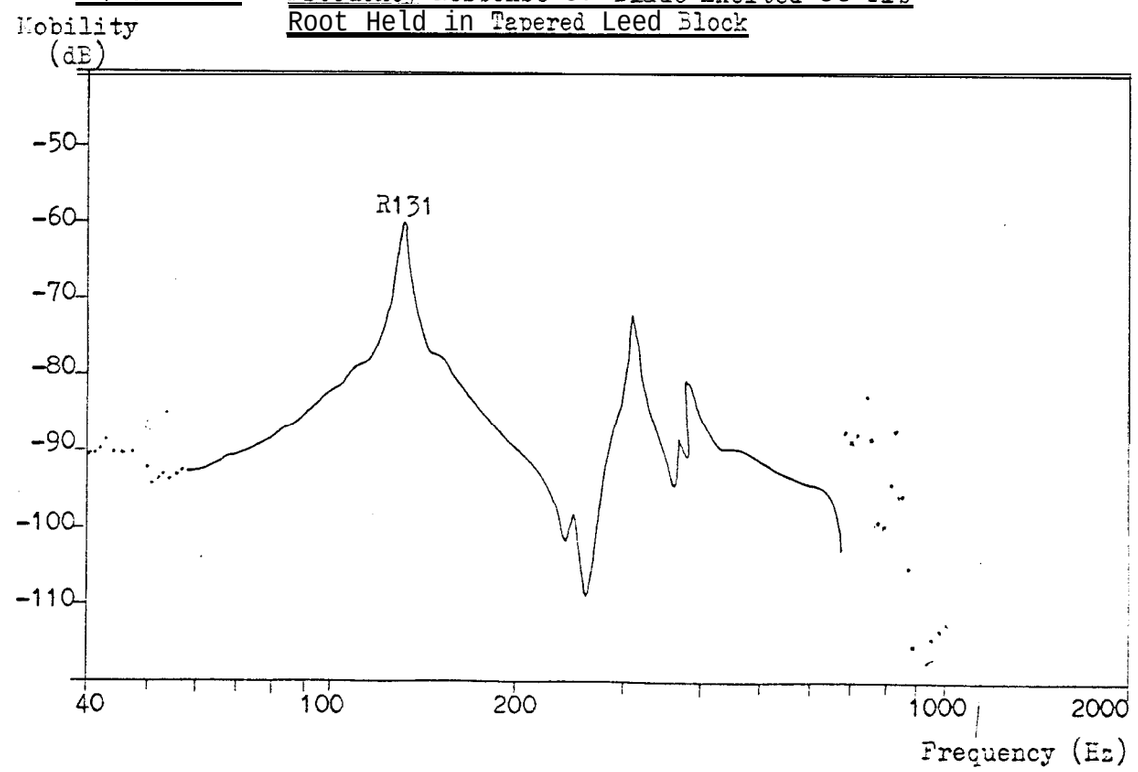

Figure 7.32 Frequency Response of Blade Excited at Tip Root Held in Block 7B

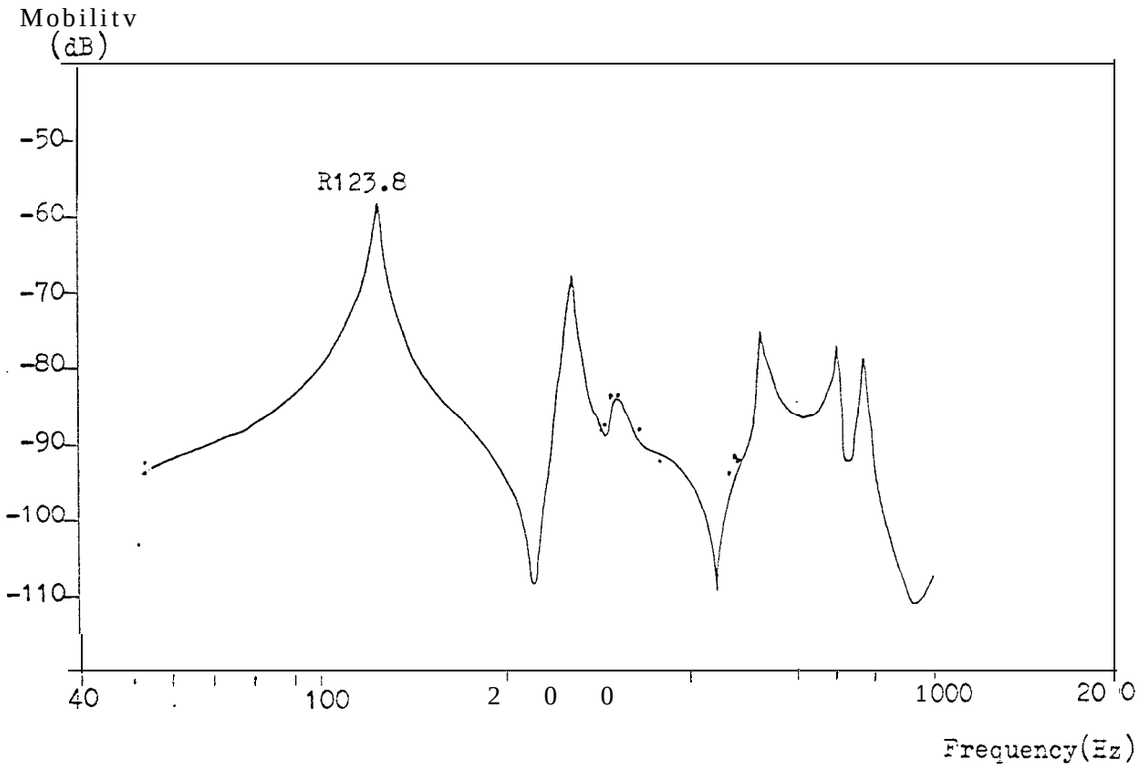

Figure . Frequency Response of Blade Excited at Root Held in Block 7B

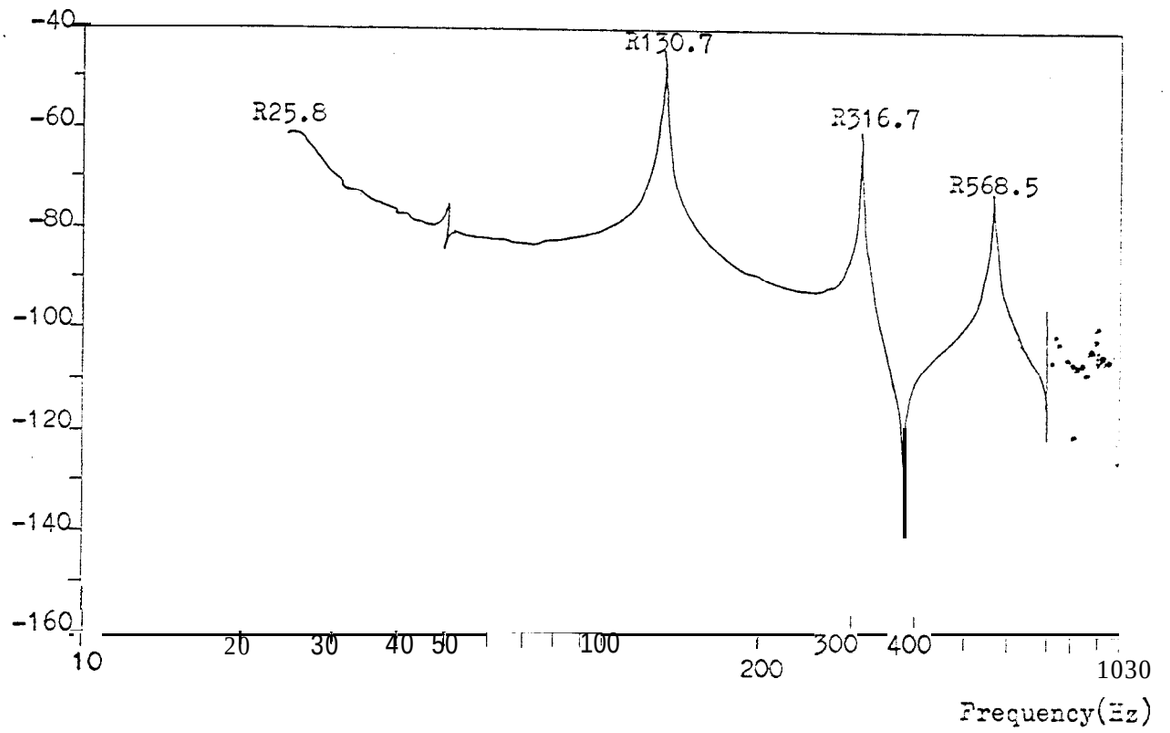

Table 7.15 Modal Constants - Configuration B2

Mode No.	Frequency (Hz)	Modal Constants	
		1 Upper	2 Lower
1	0	1.73535	1.52352
2	377.0	0.480547	-0.0882276
3	792.1	0.257250	-0.0628592
4	924.8	0.141726	-0.0697775
5	1505	-0.0774792	0.0241265

Table 7.16 Modal Constants - Configuration Al

Mode No.	Frequency (Hz)	Modal Constents	
		1 Upper	2 Lower
1	0	1.97652	1.51447
2	399.5	0.0828177	0.0166235
3	786.4	0.0152411	0.00358095
4	987.4	0.0255485	0.00582885
5	1460	0.302733	-0.269407

Table 7.17 Predicted Cantilever Frequencies Related to Rigid Body Modal Constants - Configuration A1

Row No.	Corresponding Figure	$_1A_1$	$_1A_2$	$_1A_{xx}$	$_1A_{\theta x}$	$_1A_{\theta\theta}$	Cantilever Frequency
1	7.24	1.97652	1.51447	1.7455	9.2410	97.2737(i)	112.5
2		"	"	"	"	98.3939(ii)	113.8
3	7.25	1.76208	1.45521	**1.60265**	6.13741	64.6043(i)	300.6
4		"	"	"	"	51.5256(ii)	270.5
5	7.26	1.75315	1.46368	1.61142	5.90941	62.2043(i)	229.0
6		"	"	"	"	47.5881(ii)	187.7

(i) Derived from equation $_1A_{\theta\theta} = {}_1A_{\theta x}/EX$

(ii) Derived from equation $_1A_{ee} = {}_1A_{\theta x}{}^2/({}_1A_{xx} - 1/m)$

Table 7.18 Measured Cantilever Frequencies Related to Method of Clamping

Method of Clamping		Cantilever Frequencies (Hz)		
Tip Excitation	Root Held in Machined Block	**128.9**	315.5	363.5
	Root Held in Lend Wedge	131.0	310.0	380.5
	Root Held in Block 7B	123.8	259.0	306.0
Root Excitation	" " " " "	130.7	316.1	568.5

6. CONCLUSIONS

6.1 Summary of Conclusions of Preceding Chapters

The concept of the response surface has been introduced in Chapter 1 in order to help the visual interpretation of vibration data which can be extracted from measurements on a structure or fron corresponding theoretical predictions. The response surface also illustrates resonance, antiresonance 2nd mode shape and proves to be of value when different methods of vibration analysis are compared.

The matrix models which can be formulated fror vibration data have been classified as nobility, modal or spatial 2nd their inter-relationships and utility have been discussed. It has been shown in Chapter 2 that data selected from the response surface of a lightly-damped body with clearly-defined resonances and mode shapes can be identified in modal terms. The resulting modal model may be used directly to regenerate vibration date, thus giving a considerable reduction of required data storage.

Modal models of related coordinate responses have been subsequently transformed into the spatial model expressed in terms of specified physical coordinates. Difficulties arise when the structural response in the frequency range of interest is effected by remote nodes of unknown frequencies and oode shapes. It has beer? demonstrated that high- and low-frequency residual terms improve the modal model, particularly for the case of continuous structures which have unlimited numbers of modes. Low-frequency residuals are often associated with free-free structures whose low-frequency behaviour is dominated by rigid-body modes of zero frequency, and these are completely specified in Appendix A3 in terms of mode shapes. This novel formulation is valuable when ttese modes have to be separated before a successful spatial model can be made. High-frequency residuals cannot be incorporated directly ictc spatial models since they do not have meaningful node snapes. A good approximation

can be made, however, by representing a point high-frequency residual 2s a spring 2nd by neglecting transfer residuals. This proves to be 2 simple 2nd powerful innovation.

The theoretical tools of spatial model identification hrve beer? evaluated in Chapter 3 by building spatial models of lumped-parameter systems which have a finite number of modes. It has been shown that the modelling process gives accurate results when all modaldataare included, but if the highest frequency node is ommitted, the resultant truncated data give only approximate representation which is more sensitive to changes of Stiffness than of mass. Modelling is particularly inaccurate if the points of interest - the coordinates of the spatial model - are located at or near nodes of one or more modes. The centre of a symmetrical system is particularly poor in this respect.

The systems considered in Chapter 4 are a step nearer reality in that they are ideal beams with unlimited numbers of modes. Fair results are obtained for spatial models without high-frequency residuals. The incorporation of such residuals as additional springs then gives excellent fit between ideal data and those predicted from the spatial model, thus demonstrating conclusively the inherent accuracy and utility of the spatial modal and that the identification process is numerically well-conditioned. It may be concluded that if vibration data is accurately measured, it can also be accurately modelled by this method. Most stringent comparisons between model prediction and ideal calculation have been made in natural frequencies, mode shapes and frequency response and remarkable coincidence achieved. The range of validity of the spatial model is clearly related to the number of coordinates and therefore the number of modes that it encompasses.

Attention has been turned in Chapter 5 to techniques for the measurement of the required data for application to actual structures. Develoments have been made in the methods of measuring rotational mobilities

using small two-part exciting blocks in particular. Certain defects of accelerometers - transverse sensitivity and base strain sensitivity - have been encountered 2nd circumvented as reported in Chapter 6 by application of the modelling techniques of Chapter 2. These are examples of the successfai application of derivation of one response from separate but related responses and of the advantage of an intimate connection between experiment and analysis. A conclusion of this section is that accelerometers with low transverse 2nd base strain sensitivities should be used, especially if rotational mobilities are to be measured.

Finally, in Chapter 7, the techniques and hardware developed earlier have been applied to experimental structures. In the case of the Long and Short Beams it has been shown that the measurements give data adequate for successful modelling of the individual beams, although only two bending modes can be included for the Short Beam. The two-accelerometer process used does not allow for the inclusion of residuals of rotational quantities and this omission reduces the accuracy of the eventual model of the Coupled Beam, although this result can still be pronounced 'good'. Again, the comparison with ideal results has been made not only for natural frequencies, the limit of many predictive methods, but also for rode shapes 2nd frequency responses. A valuable feature of this modelling process is the ability to cancel completely the inertia effects of the transducers 2nd exciting blocks after the spatial model has been constructed.

The turbine blade is 2 complex, asymmetrical, virtually-undamped test piece. It is recognised that the attempt to model its behaviour using analysis in two, rather than three, dimensions is an over-simplification but it Is considered that there is value in applying the modal modelling techniques of this thesis to 2 structural component of such complexity. Despite the obvious limitations, the first cantilever frequency 2s predicted using 2 novel search technique based on the norm of

the free-free mobility matrix is between 9% and 17% of the cantilever frequency measured directly. In this exercise it has been shown that the mobility model produces a successful match of regenerated response data to the original raw measured data and that the partial nodal model based on the mobility model gives useful natural frequency predictions although it Coes not have the power of the spatial model also to give estimates of mode shape and frequency response.

E.2 Applicability of Techniques and Future Work

The identification of spatial models has been successfully demonstrated for lightly-damped structures 2nd the limitations explored. The technique is commendably economical of computer time and both allows and requires the judgement of the analyst during its application. If damping is tpo large for this method of identification to be sufficiently accurate then other more elaborate and time-consuming methods are available, although several years of industrial use of the method have shown its versatility in treating many practical problems.

It may be concluded that there is 2 wide range of test pieces, particularly structural components, for which the identification 2nd spatial modelling of this thesis can be effected accurately and quickly. The spatial models of substructures can easily be linked together using standard computer routines and the resultant model of the complete structure will have good estimates of the frequencies of resonance and anti-resonance of the assembly, although the assembled structure may introduce sufficient additional damping at the connection points to make the prediction ofresponse level in near-resocance regions somewhat inaccurate.

There are some aspects of this work which deserve further attention. The concept of the response surface could be applied with sone modification to structures with more than the one significant spatial dimension of the slender bean used here as an example. It is evident that the

bird's eye view of the response surface which is essentially two- rather than three-dimensional offers a coherent picture of antiresonance lines which could be manipulated in the design process of modifying structures to meet vibration specifications. It is also apparent that antiresonance theory in general is capable of further development and there may well be opportunity in such studies to use approximations and residual terms analagous to those used in the spatial modelling of this thesis.

Finally, it is the author's firm opinion that analytical techniques should not be kept divorced from experimental methods since one aspect of study keeps the other within reasonable bounds. This view is opposed to current industrial practice in which it is common to find vibration analyst and experimental tester in separate departments, and further, it often happens that the analyst makes use of packaged computer routines whose assumptions and inner workings are not in his control. In conclusion it is asserted that reasoned progress in the design of structures with improved vibration properties will come most surely with an approach in which a continuous balance is made between experiment and analysis.

REFERENCES

1. GROOTENHUIS, P. - 'Trends in Design for the Shock and Vibration Environment', S.E.E. Symposium, 'Environmental Engineering Today', Wembley, London, Vol. 3, pp.85-99. (9- 11 May) 1979
2. HURTY, W.C. & RUBINSTEIN, M.F. - 'Dynamics of Structures', Prentice-Hall, Englewood Cliffs, N.J. 1964
3. MEIROVITCH, L. - 'Analytical Methods in Vibrations', MacMillan, New York. 1967
4. EWINS, D.J. - 'Measurement and Application of Mechanical Impedance Data', Journal of the Society of Environmental Engineers, Part 1 'Introduction & Ground Rules', Dec. 1975, Part 2 'Measurement Techniques', Mar. 1976 and Part 3 'Interpretation and Application of Measured Data', June 1976
5. BISHOP, R.E.D. & JOHNSON, D.C. - 'The Mechanics of Vibration', C.U.P. 1960
6. SALTER, J.?. - 'Steady State Vibration', Kenneth Mason Press. 1969
7. McCALLION, E. - 'Vibration of Linear Mechanical Systems', Longmans. 1973
8. BISHOP, R.E.I). & GLADWELL, G.M.L. - 'An Investigation into the Theory of Resonance Testing', Phil. Trans. Royal Soc. London, Series A, No. 1055, Vol. 255, pp. 241 - 280. 1963
9. SILVA, J.M.M. - 'Measurements an?. Applications of Structural Mobility Data for the Vibration Analysis of Complex Structures', Ph.D. Thesis, Department of Mechanical Engineering, Imperial College of Science & Technology, London, S.W.7. March 1978
10. BEARDS, C.F. - 'The Control of Structural Vibration by Frictional Damping in Joints', S.E.E. Symposium, 'Environmental Engineering Today', Wembley, London, Vol. 3, pp.35-42. 1979 (9 - 11May)

11. GAUKROGER, D.R., HERON, I:.?. & SKINGLE, C.W. - 'The Processing of Response Data to Obtain Modal Frequencies and Damping Ratios', Jnl. Sound Vib., 35(4), 599 - 571. 1974

12. GOYDER, E.G.D. - 'Structural Modelling by the Curve Pitting of Measured Frequency Response Data', I.S.V.R. Technical Report No.87 Oct. 1976

13. KLOSTERMAN, Albert L. - 'On the Experimental Determination and Use of Modal Representations of Dynamic Characteristics', Ph.D. Thesis, University of Cincinatti. 1971

14. FLANNELLY, W.G., BERMAN, A. & BARNSBY, R.M. - 'Theory of Structural Dynamic Testing Using Impedance Techniques', U.S.A.A.V.L.A.B.S. Technical Report 70 - 63. 1970

15. DONE, G.T.S. & HUGHES, A.D. - 'Reducing Vibration by Structural Modification', Proceedings of the First European Rotorcraft and Powered Lift Aircraft Form, Southampton, England. (To be published in 'Vertical'). 22 - 24 Sept. 1975

16. DONE, G.T.S., HUGHES, A.D. & WEBBY, J. - 'The Response of a Vibrating Structure as a Function of Structural Parameters - Application and Experiment', J.S.V. 49 (2), 149 - 159. 1976

17. NYQUIST, a. - 'Regeneration Theory', Bell Systen Technical Journal, Vol. 11, pp. 126 - 147. 1932

18. KENNEDY, Charles C. & PANCU, C.D.P. - 'Use of Vectors in Vibration Measurement and Analysis*, Jnl. Aero. Sci. 14, 11, pp. 603 - 625. 1947

19. BODE, H.W. - 'Relations Between Attenuation and Fhsse in Feedback Amplifier Design', Bell Systeo Technical Journal, Vol. 19. 1940

20. KLOSTERMAN, Albert L. & LEMON, Jason R. - 'building Block Approach to Structural Dynamics', A.S.M.E., 69 - Vibr. - 30. 1969

21. SAINSBURY, M.G. - 'User's Guide for the Structural Dynamic Analysis Computer Program COUPLE1', Dynamics Group Report, Mechnical Engineering Department, Imperial College. May 1975
1. The Basic Dynamic Stiffness Coupling Program
2. Special Subroutines for Standard Types of Component
3. Miscellaneous Worked Examples

22. ASTROM, K.J. & EYKHOFF, P. - 'System Identification - A Survey'. kutomatica, Vol. 7, Part 2, pp. 123 - 162. Mar. 1971

23. BEKEY, G.A. - 'System Identification -an Introduction and a Survey', Simulation, pp. 151 - 166. Oct. 1970

24. YOUNG, J.P. & ON. F.J. - 'Mathematical Modelling via Direct Use of Vibration Data', S.A.E. paper No. 690615. 1969

25. COLLINS, J.D., YOUNG, J.P. & KIEFLING, L. - 'Methods and Applications of System Identification in Shock and Vibration', A.S.M.E. Winter Meeting, pp. 45 - 71. 1972

26. FLANNELLY, W.G. & BERMAN, 4. - 'The State of the Art of System Identification of Aircraft Structures', A.S.M.E. Winter Meeting, pp. 121 - 131. 1972

27. EWINS, D.J. - 'Whys and Wherefores of Modal Testing', S.E.E. Conference 'Modal Testing Using Digital Techniques', Cranfield. 6 June 1978.
Journal of S.E.E. pp. 3-15, September 1979

28. BROCH, J.T. - 'The Application of B. & K. Equipment to Mechanical Vibration and Shock Measurements', Bruel & Kjaer Ltd., Naerum, Denmark. 1972

29. QUACKENBUSH, R.E. (ed.) - 'Vibration Measurements Handbook', Zndevco - Dynamic Instrument Division, Pasadena, California. 1970

30. KERLIN, R.L. & SNOWDON, J.C. - 'Driving Point Impedances of Cantilever Beams - Comparison of Measurement and Theory', Jcl. Acoustical Soc. of America, 47, No. 1, Pt. 2, pp. 220 - 228. 1970

31. SAINSBURY, M.G. - 'Experimental and Theoretical Techniques for the Vibration Analysis of Damped Complex Structures', Ph.D. Thesis, Department of Mechanical Engineering, Imperial College of Science and Technology, London, S.W.7. Sept. 1976

32. MUSTAIN, R.W. - 'Survey of Modal Vibration Test/Analysis Techniques', A.S.M.E. paper 760870. 1976

33. LEWIS Robert C. & WRISLEY, Donald L. - 'A System for the Excitation of Pure Natural Nodes of Complex Structure', Journal Aero. Sci., Vol. 17, pp. 705 - 722. 1950

34. FRAEJIS de VEUBEKE, B.M. - 'A Variational Approach to Pure Mode Excitation based on Characteristic Phase Lag Theory', A.G.A.R.D. Report No. 39 (N.A.T.O. Advisor; Group for Aeronautical Research & Development). 1956

35. TRAILL-NASH , R.W. - 'On the Excitation of Pure Natural Modes in Aircraft Resonance Testing', Journal Aero/Space Science, Vol. 25, pp. 775 - 778. 1958

36. ASHER, Gifford W. - 'A Method of Normal Mode Excitation Utilising Admittance Measurements', Dynamics& Aeroelasticity, Proc. Mat. Specialists Meeting (Inst. Aeronaut Sci.), Fort Worth Texas, pp. 69 - 76. 1958

37. IBANEZ, P. - 'Force Appropriation by Extended Asher's Method', S.A.E. Paper No. 760873. 1976

38. VRIES, G. de, & BEATRIX, G. - 'General Measuring Processes of Vibratory Characteristics of Lightly Damped Linear Structures', Progress in Aeronautical Sciences, Vol. 9, Perzamon Press, Oxford & New York. 1968

39. SLOANE, E. & KcKEEVER, B.- 'Modal Survey Techniques and Theory', S.A.E. Paper No. 751067. 1975

40. SMITH, S. & WOODS, A.A. - 'A Multiple Driver Admittance Technique for Vibration Testing of Complex Structures', S.V.B. 42 (3), pp. 15 - 23. 1972

41. GABRI,B.S.& MATTHEWS, J.T. - 'Normal Mode Testing Using Multiple Exciters under Digital Control', S.E.E. Symposium, 'Environmental Engineering Today', Wembley, London, Vol. 1, pp. 97 - 110. 1979 (9 - 11 Lay)

42. KELLER, A.C. & ANDRESS, E.A. - 'Multiple Shaker Production Testing', S.E.E. Symposium, 'Environmental Engineering Today', Wembley, London, Vol. 3, pp. 23 - 34. 1979 (9 - 11 May)

43. COOLEY, J.W. & TUKEY, J.W. - 'An Algorithm for the Machine Calculation of Complex Fourier Series', Math. of Computing, Vol.19, pp. 297 - 301. 1965 (April)

44. RAMSAY, Kenneth A. - 'Effective Measurements for Structural Dynamics Testing', Part I 'Sound & Vibration', pp. 24 - 35. Nov. 1975. Part II - available fron Hewlett Packard Ltd., Winnersh, Wokingham, Berks, RG11 5AR (Wokingham 784774)

45. SISSON, T, SIMMERMAN, R. & MARTZ, J. - 'Determination of Modal Properties of Automotive Bodies and Frames Using Transient Testing Techniques', S.A.E. Paper No. 730502. 1973

46. PETERSON, E.L. & KLOSTERMAN, A.L. - 'Obtaining Good Results from an Experimental Modal Survey', Journal of S.E.E.,pp. 3 - 10. Mar. 1978. Also S.E.E.C.O. 77 Apr. 1977

47. BROWN, D., CARBON, G. & RAMSEY, K. - 'Survey of Excitation Techniques Applicable to the Testing of Automotive Structures', S.A.E. Report 770029 (International Automotive Engineering Congress & Exposition, Detroit, Feb. 26 - Mar. 4 1977). 1977

48. WHITE, 9.G. - 'Evaluation of the Dynamic Characteristics of Structures by Transient Testing', J. Sound Vib. 15 (2) 147 - 161, 1971

49. WHITE, E.G. - 'Transient Testing Techniques and the Dynamic Analysis of Structures', S.E.E. Seminar 'Modal Testing using Digital Techniques', Cranfield. June 6, 1978

50. SKINGLE, C.W. - 'A Method for Analysing the Response of a Resonant System to a Rapid Frequency Sweep Input', Royal Aircraft Establishment Technical Report No.66379. 1966 (Dec.)

51. WILLIAMS, R. & GABRI, B.S. - 'Digital Frequency Analysis of Engineering Signals', Journal of S.E.E., pp. 3 -15. June 1978

52. THRANE, N. - 'The Discrete Fourier Transform and F.F.T. Analysers' B . & K. Technical Review, No.1, Bruel & Kjaer, Naerum, Denmark. 1979

53. THRANE, N. - 'Analysis of Impulsive Signals by use of Digital Techniques', S.E.E. Symposium, 'Environmental Engineering Today', Wembley, London. 1979 (9 - 11 May)

54. LEPPERT, E.L., LEE, S.E., DAY, F.D., CHAPMAN, P.C. & WADA, B.K. - 'Comparison of Modal Test Results: Multipoint Sine Versus Single Point Random', S.A.E. Paper Kc. 760879. 1976

55. HANNA, G.A., STRETHER SMITH JR. & STROUD. R.C. - 'An Evaluation of Excitation and Analysis Methods for Modal Testing', A.S.M.E. Paper 760872. 1976

56. WILLIAMS, J. - 'The Gse of Discrete Frequency Testing for Modal Analysis of Engineering Structures', S.E.E. Symposium 'Signal Processing for Vibration, Shock and Noise', Imperial College, London. (Apr. 4 - 6) 1977.

57. GAUKROGER, D.R., SKINGLE, C.W. & ARROW K.H. - 'Numerical Analysis of Vector Response Loci', Jnl. Sound Vib. 29 (3), pp.341-343. 1973

58. DAT, Rolland & MEURZEC, Jean-Louis - 'The Application of a Smoothing Technique to Analyse Frequency Response Measurements fcr a Linear System', R.A.E. Library Translation, 1703, Translator D.R. Gaukroger. 1972

59. 't MANNETJE, J.J. - 'Transfer-Function Identification using a Complex Curve-Fitting Technique', J.M.E.S. 15 No. 5 pp.339-345. 1973

60. FLANNELLY, W.G. McGARVEY, J.E. & BERMAN, A. - 'A Theory of Identification of the Parameters in the Equations of Motion of a Structure Through Dynamic Testing', Structural Dynamics Symposium, Loughborough University. 25 - 25 Mar. 1970

61. O'HARA, G.J. & REMMERS, G.M. - 'Measurement of a Structure's Modal Effective Mass', S.V.B. 39, pp. 143 - 151. 1969

62. NEUBERT, V.H. - 'Series Solutions for Structural Mobility', Acoustical Society of America Journal, Vol. 38, pp. 867-876. 1965

63. BICT, M.A. - 'Coupled Oscillations of Aircraft Engine - Propeller Systems', J.A.S., Vol. 7, Part 9, pp. 376 - 382. July 1940

64. RANEY, J.P. - 'Identification of Complex Structures using Near-Resonance Testing', S.V.B. 38 (2), pp. 23 - 32. Aug. 1968

65. HARDENBERG, J.F. - 'The Transmission of Vibrations Through Structures', Ph.D. Thesis, Imperial Coiiege. 1971

66. HEMINGWAY, N.G. - 'Vibration and Noise Transmission in a Vehicle Suspension', Ph.3. Thesis' C.N.A.A., Hatfield Polytechnic, Sept. 1975.

67. ROSS, Ronald G. - 'Synthesis of Stiffness and i-lass Matrices from Experimental Vibration Modes', A.S.M.E. Paper 710787, pp. 2627 - 2635. 1971

68. IBANEZ, F. - 'Methods fcr the Identification of Dynamic Farameters of Mathematical Structural Models from Experiment21 Data', Nuclear Engineering & Design (27). 1974

69. BERMAN, Alex & FLANNELLY, William G. - 'Theory of Incomplete Models of Dynamic Structures', A.I.A.A. Journal 9 No. 8, pp.1481-1487. 1971

70. FLANNELLY, W.G. - 'Truncated Models and their Use in Predicting Changes in Mass and Stiffness', Research Note 72 - 8, Kaman Aero-space Corporation. 12 Oct. 1972

71. FLANNELLY, W.G. & GIANSANTE, N. - 'Experimental Verification of System Identification', U.S.A.A.M.R.D.L. - TR - 74 - 64, Report produced by Kaman Aerospace Corp.

72. THOREN, A.R. - 'Derivation of Mass and Stiffness Matrices from Dynamic Test Data', A.I.A.A./A.S.M.E./S.A.E., 13th Structures, etc. Conference, San Antonio, Texas, A.I.A.A. Paper No. 72346. Apr. 10-12 1972

73. BAGLEY, R.L. - ' Inverse Eigenvalue Method of Mechanical Admittance Analysis', M. I.T. Report TN 1973-49 AD 771 799 MICRO FICHE 1973

74. BAGLEY, R.L. - 'Antiresonant Frequency and the Measurement of Mechanical Admittance Data', M.I.T. Report TN 1973-53 AD 773 307 MICRO FICHE 1973

75. GOYDER, H.G.D. - 'Vibration Analysis using Experimental Data and Approximate Methods with Consideration of Power Flow from Machinery into Building Structures', Ph.D. Thesis, Institute of Sound and Vibration Research, University of Southampton. 1979

76. GERASIMOV, M.M. - 'The Face Finder', Hutchinson & Co. (Publishers) Ltd., London, W.1. 1971

77. EWINS, D.J. - 'Estimation of Resonant Peak Amplitudes', J.S.V. 43 (4), 595 - 605. 1975

78. STRANG, G. - 'Linear Algebra and its Applications', Academic Press, New York. 1976.

79. FLANNELLY, W.G., BERMAN, A. & GIANSANTE, N. - 'Research on Structural Dynamic Testing by Impedance Methods', Volume I - 'Structural System Identification from Multipoint Excitation', Kaman Aerospace Corporation, U.S.A.A.M.R.D.,. Technical Report 72-63A, Eustis Directorate, U.S. Army Air Mobility Research and Development Laboratory, Fort Eustis, Virginia. 1972 (Nov.)

60. ALBASINY, E.L. & RALL, L.B. (editor) - 'Error in Digital Computation', Vol. 1, John Wiley, Proceedings et University of Wisconsin. Chapter: 'Error in Digital Solution of Linear Problems' Oct. 1964

61. FLANNELLY, W.G., BARTLETT, F.D. & FORSBERG, T.W. - 'Laboratory Verification of Force Determination - 2 Potential Tool for Reliability Testing', U.S.A.A.M.R.D.L. - TR - 76 - 38, Report produced by Kaman Aerospace Corp. Jan.1977

62. POTTER, R. & RICHARDSON, M. - 'Mass, Stiffness 2nd Damping Matrices from Measured Modal Parameters', I.S.A. Paper No. 74-630. 1974

63. RICHARDSON, M. & HENISHERN, J. - 'Identifying Modes of Large Structures fro-, Multiple Input 2nd Response Measurements,S.A.E. Paper No. 760875. 1976

64. EWINS, D.J. & GLEESON, P.T. - 'Experimental Determination of Multi-Directional Mobility Data for Beams',S.V.B.45. 1975

65. MALECI, G. - 'System Identification of 2 Beam Loaded by Concentrated Masses', Dynamics Group Internal Report, imperial College, Department of Mechanical Enginesring, Nov.1977

66. EWINS, D.J. - 'Handbook for the Computer-Controlled Mechanical Impedance Measurement Facility', Dynamics Group Handbook, Imperial College, Department of Mechanical Engineering.

67. ANON - Accelerometer Handbook - supplied with the transducer. Bruel & Kjaer Ltd.

68. PENNINGTON, D. - Piezoelectric Accelerometer Handbook, published by Endevco Ltd. 1965

69. HARRIS, C.M. & CREDE, C.E. - 'Shock 2nd Vibration Handbook', McGraw-Hill. 1961

70. ROCKWELL, D.W. & RAMBOZ, J.H. - 'Measurement of Accelerometer Transverse Sensitivity', S.V.B. 35(4), pp.73 - 97. Feb. 1966

91. SILVA, J.M.M. - 'On the Influence of the Push-Rod in Mechanical Impedance Testing', Imperial College Mechanical Engineering Dept., Dynamics Group Report. Oct. 1975

92. SILVA, J.M.M. - 'The Influence of the Joint on the Vibration Response of a Cross-Beam Assembly', M.Sc. Thesis, Imperial College of Science and Technology. Dec. 1974

93. EWINS, D.J. - 'The Effects of Detuning upon the Vibrations of Bladed Discs', Ph.D. Thesis, Trinity College, Cambridge. Nov. 1966

94. EWINS, D.J. - 'A Study of the Vibration Modes of a Bladed Turbine Wheel', I.Mech.E./Conference 'Vibrations in Rotating Systems'. 1972

95. SRINIVASAN, A.V. (Ed.) - 'Structural Dynamic Aspects of Bladed Disc Assemblies', A.S.M.E. Publication. 1976

96. COTTNEY, D.J.) 'The Receptance Analysis of Disc, Blade and Shroud Vibrations', Ph.D. Thesis, Department of Mechanical Engineering, Imperial College of Science & Technology, S.W.7. 1975

97. CONTE, S.D. & de BOOR, C. - 'Elementary Numerical Analysis', McGraw Hill, 2nd Ed. 197s

Appendix A1 Computer Programs Referenced in Text

Program	Code	Author	Introduced in Section	Brief Description or Function
ADFLEX	2	PTG	4.3.2	Addition of Flexibility terms to response
COUPLE1	2	MGs	1.3.3	Generetion of frequency response of structure formed by Coupling of substructures
EIGEN	2	PTG	3.1.3	Calculation of modal data, eigenvalues and -vectors, from spatial model, i.e. $[\Phi]$, $[\omega_r]$ from $[M]$, $[K]$
EMMAY	1,2	PTG	2.3.1	Calculation of spatial model from nodal data, i.e. $[M]$, $[K]$ from $[\Phi]$, $[\omega_r]$
FRERES	2	PTG	1.2.2	Generation of suite of Frequency Responses from beam nodal data
IDENT	1,2	PTG	2.1.1	Identification of modal date from frecuency response
INCAN	1	PTG	5.2.2	Inertia Cancellation following identification
MOB2	1	MGS/JMMS	5.1.1	Measurement of point and transfer mobilities
PICASO	2	JV	1.2.2	Graphics: 3D views of surface stored as array of data
PM2/1	1	MGS	5.2.1	Measurement of translational and rotational Point Mobilities

COUPLE1 Subroutines

MATIN1	1,2	MGS	2.1.1	Matrix Inversion Jordan's method with partial pivoting
ZMAK2	2	MGS	3.1.2	Generates mobility properties of $[M]$, $[K]$, $[H]$
ZFLAX1	2	MGS	4.1.4	Generates mobility properties of Bernouilli-Euler beam
ZFILE	2	MGS	4.3.2	Coupling based on response data stored on file

Code 1 - Written in FOCAL language for minicomputer

Code 2 - Written in FORTRAN language for mainframe computer

Appendix A2. (a) Flow Chart of Prog-ram IDENT

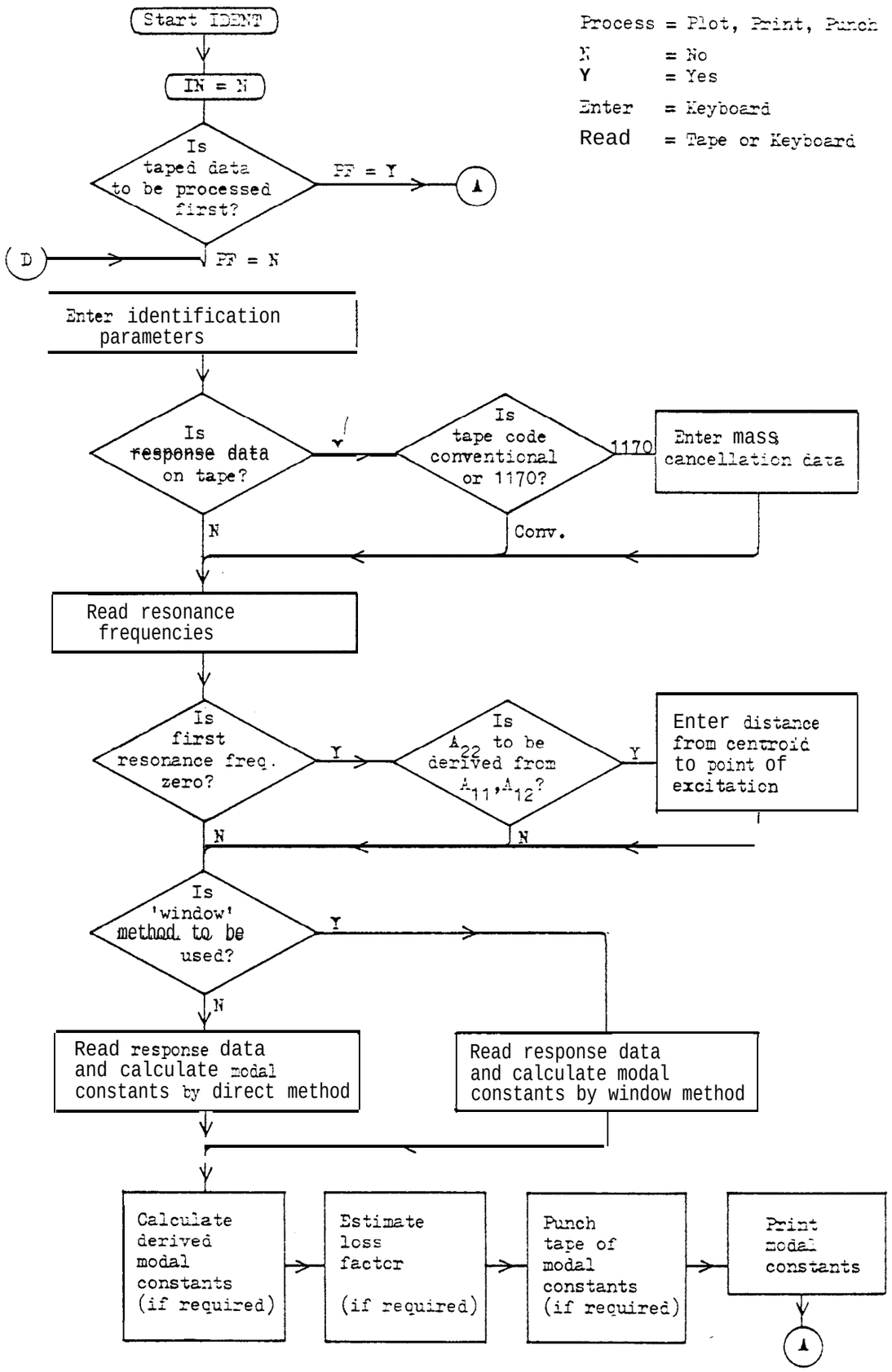

(a) Flow Chart of Program IDENT (continued

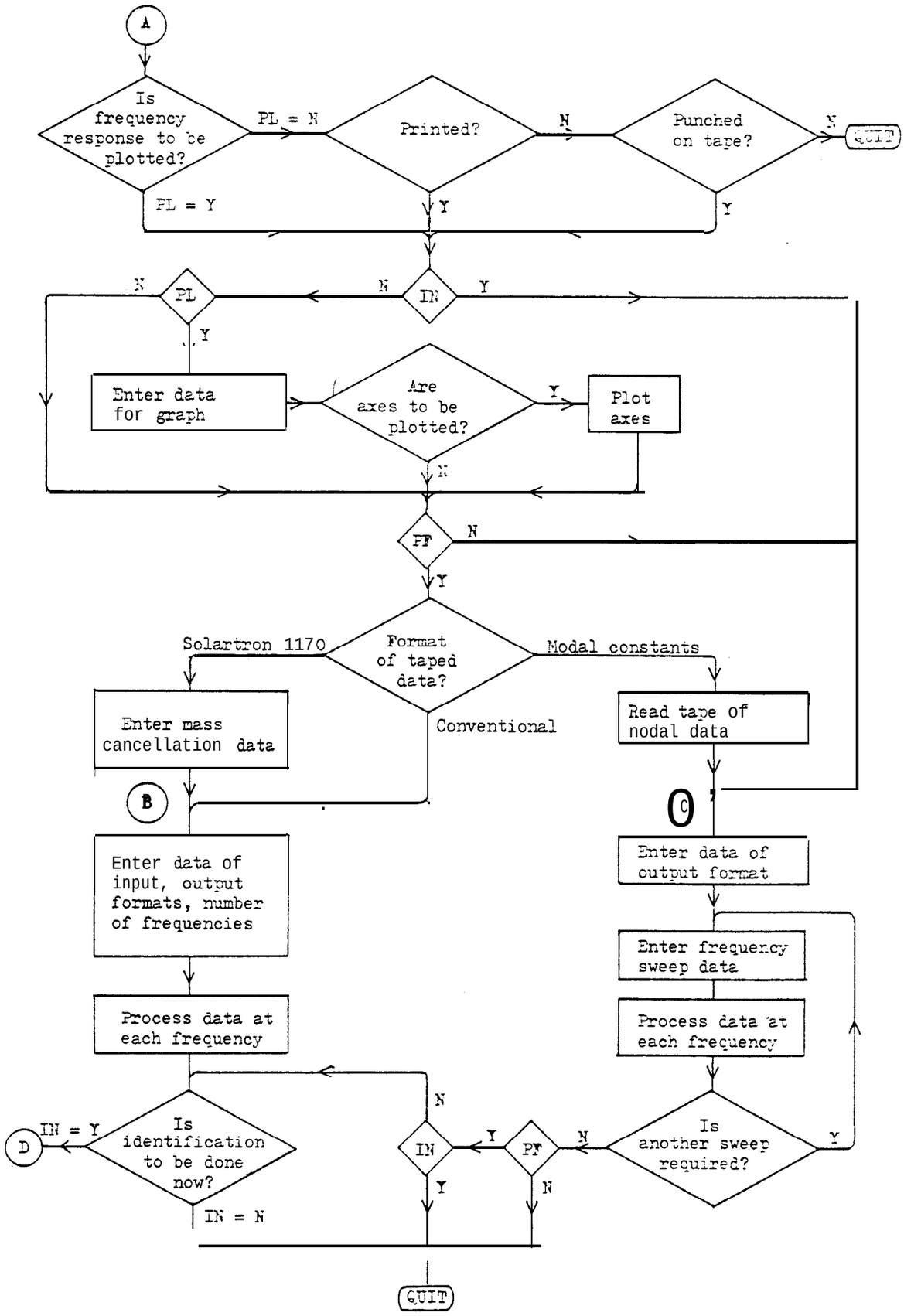

(b) Flow Chart of Program INCAN

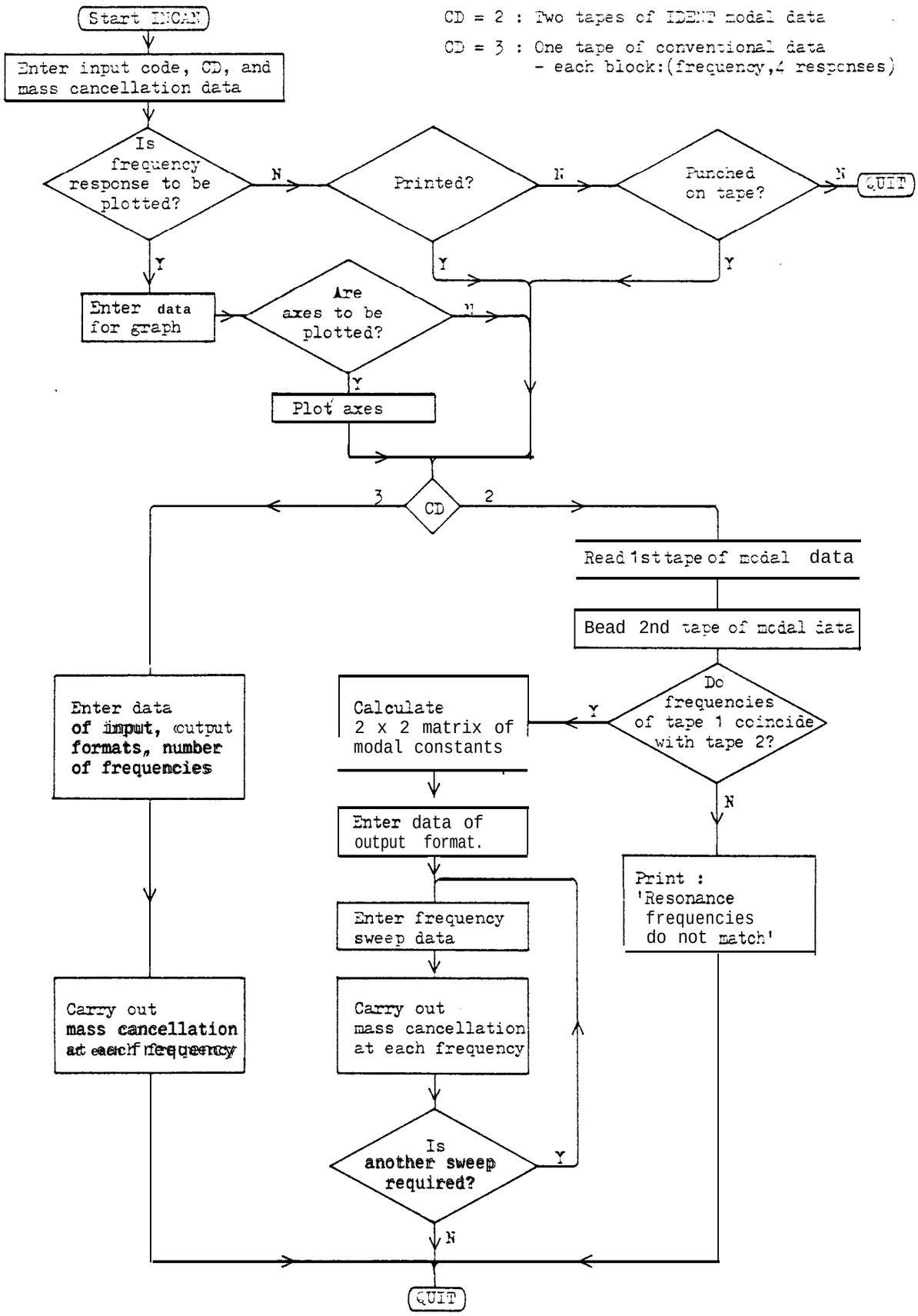

APPENDIX A3 Rigid Body Motion

A3.1 Basic Configuration

The basic configuration of a rigid body is shown in Figure A3.1. The point G is the centroid of the body which has mass m. X, Y and Z are principal axes and the corresponding mass moments of inertia are I_X, I_Y and IZ.

The equation of motion of the body in terms of centroidal forces is:-

$$\begin{Bmatrix} \ddot{X} \\ \ddot{Y} \\ \ddot{Z} \\ \ddot{\alpha} \\ \ddot{\beta} \\ \ddot{\theta} \end{Bmatrix}_G = \begin{bmatrix} 1/m & & & & & \\ & 1/m & & & & \\ & & 1/m & & & \\ & & & 1/I_X & & \\ & & & & 1/I_Y & \\ & & & & & 1/I_Z \end{bmatrix} \begin{Bmatrix} F_X \\ F_Y \\ F_Z \\ M_\alpha \\ M_\beta \\ M_\theta \end{Bmatrix}_G$$

$$\text{or} \quad \{\ddot{X}\}_G = [1/m] \{F\}_G \qquad (A3.1)$$

A3.2 Displacement Transformation from G to P

The point 3 has position coordinates (X_P, Y_3, Z_P) with respect to the centroid as origin.

The displacements at G end P are related by the equation:-

$$\begin{Bmatrix} X \\ Y \\ Z \\ \alpha \\ \beta \\ \theta \end{Bmatrix}_P = \left[\begin{array}{ccc|ccc} 1 & 0 & 0 & 0 & Z_P & -Y_P \\ 0 & 1 & 0 & -Z_P & 0 & X_P \\ 0 & 0 & 1 & Y_P & -X_P & 0 \\ \hline 0 & 0 & 0 & 1 & 0 & 0 \\ 0 & 0 & 0 & 0 & 1 & 0 \\ 0 & 0 & 0 & 0 & 0 & 1 \end{array}\right] \begin{Bmatrix} X \\ Y \\ Z \\ \alpha \\ \beta \\ \theta \end{Bmatrix}_G$$

$$\text{or} \quad \{X\}_P = [T_{PG}] \{X\}_G \qquad (A3.2)$$

Figure A3.1 Principal Axes and Moments of Inertia of Rigid Body

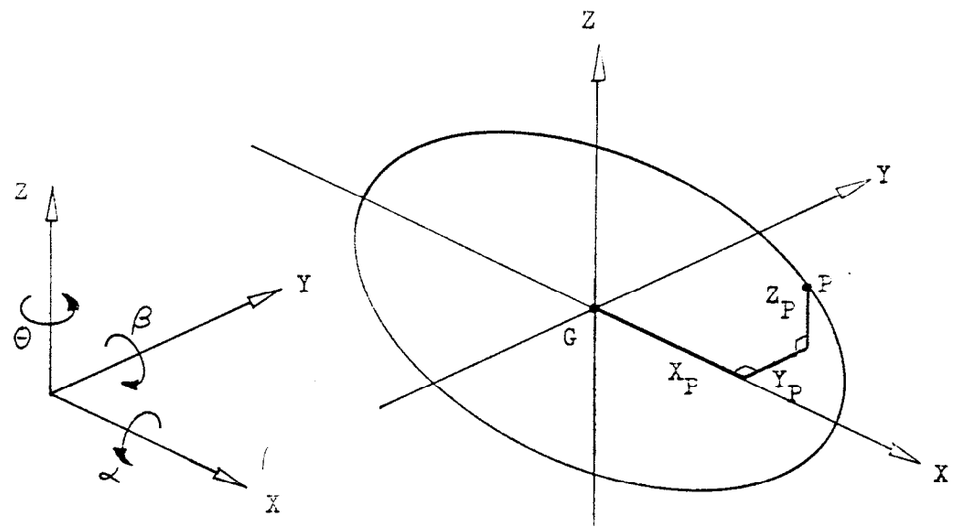

Figure x3.2 Rotation About the X Axis

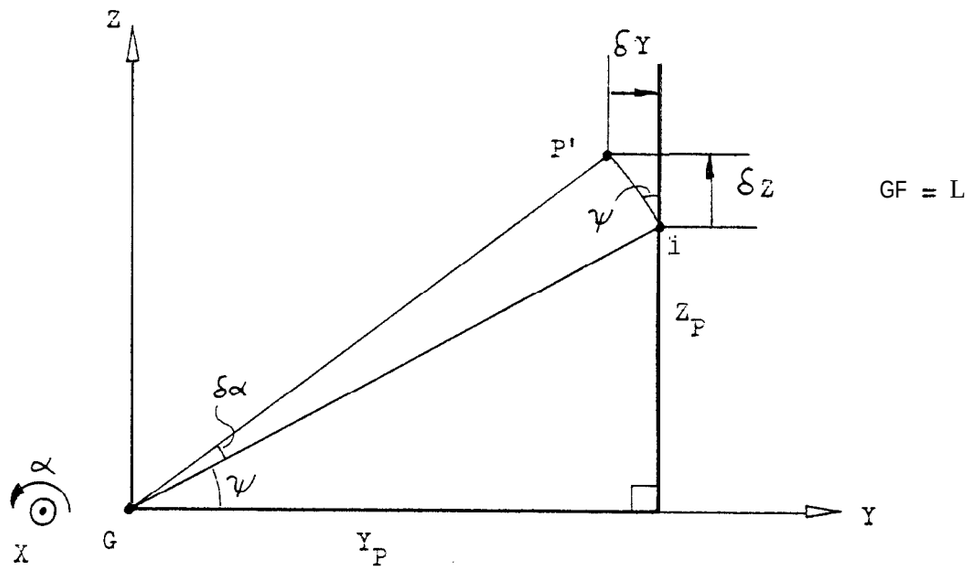

A small rotation $\delta\alpha$ moves P to P', arc length $L\delta\alpha$

$$\delta X = 0$$

$$\delta Y = -L\delta\alpha \sin\psi = -Z_P\,\delta\alpha$$

$$\delta Z = L\delta\alpha \cos\psi = Y_P\,\delta\alpha$$

$$\delta\alpha = = 1\,\delta\alpha$$

$$\delta\beta = 0$$

$$\delta\theta = 0$$

A3.3 Force *Transformation from G to P

There is also a transformation relating the forces at P and G:-

$$\{F\}_G = [U_{GP}] \{F\}_P \qquad (A3.3)$$

The system may be allowed small displacements (δX, SY, ...)G and (SX, δY, δZ, ...)$_P$ and application of the principle of virtual work gives:-

$$(F_X \delta X + F_Y \text{by} + F_Z \delta Z + \ldots)_G = (F_X \delta X + F_Y \delta Y + \ldots)_P$$

or $$\{\delta X\}_G^T \{F\}_G = \{\delta X\}_P^T \{F\}_P \qquad (A3.4)$$

'But $\{\delta X\}_P = [T_{PG}] \{\delta X\}_G$ from (A3.2)

Therefore $$\{\delta X\}_P^T = \{\delta X\}_G^T [T_{PG}]^T \qquad (h3.5)$$

Substitute (A3.3) and (A3.5) in (63.4) to get:-

$$\{\delta X\}_G^T [U_{GP}] \{F\}_P = \{\delta X\}_G^T [T_{PG}]^T \{F\}_P$$

from which it follows that $[U_{GP}] = [T_{PG}]^T$

Thus $$\{F\}_G = [T_{PG}]^T \{F\}_P \qquad (A3.6)$$

Similarly for another point, Q:-

$$\{X\}_Q = [T_{QG}] \{X\}_G \qquad (A3.7)$$

$$\{F\}_G = [T_{QG}]^T \{F\}_Q \qquad (A3.8)$$

A3.4 Responses at P Arising from Forces Applied at Q

The motions at P caused by forces at Q can be obtained by substituting equations (A3.2) and (A3.8) in equation (A3.1) to get:-

$$\{\ddot{X}\}_P = [T_{PG}] \{\ddot{X}\}_G = [T_{PG}] [1/m] [T_{QG}]^T \{F\}_Q = [I_{PQ}] \{F\}_Q \qquad (A3.9)$$

where $[I_{PQ}] = [T_{PG}] [1/m] [T_{QG}]^T$

$[I_{PQ}]$ is a matrix of rigid body inertence terms which is written in full in the following equation:-

$$
\begin{Bmatrix} \ddot{X} \\ \ddot{Y} \\ \ddot{Z} \\ \ddot{\alpha} \\ \ddot{\beta} \\ \ddot{\theta} \end{Bmatrix}_P =
\begin{bmatrix}
\frac{1}{m} + \frac{Z_P Z_Q}{I_Y} + \frac{Y_P Y_Q}{I_Z} & -\frac{Y_P X_Q}{I_Z} & -\frac{Z_P X_Q}{I_Y} & 0 & \frac{Z_P}{I_Y} & -\frac{Y_P}{I_Z} \\
-\frac{X_P Y_Q}{I_Z} & \frac{1}{m} + \frac{Z_P Z_Q}{I_X} + \frac{X_P X_Q}{I_Z} & -\frac{Z_P Y_Q}{I_X} & -\frac{Z_P}{I_X} & 0 & \frac{X_P}{I_Z} \\
-\frac{X_P Z_Q}{I_Y} & \frac{Y_P Z_Q}{I_X} & \frac{1}{m} + \frac{Y_P Y_Q}{I_X} + \frac{X_P X_Q}{I_Y} & \frac{Y_P}{I_X} & -\frac{X_P}{I_Y} & 0 \\
0 & -\frac{Z_Q}{I_X} & \frac{Y_Q}{I_X} & \frac{1}{I_X} & 0 & 0 \\
\frac{Z_Q}{I_Y} & 0 & -\frac{X_Q}{I_Y} & 0 & \frac{1}{I_Y} & 0 \\
-\frac{Y_Q}{I_Z} & \frac{X_Q}{I_Z} & 0 & 0 & 0 & \frac{1}{I_Z}
\end{bmatrix}
\begin{Bmatrix} F_X \\ F_Y \\ F_Z \\ M_\alpha \\ M_\beta \\ M_\theta \end{Bmatrix}
$$

(x3.10)

The first three terms on the leading diagonal of this matrix each have three components. The inertance $(\ddot{X}_P/F_{XQ})$, for example, has components corresponding to three rigid body nodes; one ten involving translation in the X direction, one involving rotation about the Y axis and the third involving rotation about the Z axis.

A3.5es **at** Q in Terns of Responses at P

This reciprocal relationship is of some interest.

Equation (x3.1)

$$\{F\}_G = [m]\{\ddot{X}\}_G \qquad (A3.11)$$

$$\{X\}_Q = [T_{QG}]\{X\}_G \qquad (A3.12)$$

$$\{F\}_G = [T_{QG}]^T\{F\}_Q \qquad (A3.13$$

$$\{F\}_Q = [T_{QG}]^{-T}\{F\}_G$$

$$= [T_{QG}]^{-T}[m][T_{PG}]^{-1}\{\ddot{X}\}_P = [MB]\{\ddot{X}\}_P \qquad (A3.14)$$

where $[MB]$ is a matrix of inertia term.

$$\text{Now} \quad \left[T_{PG}\right]^{-1} = \left[\begin{array}{ccc|ccc} & & & 0 & -Z_P & Y_P \\ & I & & Z_P & 0 & -X_P \\ & & & -Y_P & X_P & 0 \\ \hline & & & & & \\ & 0 & & & I & \end{array}\right] \qquad \text{(A3.15)}$$

$$\left[\begin{matrix} m & & \\ & m & \\ & & m \end{matrix}\right]\left[T_{PG}\right]^{-1} = \left[\begin{array}{ccc|ccc} m & & & 0 & -mZ_P & mY_P \\ & m & & mZ_P & 0 & -mX_P \\ & & m & -mY & mX_P & 0 \\ \hline & & & I_X & & \\ & 0 & & & I_Y & \\ & & & & & I_Z \end{array}\right] \qquad \text{(x3.16)}$$

$$\left[T_{QG}\right]^{-1}\left[\begin{matrix} m & & \\ & m & \\ & & m \end{matrix}\right]\left[T_{PG}\right]^{-1} = \left[\begin{array}{ccc|ccc} & & & & & \\ & I & & & 0 & \\ & & & & & \\ \hline 0 & Z_Q & -Y_Q & & & \\ -Z_Q & 0 & X_Q & & I & \\ Y_Q & -X_Q & 0 & & & \end{array}\right]\left[\begin{array}{ccc|ccc} m & & & 0 & -mZ_P & mY_P \\ & m & & mZ_P & 0 & -mX_P \\ & & m & -mY_P & mX_P & 0 \\ \hline & & & I_X & & \\ & 0 & & & I_Y & \\ & & & & & I_Z \end{array}\right] = \left[MB\right] \qquad \text{(A3.17)}$$

$$\left[MB\right] = \left[\begin{array}{ccc|ccc} m & 0 & 0 & 0 & -mZ_P & mY_P \\ 0 & m & 0 & mZ_P & 0 & -mX_P \\ 0 & 0 & m & -mY_P & mX_P & 0 \\ \hline 0 & mZ_Q & -mY_Q & I_X+m(Z_QZ_P+Y_QY_P) & -mY_Q X_P & -mZ_Q X_P \\ -mZ_Q & 0 & mX_Q & -mX_Q Y_P & I_Y+m(Z_QZ_P+X_QX_P) & -mZ_Q Y_P \\ mY_Q & -mX_Q & 0 & -mX_Q Z_P & -mY_Q Z_P & I_Z+m(Y_QY_P+X_QX_P) \end{array}\right] \qquad \text{(A3.18)}$$

$$= \left[I_{PQ}\right]^{-1} \qquad \text{see (A3.10)}$$

i-3.6 Rigid Body Mode Shapes

The contribution to receptance arising from rigid body motion may be expressed by modifying equation (1.18), setting λ_r equal to zero and substituting s for r:-

$$\alpha_{jk}(\omega) = \sum_{s=1}^{6} \frac{{}_s\phi_j \; {}_s\phi_k}{-\omega^2} \qquad (A3.19)$$

where s corresponds to each of six possible rigid body modes in turn, denoted by X, Y, Z, α, β, θ.

Each term of the form ${}_s\phi_j$ is an element of a mode shape vector ${}_s\{\phi\}$. The suffix j denotes in the general case a coordinate which is one of the six possible coordinates of one of the points of interest. Initially, we k-ill consider only one point, such as F in Figure A3.1, and express the 'mode shape' of elements at P :-

$$\{\phi\}_P = \begin{Bmatrix} X_P \\ Y_P \\ Z_P \\ \alpha \\ \beta \\ \theta \end{Bmatrix} \qquad (x3.20)$$

In the rigid body mode involving translation along the X axis all displacements are zero except the first. The mode shape vector related to point P is thus:

$${}_X\{\phi\}_P = C_x \begin{Bmatrix} 1 \\ 0 \\ 0 \\ 0 \\ 0 \\ 0 \end{Bmatrix} \qquad (A3.21)$$

where C_x is a scaling factor.

Equation (A3.3) can be transposed:

$$ {}_X\{\phi\}_P^T = C_x \{1 \quad 0 \quad 0 \quad 0 \quad 0 \quad 0\} \qquad (A3.22) $$

Similar equations apply to translations along the other axes:

$$ {}_Y\{\phi\}_P^T = C_y \{0 \quad 1 \quad 0 \quad 0 \quad 0 \quad 0\} \qquad (A3.23) $$

$$ {}_Z\{\phi\}_P^T = C_z \{0 \quad 0 \quad 1 \quad 0 \quad 0 \quad 0\} \qquad (A3.24) $$

The rotational rigid body modes are a little more complicated. Consider, for example; a small rotation α about the X axis as sketched in Figure h3.2.

It can be seen that in addition to α, the coordinates Y and Z are affected by the rotation whose mode shape is given by:

$$ {}_\alpha\{\phi\}_P^T = C_\alpha \{0 \quad -Z_P \quad Y_P \quad 1 \quad 0 \quad 0\} \qquad (A3.25) $$

Similar geometric considerations lead to the equations:

$$ {}_\beta\{\phi\}_P^T = C_\beta \{Z_P \quad 0 \quad -X_P \quad 0 \quad 1 \quad 0\} \qquad (A3.26) $$

and

$$ {}_\theta\{\phi\}_P^T = C_\theta \{-Y_P \quad X_P \quad 0 \quad 0 \quad 0 \quad 1\} \qquad (A3.27) $$

A3.7 Normalisation

Normalisation may be carried out by rewriting equation (1.8):-

$$ [\Phi]_P^T [MB]_P [\Phi]_P = [I] \qquad (A3.28) $$

in which $[\Phi]_P$ is the ensemble of the rigid-body mode shape vectors above and $[MB]_P$ is the matrix of inertia terms of equation (A3.18) with Q = P, for the case of point excitation.

The multiplication of the LHS of equation (k3.28) gives a diagonal matrix with elements of the form mC_x^2.

It follows that:- $C_x = C_y = C_z = 1/\sqrt{m}$ (A3.29)

and $C_\alpha = 1/\sqrt{I_X}$, $C_\beta = 1/\sqrt{I_Y}$, $C_\theta = 1/\sqrt{I_Z}$ (A3.30)

A3.8 Normalised Rigid Body Mode Shapes

The sir node shapes related to point P are:

Mode X Y Z

$$ {}_X\{\phi\}_P = \frac{1}{\sqrt{m}}\begin{Bmatrix}1\\0\\0\\0\\0\\0\end{Bmatrix}, \quad {}_Y\{\phi\}_P = \frac{1}{\sqrt{m}}\begin{Bmatrix}0\\1\\0\\0\\0\\0\end{Bmatrix}, \quad {}_Z\{\phi\}_P = \frac{1}{\sqrt{m}}\begin{Bmatrix}0\\0\\1\\0\\0\\0\end{Bmatrix} $$

Mode α β θ

$$ {}_\alpha\{\phi\}_P = \frac{1}{\sqrt{I_X}}\begin{Bmatrix}0\\-Z_P\\Y_P\\1\\0\\0\end{Bmatrix}, \quad {}_\beta\{\phi\}_P = \frac{1}{\sqrt{I_Y}}\begin{Bmatrix}Z_P\\0\\-X_P\\0\\1\\0\end{Bmatrix}, \quad {}_\theta\{\phi\}_P = \frac{1}{\sqrt{I_Z}}\begin{Bmatrix}-Y_P\\X_P\\0\\0\\0\\1\end{Bmatrix} \qquad (A3.31) $$

A3.9 Modal Constants

The 6 x 6 matrices of modal constants relating two points P and Q can be written using equation (2.24) ES follows:

$$ {}_X[A]_{PQ} = \frac{1}{m}\begin{Bmatrix}1\\0\\0\\0\\0\\0\end{Bmatrix}\{1\ 0\ 0\ 0\ 0\ 0\} = \frac{1}{m}\begin{bmatrix}1&&&&&\\&0&&&&\\&&0&&&\\&&&0&&\\&&&&0&\\&&&&&0\end{bmatrix} \qquad (A3.32) $$

Similarly,

$$ {}_Y[A]_{PQ} = \frac{1}{m}\begin{bmatrix}0&&&&&\\&1&&&&\\&&0&&&\\&&&0&&\\&&&&0&\\&&&&&0\end{bmatrix} \qquad (A3.33) $$

and

$$ {}_Z[A]_{PQ} = \frac{1}{m}\begin{bmatrix}0&&&&&\\&0&&&&\\&&1&&&\\&&&0&&\\&&&&0&\\&&&&&0\end{bmatrix} \qquad (A3.34) $$

For the rotational nodes:

$$\alpha[A]_{PQ} = \frac{1}{I_X} \begin{Bmatrix} 0 \\ -Z_P \\ -Y_P \\ 1 \\ 0 \\ 0 \end{Bmatrix} \{0 \quad -Z_Q \quad Y_Q \quad 1 \quad 0 \quad 0\} = \frac{1}{I_X} \begin{bmatrix} 0 & & & & & \\ 0 & 0 & 0 & 0 & 0 & 0 \\ 0 & Z_P Z_Q & -Z_P Z_Q & -Z_P & 0 & 0 \\ 0 & -Y_P Z_Q & Y_P Y_Q & Y_P & 0 & 0 \\ 0 & -Z_Q & Y_Q & 1 & 0 & 0 \\ 0 & 0 & 0 & 0 & 0 & 0 \\ 0 & 0 & 0 & 0 & 0 & 0 \end{bmatrix}$$

(A3.35)

and

$$\beta[A]_{PQ} = \frac{1}{I_Y} \begin{Bmatrix} Z_P \\ 0 \\ -X_P \\ 0 \\ 1 \\ 0 \end{Bmatrix} \{Z_Q \quad 0 \quad -X_Q \quad 0 \quad 1 \quad 0\} = \frac{1}{I_Y} \begin{bmatrix} Z_P Z_Q & 0 & -Z_P X_Q & 0 & Z_P & 0 \\ 0 & 0 & 0 & 0 & 0 & 0 \\ -X_P Z_Q & 0 & X_P X_Q & 0 & -X_P & 0 \\ 0 & 0 & 0 & 0 & 0 & 0 \\ Z_Q & 0 & -X_Q & 0 & 1 & 0 \\ 0 & 0 & 0 & 0 & G & 0 \end{bmatrix}$$

(A3.36)

and

$$\theta[A]_{PQ} = \frac{1}{I_Z} \begin{Bmatrix} -Y_P \\ X_P \\ 0 \\ 0 \\ 0 \\ 1 \end{Bmatrix} \{-Y_Q \quad X_Q \quad 0 \quad 0 \quad 0 \quad 1\} = \frac{1}{I_Z} \begin{bmatrix} Y_P Y_Q & -Y_P Y_Q & 0 & 0 & 0 & -Y_P \\ -X_P Y_Q & X_P X_Q & 0 & 0 & 0 & X_P \\ 0 & 0 & 0 & 0 & 0 & 0 \\ 0 & 0 & 0 & 0 & 0 & 0 \\ 0 & 0 & 0 & 0 & 0 & 0 \\ -Y_Q & X_Q & 0 & 0 & 0 & 1 \end{bmatrix}$$

(A3.37)

The total array of modal constants is given by:

$$[A]_{PQ} = X[A]_{PQ} + Y[A]_{PQ} + Z[A]_{PQ} + \alpha[A]_{PQ} + \beta[A]_{PQ} + \theta[A]_{PQ}$$

(A3.38)

It can be seen that:

$$[A]_{PQ} = [I_{PQ}] \quad \text{of equation (A3.10)}$$

It should be remembered thet all the elements of these matrices express transfer relationships between points P and Q.

A3.10 Example: Rigid Body Mode Shapes of Long Beam

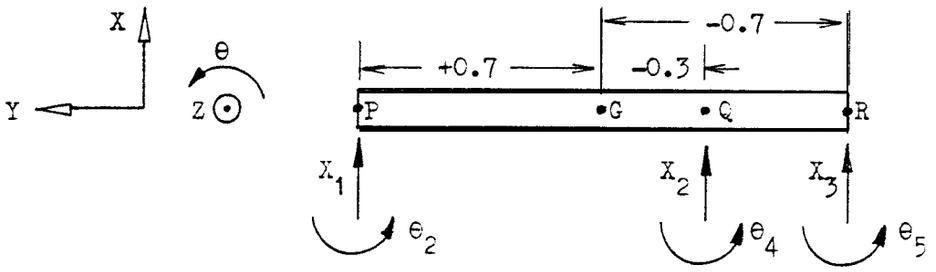

The beam has mass m =8.74 kg ; $1/\sqrt{m}$ = **0.3382** $kg^{-\frac{1}{2}}$

The centroidel mass moment of inertia is:

$$I_Z = 8.74\,(1.4)^2/12 = \mathbf{1.428}\ kgm^2\ ;\quad \mathbf{1}/\sqrt{I_Z} = \mathbf{0.6370}\ kg^{-\frac{1}{2}}\ m^{-1}$$

The translational rigid body mode referred **to** X, **6** coordinates at points P, Q and R is given by:

$$X\{\phi\} = \frac{1}{\sqrt{m}}\begin{Bmatrix}1\\0\\1\\0\\1\\0\end{Bmatrix} = \begin{Bmatrix}0.3382\\0\\0.3382\\0\\0.3382\\0\end{Bmatrix}$$

and for the rotational rigid body mode:

$$\theta\{\phi\} = \frac{1}{\sqrt{I_Z}}\begin{Bmatrix}-Y_P\\1\\-Y_Q\\1\\-Y_R\\1\end{Bmatrix} = \mathbf{0.8370}\begin{Bmatrix}-0.7\\1\\+0.3\\1\\+0.7\\1\end{Bmatrix} = \begin{Bmatrix}-.5859\\\mathbf{.E370}\\.2511\\.8370\\.5859\\.8370\end{Bmatrix}$$

These vectors correspond closely with those in Table 4.9(e).

Appendix A4 Notes on Truncated-Data Matrices

It was pointed out in section 3.3.2 that the truncated mode shape matrix had elements close in value to the corresponding part of the full $[\Phi]$ matrix. The following development, arising from a formulation in reference (79), is based on a partitioned $[\Phi]$ matrix and shows how the truncated $[\Phi]$ matrix leads to mass and stiffness matrices with no zero elements and with negative off-diagonal mass values.

Mass Matrices

We have already established:-

$$[\Phi]^T[M][\Phi] = [I] \tag{1.8}$$

and

$$[M] = [\Phi]^{-T}[\Phi]^{-1} \tag{1.12}$$

Suppose that of the total number of modes n a number r were measurable, giving a mode shape matrix $[\Phi_{rr}]$ of size r x r.

A mass matrix $[M^*]$ could be calculated:-

$$[M^*] = [\Phi_{rr}]^{-T}[\Phi_{rr}]^{-1} \tag{44.1}$$

The matrix $[\Phi_{rr}]$ is the left upper partition of the complete matrix $[\Phi]$. The truncated-data mode shape matrices calculated in section 3.3.2 are similar to, but not identical with, the left upper portions of the corresponding complete matrices. However, the similarity is near enough for the analysis below to be relevant.

Equation (1.6) can be written:-

$$\left[\begin{array}{c|c} \Phi_{rr}^T & \Phi_{nr}^T \\ \hline \Phi_{rn}^T & \Phi_{nn}^T \end{array}\right]\left[\begin{array}{c|c} M_{rr} & 0 \\ \hline 0 & M_{nn} \end{array}\right]\left[\begin{array}{c|c} \Phi_{rr} & \Phi_{rn} \\ \hline \Phi_{nr} & \Phi_{nn} \end{array}\right] = \left[\begin{array}{c|c} I & 0 \\ \hline 0 & I \end{array}\right] \tag{A4.2}$$

giving

$$\left[\begin{array}{c|c} \Phi_{rr}^T & \Phi_{nr}^T \\ \hline \Phi_{rn}^T & \Phi_{nn}^T \end{array}\right]\left[\begin{array}{c|c} M_{rr}\Phi_{rr} & M_{rr}\Phi_{rn} \\ \hline M_{nn}\Phi_{nr} & M_{nn}\Phi_{nn} \end{array}\right] = \left[\begin{array}{c|c} I & 0 \\ \hline 0 & I \end{array}\right] \tag{A4.3}$$

Evaluating the submatrix in the first row, first column:-

$$[\Phi_{rr}]^T[M_{rr}][\Phi_{rr}] + [\Phi_{nr}]^T[M_{nn}][\Phi_{nr}] = [I] \tag{A4.4}$$

Premultiplying by $[\Phi_{rr}]^{-T}$ and postmultiplying by $[\Phi_{rr}]^{-1}$ and using equation (h4.1) we get:-

$$[K^*] = [\Phi_{rr}]^{T}[\Phi_{rr}]^{-1} = [M_{rr}] + [\Phi_{rr}]^{-T}[\Phi_{nr}]^{T}[K_{nn}][\Phi_{nr}][\Phi_{rr}]^{-1} \quad (A4.5)$$

Write $[\Phi_{nr}][\Phi_{rr}]^{-1} = [\theta]$ of order (n-r) x (r) (A4.6)

Then $[\theta]^{T} = [\Phi_{rr}]^{-T}[\Phi_{nr}]^{T}$ of order (r) x (n-r) (A4.7)

Thus equation (A4.5) becomes:-

$$[K^*] = [K_{rr}] + [\theta]^{T}[K_{nn}][\theta] \quad (A4.8)$$

The matrices $[\Phi_{rr}]$ and $[\Phi_{nr}]$ are in general fully populated, although they may have certain elements zero. They are, in principle, measurable even if limited frequency range means that only r modes can be measured since the number of measurement points need not be limited to coincide with the number of measured modes. It follows that the matrices $[\theta]$ and $[\theta]^{T}[K_{nn}][\theta]$ will also be fully populated with elements of either sign. It is thus to be expected that the matrix K_{ij}^* arising out of truncated data calculations will be fully populated and have some negative values.

It is clear also from equation (A4.8) that $[K^*]$ contains information about the total mass of the system since it features both $[M_{rr}]$ and $[K_{nn}]$.

Stiffness Matrices

For an undamped system we my write equation (1.12) : -

$$[\Phi]^{T}[K][\Phi] = [\omega_r^{2}] \quad (A4.9)$$

and

$$[K] = [\Phi]^{-T}[\omega_r^{2}][\Phi]^{-1} \quad (2.48)$$

Using $[\Phi_{rr}]$ to denote the truncated mode shape matrix of the previous section we can define:-

$$[K^*] = [\Phi_{rr}]^{-T}[\omega_{rr}^{2}][\Phi_{rr}] \quad (A4.10)$$

Equation (A4.9) may be written in partitioned form:-

$$\left[\begin{array}{c|c} \Phi_{rr}^T & \Phi_{nr}^T \\ \hline \Phi_{rn}^T & \Phi_{nn}^T \end{array}\right] \underbrace{\left[\begin{array}{c|c} K_{rr} & K_{rn} \\ \hline K_{nr} & K_{nn} \end{array}\right] \left[\begin{array}{c|c} \Phi_{rr} & \Phi_{rn} \\ \hline \Phi_{nr} & \Phi_{nn} \end{array}\right]}_{\left[\begin{array}{c|c} (K_{rr}\Phi_{rr} + K_{rn}\Phi_{nr}) & (K_{rr}\Phi_{rn} + K_{rn}\Phi_{nn}) \\ \hline (K_{nr}\Phi_{rr} + K_{nn}\Phi_{nr}) & (K_{nr}\Phi_{rn} + K_{nn}\Phi_{nn}) \end{array}\right]} = \left[\begin{array}{c|c} \omega_{rr}^2 & 0 \\ \hline 0 & \omega_{nn}^2 \end{array}\right] \qquad \text{(A4.11)}$$

Again, evaluating the submatrix of the first row, first column :-

$$\left[\Phi_{rr}\right]^T\left[K_{rr}\right]\left[\Phi_{rr}\right] + \left[\Phi_{rr}\right]^T\left[K_{rn}\right]\left[\Phi_{nr}\right] + \left[\Phi_{nr}\right]^T\left[K_{nr}\right]\left[\Phi_{rr}\right] + \left[\Phi_{nr}\right]^T\left[K_{nn}\right]\left[\Phi_{nr}\right] = \left[\omega_{rr}^2\right] \qquad \text{(A4.12)}$$

As before, premultiply by $\left[\Phi_{rr}\right]^{-T}$ and postmultiply by $\left[\Phi_{rr}\right]^{-1}$ to get, after substitution of $\left[\theta\right] = \left[\Phi_{nr}\right]\left[\Phi_{rr}\right]^{-1}$ we can obtain, using equation (A4.10) :

$$\left[K^*\right] = \left[K_{rr}\right] + \left[K_{rn}\right]\left[\theta\right] + \left[\theta\right]^T\left[K_{nr}\right] + \left[\theta\right]^T\left[K_{nn}\right]\left[\theta\right] \qquad \text{(kS.13)}$$

This equation is rather more complicated than (A4.5), but it has similar features. The matrix $\left[K^*\right]$ will have non-zero terms corresponding to zeroes of the original $\left[K\right]$ and it has contributions from all elements of the original $\left[K\right]$.

Check Calculations

Three calculations using program EMMAY were made using as input, first the complete rode shape matrix $\left[\Phi\right]$ and then corresponding truncated natrices $\left[\Phi_{44}\right]$ and $\left[\Phi_{33}\right]$. Thedata,of6 figure accuracy, were that of the exact rode shape matrix of the Asymmetrical Grounded System 2 s presented in Table 3.1(e). The results are shown in Table A4.1.

Table A4.1

r	5	4	3
ΣM	5.99998	**5.33567**	27.5200
ΣK	0.999997	1 ● 00092	**9.41451** x 10^6

where ΣM is the summation of all elements of the mass netrix

ΣK is the summation of all elements of the stiffness matrix

The closeness of the figures of the second column to those of the first is remarkable, leading one to suspect that the equivalence could be proved. Extensive algebra, not shown here, fails to produce such proof and the figures of the third column indicate very forcibly that such proof is impossible. There may be, however, a criterion of goodness of a cosmodel in terms of the nearness of ΣM to the system total mass.

APPENDIX A5 A Note on NORMS

A5.1 The Norm of a Vector

This is a single, real, not-negative number written $\|x\|$. It is a measure of the 'length' or size of a vector $\{x\}$.

According to Albasiny [80] it has the following properties:-

$$\|x\| > 0 \quad \text{if } x \neq 0\,, \quad \|0\| = 0, \quad \text{etc.}$$
$$\|cx\| = |c|\|x\| \quad \text{where c is a scalar} \tag{A5.1}$$
$$\|x + y\| \leq \|x\| + \|y\|$$

from which it may be deduced that:

$$\|x - y\| \geq \left|\|x\| - \|y\|\right| \tag{A5.2}$$

The general case is expressed by the Hölder norm:

$$\|x\|_k = \left[\sum_{i=1}^{N} |x_i|^k\right]^{1/k} \quad \text{for } (k \geq 1) \tag{A5.3}$$

where x_i is the i^{th} component of vector $\{x\}$ which has N elenents.

The three most common rector norm follow by substituting k = 1, 2, ∞ in (A5.3).

$$\left.\begin{aligned} \|x\|_1 &= |x_1| + |x_2| + \ldots |x_N| \\ \|x\|_2 &= (|x_1|^2 + |x_2|^2 + \quad |x_N|^2)^{\frac{1}{2}} \\ \|x\|_\infty &= \text{maximum } |x_i| \end{aligned}\right\} \tag{A5.4}$$
$$i = 1, 2, \ldots N$$

The second of these is the Euclidean norm which could be written:

$$\|x\|_E = \|x\|_2 = (x_1^2 + x_2^2 + \quad x_N^2)^{\frac{1}{2}} = (\{x\}^T\{x\})^{\frac{1}{2}} \tag{A5.5}$$

This definition (A5.5)is compatible with those of Strang [78], Bishop et al. [5] and Conte [97].

65.2 The Norm of a Matrix

Again this is a number intended to express the 'size' of a matrix. According to Albasiny [80], the nom of $[A]$ is $\|A\|$ which nay be substituted for $\|x\|$ in equations (Z.5.1) and (X5.2). Additionally, matrix noms satisfy the inequality:

$$\|AB\| \leq \|A\| \quad \|B\| \tag{X5.6}$$

Vector and matrix norms are related by the compatibility condition:

$$\|Ax\| \leq \|A\| \quad \|x\| \tag{x5.7}$$

Each vector nom has an associated matrix nom:

$$\|A\|_1 = \max_j \sum_{i=1}^{N} |a_{ij}|$$

$$\|A\|_2 = (\text{maximum eigenvalue of } [A]^H[A])^{\frac{1}{2}} \tag{A5.8}$$

$$\|A\|_\infty = \max_i \sum_{j=1}^{N} |a_{ij}|$$

where $[A]^H$ is the Hermitian conjugate of $[A]$ and a_{ij} is the (i,j) elenent of $[A]$ which has N^2 elenects.

$\|A\|_2$ is the 'spectral nom' of $[A]$ and is difficult to compute.

The Euclidean norm is given by:

$$\|A\|_E = \left(\sum_{i=1}^{N} \sum_{j=1}^{N} |a_{ij}|^2 \right)^{\frac{1}{2}} \tag{A5.9}$$

and is easy to compute. Although it can be up to N^2 times bigger than $\|A\|_2$ it does obey ecuetion (A5.7), which could be written:

$$\|Ax\|_2 \leq \|A\|_E \quad \|x\|_2 \tag{A5.10}$$

Strang [78] uses a related equation in his definition of the norm of a matrix:

$$\|A\| = \max_{x \neq 0} \frac{\|Ax\|}{\|x\|} \tag{A5.11}$$

He defines a 'condition number': $c = \|A\| \|A^{-1}\|$ (45.12)

which indicates the amount of round-off errors in the inversion of $[A]$.

If $[A]$ is symmetric positive definite then the condition number may be simply defined as a ratio of smallest and largest eigenvalues:

$$c = \lambda_N/\lambda_1 = \lambda_{max}/\lambda_{min} \qquad (A5.13)$$

No. of sig. figs. lost in inversion $\simeq \log_{10} c$ (A5.14)

He comments that the determinant of a cstrix is a terrible (sic) measure of ill-conditioning.

A5.3 The Norm of a Determinant of a Matrix

Conte [97] observes that an indicator of ill-conditioning is the 'smallness' of the determinant of the matrix, but realises that 'small' is defined only in a relative sense. He suggests that the determinant can **be** normalised by dividing each row by its length.

Thus $x_k = (a_{k1}^2 + a_{k2}^2 + \quad + a_{kN}^2)^{\frac{1}{2}}, k = 1,2 \quad N$ (A5.15)

is the length of the k^{th} row

$$\text{and Norm } |A| = \begin{vmatrix} a_{11}/x_1 & a_{12}/x_1 \cdots & a_{1N}/x_1 \\ a_{21}/x_2 \ldots & & \\ \ldots\ldots & & \\ a_{N1}/x_N \ldots\ldots & & a_{NN}/x_N \end{vmatrix} = \frac{|A|}{x_1\, x_2 \cdots x_N} \qquad (A5.16)$$

where $-1 \leqslant \text{Norm } |A| \leqslant +1$

A matrix $[A]$ is then seid to be ill-conditioned if Norm $|A|$ is small compared to unity.

This norm is used by Sainsbury in the program COUPLE1 [21] and by **the** author in Chapter 7 in the search for cantilever frequencies of a turbine blade.

Thereseemsto be no reedy relationship between this norm of the determinant and the differently defined norm of the associated matrix.

$$\text{if } [A] = \begin{bmatrix} a_{11} & a_{12} \\ a_{21} & a_{22} \end{bmatrix}, \text{then} \begin{cases} x_1 = \sqrt{a_{11}^2 + a_{12}^2} \\ x_2 = \sqrt{a_{21}^2 + a_{22}^2} \end{cases}$$

$$\text{Norm } |A| = \frac{(a_{11}\, a_{22} - a_2\, a_{12})}{x_1\, x_2} \leqslant 1$$

$$\text{whereas } \|A\|_E = \sqrt{x_1^2 + x_2^2}$$

APPENDIX A5 Published Paper

Bulletin 45
(Part 5 of 5 Parts)

REPRINTED FROM

THE SHOCK AND VIBRATION BULLETIN

JUNE 1975

A Publication of
THE SHOCK AND VIBRATION
INFORMATION CENTER
Naval Research Laboratory, Washington, D.C.

Office of
The Director of Defense
Research and Engineering

EXPERIMENTAL DETERMINATION OF MULTIDIRECTIONAL MCBILITY DATA FOR BEAMS

D. J. Ewins,
Imperial College of Science and Technology,
London, England

and

P. T. Gleeson,
Middlesex Polytechnic and Imperial College,
London, England

When mobility data is to be used for prediction Of the vibration properties of coupled structures, it is necessary to consider all tne directions of vibration which are significant at each coupling point. In particular, when analysing beam-like structures it is necessary to include both translational and rotational nobilities. Often it is necessary to obtain such data by experiment and although techniques are established for measuring translational vibration, it is difficult to measure rotational mobilities with sufficient accuracy. A method is presented here which enabies the required rotational mobilities to be derived from measurements of translational mobilities. Results show that derivation of rotational data is more accurate than direct measurement, especially at low frequencies.

1. INTRODUCTION

When a complete structure is analysed in order to predict its vibration characteristics, it is usually more convenient to break that structure down into its basic component parts. Each of these may then be analysed individually in as much (or as little) detail as its complexity demands. An analytical model of the complete structure may then be generated by combining all the individual component analyses using an impedance or mobility coupling process.

However, it is often found that some of the components in engineering structures are not amenable to (or even defy) theoretical analysis. In this case, in order to make an analysis of the complete structure, recourse may be made to experimental measurement of the necessary data. This situation is often encountered when using non-metallic components (rubber or polymers), or when attaching additional components onto an existing and complex structure such as an air-frame or a bulkhead in a ship. If such a procedure is to be undertaken Successfully, very careful consideration must be given to the choice of (a) which mobility data should be measured, and (b) how these may be obtained accurately. The main limitation of conventional mobility or impedance measuring techniques is that they consider motion in one translational direction only, while practical structures usually vibrate in several directions simultaneously (translational and rotational).

Previous work (1) has illustrated this basic problem and presented 2 method for measuring the type of multi-directional mobility data which may be required. The results were encouraging, although not perfect, but the measurement method was difficult 2nd relatively lengthy. Another, similar, method fcr measuring such comprehensive mobility data has been reported (2), but this also is fairly complex.

Further work has now been undertaken with the objectives of deveicsing the measurement technique described in (1): (a) by applying it to a wider variety of structures, in particular to smaller ones; (b) by improving the accuracy of the measured data; and (c) by simplifying tne procedure so that it may be undertaken with conventional impedance testing equipment.

The present paper describes this development.

2. CASE STUDY

As previously, a specific example was chosen with wnich to test and demonstrate the various aspects of the measurement method. A very simple structure was selected - a uniform steel beam, C, which wasformed by joining two different uniform beams A and B, end to end. The experiment consisted of:

(i) measuring the tip mobility data for beam A; ;

(ii) measuring similar data for beam B;

(iii) using the above data to predict the properties of the combined beam C, and then comparing these with the actual properties.

The underlying philosophy of this experiment was that unless such a simple system as that described above could be measured and analysed successfully, there was little point in attempting to apply such techniques.to more complex practical structures.

Chosen Beams

It was decided to use steel beams of rectangular cross section for the test pieces so that the theoretical mobility values could be readily calculated. Steel was selected because of its availability and also because, being very lightly damped, it would offer a wide dynamic range of response and thus tax the measurement system. Several considerations were made in deciding upon the dimensions of the two beams. As mentioned above, one object of this study was to test the basic multi-directional mobility measurement technique on smaller components than previously. Also, there were frequency constraints to be imposed in order to keep within the range in wnich accurate measurements. could be reliably expected. This range had a lower bound of 50 Hz (mains frequency) and an upper one of about 1000 Hz, above which transducers and drive rods can begin to cause problems. Tnus the decade 80 - 800 Hz was selected as the 'central' frequency range.

The beams were to be tested in a free-free configuration; this naving boundary conditions which can be most closely achieved in an experiment. The longer of the two beams was chosen with a section of 25 mm x 31 mm and a length of 1.4 m. For bending vibration in its stiffer plane (i.e. with 31 mm as the thickness), this beam has calculated natural frequencies at 86, 237, 464 and 767 Hz. The shorter beam was chosen to have the same cross section and a length of 0.65 m. This beam has its first two natural frequencies at 399 and 1100 Hz, deliberately chosen so as not to coincide with those of the long beam.

3. DIRECT MEASUREMENT OF MOBILITY DATA

Basic Measurement Method

The response of the test piece tc a harmonic input force and a harmonic couple M, applied at point P, are the velocity $\dot{X}$ and the angular velocity $\dot{\theta}$.

These are related by the mobility equation:-

$$\begin{Bmatrix} \dot{X} \\ \dot{\theta} \end{Bmatrix} = \begin{bmatrix} \frac{\dot{X}_f}{F} & \frac{\dot{X}_m}{M} \\ \frac{\dot{\theta}_f}{F} & \frac{\dot{\theta}_m}{M} \end{bmatrix} \begin{Bmatrix} F \\ M \end{Bmatrix} = \begin{bmatrix} Y_{xx} & Y_{x\theta} \\ Y_{\theta x} & Y_{\theta\theta} \end{bmatrix} \begin{Bmatrix} F \\ M \end{Bmatrix}$$

or

$$\{\dot{X}\} = [Y]\ \{F\} \qquad (1)$$

In general, F and M are complex quantities incorporating both magnitude and phase information of steady-state sinusoids and it follows that $\dot{X}$, $\dot{\theta}$ and all four elements of the mobility matrix, $[Y]$, are also complex,

For measurement of these mobility data, the inputs F and M are applied to the structure by an 'exciting block' which is fixed to the test piece at P and which enabies F, M and the responses $\dot{X}$ and $\dot{\theta}$ to be deduced from the outputs of accelerometers mounted symmetrically on the block. See Fig. 1.

The responses $\ddot{X}$ and $\ddot{\theta}$ at point P are related to the accelerations a_A and a_B measured by the accelerometers by the equations:-

$$\ddot{X} = (a_A + a_B)/2, \quad \ddot{\theta} = (a_A - a_B)/2s$$

where s is the distance of offset of each accelerometer from P.

These equations may be expressed as a matrix equation:

$$\begin{Bmatrix} \ddot{X} \\ \ddot{\theta} \end{Bmatrix} = \begin{bmatrix} 1/2 & 1/2 \\ 1/2s & -1/2s \end{bmatrix} \begin{Bmatrix} a_A \\ a_B \end{Bmatrix}$$

or

$$\{\ddot{X}\} = [T]\ \{a\} \qquad (2)$$

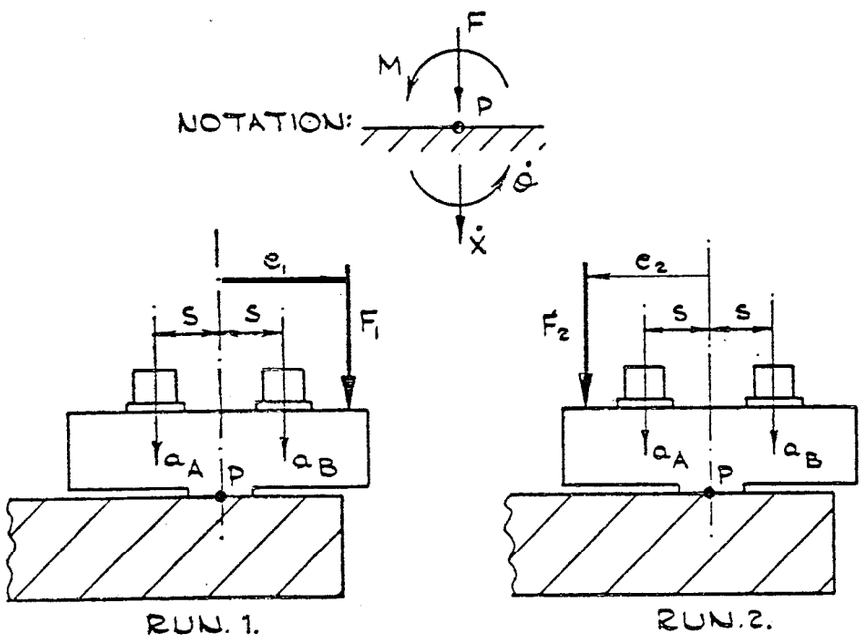

FIG.1. BASIC MEASUREMENT CONFIGURATION.

Data are obtained in each of two test runs at a discrete number of frequencies. In Run 1 a force F_1 is applied to the block at a point offset a distance e_1 from P, and in Run 2 a force F_2 is applied at a point which is a distance e_2 from P. (e_1 and e_2 need not be symmetrical about P).

The coordinate system has X positive downwards and θ positive anti-clockwise. Since F and M are the force and couple inputs applied to the test piece at P, their relationship to F_1 and F_2 can be determined by regarding the exciting block as a free body with an input F_1 or F_2 above the block and $-F$, $-M$ input at P (See Fig. 1).

Thus, in Run 1, resolving vertical forces:

$$F_1 - F = m\ddot{X}_1$$

and taking moments about P:

$$e_1 F_1 - M = I_p\ddot{\theta}_1$$

where m is the mass of the block (including accelerometers) and I_p its moment of inertia about P.

Thus: $$\begin{Bmatrix} F \\ M \end{Bmatrix} = \begin{Bmatrix} F_1 - m\ddot{X}_1 \\ e_1 F_1 - I_p\ddot{\theta}_1 \end{Bmatrix}$$

Equation (1) may now be rewritten as:

$$\begin{Bmatrix} \dot{X}_1 \\ \dot{\theta}_1 \end{Bmatrix} = [Y] \begin{Bmatrix} F_1 - m\ddot{X}_1 \\ e_1 F_1 - I_p\ddot{\theta}_1 \end{Bmatrix}$$

Dividing through by F_1 and writing $\ddot{X}/j\omega = \dot{X}$; $\ddot{\theta}/j\omega = \dot{\theta}$ we get:

$$1/j\omega \begin{Bmatrix} (\ddot{X}/F)_1 \\ (\ddot{\theta}/F)_1 \end{Bmatrix} = [Y] \begin{Bmatrix} 1 - m(\ddot{X}/F)_1 \\ e_1 - I_p(\ddot{\theta}/F)_1 \end{Bmatrix} \quad (3)$$

Similarly for Run 2:

$$1/j\omega \begin{Bmatrix} (\ddot{X}/F)_2 \\ (\ddot{\theta}/F)_2 \end{Bmatrix} = [Y] \begin{Bmatrix} 1 - m(\ddot{X}/F)_2 \\ e_2 - I_p(\ddot{\theta}/F)_2 \end{Bmatrix} \quad (4)$$

Combining (3) and (4):

$$1/j\omega \begin{bmatrix} (\ddot{X}/F)_1 & (\ddot{X}/F)_2 \\ (\ddot{\theta}/F)_1 & (\ddot{\theta}/F)_2 \end{bmatrix} =$$

$$[Y]\left(\begin{bmatrix}1 & 1\\ e_1 & e_2\end{bmatrix}-\begin{bmatrix}m & 0\\ 0 & I_p\end{bmatrix}\begin{bmatrix}(\ddot{X}/F)_1 & (\ddot{X}/F)_2\\ (\ddot{\theta}/F)_1 & (\ddot{\theta}/F)_2\end{bmatrix}\right) \quad (5)$$

We may write $\begin{bmatrix}1 & 1\\ e_1 & e_2\end{bmatrix} = [T]$, a transformation matrix.

and $\begin{bmatrix}m & 0\\ 0 & I_p\end{bmatrix} = [M]$, a matrix of block inertial properties

Using equation (2), we have:

$$\begin{bmatrix}(\ddot{X}/F)_1 & (\ddot{X}/F)_2\\ (\ddot{\theta}/F)_1 & (\ddot{\theta}/F)_2\end{bmatrix} = [T]\begin{bmatrix}(a_A/F)_1 & (a_A/F)_2\\ (a_B/F)_1 & (a_B/F)_2\end{bmatrix}$$

$$\text{or} \quad [In] = [T]\,[In_m] \quad (6)$$

where $[In]$ is a matrix of Inertance quantities

and $[In_m]$ is the matrix of those Inertance quantities which are measured experimentally.

Thus equation (5) may be rewritten:-

$$1/j\omega[T][In_m] = [Y]([\mathrm{I}]-[M][T][In_m])$$

$$\text{and so } [Y] = 1/j\omega[T][In_m]\,([\mathrm{I}]-[M][T][In_m])^{-1} \quad (7)$$

The required matrix of mobility parameters is obtained here in terms of $[T]$, $[\mathrm{I}]$ and $[M]$ which are constant for a given test configuration, together with $[In_m]$ which incorporates data measured at angular frequency ω in the two test runs. The resulting mobility data, $[Y]$, has thus been fully corrected to account for the mass and inertia of the added block and transducers.

Measuring System

The experiments reported here were carried out using a digital transfer function analyser (DTFA) interfaced with a mini-computer, together constituting a system capable of handling the large amount of data and computation involved. The peripheral equipment consisted of a teletype with a read/write facility together with a high-speed punch, a high-speed reader and an X - Y plotter.

The oscillator of the DTFA supplied a conventional shaker via a power amplifier. The coupling of the shaker to the force transducer mounted on the exciting block was made through a short flexible push rod made of steel 1 mm diameter and 25 mm long. This allowed the test structure to rotate slightly when the applied force did not pass through its centre of gravity without being restrained by an unknown couple.

During Run 1 the force was input at a distance e_1 from P and the inertance data at each of the test frequencies were stored on tape. The force input was then moved to a distance e_2 from P. At each test frequency during Run 2, inertance data were again measured and combined with the corresponding data read from the Run 1 tape. The matrix calculation for the four complex components of the mobility matrix $[Y]$ was carried out and the results printed on the teletype and also punched on tape. Graphs of the mobility data versus frequency were subsequently made from the taped data.

Development of Exciting Blocks

Each exciting block was designed to be used with a Bruel and Kjaer type E200 Force Transducer and Endevco type 23DE Accelerometers.

Easel on earlier tests (1), block Mk. 4 was designed to provide the smallest, lightest block which could have two accelerometers on its upper surface, equidistant from the measuring point P, and also have two positions for the force gauge. A drawing of this block is shown in Fig. 2. The foot of the block has dimensions 24 by 32 mm which closely matches the section of the test beam to which it was attached (with adhesive) during the tests.

The results of tests using the Kk.4 block were poor in the measurement of the rotational mobilities, of $(\dot{\theta}/M)$ in particular. It was thought that the measurement of $\dot{\theta}$ could be improved by increasing s (the accelerometer offset) from 25 mm to 50 mm and the rotational signal level could be increased by shifting the force transducer in Run 1 from 0 to 50 mm. Thus a Mk. 5 block was designed which had the accelerometers and the force transducer mounted back-to-back as shown in Fig. 3. The foot of this block (30 mm by 32 mm,) was slightly wider than the test beams but it was thought necessary to ensure adequate stiffness at the ends of the block by making the 'skirts' 6 mm thick.

Block Mk. 5 was used extensively in measuring the four mobility parameters of the beams. As before, the rotational quantities were obtained less accurately

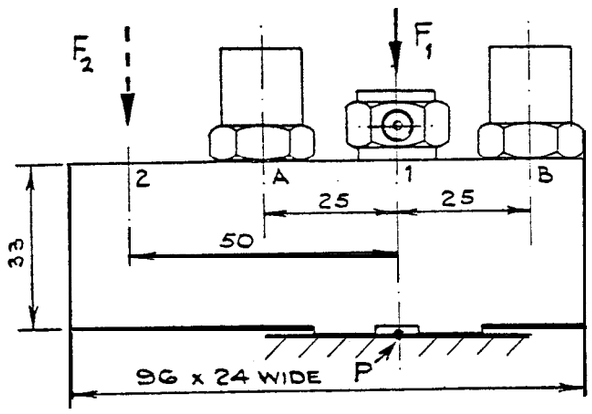

2, A, 1, 0, ARE HOLES DRILLED & TAPPED $\frac{10}{32}$ UNF

A & B FOR ACCELEROMETERS ENDEVCO 233 E

1 & 2 FOR FORCE GAUGES B&K 6200.

FIG. 2. EXCITING BLOCK. MARK 4.

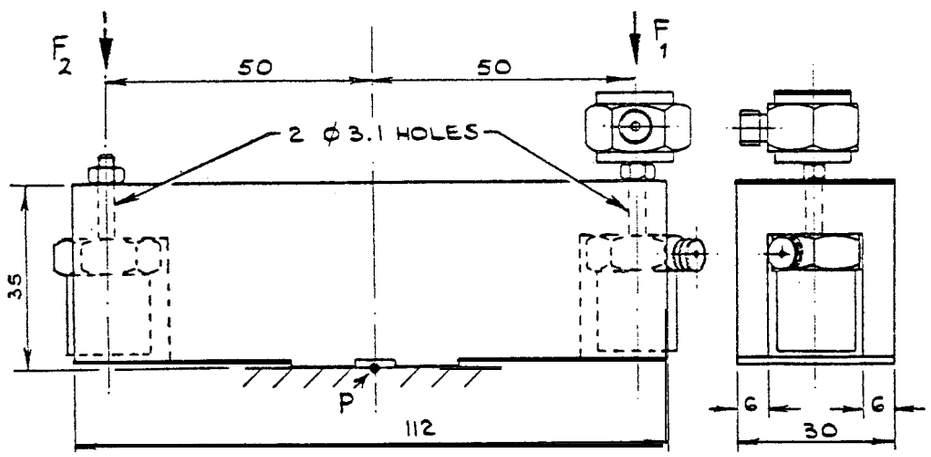

FIG.3. EXCITING BLOCK. MARK 5.

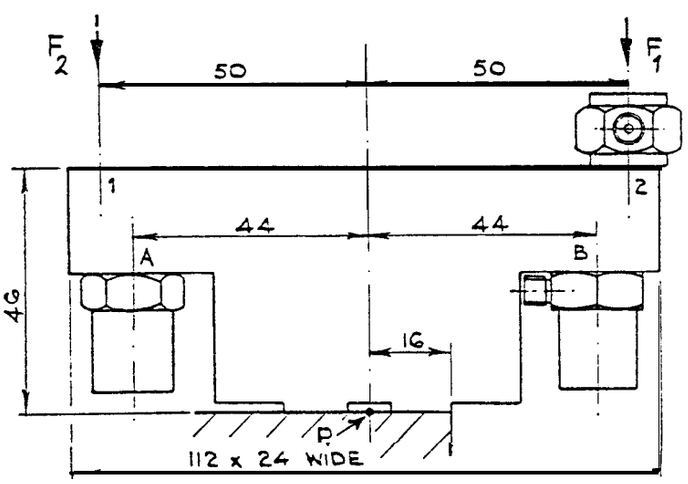

ALL DIMENSIONS IN mm.

FIG.4. EXCITING BLOCK. MARK 6

than tne translational, with ($\dot{\theta}$/M) generally being poor, especially at low frequencies. Two factors were significant:-

(a) The transverse sensitivity of the accelerometers gave rise to signals comparable to the small difference signals associated with $\ddot{\theta}$ measurement; and

(b) There appeared to be direct interference between the force gauge and the accelerometer when *the* transducers shared a common mounting stud.

The first factor was minimised by the use of accelerometers selected to have *a* transverse sensitivity of less than 1.0%.

Tne second factor was corrected by the design of block Nk. 6, which has the same essential features as block Mk. 5 but does not use a common mounting stud for both force gauge and accelerometer. This block is shown in Fig. 4: it has no 'skirts' but has a thicker top section to provide sufficient stiffness.

All the measurements reported in this paper were made using block Mk. 6.

Measured Mobilities of Long and Short Beams

In order to measure the nobilities of the long beam, the Mk. 6 exciting blockwas attached by adhesive to the beam such that the test point, P, was as close as possible (0.016 m) to the tip. Measurements were made at 76 discrete frequencies *in* the range 31.6 Hz to 1000 Hz and are presented in Fig. 5 in which the continuous line shows the theoretical response for the beam tip, computed using closed-form receptance formulae, and the points are the measured data.

The measured responses for ($\dot{X}$/F), ($\dot{\theta}$/F) and ($\dot{X}$/M) show a little scatter but are accurate to within a-bout 2 dB up tc 800 Hz. The ($\dot{\theta}$/M) response is inaccurate below the first response and shows an antiresonance at about 57 Hz whereas the theoretical antiresonance is well below 30 Hz. Above tne first resonance at 86 Hz, however, the measured ($\dot{\theta}$/M) response is reasonably accurate. Tne results of otner tests on this beam have very similar features.

A number of corresponding tests were carried out on tne short beam and *the results* are shohn in Fig. 6. These show very good correlation between the measured data and the theoretical tip response for the ($\dot{X}$/F), ($\dot{\theta}$/F) and ($\ddot{X}$/M) mobilities. Tne biggest discrepancies are in the location of the antiresonances, but this is probably a result of the measurement point not being quite at the tip of the beam, but 0.016 m inboard. (A theoretical calculation was made for a point 0.016 m along a 0.65 beam. This showed antirescnances exactly coincident with those cf the measured data. The resonances of course, were unchanged and remained in close coincidence with the measured data points). Tne($\dot{\theta}$/M) response is reasonably accurate above 200 Hz but has a considerable error of about +8 dB below that frequency.

In general, it can be seen that the two rotational responses ($\dot{\theta}$/F) and ($\dot{\theta}$/M) are the more-difficult to measure accurately and (e/K:), which invoives two rotational quantities, is unlikely tc be accurate at frequencies below the first resonance. Tne $\ddot{\theta}$ data *depends on* the difference between the signals of the 2 accelerometers, which have theiefore to be accurately matched and carefully calibrated. Any spuriccs response which has oniy a slight effect on the $\ddot{X}$ data (which depends on the sum of the accelerometer signals) will have a major effect cn the $\ddot{\theta}$ value. In most cases it is also true to say tnat the expected values of acceleration due to rotation are much smaller than those due to translation.

4. ANALYSIS C? THE COUPLED BEAMS

Coupling of Ccmoonents

Components A and B have mobility properties given by:-

$$\{\dot{X}_A\} = [Y_A]\{F_A\} \quad (8)$$

and $$\{\dot{X}_B\} = [Y_B]\{F_B\} \quad (9)$$

Where $[Y]$is a mobility matrix for the point on the structure which is of interest.

When the components are coupled (to form A + B) their respective motions at the coupling point must be identical:-

$$\{\dot{X}_A\} = \{\dot{X}_B\} = \{\dot{X}_C\} \quad (10)$$

snc considering the equilibrium at the point of connection :-

$$\{F_A\} + \{F_B\} = \{F_C\} \quad (11)$$

where $\{F\}$ is the net force exerted on the coupled structure.

Tne mobility cf the combination, $[Y_C]$, features in the equation:-

$$\&) \quad = [Y_C]\{F_C\}$$

FIG. 5 MOBILITY PROPERTIES OF THE LONG BEAM: I

—— Theoretical . . . Direct Measurements

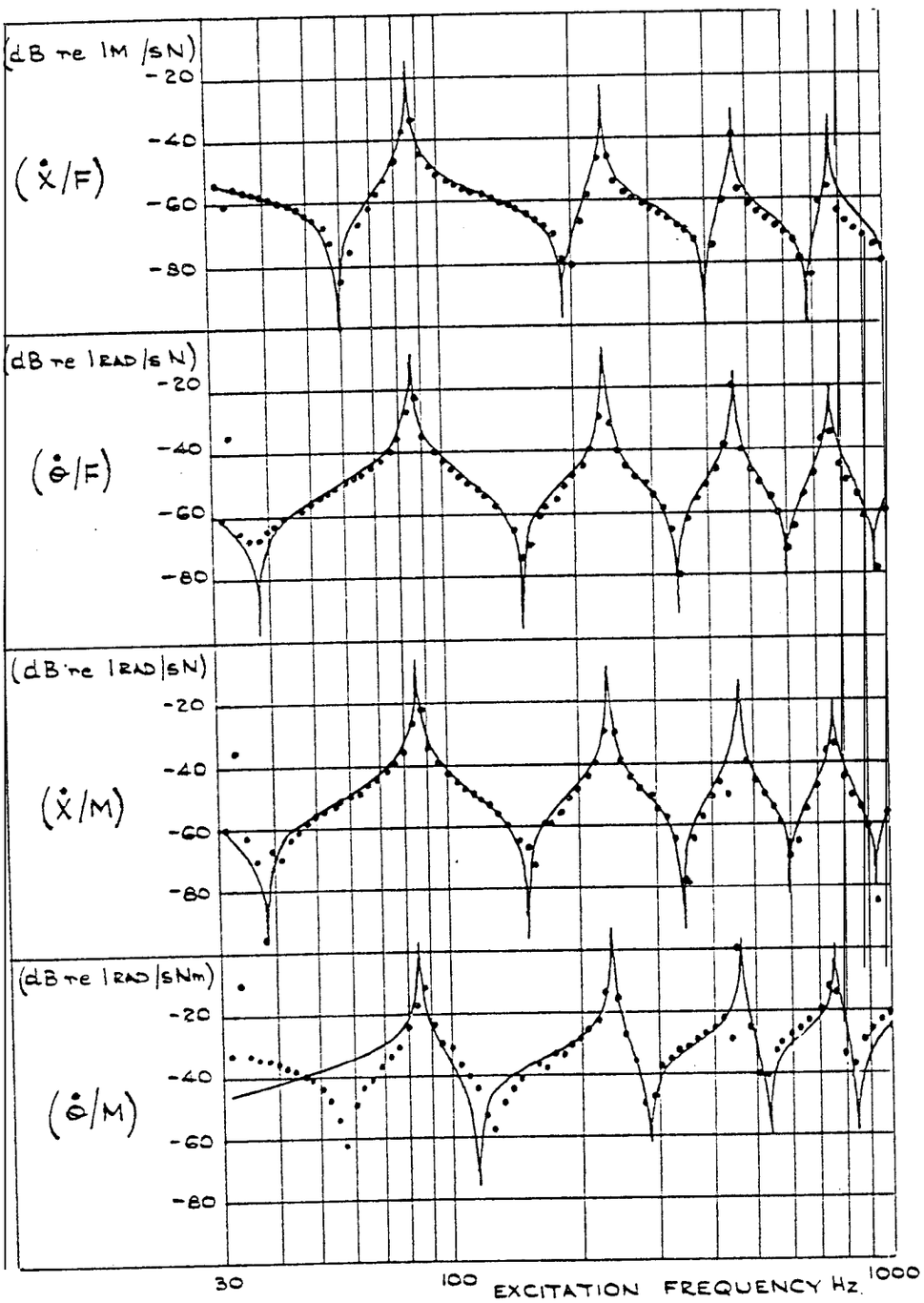

FIG. 6 MOBILITY PROPERTIES OF THE SHORT BEAM: I

——— Theoretical ... Direct Measurements

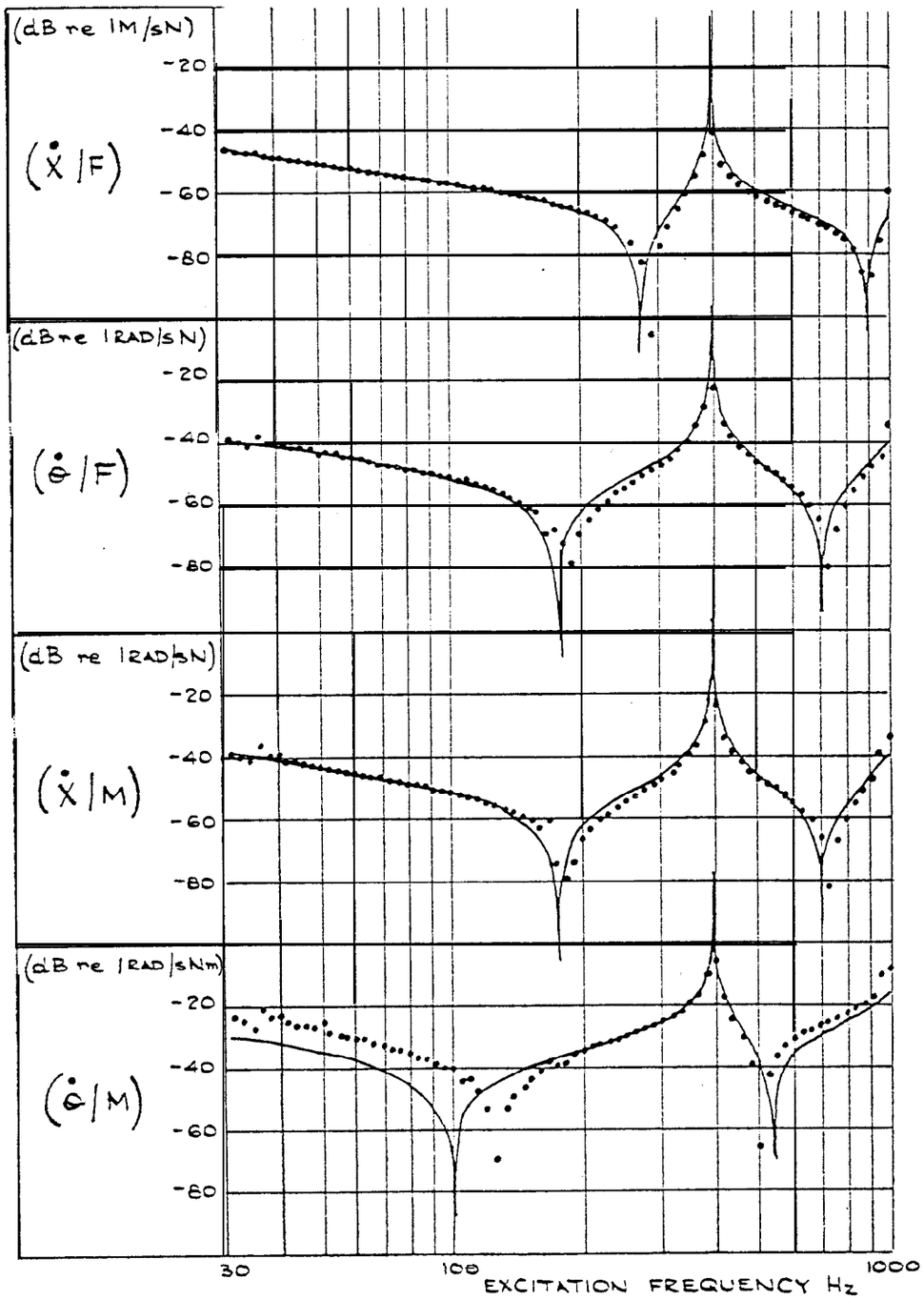

$$= [Y_C]\ (\{F_A\} + \{F_B\})$$

$$= [Y_C]\ ([Y_A]^{-1} + [Y_B]^{-1})\ \{\dot{X}_C\} \quad (12)$$

$$\therefore [Y_C] = ([Y_A]^{-1} + [Y_B]^{-1})^{-1} \quad (13)$$

Calculation of the mobility matrix of an assembly for any particular frequency thus involves inverting the mobility matrix of each component (for that frequency); adding the two resultant impedance matrices and then re-inverting.

This process has to be carried out at each frequency data point.

Coupled-Beam Analysis Using Raw Data

The measured data used for Fig. 5 and 6 were combined, frequency by frequency, in a calculation of the mobility responses at the point of connection between the long beam (1.4 m) and the short beam (0.65 m). The computation involved reading data simultaneously from two tapes; then inverting and adding two matrices; inverting the result and punching out the data produced. This process took about 30 seconds per resultant data point, the major part of the time being occupied by the teletype reading taped data.

The result of this direct calculation is shown as Fig. 7 together with the theoretical values of the mobility at a point 0.65 m along a 2.05 m beam. The predicted results are extremely poor for all four mobility parameters except in the range 180 Hz to 400 Hz. Examination of the input data shows that this is the only frequency range for which the $(\dot{e}/M)$ response of the short beam is accurate. The other seven mobility parameters have wider ranges of reasonable accuracy. Thus it is concluded that if any of the eight input mobility parameters is inaccurate at a particular frequency, the all the calculated mobilities of the combined structure will probably be wrong at that frequency.

The $(\dot{e}/M)$ responses were confirmed as the chief sources of error by another calculation in which the raw $(\dot{e}/M)$ data of both subsystems were replaced by theoretical $(\dot{e}/M)$ data. The result of this exercise is shown in Fig. 8 which illustrates a considerable improvement in accuracy when compared with Fig. 7, especially below 50 Hz. The overall accuracy, however, is still not acceptable since there are ranges where the scatter is considerable, (80 - 100 Hz; 120 - 140 Hz; 400 - 500 Hz, for example).

Improvement in the resultant coupled data could evidently be made first, by smoothing, and second, by improving the accuracy of the rotational mobilities $(\dot{e}/F)$ and $(\dot{e}/M)$ for the two component subsystems.

5. COUPLED-BEAM ANALYSIS USING SMOOTHED DATA

Smoothing Technique

The first attempt to improve the component data was by a simple smoothing process. In this, the experimental mobility 'curve' is curve-fitted by a suitable equation which thus smoothes out random scatter in the data. The appropriate equation is formed by identifying from the experimental data the main modes of vibration of the test structure. Modal identification provides a simple representation of a system with n resonances as an assembly of n single-degree-of-freedom oscillators, each resonating at one of the n resonant frequencies and weighted by a modal constant. The method of modal identification used here was based on the treatment developed by A. L. Klosterman (3) and is summarised in Appendix 1. There it is shown that the modal constants for a system with n dominant modes can be determined by matrix manipulation involving measured mobility data obtained at n discrete non-resonant frequencies. In the present study, this data could of course be selected from that already measured. Once the n modal constants (e.g. $A_1, A_2 \ldots A_n$ for (X/F)) have been determined, the identified frequency response can be regenerated by summing the contribution from each mode in turn at each frequency.

The raw data for the long beam was examined and five resonant frequencies (0, 86, 234, 457 and 758 Hz) estimated. Data measured at the n off-resonant frequencies of 31.6, 69.2, 120, 302 and 724 Hz were taken and used to calculate modal constants from which the smoothed curves of Fig. 9 were calculated. These are seen to be quite similar to the raw data of Fig. 5 except above 758 Hz, the highest resonant frequency used. Above that frequency, the curves approach the 20 dB/decade mobility line of a mass, because the dominant contribution is from the highest mode included in the identification which is mass-like above its resonant frequency.

In the case of the short beam, the resonant frequencies were estimated from the raw data to be 0, 394 and 1100 Hz and data measured at 31.6, 209 and 603 Hz were used in the modal calculations giving the results shown in Fig. 10

FIG. 7 MOBILITY PROPERTIES OF THE COUPLED BEAM: I

——— Theoretical ... Predicted from direct measurements on component beams

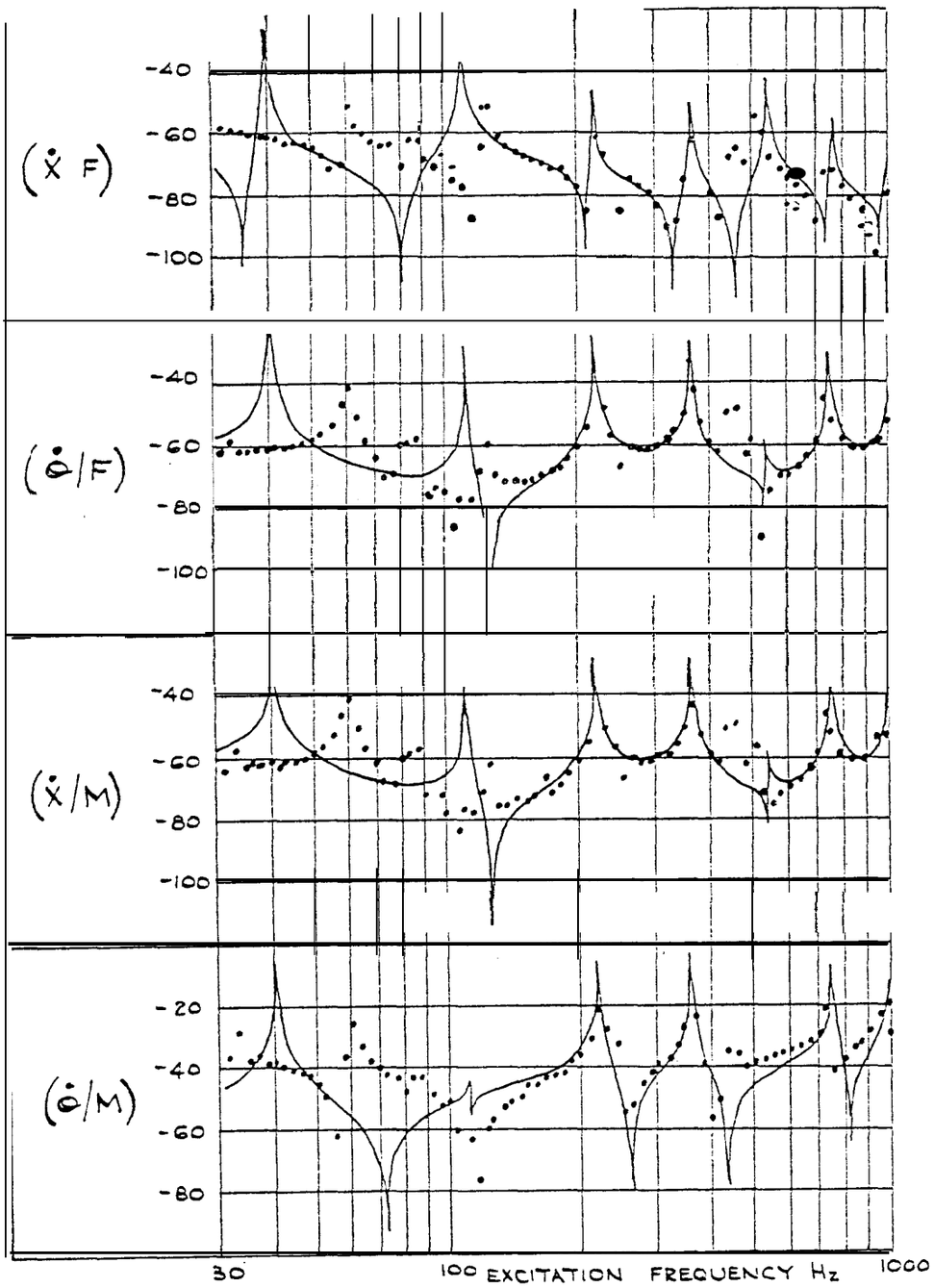

FIG. 8 MOBILITY PROPERTIES OF THE COUPLED BEAM: II

——— Theoretical ... Predicted from direct measurements plus theoretical (θ/M) data

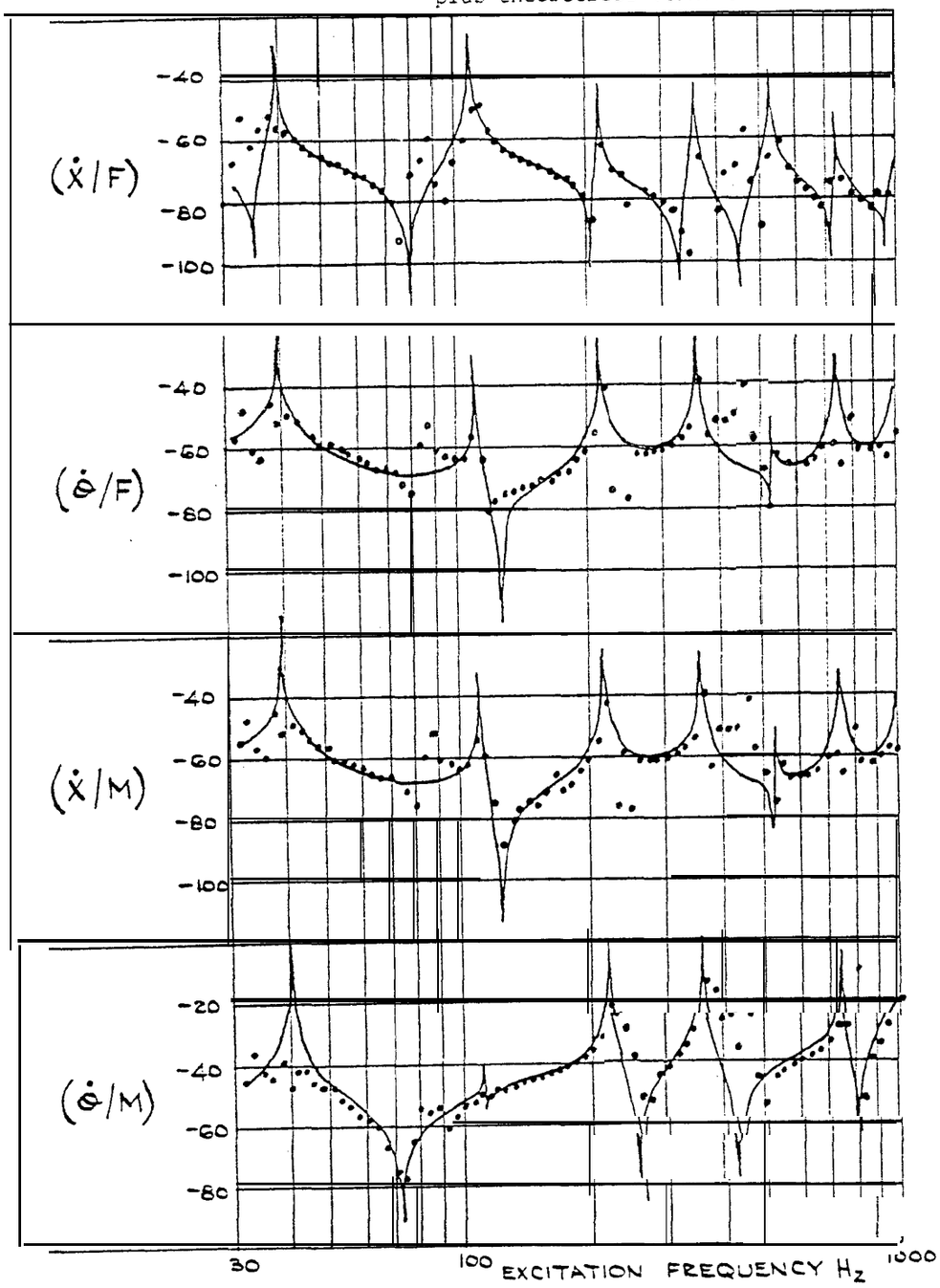

FIG. 9 MOBILITY PROPERTIES OF THE LONG BEAM: II

——— Theoretical . . . Smoothed measurements

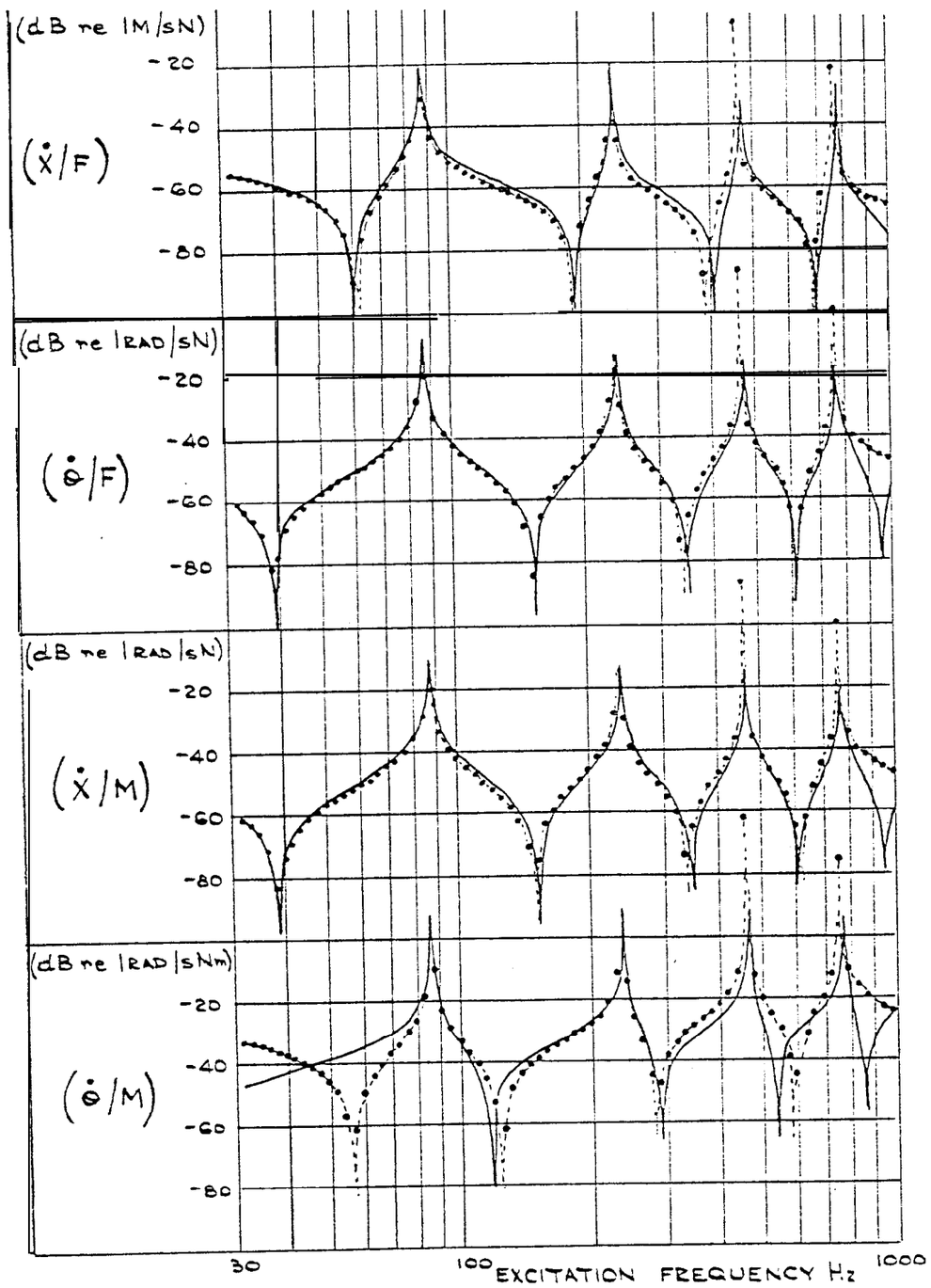

FIG. 10 MOBILITY PROPERTIES OF THE SHORT BEAM: II

Theoretical . . . Smoothed measurements

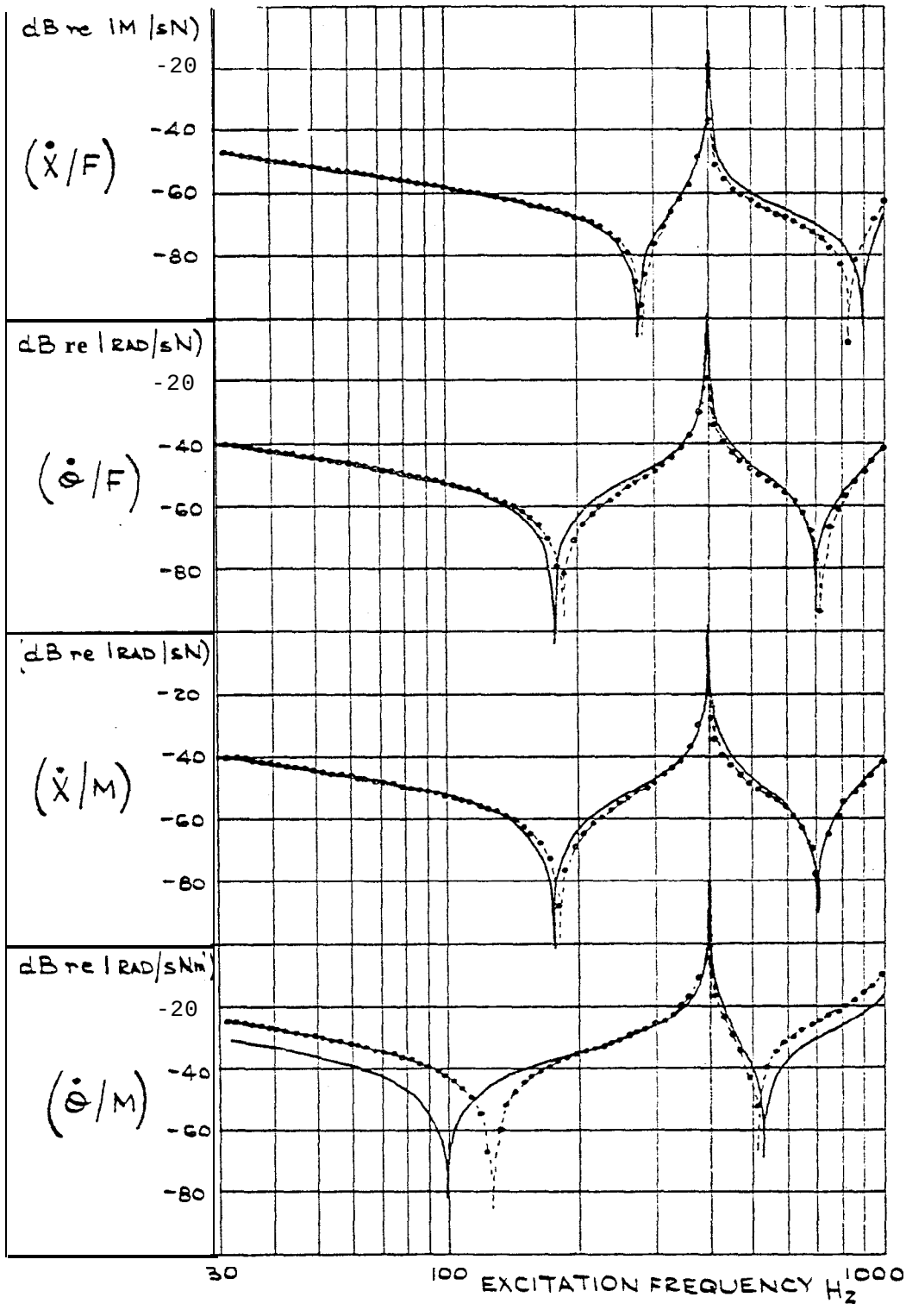

which is recognisably a smoothed version of Fig. 6. There is no high frequency discrepancy on this plot because the highest mode used is at a frequency higher than the range limit of 1000 Hz. In general, smoothing by modal identification gives acceptable accuracy provided that the number of modes identified is one more than the number of modes which lie within the frequency range of interest.

Coupled-Beam analysis using smoothed data

The smoothed data of Fig. 9 and 10 were coupled using exactly the same process as before to produce a predicted set of responses for a 2.05 m beam. The results are presented in Fig. 11 but although having less scatter, they are not otherwise any improvement in the unsmoothed results in Fig. 7.

However, there was one advantage in using smoothed data at this stage, and that was in the computation time which was considerably reduced since much less data needed to be handled. Printing of the output on the teletype took the greater part of the time, the process taking about 12 seconds per resultant data point (compared with 33 seconds previously).

6. ALTERNATIVE METHOD OF DETERMINING ROTATIONAL MOBILITIES

A method was now sought by which the accuracy of $(\dot{\theta}/F)$ and $(\dot{\theta}/M)$ mobility data could be improved. As the rotational motion (θ, $\dot{\theta}$ or $\ddot{\theta}$) is evidently very difficult to measure accurately, some alternative means of deriving the appropriate mobilities was required.

Referring to the modal identification analysis presented in Appendix 1, we find a particularly interesting and useful result. For each mode identified, there are four constants - A_r, B_r, C_r and D_r - which relate to the contribution of the r^{th} mode to the $(\dot{X}/F)(\dot{\theta}/F)$ $(\dot{X}/M)$ and $(\dot{\theta}/M)$ mobilities respectively. Now it is shown in the kppendix that these four constants are very simply related by:

$$B_r = C_r \text{ and } Dr = C_r^2/A_r$$

(The special case of the zero-frequency mcdes possessed by a free-free structure is treated in Appendix 2, resulting in

$$B_1 = C_1 \text{ and } D_1 = C_1^2/(A_1 - 1/m)$$

where m is the mass of the structure).

Because of the greeter difficulty in measuring rotation than translations, it is possible to derive more accurate values for A_r and C_r from (X/F) and $(\dot{X}/M)$ data) than for B_r and D_r. However, it is clear from the above relationships that these latter constants may be immediately determined from A_r and C_r.

Thus the mobilities $(\dot{\theta}/F)$ and $(\dot{\theta}/M)$ can be derived from measurements of $(\dot{X}/F)$ and $(\dot{X}/M)$ using the modal identification techniques, without measuring rotetions directly.

Calculations using the relationships between the modal constants developed above were carried out for both beams and the results are shown in Figs. 12 and 13. In these, there are only three distinct responses presented since $(\dot{\theta}/F)$ is now automatically identical to $(\dot{X}/M)$ (since $B_r = D_r$).

When the derived $(\dot{\theta}/M)$ response of Fig. 12 is compared With the smoothed $(\dot{\theta}/M)$ response of Fig. 9, it is immediately apparent that the accuracy at low frequencies below the first resonance at 86 Hz, where the Fig. 9 response is very poor, is now greatly improved and at higher frequencies up to 800 Hz, where Fig. 9 was quite good, it is a little further improved.

Similar observations apply to the comparison of $(\dot{\theta}/M)$ responses of Figs. 10 and 13 for the short beam. The accuracy of the Fig. 13 curve is less than that of Fig. 12 because fewer modes are included, but most significantly the $(\dot{\theta}/M)$ response is accurate around 30 Hz.

The conclusion of this section is that better $(\dot{\theta}/M)$ resuits may be obtained by identifying the A_r and C_r modal constants from $(\dot{X}/F)$ and $(\dot{X}/M)$ measurements and then calculating B_r and D_r than by trying to identify B_r and D_r directly from the inevitably less reliable $(\dot{\theta}/F)$ and $(\dot{\theta}/M)$ raw data.

7. COUPLED-BEAM ANALYSIS USING DERIVED DATA

The four mobility responses for the combined beam were again computed, this time using the derived B_r and D_r constants together with the identified A_r and Cr constants. Xgain these are only three distinct responses presented in Fig. 14 because $(\dot{\theta}/F)$ and (X/M) are taken as identical,

This coupled data is inaccurate above 800 Hz, the highest frequency for which the data for the long beam is reliable. Below 600 Hz the fit of the smoothed and derived data to the curve calculated from closed-form receptance

FIG. 11 MOBILITY PROPERTIES OF THE COUPLED BEAM: III

——— Theoretical ... Predicted from smoothed measurements on component beams.

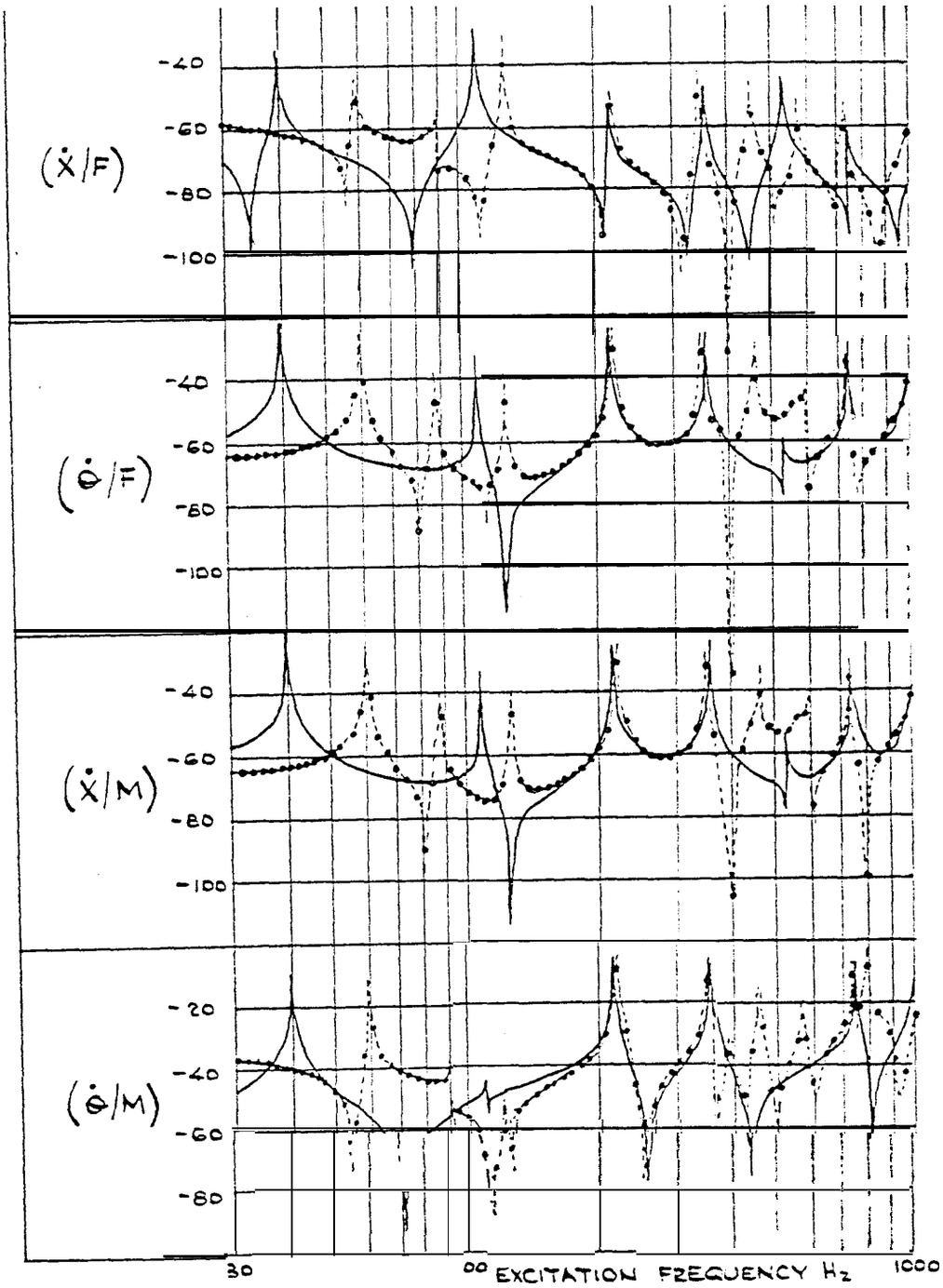

FIG. 12 MOBILITY PROPERTIES OF THE LONG BEAM: III

Theoretical ·..Smoothed measurements for (X/F)(X/M)
Derived measurements for ($\dot{\theta}$/F)($\dot{\theta}$/M)

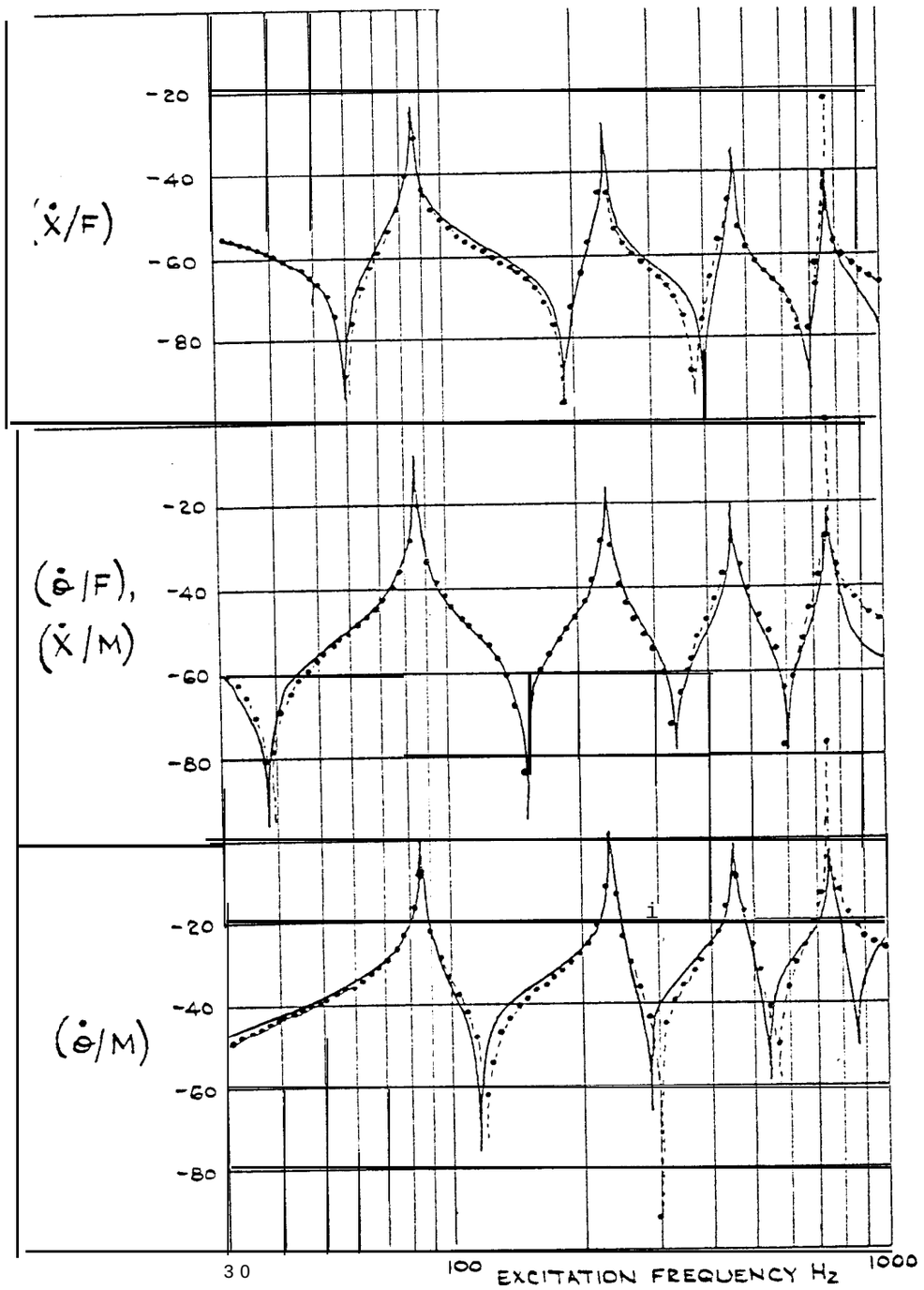

FIG 3 MOBILITY PROPERTIES OF THE SHORT BEAM: III

Theoretical ... Smoothed Measurements for $(\dot{X}/F)(\dot{X}/M)$
Derived measurements for $(\dot{\theta}/F)(\dot{\theta}/M)$

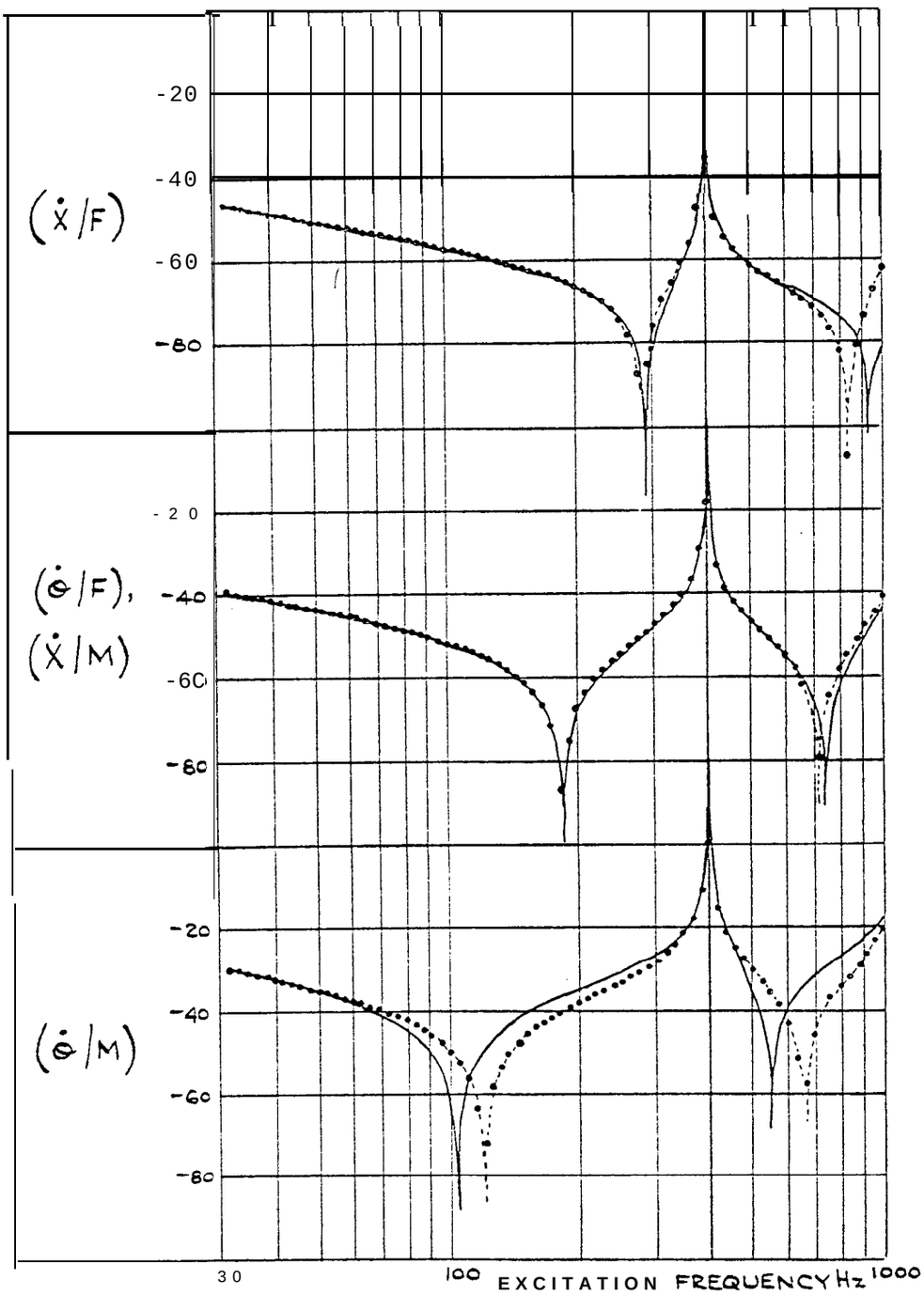

FIG. MOBILITY PROPERTIES OF THE COWLED BEAM: IV

——— Theoretical . . . Predicted from Smoothed/derived measurements on component beams.

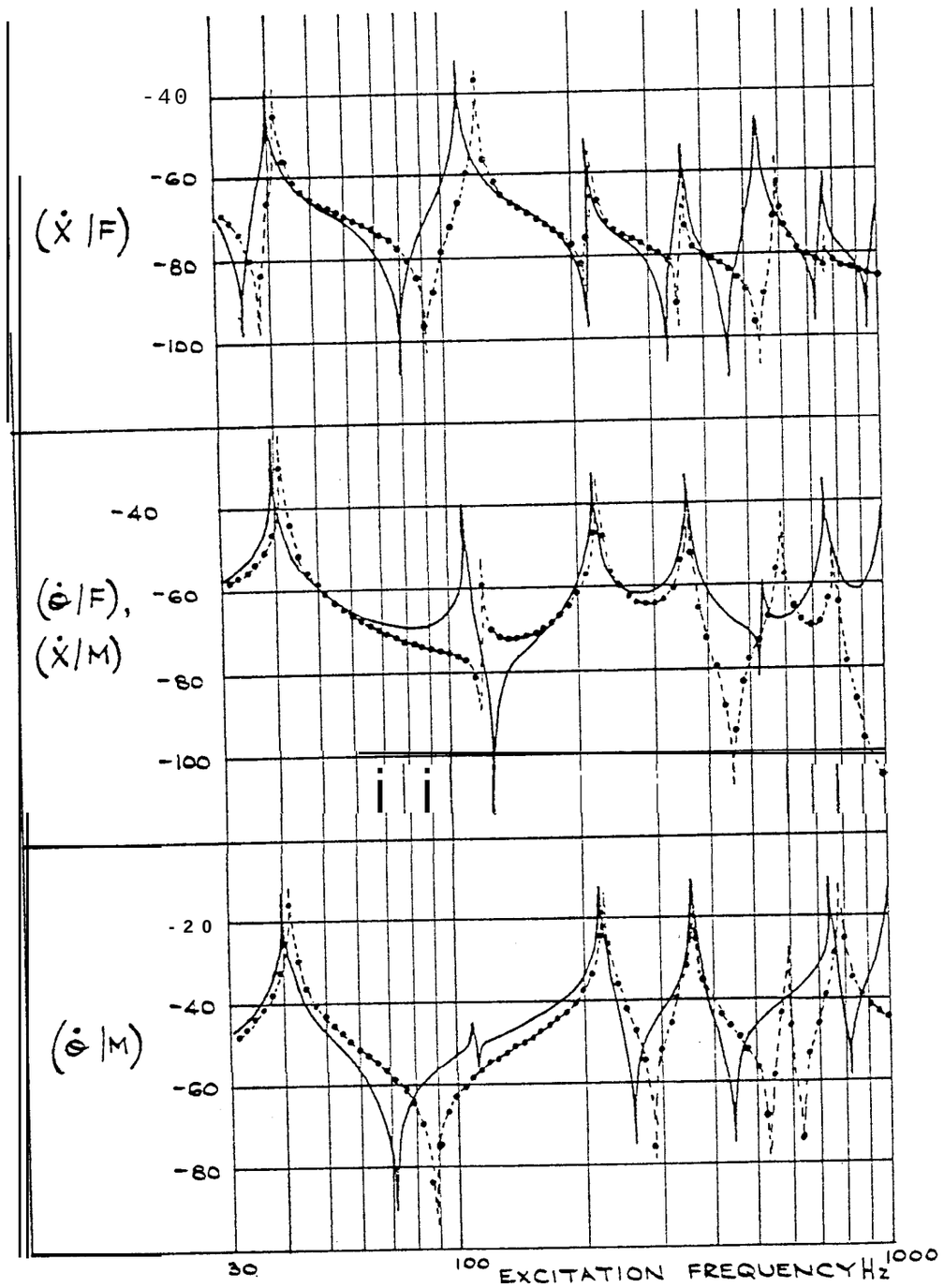

formulae is much better than either of the previous examples shown in Figs. 7 and 11. In particular, these results accurately predict the low frequency resonance at 42 Hz (close to the theoretical value of 40 Hz) which is absent from the earlier coupled-beam results. The other 5 resonances are also indicated with reasonable accuracy for the mobility ($\dot{X}/F$), and this response has the right general shape and level up to 800 Hz. The ($\dot{\theta}/F$), ($\dot{X}/M$) responses maintain good shape up to 400 Hz, although the resonance at 120 Hz is only just noticeable. The 120 Hz resonance is missed altogether from the ($\dot{\theta}/M$) response but it should be noted that the corresponding theoretical resonance is very small.

The identification and derivation process is thus more accurate for low frequencies than for high which may be explained by the inherently greater accuracy of low frequency modal constants, The results are felt to be significant mainly because it has not been possible to measure ($\dot{\theta}/M$) at all accurately at frequencies below the first resonance by any other method.

8. CONCLUSIONS

It has been demonstrated again that when experimentally determined mobility (or impedance) data are required for further analysis, due consideration must be given to all the directions in which the test structure vibrates. In particular, for beams it is necessary to include the rotational motion as well as the translational.

Measurement of rotational mobility data is hindered by the difficulty of measuring rotational response. However, a method has been presented which enables the determination of such rotational mobility data from measurements of translational responses only, thereby obviating the need to measure angular motion. The technique involves simply making two otherwise conventional mobility measurements, plus some analysis.

REFERENCES

1. 3. J. Ewins and M. G. Sainsbury, "Mobility Measurement for the Vibration Analysis of Connected Structures", Shock and Vibration Bulletin, 42, Pt 1, 1972.

2. J. E. Smith, "Measurement of the Total Structural Mobility Matrix", Shock and Vibration Bulletin, 40, 1970.

3. A. L. Klosterman, "On the Experimental Determination and Use of Modal Representations of Dynamic Characteristics", University of Cincinatti, Ph.D. Thesis, 1971.

APPENDIX I. The Response of a Multi-Degree of Freedom System to Sinusoidal Excitation

The response of a n-degree of freedom system to steady-state sinusoidal excitation at an angular frequency ω, can be written in generalized coordinates q_1, q_2 etc., see ref. (3):

$$\{Q\} = \sum_{r=1}^{n} \frac{\{\psi_r\}^T \{F\} \{\psi_r\}}{m_r (\Omega_r^2 - \omega^2)} = \sum_{r=1}^{n} Y_r \{\psi_r\} \quad \text{(i)}$$

where $\{Q\}$ is a column vector of response amplitudes
$\{F\}$ is a column vector of input force amplitudes
and Ω_r is the r th eigenvalue
$\{\psi_r\}$ is the eigenvector of the rth mode
m_r is the mass of the r th mode

We are particularly interested in the response Q_i caused by the single excitation F_j:

$$Q_i = \sum_{r=1}^{n} \frac{(\psi_{rj} F_j)(\psi_{ri})}{m_r (\Omega_r^2 - \omega^2)} \quad \text{(ii)}$$

giving

$$(Q_i/F_j) = \sum_{r=1}^{n} \frac{\psi_{rj} \psi_{ri}}{m_r (\Omega_r^2 - \omega^2)} \quad \text{(iii)}$$

We wish to consider two responses, $X (=Q_1)$ and $\theta (=Q_2)$, and two forces, $F (=F_1)$ and $M (=F_2)$

The system being considered is continuous but we may assume that at low frequencies only a finite number of modes need be included.

Thus we can write:-

$$(X/F) = \sum_{r=1}^{n} \frac{A_r}{(\Omega_r^2 - \omega^2)} \quad \text{(iv)}$$

$$(e/F) = \sum_{r=1}^{n} \frac{B_r}{(\Omega_r^2 - \omega^2)} \quad \text{(v)}$$

$$(X/M) = \sum_{r=1}^{n} \frac{C_r}{(\Omega_r^2 - \omega^2)} \quad \text{(vi)}$$

$$(\theta/M) = \sum_{r=1}^{n} \frac{D_r}{(\Omega_r^2 - \omega^2)} \qquad \text{(vii)}$$

Where $A_r = \phi_{r1}^2/m_r$; $B_r = \phi_{r2}\,\phi_{r1}/m_r$;

$$C_r = \phi_{r1}\,\phi_{r2}/m_r;\ D_r = \phi_{r2}^2/m_r \qquad \text{(viii)}$$

It follows that $B_r = C_r$ and $D_r = C_r^2/A_r$ (ix)

Thus all four modal constants may be deduced from A_r and C_r.

MODAL IDENTIFICATION

This is the process of determining the modal constants from measured impedance data.

Equation (iv) may be rewritten by substituting $-\omega^2 X = \ddot{X}$ to give

$$(\ddot{X}/F) = \sum_{r=1}^{n} \frac{-\omega^2 A_r}{(\Omega_r^2 - \omega^2)}$$

$$= \sum_{r=1}^{n} \frac{A_r}{(1 - \Omega_r^2/\omega^2)}$$

This quantity is the Inertance, the ratio of acceleration to force, the two quantities measured in impedance tests.

There are n modes being considered, and thus there are n resonant frequencies which must be known. Inertance data must be obtained at n non-resonant angular frequencies, $\omega_1, \omega_2, \omega_3 \ldots \omega_n$.

The matrix equation relating these quantities is

$$\begin{bmatrix} (\ddot{X}/F)_1 \\ (\ddot{X}/F)_2 \\ (\ddot{X}/F)_3 \\ \vdots \\ (\ddot{X}/F)_n \end{bmatrix} = \begin{bmatrix} \frac{1}{(1-\Omega_1^2/\omega_1^2)} & \frac{1}{(1-\Omega_2^2/\omega_1^2)} & \cdots & \frac{1}{(1-\Omega_n^2/\omega_1^2)} \\ \frac{1}{(1-\Omega_1^2/\omega_2^2)} & \cdots & & \frac{1}{(1-\Omega_n^2/\omega_2^2)} \\ \frac{1}{(1-\Omega_1^2/\omega_3^2)} & \cdots & & \cdots \\ \vdots & & \vdots & \\ \frac{1}{(1-\Omega_1^2/\omega_n^2)} & \cdots & & \frac{1}{(1-\Omega_n^2/\omega_n^2)} \end{bmatrix} \begin{bmatrix} A_1 \\ A_2 \\ A_3 \\ \vdots \\ A_n \end{bmatrix}$$

or

$$\{I_A\} = [R]\,\{A\}$$

similarly there are equations for the other modal constants:-

$$\{I_B\} = [R]\,\{B\};\ \{I_C\} = [R]\,\{C\} \quad \text{and} \quad \{I,\} = [R]\,\{D\}$$

The modal constants can thus be determined by inverting the R matrix and then pre-multiplying the appropriate response matrix

$$\{A\} = [R]^{-1}\,[I,) \quad \text{and so on.}$$

APPENDIX II. Solid Body Response

If the system is free-free it has a resonance at zero frequency ($\Omega_1 = 0$). Tne motion is, of course, that of a solid body. The relationships expressed in eouation (ix) do not hold for this case-and it is necessary to study the geometry of the motion to discover the corrections needed.

The body has mass m and moment of inertia I_G about its centroid G.

In the first instance the effect of pure input couple M on the angular response θ and the translational response X_P of point P are required. (Fig. 15.)

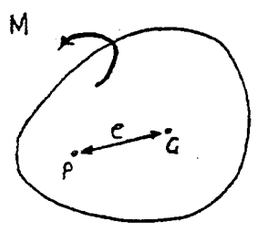

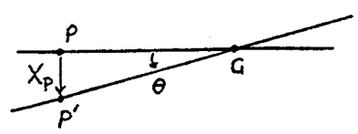

Fig. 15. Effect of Couple Input on Solid Body

Pure couple M produces rotation but no translation of G.

$M = I_G \ddot{\theta}$ $\quad \therefore (\ddot{\theta}/M) = 1/I_G$

$M = I_G(\ddot{X}_P/e)$ $\therefore (\ddot{X}_P/M) = e/I_G$

Secondly, the effect of the input force F acting at P is required.(Fig.16)

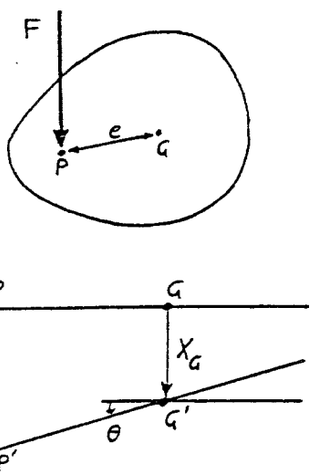

Fig. 16. Effect cf Force Input on Solid Body

Force input at F produces both rotation and translation cf G.

$X_P = e\,\theta + X_G$

$X_G = X_P - e\,\theta$

$F\,e = I_G \ddot{\theta}$ $\quad \therefore (\ddot{\theta}/F) = e/I_G$

$F = m\,\ddot{X}_G = m\,(\ddot{X}_P - e\,\ddot{\theta})$

$= m\,(\ddot{X}_P - e\,(e\,F/I_G))$

$\therefore F(1 + m\,e^2/I_G) = m\,\ddot{X}_P$

$\therefore (\ddot{X}_P/F) = 1/m + e^2/I_G$

It follows that $A_1 = 1/m + e^2/I_G$

$B1 = e/I_G$

$C_1 = e/I_G$

$D_1 = 1/I_G$

Thus $B1 = C1$ and $D_1 = C_1^2/(A_1 - 1/m)$